UAB
Universitat Autònoma de Barcelona

All about bones: bioarchaeological insights into social inequality and complexity during the Early Bronze Age

A multidisciplinary approach to Northern Mesopotamia and Northeastern Iberian contexts

ALICIA GLUITZ

ADVERTIMENT. L'accés als continguts d'aquesta tesi queda condicionat a l'acceptació de les condicions d'ús establertes per la següent llicència Creative Commons: https://creativecommons.org/licenses/?lang=ca

ADVERTENCIA. El acceso a los contenidos de esta tesis queda condicionado a la aceptación de las condiciones de uso establecidas por la siguiente licencia Creative Commons: https://creativecommons.org/licenses/?lang=es

WARNING. The access to the contents of this doctoral thesis it is limited to the acceptance of the use conditions set by the following Creative Commons license: https://creativecommons.org/licenses/?lang=en

UAB
Universitat Autònoma de Barcelona
Departament de Prehistòria

All about bones: bioarchaeological insights into social inequality and complexity during the Early Bronze Age

A multidisciplinary approach to Northern Mesopotamia and Northeastern Iberian contexts

PhD in Prehistoric Archaeology

ALICIA GLUITZ

SUPERVISOR:

Dr. Miquel Molist Montañà

2025

ABSTRACT

All about bones: bioarchaeological insights into social inequality and complexity during the Early Bronze Age. A multidisciplinary approach to Northern Mesopotamia and Northeastern Iberian contexts.

The present study investigates the manifestation of social inequalities during the Early Bronze Age through comprehensive bioarchaeological analysis of human remains from three strategically selected archaeological sites: Gird Lashkir and Gir-e Gomel in northern Mesopotamia, and Plaça de la Gardunya in northeastern Iberia. Despite their geographical separation, these sites share common characteristics of emerging urbanism, increasing social complexity, and limited published archaeological data, making them ideal case studies for evaluating multidisciplinary approaches to understanding ancient societies.

A comprehensive methodological framework was employed, integrating archaeothanatological analysis, anthropological examination, dental microwear analysis, and stable isotope analyses of bone collagen and tooth enamel hydroxyapatite. This multifaceted approach facilitated reconstruction of burial practices, social organization, health status, dietary patterns, and residence patterns across the studied populations.

The results reveal contrasting social dynamics between the two regions. Northern Mesopotamian sites (Gird Lashkir and Gir-e Gomel) exhibited clear evidence of hierarchical social organization through differential burial treatments, ornamental assemblages, and grave goods distribution, with cylinder seals and exotic materials indicating complex trade networks and ascribed status inheritance. Conversely, Plaça de la Gardunya demonstrated egalitarian social organization characterized by collective burial practices in hypogea with no differential treatment of individuals.

Dietary analysis through dental microwear patterns and stable isotope signatures revealed omnivorous subsistence strategies across all populations, with consumption of C_3 plants and domesticated animal proteins. Despite evidence of social stratification in northern Mesopotamia, no significant dietary differentiation was observed based on age, sex, or social status, suggesting an egalitarian access to food. Mobility patterns identified through oxygen and strontium isotope analysis indicated local populations and non-local individuals, suggesting regional demographic mobility.

This research demonstrates the effectiveness of integrative bioarchaeological approaches in elucidating complex social realities and challenges assumptions about the relationship between social stratification and resource access in Early Bronze Age societies. The findings contribute to broader understanding of prehistoric social organization and highlight the importance of multidisciplinary methodologies in archaeological interpretation.

RESUMEN

Todo sobre los huesos: perspectivas bioarqueológicas sobre la desigualdad y la complejidad social durante la Edad del Bronce Antiguo. Un enfoque multidisciplinar para los contextos del norte de Mesopotamia y el noreste de la Península Ibérica.

El presente estudio se centra en investigar la manifestación de las desigualdades sociales durante la Edad del Bronce Antiguo a través de análisis bioarqueológicos de los restos humanos procedentes de tres yacimientos arqueológicos estratégicamente seleccionados: Gird Lashkir y Gir-e Gomel en el norte de Mesopotamia, y Plaça de la Gardunya en el noreste de la Península Ibérica. A pesar de su lejanía geográfica, estos yacimientos comparten características comunes de urbanismo emergente, creciente complejidad social y una limitación de datos arqueológicos publicados, convirtiéndolos en casos de estudio ideales para evaluar enfoques multidisciplinarios en la comprensión de las sociedades del pasado.

Se ha utilizado un marco metodológico que integra análisis arqueotanatológicos, análisis antropológicos, análisis del patrón de microdesgaste dental y análisis de isótopos estables en muestras de colágeno de hueso y de hidroxiapatita del esmalte dental. Este enfoque ha permitido reconstruir las prácticas funerarias, la organización social, el estado de salud, los patrones dietéticos y los patrones de residencia de las poblaciones estudiadas.

Los resultados revelan dinámicas sociales que contrastan entre las dos regiones. Los yacimientos del norte de Mesopotamia (Gird Lashkir y Gir-e Gomel) exhiben evidencias claras de una organización social jerárquica a través de tratamientos funerarios diferenciados, conjuntos ornamentales y distribución de ajuares, con sellos cilíndricos y materiales exóticos indicando redes de intercambio complejas y herencia de estatus adscrito. Por otro lado, Plaça de la Gardunya demuestra poseer una organización social igualitaria caracterizada por prácticas funerarias colectivas en hipogeos sin tratamiento diferencial de los individuos.

El análisis dietético a través de los patrones de microdesgaste dental y las señales de isótopos estables han revelado la práctica de estrategias de subsistencia omnívoras en todas las poblaciones, con un consumo de plantas tipo C_3 y de proteínas animales de especies domesticadas. A pesar de la evidencia de estratificación social en el norte de Mesopotamia, no se ha observado una diferenciación significativa al acceso de alimentos basada en la edad, el sexo o el estatus social, sugiriendo un acceso igualitario. Los patrones de movilidad identificados a través del análisis de isótopos estables de oxígeno y de estroncio han indicado la existencia de individuos locales y no locales, sugiriendo mobilidad demográfica regional.

Esta investigación demuestra la efectividad de los enfoques bioarqueológicos para dilucidar realidades sociales complejas y desafía las suposiciones sobre la relación entre estratificación social y acceso a los recursos alimenticios en las sociedades de la Edad del Bronce Antiguo. Los hallazgos contribuyen a una comprensión más amplia de la organización social en el pasado y destacan la importancia de metodologías multidisciplinares en la interpretación arqueológica.

RESUM

Tot sobre els ossos: perspectives bioarqueològiques sobre la desigualtat i la complexitat social durant l'Edat del Bronze Antic. Un enfocament multidisciplinari pels contextos del nord de Mesopotàmia i del nord-est de la Península Ibèrica.

El present estudi investiga la manifestació de les desigualtats socials durant l'Edat del Bronze Antic a través de l'anàlisi bioarqueològica de les restes humanes procedents de tres jaciments arqueològics estratègicament seleccionats: Gird Lashkir i Gir-e Gomel al nord de Mesopotàmia, i Plaça de la Gardunya al nord-est de la Península Ibèrica. Tot i la seva llunyania geogràfica, aquests jaciments comparteixen característiques comunes d'urbanisme emergent, complexitat social creixent i limitades dades arqueològiques publicades, convertint-los en casos d'estudi ideals per avaluar enfocaments multidisciplinaris en la comprensió de les societats del passat.

S'ha utilitzat un marc metodològic multidisciplinar que integra l'anàlisi arqueotanatològica, l'anàlisi antropològic, l'anàlisi del patró de microdesgast dental i l'anàlisi d'isòtops estables de col·lagen ossi i hidroxiapatita de l'esmalt dental. Aquest enfocament ha facilitat la reconstrucció de les pràctiques funeràries, l'organització social, l'estat de salut, els patrons dietètics i els patrons de residència de les poblacions estudiades.

Els resultats revelen dinàmiques socials contrastants entre les dues regions. Els jaciments mesopotàmics del nord (Gird Lashkir i Gir-e Gomel) han exhibit evidència clara d'organització social jeràrquica a través dels tractaments funeraris diferenciats, conjunts ornamentals i distribució d'aixovars, amb segells cilíndrics i materials exòtics indicant xarxes d'intercanvi complexes i herència d'estatus adscrit. Per altra banda, Plaça de la Gardunya ha demostrat una organització social igualitària caracteritzada per pràctiques funeràries col·lectives en hipogeus sense tractament diferencial dels individus.

L'anàlisi dietètica a través de patrons de microdesgast dental i de les senyals dels isòtops estables han revelat estratègies de subsistència omnívores en totes les poblacions, amb consum de plantes de tipus C_3 i de proteïnes d'animals domesticats. Tot i l'evidència d'estratificació social al nord de Mesopotàmia, no es va observar un accés diferencial significatiu als recursos alimentaris basat en l'edat, el sexe o l'estatus social, suggerint un accés igualitari als aliments. Els patrons de mobilitat identificats a través de l'anàlisi d'isòtops d'oxigen i estronci han indicat l'existència d'individus locals i no locals, suggerint una mobilitat demogràfica regional.

Aquesta recerca demostra l'efectivitat dels enfocaments bioarqueològics per dilucidar realitats socials complexes i desafia les suposicions sobre la relació entre estratificació social i accés a recursos en les societats de l'Edat del Bronze Antic. Les troballes contribueixen a una comprensió més àmplia de l'organització social prehistòrica i destaquen la importància de metodologies multidisciplinàries en la interpretació arqueològica.

DEDICATORY

This PhD thesis manuscript is dedicated to many people, especially those who are no longer with us. To my father, Antonio Domínguez Carballo, who passed away on January 17, 2024, for his role as a loving parent. As he promised, he will watch over us from the field of flowers in the afterlife, alongside Rosa, Nevy, Suicune, Manchitas, and Spirit—my beloved family dogs. To my loving mother, Margareta Gluitz, who has always supported my career and has been my role model in life. To my fiancé, Iván Molina Jiménez, who supported me unconditionally during my predoctoral studies and provided valuable scientific advice. And to my beloved cat, Rando, who woke me up every day at six o'clock during the final stages of writing this manuscript.

To my closest family members: my brother, Alejandro Domínguez Domínguez; my sister, Sonia Domínguez Domínguez; my nephew, Hugo Domínguez Martínez; my aunt, Marisa Domínguez Carballo; my uncle, Fico Carrera Álvarez; my father-in-law, Domingo Molina Burgueño; and my mother-in-law, Pilar Jiménez Peralta. You have allowed me to grow and flourish in both my personal life and my career as an archaeologist.

I would also like to thank my lifelong friends, Vanessa Cornago, Ferran Hüttner, Alba Calderón, Estanis Riquer, and Mónica Boned, for always giving me the best advice and helping me clear my head in the best company.

ACKNOWLEDGEMENTS

This space is dedicated to all the contributors to this PhD thesis. I would like to acknowledge the following key figures:

Miquel Molist Montaña, who accepted me as a PhD student in the SAPPO-GRAMPO Research Group and granted me access to countless interesting research opportunities. He allowed me to excavate, study, and explore Iraqi Kurdistan; supervised the current PhD project; and funded the analyses included in this study.

Anna Bach Gómez for being an inspiring female archaeologist, for her constant insightful guidance, and for giving me the chance to excavate in multiple sites in Iraqi Kurdistan and Catalonia.

Daniele Morandi Bonacossi, *Francesca Simi*, *Katia Gavagnin*, and all the team members of the Kurdish-Italian Gir-e Gomel Archaeological Project (KIGAP) are owed gratitude for the opportunity to study samples of Gir-e Gomel and for their kind reception.

André Colonese, *Krista McGrath*, *Luis Pezo Lanfranco*, *Alice di Muro* and *Thiago Fossile* for being my mentors in stable isotope analyses, for teaching me the fundamentals of bone collagen extraction and analysis, and for grating me the spaces necessary to perform this type of analyses.

Ferran Estebaranz Sánchez for being my mentor in dental microwear patterns and for teaching me the fundamentals of traceology applied to human teeth.

Adrià Breu Barcons, *Roger Alcàntara Fors*, *Joaquim Sisa López de Pablo*, *Ivan Gironès Rofes*, and *Andreu Monforte Barberán* for sharing marvelous moments in both the lab and in the field, for teaching me about their specializations in archaeology, and for providing valuable advice and review on my research.

Francesc Xavier Garcia Ramis for providing data on the chronological and geographical background of the Ninevite 5 period, for assisting in the sample collection for stable isotope analysis, for collaborating in the dental casting of both Gird Lashkir and Gir-e Gomel settlements, for executing archaeological surveys in Erbil, for avoiding my unexpected death in Duhok, and for being one of the most caring team members I have encountered. Equipo Cotas, Equipo Sombra, and Team Liquid will always be remembered.

Biel Soriano Elias, *Olivia Orri Orri*, and *Míriam Gómez Andreu* for their great companionship both in the lab and during fieldwork, for their assistance in inventorying the anthropological remains of Plaça de la Gardunya, and for the creation of a ton of maps that are included in this manuscript.

Caterina Sabán Vinyals, *Àstrid Ortega Forn*, *Ana Sanmiguel de la Fuente*, and *Lara Marín González* for assisting in the elaboration of the inventory of the anthropological remains of Plaça de la Gardunya, for their assistance in dental casting, for the identification of anthropological remains from the site of Gird Lashkir, and for all the good moments we have shared together.

The team members of the Department of Archaeology of the Salahaddin University-Erbil, including *Hawkar Ahmed Abdulrahman*, *Abdullah Bakr Othman*, and *Abas Ali Mahmood*, the archaeologists *Carolyne Douché*, *Belana Maaruf Rashid*, and *Saya Agha*, the director of Erbil Antiquities *Nader Babakr*, as well as the curators *Amer Shwany* and *Ali Banishari*, for sharing so many fieldwork and lab work together and for teaching me about their past, their culture and traditions.

CHAPTER ABSTRACT

CHAPTER 1: Research background

In the first chapter of the study, a comprehensive description of the areas of study and the chronology is presented. The periodization of both the territories of Northern Mesopotamia and Northeastern Iberia remains an area of ongoing research, with unresolved issues that require further examination. The study cases of Gird Lashkir, Gir-e Gomel, and Plaça de la Gardunya are discussed, providing deeper insights into habitat, subsistence economy, craftsmanship, social structure, and funerary practices, in order to better define the sites under study. These definitions further underscore the existing gaps in the scientific community's understanding of these societies. The central and ancillary objectives of the present study are as follows. Firstly, a multidisciplinary approach will be employed to investigate societies undergoing analogous politico-economic complexification processes. Secondly, an exploration of funerary practices will be conducted. Thirdly, the biological profile of individuals belonging to these populations will be determined. Finally, dietary trends and residential patterns will be observed as proxies to ascertain a certain degree of social differences in terms of age, sex, and social status.

CHAPTER 2: Methodological framework

The second chapter of the present PhD project consists of the presentation of the diverse disciplines that will be employed to study the skeletal remains of the three case studies. Each area of study is accompanied by a definition and an exposition of the prevailing best practices and methodologies. Archaeothanatology, defined as the study of funeral customs and their social implications, is the scientific discipline that provides insights into the burial practices of the studied societies, offering a perspective on the social status of the deceased within their respective communities. Osteology is defined as the study of human bones. A thorough analysis of the skeletal remains can provide a detailed biological profile of the deceased, including age, sex, stature, injuries, diseases, and activity markers. Traceology offers a methodological framework for the analysis of past dietary trends. This approach entails the observation and analysis of dental microwear patterns, which are the result of abrasive microtraces created during the mastication process of food by the postcanine dentition. The paleoproteomics approach entails the assessment of taxonomic classifications of animal remains through the analysis of bone collagen.

Consequently, this methodology serves as a solution for overcoming the challenges associated with taxa determination in osteology. Determining the animal taxa in question will be crucial for conducting subsequent stable isotope analysis on bone collagen and tooth enamel hydroxyapatite. The analysis of carbon and nitrogen stable isotopes has been demonstrated to provide a more comprehensive understanding of dietary patterns, offering insights into the consumption of plants and animal protein. This analysis serves as a complementary method to the assessment of dental microwear patterns, providing a more nuanced interpretation of dietary habits and nutritional sources. The analysis of oxygen and strontium stable isotopes is a method of exploring residence patterns. This analysis provides information on the consumption of water from specific hydrological resources and on the location of the population in their early childhood by the isotopic signatures of the geological formations. Finally, the histology of bone and tooth enamel hydroxyapatite is introduced in order to define the impact of diagenetic alterations on skeletal remains. Additionally, the role of sample pretreatments as quality controls in removing contaminants and ensuring the reliability of stable isotope analyses is discussed.

CHAPTER 3: Materials and methods

The third chapter compiles the information concerning the samples that have been collected for the three case studies, as well as provides an exhaustive explanation of the methodologies and techniques applied for each discipline incorporated into the study. A comprehensive description of the containers and their contents has been included in order to carry out the archaeothanatological analysis and to assess the social status of the deceased. The biological profile of the deceased has been ascertained through a comprehensive analysis of age, sex, stature, paleopathologies, and enthesopathies. A comprehensive study of the individuals belonging to Gird Lashkir has been conducted by the PhD candidate and the team members of SAPPO-GRAMPO Research Group through excavation and further study. The population from Gir-e Gomel has been the subject of study through published anthropological reports. The population of Plaça de la Gardunya has been studied by means of an inventory of the skeletal remains, combined with anthropological reports. For the purpose of analyzing dental microwear patterns and stable isotopes, the three study cases were sampled and studied using the same methodologies. However, the availability of isoscapes and reference databases for each territory has necessitated the implementation of distinct strategies for the statistical analyses applied to each assemblage. ZooMS analysis has been conducted on animal samples whose taxa could not be determined by

an osteological analysis. The objective of this analysis was to enhance the results of the stable isotope analyses.

CHAPTER 4: Results

The fourth chapter presents the integrated results of multiple analytical methodologies applied to the skeletal assemblages of Gird Lashkir, Gir-e Gomel and Plaça de la Gardunya, encompassing both traditional and innovative approaches to bioarchaeological research. The comprehensive analytical framework integrates an archaeothanatological examination and an anthropological analysis, which facilitates the reconstruction of funerary customs and the biological profile of the buried individuals. The application of specialized methodologies, including analyses of dental microwear patterns and stable isotopes, provides further insight into dietary patterns and residential mobility. The procurement of reliable results has been achieved through the implementation of rigorous quality control protocols, including taxonomical identification using zooarchaeology by mass spectrometry, and bone collagen preservation. A thorough examination of diagenetic and taphonomic changes, which are used to assess postmortem alterations in bone and tooth enamel that result from physical and chemical changes, are also presented.

CHAPTER 5: Discussion and conclusions

dietary patterns through dental microwear analysis and stable isotope analyses, as well as residence patterns through stable isotope analyses. Further and future analysis to better understand the studied populations are suggested.

The fifth and final chapter presents a comprehensive synthesis and interpretation of the multidisciplinary bioarchaeological evidence, integrating findings across several analyses to reconstruct the lives of the studied populations. This synthesis draws together insights into burial customs, social organization, health status, and lifestyle adaptations. Dietary reconstruction is achieved through dental microwear analysis and stable isotope analyses to determine subsistence strategies. Residence patterns and population mobility are explored through strontium and oxygen isotope analyses, revealing insights into settlement dynamics. The chapter concludes by

identifying methodological limitations and proposing future research directions, including expanded isotopic sampling strategies, and additional analyses to further elucidate the complex social and biological dynamics of these communities.

INDEX

Dedicatory I

Acknowledgements II

Chapter abstract IV

Index 1

Chapter 1: Research background 3

1.1 Northern Mesopotamia 4

1.1.1 Periodizing the Early Bronze Age in the first half of the 3rd millennium BCE: each to their own 5

1.1.2 Characteristics of the first half of the 3rd millennium BCE 10

1.1.3 The site of Gird Lashkir 17

1.1.4 The site of Gir-e Gomel 21

1.2 Northeastern Iberia 25

1.2.1 Beyond the three-age system: rethinking the periodization of the Bronze Age in the Iberian Peninsula 26

1.2.2 Characteristics of the Early Bronze Age 29

1.2.3 The site of Plaça de la Gardunya 34

1.3 Objectives 42

Chapter 2: Methodological framework 45

2.1 Archaeothanatology: reconstruction of mortuary practices 46

2.2 Osteology: bones as witnesses of life 48

2.3 Traceology: decoding diet through dental microwear 55

2.4 Paleoproteomics: identifying taxa with ZooMS 61

2.5 Stable isotopes: tracing diet and residence patterns 63

2.5.1 Diet 65

2.5.2 Residence patterns 74

2.6 Histology and taphonomy of bone hydroxyapatite: establishing quality controls for stable isotope analysis 80

2.6.1 Histology of bone 80

2.6.2 Histology of tooth enamel 81

2.6.3 Taphonomy: diagenetic alterations of skeletal remains 83

2.6.4 Efficacy of sample pretreatments to remove diagenetic alterations 84

Chapter 3: Materials and methods 90

3.1 Archaeothanatology and biological profile 91

3.1.1 Gird Lashkir 91

3.2.2 Gir-e Gomel 198
3.2.3 Plaça de la Gardunya 212
3.3 Dental microwear pattern 233
3.3.1 Materials 233
3.3.2 Methods 235
3.4 ZooMS 240
3.4.1 Materials 240
3.4.2 Methods 240
3.5 Stable isotopes 242
3.5.1 Materials 242
3.5.2 Methods 252
Chapter 4: Results 272
4.1 Burial customs 273
4.1.1 Gird Lashkir 274
4.1.2 Gir-e Gomel 288
4.1.3 Plaça de la Gardunya 291
4.2 Dental microwear pattern 294
4.2.1 Gird Lashkir and Gir-e Gomel 294
4.2.2 Plaça de la Gardunya 307
4.2.3 Concluding remarks 323
4.3 ZooMS 326
4.4 Stable isotopes 327
4.4.1 Diet 327
4.4.2 Residence patterns 344
4.4.3 Concluding remarks 362
Chapter 5: Discussion and conclusions 365
5.1 Burial practices 366
5.2 Social organization 367
5.3 Health and lifestyle 368
5.4 Dietary patterns through dental microwear analysis 369
5.5 Dietary patterns through stable isotope analyses 370
5.6 Residence patterns through stable isotope analyses 372
5.7 Conclusion 373
References 375

CHAPTER 1: RESEARCH BACKGROUND

1.1 NORTHERN MESOPOTAMIA

The northeastern region of Mesopotamia encompasses the northern and northeastern territories of the contemporary countries of Iraq and Syria, respectively. The geographical area is delimited to the east by the Zagros Mountains, and to the south and west by the Euphrates River. The Tigris flows across the region, creating fertile agricultural areas. In comparison to the southern region, northern Mesopotamia is characterized by drier conditions and a less extensive development of irrigation channels. The area has been inhabited since the Paleolithic period by human communities, and it has been the cradle of civilization, having given rise to the earliest complex urban societies. The late prehistoric periods are distinguished by the emergence and development of social inequalities, during which figures described as an elite or of high status began to accumulate privileges, goods, and powers (such as the coercive), among others. These individuals exercised control over low-ranked individuals in all aspects. These changes, which are unprecedented in the history of humankind, have attracted the interest of researchers, particularly those from the southern region, who are drawn to the emergence of the first written texts. However, the political and belligerent contexts of the territory have rendered research highly challenging.

In the last decade, the northern Mesopotamian region has garnered significant scholarly interest, leading to the development of numerous international collaborative research projects. This renewed focus is largely attributed to the revitalization efforts in the Kurdistan region of Iraq (Molist et al., 2024). Those investigating the early emergence of social complexity must deal with a more complicated archaeological record, as written sources are absent in the area. However, communities were in contact with the southern territories, which began using cuneiform writing as a form of organization, administration, and contact.

1.1.1 Periodizing the Early Bronze Age in the first half of the 3rd millennium BCE: each to their own

The Early Bronze Age in northern Mesopotamia emerged during the 3rd millennium BCE and followed the Chalcolithic period, which is known as the Late Chalcolithic in the north and the Uruk period in the south of Mesopotamia. This period extends from 3100 to 2154 BCE, which corresponds to the emergence of the Ninevite 5 culture and the collapse of the Akkadian Empire. The Early Bronze Age has been conventionally divided into two distinct periods: the earlier Early Bronze Age and the later Early Bronze Age. The first of these is characterized by the low complexity that societies present, with small villages and an absence of satellite cities. The phenomenon of necropolises with substantial extensions is becoming increasingly prevalent. In contrast, the second phase is distinguished by the emergence of new and expanding urban settlements, the standardization of craftsmanship across the territory, and the appearance of chamber graves with multiple burials in the necropolises (Helwing, 2012).

The Ninevite 5 period is named after the fifth stratigraphic layer present in the Ishtar Precinct, at the site of Tell Kuyunjik, which is located in Nineveh, a city in the modern-day city of Mosul in northern Iraq (Grossman, 2014; Thomson & Mallowan, 1933). In the 1930s, Max Mallowan undertook the excavation of the site, thereby establishing chronostratigraphic layers that included archaeological index fossils and building types. The Ninevite 5 period, which spans from 3000 to 2500 BCE, has been distinguished by the presence of distinctive pottery styles (Mallowan, 2008). Mallowan established a precedent, and subsequent researchers who identified comparable pottery assemblages in their respective sites ascribed the presence of a Ninevite 5 period and culture to other archaeological sites (**Figure 1**). The accumulation of knowledge over the course of nearly a century has enabled a more profound comprehension of this chronocultural horizon, which spread throughout the north of Mesopotamia. Broadly speaking, the Ninevite 5 period can be divided into two subperiods: the Early and the Late Ninevite 5. Nevertheless, some authors have proposed additional and more complex subdivisions depending on the pottery trends from each region and site, including a transitional phase from the Late Chalcolithic to the Ninevite 5, an Early phase, a Middle phase, and a Late phase (Calderone & Weiss, 2003; Numoto, 1993; Roaf, 1988; Rova, 2003a; Smogorzewska, 2016).

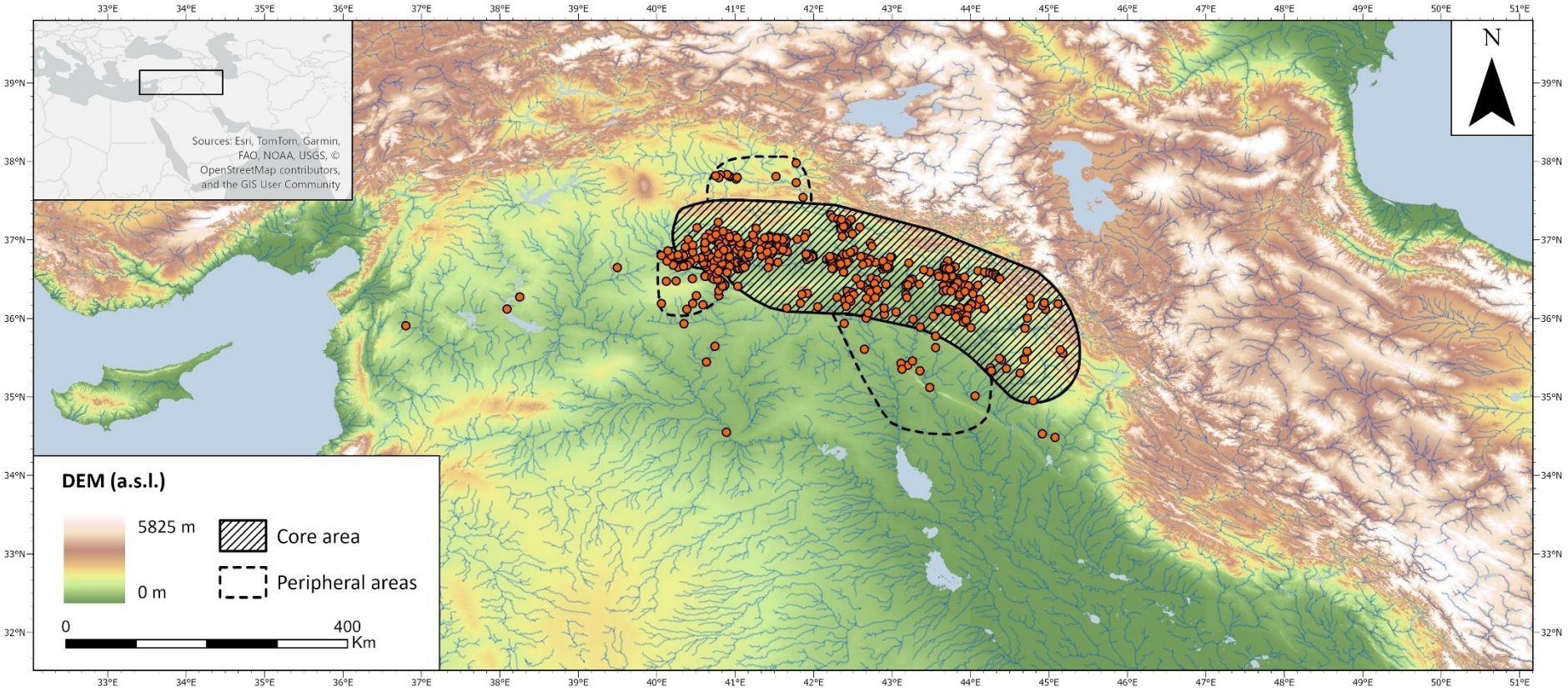


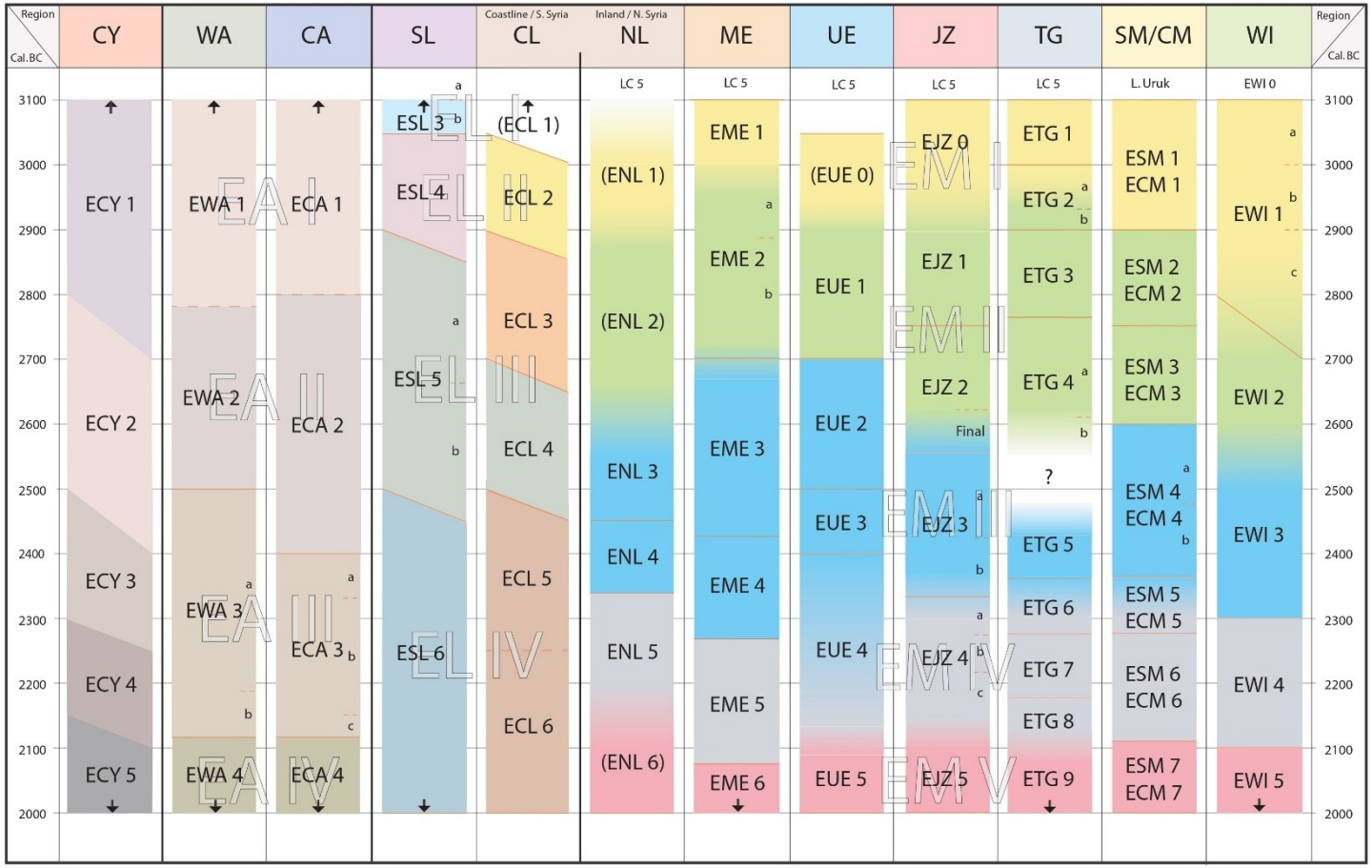
Figure 1. Sites with human occupations during the Ninevite 5 period in northern Mesopotamia. Database by courtesy of *Garcia-Ramis (2024)*. Map by courtesy of Biel Soriano Elias.

The Early Ninevite 5 period is characterized by the presence of painted pottery, which was initially believed to have originated in the Iranian plateau, with parallels observed at the sites of Tepe Siyalk and Tepe Hissar (Mallowan, 1964). Further findings and analysis in the sites of Chagar Bazar, Tell Chuera, Tell Asmar, Nuzi, Tell Brak, Tell Leilan, Tell Karrana 3, Tell Thuwaij, Tell Fisna, Tell Mohammad Arab, among others, demonstrated parallels from local Late Chalcolithic pottery styles, thereby rejecting the initial hypothesis of an exogenous origin (Fujii et al., 1989; Grossman, 2014; Oates, 1982; Roaf, 1984, 1988; Rova, 2003b, 2013; Schwartz, 1982; Wilhelm & Zaccagnini, 1993). This early phase has been determined to correspond to the South Mesopotamian periodization of Jemdet Nasr (Rova, 2013). The pigments used in the paint were primarily black or ochre, with carinated rims and bases featuring high rings identified as the dominant forms (Arrivabeni, 2019). Ceramists used vegetal-tempered pastes (Grossman, 2014). The presence of incised pottery is minimal in comparison to painted pottery (Roaf, 1988; Rova, 2003a). The Late Ninevite 5 period is distinguished by the presence of incised and excised pottery, accompanied by a gradual decline in painted pottery (Garcia-Ramis, 2024). The most common forms are bowls of small capacity with a beaded lip and pointed or pedestal base, and the pastes were mineral-tempered (Grossman, 2014).

The employment of the term "Ninevite 5" to characterize a specific period and its associated cultural phenomena has proven to be a contentious subject, due to a multitude of factors. The initial approach entails the standardization of a term grounded in chronostratigraphic and index fossil evidence. The use of this terminology delineates a society based on the type of craftsmanship they produce. No further analysis based on defining social aspects is considered, thus framing a community only by a couple of traits. The application of chronostratigraphy to extensive geographical areas gives rise to challenges, prompting researchers to reevaluate the reliability of absolute ^{14}C dates. This is particularly evident when Ninevite 5 pottery is observed to exhibit earlier or later chronologies than those initially determined by the research community. A further issue is the multiplicity of terms and periods in existence, which are determined by factors such as region, site, and the classic nomenclature selected by the researcher. It is possible to identify the application of periodizations of Southern Mesopotamia to Northern Mesopotamia, including the Early Dynastic periods (Bieliński, 2010, 2012; Mallowan, 2008). In regions where Ninevite 5 materials are present in low percentages compared to local materials, local terminology is employed. This is exemplified in the northeastern region of Syria, where the prevailing scholarly consensus favors the use of the term Early Jazira (Rova, 2003a). A similar approach is adopted in the Upper Tigris region of modern-day Turkey, where the terms EBA 1 and EBA 2 are widely accepted. The first phase, spanning from 3000 to 2750 BCE, is designated as Early Bronze

Age 1, while the second, extending from 2750 to 2500 BCE, is referred to as Early Bronze Age 2 (Laneri, 2016). In recent times, the ARCANE project (Associated Regional Chronologies for the Ancient Near East and the Eastern Mediterranean) has sought to establish a reliable relative and absolute chronology for multiple regions, including as the Jazira region (Northeastern Syria), the Tigridian region (Northern Mesopotamia and Southeastern Anatolia), Central/Southern Mesopotamia, Middle Euphrates (Central Syria), and Western/Central/Eastern Anatolia, among numerous others (Finkbeiner et al., 2015; Lebeau, 2012; Rova, 2019). A notable outcome of their research endeavors has been the formulation of a comprehensive periodization table, encompassing all the regions that have been examined, along with the corresponding equivalences (***Table 1***).

Table 1. Relative and absolute chronologies for the Near Eastern regions and its equivalences. Extracted from the ARCANE Project website.



EA (Early Anatolian) – EL (Early Levantine) – EM (Early Mesopotamian)* Cultural Horizon Table**, v. 5.4.6

The regional phases or sub-phases reflect changes in the material culture (predominantly ceramics), and/or the level of urbanisation, and refer to the comparative stratigraphy of chronological benchmarks, at a regional and inter-regional level. Use of the same colour denotes the existence of strong cultural links or parallel phenomena between neighbouring regions.

The absolute dates are based on the harmonised radiocarbon data.

E : Early, CY : Cyprus, WA : Western Anatolia, CA : Central Anatolia, SL : Southern Levant, CL : Central Levant, NL : Northern Levant, ME : Middle Euphrates, UE : Upper Euphrates, JZ : Jezirah, TG : Tigridian Region, SM : Southern Mesopotamia, CM : Central Mesopotamia, WI : Western Iran.

* EMI (Early Mesopotamian/Iranian) for WI, ** EA, EL, EM & EMI are labels proposed by M. Lebeau and adopted by the ARCANE community at the Bern final meeting, on December 8-11, 2011.

1.1.2 Characteristics of the first half of the 3rd millennium BCE

The first archaeological projects in Iraqi Kurdistan have centered on surveying the area to identify potential sites, particularly in regions where the construction of a dam was imminent (e.g., Eski-Mosul Dam), as flooding and erosion could potentially impact archaeological sites. Consequently, numerous salvage initiatives were undertaken, promoted by the government and heritage ministries (Garcia-Ramis, 2024). In the last decade, collaboration with international universities has promoted the survey of many more sites and the excavation of sites with occupation in all chronological periods. Despite the significant research conducted, excavations are often confined to small areas or trenches due to the vast extent of the sites involved, resulting in limited information available for each period. Consequently, to achieve a comprehensive understanding and interpretation of this region's archaeological period, it is crucial to persist in research activities and to encourage specialists in all archaeological disciplines to study the remains, which serve as a substantial information source.

The following review aims to shed light on the current state of research by offering a comprehensive overview of the findings concerning habitat, subsistence economy, craftsmanship, and funerary practices from the first half of the 3rd millennium BCE, a period referred to as the Ninevite 5 period.

1.1.2.1 Habitat

Communities from the first half of the 3rd millennium BCE settled in plain areas, typically in locations where there had been long-lasting occupations. The demolition of buildings is typically executed after a period of one or two generations, with the subsequent construction of new structures occurring on the remnants of the former architecture, gradually forming a mound (referred to as a *tell* in Arabic, *gir*/*gird* in Kurdish, or *tepe*/*höyük* in Turkish). The distribution of buildings is such that they are found both in the lower city and the citadel. However, the buildings which are located in the citadel are more prone to destruction due to erosion and taphonomical issues caused by the mound's slope.

The classification of architecture is typically based on its function. Domestic buildings are typically pluricellular in nature, with each room exhibiting a rectangular or quadrangular floor plan. The construction of the walls is characterized by their rectilinear form and the use of rectangular mudbricks, which are of standardized dimensions. However, a single wall may contain multiple

mudbrick measures and rows, resulting in variations in width. The exterior surfaces are covered in mud plaster. In some cases, the foundation of the walls would also be composed of stone. Domestic floors were prepared with pebbles and lime inclusions. The rooms were designed to serve distinct functions, such as a kitchen, storage space, workshop, living area, and so forth. Access to each room was typically facilitated by doors placed in the corner of one of the building's longer walls. The architectural design of these structures included open courtyard areas, which functioned as communal spaces for activities such as threshing agricultural produce (Ławecka, 2019). The urbanism and distribution of domestic buildings within the settlement remains uncertain due to the paucity of archaeological information. It has been observed that residential architecture in this region tends to exhibit a uniform orientation, with a deliberate spacing between buildings to create passageways.

Architectural elements associated with food processing include granaries and ovens. Granaries are a common architectural element in rural areas, often taking the form of either grain stores or grill plan structures. These facilities are designed to ensure proper ventilation and protection of agricultural produce. These structures were erected in open spaces and appear to lack any direct association with specific domestic buildings. These containers are typically found in villages, suggesting that household-based storage systems are employed in small agrarian communities. Large circular ovens and kilns, the latter used for firing pottery, are located in both domestic and courtyard areas. The walls are made of mudbrick, leaving a small space as the entrance. Architectural elements related to defense systems, such as small defensive walls, are often observed in small settlements. However, these structures do not currently meet the criteria for being classified as fortification walls (Ławecka, 2019; Roaf, 2003).

1.1.2.2 Subsistence economy

Agriculture and livestock constituted the primary means of subsistence for these communities. Archaeobotanical remains recovered at the sites provide evidence of the cultivation of various cereals and lentils, including barley (*Hordeum* vulgare), einkorn wheat (*Triticum monococcum*), emmer wheat (*Triticum dicoccum*), durum wheat (*Triticum durum*), lentils (*Lens culinaris*), chickpeas (*Cicer arietinum*), field peas (*Pisum sativum*), bitter vetches (*Vicia ervilia*), and grass peas (*Lathyrus sativus*) (McCorriston & Weisberg, 2002; Riehl et al., 2008; Wetterstrom, 2003). Livestock was comprised of domesticated animals, including sheep, goats, pigs, and cattle (Forest, 2003; Piątkowska-Małecka & Smogorzewska, 2010; Wetterstrom, 2003). The gathering of wild

flora taxa was also very common, and a wide range of species were collected in large quantities (Wetterstrom, 2003), including wild legumes such as medick (*Medicago* sp.), ray-podded medick (*M. radiata*), *Trigonella* sp., milkvetch (*Astragalus* sp.), and fruits like fig (*Ficus carica*) and grapes (*Vitis vinifera*) (Molist, Breu, et al., 2019a).

1.1.2.3 Craftsmanship

The pottery repertoire plays a significant role in Ninevite 5 contexts due to the high level of standardization in its production. The practice of crafting traditions is subject to variation depending on the specific phase of the period under consideration. This variation can be used as an index fossil for relative chronology in archaeological contexts. Pottery vessels were made either by coiling or by using the fast wheel (Forest, 2003; Grossman, 2014). A vessel typology that is evident throughout the entire Ninevite 5 period is the jar, characterized by its diminutive dimensions and its biconical, globular, ovoid, or heart-shaped morphology. The bases are flattened, rounded, pointed, ringed, and pedestalled. The decoration of jars can be achieved through various methods, including the application of paint, incisions, or excisions, often in the form of rocker motifs. The surface finishes were composed of slip or wet-smoothing techniques. In the context of storage vessels, large undecorated jars with globular or ovoid shapes are frequently observed. The bases tend to be rounded, and their short necks tend to flare outwards. In the culinary domain, burnished pots were identified as the prevailing morphology. In the process of ceramic production, various materials such as chaff, grit, and plant fibers were incorporated into the clay mixture as tempering additives. These materials enabled firing the vessels at lower firing temperature within the kiln (Grossman, 2014).

The Early Ninevite 5 period is characterized by its Painted Ware (Forest, 2003). A variety of vessel morphologies, including the bowl, the cup, and the jar, were common in this phase. Bowls and cups are characterized by their various forms, including carinated, round, concave, or straight sides. Rims were traditionally either rounded or beaded, while bases were often flat, ringed, pedestalled, rounded, or pointed. In the process of clay fabrication, vegetal tempers are incorporated into the mixture. The application of decoration typically occurs through the use of paint on the exterior surfaces, employing monochrome tones such as black, dark red, or dark purple. The pigments were created by combining clay with iron oxide. The most prevalent motifs included geometric, linear, rib, and animal patterns. A small percentage of vessels were decorated with incisions rather than paint. Incised motifs exhibited linear designs in the form of notches,

zigzags, or rib patterns, arranged in horizontal bands and triangles. In certain instances, animal motifs are also present, filled with incised lines (Grossman, 2014).

The Late Ninevite 5 period is defined by its Gray Ware, which is an attempt to emulate the metallic ware (Forest, 2003). Vessels exhibit the morphologies observed in the Early phase, but the carinated type gradually fall in disuse. The most prevalent vessel types are the bowl with an outturned rim and pointed bases, and the chalice with feet or pedestal, both with reduced dimensions. The clays employed in these processes are mixed with mineral tempers. It has been observed that the decorative elements undergo a transition from paint to incision and excision. Incised decoration is typically observed on bowls and cups with thin walls, which are classified as fine ware. The most prevalent motifs were geometric and linear patterns made with rounded or triangle-tipped tools, distributed in horizontal bands, triangles, and rock patterns. Excised decoration includes rib motifs in vertical and diagonal crossed patterns, and this technique could be mixed with incision in some cases (Grossman, 2014).

The production of lithic technology can be distinguished between microlithic and macrolithic artifacts. Microlithic elements were manufactured on flint or on obsidian materials using the knapping and pressure flaking methods. The cores were reduced to produce various tools, including blades, sickle blades, projectile points, and scrapers. A significant number of blades, including sickle blades, have been discovered with bitumen adhered to one side. This adhesion serves the primary purpose of attaching the blade to a handle. Lithic tools were used in a broad array of activities, including crop harvesting, threshing, cutting, animal butchering, and hunting (Thomalsky, 2019; van Gijn, 2003). As has been previously documented, chipping debris is often present in areas where flint reduction has occurred. This phenomenon has been observed in various sites, including Gird Lashkir. Macrolithic artifacts were closely related to food processing, such as saddle querns and handstones.

Metallurgy in the first half of the 3rd millennium BCE was scarce, and a limited variety of artifacts were created, including tools and ornaments. In the case of tools, stone casts found in sites such as Gird Lashkir exhibit the manufacture of axes and chisels (Molist, Gómez-Bach, et al., 2019). At the site of Tell Mohammed Arab, a copper/bronze arrowhead with a flat rhomboid morphology was discovered. In the case of ornaments, necklace beads (Tell Mohammad Arab, Gird Lashkir), copper/bronze/lead loop earrings (Gird Lashkir), pins with and without eyelets (Telul-et Thalathat V, Gird Lashkir), and toggle pins were produced (Muhly & Stech, 2003; Rutkowski,

2019). Only one example of a glyptic element was found in Tell Karrana 3, in the form of a cylinder seal (Rutkowski, 2019). Despite the apparent scarcity of metallic materials during this period, metallurgy did not truly become dominant or significant until the latter half of the 3rd millennium BCE. This period was characterized by the large-scale production of weapons, which played a pivotal role in the development of metallurgy. (Rutkowski, 2019).

The artistic expression of the region is manifested in the terracotta figurines and glyptic art forms. The figurines are predominantly of a zoomorphic nature, featuring representations of bulls (Tell Mohammad Arab, Tell Jumbur, Kenantepe), rams (Tell Jumbur), and equids (Gird Lashkir) (Molist, Gómez-Bach, et al., 2019; Tonussi, 2019). Chariots equipped with wheels have also been unearthed in sites such as Gird Lashkir. The existence of glyptic art related to administrative technology is well-documented. During the first half of the 3rd millennium BCE, a variety of styles emerged, yet the Glazed Steatite and Piedmont styles, along with geometric motifs, predominated. Its provenance is believed to be Central Mesopotamia and Western Iran; however, it was locally produced. The transition from the Late Chalcolithic 5 to the Ninevite 5 period is characterized by seals and impressions featuring geometric, human, and animal motifs, occasionally depicting both human and animal forms simultaneously. The appearance of Painted Ware in the early stages of Ninevite 5 coincided with the production of quadruped animals and scorpion motifs. The most prevalent animal scenes depicted are the schematic striding horned quadrupeds. Evidence suggests that scenes depicting both humans and animals (e.g., felines) are associated with styles characteristic of Central and Southern Mesopotamia during the Early Dynastic I and II periods. When humans are depicted alone, they are often shown holding hands and dancing. In the later phases of Ninevite 5, seals are decorated with various patterns, including geometric motifs, file cuts, interlocking triangles, arcades, dotted circles, and concentric circles. The depiction of the human figuration has been limited to the site of Kenantepe (Pittman, 2019).

1.1.2.4 Social structure

The development of a writing system in the southern region of Mesopotamia is indicative of the social structure's constant evolution and complexity within its communities. Conversely, the paucity of such vestiges in the northern region calls for a meticulous examination of the diverse material remains unearthed during archaeological excavations. The current state of research in the field of early urbanism and architecture does not yet permit a definitive conclusion regarding

the presence of complexification. However, it is evident that living and working areas were specialized, with buildings designed for specific functions, such as granaries or workshops, located within courtyard areas. Evidence of social complexity is further demonstrated by the gradual demographic increase in cities and the proliferation of small villages, which are often regarded as satellite settlements depending on one another. If a political administration had existed during this period, scholars debate regarding the control over agricultural produce by an elite group. Some researchers argue in support of the control and redistribution of agricultural produce, attributing this position to the presence of cylinder seals (Bolt & Green, 2003). Conversely, this hypothesis has been rejected by other scholars due to the domestic nature of granaries in agricultural villages (Ławecka, 2019). Additional evidence of social complexity is indicated by the standardization and dissemination of the Ninevite 5 pottery styles. The existence of a specific social stratum responsible for the production, transportation, and trade of vessels is also indicative of social hierarchy. Glyptic elements, such as cylinder seals, have been identified as the most evident sign of the existence of local centralized administrations that controlled production and distribution of goods, probably limited to the movement of storage containers (Pittman, 2019). The motifs depicted in the seals have been identified as indicative of various factors, including but not limited to origin or destination of goods, private property rights, or lineage (Bolt & Green, 2003). In the subsequent phases of the Early Bronze Age, urbanization and increased political complexity are believed to have flourished in northern Mesopotamia (Schwartz, 2003).

The funerary register is perhaps the most evident in this process of social complexification. The northern Mesopotamian societies of the Early Bronze Age experienced a period of complexification, marked by the emergence of a vertical, hierarchical social structure, where individuals were assigned a specific status at birth (Forest, 2003).

1.1.2.5 Funerary practices

Burials from the first half of the 3rd millennium BCE are found both *intra* and *extra muros*: beneath the rooms of domestic buildings, under the use level of courtyard areas, and in necropolises (Valentini, 2019). Five distinct categories of graves have been documented in the region, encompassing simple pits, cists, shaft graves, chamber graves, and ceramic containers. Simple pits are typically characterized by their oval or rectangular form, with minimal evidence of surface preparation, except in certain instances where plaster and reed matting, along with pebbles, have been observed in the walls and floors, respectively. Customarily, the deceased were

covered directly with soil; however, in some cases, the pit was covered with stone slabs, mudbricks, or a perishable material, which could affect the anatomical connection of the buried individuals. Cist graves are characterized by a rectangular shape, defined by four walls and a stone slab cover. The use of mudbricks as building material and pebbles for paving the floors is less common. Shaft graves are composed of a single or multiple burial chambers, with an approximate vertical shaft depth of 2 meters, both divided by a mudbrick wall. Chamber graves bear a resemblance to cist graves, yet a distinguishing characteristic is the presence of a corbelled vault in their cover. Access shafts were excavated on the shorter side of the grave to facilitate access. In the case of ceramic containers, individuals were placed in deep jars, pithoi, or cooking pots, which were placed inside a simple pit. The remains were covered with an inverted large bowl or by a rim sherd. Unlike other types of burials, which are located both intra and *extra muros*, ceramic containers are always located *intra muros* (Bolt & Green, 2003; Valentini, 2019).

The deceased were buried in single, double, or multiple graves, typically in primary deposition. However, secondary deposition has also been observed in certain locations, including Gird Lashkir. Burials encompass all sexes and ages, with newborns being placed within pots. The orientation of the individuals exhibits significant variability. The positioning of the deceased is usually in a supine or lateral decubitus, with the arms and legs flexed or hyperflexed to one side. Research has identified the presence of certain comfort elements in burial sites, including reed mats (Bolt & Green, 2003). Among the comfort elements found in the graves is the presence of reed mats and cushions. The presence of phytoliths on the long bones indicates that the deceased was wrapped in funerary shrouds. Ornamental items such as earrings, pendants, hair rings, pins, and beaded necklaces composed of diverse materials (carnelian, quartz, rock crystal, faience, bronze, silver, gold, to name a few) were worn. Grave goods can take various forms, including pottery vessels, animal offerings, cylinder seals, pins, lithic tools, and natural stones (Bolt & Green, 2003). In contrast, the presence of bone objects and stone vessels is less prevalent (Valentini, 2019).

According to Schwartz (2003) , the funerary record provides evidence of a five-tier hierarchical social stratification based on the wealth of grave offerings. The presence of grave goods was not observed among the poorest individuals. The second category would include individuals with only pottery vessels. Middle-class individuals would have pottery vessels and stone ornaments. The fourth category would contain pottery vessels and copper pins. The highest-ranking social class would include pottery vessels, cylinder seals, and stone and metal ornaments.

1.1.3 The site of Gird Lashkir

Gird Lashkir is an archaeological site located in the eastern plains of the city of Erbil (ancient Arbela), in modern-day Iraqi Kurdistan (**Figure 2**). It was first included in the *Atlas of the Archaeological Sites in Iraq*, published by the General Directorate of Antiquities in 1976 (Gómez-Bach et al., 2019; Molist, Breu, et al., 2019b; Molist et al., 2024). The archaeological research project is being carried out in collaboration with the research group Seminari d'Arqueologia Prehistòrica del Pròxim Orient – Grup de Recerca Arqueològica a la Mediterrània i al Pròxim Orient (SAPPO-GRAMPO), from the Department of Prehistory at the Autonomous University of Barcelona, and the Department of Archaeology at the Salahaddin University. The mound extends over an area of 4 hectares and reaches a height of 14 meters (Breu et al., 2019; Molist, Gómez-Bach, et al., 2019). However, the extent of the lower city remains to be determined. Initially, two surveys were conducted in 2013 and 2014, respectively, and 12 trenches were excavated in 2015 and 2016. These were performed to observe the stratigraphy of the settlement (**Figure 3**). While some Ubaid and Halaf pottery sherds from the 6th millennium BCE were found during the surveys (Molist, Gómez-Bach, et al., 2019), fieldwork has established the earliest occupation period as the Late Chalcolithic 2, dating to the 4th millennium BCE (Molist et al., 2024), extending up to the Early Islamic period (Molist, Gómez-Bach, et al., 2019). In recent years, fieldwork has focused on sectors 3 and 4, which yield a substantial Ninevite 5 occupation.

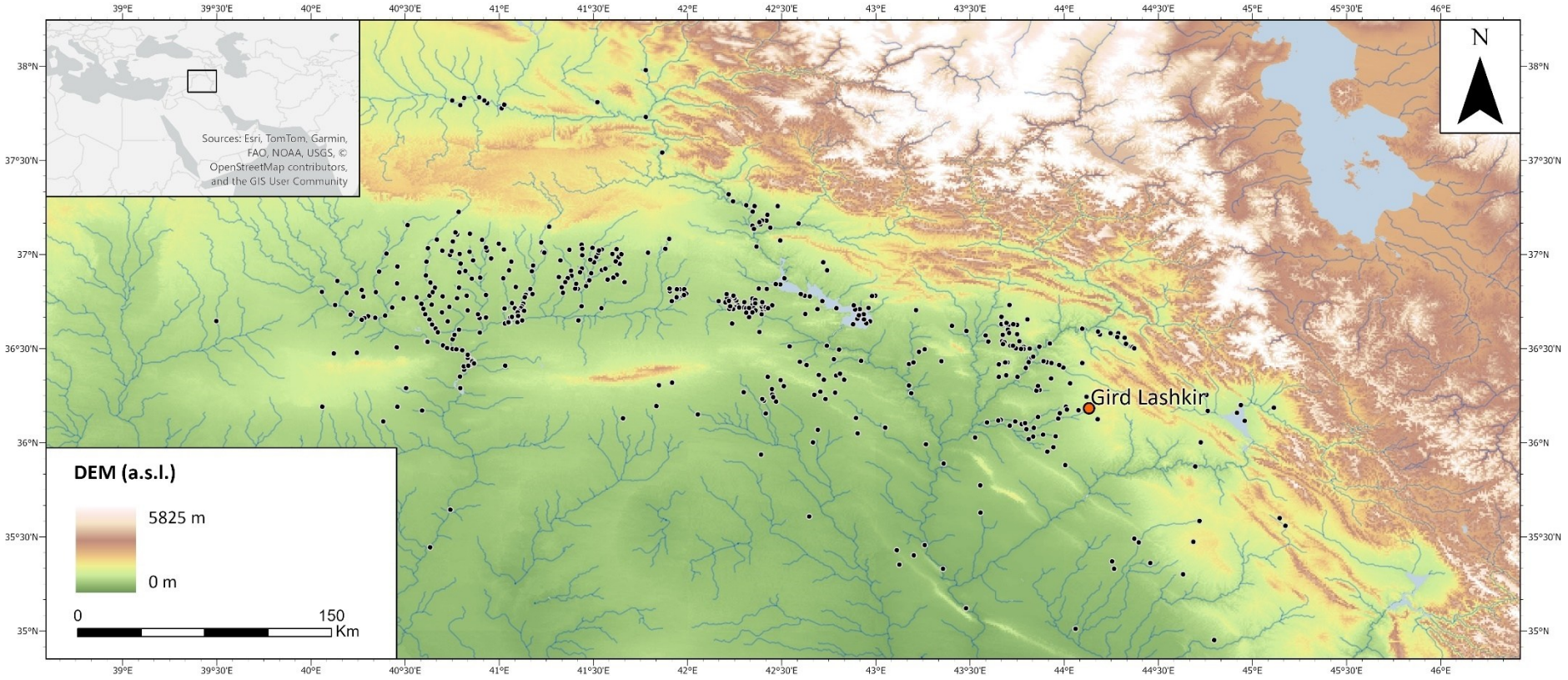


Figure 2. The site of Gird Lashkir within the sites with Ninevite 5 occupation. Map by courtesy of Biel Soriano Elias.

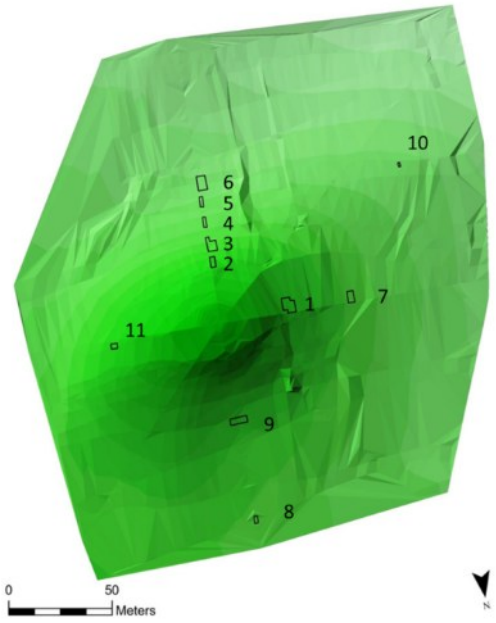


Figure 3. Location of the 12 trenches of Gird Lashkir. Extracted from *Molist, Gómez-Bach, et al. (2019)*.

The relative chronology of the human occupation of the first half of the 3rd millennium BCE has been established due to the presence of Ninevite 5 pottery assemblages, ranging from 3000 to 2500 BCE (Molist, Gómez-Bach, et al., 2019). Nevertheless, ^{14}C dating on a charred seed of barley has provided a chronology of 2885 to 2665 cal. BCE (Molist, Breu, et al., 2019b).

The architectural evidence has provided more than five constructive phases. The site is predominantly composed of domestic buildings characterized by pluricellular rectangular rooms (Molist et al., 2023). Each room is dedicated to a specific function, including living spaces, kitchen areas, grain storage, and so forth (Molist et al., 2024). However, within the same wall, the arrangement of mudbricks can vary in terms of measurement and arrangement, resulting in a wall with a range of widths. The interior and exterior surfaces of the walls were plastered with a layer of mud. The floor could be paved with beaten earth, with pebble inclusions, or with mudbricks (Molist et al., 2023). Benches, the function of which is unclear, were affixed to the corners of the walls. The doors were positioned along the long side of the room, in proximity to a corner, and were constructed from perishable materials that rotated within stone door-sockets. The rooftops may have been constructed from perishable materials, such as reeds, as evidenced by the presence of phytolith concentrations. The orientation of domestic buildings has been observed to align with the prevailing architectural styles of preceding phases. The presence of multiple

constructive phases suggests that these structures may have endured for one or two generations. The paucity of evidence pertaining to urban architecture precludes definitive conclusions regarding the configuration of the buildings. Domestic structures were situated within courtyard areas, which functioned as spaces for lithic knapping and threshing activities.

An archaeobotanical study of charred seeds has provided evidence of the cultivation of cereals and lentils, including einkorn wheat (*Triticum monococcum*), emmer wheat (*Triticum dicoccum*), barley (*Hordeum vulgare*), and lentils (*Lens culinaris*, *Mendicago* sp., *M. radiata*, and *Trigonella* sp.). The collection of wild taxa has also been documented, likely serving as fodder for domesticated herbivores (Molist, Breu, et al., 2019b). The presence of domestic animals has been evidenced through the analysis of archeozoological remains; these include species such as goats (*Capra hircus*), sheep (*Ovis aries*), pigs (*Sus domesticus*), cattle (*Bos taurus*), and equids (*Equus* sp., and *Equus hemionus*). Given the abundance of remains, it can be deduced that the most prevalent animal consumed would be pig, followed by goat, and to a lesser extent, cattle and sheep (Molist et al., 2023). The slaughter of cattle, pigs, and ovicaprids occurred at early ages to yield primary products, while ovicaprids were also slaughtered at older ages for the consumption of secondary products (Molist, Breu, et al., 2019b; Molist, Gómez-Bach, et al., 2019). The hunted species included primarily wild goats (*Capra aegagrus*), gazelles (*Gazella gazella*), and hares (*Lepus* sp.). It has also been documented that gastropods, bivalves, and crustaceans were consumed (Molist, Breu, et al., 2019b).

The pottery assemblages are typically from the Ninevite 5 period (Bakr Othman & Ali Mahmood, 2023; Molist et al., 2023, 2024) The repertoire includes fine Painted, Incised, and Excised Ware, as well as cooking coarse ware and large jars for storage. These artifacts belong to all phases of the first half of the 3rd millennium BCE. A significant quantity of bitumen lumps have been retrieved from the interior surfaces of pottery vessels (Molist, Breu, et al., 2019b). The analysis of its biomarkers has revealed an origin in the central Mesopotamian region and, to a lesser extent, in the northeastern Mesopotamian region (Breu et al., 2022). The microlithic materials recovered consist of local flint and obsidian, which were knapped to obtain blades primarily used as sickles (Molist, Gómez-Bach, et al., 2019). Macrolithic materials are composed of saddle querns and handstones (Gómez-Bach et al., 2019; Molist, Breu, et al., 2019b). Evidence of metallurgical practices is present in the form of a univalve cast crafted from sandstone, featuring two flat axes, a chisel, and a needle. The hypothesis that the smelting process occurred at the site is substantiated by the evident signs of rubefaction on the cast, a direct consequence of its con-

tinuous wear (Molist, Breu, et al., 2019b; Molist, Gómez-Bach, et al., 2019). The artistic expression of the community that inhabited at Gird Lashkir is evidenced by ten terracotta figurines, nine of which are zoomorphic nature and one of which is a four-wheeled chariot, the wheels of which have not been preserved. The species represented include cattle and a horse (Gómez-Bach et al., 2019; Molist, Breu, et al., 2019b; Molist, Gómez-Bach, et al., 2019).

With respect to the funerary practices observed within the citadel, individuals were buried beneath the floors of domestic buildings or in courtyard areas (Molist et al., 2023). In the lower mound, individuals were buried *extra muros*. The burials included individuals of all ages and sexes. Newborns were buried in a seated position within ceramic containers in a simple pit, sometimes with a lid covering the entrance. Children and adults were buried in simple pits, with some instances of mudbrick walls being reused. Deceased were placed in a supine or lateral decubitus position, with both upper and lower limbs flexed or hyperflexed to one side. The distribution of grave goods varied among individuals, exhibiting differences in quantity and quality. These goods included pottery vessels, animal offerings, raw materials, flint cores, stone pendants, and necklaces. The latter featured beads made of diverse morphologies and materials, such as semi-precious and local stones, bronze rings, and exogenous shells. Other notable grave goods included bronze or lead earrings, and cylinder seals adorned with geometric motifs (Molist et al., 2024). The presence of valuable grave goods and cylinder seals in some adult and child burials serves as evidence of inherited status and social inequality characteristic of a hierarchical society. The shared geometric motifs in cylinder seals serve as indicative evidence of lineage or shared private property by a segment of the population (Molist et al., 2023).

The sum of all the archaeological evidence indicates that Gird Lashkir was an active agent in exchange networks of products, such as tools, ornaments, semi-precious stones, obsidian, and bitumen (Breu et al., 2022). These networks encompassed the surrounding area, including southern Mesopotamia, the Zagros mountains, Western Iran, the Euphrates valley, and the Levant (Molist et al., 2023).

1.1.4 The site of Gir-e Gomel

Gir-e Gomel, also referred to by the Kurdish inhabitants as Tell Jomel, is an archaeological site located in the Navkur Plain, in proximity to the river Gomel, in Iraqi Kurdistan (**Figure 4**). The survey and excavation project, titled *The Kurdish-Italian Gir-e Gomel Archaeological Project (KIGAP)*, has been carried out since 2012 in collaboration with the University of Udine and the

Directorate of Antiquities of Duhok. The initial phase of fieldwork involved the excavation of three areas, designated as Operations 1, 2, and 3, with the objective of establishing the chronostratigraphy of the site. The mound is constituted by a citadel that reaches a height of 40 meters and a lower city that expands approximately 35 hectares. The site contains a substantial occupation chronology, spanning from the Late Chalcolithic 1-2 to modern times. Occupation from the first half of the 3rd millennium BCE has been documented in Operations 1 and 3, providing an absolute chronology of 2750 to 2000 cal. BCE. In the stratigraphy of the site, this period corresponds to Phases 23 and 24 for Operation 1, and Phase 3 for Operation 3.

The evidence of occupation is reduced to a necropolis area, concentrated in Operation 1, a burial in Operation 3, and a kiln for pottery firing also in Operation 3 (Morandi Bonacossi et al., 2018). To date, no evidence of architecture or subsistence economy has been recovered. Notwithstanding, the environmental conditions of the Navkur Plain are conducive to the practice of both extensive and intensive agriculture, a fact attributable to the presence of the rivers Al-Khazir and Gomel, as well as fertile soils.

The burial record consists of eight graves, all of which are simple pit burials with single primary inhumations. Operation 1 encompasses seven graves, specifically Graves 24, 45, 46, 47, 48, 49, and 51. Grave 24 is located isolated in the northwestern part of the excavated area, while the other six graves are concentrated in the southeastern part. The six graves were disturbed during the construction of a massive vaulted funerary chamber with access shaft in the Middle Bronze Age (Grave 44). The chamber measured 4.15 meters in length and 2.26 meters in width, and was constructed using baked bricks. Operation 3 encompasses Grave 42 and is thought to also belong to the first half of the 3rd millennium BCE (Morandi Bonacossi et al., 2018). The high degree of variability in grave goods belonging to each individual can be related to the presence of a hierarchical societal structure.

Grave 24 is ascribed to Phase 24. ^{14}C dating at 2σ has yielded an absolute chronology of 2877 - 2580 cal. BCE (Morandi Bonacossi et al., 2025). This piece of evidence has been crucial to date the grave, as grave goods do not allow to discern whether the burial occurred during the Ninevite 5 period or the early stages of the Akkadian period (Morandi Bonacossi et al., 2018).

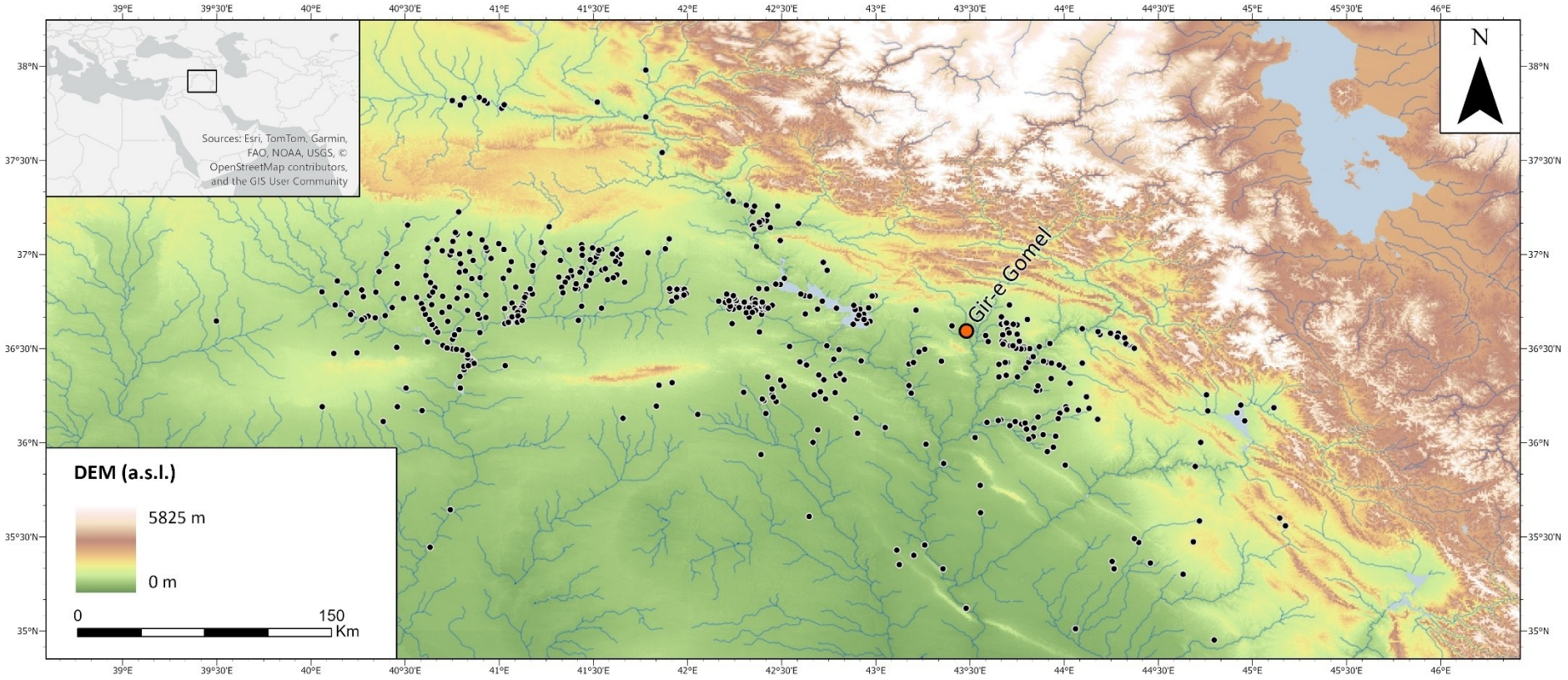


Figure 4. The site of Gir-e Gomel within the sites with Ninevite 5 occupation. Map by courtesy of Biel Soriano Elias.

The superposition of the graves located below the Middle Bronze Age Grave 44, in conjunction with radiocarbon dating, allows for the identification of two distinct burial phases (**Figure 5**). The first burials occurred during the mid-late first half of the 3rd millennium BCE, with grave goods providing a relative chronology of Ninevite 5. This phase is designated as 24b and comprises Graves 49 and 51. ^{14}C dating at 2σ of Grave 51 from two different long bone samples have yielded an absolute chronology ranging from 2847 to 2463 cal. BCE (Morandi Bonacossi et al., 2025). The second phase of inhumations occurred phase 24a, and it is comprised of Graves 45, 46, 47 and 48. ^{14}C dating at 2σ of Grave 48 has provided an absolute chronology of 2623 - 2464 cal. BCE (Morandi Bonacossi et al., 2025). During this period, a large circular fireplace was placed in the center of all the burials, which may have been related to funerary customs.

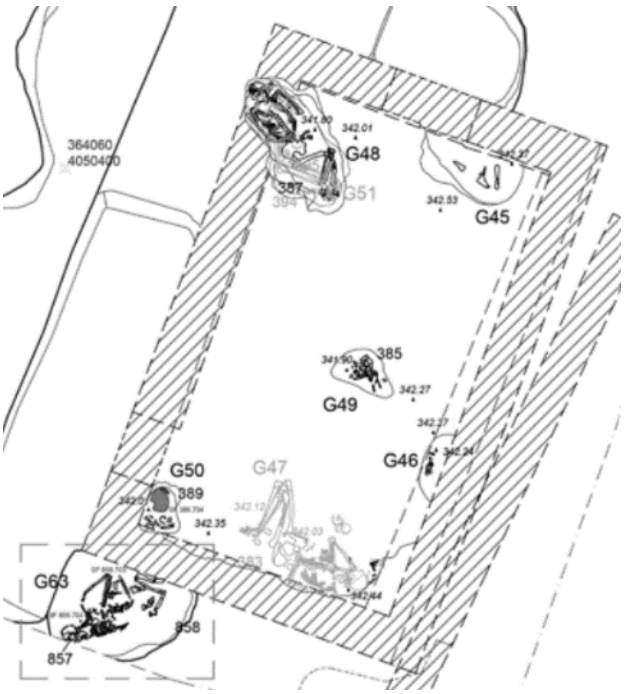


Figure 5. Ground plan of the Early Bronze Age burials disturbed by the construction of the Middle Bronze Age Grave 44. Image extracted from *Morandi Bonacossi et al. (2025)*, Fig. 24.

1.2 NORTHEASTERN IBERIA

The northeastern region of the Iberian Peninsula is currently part of the countries of Spain and Andorra. The Pyrenees serve as a geographical and historical boundary, demarcating the region from contemporary France. This territory has been inhabited by human communities since the Paleolithic period, and over time, it has become the homeland of multiple migrant communities. The region's optimal climate and geography have contributed to a relatively peaceful coexistence among these communities during the prehistoric period. The northeastern region of the Iberian Peninsula has garnered significant attention from local researchers, leading to a substantial proliferation of archaeological fieldwork and subsequent analysis since the early 1900s. While certain prehistoric periods have attracted greater scholarly attention than others, the Early Bronze Age remains one of the most under-studied periods due to the scarcity of archaeological remains in the region. The Paleolithic period is a subject of interest to the research community due to its significance in the study of the initial human presence in the region. The Neolithic period, on the other hand, is a subject of interest due to the significant socioeconomic change it represents, from a hunter-gatherer society to an agricultural and livestock-based economy. The prehistoric Age of Metals, which is comprised of the Chalcolithic and the Bronze Age periods, is characterized by the significant impact of metal artifacts on society. However, recent research trends have focused on ancient DNA and migration-related topics. The Bell Beaker and Urnfield culture communities, which are from the Chalcolithic and the Late Bronze Age periods, respectively, have been the focus of more extensive research. It is also noteworthy that these periods have yielded more remarkable archaeological remains than those discovered in the Early Bronze Age. This characteristic renders the latter a less appealing subject for archaeological study. Despite the scarcity of remains, researchers have been able to obtain valuable information about the living and death of these communities, including habitat, subsistence economy, craftsmanship, and funerary practices. The insights regarding these societies will be reflected in the research presented herein.

1.2.1 Beyond the three-age system: rethinking the periodization of the Bronze Age in the Iberian Peninsula

The three-age system continues to be used as a method for periodizing European prehistory since Thomsen popularized it in the 19th century (Ayarzagüena Sanz, 2000; Bahn, 2008; Eskildsen, 2019). A problematic aspect of this approach is that it perpetuates an evolutionary thought that conceptualizes the progression of human societies through a cyclical pattern of technological development, use, and subsequent obsolescence, eventually giving rise to a new technological innovation. This perspective prompts critical scrutiny, as it exclusively focuses on the stages marked by diagnostic fossils, while disregarding other pivotal factors that mirror shifts in human lifestyles (Eskildsen, 2019; Maya, 1997). Following Thomsen's proposal, the academic community endured a protracted period before the first systematization of Bronze Age periodization in the Iberian Peninsula was presented by archaeologist Luis Pericot at the 1949 National Archaeology Congress. Pericot used the periodization proposed for the Argaric culture as a point of reference and extrapolated it to the rest of the peninsula. In doing so, he divided the Bronze Age into three major periods: the first period, Bronze I, was defined by the site of Los Millares and the pre-Argaric period. The second period, Bronze II, was defined by the Argaric period as a reference point. The third and final period, Bronze III or Final, was characterized by the post-Argaric period and the introduction of Urnfield culture. Subsequent to Pericot's proposition, other archaeologists initiated a reevaluation of this periodization. Joan Maluquer de Motes acknowledged that it was difficult to distinguish between Bronze I and Bronze II in the northeastern Iberian Peninsula due to the continuity observed in the archaeological record (Maya, 1997). This lack of consensus and the resulting dissatisfaction within the academia led to the adoption of numerous alternative periodizations within the discipline, many of which were based on prior divisions and lacked strict consensus (**Figure 6**). However, it should be noted that the periodizations proposed by Guilaine and his contemporaries did not fully align with the material reality of archaeological sites, which varies significantly by geographic region (Almagro-Gorbea, 1997). This is because scholars relied exclusively on diagnostic fossils, particularly the presence of specific morpho-technical ceramic styles, to assign a site to the Early or Middle Bronze Age (Maya & Petit, 1986; Soriano, 2013). However, given the intermittent nature of these diagnostic fossils across northeastern Iberian settlements (Maya & Petit, 1986) and the scarcity of radiocarbon dates, it remains challenging to ascertain a clear distinction between Early and Middle Bronze Age in specific regions (Maya, 1997).

In order to address the inconsistency in the archaeological record between the end of the Chalcolithic and the beginning of the Final Bronze Age, (Maya, 1997) proposed a theoretical framework for the integration of the Early and Middle Bronze periods into a single phase: the Initial Bronze. This period was characterized by the introduction of the use of bronze and the emergence of the new funerary practice of cremation and the Urnfield culture (López-Cachero & Rovira Hortalà, 2018; Maya, 1997). Maya's term was met with enthusiasm by archaeologists working within specific northeastern Iberian regions, such as the Barcelona plain, where the archaeological evidence remained non-distinctive (Daura et al., 2017a; Gómez et al., 2015). Conversely, in other regions, such as the western part of the northeastern peninsula, the distinction between Early and Middle Bronze persisted due to the presence of material differences between these two periods.

Since the 1990s, the increasing accessibility of radiocarbon dating facilitated the proposal of periodizations that integrated these dates with the archaeological evidence. Studies such as that of Barceló (2008) various duration intervals are proposed for each period based on radiocarbon dates from different archaeological materials (such as charcoal or bone) with a standard deviation of less than 100 years. This development contributed to a more nuanced characterization of the various phases of the Bronze Age. However, the challenges that previously hindered precise definition —including the Hallstatt plateau dilemma— have prompted researchers to employ the periodization that most effectively aligns with their material records and study area (Almagro-Gorbea, 1997; Soriano, 2013). This persistent ambiguity regarding the early stages of the Bronze Age has prompted researchers, such as Soriano (2013), to adopt a holistic approach in identifying potential phases. In their doctoral thesis, an analysis that incorporated diagnostic fossils, variations in social manifestations (e.g., housing, production, funerary practices), and radiocarbon dating was conducted. Nevertheless, the evidence from the Barcelona plain still does not fully align with the model periodization he proposes.

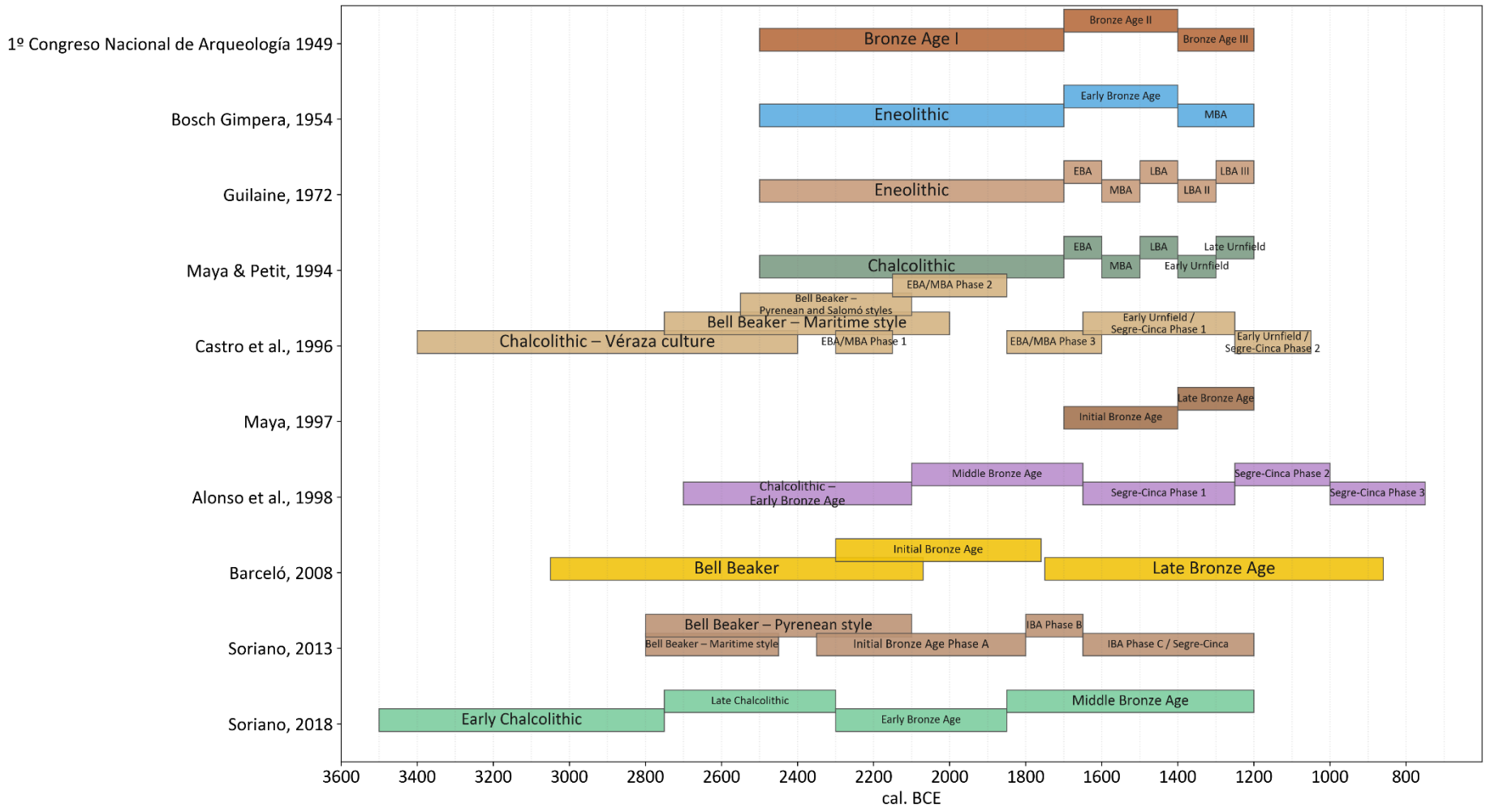


Figure 6. Periodization of the Early Bronze Age according to different researchers.

1.2.2 Characteristics of the Early Bronze Age

The archaeological sites with Initial or Early Bronze Age and Middle Bronze Age occupations have been the focus of extensive research in the northeastern Iberian Peninsula. However, this period has not yielded, or has not preserved, as many material remains as the preceding and subsequent periods. This paucity of evidence has prompted researchers to concentrate their efforts on individual sites rather than adopting a more comprehensive approach. There have been various attempts to synthesize the extant data from this period but, as time progresses, this information becomes outdated due to the discovery of new sites and their archaeological records. The following review will elucidate the findings regarding habitat, subsistence economy, craftmanship and funerary practices.

1.2.2.1 Habitat

The territory exhibits a gradual increase in open-air settlements located in plains and in proximity to watercourses. Two geographical regions can be distinguished: the Western Depression, and the Pre-coastal and Coastal regions. In the former, settlements can be found at elevated positions and make use of stone as a building material. The use of stone, a durable material, suggests a high degree of sedentarization among these communities. In contrast, the Pre-coastal and Coastal regions feature settlements situated on flat land or gentle elevations, and build using perishable materials such as mudbricks or plant elements. An exception can be found at the site of Caserna de Sant Pau del Camp, in which a hut built with stone walls was found (Granados et al., 1993). Rock shelters or caves were also used to inhabit, as evidenced by sites such as Cova de les Pixarelles, Cova del Toll (Maya, 1997), Cova del Frare (Martín et al., 1981), or Bauma del Serrat del Pont (Alcalde et al., 1998). However, the importance of these rock shelters or caves as residence areas declined over time. Evidence from sites such as Cova de Can Sadurní suggests that these types of sites were also used as seasonal livestock shelters (Soriano, 2013).

(Granados et al., 1993). Rock shelters or caves were also used to inhabit, as evidenced by sites such as Cova de les Pixarelles, Cova del Toll (Maya, 1997), Cova del Frare (Martín et al., 1981), or Bauma del Serrat del Pont (Alcalde et al., 1998). However, the importance of these rock shelters or caves as residence areas declined over time. Evidence from sites such as Cova de Can Sadurní suggests that these types of sites were also used as seasonal livestock shelters (Soriano, 2013).

1.2.2.2 Subsistence economy

Societies in the northeastern Iberian Peninsula employed a broad-spectrum subsistence economy, being the cultivation of cereal and legumes the main source of their diet. Archaeobotanical analysis on plant taxa has determined the cultivated species, which included naked wheat (*Triticum aestivum* and *Triticum durum*), hulled barley (*Hordeum vulgare*, and *Hordeum vulgare nudum*), emmer wheat (*Triticum dicoccum*), club wheat (*Triticum compactum*), pea (*Pisum sativum*), broad bean (*Vicia faba*), and bitter vetch (*Vicia ervilia*), the latter of which was used as animal feed (Alonso, 1997, 2000). The cultivated produce was stored in silos, pits and granaries. In certain flatland settlements, both in the Coastal region and the Lleida Plain, the phenomenon of "silo fields" emerged. It entailed the construction of numerous large-capacity silos and pits within a single settlement, occupying a substantial territory and thereby creating the largest living spaces ever in the area (Soriano, 2013). Notable examples of these silo fields include sites such as Can Roqueta (Boquer et al., 1990), Minferri (Alonso & López, 2000), and Bòbila Madurell (Martín et al., 1988; Maya, 1997). These structures were mostly used to store cereals, and were accompanied by combustion structures, hut floors with or without postholes, and irregular plant cuttings interpreted as clay extraction pits. Another significant innovation of this period was the construction of grill-plan buildings (Soriano, 2013), which are interpreted as raised granaries designed to protect grain from ground moisture and promote air circulation for the drying process (Carlús et al., 2010; Gómez & Molist, 2016). The first ones to appear in the northeast of the Iberian Peninsula were in the plain of Barcelona, but this type of buildings date back to the Neolithic period in Anatolia (*ca.* 8000 – 6500 cal. BCE). The presence of grill-plan buildings is evident, given the area's high humidity and proximity to water resources, including the Mediterranean Sea and rivers. The orientations of the granaries were chosen to facilitate optimal soil drainage and air circulation (Carlús et al., 2010).

The gathering of plants provided a variety of fruits, including acorn (*Quercus* sp.), blackberry (*Rubus fruticosus*), blackthorn (*Prunus spinosa*), and mastic (*Pistacia lentiscus*) (Alonso, 2000). Both cultivated and gathered plant products were commonly processed using stone mills to optimize consumption and storage. The gathering of animals was frequent and consisted of collecting mollusks of the class gastropod (*Patella* sp.), and bivalvia (*Glycymeris glycymeris*, and *Acanthocardia tuberculata*). However, there is a debate among researchers whether these species of mollusks were collected for food purposes or not. A high percentage of bivalves have a high level of erosion, which is a condition typical of bivalves that have been dead for a long time. The gathering of eroded mollusks would imply obtaining raw materials and not for dietary purposes. On the other hand, the gastropods have tear marks, so it could be inferred that they were

collected from the rocks with the purpose of being consumed (Gómez et al., 2014). In this period, an increase in the collection of bivalves and a decrease in the collection of gastropods is evidenced. This phenomenon suggests a change in the coastal landscape, with an increase in the volume of coastal sand that would have covered the rocks on which the limpets would inhabit (Gómez et al., 2015; Gómez & Molist, 2016).

The exploitation of livestock was significant, involving various species, such as ovicaprids (*Ovis aries* and *Capra hircus*), bovids (*Bos taurus*), pigs (*Sus domesticus*), and equids (*Equus caballus*). Resources from both males and females at young and older ages were used. The primary products consumed were hide, meat, fat and bone marrow; and the secondary products consumed were milk and wool. Animals were also used for their draft power. Culinary practices encompassed methods such as boiling, roasting, drying, and salting (Alonso, 1997; Andúgar Martínez & Saña Seguí, 2004; Soriano, 2013).

Hunting was not a specialized activity; rather, it served as an important dietary supplement in certain locations, as it has been evidenced for sites such as Carretelà (Aitona). Hunted species were very diverse, including fox (*Vulpes vulpes*), deer (*Cervus elaphus*), rabbit (*Oryctolagus cuniculus*), fallow deer (Dama dama), wild boar (*Sus scrofa*), and hare (*Lepus* sp.), among others (Andúgar Martínez & Saña Seguí, 2004). The evidence of fishing is scarce: a fishing net weight of triangular morphology was found at the site of Carrer de la Riereta 37-37 bis (Bofill, 2016). In this chronology, ichthyofaunal remains have not yet been discovered (Gómez et al., 2014).

1.2.2.3 Craftsmanship

The lithic industry encompasses a wide array of artifacts, ranging from macro- to microlithics, both of which are associated with agricultural production and produce processing. Some examples are grinding tools (saddle querns and grinding stones), hoes, axes, lithic flakes, hammerstones, scrapers and sickle blades (Aguelo & Huertas, 2006; Bofill, 2016; Bordas, 2016; Gómez & Molist, 2016; Granados et al., 1993; Nadal & Castillo, 2010; Piera et al., 2005; Suau & Matas, 2010; Velasco et al., 2017).

The repertoire of pottery vessels includes both the known as “generic pottery” and Epi-Bell Beaker pottery. The most common forms are hemispherical, globular or double cone, carinated and with a flat or umbilicated base. These vessels are typically characterized by their small size. Some vases have perforations in the base area, which have been interpreted as either cheese strainers. A diverse variety of surface finishes were used. In the case of generic pottery, the

surfaces were characterized by a smooth or burnished finish. The majority of these vessels were not decorated; however, some were embellished with rough clay applications and cords. The Epi-Bell Beaker pottery, characteristic of the Northeastern Group, exhibits decorative motifs that draw inspiration from the Bell Beaker tradition (Gómez et al., 2015). Potters employed various decoration techniques, including incision, fingertip impressions, barbed wire impressions, and point-and-line decorations, which is also referred to as the boquique technique (Maya & Petit, 1986; Soriano, 2013). Evidence of boquique designs filled with white paste to give a more visually appealing appearance have been found at sites such as Mercat de Santa Caterina (Gómez et al., 2015). Exterior decorations include dots, garlands with or without fringes, solar schematizations, zigzag patterns, spikes or half-spikes, crescent shapes, notches, continuous and dashed lines (Daura et al., 2017a; Maya & Petit, 1986). The arrangement of these motifs frequently occurs in bands. Smooth cords are also used as decorative elements in Epi-Bell Beaker ceramics. It has been observed that both generic and Epi-Bell Beaker pottery may include grasping elements, such as knobs, strap handles, or lugs. Additionally, evidence of pottery vessels influenced by neighboring regions has been documented. The Pyrenees region is renowned for its distinctive polypod vessels, while the Italic region is characterized by its button appendages. The pottery from the Levantine region is distinguished by their twin vessels, which are characterized by the presence of an inner bowl situated adjacent to the handle (Soriano, 2013).

Both the lithic and pottery industries exhibit no signs of production specialization or uneven distribution of artifacts at the inter-site level. However, metallurgy exhibits signs of pronounced specialization in certain archaeological sites. One of the earliest examples is Minferri (Rovira, 2006). While most sites only yield finished objects (Soriano, 2013, 2018), Minferri has tools related to the entire metallurgical process: extraction, reduction, smelting, and finishing. The hierarchization of metallurgical production suggests the presence of social asymmetries at an inter-site level. The production of silver or gold objects was scarce, limited to spiral ornaments and rings (Soriano, 2013). Conversely, bronze and copper artifacts were more prevalent, including flat axes (Minferri, Forat de la Tuta, Can Roqueta II), flanged axes (Cova B d'Olopte), daggers (Cova de les Encantades de Martís), riveted daggers (Cova d'Aigües Vives, Cova de Font Major, Cova de les Grioteres), and arrowheads (Camp Cinzano I). Cova del Batllevell, Balma del Serrat del Pont, Vall de Ribes, Mas d'en Boixos I, Forat de la Tuta), awls (Minferri, Cova del Toll, Cova de la Pesseta), beads (Cova del Toll), spiral ornaments (Cova de Montanissell), diadems (Cova de Montanissell), and perforated discs (Plana d'Ancosa) (Balaguer et al., 2011; Daura et al., 2017b; Soriano, 2013; Soriano et al., 2019; Soriano & Chamón, 2012).

The craft of ornaments was based on bone and shell materials. The production of beads for pendants and bracelets, V-perforated buttons (both plain and decorated with *oculi* motifs), and arrowheads also emerged during this period (Soriano, 2013).

1.2.2.4 Funerary practices

A wide range of funerary practices coexist during this period, including the reuse of previous funerary structures, such as in the sites of Cova Cervereta and Cova de la Pesseta (Soriano, 2018). The most prevalent funerary practice was multiple inhumations in megalithic graves with Catalan gallery, with cist, or with funerary chambers; in paradolmens, hypogea, and tumuli (Gómez & Molist, 2016; Soriano, 2013). Hypogea began to appear in the northeast of the Iberian Peninsula from the Chalcolithic period, between 2750 and 2300 cal. BCE, associated with the Bell Beaked societies (Soriano, 2018). Hypogea were particularly prevalent in the Costal and Pre-coastal regions, as evidenced by sites such as Can Roqueta II (Sabadell), Carrer de la Riereta 37-37 bis (Barcelona), Aeroport de Sabadell, Mas Vilalba (Roca del Vallès), Plana del Castell-Parc de l'Alba (Cerdanyola del Vallès), Plaça de la Gardunya (Barcelona), Pla de la Bruguera – SONY distribution centre (Castellar del Vallès), and Solar del Pou de la Figuera (Barcelona) (Carlús & Nadal, 2008; Guàrdia & Francès, 2017). In addition to multiple burials, simple, double, or triple burials in simple pits or reused silos have been found, as evidenced by the sites of Can Castellví, and Institut de Batxillerat Antoni Pous (Maya, 1997; Soriano, 2013). Multiple and simple inhumations were placed in both primary and secondary positions (Gómez & Molist, 2016). Furthermore, there is evidence suggesting the practice of cremation in sites such as Forat de la Conqueta, although the intentionality of these cremations remains unclear (Soriano, 2018). Some individuals were interred in a seemingly careless manner, as evidenced by one individual at Camp Cinzano, who was positioned vertically in a pit, with their head facing downward and their feet directed toward the opening (Soriano, 2018).

When silo fields were abandoned, they were reused as burials. The inhumations contained modest grave goods, including undecorated and Epi-Bell Beaker-decorated ceramic vessels, twin vessels, tools made of copper, bronze, bone, and flint, V-perforated buttons (mostly undecorated, and some decorated with the *oculi* motif), bone and stone ornaments, and meal offerings from domesticated animals (Soriano, 2018). As time progressed, there was a slight rise in the quantity of grave goods present in multiple individualized burials, and in simple inhumations. New pottery forms with French and Italian influences emerged, including polypod and button appendix vessels.

With regard to the social asymmetries observed in the funerary record, the research community is divided between two hypotheses. The first claims that the presence of scarce grave goods in burials is a reflection of egalitarian societies, when comparing the Early Bronze Age with the Bell Beaker communities of the Chalcolithic. They had noticeable differences in the quantity and quality of grave goods between individuals, indicating high social inequalities. The funerary practice of secondary multiple inhumations is also interpreted as a reflection of a collective rather than individualistic society (Soriano, 2018). In contrast, the second hypothesis claims that these societies were socially unequal at the end of the Early Bronze Age. There would be three social categories: the first includes individuals of all ages and sexes buried in simple graves or in hypogea, inhumed in multiple individualized forms. Faunal remains are interpreted as grave goods or as evidence of commensality. The presence of children in these contexts suggests the possibility of inherited status. The second category comprises the majority of the population and is characterized by multiple burials in a secondary deposition without grave goods. The third category includes "thrown" individuals and isolated human bones mixed with waste, without grave goods (Soriano, 2013, 2018). An example can be seen at the Plaça de la Gardunya site, where numerous scattered bones of children and adults were found in small pits. Hypogea are thought to have been reserved for members of the same lineage, serving as a restricted space for a specific segment of the population (Chambon, 2016; Suau & Matas, 2010). However, this hypothesis has yet to be confirmed by ancient DNA analysis (Soriano, 2018).

1.2.3 The site of Plaça de la Gardunya

Plaça de la Gardunya is an archaeological site located within the district of Ciutat Vella, in the Raval area (***Figure 7***). The initial excavations were conducted from 2010 to 2012 by Conatus S.L., with the objective of constructing a subterranean parking facility behind the Boqueria market. Radiocarbon dates exhibit a significant range, indicating a continuous use of the site over time as a necropolis (***Table 2***). The fieldwork, conducted in eight sectors, revealed a variety of structures dating back to the Early Bronze Age, such as postholes, buildings, pits, silos, combustion structures, paleochannels, and cuts. These structures are associated with residential, storage, and food production purposes (Velasco et al., 2017).

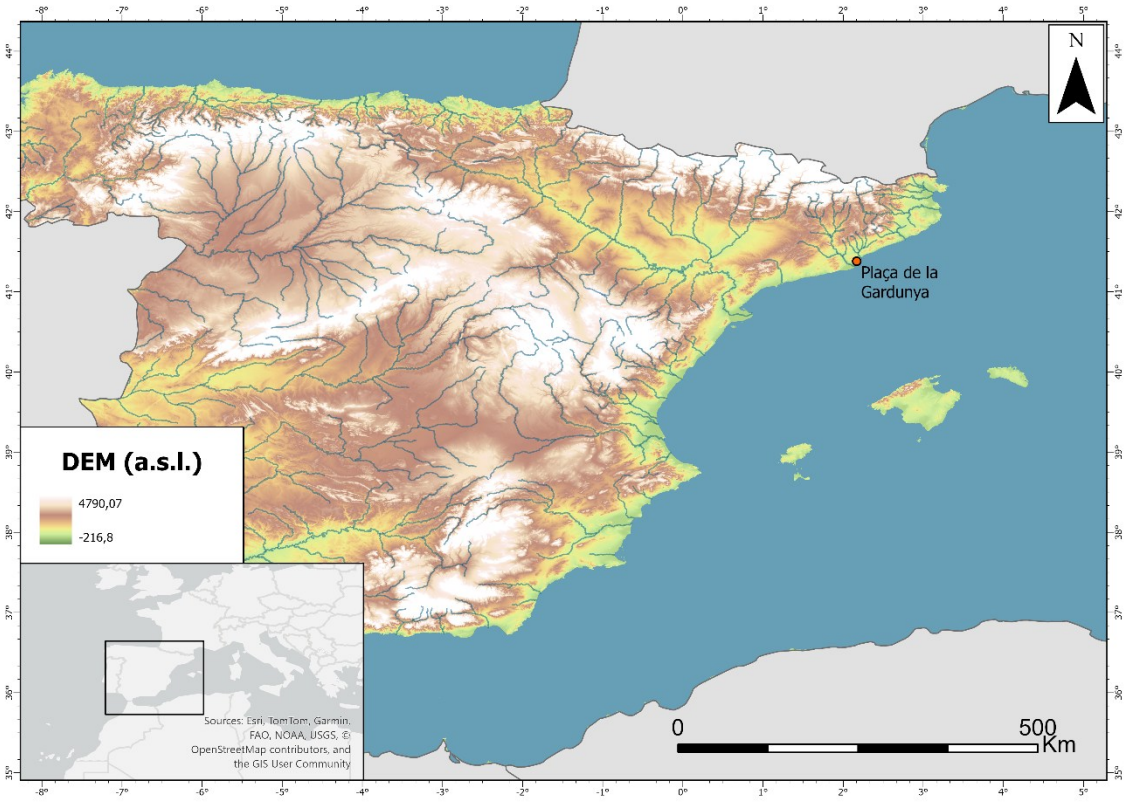


Figure 7. Location of the site of Plaça de la Gardunya in the Iberian Peninsula. Map by courtesy of Biel Soriano Elias.

Table 2. Radiocarbon dates of various individuals from the necropolis of Plaça de la Gardunya.

Grave	Individual	Sample	^{14}C cal. BCE (2σ)	Reference
3/4	4390	Rib	1737 - 1534	Gómez et al. (2015)
1	50700	Rib	1918 - 1748	Velasco et al. (2017)
2	50619	Rib	1881 - 1692	
5	4429	Skull	2028 - 1878	
	4462	Rib	2028 - 1878	
	4437	Rib	1980 - 1775	
	4427	Skull	2031 - 1888	
	4406	Rib	2281 - 2038	

Sectors 4 and 5 of the site contain the majority of graves. In Sector 4, the following graves have been identified: 2, 3/4, 5, and 7. In Sector 5, graves 1 and 2 have been identified. The information published about these graves is summarized as follows.

1.2.3.1 Grave 2 (Sector 4)

Grave 2 from Sector 4 has not preserved its original morphology due to the destruction of the upper portion of the structure by the action of heavy machinery. It may have been a hypogeum or a simple pit. It contains the multiple successive inhumations of 12 individuals, two of whom were placed in primary disposal, in a right lateral decubitus position with flexed limbs, and in anatomical connection (Velasco et al., 2017). They were oriented from east to west and had pottery as grave goods. Four of the individuals possess phenotypic pathologies in the upper and lower extremities related to metabolic rickets or congenital rickets of the achondroplasia or hypochondroplasia type. Metabolic rickets has been linked to a deficiency in vitamin D, while congenital rickets has been linked to DNA mutations that directly result in limb shortening.

1.2.3.2 Grave 3/4 (Sector 4)

Grave 3/4 from Sector 4 is a double-chambered hypogeum, the entrance to which is sealed with medium-sized stones (***Figure 8***). The grave was partially destroyed by a screen wall built for the parking lot, and by a wall from the late Middle Ages. 56 individuals were buried in this funerary structure, 37 in chamber A and 14 in chamber B. In chamber A, two individuals were buried simultaneously and disposed in a lateral decubitus flexed to the left: one oriented from east to west and the other from southeast to northwest. A third individual was buried in a secondary disposal and was also oriented from southeast to northwest. The following archaeological materials have been recovered from the chamber and have been determined not to be grave goods: five fragments of pottery decorated with Epi-Bell Beaker motifs, a complete pottery vessel, and carpological remains. Chamber B is partially damaged by the screen wall of the underground parking lot. The burial exhibits two distinct phases of use. In the earliest phase of use (SU 4430), a total of 14 individuals were buried, exhibiting minimal or no anatomical connection. Over time, a layer of earth was accumulated on top of the burial chamber. Subsequently, it was reused for the burial of 5 additional individuals. Two of these, located in the entrance area, remained at primary disposal. One of them was buried in a prone decubitus position with flexed limbs, and oriented northwest to southeast, while the other was buried in a prone decubitus position and

oriented southeast to northwest (Velasco et al., 2017). One individual buried in secondary disposal was placed in a prone decubitus position and oriented from west to east. A total of 87 bone buttons with V-perforation have been identified as grave goods. Of these, 19 are not decorated, while 3 exhibit the *oculi* decoration motif, which consists of concentric circles. The remaining 68 bone buttons were crafted from materials such as tooth, ivory, long bone, and deer antler. The V-perforated buttons have been suggested to have been part of the clothing of the deceased. However, an alternative hypothesis proposes their use as closures for funerary shrouds (Soriano, 2018). A comprehensive analysis of the spatial distribution of the buttons, a topic that has not yet been studied, could resolve the debate. In the most recent burial phase of chamber B (SU 4328), 5 individuals were buried with minimal or no anatomical connection. One of the deceased was in a left lateral decubitus position with flexed limbs (Velasco et al., 2017), oriented from north to south. Grave goods include two pottery vessels, 38 lithic remains, and a fragment of a bovid mandible.

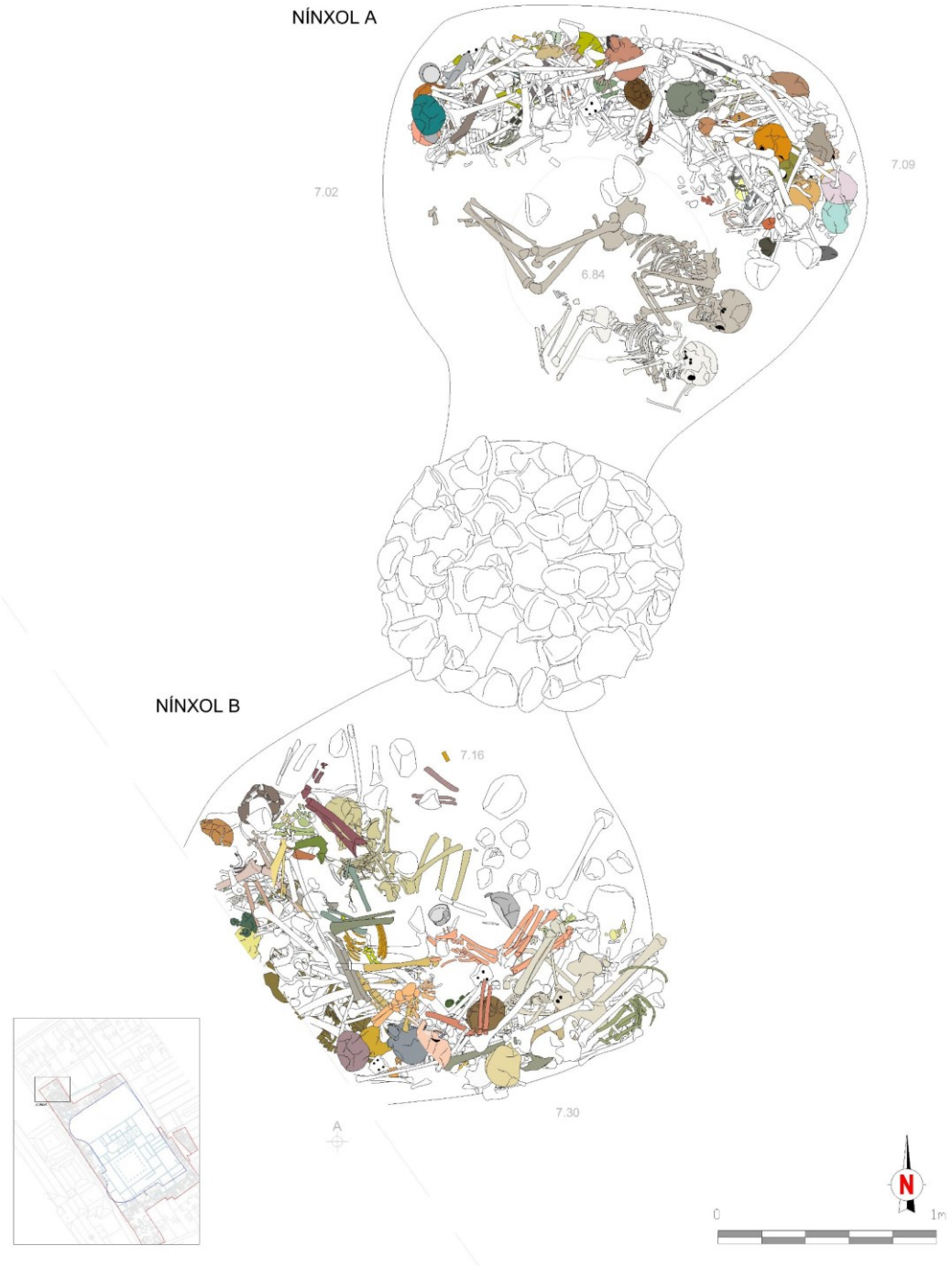


Figure 8. Floor plan of Grave 3/4. Colored bones belong to the same identified individual. Illustration commissioned by the SAPPO-GRAMPO Research Group, elaborated by Noemi Terrats.

1.2.3.3 Grave 5 (Sector 4)

Grave 5 from Sector 4 is a structure composed of four simple pits, which contain infant burials in secondary disposal. The fifth simple pit remains under discussion, as archaeologists are uncertain whether it should be incorporated into Grave 5 or described independently. It is hypothesized that these pits initially served as habitat spaces and subsequently functioned as funerary spaces, given their irregular morphology. The individuals buried in these pits are not completely preserved, as it appears that the bones were previously selected for burial. The simple pit with the stratigraphic unit 4470 contains the burial of 4 child individuals who lack anatomical connection. The grave goods include 6 pottery fragments with Epi-Bell Beaker decoration and animal remains. The simple pit with the stratigraphic unit 4469 contains the burial of 3 child individuals who lack anatomical connection. The grave goods include 1 pottery vessel and remains of lithic reduction. This pit cuts and partially covers the simple pit 4470. The simple pit with the stratigraphic unit 4471 contains the burial of various bones from child individuals, whose minimum number is unknown. The associated grave goods are 2 bovid horns and 4 small undecorated pottery vessels. The simple pit with the stratigraphic unit 4461 contains the burial of 2 child individuals who lack anatomic connection. This pit is cut and partially covered by a combustion structure. Lastly, the simple pit with the stratigraphic unit 4405 contains the burial of 8 human bone fragments of subadult individuals, lacking anatomical connection. They are associated with animal remains.

1.2.3.4 Grave 7 (Sector 4)

Grave 7 of Sector 4 has not been published, thus any type of burial record for this grave is unknown.

1.2.3.5 Grave 1 (Sector 5)

Grave 1 of Sector 5 is a hypogeum whose burial chamber was affected by a cut made in the 16th century CE (***Figure 9***). It contains the multiple burials of 8 individuals in secondary disposal. It remains uncertain whether the inhumations were successive or simultaneous. Two individuals, 50616 and 50700, were in a loose anatomical connection and its sex was not determined. The position of two individuals has been ascertained: 50616 was in a right lateral decubitus position,

while 50700 was in a prone decubitus position (Velasco et al., 2017). The funerary structure did not contain any grave goods.



Figure 9. Southeastern section of Grave 1 (Sector 5) with the presence of the buried individuals. Intellectual property of the SAPPO-GRAMPO Research Group.

1.2.3.6 Grave 2 (Sector 5)

Lastly, Grave 2 of Sector 5 consists of a hypogeum, the entrance to which is sealed with medium-sized stones (***Figure 10***). The funerary chamber was affected by a cut made in the 16th century CE and by the construction of the underground parking lot in 1960. It is characterized by an oval floor plan and a flat bottom. It contains the multiple inhumations of 5 individuals. Despite the presence of pottery fragments in the access shaft, it has not been found in the burial chamber, indicating the absence of grave goods. Three of the individuals are primary disposals, while the other two consist of secondary disposals. In the case of the deceased in primary disposal, the slight sedimentation observed between the individuals is an indicative of a possible simultaneous burial. These three individuals were oriented southwest to northeast, with two of them placed in a left lateral decubitus position with flexed limbs, while another was found in a prone decubitus position with flexed legs to the left side (Velasco et al., 2017).

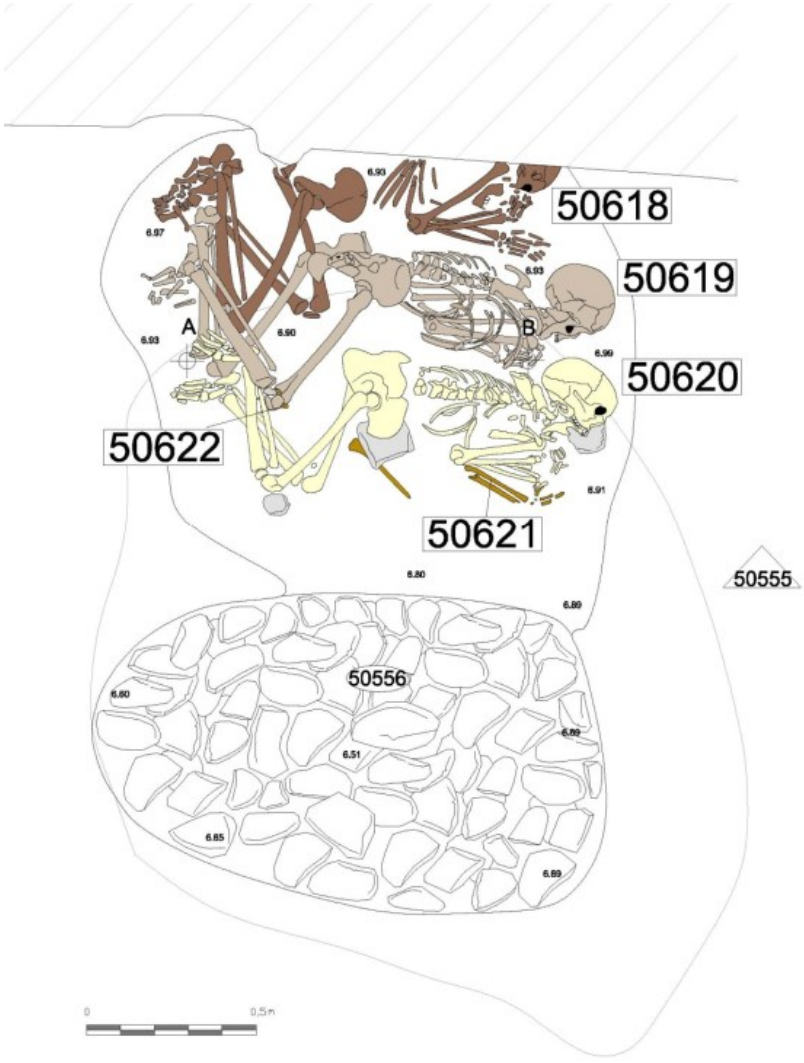


Figure 10. Floor plan of Grave 2 (Sector 5) with detailed information about the buried individuals. Illustration commissioned by the SAPPO-GRAMPO Research Group, elaborated by Noemi Terrats.

1.3 OBJECTIVES

The present thesis encompasses comprehensive multiapproach analyses conducted on three specific and carefully selected study cases, consisting of the archaeological sites of Gird Lashkir, Gir-e Gomel, and Plaça de la Gardunya. The three case studies under consideration share several significant characteristics and common problematics among them, rendering them particularly suitable for analysis. The societies that inhabited these sites correspond to the Early Bronze Age period. Gird Lashkir and Gir-e Gomel are located in the region of northern Mesopotamia, while Plaça de la Gardunya is situated in the northeastern area of the Iberian Peninsula.

These territories are particularly notable for representing key regions where the emergence of early urbanism and increasing social complexity took place, and were simultaneously undergoing similar politico-economically transformative processes during this period. Furthermore, a paucity of archaeological remains is observed in all three sites, accompanied by scarce published data available in academic literature. This has consequently led to archaeological research that is lacking a comprehensive holistic approach. This methodological deficit has perpetuated a state of persistent uncertainty, giving rise to a multitude of unanswered questions concerning the daily lives, social structures, and cultural practices of these ancient populations. Despite these fundamental similarities in archaeological context and research challenges, these societies were governed by very different and distinctive social dynamics, and are geographically located very far away from one another across different continental regions. Given their distinct cultural development and geographic distribution, they serve as ideal case studies for evaluating the efficacy of a multidisciplinary approach applied to human remains. This approach aims to provide reliable data that can significantly contribute to the interpretation of the complex socioeconomic dynamics of these past societies.

In light of this framework in mind, the principal objective of this thesis is to elucidate the existence and manifestation of social inequalities during the Early Bronze Age, specifically within two distinctly different geographical and cultural contexts such as northern Mesopotamia and northeastern Iberia. This investigation will be conducted through the detailed examination of the active agents of society: the deceased individuals recovered from the archaeological sites of Gird Lashkir, Gir-e Gomel, and Plaça de la Gardunya. Access to a greater number of potentially relevant sites was unfortunately precluded by the current unavailability of archaeological materials from sites located in regions experiencing ongoing political instability or active war conflicts, as clearly evidenced in the challenging case of northern Mesopotamia, and additionally by the general absence of adequate samples in northeastern Iberia.

In this methodological sense, the multidisciplinary approach has consisted of performing multiple complementary analyses on human skeletal remains, with each analytical method providing different information about both the life experiences and death circumstances of each individual. When these methodologies are combined and interpreted together, they provide substantially deeper insight into many aspects that are somehow intrinsically linked to the physical expression and manifestation of social inequalities within these past communities.

Each analytical approach has been applied with the pursuit of its own specific objectives, which will collectively allow to prove the presence or absence of social inequalities as they are expressed in the studied human bodies. First of all, a comprehensive archaeothanatological methodology has been systematically implemented to accurately reconstruct the burial customs of the population and to obtain detailed information about the social implications of the burial treatment of the deceased individuals. This methodology will essentially reveal their social statuses within their respective communities. The results will be obtained through the application of a standardized archaeothanatological analysis, which will meticulously record the investment of time and labor dedicated to each individual grave, the comfort elements placed in the burials, and the presence or absence of ornaments and grave goods including, if present, their precise quantity, material quality, spatial distribution, and geographical provenance. Taphonomic processes will be also systematically recorded and analyzed, as some elements of the burial, including the container and the contents, could be significantly affected by anthropic or diagenetic alterations over time.

Following the archaeothanatological approach, a detailed anthropological study will be conducted in order to ascertain the complete biological profile of the individuals. This comprehensive biological profile will be systematically elaborated by recording the presence and preservation state of the skeletal remains of each grave, as well as using several established methodologies to determine age, sex, and stature of the deceased individuals. A subsequent examination of the bones will be conducted to discern paleopathologies and enthesopathies, which are indicative of injuries, diseases, nutritional deficiencies, and musculoskeletal stress. These health indicators, when evaluated collectively, facilitate a precise interpretation of the individual's health state and activity markers over the course of their lifetime.

While the two primary analyses will provide valuable insight into the individuals and their social differences, two additional methodologies have been applied in this thesis to gain even deeper and more nuanced knowledge. These analyses entail the examination of dental microwear patterns and the analysis of stable isotopes. A dental microwear pattern analysis will be conducted

to observe the abrasiveness of the consumed diet at both an intra-population and a population level. Determining factors will include age, sex, and social status. This analysis will enable the association of a particular abrasive microwear pattern with a specific diet, as well as the establishment of dietary trends among different societies. Additionally, it will serve to observe specific dietary patterns indicative of differential access to food resources within these communities.

A comprehensive stable isotopic analysis of bone collagen and tooth enamel hydroxyapatite will yield the distinctive isotopic signatures of carbon and nitrogen. The former method allows for the identification of consumed plants, with the taxonomical identification of archaeobotanical remains serving as a reference point for inferring species. The latter method provides concrete evidence regarding the animal protein consumed, with the presence of faunal remains at the sites providing a contrast. The variability will be observed at two levels: first, among different age groups, sexes, and social statuses of a population; second, among the total population. This will provide another valuable proxy for the establishment of dietary trends and for the observation of differential access to food among different social groups.

The analysis of stable isotopes will also provide crucial insights into mobility and residence patterns through the analysis of oxygen and strontium from tooth enamel hydroxyapatite. This will facilitate a more nuanced understanding of the demographic composition of the site, distinguishing between local and exogenous populations. Additionally, it will allow for the observation of mobility trends within specific demographic groups. The isotope signature of strontium exhibits a close correlation with the geological composition of the region, while the isotope signature of oxygen reflects the hydrological resources from which the individuals obtained water during their lifetime.

The results of the dental microstriation pattern and the stable isotopic analyses will be corroborated by the application of rigorous quality control protocols. These protocols will ensure the reliability and validity of the results. Both bone collagen and tooth enamel hydroxyapatite will undergo different standardized procedures for the removal of diagenetic contaminants. Bone collagen samples will be subjected to a rigorous set of criteria, encompassing collagen yield, the percentage of preserved carbon and nitrogen isotopes, and the C:N atomic ratio. Tooth enamel hydroxyapatite samples will undergo FTIR-ATR analysis to detect alterations in the inorganic part of the bone lattice due to diagenetic alterations. With regard to the examination and assessment of dental microstriation patterns and stable isotope analyses, taphonomic and diagenetic changes in the skeletal remains will also be investigated and evaluated to a specific cause, if possible.

CHAPTER 2: METHODOLOGICAL FRAMEWORK

2.1 ARCHAEOTHANATOLOGY: RECONSTRUCTION OF MORTUARY PRACTICES

Archaeothanatology is a scientific discipline that employs a holistic approach to the analysis of graves. Its objective is the reconstruction of burial customs of past populations. Consequently, the focus is on the examination of human remains and the associated practices concerning the management and treatment of the deceased (Duday, 2009). This is particularly important in the analysis of complex funerary contexts, as only an accurate archaeothanatological study can ensure the proper interpretation of the deposition of remains (Blaizot, 2022). The reconstruction of past burial customs requires a dual approach, encompassing both the characteristics of the container and the contents. The term "container" is used to define the built space in which the deceased will be deposited. The term "content" is defined as all elements contained within the container. These comprise the deceased's skeletal remains, accompanying attire, ornaments, grave goods, and comfort items such as mats, cushions, and blankets.

A meticulous excavation process is necessary for an accurate record of burials, ensuring that all elements are preserved in their original state. Therefore, the burial container must be clearly delineated, with each bone of the skeleton being identifiable and maintained in its original placement. Additionally, grave goods, ornaments, and other comfort items must be excavated until they are fully visible. Subsequent to the excavation, three phases must be followed (Boulestin, 2022). The first phase consists of data collection. During this phase, the number, nature, and organization of human bones, ornaments, and grave goods must be recorded. The specific terminology employed must be clearly defined by the researcher, as discrepancies still exist due to the lack of consensus among scholars regarding the use of French or English terminology. It is necessary to pay particular attention to the definition of the terms “skeletal articulation”, “orientation”, “deposition”, “position”, “number of buried individuals”, “temporality of burial use”, and “form of disposal” when employing them. Upon completion of data collection, the second phase commences. It involves the reconstruction of the final deposition of the burial and the manner in which the assemblage was constituted (**Figure 11**). During this phase, a taphonomic analysis must be performed, taking into account any anomaly related to the decomposition stages of the body (Blaizot, 2022). In a biotic environment, the perishable elements that comprise the burials gradually decay over time. For instance, the phenomenon of bone articulation remaining in primary position is observed in scenarios where the body is entirely constrained within a filled space, such as when covered by soil. Conversely, if bones are found disarticulated, it is indicative of the deceased's position in a void space during the process of organic matter decomposition, allowing for bone displacement as soft tissues dissipate (Duday, 2009). A variety

of taphonomic factors have the capacity to induce bone displacement and alter bone preservation. Disturbances may be attributed to a variety of causes, including the collapse of burial structures, the construction of more modern structures, the activity of small animals, or the action of weathering agents. The third and final phase involves the interpretation of the burial customs, the results of which are contingent upon a theoretical school of thought.

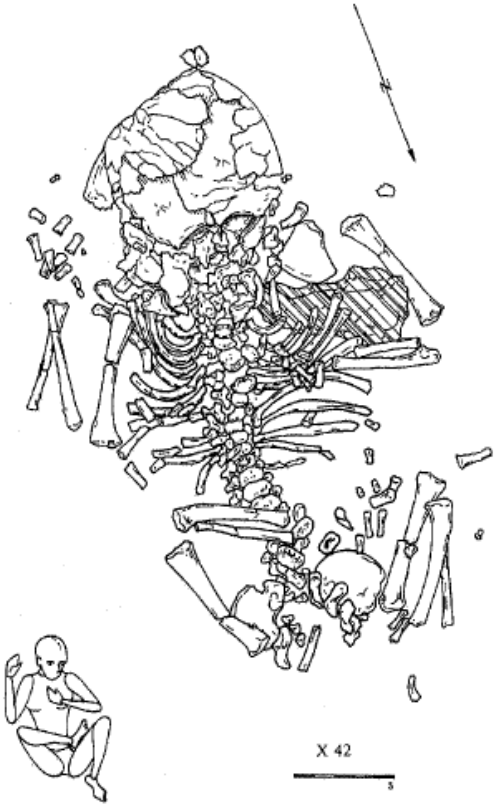


Figure 11. Drawing of the bone position, as well as the archaeothanatological reconstruction of the original body deposition from the burial of a newborn individual located in Plan de la Tour site (Gard, France). Extracted from Duday (2009), Figure 47.

Once mortuary practices have been defined, further research can be conducted on funerary practices. Such research can explore intra-group social dissymmetries in terms of sex, age, or wealth, as well as differences in funerary practices across different populations.

2.2 OSTEOLOGY: BONES AS WITNESSES OF LIFE

Osteology is the discipline that studies human bones. The inorganic composition of bone renders it among the most resilient remains, making it a valuable subject for study across numerous scientific fields, including medicine, forensics, biology, paleontology, anthropology, and archaeology. The analysis of the morphology and the marks left behind in bones can provide information about the soft tissues that were attached to them. A thorough analysis of skeletal remains can provide significant insights into the biological profile of individuals, encompassing factors such as sex, age, and stature, in addition to the presence of pathologies. The interpretation of the recovered details of the biological profile will provide information about health, demographic statistics, and can also provide information about possible social dissymmetries.

The elaboration of a biological profile starts with a meticulous excavation process, during which each bone of the skeleton is identified. Subsequent to the recovery of all relevant archaeothanatological information, determination of sex, age, and stature can be initiated directly during fieldwork, provided that the preservation of bones is severely compromised. In the presence of well-preserved bones, they can be collected for further study in the laboratory. The determination of sex can be made through the observation of sexual dimorphism, which is present in the morphology of bones (Buikstra & Ubelaker, 1997; Shook et al., 2024). The most reliable indicators are found in the *os coxae*, especially in the subpubic region, the greater sciatic notch, and the preauricular sulcus. In the subpubic region, three Phenice's traits (1969) are observed (**Figure 12**). The first trait is considered the most reliable indicator, as the presence of a ventral arc indicates female sex, and the absence indicates male sex. Secondly, the subpubic concavity is concave in females and convex in males. Finally, the presence of a ridge in the ischiopubic ramus has been identified as an indicator of female morphology, while a broad and flat morphology is suggestive of male morphology. For the greater sciatic notch, a greater and broader morphology indicates female sex, while a smaller and narrower morphology indicates male sex. The scoring system employed ranges from 1 to 5, with 1 representing a typical female morphology and 5 representing a typical male morphology (**Figure 13**). The preauricular sulcus is observed more frequently in female individuals than in males. The scoring system ranges from 1 to 4, with 1 representing the typical female morphology and 5 representing the typical male morphology (**Figure 14**).

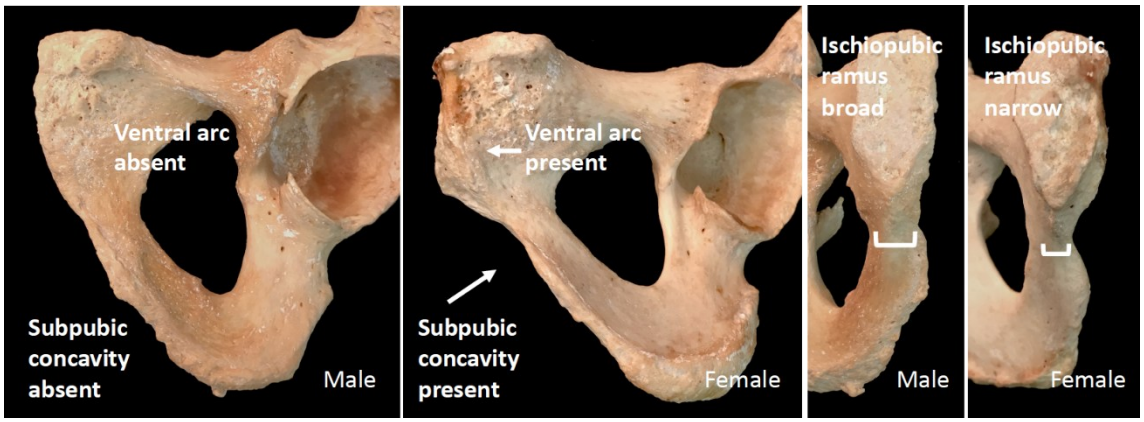


Figure 12. Phenice's traits. Extracted from *Shook et al. (2024)*, Figure 15.4.2.

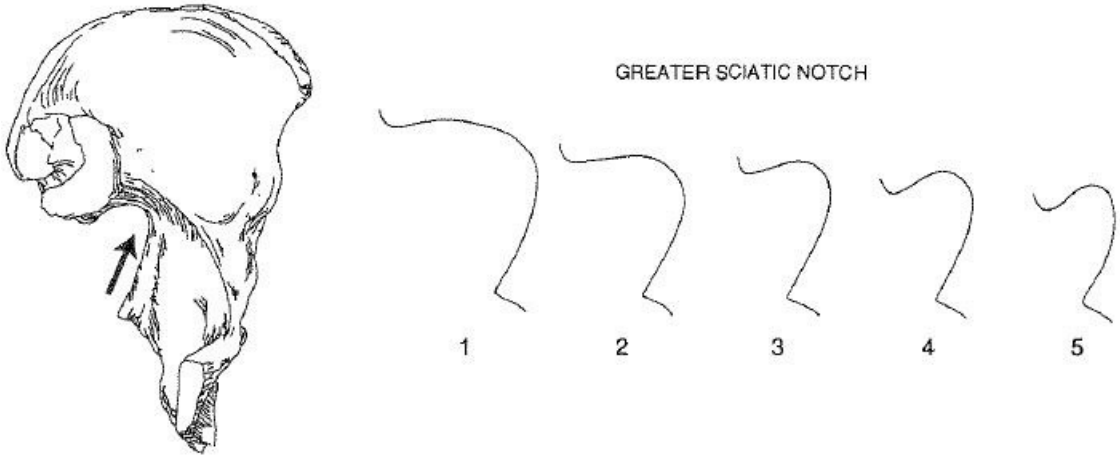


Figure 13. Sexual dimorphism and scoring system for the greater sciatic notch. Extracted from Buikstra & Ubelaker (1997), Figure 2.

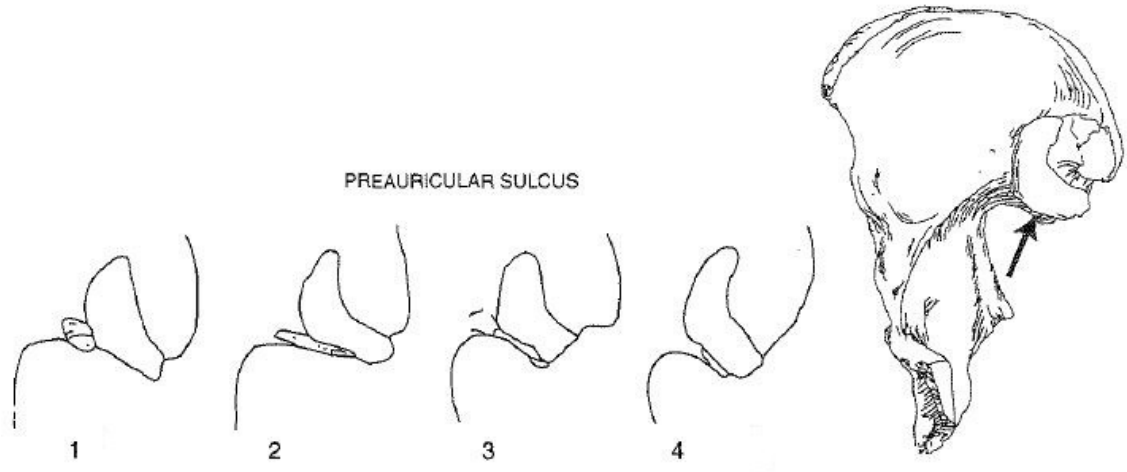


Figure 14. Sexual dimorphism and scoring system for the preauricular sulcus. Extracted from Buikstra & Ubelaker (1997), Figure 3.

Cranial traits can also be recorded to estimate sex, but it may always serve as an auxiliary method and its reliability cannot be determined without corroboration from the *os coxae* features. Five characteristics are typically observed (**Figure 15**): the nuchal crest, the mastoid process, the supraorbital margin, the glabella, and the mental eminence. The five-character traits are scored on a scale of 1 to 5, with 1 representing the typical female morphology and 5 representing the typical male morphology. The nuchal crest must be observed in the occipital surface, and the presence of a bony projection must be discerned. The presence of a smooth surface is indicative of female sex, while the presence of a hook-shaped bone projection is indicative of male sex. The mastoid process, located in the temporal bone, is evaluated for its volume. Female sex is characterized by its small projection and volume, while male sex is characterized by its massive and projected mastoid process. The thickness of the supraorbital margin is then evaluated. A sharp border has been shown to be associated with females, while a rounded and thick border has been shown to be associated with males. In relation to the glabella, the presence of small prominence or projection is indicative of female individuals, while massive prominence is associated with males. A non-projected mental eminence has been observed to be associated with females, while a massive mental eminence has been observed to be associated with males.

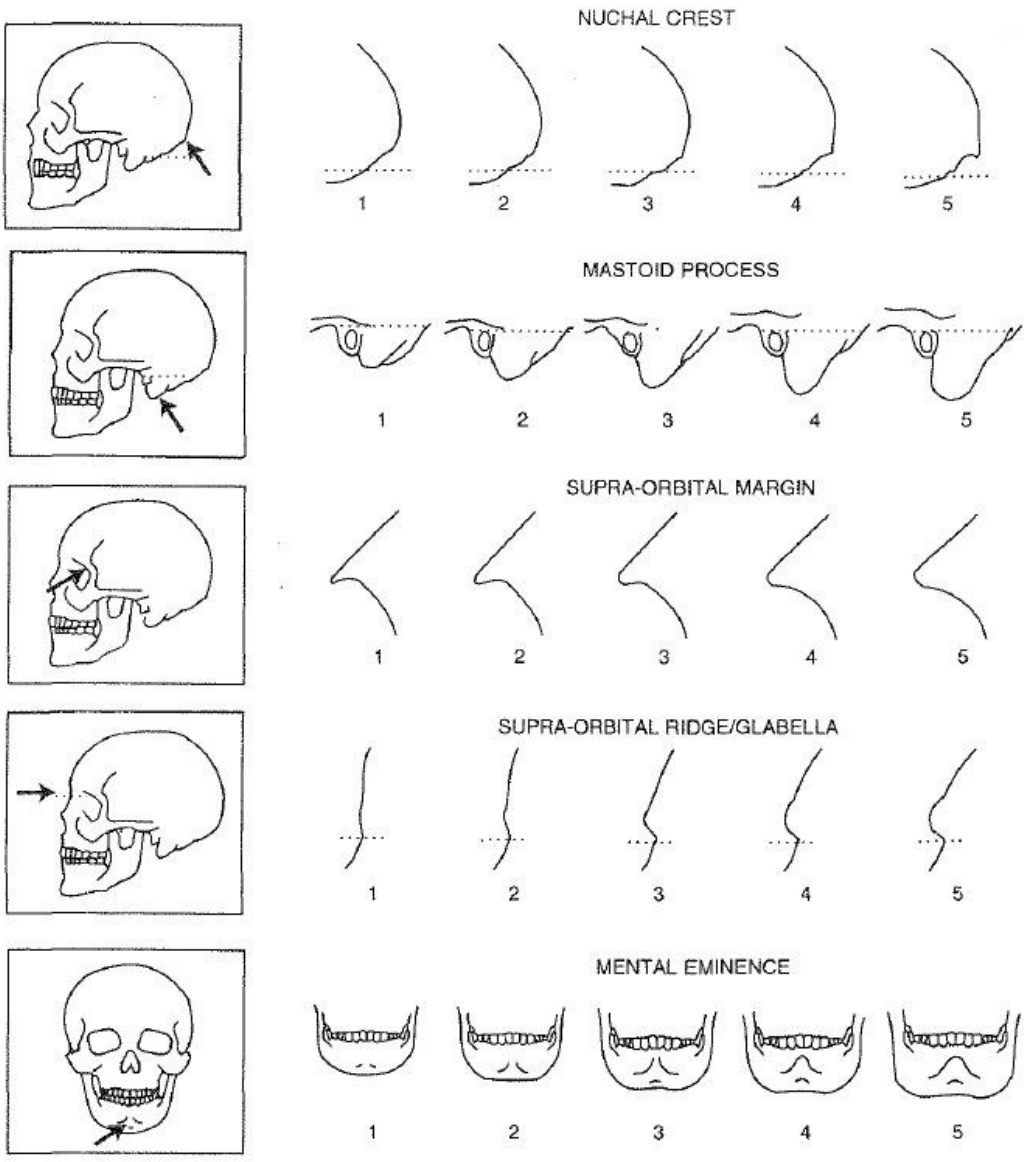


Figure 15. Sexual dimorphism and scoring system for cranial traits. Extracted from Buikstra & Ubelaker (1997), Figure 4.

The determination of age can be made using a variety of indicators (Buikstra & Ubelaker, 1997; Schaefer et al., 2009). These include the following: the development of bones (also known as bone fusion or epiphyseal closures), the eruption of teeth, the wear of teeth, the closure of cranial sutures, the morphology of the pubic symphysis, the morphology of the auricular surface, the morphology of the sternal end of the ribs, and measures of long bones, among many others. It is important to determine age using multiple indicators, as this can provide a more accurate assessment. Epiphyseal fusion, in conjunction with dental eruption, serves as a pair of indicators that are particularly well-suited for the estimation of age in subadult individuals. In the context

of bone development, the epiphyseal fusion manifest at a distinct age range for each bone. The comprehensive interpretation of age-at-death is best achieved through the recording of the epiphyseal fusion stage in every bone. A similar phenomenon occurs during tooth eruption, wherein teeth form and erupt at specific ages, including both decidual and permanent teeth. A precise age at death can be ascertained through meticulous observation of the developmental and eruption stages of the various teeth (Hillson, 2023). In adult individuals, the most reliable indicators of age are tooth wear, the morphology of the pubic symphysis, and, to a lesser extent, the cranial sutures. In the context of a complete skull, the presence of up to 17 distinct cranial sutures can be documented. Stages are classified into the following categories: open, minimal closure, significant closure, and complete obliteration. The estimated age will be determined by the final score (Meindl & Lovejoy, 1985). The assessment of tooth attrition can be conducted through the methodologies established by Brothwell (1981) for molars, and by Lovejoy (1985) for all tooth (**Figure 16**). The morphology of the public symphysis has been defined for both male and female individuals at different ages. A correlation between distinct attributes and the various developmental phases of the symphyseal surface has been established. The prevailing methodologies employed in this study are rooted in the approaches developed by Todd (1920) and Brooks & Suchey (1990). Todd's approach encompasses only male morphologies, whereas Brook & Suchey's method encompasses both male and female morphologies.

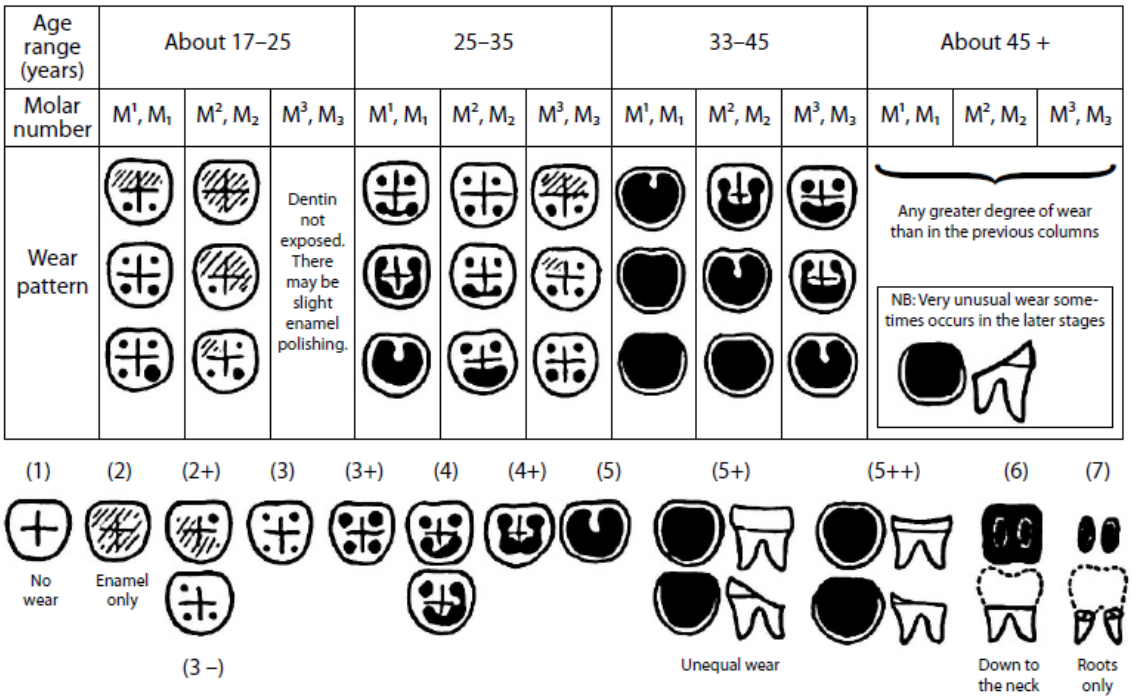


Figure 16. Brothwell's method for scoring molar attrition. Extracted from T. D. White et al. (2012), Figure 18.6.

Stature estimation is achieved through the measurement of various bones' lengths. Regression equations are required for each population, as several variations exist. The most frequently referenced equations in the field were published by Trotter & Gleser (1958), Genovés (1967), and Trotter (1970). The measures are based on East Asian males who fought in the Korean War, modern Mexican males, and data from the Terry Collection, which includes 255 male individuals and 710 white male North American soldiers who fought in World War II. When studying other populations, these equations must be taken with caution and considered as an initial approximation.

Following an estimation of the individual's sex, age, and stature, a more detailed analysis of the bones can be conducted to obtain further data regarding health status. This objective can be accomplished through paleopathological analysis. Paleopathology is the discipline that studies diseases, trauma, degenerative conditions, nutritional deficiencies and other indicators of dietary stress, age-related bone loss, work indicators, and antemortem cultural modifications in human bones. The presence of pathologies can be observed in any bone, manifesting in a variety of forms. The etiology encompasses a wide spectrum of potential causes, including but not limited to diseases, infections, musculoskeletal stress markers, genetic conditions, trauma, age, congenital disorders, metabolic diseases, dysplasia, tumors, nutritional, hormonal, or metabolic imbalances (T. D. White et al., 2012). In the field of paleopathology, it is important to differentiate between normal and abnormal variations in bone, as well as to ascertain whether bone has been impacted by postmortem taphonomic alterations (**Figure 17**). The methodology entails the systematic execution of three distinct phases. The first phase involves the meticulous documentation of the identified abnormalities. The nomenclature employed for each anomaly is unique and specific. The second step in the process entails the identification of the potential underlying causes of these observed changes. In the third and final phase, a differential diagnosis must be proposed (Klaus & Lynnerup, 2019). Given that numerous potential etiologies can induce analogous manifestations within the skeletal system, formulating precise differential diagnoses often poses a considerable challenge. A relevant example can be found in the defects in tooth enamel development, also known as hypoplasia. These defects can be caused by more than a hundred conditions (Schultz et al., 1998; T. D. White et al., 2012). The text will not delve into the intricacies of all bone anomalies, as doing so would simply replicate one of the numerous existing paleopathology handbooks. A variety of handbooks and articles on the subject can be consulted, including works by Baxarias & Herrerín (2008) and Buikstra (2019).



Figure 17. Distal fragment of the left fibula from Grave 6.2 of the site of Gird Lashkir. Presence of fibular *osteochondritis dissecans* at the articular face of the external malleolus.

Furthermore, an analysis encompassing the observation of enthesopathies can serve as a means to determine an individual's lifestyle. Enthesopathies are defined as injuries that occur at the entheses, where tendons and ligaments attach to the bone. When a muscle is under continuous stress, the tendons or ligaments undergo different tensions that provoke the remodeling of the entheses in the form of bony growths, also called enthesophytes. These injuries are considered as musculoskeletal stress or activity markers, resulting from prolonged high-intensity physical activity (Baxarias & Herrerín, 2008). However, it is important to consider other potential etiologies, including inflammation, trauma, degenerative diseases, endocrine disorders, and metabolic conditions (Resnick & Niwayama, 1983).

2.3 TRACEOLOGY: DECODING DIET THROUGH DENTAL MICROWEAR

Traceology is the discipline that studies event traces during an episode (Ristenbatt et al., 2022). Its application in numerous scientific fields, including forensic science, criminalistics, paleoanthropology, and archaeology, underscores its multifaceted nature. In archaeometry, traceology is employed to discern patterns of manufacture, use, maintenance, and disuse of artifacts such as vessels, ornaments, tools, and weapons, among others. In zooarchaeology, it serves as a means to discern patterns associated with the butchering of animals. In anthropology, the analysis of bones is employed to elucidate dietary trends and taphonomic processes. In order to perform a traceological analysis, two phases must be followed. The initial phase involves the documentation of traces through a series of processes, including detection, recognition, identification, and individualization. Based on their size, the traces can be classified into two distinct groups. Firstly, traces of sufficient magnitude to be quantifiable in millimeters (mm) or centimeters (cm) are designated as macrotraces, macrowear, or mesowear. Secondly, traces small enough to be measured in micrometers (µm) are known as microtraces. The second phase involves the attribution of a source for each trace and the evaluation of the created physical record to reconstruct a specific event action (Ristenbatt et al., 2022). The application of experimental archaeology is of significant value in the elaboration of trace collections with controlled data. The information obtained during experimental archaeology is classified into different patterns that will be used as a reference for assessing an action to a trace.

In the field of anthropology, teeth are among the most extensively studied human bones. This is due to its inorganic nature, which renders teeth among the most resistant structures. Furthermore, teeth contain a substantial amount of information regarding diet and environmental conditions. In traceology, a specific emphasis is placed on the observation of traces present in teeth, particularly in the enamel surfaces. Traces in tooth enamel are referred to as dental microwear due to their small size. The primary focus of analyses is the study of the microtraces present on the occlusal and buccal surfaces of postcanine dentition (Estebaranz-Sánchez et al., 2008). The traces observed can take form of pits and striations. Their appearance is caused by food particles and external matter (such as phytoliths, grit, sand or dust) in the mastication process. The size and hardness of traces are highly variable (Calandra et al., 2019; Hernando, Fernández-Marchena, et al., 2020; Romero & De Juan, 2012; Schulz-Kornas et al., 2020). Pits are formed when particles are driven or compressed into the surface of the enamel, whereas striations are formed when particles are sheared or dragged between opposing enamel surfaces during the mandibular movements associated with mastication (Mahoney, 2006). Therefore, the study of

dental microwear is a suitable and reliable proxy of dietary habits due to the direct evidence nature of the traces (Romero & De Juan, 2012; Teaford, 2007).

The initial identification of microtraces associated with food was conducted by dentists and paleontologists from the 1920s to the 1960s. Through the use of optical microscopy (OM), it was observed that the orientation of the striae reflected the direction of the chewing movements (Simpson, 1926; Teaford, 2007). The analysis entailed a qualitative classification of surface features as polished, pitted, or scratched (Dahlberg & Kinzey, 1962; Hernando, Fernández-Marchena, et al., 2020). In the late 1970s, further studies established a direct correlation between abrasive patterns and diet, as evidenced by the size of pits and striae. Nonetheless, Optical Microscopy exhibited numerous limitations. Due to the curvature of the teeth's surface, the microscope was unable to achieve adequate focus for the entirety of the sample. A further issue was the brightness of the enamel surface and the low image resolution. The limitations were subsequently overcome by the implementation of scanning electron microscopy (SEM) (Walker et al., 1978), a technique that facilitated the acquisition of high-resolution images and their automated quantification through the utilization of specialized software packages. This advancement enabled a more precise determination of the size and orientation of the microtraces (Ungar, 1995). In the early 2010s, researchers discovered an automated technique for interpreting dental microwear using Confocal Laser Scanning Microscopy (CLSM). This method enabled the acquisition of precise surface textures and the measurement of complexity (*Asfc*) and anisotropy (*epLsar*) of the traces (Hernando et al., 2022). Recent studies have revindicated the use of OM against SEM or CLSM due to the elevated cost and time-consumption of sample preparation and analysis. The results indicate that the recent advancements in equipment and software have effectively overcome the limitations of OM observed during the 1970s. OM has been shown to detect a greater number of horizontal striations in comparison to SEM, and the enhancement in resolution ensures optimal image quality, thereby producing reliable results in the field of microwear analysis (Hernando, Fernández-Marchena, et al., 2020).

The traceological study of postcanine dentition begins with a meticulous cleansing of the tooth enamel surfaces using ethanol, a process that removes any adherent dirt. Tooth examination is appropriate when the observation method does not entail alterations to the tooth surface. Conversely, in the event of tooth alteration, the creation of a replica is recommended. An impression material, such as silicone, is applied to the surfaces, creating a mold. The mold is then filled with resin to create a precise replica of the original tooth. The efficacy of the technique has been demonstrated through its capacity to reproduce features at the fraction of a micron level in both *in vitro* and *in vivo* specimens, thereby substantiating its status as a high-resolution method. The

original or replica sample is examined through binocular lenses at 40× magnification to identify the presence of microwear related to food abrasion. All identified teeth are then usually subjected to further examination using a Scanning Electron Microscope or a Confocal Laser Scanning Microscope. In the context of SEM, it is imperative that replicas undergo a sputter-coating procedure with gold-palladium to enhance electrical conductivity. Thereafter, micrographs at 100× magnification for the buccal surface and 500× magnification for the occlusal surface are obtained (**Figure 18**) (Galbany et al., 2004; Romero & De Juan, 2012).

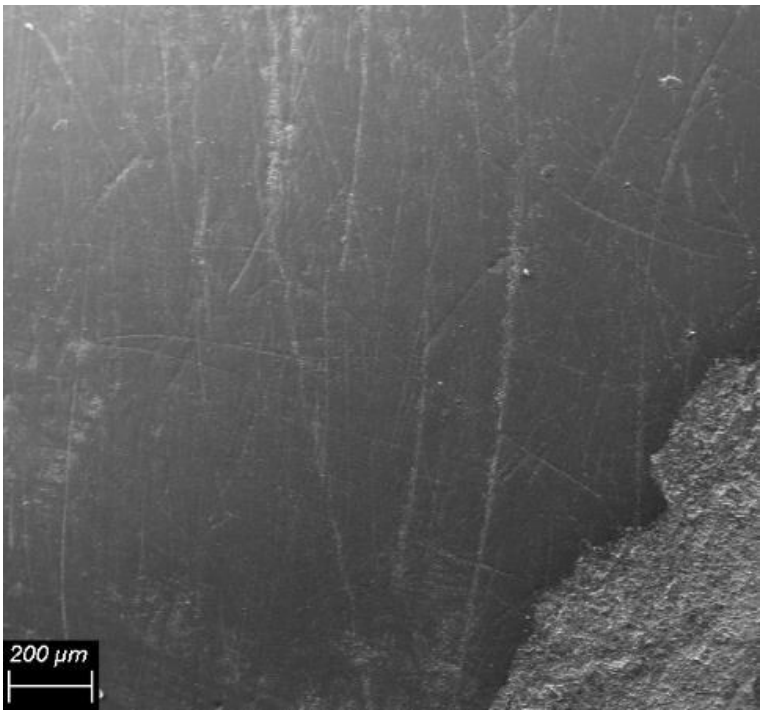


Figure 18. Scanning Electron Microscope image of a third molar from the left side of the mandible. It belongs to the individual buried at Grave 5, from the site of Gird Lashkir. The micrograph displays the buccal surface of the crown at 100× magnification. Microwear, as well as degraded enamel, can be observed.

Depending on the side under observation, striations and pits are counted, measured in size (width and length in µm), oriented (0º to 180º), and density is calculated. For the occlusal surface, the preferrable study areas are Phase I and Phase II, facets from 4 to 9. For the buccal surface, the standard study area is the medial third of the surface under the cusp tip (**Figure 19**) (Romero & De Juan, 2012). The buccal surface is less affected by attrition during mastication, thus providing more dietary information than the occlusal surface, which yields more information about biomechanical factors (Pérez-Pérez et al., 1994).

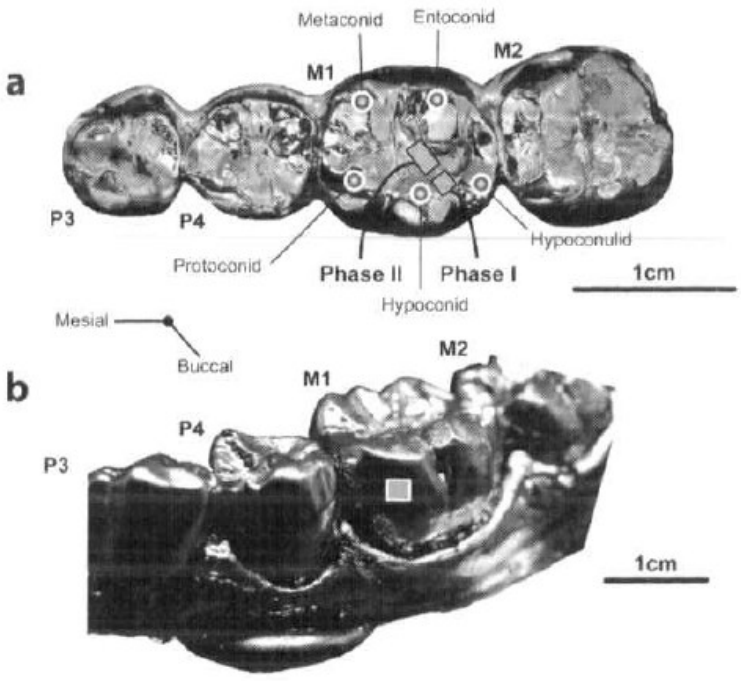


Figure 19. Postcanine dentition of an adult human individual. a) Occlusal view with squares marking the preferred study areas (Phase I and Phase II, facets 4 to 9). b) Occlusal-buccal view with a square marking the standardized study area. Extracted from Romero & De Juan (2012), Figure 14.2.

To ensure accuracy and reliability, special attention must be paid during measurement to avoid variability errors. Four distinct categories of errors have been identified: instrumental, specimen, human, and clerical errors. These errors can manifest at both the interobserver and intraobserver levels. Adequate measuring devices with a low instrumental error, a high observer experience, and the repetition of measurements have been identified as effective practices for reducing measurement error. Repeated measurements yield a mean value, which results in low measurement error and standard deviation (Pérez-Pérez et al., 1990).

After the collection of the relevant data, a microwear pattern must be ascertained for each tooth that has been observed. The identified patterns must then be compared with existing pattern collections representing known diets. A diet consisting of meat has been observed to exhibit a pattern with low density and vertical striations, while a diet consisting of plant foods has been shown to have a more horizontal and high density of striations due to its abrasive nature (Alrousan et al., 2013; Pérez-Pérez et al., 1994; Romero & De Juan, 2012).

When using a CLSM, a scale-sensitive fractal analysis is performed to observe the microwear texture from the replicated samples at a 100× magnification (**Figure 20**) (Hernando et al., 2022).

The study focuses on two parameters: the Area-scale fractal complexity (*Asfc*) and the exact proportion of Length-scale anisotropy of relief (*epLsar*) (Schmidt et al., 2019; Scott, 2005). *Asfc* is a measure of the roughness of the enamel surface, while *epLsar* is a metric for the alignment of features across the enamel surface. A high *Asfc* complexity and high *epLsar* values are related to abrasive diets caused by the chewing of hard foods (El-Zaatari, 2010) or to the erosion from acids associated with diet (Hara et al., 2016; K. L. Krueger et al., 2021; Ranjitkar et al., 2017). Low *Asfc* complexity is related to the mastication of soft or finely processed foods (El-Zaatari, 2010; Schmidt et al., 2019).

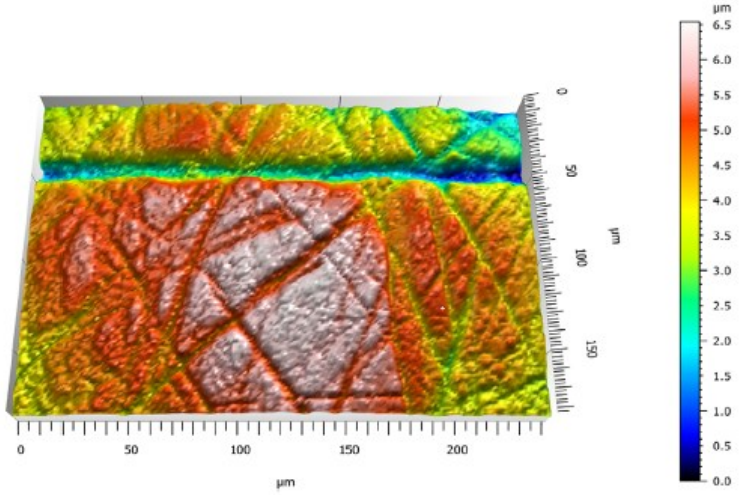


Figure 20. 3D view of the buccal surface from an individual of Cova de la Guineu. Extracted from Hernando et al. (2022), Figure 2.

Post-mortem taphonomic and diagenetic alterations on tooth enamel are frequently encountered in buried teeth (**Figure 21**). Physical alterations have been shown to cause fissures in the crown, typically resulting from disruptive temperature changes. Another alteration is manifested as evenly dispersed pits and parallel scratching along the enamel surface, which have been attributed to the interaction with small soil particles. Chemical alterations result in the deterioration of the enamel surface at various levels. Minimal alterations result in cracking that exhibits a patched pattern, leading to the erasure of the existing microwear related to food abrasion. Moderate alterations, primarily caused by weathering conditions, result in the erosion of the enamel surface, leading to enamel prism exposure. Intense alterations result in the erosion of the enamel surface to the extent that *perykimata* or enamel growth lines become exposed (Martínez & Pérez-Pérez, 2004).

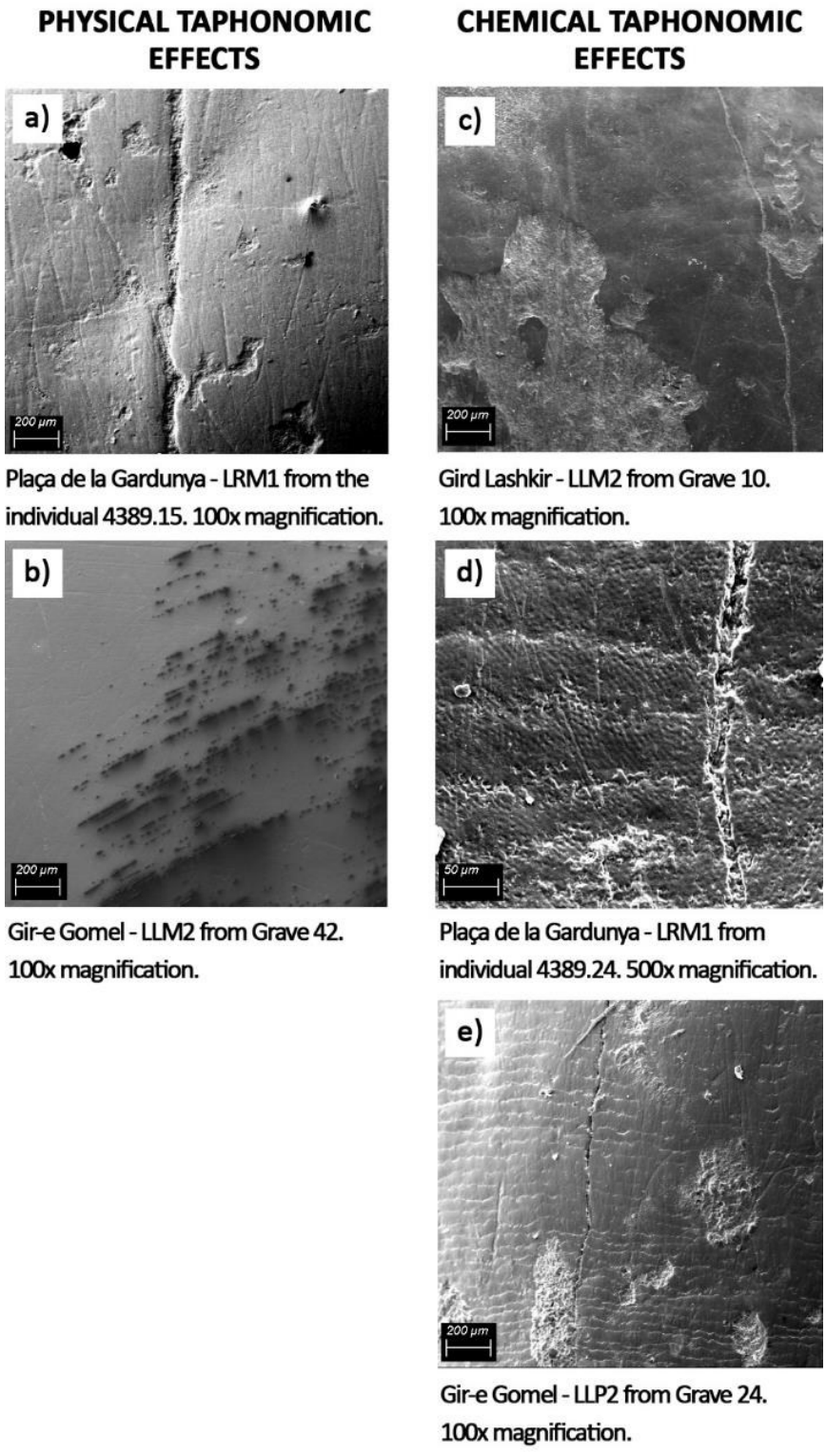


Figure 21. The most common post-mortem taphonomic effects in tooth enamel surfaces are caused by physical and chemical agents. Physical effects encountered are usually a) fissures dividing the crown into two pieces, and b) scratches caused by soil particles. Chemical effects encountered are usually c) erosion or destruction of the enamel surface, d) exposure of enamel prisms, and e) exposure of *perykimata*.

2.4 PALEOPROTEOMICS: IDENTIFYING TAXA WITH ZOOMS

Zooarchaeology by Mass Spectrometry (ZooMS) is an analytical technique that enables the taxonomic identification of a wide range of archaeological materials at the family, subfamily, and genus levels. This method is particularly effective in cases where morphological identification is challenging due to the poor state of preservation of the bones or in worked bone objects that have lost their original morphology (Buckley, 2018). The identification of the species that comprise the archaeological record is of significant importance, as the presence of patterns provides crucial insights into various aspects of human behavior, including animal husbandry, animal exploitation, dietary trends, craftsmanship, symbolism, and trade networks (Brandt et al., 2018; Janzen et al., 2021; McGrath et al., 2019). ZooMS is a technique that lends itself to the analysis of well- and poorly preserved samples due to its noninvasive and minimally destructive nature (Richter et al., 2022). It possesses several distinct advantages over DNA analysis. Firstly, proteins are significantly more abundant and have a longer survival time. Secondly, it is more successful in warmer environments. Finally, it is cost-effective (Buckley, 2018).

To perform ZooMS analysis, bone samples are used to extract collagen, specifically Type I (Buckley et al., 2009). Collagens are the most abundant proteins in mammal tissues, accounting for approximately 30% of the total protein mass. Of the 28 distinct collagen types, Type I is the most abundant, comprising approximately 95% of the total collagen content in bone (Henriksen & Karsdal, 2019). Bone samples are powdered to yield better results. Two methods can be employed to obtain ZooMS fingerprints. The first method involves the decalcification of the bone using an acid, such as hydrochloric acid (HCl). Thereafter, the ultrafiltration process is employed to transfer the acid-soluble collagen into a buffer that is compatible with enzymatic digestion. The second method involves the gelatinization of acid-insoluble collagen in a buffered solution that is compatible with the enzyme digestion and mass spectrometric analysis that follows. Following the completion of the enzymatic digestion process in both methods (a process typically performed with the protease trypsin), the peptide solution is subjected to acidification, and subsequently undergoes a purification procedure via SPE. The sample is then ready to be analyzed by a soft-ionization mass spectrometer (Buckley, 2018). The development of ZooMS in the late 1980s resulted in the integration of a Matrix-Assisted Laser Desorption/Ionization (MALDI) to the mass spectrometer, whose soft ionization enabled the analysis of small, ionized proteins and peptides without the challenges associated with fragmentation. In addition, it has shown to be less prone to sample contamination (Buckley, 2018). The time-of-flight (TOF) analyzer, initially developed in the late 1940s but not popularized until the 1990s, was coupled with the MALDI, enabling the measurement of the ion's mass-to-charge ratio by time-of-flight (Aebersold &

Goodlett, 2001). When samples are analyzed by mass spectrometry, the result is a spectrum in which peptide masses between 800 and 3500 Da (dalton, also known as unified atomic mass unit) are measured. These masses correspond to amino acids ranging in length from approximately 8 to 30. The peaks of the spectrum are indicative of mass-to-charge ratios (m/z) to a specific peptide sequence, which is referred to as a peptide mass fingerprint. The fingerprints of vertebrate collagens are generally composed of 50 to 100 peaks, corresponding to approximately 40% of the available sequences of α1(I) and α2(I) collagen chains. These chains constitute the triple helical structure of collagen Type I (Buckley, 2018). Each resulting fingerprint is unique to each taxon and can be interpreted by comparison with published databases of known analyzed species (**Figure 22**) (Richter et al., 2022).

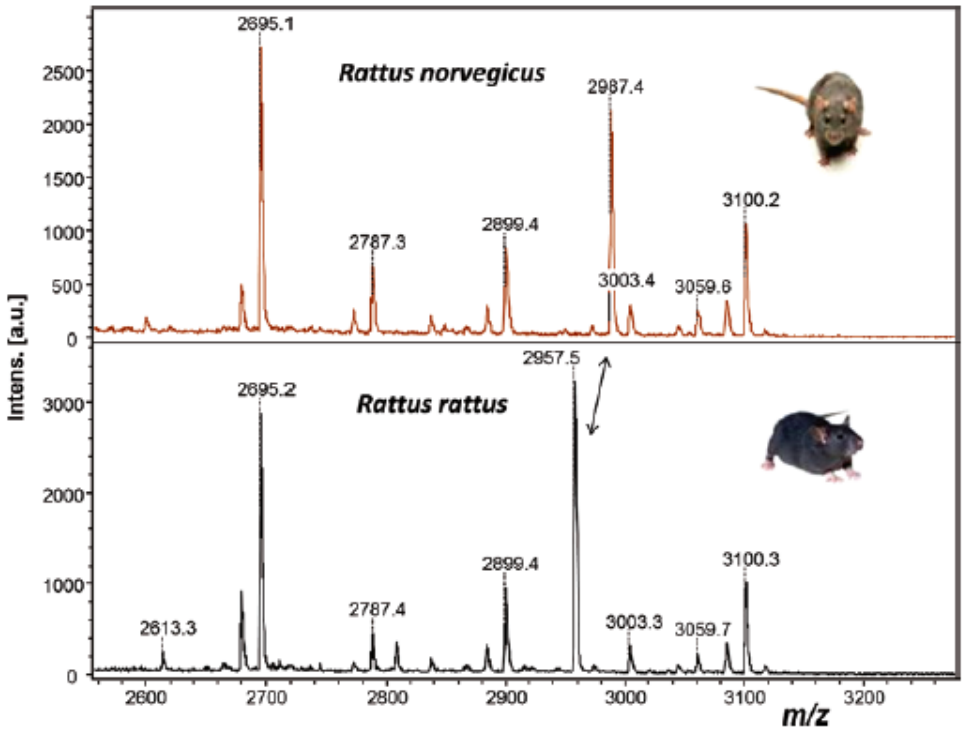


Figure 22. Peptide mass fingerprints of two rat species, Rattus norvegicus and Rattus rattus. The arrow shows the peptide markers that distinguish both species. Extracted from Buckley (2018), Figure 12.2.

2.5 STABLE ISOTOPES: TRACING DIET AND RESIDENCE PATTERNS

Stable isotope analysis is a technique employed in many disciplines, including environmental, forensic, paleontological and archaeological sciences. It consists of measuring the abundance of the stable isotopes present in the different chemical elements that are able to reveal information about residence, migration, diet, nutrition, breastfeeding, weaning ages, diseases, population growth, among others. The results of stable isotope analysis have demonstrated to make a significant contribution to the reconstruction of past human lives (Katzenberg & Waters-Rist, 2019). The most common chemical elements under study in stable isotope analyses are carbon, nitrogen, oxygen, strontium and sulfur. All of these chemical elements appear in nature with different variations in their atomic mass, which means that the number of neutrons in the atom varies, while the number of protons and electrons remains invariable. Each variation in atomic mass from the same atom is identified as an isotope. To identify each isotope, the atomic mass of the chemical element is typically encountered noted in superscript at the upper left of the chemical symbol or standard nomenclature established by the IUPAC (International Union of Pure and Applied Chemistry). For example, the chemical element of carbon has fourteen different known isotopes, ranging from ^{8}C to ^{20}C, as well as ^{22}C. Twelve of them are radioactive (also known as radioisotopes), meaning they undergo a radioactive decay throughout time. One of the most studied is ^{14}C, whose radioactive decay allows to obtain radiocarbon dates. Only two isotopes of carbon, ^{12}C and ^{13}C are stable, meaning they don't undergo a radioactive decay, thus having long half-lives. Different isotopes from the same element have different abundance ratios on Earth. To report the changes in isotopic abundance, the delta notation (δ) has been adopted. It measures the difference between the isotope ratio of the sample analyzed compared with a standard material (**Equation 1**). These standard materials have an unchanging isotope ratio, which is crucial when crossing data analyzed in several laboratories. Since variations in atomic percentages are very small, abundance is expressed in units per mil (‰) (Meier-Augenstein, 2010).

$$\delta R \; in \; ‰ = \left\{ \frac{R_{(sample)}}{R_{(standard)}} - 1 \right\} \times 1000$$

Equation 1. Calculation of the delta notation. R is the ratio of the heavier isotope over the lighter.

Standards can be international reference materials or working standards. International reference materials have been selected and normalized according to the IAEA (International Atomic Energy Agency) guidelines. The primary standards most typically used are the Vienna PeeDee

Belemnite (VPDB), Vienna Standard Mean Ocean Water (VSMOW), and atmospheric air (Air). Carbon isotopes are usually referred to the VPDB standard, Nitrogen, to Air, and Oxygen, to VSMOW. Working standards, also called internal laboratory standards, are materials calibrated against the international reference standards. An example could be caffeine (IAEA-600) or calcite (IAEA-603). By definition, δ values of standard references are equal to zero.

Isotopes undergo mass discrimination when physical or chemical reactions occur. This process, also called isotopic fractionation, causes lighter and heavier isotopes to distribute unequally. The most common effects are related to equilibrium, physicochemical, and chemical processes. During equilibrium fractionation, a pair of isotopes exchange the position in which they originally concentrated to where it is most strongly bonded in the process of formation and breakage of molecule bonds. This process occurs for example when vapor water transforms into liquid precipitation. During physicochemical fractionation, also called thermodynamic isotopic effects, molecules from chemical bonds do not form or break. During this process, the molecules of lighter isotopes react faster than the heavier isotopes, as the breakage of the bonds requires less energy (Katzenberg & Waters-Rist, 2019). Some physicochemical processes are diffusion, evaporation, condensation, or two-phase partitioning. In contrast to physicochemical fractionation, during chemical fractionation molecules from chemical bonds form and break. Nevertheless, molecules react in the same manner as in physicochemical fractionation, with lighter isotopes reacting faster than heavier isotopes due to bond strength and length. The associated kinetic effects determine the degree of isotopic fractionation (Meier-Augenstein, 2010). One kinetic effect is photosynthesis.

The sampling method in stable isotope analysis is very important. Depending on the bone selected, the information provided will be different. Bone is in constant remodeling process by the bone cells, osteoblasts and osteoclasts. Each bone has a determined turnover time, meaning that all the tissue is completely substituted by new bone in a certain time-span. For example, femurs are completely remodeled every 20-25 years, while ribs do so every 5 years (Meier-Augenstein, 2018). Therefore, sampling a femur will provide information about a long span of time, while sampling the rib will provide information about the last 5 years of life of the individual. The only bones that do not remodel since its formation is tooth enamel, whose materials are fixed at formation time and remain undisturbed until postmortem diagenetic processes. Sampling teeth will provide information about the early life of an individual (Meier-Augenstein, 2010).

The two first stable isotopes explored in archaeological research have been carbon and nitrogen, and it has not been until recent that strontium and oxygen stable isotopes have also been studied to gain insight on mobility and residence patterns (Katzenberg & Waters-Rist, 2019).

2.5.1 Diet

The application of stable isotope analysis in the study of prehistoric diet dates back to 1977, when an investigation by Vogel and van der Merwe into the introduction of maize into agriculture in New York employed the use of carbon isotopes (Vogel & van Der Merwe, 1977). Six years later, in 1983, Sullivan and Krueger published an article about animal diet reconstruction based on bone hydroxyapatite (Sullivan & Krueger, 1983). In 1985, DeNiro conducted a study on the carbon and nitrogen isotopes present in the bone collagen of animals with a controlled diet. This and subsequent contributions have been instrumental in enhancing our understanding of isotopic analysis and the interpretation of prehistoric diets (DeNiro, 1985). It has been demonstrated that the isotopic composition of collagen serves as a reliable biological marker, offering insights into the dietary patterns of organisms, particularly with regard to the consumption of protein-rich foods, differentiating marine from terrestrial diets, and discerning breastfeeding and weaning ages (Katzenberg & Waters-Rist, 2019; Koch et al., 1997; Meier-Augenstein, 2010). The richness of data interpretation has rendered bone collagen the preferred sample for stable carbon and nitrogen isotope analysis. As indicated by the works of Ambrose (1990) and van Klinken (1999), collagen contains between 11 and 17% nitrogen and between 35 and 47% carbon by weight.

However, subsequent studies on bone hydroxyapatite samples exhibited contradictory stable carbon isotope results, predominantly attributable to contamination resulting from diagenetic processes. Accordingly, Lee-Thorp and van der Merwe proposed in 1987 the implementation of pretreatment methods in both bone and tooth enamel to assess diagenesis. The samples in this study consisted of herbivorous species with known dietary patterns. The results demonstrated the efficacy of pretreatments in removing diagenetic carbonates, providing biogenic signatures, and yielding reliable, stable isotopic values for carbon in samples dating back to 3 million years (Lee-Thorp & van der Merwe, 1987). Since that time, numerous research efforts have centered on identifying methodologies for the removal of exogenous matter from archaeological samples, a phenomenon attributable to diagenesis and taphonomic alterations. Pestle et al. (2014) conducted a study in which the reliability of the results from bone collagen and bone hydroxyapatite

was observed. To do so, the same sample was sent to 21 different laboratories. The results obtained from the analysis of carbon and nitrogen stable isotopes indicated that bone collagen provides reliable results, while bone hydroxyapatite exhibited significant inter-laboratory variability.

2.5.1.1 Carbon

The chemical element of carbon is encountered in nature in 14 different isotopes, going from ^{8}C to ^{20}C, and ^{22}C. Only two of them are considered stable, ^{12}C and ^{13}C, while the rest are radioisotopes. ^{12}C is the most abundant, with an approximate of 98.93%, while ^{13}C has an abundance of 1.07%. In stable isotope analysis, the ratio between the pair of isotopes ^{13}C and ^{12}C is calculated. Typically, the delta notation (δ) is used to report the changes in isotopic abundance, but plant scientists can also use the discrimination notation (Δ) instead of the delta notation, as it is a means or normalizing data through an equation which removes the effect of plant fractionation in the results. Carbon isotopes are found in many reservoirs or sinks, such as the atmosphere, oceans, or soil. The oceans contain approximately 50 times more CO_2 than the atmosphere (Meier-Augenstein, 2010). The carbon cycle ensures the transfer of carbon from one reservoir to another. Plants are one of the main organisms in carbon fixation through the metabolic process of photosynthesis by means of diffusion and carboxylation. The enzyme ribulose-1,5-bisphosphate carboxylase/oxygenase (RuBisCo) captures the inorganic carbon dioxide (CO_2) from the atmosphere, which has a $\delta^{13}C$ isotopic signature of ≈ -8‰ (O'Leary, 1988; Richards, 2015), and through chemical reactions occurring during the Calvin cycle, transforms it into glucose. Plants have different photosynthetic pathways when fractioning carbon isotopes during CO_2 fixation and are usually classified into three major groups: C_3, C_4, and CAM. Depending on the photosynthetic pathway, the resulting $\delta^{13}C$ isotopic signature of the plant will vary.

Plants with a C_3 photosynthetic pathway undergo a series of chemical reactions known as the Calvin cycle. CO_2 is transported into the stoma of the chloroplast, where it reacts with ribulose 1,5-biphosphate (RuBP), a five-carbon acceptor molecule, producing two molecules of 3-phosphoglycerate (3-PGA), each containing 3 carbon atoms (Sage & Sage, 2013). The two molecules of 3-PGA are catalyzed by a separate enzyme, producing hexose (a monosaccharide, also known as simple sugar) and regenerating RuBP. The production of 3-PGA gives its name to the C_3 photosynthetic pathway (M. G. Simpson, 2019). The resulting $\delta^{13}C$ isotopic signature of glucose in leaves is ≈ -28‰ (O'Leary, 1988; Richards, 2015), having a net isotopic fractionation of ≈ -20‰ (O'Leary, 1988). Plants following the C_3 photosynthetic pathway are most of the land plants

(trees, shrubs, herbs, temperate grasses) and quite a few aquatic plants. Some C_3 plant crops are wheat and rice.

The C_4 photosynthetic pathway, also known as the Hatch-Slack pathway, was an evolutionary modification of the preexisting C_3 photosynthesis (Sage & Sage, 2013). CO_2 is fixated in mesophyll cells by the enzyme phosphoenolpyruvate carboxylase (PEPC), producing oxaloacetate, a C_4-dicarboxylic acid, giving name to the photosynthetic pathway (Meier-Augenstein, 2010). A series of chemical reactions produces malic acid, a four-carbon molecule that transports the CO_2 into the bundle sheath cells. RuBP fixes it to the new cell to proceed with the Calvin cycle. C_4 plants are mostly encountered in areas of drought or high light intensity. Under low rainfall conditions, stomata from C_4 plants close to avoid losing moisture, causing less CO_2 entrance. Nevertheless, as PEPC fixes CO_2 better than RuBP, CO_2 transportation into the cell is more efficient than in C_3 plants (M. G. Simpson, 2019). The resulting $\delta^{13}C$ isotopic signature of glucose in leaves is ≈ -14‰ (Meier-Augenstein, 2010; O'Leary, 1988; Richards, 2015), having a net isotopic fractionation of ≈ -6‰ (O'Leary, 1988). Plants following a C_4 photosynthetic pathway are angiosperms, in cultivated species such as millet, maize, sugarcane, and sorghum (Katzenberg & Waters-Rist, 2019).

The last photosynthetic pathway is CAM, an acronym for Crassulacean Acid Metabolism. CO_2 fixation happens in a similar way as in the C_4 photosynthetic pathway, with the difference that it is divided in two stages. At night, stomata open and PEPC fixes atmospheric CO_2 inside vacuoles from the mesophyll cells to form malic acid. Then, during the day, stomata close and the CO_2 is released into the chloroplasts, where the Calvin cycle is produced (M. G. Simpson, 2019). The resulting $\delta^{13}C$ isotopic signature of glucose in leaves is ≈ -20 to -10‰ (O'Leary, 1988; Richards, 2015), having a net isotopic fractionation of ≈ -12 to -2‰ (O'Leary, 1988). CAM plants are adapted to arid conditions, and compose a great number of angiosperms, such as Cactaceae, Bromeliaceae (pineapple), as well as aquatic plants.

Aquatic plants derive their carbon from the dissolved atmospheric CO_2 in water, which is dependent on its pH. Seawater has a pH of 8, having a net isotopic fractionation of ≈ +9‰ resulting in a $\delta^{13}C$ isotopic signature of ≈ +1‰. Freshwater lakes have a pH of 6, having a net isotopic fractionation of ≈ -7‰ and resulting in a $\delta^{13}C$ isotopic signature of ≈ -15‰. When carbon is fixated into seawater particulate organic matter, the net carbon isotopic fractionation of ≈ -23‰ results in a $\delta^{13}C$ isotopic signature of ≈ -22‰. Organisms like algae have a $\delta^{13}C$ isotopic signature of ≈ -22 to -10‰, and plankton is more carbon depleted, showing $\delta^{13}C$ isotopic signatures of ≈ -

31 to -18‰. For freshwater particulate organic matter, the net carbon isotopic fractionation of ≈ -20‰ results in a $\delta^{13}C$ isotopic signature of ≈ -35‰ (Meier-Augenstein, 2010).

Once plants have fixated carbon into their cells, animals from both terrestrial and aquatic ecosystems fixate carbon into their tissues through ingestion, determined by the macronutrient flows and the complexity of food webs. In terrestrial ecosystems, herbivores eat vegetation and absorb the carbon into their tissues through secondary fractionation. Proteins from herbivore animals derive from plant proteins and carbohydrates, which are fixated into the collagen matrix of bone. The net isotopic fractionation is of ≈ +5‰, and the resulting $\delta^{13}C$ isotopic signature will reflect bulk diet (Hedges, 2003; H. W. Krueger & Sullivan, 1984; Lee-Thorp et al., 1989). The $\delta^{13}C$ isotopic signature of hydroxyapatite will reflect the contribution of carbohydrates to bulk diet, which has a net isotopic fractionation of ≈ +12‰ (H. W. Krueger & Sullivan, 1984; Lee-Thorp et al., 1989). Carnivore animals implement carbon into their tissues when consuming meat from other animals. Proteins from carnivore animals derive from proteins and lipids from herbivore animals, which are fixated into the collagen matrix of bone (Hedges, 2003). The net isotopic fractionation is of ≈ +5 to +8‰, and the resulting $\delta^{13}C$ isotopic signature will the ingested protein routed in collagen. The $\delta^{13}C$ isotopic signature of hydroxyapatite will reflect the contribution of lipids and proteins to bulk diet, which has a net isotopic fractionation of ≈ +8 to +12‰ (Ambrose & Norr, 1993; H. W. Krueger & Sullivan, 1984; Lee-Thorp et al., 1989). Omnivores obtain their carbon by ingesting plants and meat. The $\delta^{13}C$ isotopic signature of bone collagen will reflect the ingested protein routed in collagen, derived primarily from animal proteins, and from plants in a secondary manner. The $\delta^{13}C$ isotopic signature of hydroxyapatite will reflect the contribution of the whole diet energy, composed by lipids, carbohydrates and proteins (Ambrose & Norr, 1993; Jim et al., 2006a; H. W. Krueger & Sullivan, 1984; Sullivan & Krueger, 1983; Webb et al., 2017a). In aquatic ecosystems, atmospheric CO_2 is fixed to water through dissolution, and plants and other particulate organic matter fix carbon into their cells. The complexity in food webs is greater than in terrestrial ecosystems: much more trophic levels are present due to many animals being opportunistic and size-based feeders. Therefore, net isotopic isotopic fractionation is more challenging to calculate, but it is clear that marine plants and animals are more isotopically carbon enriched than terrestrial specimens (Lee-Thorp et al., 1989; Richards, 2015).

The net isotopic fractionations (**Figure 23**) and the isotopic signatures of $\delta^{13}C$ (**Figure 24**) can be observed in the following diagrams, elaborated with data published by (Ambrose & Norr, 1993; Hedges, 2003; Jim et al., 2006b; H. W. Krueger & Sullivan, 1984; Lee-Thorp et al., 1989; Meier-Augenstein, 2010; O'Leary, 1988; Richards, 2015; Sullivan & Krueger, 1983; Webb et al., 2017b).

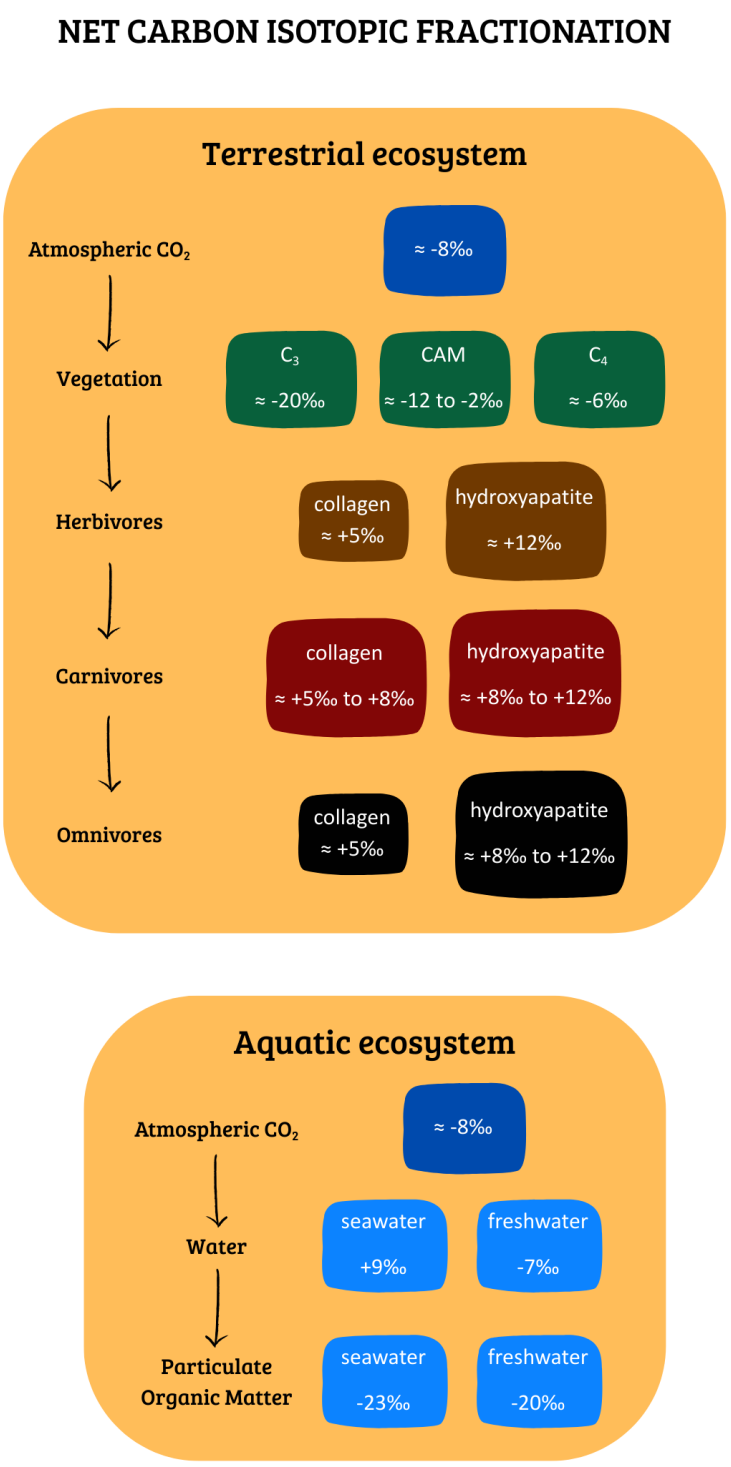


Figure 23. Net carbon isotopic fractionation.

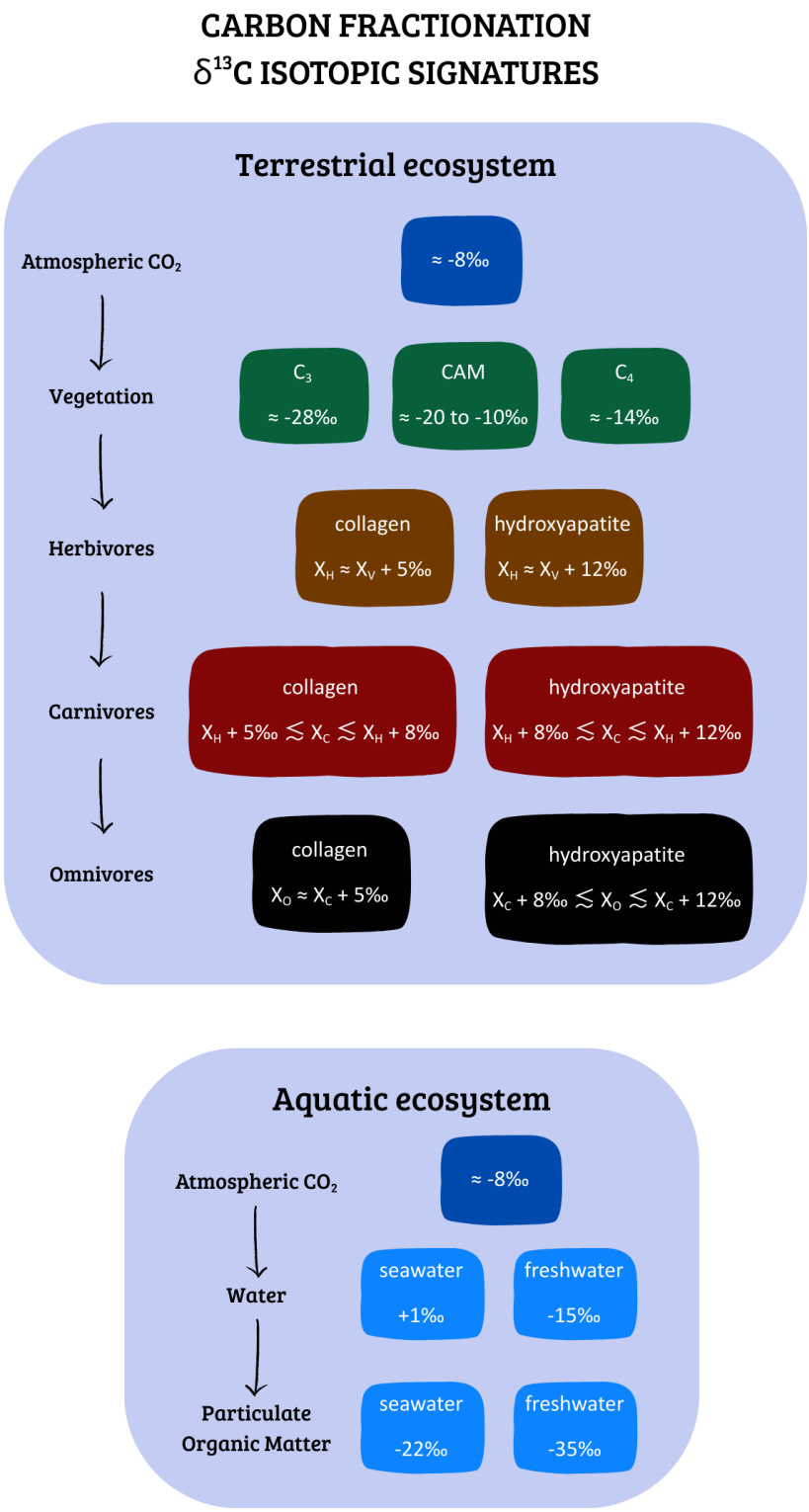


Figure 24. $\delta^{13}C$ isotopic signatures after carbon fractionation.

To obtain the $\delta^{13}C$ isotopic signature of herbivores, carnivores and omnivores, the preferred sample tissues in archaeology are bone collagen and tooth enamel hydroxyapatite. Carbon is found as structural and as absorbed carbonate. In structural carbonate, inorganic carbon derived

primarily from lipids and carbohydrates is dissolved in blood, and substitutes the phosphate position in the crystal lattice. In absorbed carbonate, carbon is absorbed on to hydration layers and crystal surfaces (Ambrose & Norr, 1993; Hedges, 2003; Lee-Thorp et al., 1989). The $\delta^{13}C$ isotopic signatures of bone collagen and hydroxyapatite are expected to have an offset depending on the trophic level of the analyzed individual. The so-called hydroxyapatite-collagen spacing has shown that hydroxyapatite is isotopically more enriched than bone collagen in herbivore, carnivore and omnivore animals. Many equations have been developed (**Equation 2**, **Equation 3**, and **Equation 4**), and slight variations are due to environmental differences from the samples origin (France & Owsley, 2015; Hedges, 2003; H. W. Krueger & Sullivan, 1984; Lee-Thorp et al., 1989; Lee-Thorp & van der Merwe, 1987).

$$\textbf{Herbivores}: \delta^{13}C_{ap} = \delta^{13}C_{col} + 7‰$$

$$\textbf{Carnivores}: \delta^{13}C_{ap} = \delta^{13}C_{col} + 3‰$$

Equation 2. Hydroxyapatite-collagen spacing in herbivore and carnivore animals (H. W. Krueger & Sullivan, 1984).

$$\textbf{Herbivores}: \delta^{13}C_{ap} \backsimeq \delta^{13}C_{col} + 6.8‰$$

$$\textbf{Carnivores}: \delta^{13}C_{ap} \backsimeq \delta^{13}C_{col} + 4.3‰$$

$$\textbf{Omnivores}: \delta^{13}C_{ap} \backsimeq \delta^{13}C_{col} + 5.2‰$$

Equation 3. Hydroxyapatite-collagen spacing in herbivore (± 1.35‰), carnivore (± 1‰) and omnivore animals (± 0.8‰) *(Lee-Thorp et al., 1989)*.

$$\textbf{Human}: \delta^{13}C_{ap} \backsimeq \delta^{13}C_{col} + 5.4‰$$

Equation 4. Hydroxyapatite-collagen spacing in humans (± 1.1‰) (France & Owsley, 2015).

Nevertheless, some studies propose that the $\delta^{13}C$ isotopic signature of collagen or hydroxyapatite cannot be interpreted in an isolated form, but plotted against each other with regression lines of known C_3 diet, C_4 diet, and marine diet protein. The position on each line indicates the energy source of the studied individual (C_3, C_4 or mixed) (Kellner & Schoeninger, 2007).

2.5.1.2 Nitrogen

The chemical element of nitrogen is encountered in nature in 15 different isotopes, going from ^{9}N to ^{23}N. Only two of them are considered stable, ^{14}N and ^{15}N, while the rest are radioisotopes. ^{14}N is the most abundant, with an approximate of 99.636%, while ^{15}N has an abundance of 0.364%. In stable isotope analysis, the ratio between the pair of isotopes ^{15}N and ^{14}N is calculated. Only 2.02% of nitrogen on Earth is found in the atmosphere. Atmospheric nitrogen is encountered as N_2, being very stable and relatively unreactive, conforming the major sink on Earth. The $\delta^{15}N$ isotope signature of atmospheric air is constant, 0.0036765, becoming air the standard reference for nitrogen in stable isotope analysis. 97.98% of nitrogen is bound in rocks (Meier-Augenstein, 2010).

The nitrogen cycle consists of the fixation of atmospheric nitrogen into the biosphere through various processes, including nitrogen fixation, assimilation, ammonification, nitrification, and denitrification. In terrestrial ecosystems (**Figure 25**), during nitrogen fixation, atmospheric nitrogen (N_2) is fixed into soil by lightning, by diazotroph bacteria and archaea organisms. Some of them maintain a symbiotic relationship with the roots of various plants, as is the case with rhizobia and legumes. Once bacteria are in the roots of the plants, nitrogenase enzymes produce ammonia (NH_3) by combining atmospheric N_2 with hydrogen. Symbiotic bacteria exchange the produced ammonia for plant carbohydrates. During assimilation, plant roots absorb nitrogen through the ammonia and the nitrate (NO_3^-) present in the soil. Plants with a symbiotic relationship with bacteria have more access to nitrogen, which leads to better plant growth and resistance to stress. During ammonification, decomposing organisms such as bacteria and fungi act upon dead plants, transforming the nitrogen released by the plant to ammonia and ammonium (NH_4^+), which consists of ammonia with an added hydrogen atom. This nitrogen release enriches the $\delta^{15}N$ isotope signature of soil, acting as a natural fertilizer. During nitrification, ammonia or ammonium is oxidized by nitrifying bacteria, composed of ammonia-oxidizing bacteria (AOB) and ammonia-oxidizing archaea (AOA), converting it to nitrite (NO_2^-) through various enzymatic processes. Then, nitrite-oxidizing bacteria (NOB) oxidize nitrite into nitrate, a molecule absorbed again by plant roots. The cycle ends with denitrification, which consists of the reduction of nitrate back into molecular nitrogen (N_2) by bacteria (J. Postgate, 1998; J. R. Postgate, 1972, 1982).

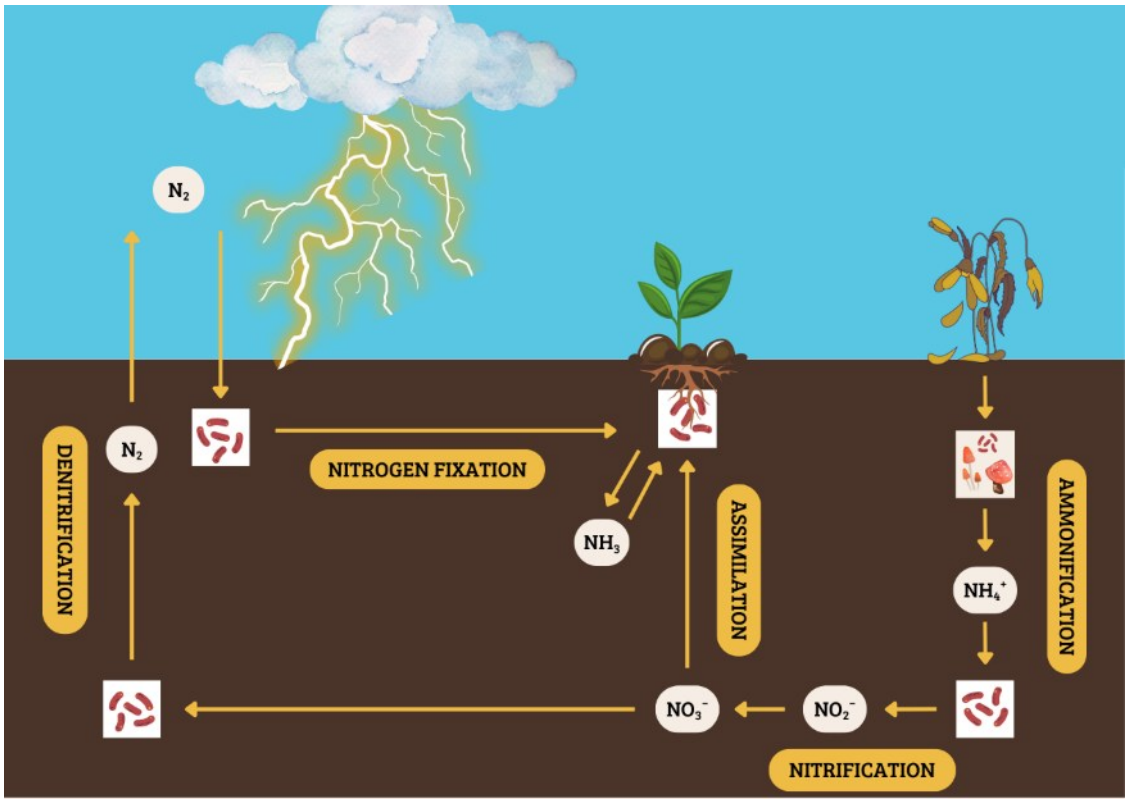


Figure 25. Diagram of the nitrogen cycle in terrestrial ecosystems.

The marine nitrogen cycle is more complex than the terrestrial cycle, but the processes involved are essentially the same (**Figure 26**). In aquatic ecosystems, nitrogen fixation occurs when precipitation drags atmospheric nitrogen into the marine water and is later fixated by cyanobacteria in the euphotic zone. This zone has sufficient light energy to allow photosynthesis processes. Then, phytoplankton undergoes the process of assimilation, in which trough photosynthesis absorbs and assimilates ammonium, nitrate and nitrite. During ammonification, heterotrophic bacteria transform organic nitrogen into ammonium in the aphotic zone, in which little or no sunlight is available. Then, during nitrification, ammonia-oxidizing bacteria oxidize ammonium into nitrite, and nitrite to nitrate. The cycle finishes with denitrification, which consists of the reduction of nitrate back into molecular nitrogen (N_2) by heterotrophic bacteria (Gruber, 2008; Zehr & Capone, 2021).

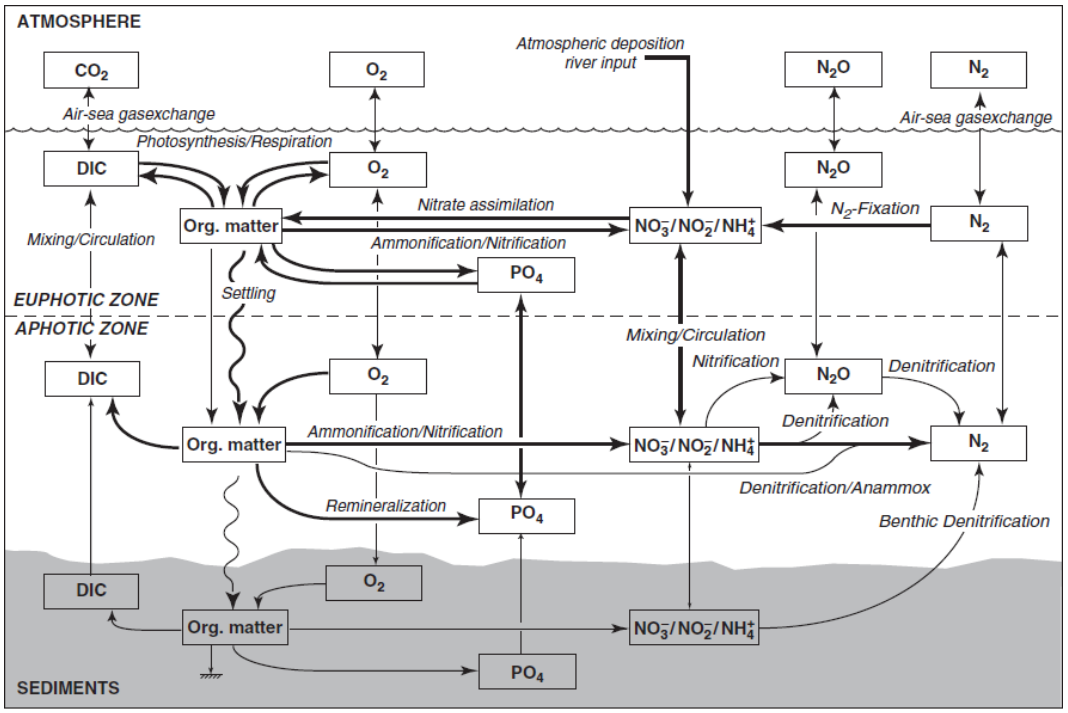


Figure 26. Diagram of the nitrogen cycle in marine ecosystems. Extracted from Gruber (2008).

When analyzing the $\delta^{15}N$ isotope signature in terrestrial ecosystems, an enrichment of 3-4‰ is expected with each shift upwards in the trophic level in comparison with the food source (Kelly, 2000). The preferred sample for nitrogen stable isotope analysis is bone collagen, as the $\delta^{15}N$ isotope signature derives from dietary proteins, reflecting the position of the consumer in the food web (Jim et al., 2006a; O'Connell et al., 2012). Another enrichment of the $\delta^{15}N$ isotope signature is also expected in societies that use organic fertilizers in soils for agriculture, such as animal waste. When analyzing the $\delta^{15}N$ isotope signature in marine ecosystems, a wider range of values is to be expected due to the complexity of both the marine nitrogen cycle and the marine food webs, in which much more trophic levels than in terrestrial ecosystems due to opportunistic and size-based feeders are involved (Meier-Augenstein, 2010).

2.5.2 Residence patterns

The analysis of residence patterns and human mobility in the field of archaeology has been achieved through the analysis of oxygen and strontium stable isotopes (Katzenberg & Waters-Rist, 2019). In the early stages of research conducted by Ericson (1985) on Chumash Native Americans, the potential of strontium in the study of past human ecology and social organization was demonstrated, thereby elucidating problems regarding migration, marital residence, and

foodstuff origins. Subsequent studies analyzing the population of Grasshopper Pueblo and Walnut Creek demonstrated that the results obtained from both human bone and tooth enamel samples were able to reflect migration patterns from early childhood to late adulthood (Price et al., 1994). The employment of oxygen stable isotopes has emerged as a more recent methodological approach in comparison to strontium (Bell et al., 2006; Fricke et al., 1995). Research conducted by Luz et al. (1984) demonstrated a correlation between the oxygen signature in mammals' bone phosphate samples and drinking water. The detection of local and non-local individuals was assessed in studies such as the one published by C. D. White et al. (2004) on population from Tlailotlacan, in bone and tooth enamel samples. Ongoing research on oxygen and strontium has sought to develop precise isoscapes, which facilitate the association of ratios from human individuals with specific geological origins.

2.5.2.1 Oxygen

The chemical element of oxygen comprises the 88.8% of the Earth's water mass, and the 21% of the Earth's atmosphere. There are 18 known isotopes of oxygen, which range from ^{11}O to ^{28}O. Three of them are stable, ^{16}O, ^{17}O and ^{18}O, which have relative abundances of 99.76%, 0.04%, and 0.21%, respectively (Meier-Augenstein, 2010). In stable isotope analysis, the ratio between the pair of isotopes ^{18}O and ^{16}O is calculated. In terrestrial mammals, oxygen is introduced to body tissues through drinking water, breathing air, and consumed food. Body water (blood) contains oxygen from meteoric water and water produced during water respiration: ⅓ comes from sugars, and ⅔ comes from atmospheric oxygen. Tooth enamel hydroxyapatite contains oxygen from meteoric water and is the most reliable source to trace drinking water.

The isotope ratio of oxygen exhibits geographical variations and is subject to various effects, including continental, altitude, and temperature effects, among others. The measurement of the isotope ratio of oxygen across different water sources can generate local and global isoscapes, thereby allowing for the correlation of the isotope ratio of different individuals with a specific geographic area. Therefore, the analysis of the stable isotope of oxygen is a suitable method for mobility studies in archaeology. During the hydrologic cycle (***Figure 27***), warm water from the ocean evaporates and enters the atmosphere, forming clouds. As ^{18}O is heavier than ^{16}O, it requires a greater amount of time to evaporate. Consequently, clouds are more depleted in ^{18}O than the ocean (Chesson et al., 2011). The continental effect is characterized by the movement of clouds inland. As water vapor cools, it undergoes a phase transition, becoming liquid

droplets that subsequently precipitate. As ^{18}O is heavier, it is the first isotope to undergo precipitation from cloud formations. Depending on the distance from the ocean at which precipitation begins, water sources will be more enriched or more depleted in the oxygen isotope ratio. Typically, the samples exhibiting the closest proximity to the ocean are more enriched in ^{18}O, while those from more distant locations demonstrate a higher enrichment in ^{16}O. This phenomenon is directly associated with the altitude effect. During the rainout of the heavier isotope, precipitation at higher elevations becomes depleted in ^{18}O (Pederzani & Britton, 2019). The temperature effect favors the enrichment of ^{16}O in colder climates, such as in glaciers. The temperature effect is also observed outside the hydrological cycle, such as in culinary practices. In the process of boiling foodstuffs, the physicochemical fractionation of evaporation results in a boiling point for ^{16}O at 100°C, which is 0.14°C faster than the boiling point of ^{18}O. Therefore, this culinary technique can affect the $\delta^{18}O$ isotopic signature of human samples, being enriched up to 1.05-1.20‰ in comparison to source water (Meier-Augenstein, 2010).

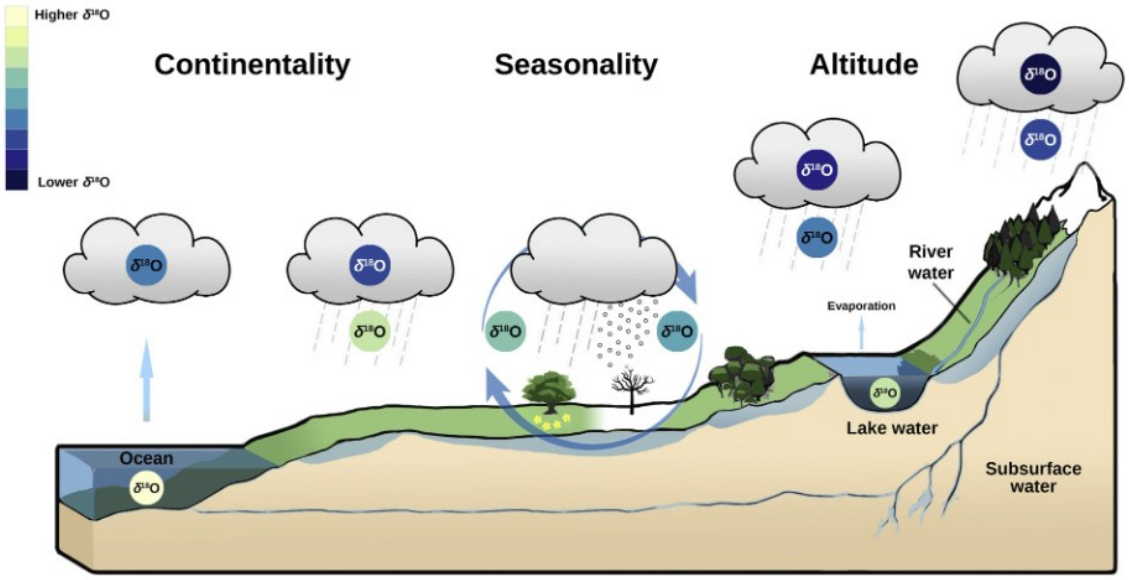


Figure 27. Changes in the isotopic ratio of oxygen during the hydrologic cycle. Extracted from *Pederzani & Britton (2019)*, Fig. 1.

Two chemical elements are analyzed for oxygen stable isotope analysis: carbonates and phosphates. As each mammal species have different fractionation processes, correction equations have to be applied for obtaining reliable isotopic signatures. Oxygen stable isotopic values from phosphate are reported in VSMOW scale, while from carbonate are reported in VPDB scale. Equations to converse from one scale to another have been developed by several researchers (**Equation 5**), being the one proposed by Coplen et al. (1983) the most recommended by the IUPAC (**Equation 6**). Equations have also been developed to transform results from carbonate

normalized in the VSMOW scale to drinking water values, such as the one published by Chenery et al. (2012), based on the equation published by Daux et al. (2008) (**Equation 7**).

$$\delta^{18}\mathrm{O}_{\mathrm{VSMOW}} = 1.03086 \times \delta^{18}\mathrm{O}_{\mathrm{VPDB}} + 30.86$$

$$\delta^{18}\mathrm{O}_{\mathrm{VPDB}} = 0.97006 \times \delta^{18}\mathrm{O}_{\mathrm{VSMOV}} - 29.94$$

Equation 5. Conversion from VSMOW scale to VPDB, and vice versa (Friedman & O'Neil, 1977).

$$\delta^{18}\mathrm{O}_{\mathrm{VSMOW}} = 1.03092 \times \delta^{18}\mathrm{O}_{\mathrm{VPDB}} + 30.92$$

$$\delta^{18}\mathrm{O}_{\mathrm{VPDB}} = 0.97001 \times \delta^{18}\mathrm{O}_{\mathrm{VSMOV}} - 29.99$$

Equation 6. Conversion from VSMOW scale to VPDB, and vice versa *(Coplen et al., 1983)*.

$$\text{Drinking water} = 1.786 \times \delta^{18}\mathrm{O}_{\mathrm{VSMOW(carbonate)}} - 54.005$$

Equation 7. Normalization of oxygen isotopic values in VSMOW scale from carbonate samples into drinking water values, also in the VSMOW scale. Equation based on the equation number 4 published by Daux et al. (2008) (Chenery et al., 2012).

Paleoenvironmental science has aimed to reconstruct the isotopic composition of local meteoric water in the past through the analysis of the phosphate present in mammal bones. Fractionation during phosphate precipitation has shown to be equal in all specimens of the same species, so equations for human bone phosphate have been developed (**Equation 8**, **Equation 9** and **Equation 10**) (Daux et al., 2008; Longinelli, 1984).

$$\delta^{18}O_{phosphate} = 0.64 \times \delta^{18}O_{water} + 22.37$$

Equation 8. Correlation equation between human bone phosphate and oxygen values of source water *(Longinelli, 1984)*.

$$\delta^{18}O_{phosphate} = 0.78 \times \delta^{18}O_{water} + 22.70$$

Equation 9. Correlation equation between human bone phosphate and oxygen values of source water (Luz & Kolodny, 1985).

$$\delta^{18}\mathrm{O}_{\mathrm{phosphate}} = 0.65 \times \delta^{18}\mathrm{O}_{\mathrm{water}} + 21.89$$

Equation 10. Unified correlation equation between human bone phosphate and oxygen values of source water *(Daux et al., 2008)*.

The reliability of the isotopic ratio of oxygen from human bone samples has been addressed by several researchers. One of the studies observed the inter-laboratory variability by analyzing the same human bone hydroxyapatite in 21 different laboratories (Pestle et al., 2014). The analysis of these samples revealed significant discrepancies, indicating a high degree of variability and unreliability of the obtained results. Consequently, the utilization of oxygen isotopic values from bone hydroxyapatite for the interpretation of residence patterns or mobility is not recommended, as variability may be attributed to environmental or biological differences. Conversely, the crystal composition of tooth enamel hydroxyapatite has been shown to exhibit a lesser degree of diagenesis when compared to bone hydroxyapatite. Accordingly, the isotope ratio of oxygen will provide the signature captured during the time formation of the teeth in early childhood.

2.5.2.2 Strontium

The chemical element of strontium is present in low concentrations on Earth. The distribution of these elements in the Earth's crust is 0.036%, decreasing to 0.0008% in the ocean and 0.00046% in human tissues. A total of 35 known strontium isotopes have been identified, ranging from ^{73}Sr to ^{107}Sr. However, only four of these isotopes are stable: ^{84}Sr, ^{86}Sr, ^{87}Sr, and ^{88}Sr. The majority of radiogenic isotopes exhibit a half-life ranging from milliseconds to a year. In stable isotope analysis, the ratio between the pair of isotopes ^{86}Sr and ^{87}Sr is calculated. Strontium is reported as $^{87}Sr/^{86}Sr$, with no additional scale required. ^{86}Sr exhibits a relative abundance of 9.86%, while ^{87}Sr has a relative abundance of 7%. Strontium is found in bedrock, soil, water, plants, and animals. In terrestrial ecosystems, strontium signatures from bedrock, soil, underground water, and precipitation are assimilated by plants via root intake. Herbivores assimilate the strontium through plant consumption and drinking water, while carnivores assimilate it primarily through herbivore consumption and secondarily through drinking water. Each assimilation process entails a fractionation factor, which is minimal due to the large atomic mass of strontium (Slovak & Paytan, 2012). In marine ecosystems, the signatures of strontium from sediments and water are assimilated by plankton. Fish that consume a diet consisting of plankton assimilate the strontium, which is subsequently transferred to other fish and marine animals throughout the food web during the process of consumption. It has been demonstrated that humans and other animals with an omnivorous diet that includes the intake of marine resources will have a wider range of variation in its strontium signatures. This is due to the fact that marine sources are more $^{87}Sr/^{86}Sr$ enriched than terrestrial ecosystems. Notwithstanding the absence

of direct consumption of marine animals, the ingestion of marine salt has been demonstrated to potentially influence terrestrial local strontium signatures (J. Burton & Katzenberg, 2019). The complex process of strontium assimilation in human tissues, derived from multiple sources, underscores the necessity for cautious interpretation of strontium signatures in relation to residence or mobility patterns.

To obtain isoscapes with reliable strontium ratios from a specific area, it is necessary to perform various sampling strategies. These include the local geology, the local fauna with a short lifespan and low-mobility, such as rodents or snails (Ericson, 1985), and, if the individuals studied are located in coastal areas, water and marine fauna.

In the analysis of strontium stable isotopes on human individuals, the most reliable results will be provided by the analysis of tooth enamel hydroxyapatite, as its large crystal sizes make it less prone to diagenetic alterations (J. Burton & Katzenberg, 2019). The data obtained will represent the isotope signature from early childhood, the moment in which tooth enamel is formed and strontium is embedded in the crystal lattice. Studies that have incorporated human samples from various global regions have demonstrated that the strontium ratio in humans exhibits a range from 0.7047 to 0.7190, with a variation of less than 0.015. The variation of the strontium ratio among humans from the same area is even smaller, with a range of only ± 0.0001 (J. H. Burton & Hahn, 2016).

2.6 HISTOLOGY AND TAPHONOMY OF BONE HYDROXYAPATITE: ESTABLISHING QUALITY CONTROLS FOR STABLE ISOTOPE ANALYSIS

The analysis of stable isotopes from bone or tooth enamel samples is subject to quality control measures to ensure the validity and reliability of the results and their interpretation. Otherwise, the results may be influenced by values associated with alterations of various origins, such as contaminating agents. The development of treatments capable of effectively addressing alterations in bone composition requires a comprehensive understanding of the processes involved in hard tissue formation and the impact of contaminants on these tissues. Therefore, the sequence of study will commence with histology and will be followed by taphonomy. Histology is the branch of biology that studies tissues at a microscopic level. Taphonomy, on the other hand, is the discipline that studies the process that affects organic matter from the moment of death until its recovery as archaeological elements. The study of diagenesis, defined as the chemical and physical alterations of biological remains post-mortem, falls within the domain of taphonomy.

2.6.1 Histology of bone

Bone tissue is a composite of collagen and hydroxyapatite, and it is structurally similar in all mammals. Collagen is a protein molecule that is ingested and constitutes 90% of the organic part of bone. A total of 28 distinct collagen types have been identified, with Type I being the most abundant. It comprises approximately 95% of the total collagen content in bone and around 80% of the total protein content in bone (Henriksen & Karsdal, 2019; Katzenberg & Waters-Rist, 2019). The remaining percentage is composed by lipids and proteoglycans (Triffit, 1980). Collagen molecules combine to form elastic fibers, which harden when they come into contact with hydroxyapatite crystals, which constitute the inorganic part of the bone.

Hydroxyapatite is a mineral form of calcium phosphate (Garvie-Lok et al., 2004; Madupalli et al., 2017; T. D. White et al., 2012), also known as Hap in the standardized nomenclature of the International Mineralogical Association (IMA). Its chemical formula can be encountered in many variations, being one example $Ca_{10}(PO_4)_6(OH)_2$ (Sun et al., 2024). In hydroxyapatite crystals, carbonate is more concentrated in the cortical ($6.86 \times 10^{-3} \pm 1.50$) than in the trabecular part of the bone ($5.74 \times 10^{-3} \pm 5.66 \times 10^{-4}$) (Camacho et al., 1999). There are two types of these carbonates that can substitute its location in the hydroxyapatite lattice: B-type carbonate (B-

CAp), and A-type carbonate (A-CAp). B-CAp substitutes into the anionic site of PO_4^{3-}, while A-CAp substitutes into the anionic site of OH^- in the crystallographic *c*-axis. The predominant composition of carbonate is attributed to B-CAp, constituting 94 - 96 wt%, while A-CAp contributes a minimal percentage (4 - 6 wt%) (Madupalli et al., 2017).

Adult bones are composed of two distinct portions: the compact and the trabecular parts. The formation of both structures is attributable to lamellar bone tissue, which is organized in lamellae. While compact bone is nourished by haversian systems, trabecular bone is nourished through blood vessels located within its porous structure. The formation and maintenance of bone tissue are the result of the actions of two distinct cell types: osteoblasts and osteoclasts. Osteoblasts are responsible for depositing osteoids, which is an uncalcified organic matter abundant in collagen proteins. Upon entering the osteoid matrix, hydroxyapatite initiates the process of calcification, leading to the formation of new bone tissue. Osteoclasts are responsible for the resorption of bone tissue (T. D. White et al., 2012). Bone tissue turnover is a continuous process that is facilitated by the continuous activity of osteoblasts and osteoclasts. This dynamic process is part of a continuous cycle of remodeling that persists until the tissue dies.

2.6.2 Histology of tooth enamel

Enamel, the most external part of the dental crown, is also the hardest structure of the human body. Its composition is predominantly inorganic (96%), with the remaining 4% consisting of organic materials and water (4%) (Farooq et al., 2021). The determination of the chemical composition of human dental enamel has proven to be a significant challenge for researchers, primarily due to the presence of substantial intra-species variations and the absence of standardization in the published data (Kono et al., 2022). Human dental enamel is composed of multiple chemical elements in different proportions. In 1984, LeGeros & LeGeros advanced a proposal, the details of which are delineated in **Table *3***.

Table 3. Chemical composition of human dental enamel. Extracted from LeGeros & LeGeros (1984).

Composition wt%	Enamel
Calcium, Ca^{2+}	36.5
Phosphorus, as P	17.7
(Ca/P) by weight	2.06
(Ca/P) molar	1.58
Sodium, Na^+	0.30
Potassium, K^+	0.08

Magnesium, Mg^{2+}	0.34
Carbonate, CO_3^{2-}	3.5
Fluoride, F^-	0.01
Chloride, Cl^-	0.30
Ignition products (950°)	Apatite + β-TCP

The inorganic component of enamel is constituted by crystals of hydroxyapatite. Its distinctive features, which include a low porosity and a substantial size of hydroxyapatite crystals (130 x 30 nm), hinder post-mortem recrystallization, thereby rendering it less prone to diagenetic alterations in comparison to bone or dentin. Bone and dentin are distinguished by the presence of smaller crystals (20 x 4 nm), high porosity, and a predominant organic composition (Koch et al., 1997; Zapanta LeGeros, 1981).

The process of enamel formation, or amelogenesis, initiates following the formation of the first layer of dentin, which is known as dentinogenesis. The process is subdivided into three distinct stages: induction, secretion, and maturation. In the inductive stage, ameloblasts are formed. These cells, characterized by their columnar and polarized morphologies, are instrumental in the subsequent formation of the mineralized enamel matrix (Sasaki et al., 2007; Smith, 2020). During the secretory stage, ameloblasts begin to synthesize enamel proteins, known as acidic enamelins. These elements promote the nucleation and regulation of the growth of hydroxyapatite crystals in the dental enamel (Sasaki et al., 2007). During Tome's process, ameloblasts lay down the crystals of the enamel matrix. In the maturation stage, ameloblasts transport material into the matrix and mineralize the enamel into mature hydroxyapatite prisms (Smith, 2020), which are arranged as shown in **Figure *28***. These prisms adopt the structure of striae of Retzius, which adopts the position of perikymata (Smith, 2020). Upon crystal formation, ameloblasts undergo a process of programmed cell death known as apoptosis (Wyllie, 1997), resulting in the absence of cells capable of repairing or regenerating the crystals (Farooq et al., 2021).

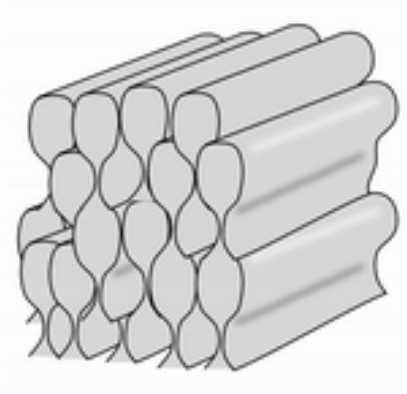


Figure 28. Arrangement of enamel rods. Extracted from Sheldahl et al. (2020), Figure 4.2.

2.6.3 Taphonomy: diagenetic alterations of skeletal remains

Human remains buried in the ground are subject to changes and alterations to different levels. Taphonomy is the discipline that studies the diagenetic process, which encompasses the chemical, physical and biological postdepositional changes that occur to organic and inorganic matter when it is exposed to external and internal geological agents. The transformations can modify the original chemical structures of the archaeological materials. Human remains, like any other material, seek to reach an equilibrium with the environmental conditions they are buried with. Remains will always be in a metastable condition, as equilibrium is never reached due to constant environmental and anthropogenic alterations (Wilson & Pollard, 2002). Establishing diagenetic changes is crucial to observe the difference between biogenic and altered signatures, as the latter will provide false or inaccurate results in bioarcheological analysis. Diagenesis occurs when trace elements migrate from soil to groundwater. Once in motion, they are transferred to the bone porewater in different concentrations, getting fixed by absorption and becoming part of the bone mineral structure (Wilson & Pollard, 2002). Exogenous carbonate minerals can dissolve or reprecipitate as a new form of a carbonate mineral (Wilson & Pollard, 2002).

Bone collagen has different degradation rates depending on the burial environment and the chronology of the remains. The oldest collagen retrieved has been from a Neanderthal individual from 120.000 years ago (Richards & Trinkaus, 2009). For carbon stable isotope analysis, an alternative to bone collagen was found in the carbonate content ($CO_3^{=}$) present in hydroxyapatite (Katzenberg & Waters-Rist, 2019).

Diagenetic changes can be established by trace element analysis, X-ray diffraction, carbonate yield (Koch et al., 1997; Zapata et al., 2006), carbon to nitrogen ratio, the percentage of a preserved isotope, or determining the level of racemization of key amino acid residues in collagen (Gron et al., 2024; Leggett et al., 2024; Lightfoot et al., 2024; Meier-Augenstein, 2010; Mendes Cardoso et al., 2024; Tsutaya et al., 2024). Some studies observe a correlation between low carbonate yields related to recrystallization of hydroxyapatite to fluorapatite, whereas high carbonate yields relate to the addition of carbonates with an exogenous provenance (Koch et al., 1997). Hydroxyapatite from tooth enamel is less susceptible to diagenetic alteration than bone hydroxyapatite (Ambrose & Norr, 1993; Lee-Thorp & van der Merwe, 1987).

Bone collagen samples have specific quality controls. The ratio of carbon to nitrogen (C/N) in collagen from modern pristine bones (not taphonomically affected) is 3.2. Therefore, for ancient

bones, a range between 2.9 to 3.6 has been proposed for well-preserved collagen, as it considers taphonomical alterations and analytical errors (DeNiro, 1985). The preservation percentage of carbon (%C) and nitrogen (%N) is also useful in establishing the preservation state of collagen, as contaminated samples are either enriched in carbon or depleted in nitrogen (Katzenberg & Waters-Rist, 2019). Another quality control is the collagen yield, defined as the difference between the weight of the extracted collagen to the weight of the original cleaned sample. A minimum of 1% is needed to establish that the sample is well-preserved (van Klinken, 1999). The amino acids present in collagen can also be studied. Diagenetic processes that cause the loss of some amino acids can alter the $\delta^{13}C$ isotopic signature of collagen (Hare & Estep, 1983).

2.6.4 Efficacy of sample pretreatments to remove diagenetic alterations

To remove diagenetic contaminants from hydroxyapatite and to avoid further recrystallization, many different pretreatments or preparation methods have been applied to archaeological samples. Diagenetic altered samples usually present high crystallinity indices, low carbonate content and contaminated with fluorine (Garvie-Lok et al., 2004). Whereas carbonate minerals are usually removed with acids due to being more soluble than hydroxyapatite (Koch et al., 1997), fluorine is less soluble and therefore won't be removed by acetic acid pretreatments (Garvie-Lok et al., 2004).

Hydroxyapatite recrystallization can occur during sample preparation and during sampling pretreatment with concentrated acids and long exposure. Fine powdered enamel samples obtained by drilling are more vulnerable to dissolution. More diluted acid solutions and shorter pretreatment times are related to lower crystallinity increase. Many studies advise not to exceed 4 hours in acid treatment, as recrystallization of the sample and mineral formation increases (Garvie-Lok et al., 2004; Lee-Thorp & van der Merwe, 1991). Studies such as Snoeck & Pellegrini (2015), and Pellegrini & Snoeck (2016) do a valuable contribution in studying the efficacy of multiple pretreatments in different sample types (bone, dentine and enamel), according to various protocols. They tested five pretreatments at different concentrations, exposure time and temperature to remove organic matter from hydroxyapatite: non-pretreated; hydrogen peroxide (H_2O_2) with a 10% and 30% concentration for 72 hours at room temperature and at 80°C; hydrazine hydrate ($N_2H_4 \cdot H_2O$) with a 95% concentration for 48 hours at 60°C; sodium hypochlorite (NaClO) with a 1%, 2.5% and 5% concentration for 72 hours at room temperature; and sodium chlorite ($NaClO_2$) with a 1.5% concentration (pH 3), for 72 hours and at room temperature. To remove

secondary minerals from hydroxyapatite, mainly diagenetic carbonates, they used two treatments: one with acetic acid (CH_3COOH) with a 0.1 M concentration (pH 2.9), for 30 minutes at room temperature; and another one with a calcium acetate ($(CH_3COO)_2Ca$) buffered acetic acid solution with a concentration of 1 M (pH 4.5), for 30 minutes at room temperature. Acetic acid has been used on samples in which pretreatments have previously been applied to remove organic matter from hydroxyapatite, as well as on non-pretreated samples. Each treatment finished with a triple rinse with Milli-Q ultra-pure water.

Results point to interesting conclusions. Regarding pretreatments for organic matter removal, H_2O_2 was only able to remove 25% of organic matter contained in the samples, making it the least efficient pretreatment method in removing organic matter. Additionally, it dissolves endogenous carbonates due to its acidic properties. The most common pretreatment used by researchers, NaClO, induced the absorption of exogenous carbonates from the environment, increasing its content. $NaClO_2$ did not remove organic matter from hydroxyapatite. $N_2H_4{\cdot}H_2O$ is the least common pretreatment used by researchers and seems to be the most efficient one of all. It removes all the organic matter in enamel samples and almost all in bone and dentine and it has almost no impact on carbonate signatures.

When it comes to sample mass loss (**Table *4***), there are major differences depending on the pretreatment applied to the samples. Pretreatments that aim to remove organic matter from hydroxyapatite, like H_2O_2, involve a 24.29-25.95% sample mass loss. NaClO is less aggressive on sample mass loss, varying between 14 and 16.29%. Unfortunately, $N_2H_4{\cdot}H_2O$'s mass loss is not reported as the protocol involves more steps that generate extra mechanical mass loss, not making it comparable to the rest of pretreatments tested. $NaClO_2$ was not tested for sample mass loss either. Regarding pretreatments that aim to remove diagenetic carbonates from hydroxyapatite, we have CH_3COOH 0.1 M, which has an average of 65.19% sample mass loss, and 1 M calcium acetate buffered acetic acid, which has an average of 28.63% sample mass loss. The latter is considerably less aggressive, making it more suitable to remove diagenetic carbonates from poorly preserved archaeological samples. Other researchers such as H. W. Krueger (1991) agrees on this statement: he observed that acetic acid pretreatment, is effective in removing the sample diagenesis and that reflects the biogenic signature of the sample, as isotopic exchanges are minimal in hydroxyapatite crystals. Therefore, carbon isotopic analysis on pretreated hydroxyapatite is a powerful tool for dietary research, even more when collagen is poorly preserved in bones or dentin. When pretreatments to remove organic matter and diagenetic carbonates are combined, using H_2O_2 or $N_2H_4{\cdot}H_2O$ first and 1 M calcium acetate buffered

acetic acid afterwards, seems to be the best method to avoid high carbonate loss from tooth enamel samples.

Table 4. Average sample mass loss for each type of pretreatment (following Pellegrini & Snoeck, 2016).

Pretreatment	*N*	Average sample mass loss
H_2O_2, 10% concentration, 72 h, 80°C	21	24.29%
H_2O_2, 30% concentration, 72 h, 80°C	21	25.95%
$N_2H_4 \cdot H_2O$, 95% concentration, 48 h, 60°C	—	Not reported
NaClO, 1%, 72 h, room temp.	21	16.29%
NaClO, 2.5%, 72 h, room temp.	21	15.10%
NaClO, 5%, 72 h, room temp.	21	14%
$NaClO_2$, 1.5% concentration (pH 3), 72 h, room temp.	—	Not reported
CH_3COOH, 0.1 M concentration (pH 2.9), 30', room temp.	16	65.19%
CH_3COOH, 1 M concentration (pH 4.5), 30', room temp.	16	28.63%

After reviewing the effectiveness of a wide range of pretreatments to remove organic matter and diagenetic carbonates, the following question is proposed: are the isotopic signatures of the pretreated samples representative of its biogenic signature, or are they biased? Isotopic analyses of carbon and oxygen carbonates on untreated and treated samples have shed light to this question. Isotopic shifts in pretreated samples are not significative if they are compared with untreated samples. Pellegrini & Snoeck (2016) observe the following results (**Table *5***). The premise is always that modern samples are taphonomically not altered and considered as the reference.

Table 5. Pretreatment effects on carbon and oxygen isotope composition (based on data from Pellegrini & Snoeck, 2016). Values compared to untreated samples. Negative values indicate depletion, and positive values indicate enrichment.

Pretreatment	Isotope	Sample type					
		Modern bone	Archaeological bone	Modern dentin	Archaeological dentin	Modern enamel	Archaeological enamel
		n = 5	*n* = 5	*n* = 1	*n* = 2	*n* = 6	*n* = 2
H_2O_2 10%	$\delta^{13}C$	-0.36 ‰	0.63 ‰	-1.15 ‰	-0.55 ‰	-0.11 ‰	-0.12 ‰
	$\delta^{18}O$	-0.11 ‰	-1.42 ‰	-0.80 ‰	-3.25 ‰	0.02 ‰	0.55 ‰
H_2O_2 30%	$\delta^{13}C$	-0.40 ‰	-1.68 ‰	-1.10 ‰	-0.58 ‰	-0.15 ‰	-0.25 ‰
	$\delta^{18}O$	-0.28 ‰	-0.98 ‰	-0.50 ‰	-1.73 ‰	0.33 ‰	0.90 ‰
$N_2H_4 \cdot H_2O$	$\delta^{13}C$	1.06 ‰	0.15 ‰	-0.20 ‰	0.93 ‰	0.22 ‰	0.08 ‰
	$\delta^{18}O$	-0.53 ‰	-0.43 ‰	-0.25 ‰	-3.48 ‰	-0.13 ‰	0.15 ‰
NaClO, 1%	$\delta^{13}C$	1.94 ‰	0.02 ‰	1.10 ‰	0.32 ‰	0.38 ‰	0.28 ‰
	$\delta^{18}O$	-1.68 ‰	-0.81 ‰	-1.70 ‰	-3.83 ‰	-1.42 ‰	-0.20 ‰
NaClO, 2.5%	$\delta^{13}C$	2.51 ‰	0.14 ‰	2.00 ‰	0.07 ‰	0.48 ‰	0.20 ‰
	$\delta^{18}O$	-2.13 ‰	-1.32 ‰	-1.00 ‰	-3.50 ‰	-1.91 ‰	-0.65 ‰
NaClO, 5%	$\delta^{13}C$	2.56 ‰	0.22 ‰	2.70 ‰	0.02 ‰	0.46 ‰	0.25 ‰
	$\delta^{18}O$	-2.88 ‰	-1.81 ‰	-2.00 ‰	-4.15 ‰	-2.06 ‰	0.02 ‰
$NaClO_2$, 1.5%	$\delta^{13}C$	Not reported					
	$\delta^{18}O$	Not reported					
CH_3COOH 0.1 M	$\delta^{13}C$	-0.28 ‰	-1.40 ‰	-1.35 ‰	—	-1.58 ‰	-0.47 ‰
	$\delta^{18}O$	0.59 ‰	0.17 ‰	-0.05 ‰	—	0.07 ‰	1.60 ‰
CH_3COOH 1M	$\delta^{13}C$	-0.23 ‰	-1.70 ‰	-1.70 ‰	—	-1.65 ‰	-0.27 ‰
	$\delta^{18}O$	1.02 ‰	0.40 ‰	0.40 ‰	—	-0.28 ‰	1.23 ‰

When applying organic matter removal pretreatments, isotopic measures on carbon present some differences. In modern bone, isotopic signatures are low depleted after using H_2O_2. Depletion is higher as the concentration of the pretreatment increases. NaClO causes high carbon enrichments, which rises as the concentration of pretreatment increases. $N_2H_4{\cdot}H_2O$ has an enrichment of 1.06 ‰. Modern dentine is highly depleted when applying H_2O_2, and highly enriched when applying NaClO pretreatments. $N_2H_4{\cdot}H_2O$ provides a relatively slightly depleted value compared to the untreated sample. Modern tooth enamel has low depletions when applying H_2O_2, small enrichments when applying NaClO and $N_2H_4{\cdot}H_2O$. When looking at archaeological samples, bone tends to have slightly enriched values (except for H_2O_2 pretreatment at 30% concentration, whose value is highly depleted). Archaeological dentine and tooth enamel are slightly depleted when applying H_2O_2 and enriched when applying NaClO and $N_2H_4{\cdot}H_2O$.

Upon observation of oxygen isotopic values, modern bone and dentine exhibit slightly depleted values after applying H_2O_2 and $N_2H_4{\cdot}H_2O$. When applying NaClO, values are highly depleted and lower as the concentration increases. Modern tooth enamel displays slightly enriched values after the use of H_2O_2, slightly enriches values after the use of $N_2H_4{\cdot}H_2O$ and highly depleted values after using NaClO. When it comes to archaeological samples, bone and dentin exhibit a wide range of depleted values, being -0.81 ‰ the highest and -4.15 ‰ the lowest. Tooth enamel is slightly enriched after applying H_2O_2, $N_2H_4{\cdot}H_2O$ and NaClO at 5% concentration, while it is slightly depleted after applying NaClO at 1% and 2.5%.

The patterns for carbon and oxygen isotopes indicate that bone and dentin samples are more susceptible to isotopic offsets after using pretreatments. Tooth enamel is the most reliable sample type, as its modern isotopic values after the use of pretreatments do not vary incredibly from the untreated samples. The same is true for archaeological tooth enamel samples. Regarding pretreatments, NaClO seems to be the most aggressive towards the samples as it causes big offsets in the isotopic signatures.

When solely diagenetic carbonates removal pretreatments are used, isotopic measures on carbon present some differences. In the case of modern bone, it exhibits slightly depleted values, showing that these pretreatments slightly alter the biogenic isotopic signature. On the contrary, modern dentine and modern tooth enamel show high carbon depletion, which shows that these acids remove biogenic carbonates and alter the biogenic isotopic value. When looking at archaeological samples, enamel displays low depleted values, while bone and dentin show higher depleted values. These results indicate that acetic acid pretreatments are too aggressive as they remove diagenetic but also biogenic carbonates, which alters the isotopic values of the sample.

This is true for modern dentin and tooth enamel, as well as for archaeological bone. For archaeological tooth enamel, acetic acid pretreatments act as diagenetic carbonates removal, not affecting the biogenic matter.

Upon observation of oxygen isotopic values, modern bone exhibits enriched values; modern dentin displays invariable or slightly enriched values; and modern enamel exhibits invariable or slightly depleted values. Archaeological bone is less enriched than modern bone, and tooth enamel is highly enriched in comparison to the modern sample. Archaeological dentin has no data available. Results indicate that acetic acid pretreatments are suitable for removing diagenetic carbonates in modern dentin and tooth enamel, maybe also for archaeological bone. Nonetheless, these types of pretreatments seem to be too aggressive towards modern bone by removing biogenic carbonates from the samples. Higher offsets may be expected from archaeological tooth enamel.

To sum up, the best organic removal pretreatments to recover reliable carbon isotope values from archaeological remains are H_2O_2 at 10% concentration for bone, $N_2H_4 \cdot H_2O$ for dentin, and H_2O_2 or $N_2H_4 \cdot H_2O$ for tooth enamel. To recover the most reliable oxygen isotope values from archaeological remains are $N_2H_4 \cdot H_2O$ for bone, H_2O_2 at 30% concentration for dentin, and H_2O_2 or $N_2H_4 \cdot H_2O$ for tooth enamel.

CHAPTER 3: MATERIALS AND METHODS

3.1 ARCHAEOTHANATOLOGY AND BIOLOGICAL PROFILE

3.1.1 Gird Lashkir

The graves that have been subjected to archaeothanatological and anthropological analyses are all the ones belonging to the first half of the 3rd millennium BCE that have been excavated since 2018 until 2024. They consist of a total of 14 burials containing 17 individuals from all age ranges and sexes. The grave numbers are Grave 2, Grave 4, Grave 5, Grave 6, Grave 7, Grave 8, Grave 9, Grave 10, Grave 11, Grave 12, Grave 13, Grave 14, Grave 15, and Grave 16. All the graves are located in Sector 3 except for Grave 12, which is located in the plain area West to the principal mound. Access to the skeletal remains have been granted and studied in its integrity. At present, the archaeothanatological and anthropological data obtained through this study are both unprecedented and unpublished.

The archaeothanatological study of the graves from Gird Lashkir has undergone the following process. The initial phase entailed direct involvement in fieldwork, encompassing the excavation and *in situ* study of Graves 5 to 16. A standardized protocol was employed to obtain archaeothanatological data. The second step entailed the retrieval of archaeothanatological data from reports and photographs of the graves previously excavated by team members from the research group. This data pertained specifically to Graves 2 and 4. Subsequent to the recovery of all pertinent data, the third step entailed the development of a database encompassing information regarding the container and the contents of each grave. Accordingly, the data incorporated in the description of the container includes the sector of the excavation in which it is situated, the structure number of the grave, the locus number where it was located, the architectural phase in which the burial was constructed, the type of container and its morphology. The data incorporated for the content description encompasses the number of buried individuals, the type of disposal, the state of preservation of the skeletal remains, the orientation of the body and the face, the position of the deceased, the skeletal articulation, and the presence of ornaments and grave goods. In the context of the number of individuals buried in a specific grave, the term "multiple burial" is employed when four or more individuals are contained within the same space. Multiple burials are defined as successive when the different deceased were buried in different moments (also known as collective burials in English terminology). Conversely, simultaneous burials entail the deposition of all the deceased in a single action, with all the remains being deposited within a single container. The form of disposal is defined as primary if the body was deposited when the skeletal remains were still in a complete anatomical articu-

lation, and as secondary if the deposition of the remains were performed after the skeletal remains were previously partially or completely disarticulated (Boulestin, 2022). Bones are defined as articulated when they are still in anatomical order, loosely articulated if bones are in anatomical order but slightly displaced, and disarticulated if bones are completely displaced from their anatomical order. The orientation of the individual is determined by cardinal and ordinal directions, with the head-to-pelvis axis serving as a constant reference point. The position indicates the manner in which the body was placed inside the burial, including the type of decubitus, as well as the status of the limbs, whether extended, flexed, or hyperflexed.

The illustration of the graves has been performed through the use of *Illustrator* software, thereby facilitating enhanced insight into the processes involved in the grave, encompassing construction, disposal, and taphonomic and/or anthropic alterations. After meticulous analysis and consideration of the archaeothanatological data, a comprehensive interpretation of the data has been developed for each individual grave.

Following the execution of the archaeothanatological analysis, the anthropological analysis was conducted for the purpose of elaborating the biological profile of Gird Lashkir's individuals. The analysis commenced with the identification of the bones, subsequently followed by the formulation of a visual recording form that systematically collected all pertinent information for each individual, in accordance with the standardized criteria established and published by Roksandic (2003). The use of red has been employed to denote the bone fragments that have been positively identified and assigned to a specific side. The utilization of the color blue serves to denote positively identified bone fragments that exhibit ambiguous siding characteristics. Finally, the utilization of green has been employed to denote bone fragments that could only be identified as belonging to a particular bone type, such as the skull or a long bone.

Subsequent to this, a comprehensive evaluation of the subjects' sex and age was conducted. A multi-proxy approach toward sex and age has been conducted. The assessment of sexual dimorphism has been approached through a variety of biological characteristics, including cranial features (Acsádi & Nemeskéri, 1970), coxal traits (Buikstra & Ubelaker, 1997), and traits from the *os pubis* (Phenice, 1969). The age of subadult individuals has been assessed trough the analysis of tooth development (AlQahtani et al., 2010; Gustafson & Koch, 1974; Schour & Massler, 1941) and epiphyseal fusion of the bones from the postcrania (Schaefer et al., 2009). The age of adult individuals has been assessed through various methods, including the analysis of cranial sutures of the vault (Meindl & Lovejoy, 1985), the observation of tooth development (AlQahtani et al., 2010; Gustafson & Koch, 1974; Schour & Massler, 1941), the assessment of dental attrition

through the Brothwell and Lovejoy systems (Brothwell, 1981; Lovejoy, 1985; T. D. White et al., 2012), the description of the development of the pubic symphysis from the *os coxae* using the Suchey-Brooks and Todd systems (Brooks & Suchey, 1990; Todd, 1920), and the observation of the epiphyseal fusion of the bones from the postcrania (Schaefer et al., 2009).

In order to estimate the stature of the individual at the time of death, the maximum length of the long bones from the upper and lower limbs was measured, as previously described by T. D. White et al. (2012). The regression equations published by Trotter (1970) have been used, as well as the modification equation for individuals over 30 years of age, when necessary.

The determination of the health status of each individual was achieved through paleopathological analysis, in which the bones of the skeleton were observed for the identification of anomalies. These anomalies were then subjected to further investigation to ascertain their etiologies and propose a differential diagnosis.

Finally, a comprehensive evaluation of the lifestyle of each individual has been achieved through an enthesopathological analysis, in which the joints have been meticulously examined to identify markers that could be associated with specific activities endured throughout the individual's lifetime.

3.1.1.1 Grave 2

3.1.1.1.1 The container



Sector	3
Structure number	2018/50
Location	Locus 63
Period	Ninevite 5 (2900 – 2550 BCE) First half of the 3rd millennium BCE Early Bronze Age
Architectural phase	This grave was buried in the transition between phases 4A and phase 3, in a moment of architectural disuse. It is located below a wall belonging to phase 3.
Type of container	Simple pit with a funerary urn.
Morphology	The simple pit is oval in shape and the funerary urn has a jar morphology.

3.1.1.1.2 The content

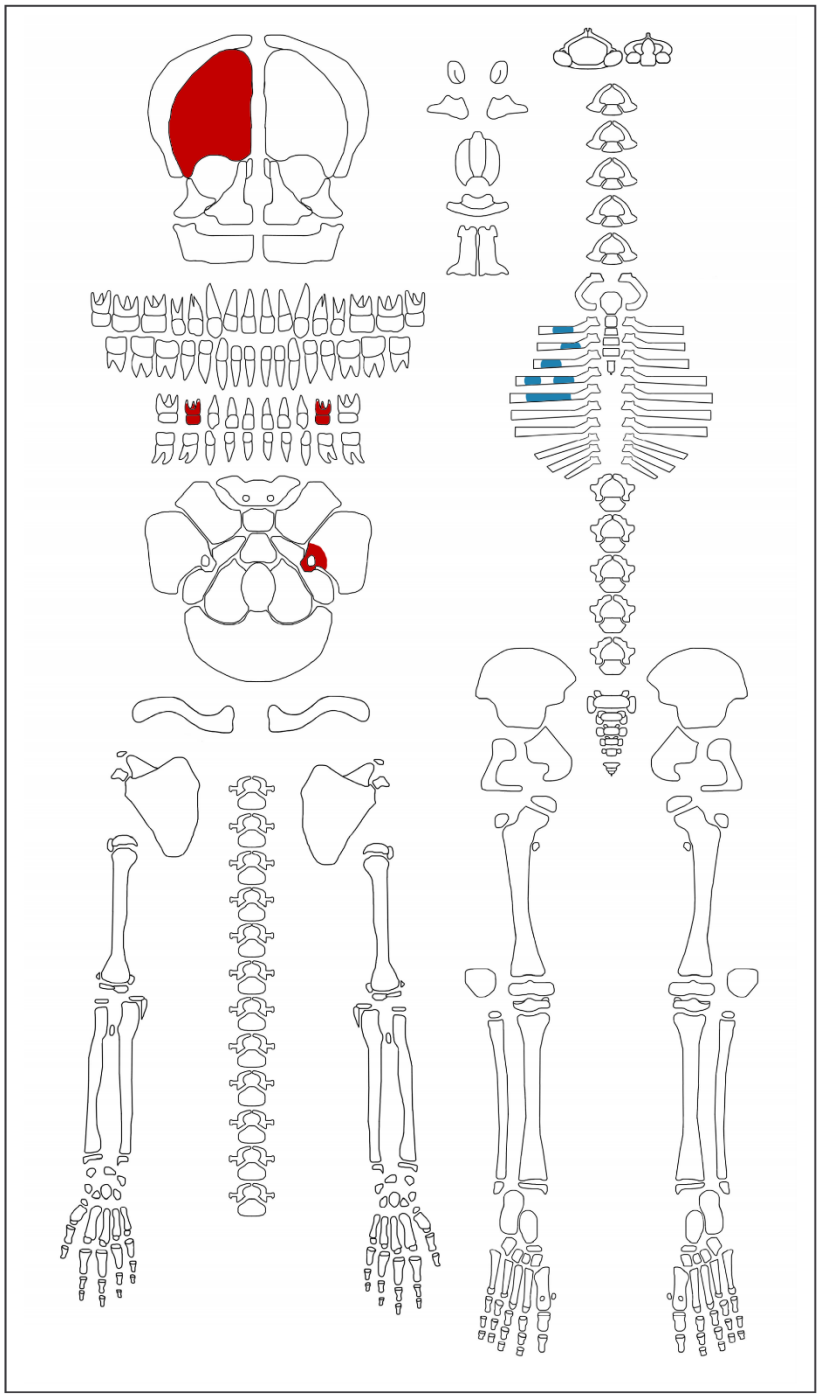
Number of buried individuals	1
Form of disposal	Primary inhumation
State of preservation	Poorly preserved

Body orientation	Not recorded
Face orientation	Not recorded
Position	Not recorded
Skeletal articulation	Not recorded
Ornaments	None
Grave goods	None

3.1.1.1.3 Osteology: bone identification

Visual recording form - Newborn (Roksandic, 2003)

GRAVE 2



3.1.1.1.4 Determination of sex

The absence of any sexual trait did not allow to determine the sex of the individual.

3.1.1.1.5 Determination of age

Age has been determined by tooth development according to Schour & Massler (1941) and Gustafson & Koch (1974). The complete crown and the almost complete root of both preserved teeth give an estimated age range of 1.5 to 2.5 years, classifying as an infant according to Buikstra & Ubelaker (1997).

3.1.1.1.6 Stature estimation

The estimation of the stature of the buried individual was not performed due to the lack of epiphyseal fusion of the long bones.

3.1.1.1.7 Paleopathologies: determination of health

The presence of paleopathologies was not detected in the observed bones.

3.1.1.1.8 Enthesopathies: determination of activity markers

The presence of enthesopathies was not detected in the observed bones.

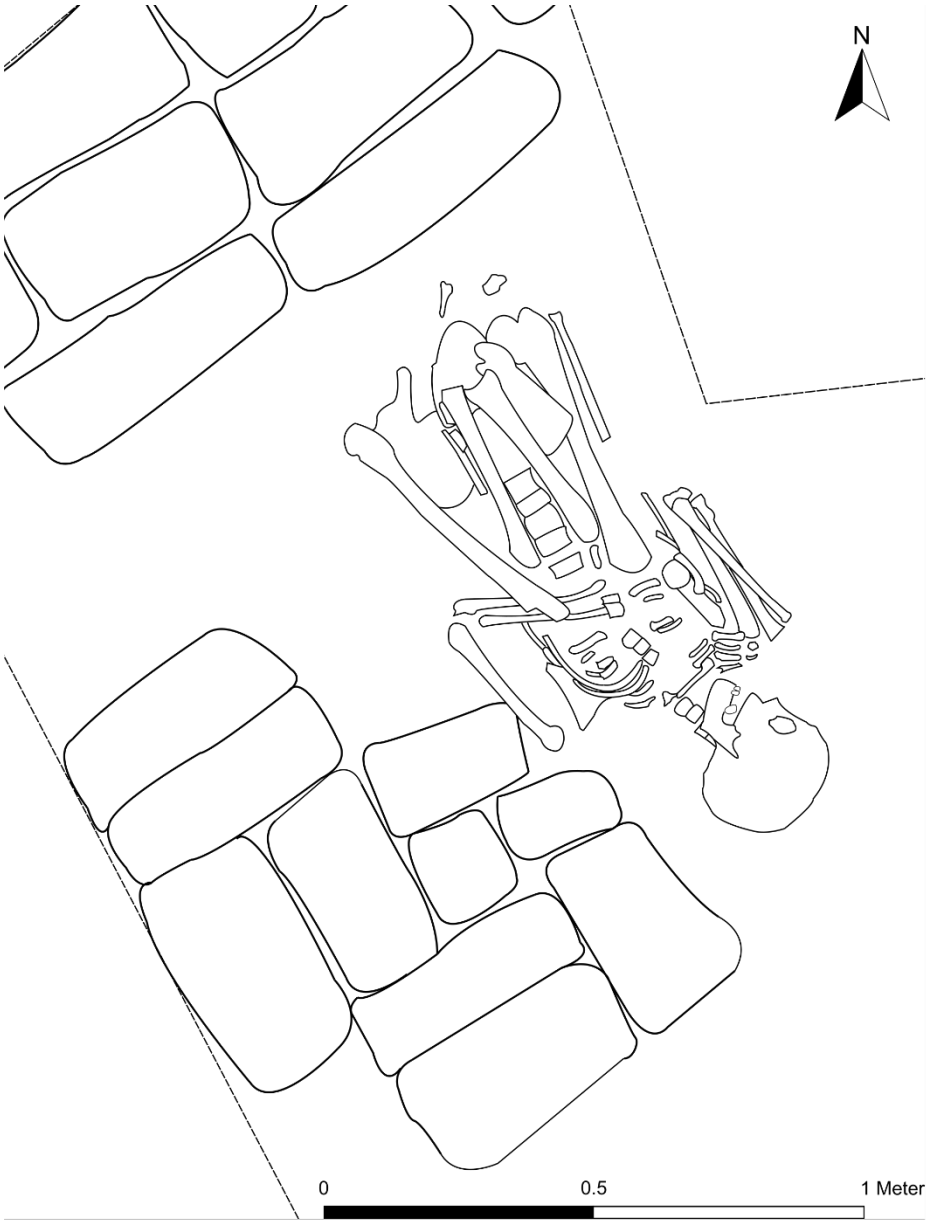
3.1.1.2 Grave 4

3.1.1.2.1 The container



Sector	3
Structure number	2019/53
Location	Locus
Period	Ninevite 5 (2900 – 2550 BCE) First half of the 3rd millennium BCE Early Bronze Age
Architectural phase	The construction of the grave occurred during the period of rapid transitional architecture, specifically phases 4B and 4A. Consequently, it can be posited that the existence of life and death within the site may have been contemporaneous.
Type of container	Simple pit
Morphology	Rectangular shape

3.2.1.1.1 The content



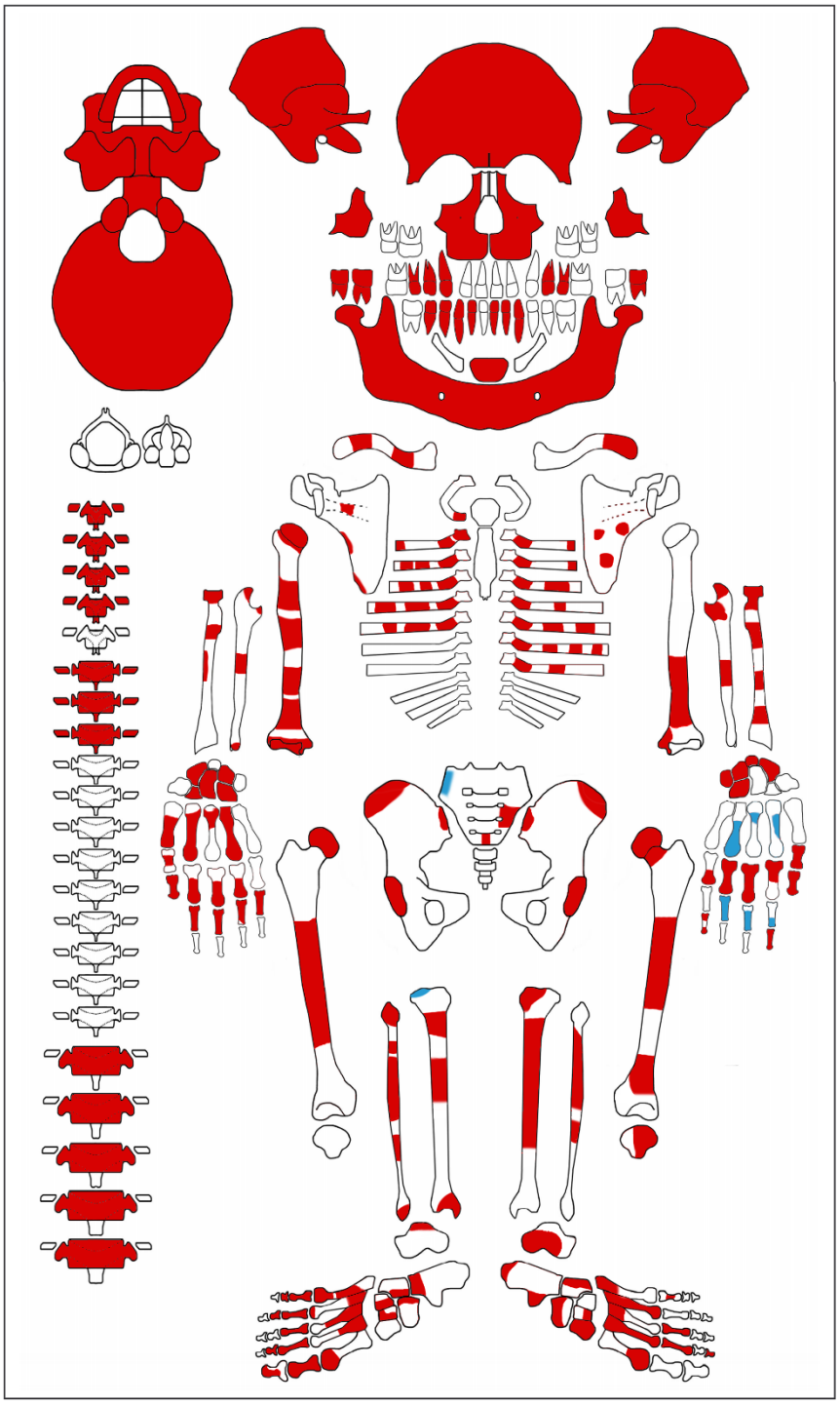
Number of buried individuals	1
Form of disposal	Primary inhumation
State of preservation	Poorly preserved
Body orientation	South-North
Face orientation	East
Position	Supine decubitus with hyperflexed legs on both sides of the body. The left arm is positioned over the sternum, while the right arm is positioned over the cervical vertebra. The skull is positioned on its right side.
Skeletal articulation	Articulated

Ornaments	None
Grave goods	One pebble on each side of the skull, one flint tool over the *os coxae* and one pottery sherd behind the fibula.

3.2.1.1.2 Osteology: bone identification

Visual recording form - Adult (Roksandic, 2003)

GRAVE 4



3.2.1.1.3 Determination of sex

The determination of sex was based on cranial features (Acsádi & Nemeskéri, 1970), which include the nuchal crest, the mastoid processes, the glabella and the mental eminence. The preserved characteristics are indicative of a probable female classification (see **Table 6**).

Table 6. Scores for the cranial features to determine sex.

Cranial feature	Right side	Center	Left side
Nuchal crest		1 (Female)	
Mastoid process	1 (Female)		2 (Probably Female)
Supraorbital margin	Not observable		Not observable
Supraorbital ridge / Glabella		2 (Probably Female)	
Mental eminence		2 (Probably Female)	

3.2.1.1.4 Determination of age

Age has been determined by dental attrition in permanent molars (M_2, M_3 and $_3M$), as defined by Brothwell (1981) and adapted in T. D. White et al. (2012). The estimated age range is between 17 and 25 years, classified as a young adult according to Buikstra & Ubelaker (1997).

3.2.1.1.5 Stature estimation

The poor state of preservation of the individual has not allowed the measurement of the long bones, and therefore the estimation of the stature of the buried individual has not been performed.

3.2.1.1.6 Paleopathologies: determination of health

Teeth present various paleopathologies, including severe attrition and defects of the enamel. Ten teeth have the dentin exposed (P^1, P^2, ^1P, ^2P, I_2, C_x, P_1, $_1I$, $_2I$ and $_xC$), and the pulp chamber is exposed on C^x. The defects in the enamel consist of linear hypoplasias present in both mandibular canines. According to the Swärdstedt (1966) equations, the enamel formation was disturbed repeatedly at the ages of 1.4, 1.8, 3.1, and 3.5 years (**Table 7**). Multiple factors can cause hypoplasia, being the most common in prehistoric societies malnutrition, psychosocial stress, or

infection during tooth development (Hillson, 2014).

Table 7. Measures of the enamel hypoplasia, only recorded in first superior incisors and inferior canines.

Tooth	Number of grooves	Distance from the groove to the cemento-enamel junction (in mm)	Height of the crown (in mm)
C_x	2	1 and 3.5	7
$_xC$	2	1.5 and 3	7

The presence of periostitis, an inflammatory reaction of the periosteum (Baxarias & Herrerín, 2008; Roberts & Buikstra, 2019), has been identified in the individual's ribs. This reaction can result from a traumatic injury or bacterial infection (Davies-Barrett et al., 2019; Ortner, 2003). New periosteal reactive bone formation in the caudal edges of the ribs is also evident. This pathology has been associated with pulmonary diseases, such as tuberculosis, given the potential for lung diseases to inflame the pleura, which can affect the bone as it attaches to the visceral surfaces of the ribs, thereby causing an inflammatory reaction on the surface of the ribs (Mariotti et al., 2015; Roberts & Buikstra, 2019). Other paleopathologies observed are osteophytes in the middle of the superior surface of the hyoid's body. On the other hand, the five bodies of the lumbar vertebrae are porous, present osteophytes and one of them is compressed in the interior surface. The sum of these conditions is related to the degenerative osteoarthritis that comes through the aging process (Rissech et al., 2006).

3.2.1.1.7 Enthesopathies: determination of activity markers

Enthesophytes can be found in various bones, including the hyoid, the lumbar vertebrae, both hands, the left patella and the left foot. Both hands show significant enthesophyte-related changes in the phalanges, as evidenced by the presence of a pronounced crest in the fibrous sheaths (also known as *vaginae fibrosae digitorum manus*) of the proximal and intermediate phalanges (from the right hand, the 4th proximal phalanx, and the 2nd and 3rd intermediate phalanges. From the left hand, the 2nd proximal hand phalanx and the 2nd, 3rd and 4th intermediate phalanges) (**Figure 29**). There is also a capsular osteophyte in the base of the 2nd distal left-hand phalanx. The crests and the osteophyte are associated with a developed pulley system in the fingers, as well as increased mechanical strain on the insertions, which may result in a stronger grip (Hermann et al., 2022). This enthesopathy is frequently linked to the manipulation and holding of tools (Baxarias & Herrerín, 2008).



Figure 29. Proximal hand phalanx of the left hand. A pronounced crest in the fibrous sheaths is observable on both sides of the palmar view of the bone.

More enthesophytes are found in the left foot, specifically in the facet for the first cuneiform and for the second cuneiform of the second metatarsal, in the facet for the third metatarsal of the fourth metatarsal, and in the lateral side of the base of the 2nd distal foot phalanx. The left patella is also affected by enthesophytes in the enthesis for the *quadriceps femoris* and the *ligamentum patellae*, which could have been caused by frequent walking or jumping.

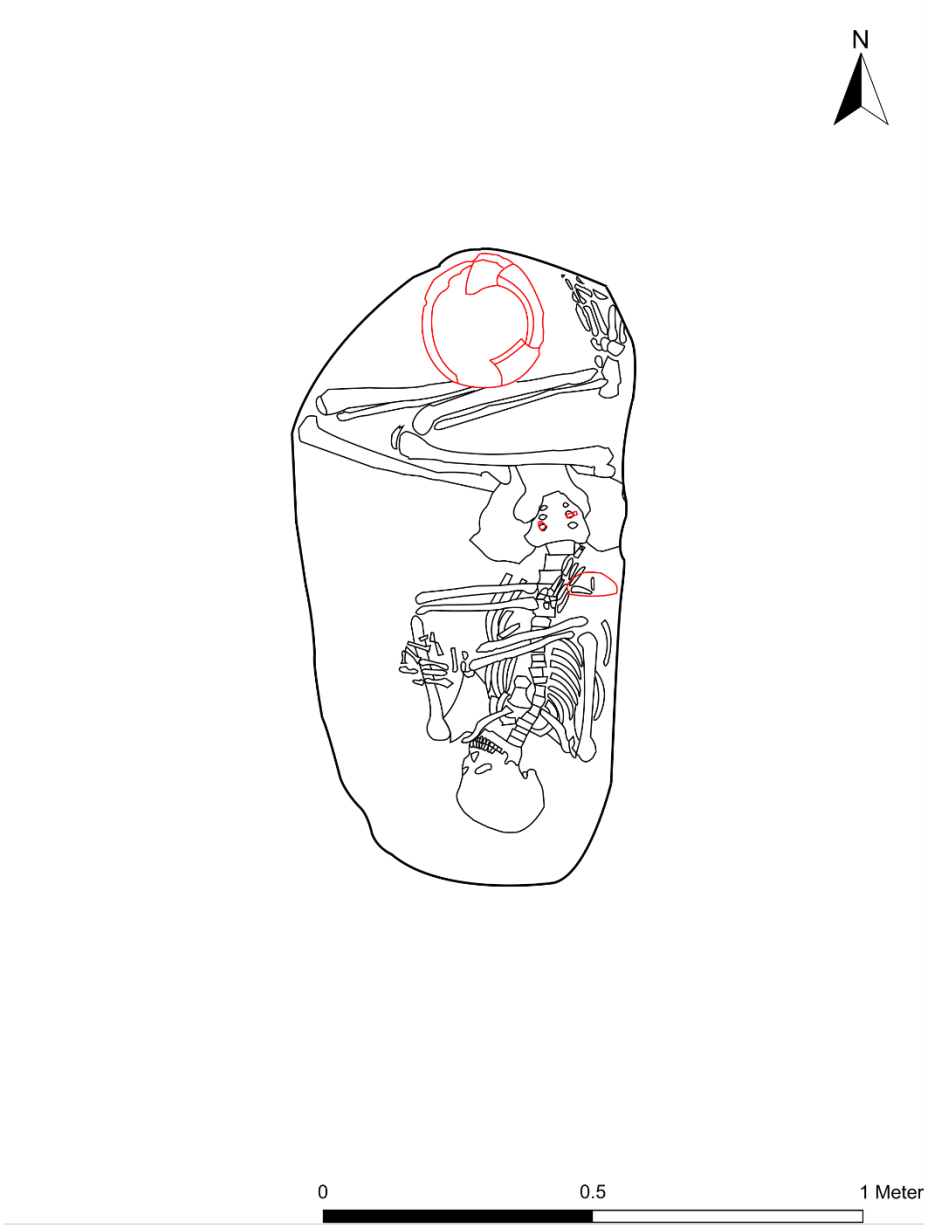
3.2.1.2 Grave 5

3.2.1.2.1 The container



Sector	3
Structure number	2021/10
Location	Locus 101.6
Period	Ninevite 5 (2900 – 2550 BCE) First half of the 3rd millennium BCE Early Bronze Age
Architectural phase	The construction of the grave occurred during the period of rapid transitional architecture, specifically phases 4B and 4A. Consequently, it can be posited that the existence of life and death within the site may have been contemporaneous.
Type of container	Simple pit
Morphology	Oval shape

3.2.1.2.2 The content



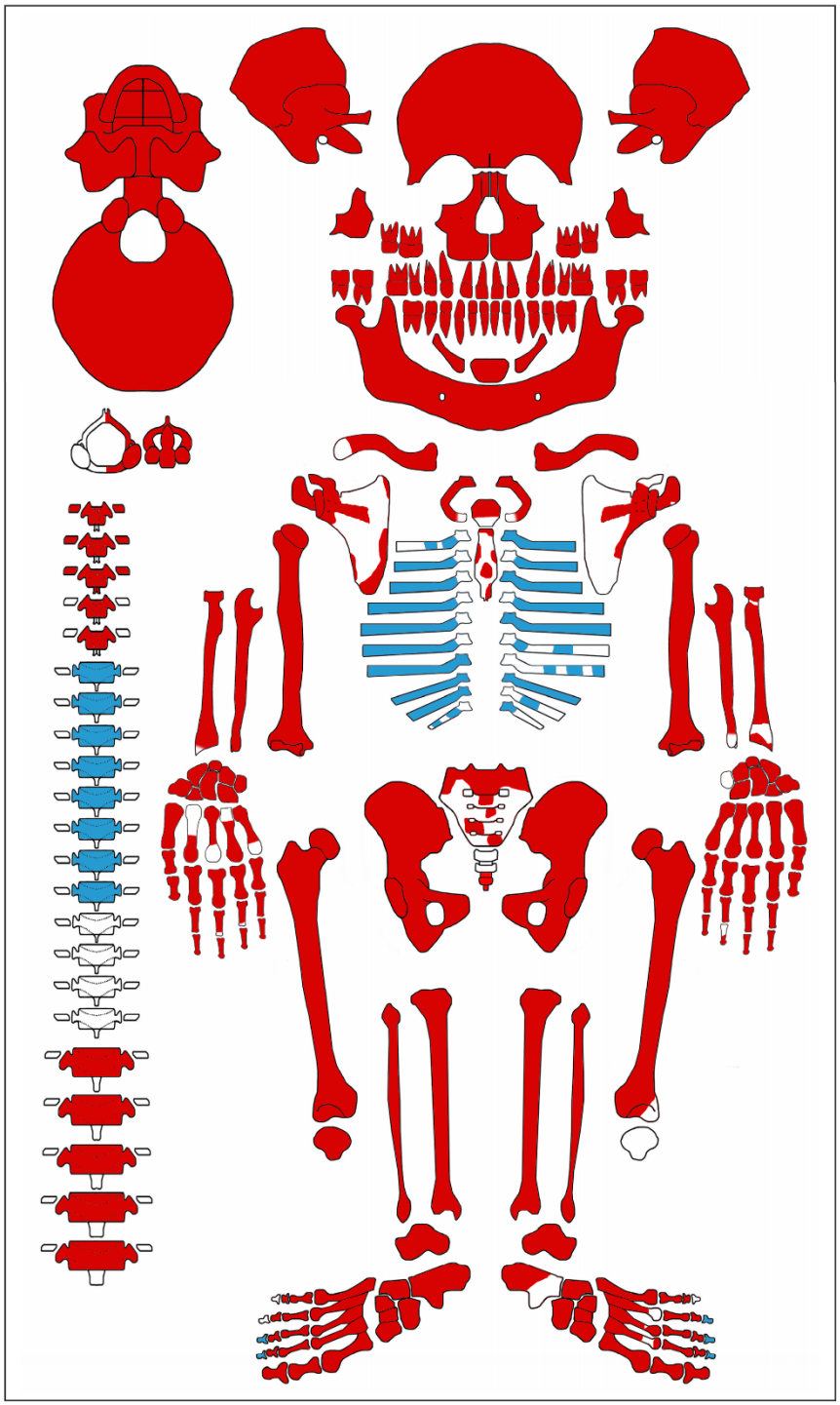
Number of buried individuals	1
Form of disposal	Primary inhumation
State of preservation	Poorly preserved
Body orientation	South-North
Face orientation	West
Position	Supine decubitus with the legs hyperflexed on the left side. The arms are crossed over the chest, with the right hand positioned over the left humerus and the left hand positioned over the abdomen. The skull is positioned on the left side.
Skeletal articulation	Articulated

Ornaments	None
Grave goods	One cylinder seal with geometric motifs (diagonal lines) and one pendant made of amygdaloidal basalt positioned above the sacrum, with a trapezium shape and rounded edges, a fragment of volcanic stone on the left hand, and a complete pottery vessel under the foot.

3.2.1.2.3 Osteology: bone identification

Visual recording form - Adult (Roksandic, 2003)

GRAVE 5



3.2.1.2.4 Determination of sex

The determination of sex was based on cranial (Acsádi & Nemeskéri, 1970) and coxal (Buikstra & Ubelaker, 1997) features. The cranial features that have been preserved include the nuchal

crest, the mastoid processes, the right supraorbital margin, the glabella and the mental eminence. The preserved characteristics are indicative of a female classification (see **Table 8**). Coxal features have been identified in both *os coxae*. In the right *os coxae*, the dimensions of the greater sciatic notch do not allow to discern between male or female sex. A thorough analysis of the *os pubis* and the Phenice traits (1969) reveals the presence of a ventral arc, of a subpubic concavity, and of a ridge in the medial aspect of the ischio-pubic ramus. These characteristics are considered female sex traits.

Table 8. Scores for the cranial features to determine sex.

Cranial feature	Right side	Center	Left side
Nuchal crest		1 (Female)	
Mastoid process	2 (Probably Female)		2 (Probably Female)
Supraorbital margin	2 (Probably Female)		Not observable
Supraorbital ridge / Glabella		1 (Female)	
Mental eminence		2 (Probably Female)	

3.2.1.2.5 Determination of age

The determination of age was based on the examination of tooth wear attrition, by the development of the pubic symphysis from both *os coxae*, as well as by the epiphyseal fusion of the left clavicle. The analysis of dental attrition in permanent molars was conducted following Brothwell (1981), which has also been adapted in T. D. White et al. (2012) (see **Table 9**). The estimated age range is between 25 and 35 years. According to the Suchey-Brooks system (Brooks & Suchey, 1990), the development of the pubic symphysis in the right *os coxae* is assigned to Phase 4. The 95% range of age is determined to be between 26 and 70 years, with a mean age of 38.2 years. The development of the pubic symphysis in the left *os coxae* is assigned to Phase 3. The 95% range of age is determined to be between 21 and 53 years, with a mean age of 30.7 years. The epiphyseal fusion of the left clavicle indicates an age of > 20-25 years. The sum of all the characteristics of age determination indicates an approximated estimated age range between 25 and 38 years, classified as a middle adult according to Buikstra & Ubelaker (1997).

Table 9. Scores of dental attrition in permanent molars (in anthropological notation).

Tooth	Score	Estimated age (in years)
^{1}M	4	25 – 35
^{2}M	2+	17 – 25
^{3}M	2	25 – 35
M^{1}	5	25 – 35
M^{2}	2+	17 – 25
M^{3}	2	17 – 25
$_{1}$M	5	25 – 35
$_{2}$M	3	25 – 35
$_{3}$M	2	25 – 35
M$_{1}$	5	25 – 35
M$_{2}$	3+	25 – 35
M$_{3}$	2	25 – 35

3.2.1.2.6 Stature estimation

In order to estimate the stature of the buried individual, the maximum length of the best-preserved and complete bones was measured (**Table 10**). The regression equations for white males, according to Trotter (1970) were employed, as well as the modification equation for individuals over 30 years of age. If the deceased was younger than 30 years of age, the estimated range of stature varied between 145.5 and 173.1 centimeters, with an average of 159.3 centimeters. In the case of a higher age, the mean would decrease to 158.8 centimeters.

Table 10. Measures from the preserved long bones (in centimeters).

Side	Bone	Length (in cm)	Side	Bone	Length (in cm)
Right	Humerus	28	Left	Humerus	28
	Radius	23.5		Radius	22
	Ulna	26		Ulna	25
	Femur	38.5		Femur	39
	Tibia	34		Tibia	34.5
	Fibula	32.5		Fibula	33

3.2.1.2.7 Paleopathologies: determination of health

The studied bones present several paleopathologies, including dental diseases, osteoarthritis

and periostitis. The dental diseases that have been observed are related with tooth decay (caries), dental calculus (tartar), periodontitis, and defects of the enamel. They have various etiologies, being poor oral health and accumulation of bacteria the principal ones, causing considerable pain and difficulties in eating (Lewis, 2018). Caries is an infectious disease that progressively destroys the crown and the root structures due to microbial activity (Ortner, 2003). It has been identified in the proximal surface of the M^3. Dental calculus consists of the buildup of hardened plaque on the surface of the tooth (Lewis, 2018), and it is present in 23 teeth. Detailed information can be seen in **Table 11**. Periodontitis consists of the loss of the supporting structures of the tooth due to the buildup of plaque bacteria, resulting of gingivitis (Lewis, 2018). Almost all teeth present horizontal and vertical periodontitis.

Table 11. Detailed information about the identified dental calculus (in anthropological notation).

Tooth	Intensity	Surface location
$_1$I	Moderate	Lingual, distal, proximal and buccal
$_2$I	Moderate	Lingual
$_x$C	Slight	Lingual, distal and proximal
$_1$P	Slight	Proximal
$_2$P	Slight	Distal
I_1	Moderate	Lingual, distal, proximal and buccal
I_2	Moderate	Lingual, distal, proximal and buccal
C_x	Moderate	Distal, proximal and buccal
C_x	Slight	Lingual
P_1	Slight	Lingual
P_2	Slight	Proximal and distal
M_3	Slight	Lingual and distal
^{2}I	Slight	Proximal
^{2}P	Slight	Proximal
^{1}M	Slight	Proximal
^{2}M	Slight	Proximal
^{3}M	Slight	Proximal
I^1	Slight	Lingual
I^2	Slight	Lingual
C^x	Moderate	Lingual
P^1	Slight	Distal
P^2	Slight	Lingual, distal and proximal
M^1	Slight	Distal and proximal
M^2	Slight	Proximal

The defects in the enamel consist of linear hypoplasias present in both mandibular canines. According to the Swärdstedt (1966) equations, the enamel formation was disturbed repeatedly at the ages of 2.2, 3.1, and 3.5 years (**Table 12**). Multiple factors can cause hypoplasia, being the most common in prehistoric societies malnutrition, psychosocial stress, or infection during tooth

development (Hillson, 2014).

Table 12. Measures of the enamel hypoplasia, only recorded in first superior incisors and inferior canines.

Tooth	Number of grooves	Distance from the groove to the cemento-enamel junction (in mm)	Height of the crown (in mm)
C_x	2	2 and 3.5	7
$_xC$	2	2 and 3	7

The vertebrae of the deceased individual are affected by degenerative osteoarthritis, osteoporosis and compression in the vertebral bodies. The presence of osteophytes, defined as fibrocartilage-capped bony outgrowths (Wong et al., 2016), are located in the lumbar vertebrae in the form of traction osteophytes (Heggeness & Doherty, 1998) in the epiphyseal rings of the vertebral bodies (**Figure 30**). Osteoporosis is characterized by reduced bone density and microarchitectural deterioration of bone tissue, leading to increased bone fragility and a high risk of fractures (Lin & Lane, 2004). The vertebral bodies exhibit signs of slight and heavy compression, suggesting that the intervertebral disks have undergone erosion over time. The sum of all these injuries is attributable to degenerative osteoarthritis that comes through the aging process (Rissech et al., 2006), which can result in a significant reduction in mobility.



Figure 30. Fourth lumbar vertebrae in its superior view. Traction osteophytes are visible in the epiphyseal ring of the vertebral body.

Degenerative osteoarthritis has had a profound impact on the tarsals of both feet, manifesting as osteophytes in various facets of the tarsals. The disease manifested with reduced mobility and pain when walking or standing. In the right foot, the calcaneus exhibits osteophytes on the facet for the cuboid; the navicular demonstrates osteophytes on the facet for the first cuneiform and the facet for the talar head; and the first cuneiform displays osteophytes on the facet for the second cuneiform. In the left foot, osteophytes are present on the talus head, navicular facet for talar head, second cuneiform facet for talar head, first cuneiform facet for talar head, and nonarticular dorsal surface (**Figure 31**). Additionally, osteophytes are found on the third cuneiform facet for talar head on the nonarticular dorsal surface. The facet for the second cuneiform is eroded in the first cuneiform of the left foot, as well as the cortical bone of the third cuneiform. The presence of osteophytes is observed not only in the tarsals but also in the phalanges of both feet. In the right foot, capsular osteophytes are present in the plantar surface of the proximal and distal hallucial phalanx; in contrast, in the left foot, they are present in all the distal phalanges.



Figure 31. Lateral side of the talus from the left foot.

The presence of periostitis, an inflammatory reaction of the periosteum, has also been identified (Baxarias & Herrerín, 2008; Roberts & Buikstra, 2019). This reaction can result from a traumatic injury or bacterial infection (Ortner, 2003). New periosteal reactive bone formation is evident in the caudal edges and heads. This pathology has been associated with pulmonary diseases, such as tuberculosis, given the potential for lung diseases to inflame the pleura, which can affect the bone as it attaches to the visceral surfaces of the ribs, thereby causing an inflammatory reaction on the surfaces of the ribs (Roberts & Buikstra, 2019). One of the right ribs exhibits periosteal tissue between the tubercle and the body, suggesting a potential healed fracture. Linked to this pathology is the presence of osteophytes in various anatomical regions of the ribs, including the neck, the tubercle, and its articular facets, as well as the sternal end. Another bone affected by periostitis is the third cuneiform of the right foot, which shows evidence of periostitis on the nonarticular dorsal surface. This condition has also been associated with degenerative osteoarthritis.

3.2.1.2.8 Enthesopathies: determination of activity markers

The presence of activity markers has been observed in the shoulder girdle, the right arm, and in both legs and feet. The lower part of the body exhibits a greater prevalence of enthesophyte-

related changes in comparison to the upper part. In the shoulder girdle region, the right scapula exhibits enthesophytes in the glenoid fossa, thereby affecting the glenohumeral joint. The right radius is affected by a perforation located in the articular fovea, which may serve as an indicator of the onset of elbow *osteochondritis dissecans*. This injury manifests in instances of repetitive high-stress forces being applied to the elbow joint. Additionally, a slight degree of robustness in the insertion with the *biceps brachii* muscle is observed, the function of which is to flex and rotate the forearm at the elbow joint. Injuries affecting the upper body have been associated with repetitive use of the right arm and/or indicative of right-handedness.

In the lower part of the body, enthesopathies affect all the bones of the legs. Both femurs exhibit a high degree of robustness in the gluteal tuberosity, the site of attachment for the gluteus maximus muscle. This muscle is responsible for extending the hip joint and rotating the thigh, and it is associated with activities such as rising from a seated position or climbing. The right femur exhibits osteophytes in the impression for the lateral head of the gastrocnemius muscle, which is inserted in the Achilles tendon. This muscle is responsible for flexing the knee and foot (Palastanga et al., 1989). The enthesophytes present in the calcaneal tuberosity of the calcaneus of both feet are linked to this muscle. The primary cause of these enthesophytes is musculoskeletal stress of the Achilles tendon. The right patella presents enthesophytes in both the posterolateral and the anteromedial sides, as well as porosity on the lateral articular facet. The last mechanical stress markers in the right leg are found in the fibula, in which enthesophytes are present in multiple ligament insertions, including the styloid process (on the insertion of the capsular ligaments of the knee), the fibular neck (on the insertion of the *soleus* muscle), the anterior superior tibiofibular ligament attachment, and the malleolar articular surface (**Figure 32**). In the left leg, the proximal tibiofibular joint is affected by biomechanical stress. The tibia and fibula both display enthesophytes along the anterior-superior surface of the tibial tuberosity and the fibular neck, respectively, where the *quadriceps femoris* and *soleus* muscles are inserted. The *quadriceps femoris* is responsible for flexing the hip and extending the knee, while the *soleus* muscle, which is inserted into the Achilles tendon, is responsible for flexing the foot and maintaining the stability of the body. The right fibula is also affected by an atypical morphology of the distal epiphysis, which could be linked to stress on the inferior tibiofibular syndesmosis attachment. This attachment plays a role in protecting the ankle joint by gripping the talus, thereby preventing displacement of the foot. The injuries observed in the lower part of the body, related to robustness in the ligament and tendon insertions, as well as injuries in the areas related to extending, flexing, and rotating the hips, the knee, and the feet, could be caused by difficulties in movement due to the degenerative osteoarthritis present in the tarsals of the individual.



Figure 32. Right fibula. Lateral surface of the proximal diaphysis with presence of enthesophytes.

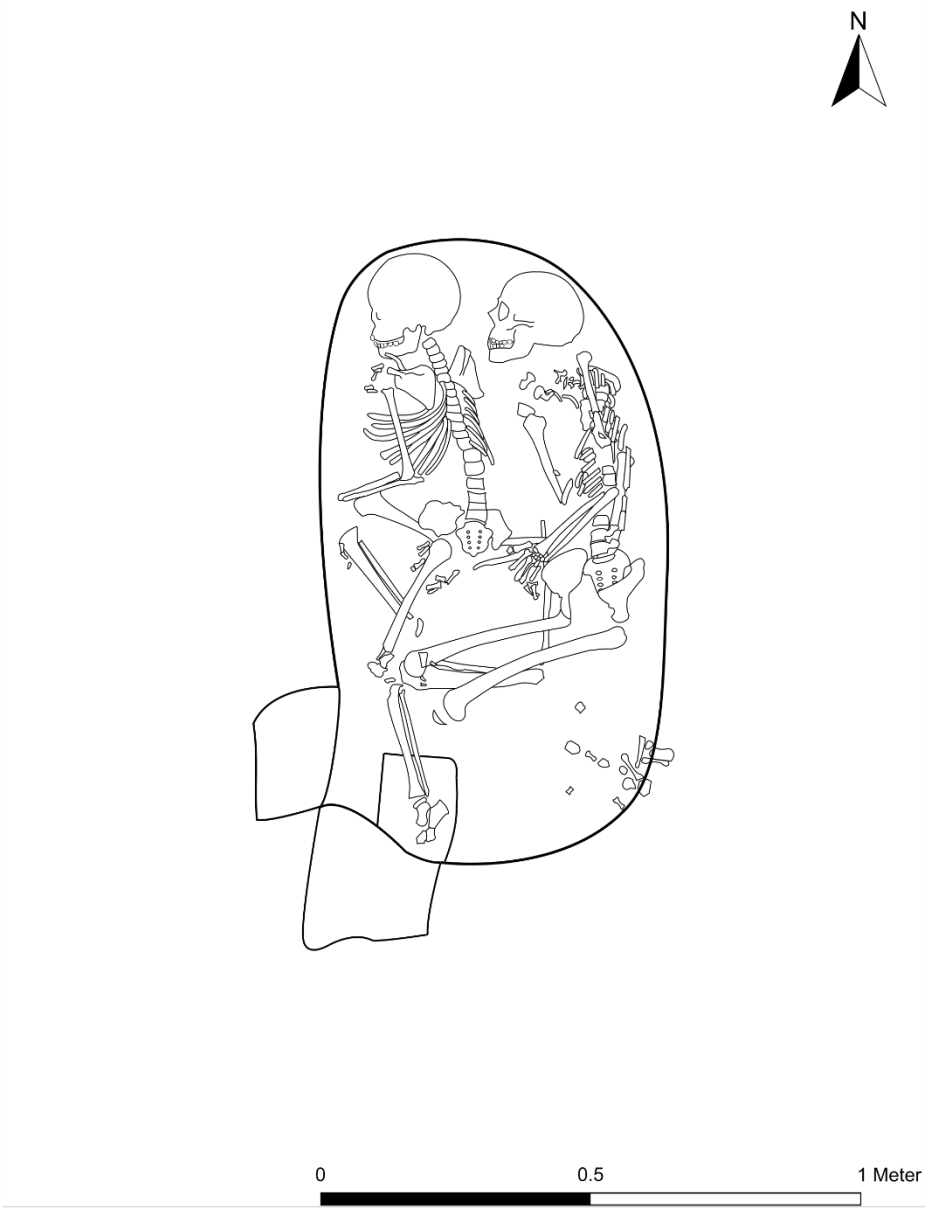
3.2.1.3 *Grave 6*

3.2.1.3.1 The container



Sector	3
Structure number	2021/20
Location	Locus 123
Period	Ninevite 5 (2900 – 2550 BCE) First half of the 3rd millennium BCE Early Bronze Age
Architectural phase	The construction of the grave occurred during the period of rapid transitional architecture, specifically phases 4B and 4A. Consequently, it can be posited that the existence of life and death within the site may have been contemporaneous.
Type of container	Simple pit
Morphology	Oval shape

3.2.1.3.2 The content



Number of buried individuals	2
Form of disposal	Primary inhumation
State of preservation	Poorly preserved
Body orientation	North-South
Face orientation	West

3.2.1.3.2.1 Individual 1 (Grave 6.1)

Position	Prone decubitus. The right arm is flexed beneath the thorax. The left arm is flexed, and the hand is positioned on the right knee. The right leg is flexed, while the left leg is extended.
Skeletal articulation	Articulated
Ornaments	None
Grave goods	None

3.2.1.3.2.2 Individual 2 (Grave 6.2)

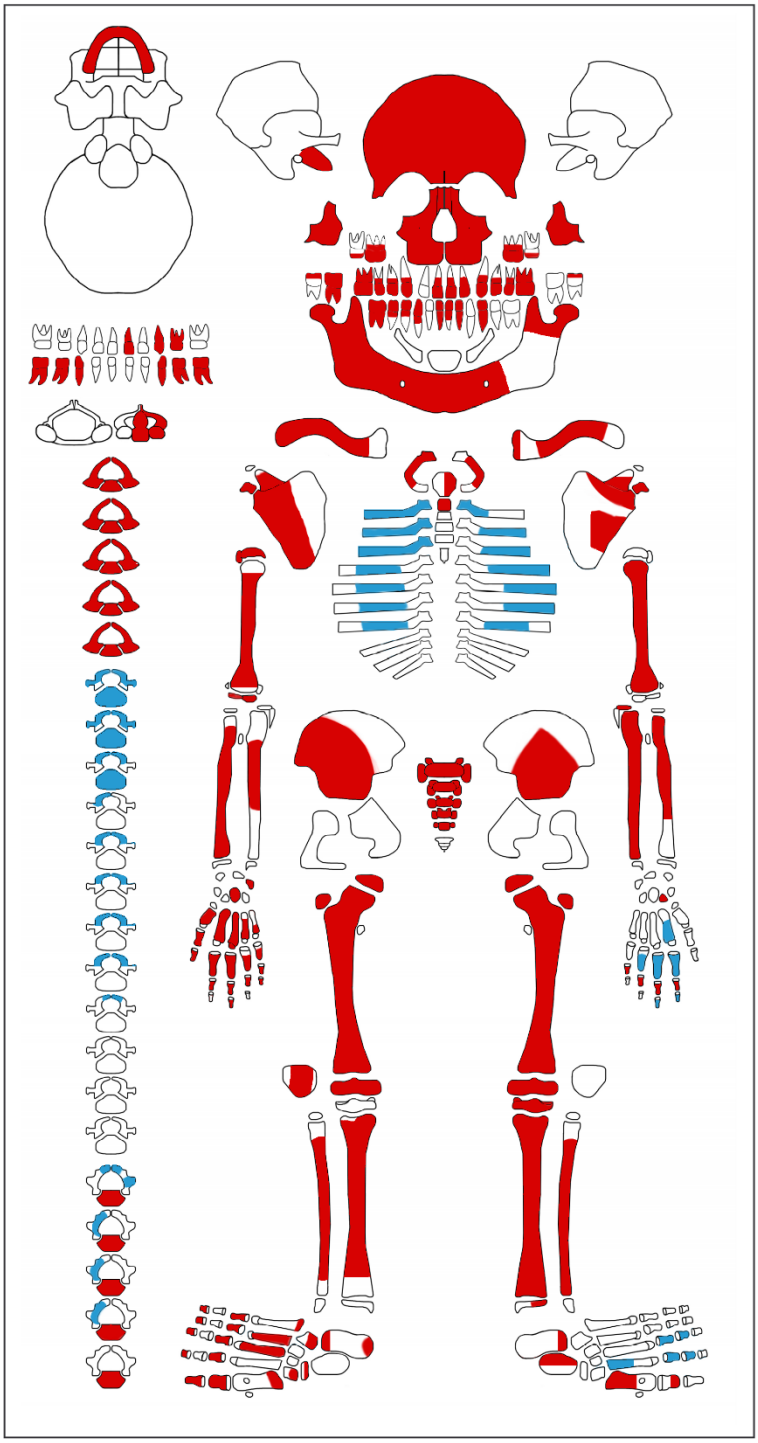
Position	Right lateral decubitus. The skull is displaced in relation to the post-crania. The right humerus is positioned at the level of the skull, while the forearm is extended from the thorax. The left arm is *in situ*, flexed from the thorax to the younger individual. The legs are hyperflexed.
Skeletal articulation	Disarticulated anatomic parts: from the skull to the thoracic vertebrae, the right arm and hand, the left tibia and fibula, and both feet. Loosely articulated anatomic parts: left arm and hand, lumbar vertebrae, hips, femurs, right tibia and fibula, and patellas.
Ornaments	None
Grave goods	None

3.2.1.3.3 Osteology: bone identification

3.2.1.3.3.1 Individual 1

Visual recording form - Child (Roksandic, 2003)

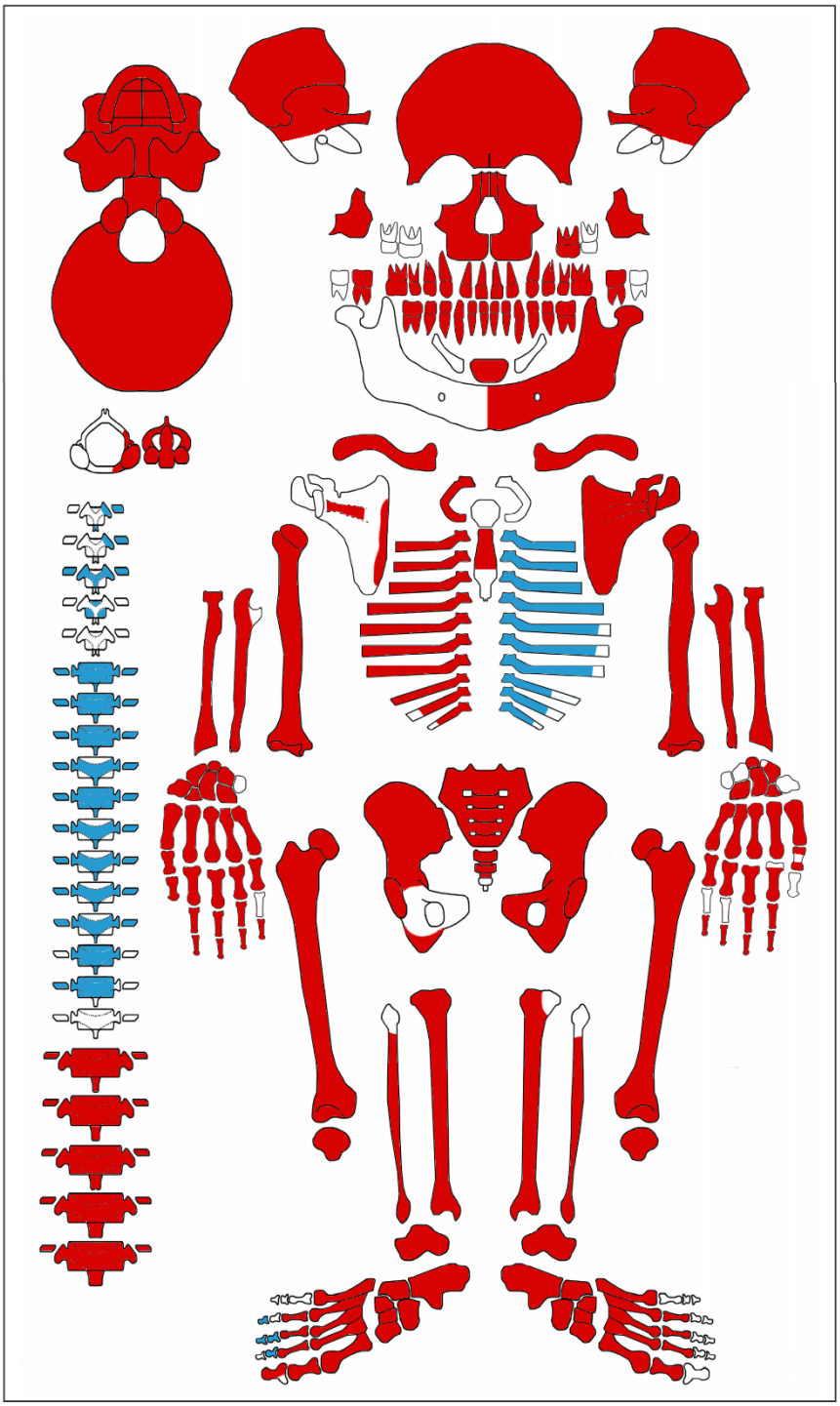
GRAVE 6 - Individual 1



3.2.1.3.3.2 Individual 2

Visual recording form - Adult (Roksandic, 2003)

GRAVE 6 - Individual 2



3.2.1.3.4 Determination of sex

3.2.1.3.4.1 Individual 1

The absence of any sexual trait did not allow to determine the sex of the individual.

3.2.1.3.4.2 Individual 2

The determination of sex was based on cranial (Acsádi & Nemeskéri, 1970) and coxal (Buikstra & Ubelaker, 1997) features. The cranial feature that has been preserved include the right mastoid process. The preserved characteristics are indicative of a female classification (see **Table 13Table 8**). The coxal features that have been preserved in both *os coxae* is the greater sciatic notch, which are broad, being characteristic of a probably female sex. The morphology of the preauricular sulcus in the left *os coxae* is also characteristic of a probably female sex. A thorough analysis of the *os pubis* and the Phenice traits (1969) in the left *os coxae* reveals the presence of a subpubic concavity, characteristic of female sex, and of a flat surface in the medial aspect of the ischio-pubic ramus, characteristic of male sex. These sum of all the features suggests the individual was probably of female sex.

Table 13. Scores for the cranial features to determine sex.

Cranial feature	Right side	Center	Left side
Nuchal crest		Not observable	
Mastoid process	2 (Probably Female)		Not observable
Supraorbital margin	Not observable		Not observable
Supraorbital ridge / Glabella		Not observable	
Mental eminence		Not observable	

3.2.1.3.5 Determination of age

3.2.1.3.5.1 Individual 1

Age has been determined by tooth development according to Schour & Massler (1941), Gustafson & Koch (1974) and AlQahtani et al. (2010), as well as epiphyseal fusion of the bones from the postcrania according to Schaefer et al. (2009). Tooth development provides an estimated age range between 9 and 13 years. Epiphyseal fusion of the cervical vertebrae and the coracoid

process of both *scapulae* provide the youngest estimated age of < 12 years. Therefore, the estimated age range is approximately 9 to 12 years, classified as a child according to Buikstra & Ubelaker (1997).

3.2.1.3.5.2 Individual 2

The determination of age was based on the examination of tooth wear attrition, on the development of the pubic symphysis, and on the epiphyseal fusion of the bones from the postcrania. The analysis of dental attrition in permanent molars was conducted following Brothwell (1981), which has also been adapted in T. D. White et al. (2012) (see **Table 14**). The estimated age range is between 17 and 25 years. According to the Todd system (1920), the development of the pubic symphysis in the right *os coxae* is assigned to the fourth phase, whose age range is determined to be between 25 and 26 years. The epiphyseal fusion of the left clavicle indicates an age of > 24-29 years. The sum of all the characteristics of age determination indicates an approximated estimated age of 25 years, classified as a young adult according to Buikstra & Ubelaker (1997).

Table 14. Scores of dental attrition in permanent molars (in anthropological notation).

Tooth	Score	Estimated age (in years)
$_1$M	1	17 - 25
$_2$M	1	17 - 25
^{1}M	3-	17 - 25
^{2}M	2	17 - 25
M^1	2+	17 - 25

3.2.1.3.6 Stature estimation

3.2.1.3.6.1 Individual 1

The estimation of the stature of the buried individual was not performed due to the lack of epiphyseal fusion of the long bones. Nevertheless, the maximum length of the best-preserved and complete bones was measured (**Table 15**).

Table 15. Measures from the preserved long bones (in centimeters).

Side	Bone	Length (in cm)	Side	Bone	Length (in cm)
Right	Humerus	Not observable	Left	Humerus	18
	Radius	Not observable		Radius	13.5
	Ulna	Not observable		Ulna	17
	Femur	Not observable		Femur	27.5
	Tibia	22		Tibia	21.5
	Fibula	21		Fibula	21.5

3.2.1.3.6.2 Individual 2

In order to estimate the stature of the buried individual, the maximum length of the best-preserved and complete bones was measured (**Table 16**). The estimated range of stature varied between 149.2 and 170.9 centimeters, with an average of 160 centimeters.

Table 16. Measures from the preserved long bones (in centimeters).

Side	Bone	Length (in cm)	Side	Bone	Length (in cm)
Right	Humerus	Not observable	Left	Humerus	30
	Radius	22		Radius	23
	Ulna	25.5		Ulna	25
	Femur	40		Femur	40.5
	Tibia	36		Tibia	Not observable
	Fibula	32		Fibula	Not observable

3.2.1.3.7 Paleopathologies: determination of health

3.2.1.3.7.1 Individual 1

The presence of paleopathologies was not detected in the observed bones.

3.2.1.3.7.2 Individual 2

Two paleopathologies have been identified in the skeletal remains of the deceased: dental diseases and an injury in the malleolar fossa of the left fibula. The defects in the enamel consist of linear hypoplasias present in both mandibular canines. According to the Swärdstedt (1966) equations, the enamel formation was disturbed repeatedly at the ages of 3.5, 4.3, and 5.8 years (**Table 17**). Multiple factors can cause hypoplasia, being the most common in prehistoric societies malnutrition, psychosocial stress, or infection during tooth development (Hillson, 2014).

Table 17. Measures of the enamel hypoplasia, only recorded in first superior incisors and inferior canines.

Tooth	Number of grooves	Distance from the groove to the cemento-enamel junction (in mm)	Height of the crown (in mm)
C_x	1	5	8
$_xC$	3	4, 5 and 7	8

The malleolar fossa of the left fibula exhibits an eroded cortical surface, characterized by the presence of porosity in the bone (**Figure 33**). The etiology of the present injury is idiopathic, as a multitude of factors have the capacity to induce it, encompassing direct trauma (e.g., a sprained ankle), repetitive microtrauma, and genetic conditions, among others. In the event that the talus or other bones are found to be pathologically affected, the presence of ankle *osteochondritis dissecans* may be considered. This condition is characterized by a lesion of the subchondral bone, leading to sequestration and delamination. This pathology has the capacity to remain asymptomatic for an extended period, but when symptoms manifest, they are characterized by intermittent pain during activities such as walking or running. (Zanon et al., 2014).



Figure 33. Medial side of the left fibula. The image shows evidence of osteochondritis dissecans at the malleolar fossa.

3.2.1.3.8 Enthesopathies: determination of activity markers

3.2.1.3.8.1 Individual 1

The presence of enthesopathies was not detected in the observed bones.

3.2.1.3.8.2 Individual 2

The presence of enthesopathies was not detected in the observed bones.

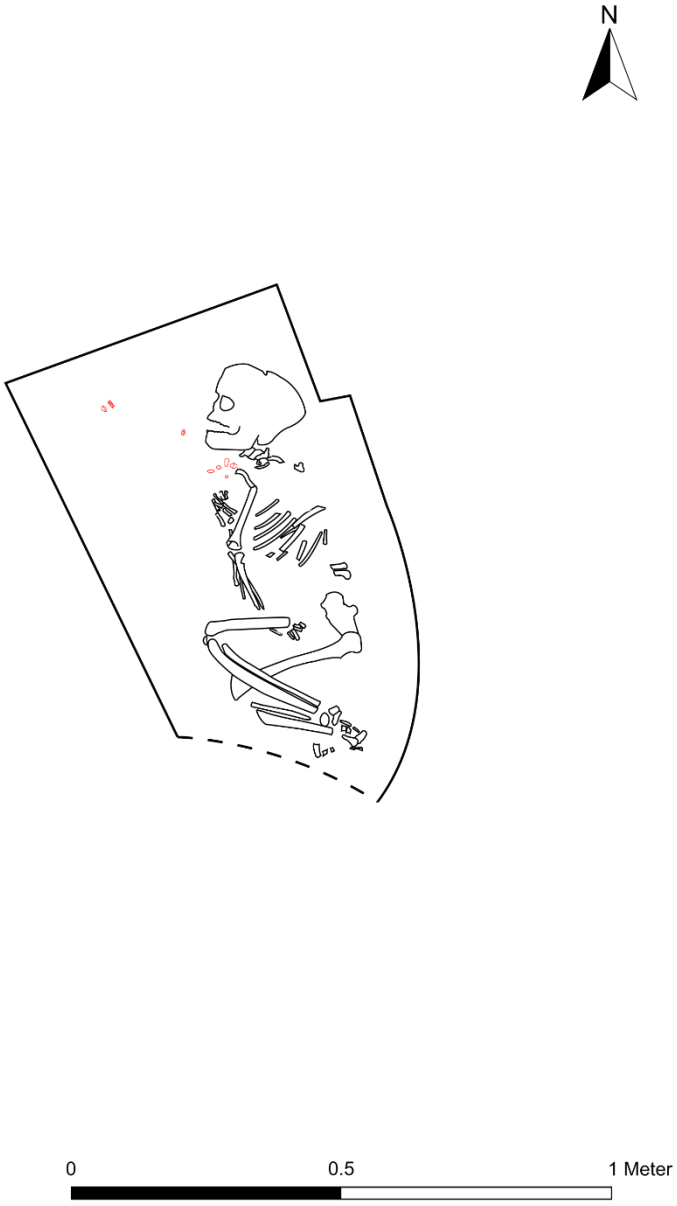
3.2.1.4 Grave 7

3.2.1.4.1 The container



Sector	3
Structure number	2022/1
Location	Locus 124.1
Period	Ninevite 5 (2900 – 2550 BCE) First half of the 3rd millennium BCE Early Bronze Age
Architectural phase	The construction of the grave occurred during the period of rapid transitional architecture, specifically phases 4B and 4A. Consequently, it can be posited that the existence of life and death within the site may have been contemporaneous.
Type of container	Simple pit
Morphology	Rectangular shape

3.2.1.4.2 The content



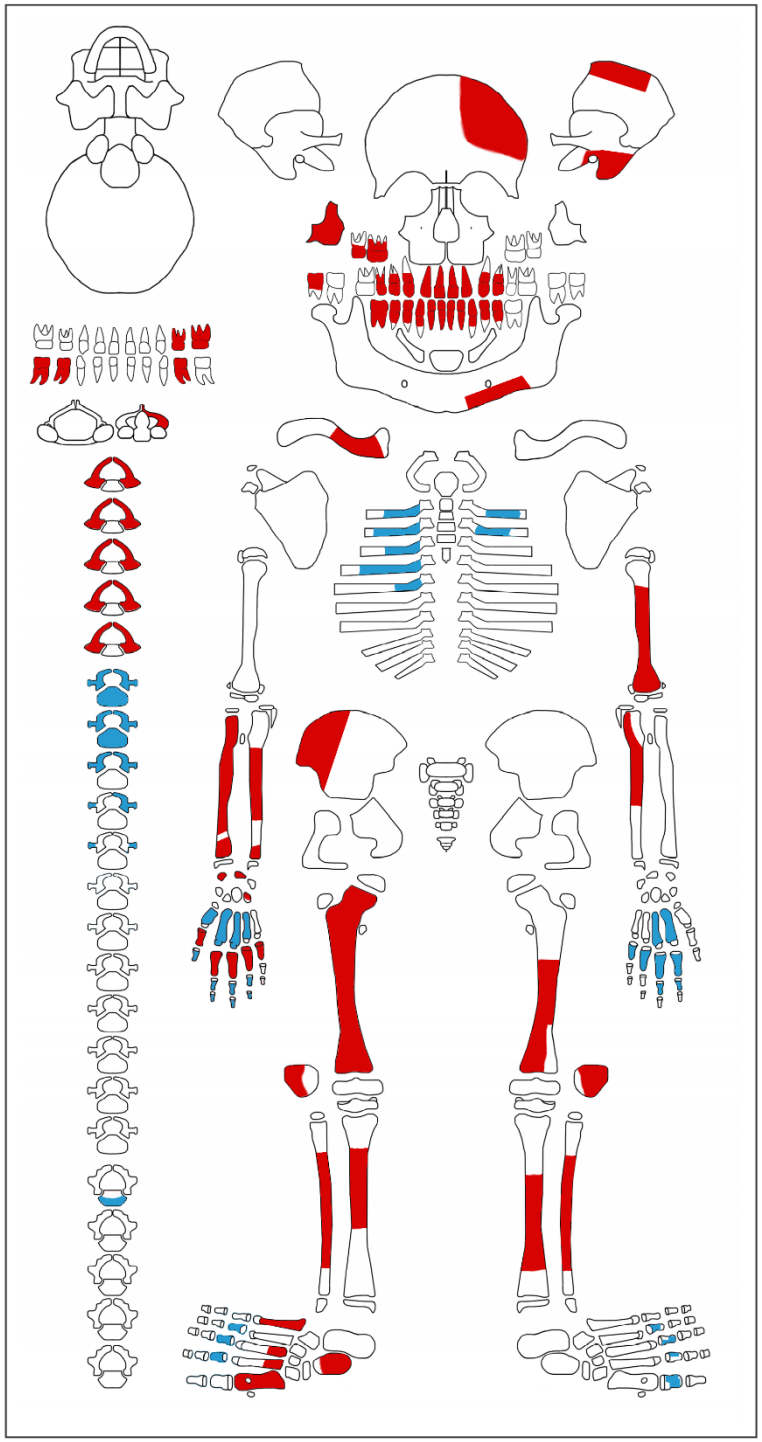
Number of buried individuals	1
Form of disposal	Primary inhumation
State of preservation	Poorly preserved
Body orientation	Northwest-Southeast
Face orientation	West
Position	Right lateral decubitus with flexed legs. The right arm is flexed toward the chest, while the left arm is extended beneath the left leg.
Skeletal articulation	Articulated

Ornaments	A necklace, composed of seven beads, was suspended from the neck. The beads exhibited a variety of morphologies, including discoid, rhomboid, trapezoid, hexagonal, and bitroncoconical shapes. The materials from which the beads were made included carnelian, lapis lazuli, amygdaloidal basalt, and a white rock.
Grave goods	A *cypraea* shell and a cylinder seal with geometric motifs (lines and rhombs with dots inside) are positioned in front of the face.

3.2.1.4.3 Osteology: bone identification

Visual recording form - Child (Roksandic, 2003)

GRAVE 7



3.2.1.4.4 Determination of sex

The absence of any sexual trait did not allow to determine the sex of the individual.

3.2.1.4.5 Determination of age

Age has been determined by tooth development according to Schour & Massler (1941), Gustafson & Koch (1974) and AlQahtani et al. (2010), by cranial sutures according to Meindl & Lovejoy (1985), as well as by epiphyseal fusion of the bones from the postcrania according to Schaefer et al. (2009). Tooth development provides an approximated estimated age of 10 years. All the cranial sutures are open, indicating a subadult age. Epiphyseal fusion has been observed in the thoracic vertebrae, the left humerus, the right radius and ulna, the right carpals and both right and left metacarpals and phalanges. The youngest estimated age of 9 to 14 years is provided by the bones of the hands. Considering tooth development as the most precise age indicator, the estimated age is approximately 10 years, classifying as a child according to Buikstra & Ubelaker (1997).

3.2.1.4.6 Stature estimation

The estimation of the stature of the buried individual was not performed due to the lack of epiphyseal fusion of the long bones. Nevertheless, he maximum length of the best-preserved and complete bones was measured (**Table 18**).

Table 18. Measures from the preserved long bones (in centimeters).

Side	Bone	Length (in cm)	Side	Bone	Length (in cm)
Right	Humerus	Not observable	Left	Humerus	14.5
	Radius	13		Radius	16
	Ulna	17		Ulna	16
	Femur	28.5		Femur	17.5
	Tibia	20		Tibia	29.5
	Fibula	19		Fibula	23

3.2.1.4.7 Paleopathologies: determination of health

The presence of paleopathologies was not detected in the observed bones.

3.2.1.4.8 Enthesopathies: determination of activity markers

The presence of enthesopathies was not detected in the observed bones.

3.2.1.5 Grave 8

3.2.1.5.1 The container

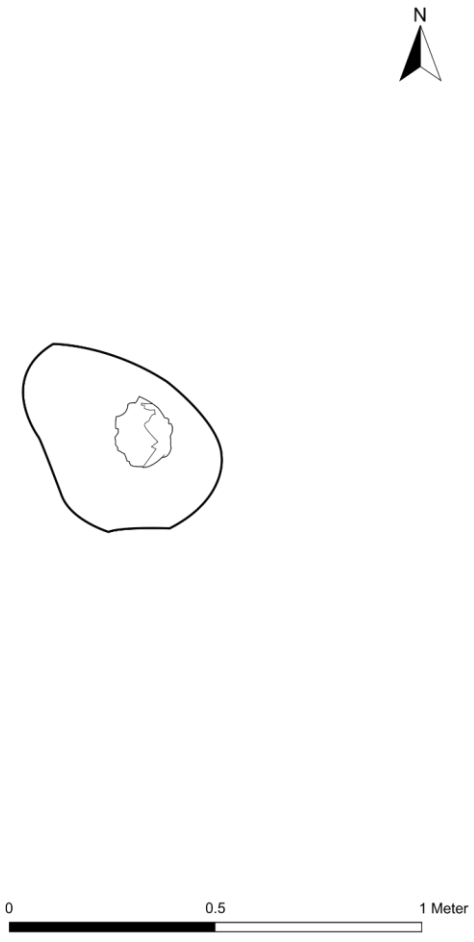


Sector	3
Structure number	2022/4
Location	Locus 127.3
Period	Ninevite 5 (2900 – 2550 BCE) First half of the 3rd millennium BCE Early Bronze Age
Architectural phase	The construction of the grave occurred during the period of rapid transitional architecture, specifically phases 4B and 4A. Consequently, it can be posited that the existence of life and death within the site may have been contemporaneous.
Type of container	Simple pit
Morphology	Oval shape

3.2.1.5.2 The content

TELL LASHKIR

Grave 8

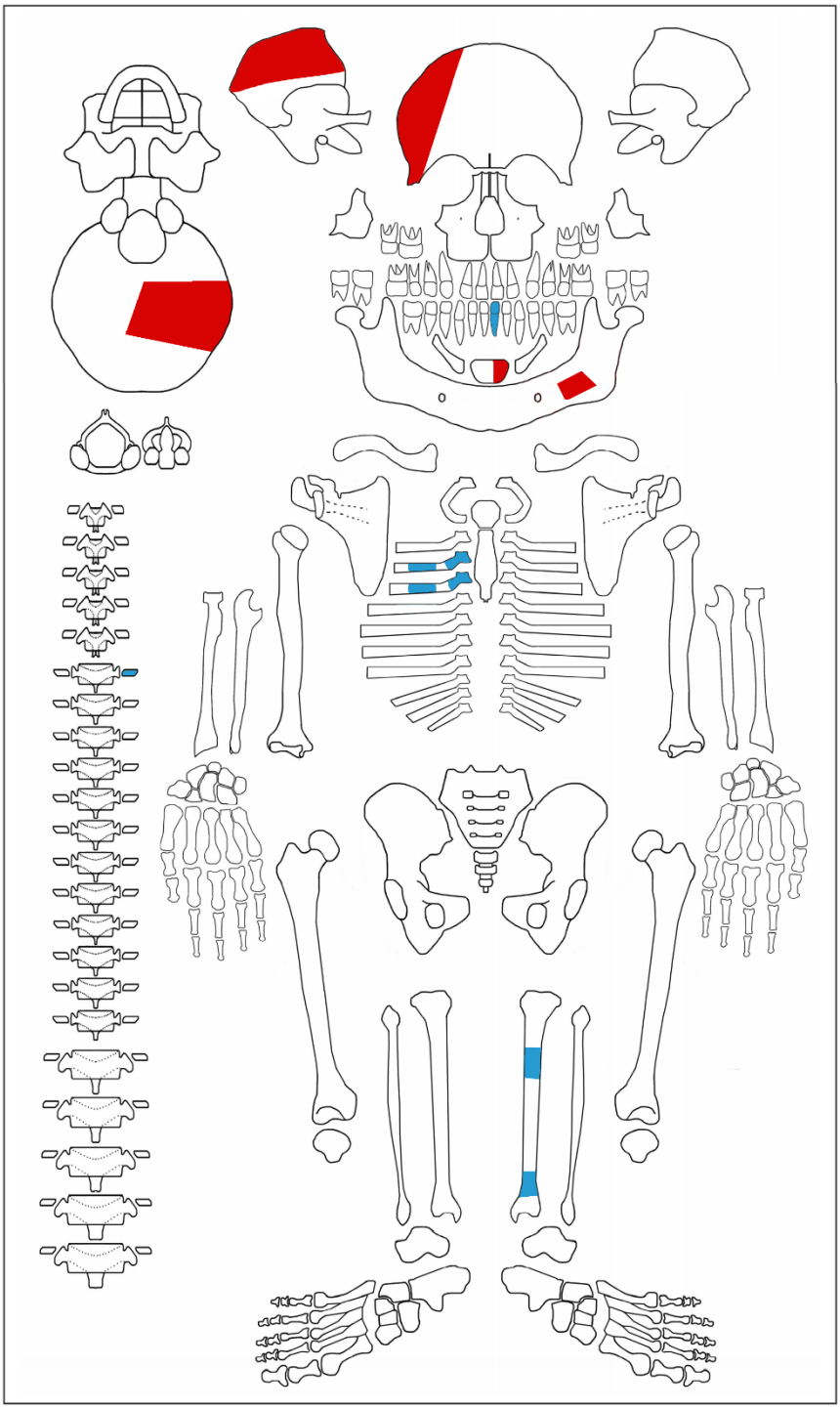


Number of buried individuals	1
Form of disposal	Secondary inhumation
State of preservation	Poorly preserved
Body orientation	Not observable
Face orientation	North
Position	Skull upside down
Skeletal articulation	Disarticulated
Ornaments	None
Grave goods	None

3.2.1.5.3 Osteology: bone identification

Visual recording form - Adult (Roksandic, 2003)

GRAVE 8



3.2.1.5.4 Determination of sex

The absence of any sexual trait did not allow to determine the sex of the individual.

3.2.1.5.5 Determination of age

The dimensions and morphology of the preserved bones only allow for the determination of adult age.

3.2.1.5.6 Stature estimation

The estimation of the stature of the buried individual could not be performed due to the lack of preserved long bones.

3.2.1.5.7 Paleopathologies: determination of health

The presence of paleopathologies was not detected in the observed bones.

3.2.1.5.8 Enthesopathies: determination of activity markers

The presence of enthesopathies was not detected in the observed bones.

3.2.1.6 Grave 9

3.2.1.6.1 The container



Sector	3
Structure number	2022/13
Location	Locus 150.2
Period	Ninevite 5 (2900 – 2550 BCE) First half of the 3rd millennium BCE Early Bronze Age
Architectural phase	The construction of the grave occurred during the period of rapid transitional architecture, specifically phases 5A and 4B. Consequently, it can be posited that the existence of life and death within the site may have been contemporaneous.
Type of container	Simple pit with a funerary urn and a lid.
Morphology	The simple pit is oval in shape and the funerary urn has a jar morphology.

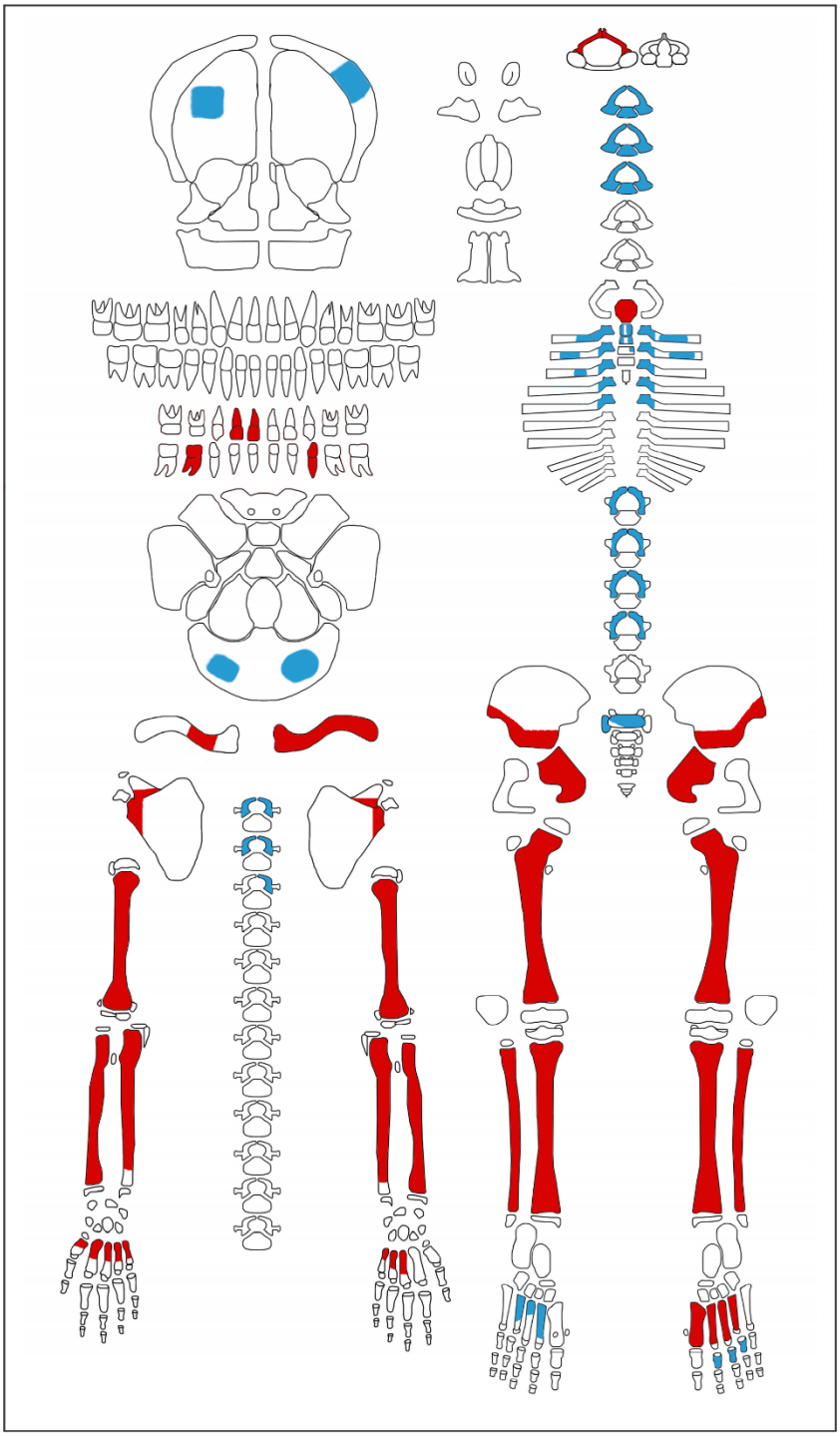
3.2.1.6.2 The content

Number of buried individuals	1
Form of disposal	Primary inhumation
State of preservation	Poorly preserved
Body orientation	East-West
Face orientation	To the ground
Position	Seated
Skeletal articulation	Disarticulated
Ornaments	None
Grave goods	None

3.2.1.6.3 Osteology: bone identification

Visual recording form - Newborn (Roksandic, 2003)

GRAVE 9



3.2.1.6.4 Determination of sex

The absence of any sexual trait did not allow to determine the sex of the individual.

3.2.1.6.5 Determination of age

Age has been determined by tooth development according to Schour & Massler (1941), Gustafson & Koch (1974) and AlQahtani et al. (2010), by epiphyseal fusion of the bones from the postcrania according to Schaefer et al. (2009), as well as by diaphyseal metrics according to Ubelaker (1984). Tooth development provides an approximate estimated age of < 2 years. Epiphyseal fusion reveals that all the bones are unfused because the epiphyses have not been yet formed, indicating an age of < 1 year. Diaphyseal metrics provide an approximate age range between newborn and < 5 months. Therefore, the estimated age range is approximately between newborn and 1 year, classified as a fetus or an infant according to Buikstra & Ubelaker (1997).

3.2.1.6.6 Stature estimation

The estimation of the stature of the buried individual was not performed due to the lack of epiphyseal fusion of the long bones. Nevertheless, the maximum length of the best-preserved and complete bones was measured (**Table 19**).

Table 19. Measures from the preserved long bones (in centimeters).

Side	Bone	Length (in cm)	Side	Bone	Length (in cm)
Right	Humerus	5.2	Left	Humerus	3.5
	Radius	4.3		Radius	3.9
	Ulna	5.1		Ulna	4
	Femur	4.5		Femur	4.9
	Tibia	3.6		Tibia	4.8
	Fibula	4.5		Fibula	3.8

3.2.1.6.7 Paleopathologies: determination of health

The presence of periostitis, an inflammatory reaction of the periosteum (Baxarias & Herrerín, 2008; Roberts & Buikstra, 2019), has been identified in the individual's ribs. New periosteal reactive bone formation has been observed in the caudal edges of two left ribs. The etiology of

the injuries is likely multifactorial, and the age of the individual is a contributing factor to the difficulty of establishing a probable cause.

3.2.1.6.8 Enthesopathies: determination of activity markers

The presence of enthesopathies was not detected in the observed bones.

3.2.1.7 Grave 10

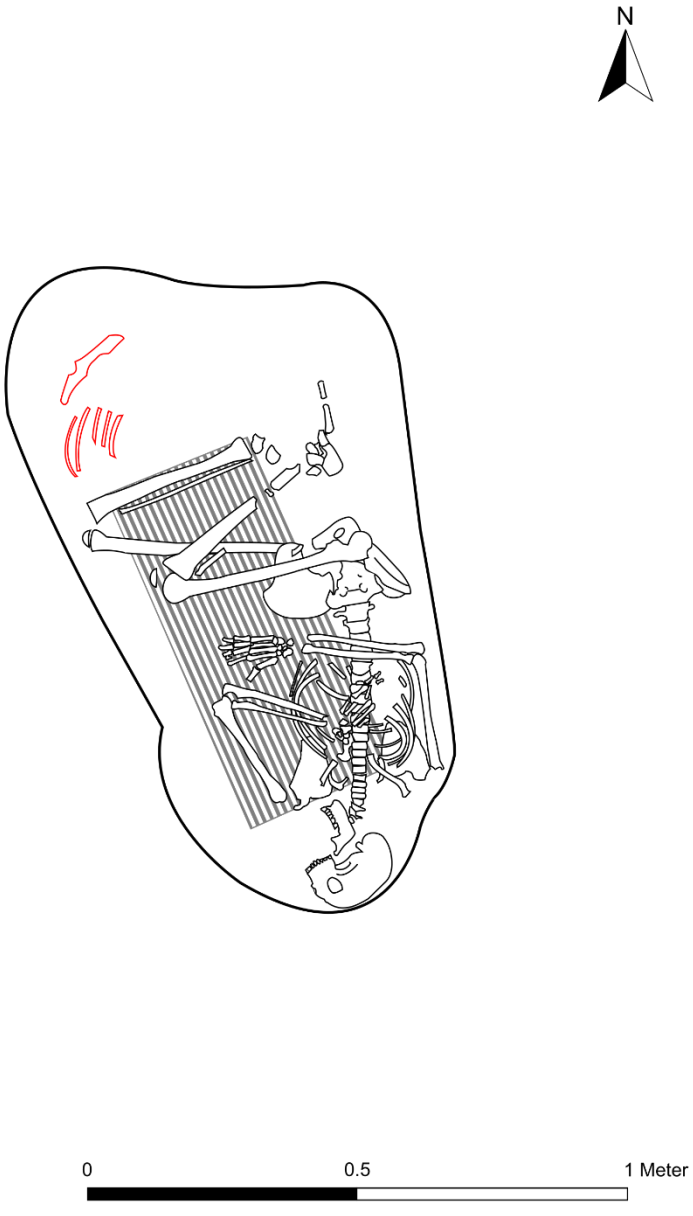
3.2.1.7.1 The container



Sector	3
Structure number	2022/15
Location	Locus 143.3
Period	Ninevite 5 (2900 – 2550 BCE) First half of the 3rd millennium BCE Early Bronze Age
Architectural phase	The construction of the grave occurred during the period of rapid transitional architecture, specifically phases 5A and 4B. Consequently, it can be posited that the existence of life and death within the site may have been contemporaneous.
Type of container	Simple pit

Morphology	Oval shape

3.2.1.7.2 The content



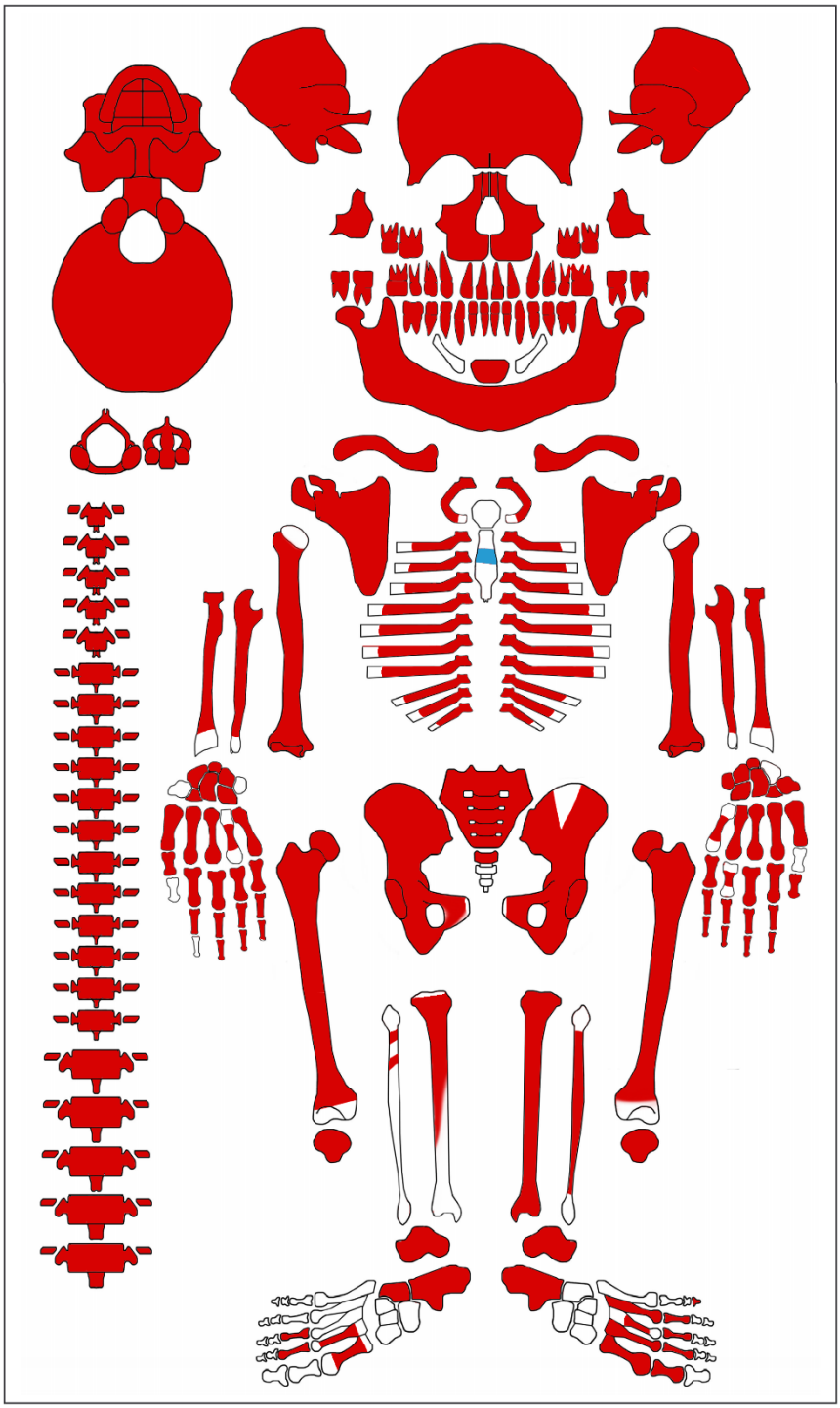
Number of buried individuals	1
Form of disposal	Primary inhumation
State of preservation	Poorly preserved
Body orientation	Northeast-Southwest
Face orientation	West
Position	Supine decubitus with the legs flexed to the left side. The left arm is positioned over the chest, while the right arm is placed over the abdomen. The right hand was held in a

	slightly closed position, while the left foot was positioned in an unnatural direction, facing the head.
Skeletal articulation	Articulated
Ornaments	None
Grave goods	A rack of pork, accompanied by the *os coxae* of a pig, positioned beneath the feet of the deceased.

3.2.1.7.3 Osteology: bone identification

Visual recording form - Adult (Roksandic, 2003)

GRAVE 10



3.2.1.7.4 Determination of sex

The determination of sex was based on cranial (Acsádi & Nemeskéri, 1970) and coxal (Buikstra & Ubelaker, 1997) features. The cranial features that have been preserved include the nuchal crest, the mastoid processes, the supraorbital margins, the glabella and the mental eminence. The preserved characteristics are indicative of a female classification (see **Table 20**). The coxal feature that has been preserved in both *os coxae* is the greater sciatic notch, which are broad, being characteristic of a female sex. The preauricular sulcus is only observable in the right *os coxae*, whose characteristics indicate a female sex. A thorough analysis of the *os pubis* and the Phenice traits (1969) in the right *os coxae* reveals the absence of the subpubic concavity, characteristic of male sex, and the presence of a ridge in the medial aspect of the ischio-pubic ramus, characteristic of female sex. The sum of all the characteristics suggest that the individual was of female sex.

Table 20. Scores for the cranial features to determine sex.

Cranial feature	Right side	Center	Left side
Nuchal crest		1 (Female)	
Mastoid process	2 (Probably female)		1 (Female)
Supraorbital margin	4 (Probably male)		3 (Indeterminate)
Supraorbital ridge / Glabella		1 (Female)	
Mental eminence		1 (Female)	

3.2.1.7.5 Determination of age

The determination of age was based on the cranial sutures in the vault according to Meindl & Lovejoy (1985), on the examination of tooth wear attrition in permanent molars following Brothwell (1981), which has also been adapted in T. D. White et al. (2012), and on epiphyseal fusion of the bones from the postcrania according to Schaefer et al. (2009)**Table 14**. The cranial sutures in the vault provide an age range between 19 to 50 years, with an average estimated age of 45.2 years (see **Table 21**).

Table 21. Cranial suture fusion sites of the vault and the given scores.

Site	Score
Midlambdoid	2
Lambda	2
Obelion	2
Anterior sagittal	2
Bregma	2

Midcoronal	2
Pterion	Not observable
Sphenofrontal	Not observable
Inferior sphenotemporal	Not observable
Superior sphenotemporal	2

Regarding the epiphyseal fusion of the bones from the postcrania, the second and third vertebrae of the sacrum are fused. The fusion of the four last vertebrae of the sacrum is complete before the age of 25 years (Ríos et al., 2008).

The analysis of the dental attrition estimates an age range between 17 and 25 years (**Table 22**). The epiphyseal fusion of the long bones indicates an estimated age of > 20 years. The results of the three methods suggest an approximated estimated age of 20 to 25 years, classified as a young adult according to Buikstra & Ubelaker (1997).

Table 22. Scores of dental attrition in permanent molars (in anthropological notation).

Tooth	Score	Estimated age (in years)
^{1}M	3+	25 – 35
^{2}M	2	17 – 25
^{3}M	2	17 – 25
M^{1}	2	17 – 25
M^{2}	2	17 – 25
$_{1}$M	2+	17 – 25
$_{2}$M	2	17 – 25
$_{3}$M	1	17 – 25
M$_{1}$	2+	17 – 25
M$_{2}$	2	17 – 25
M$_{3}$	1	17 – 25

3.2.1.7.6 Stature estimation

In order to estimate the stature of the buried individual, the maximum length of the best-preserved and complete bones was measured (**Table 23**). The regression equations for white males, according to Trotter (1970) were employed. The estimated range of stature varied between 135.2 and 163.5 centimeters, with an average of 149.3 centimeters.

Table 23. Measures from the preserved long bones (in centimeters).

Side	Bone	Length (in cm)	Side	Bone	Length (in cm)
Right	Humerus	27.5	Left	Humerus	27.5
	Radius	22		Radius	20.5
	Ulna	22.5		Ulna	23
	Femur	39.5		Femur	37.5
	Tibia	33.5		Tibia	31
	Fibula	Not observable		Fibula	27

3.2.1.7.7 Paleopathologies: determination of health

Teeth present various paleopathologies, including tooth decay (caries) and defects of the enamel. Caries has been observed on the interproximal side of the P^2, and on the occlusal and cervical sides of the $_3M$. (P^1, P^2, ^1P, ^2P, I_2, C_x, P_1, $_1I$, $_2I$ and $_xC$), and the pulp chamber is exposed on C^x. The defects in the enamel consist of linear hypoplasias present in both mandibular canines. According to the Swärdstedt (1966) equations, the enamel formation was disturbed repeatedly at the ages of 1.6 and 2.1 years (**Table 24**). A pronounced plane-form defect in the enamel is observable in one premolar and three third molars (^3M, $_1P$, $_3M$ and M_3) (see **Figure 34**). This indicates an abrupt interruption in matrix secretion for the majority of ameloblasts (Hillson, 2014). This disruption can be attributed to a stress episode, during which elevated cortisone levels inhibit protein synthesis (Lewis, 2018). Nonetheless, a multitude of factors have been identified as potential contributors to the development of hypoplasia. Among these, malnutrition, psychosocial stress, and infections during the process of tooth development have been documented as the most prevalent in prehistoric societies (Hillson, 2014).

Table 24. Measures of the enamel hypoplasia, only recorded in first superior incisors and inferior canines.

Tooth	Number of grooves	Distance from the groove to the cemento-enamel junction (in mm)	Height of the crown (in mm)
$_xC$	2	2 and 3	11



Figure 34. ^{3}M with a pronounced plane-form defect in the enamel.

Osteoporosis is characterized by reduced bone density and microarchitectural deterioration of bone tissue, leading to increased bone fragility and a high risk of fractures (Lin & Lane, 2004). Lesions related to osteoporosis have been identified in the upper limbs of the deceased. The affected bones in the arms are the proximal epiphyses of the right radius, the right ulna, and the left ulna, as well as the distal epiphysis of the left humerus. The affected bones in the hands are the fingers, including the metacarpals, the proximal phalanges and the intermediate phalanges. All these injuries can result in a significant reduction in the mobility and use of the hands and arms.

3.2.1.7.8 Enthesopathies: determination of activity markers

The presence of enthesopathies was not detected in the observed bones.

3.2.1.8 Grave 11

3.2.1.8.1 The container

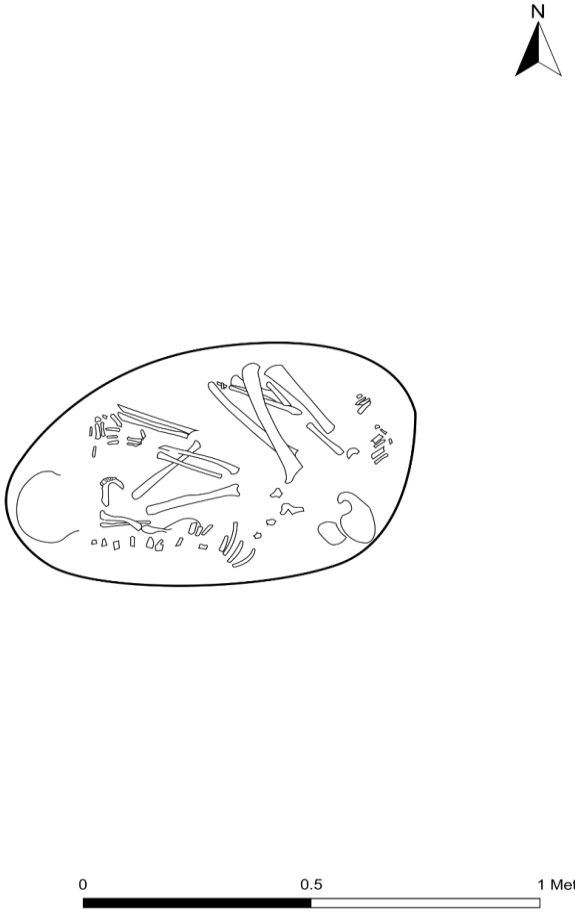


Sector	3
Structure number	2022/31
Location	Locus 157.2
Period	Ninevite 5 (2900 – 2550 BCE) First half of the 3rd millennium BCE Early Bronze Age
Architectural phase	The construction of the grave occurred during the architectural phase 5A. Consequently, it can be posited that the existence of life and death within the site may have been contemporaneous.
Type of container	Simple pit
Morphology	Oval shape

3.2.1.8.2 The content

TELL LASHKIR

Grave 11

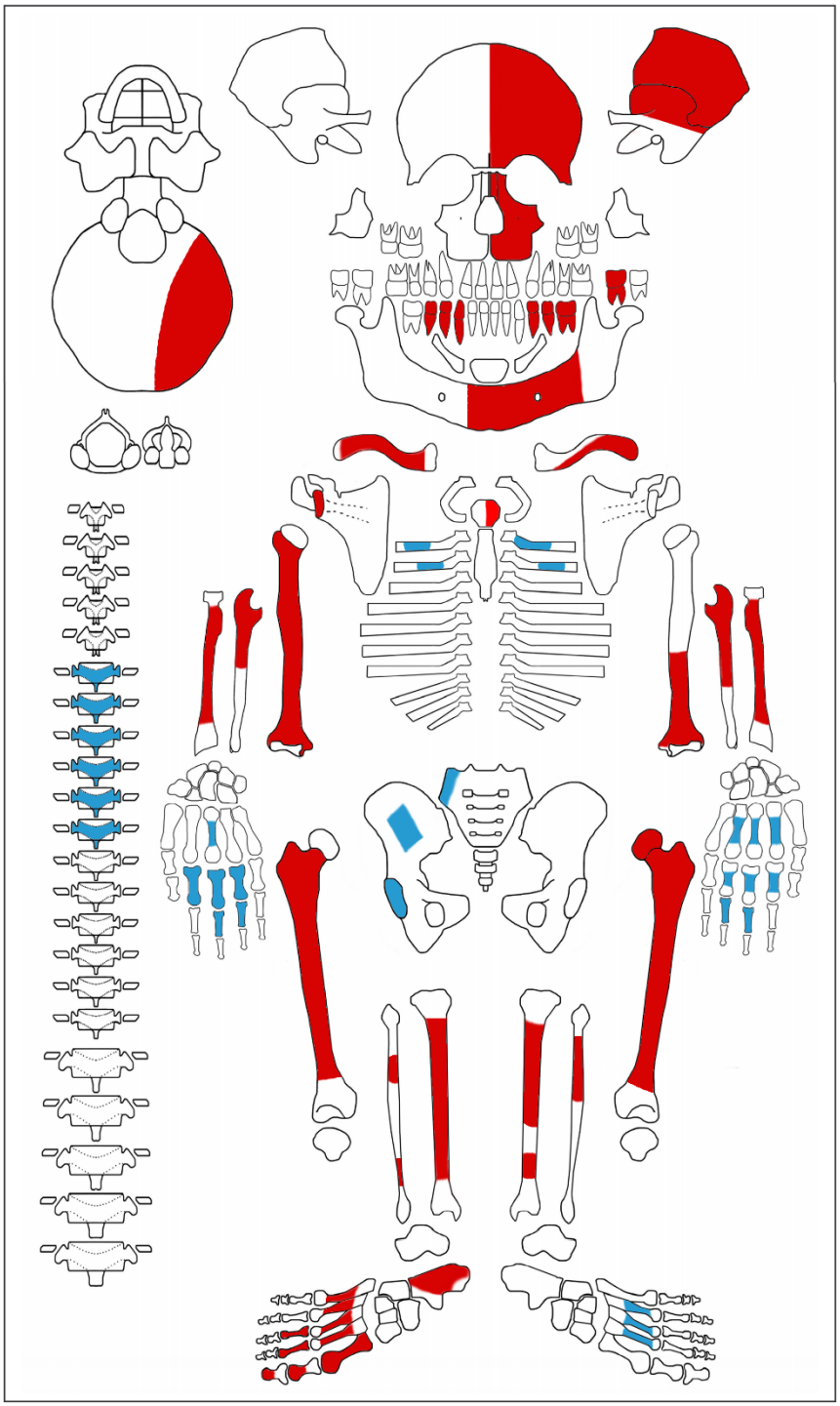


Number of buried individuals	1
Form of disposal	Primary inhumation
State of preservation	Poorly preserved
Body orientation	Southwest-Northeast
Face orientation	North
Position	Left lateral decubitus with hyperflexed limbs.
Skeletal articulation	Articulated
Ornaments	None
Grave goods	None

3.2.1.8.3 Osteology: bone identification

Visual recording form - Adult (Roksandic, 2003)

GRAVE 11



3.2.1.8.4 Determination of sex

The determination of sex was based on cranial features (Acsádi & Nemeskéri, 1970). The only

observable and preserved feature is the mental eminence, whose characteristics are indicative of a male classification (see **Table 25**).

Table 25. Scores for the cranial features to determine sex.

Cranial feature	Right side	Center	Left side
Nuchal crest		Not observable	
Mastoid process	Not observable		Not observable
Supraorbital margin	Not observable		Not observable
Supraorbital ridge / Glabella		Not observable	
Mental eminence		5 (Male)	

3.2.1.8.5 Determination of age

The determination of age was based on the examination of tooth wear attrition in permanent molars following Brothwell (1981), which has also been adapted in T. D. White et al. (2012). The analysis estimates an age range between 17 and 25 years (**Table 26Table 22**), classified as an adolescent or a young adult according to Buikstra & Ubelaker (1997).

Table 26. Scores of dental attrition in permanent molars (in anthropological notation).

Tooth	Score	Estimated age (in years)
$_1$M	2	17-25
$_2$M	2	17-25

3.2.1.8.6 Stature estimation

The estimation of the stature of the buried individual was not performed due to the poor state of preservation of the long bones.

3.2.1.8.7 Paleopathologies: determination of health

The presence of paleopathologies was not detected due to the poor state of preservation of the bones and to the presence of abundant mineral concretions.

3.2.1.8.8 Enthesopathies: determination of activity markers

The only enthesopathy detected was a moderate level of robustness in the supinator crest of the right ulna. This condition is prevalent among individuals experiencing significant labor stress in the upper extremities, with a higher incidence observed in males and on the right side of the body (Baxarias & Herrerín, 2008).

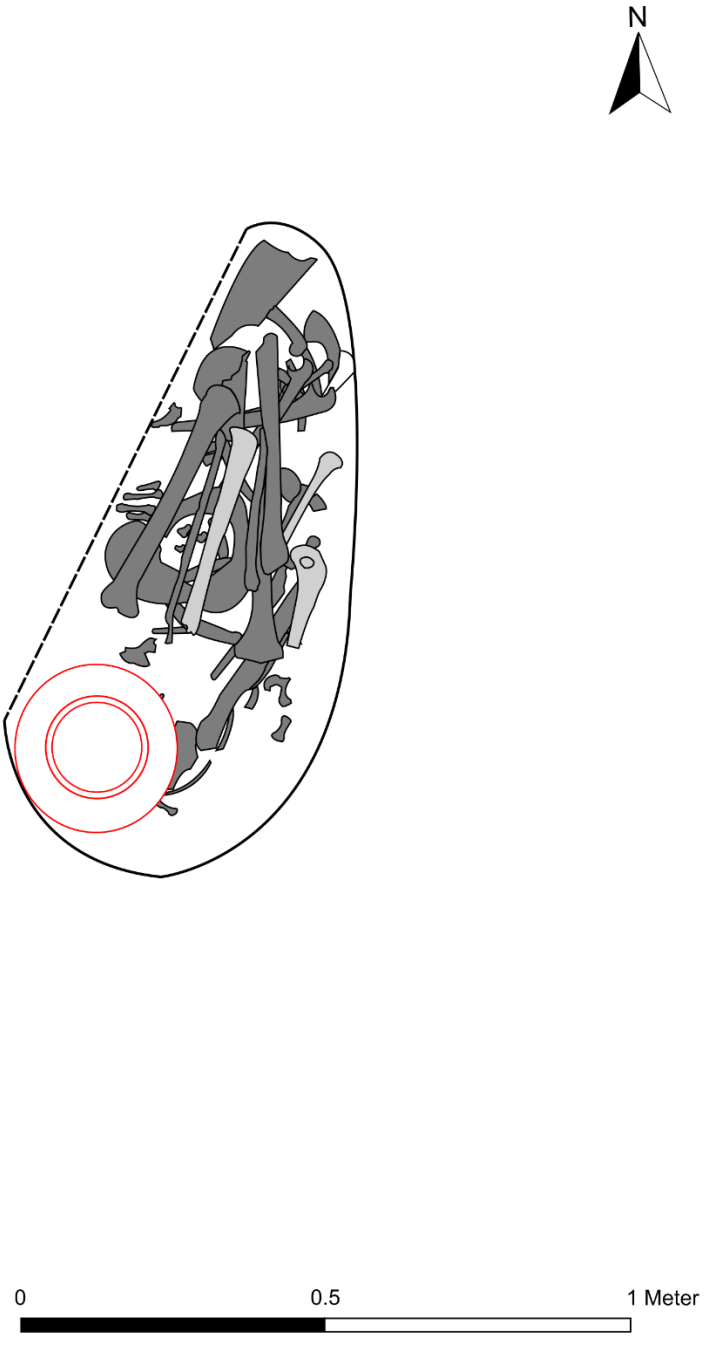
3.2.1.9 Grave 12

3.2.1.9.1 The container



Sector	Chanel
Structure number	2023/2
Location	Locus 3.5
Period	Ninevite 5 (2900 – 2550 BCE) First half of the 3rd millennium BCE Early Bronze Age
Architectural phase	Not determined
Type of container	Simple pit
Morphology	Oval shape

3.2.1.9.2 The content



Number of buried individuals	3
Form of disposal	Secondary inhumation
State of preservation	Poorly preserved
Body orientation	Not observable
Face orientation	Not observable

3.2.1.9.2.1 Individual 1 (Grave 12.1)

Position	Comingled bones
Skeletal articulation	Disarticulated
Ornaments	None
Grave goods	One jar with incised decorations

3.2.1.9.2.2 Individual 2 (Grave 12.2)

Position	Comingled bones
Skeletal articulation	Disarticulated
Ornaments	None
Grave goods	One jar with incised decorations

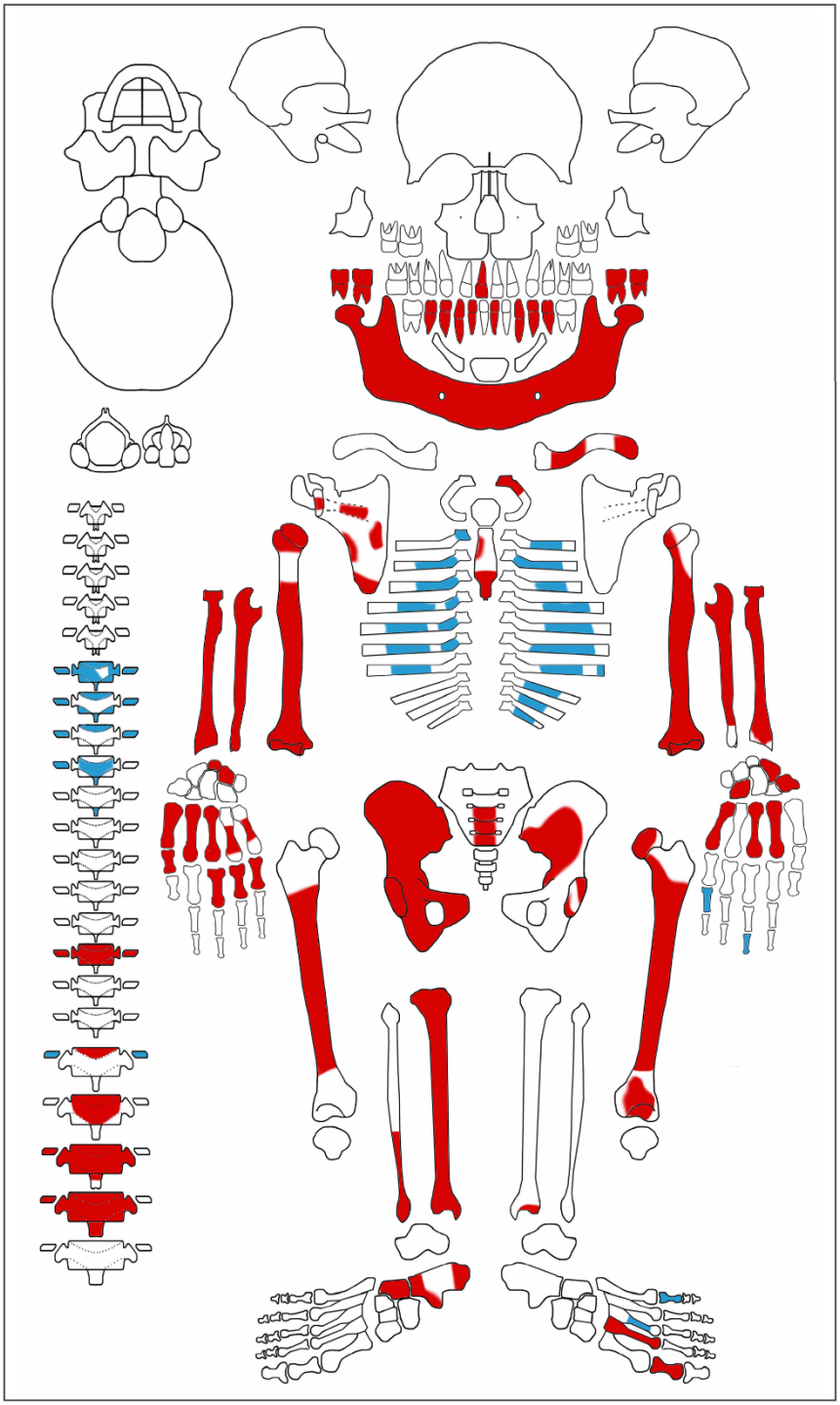
3.2.1.9.2.3 Individual 3 (Grave 12.3)

Position	Comingled bones
Skeletal articulation	Disarticulated
Ornaments	None
Grave goods	One jar with incised decorations

3.2.1.9.2.4 Individual 1

Visual recording form - Adult (Roksandic, 2003)

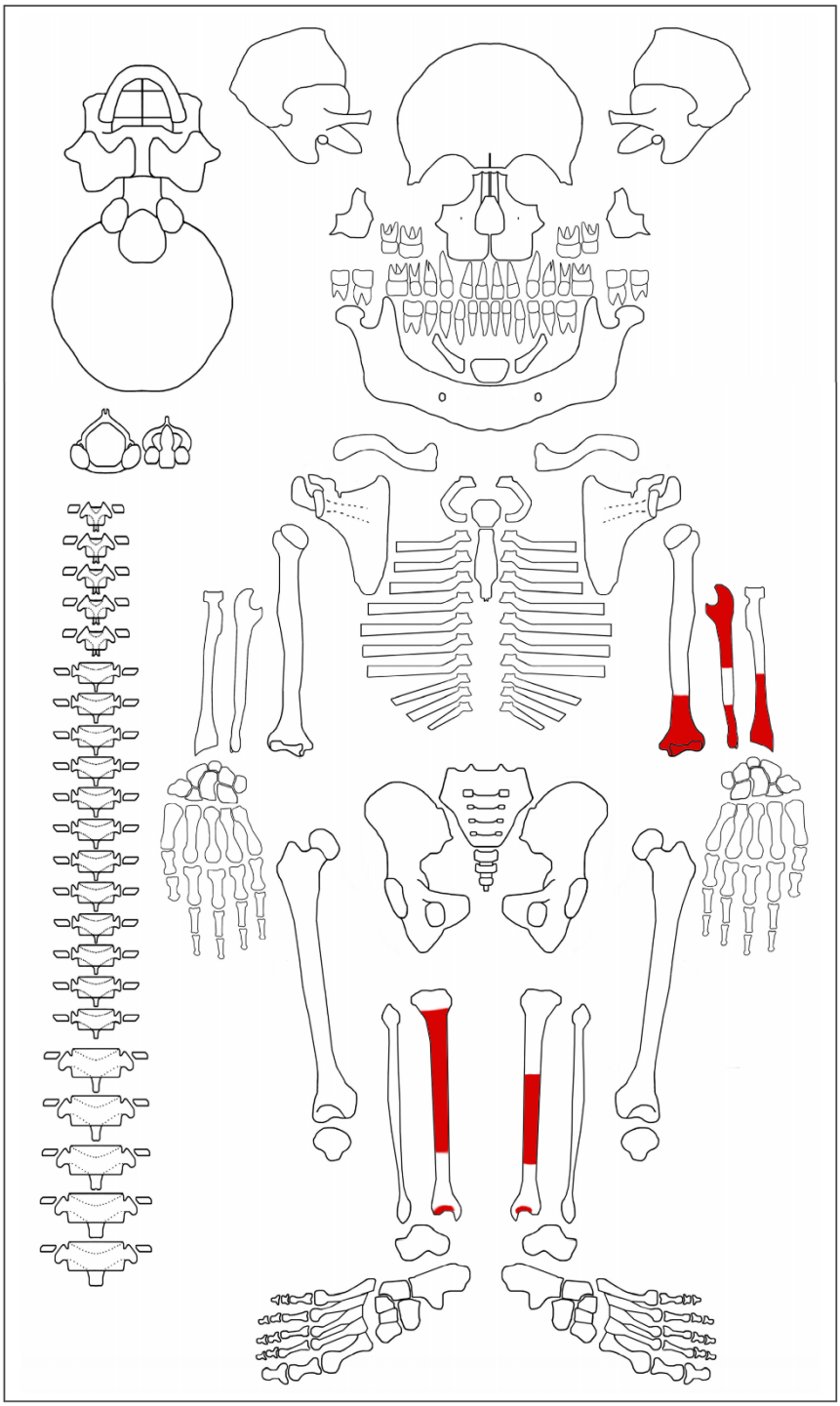
GRAVE 12 - Individual 1



3.2.1.9.2.5 Individual 2

Visual recording form - Adult (Roksandic, 2003)

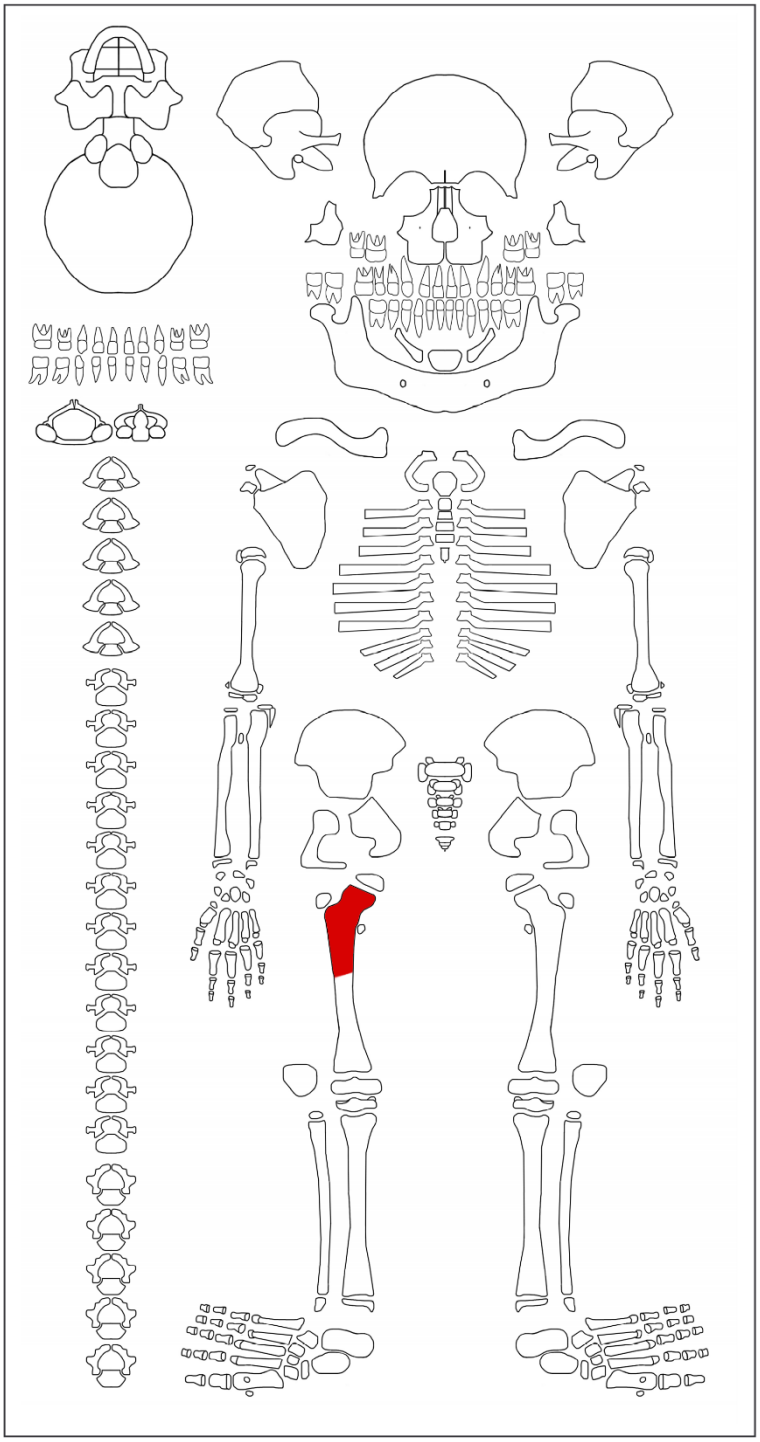
GRAVE 12 - Individual 2



3.2.1.9.2.6 Individual 3

Visual recording form - Child (Roksandic, 2003)

GRAVE 12 - Individual 3



The only bone that can be attributed to this individual is a proximal fragment of the right femur.

3.2.1.9.3 Determination of sex

3.2.1.9.3.1 Individual 1

The determination of sex was based on cranial (Acsádi & Nemeskéri, 1970) and coxal (Buikstra & Ubelaker, 1997) features. The cranial features that have been preserved include the mental eminence. The preserved characteristics are indicative of a male classification (see **Table 27**). Coxal features have been identified in both *os coxae*. The coxal feature that has been preserved in both *os coxae* is the greater sciatic notch, which are narrow, being characteristic of a male sex. A thorough analysis of the *os pubis* and the Phenice traits (1969) from the right *os coxae* reveals the absence of a subpubic concavity, and of a flat surface in the medial aspect of the ischio-pubic ramus, characteristic of male sex.

Table 27. Scores for the cranial features to determine sex.

Cranial feature	Right side	Center	Left side
Nuchal crest		Not observable	
Mastoid process	Not observable		Not observable
Supraorbital margin	Not observable		Not observable
Supraorbital ridge / Glabella		Not observable	
Mental eminence		5 (Male)	

3.2.1.9.3.2 Individual 2

The absence of any sexual trait did not allow to determine the sex of the individual.

3.2.1.9.3.3 Individual 3

The absence of any sexual trait did not allow to determine the sex of the individual.

3.2.1.9.4 Determination of age

3.2.1.9.4.1 Individual 1

The determination of age was based on the examination of tooth wear attrition, and on the development of the pubic symphysis. The analysis of dental attrition in permanent molars was conducted following Brothwell (1981), which has also been adapted in T. D. White et al. (2012)

(see **Table 28**). The estimated age range is between 33 and 45 years. According to the Todd system (1920), the development of the pubic symphysis in the right *os coxae* is assigned to the ninth phase, whose age range is determined to be between 44 and 50 years. According to the Suchey-Brooks system (Brooks & Suchey, 1990), the development of the pubic symphysis in the right *os coxae* is assigned to Phase 5. The 95% age range is determined to be between 27 and 66 years, with a mean age of 45.6 years. The sum of all the methods for age determination indicates an approximated estimated age of 44 to 45 years, classified as a middle adult according to Buikstra & Ubelaker (1997).

Table 28. Scores of dental attrition in permanent molars (in anthropological notation).

Tooth	Score	Estimated age (in years)
M_2	5+	33 – 45
M_3	5+	33 – 45

3.2.1.9.4.2 Individual 2

Age was determined by the epiphyseal fusion of the long bones. The evidence suggests an estimated age above 20 years.

3.2.1.9.4.3 Individual 3

Age was determined by the epiphyseal development of the right femur, as described by Schaefer et al. (2009). This method provides an approximate estimated age of 1 year, which corresponds to the classification of an infant, as defined by Buikstra & Ubelaker (1997).

3.2.1.9.5 Stature estimation

3.2.1.9.5.1 Individual 1

The estimation of the stature of the buried individual was not performed due to the poor state of preservation of the long bones.

3.2.1.9.5.2 Individual 2

The estimation of the stature of the buried individual was not performed due to the poor state of preservation of the long bones.

3.2.1.9.5.3 Individual 3

The estimation of the stature of the buried individual was not performed due to the lack of epiphyseal fusion of the long bones and to the scarce remains available.

3.2.1.9.6 Anatomical variations

3.2.1.9.6.1 Individual 1

Two anatomical variations have been observed in the bones of the deceased, including the mandible and the right ulna. The genial tubercles, defined as prominent insertional spines at the mandibular insertion of the geniohyoid and genioglossus muscles (Bernaerts et al., 2006), are located on the left side of the bone (**Figure 35**). These muscles are responsible for elevating the mandible and facilitating mastication. This condition has been observed to be a congenital variation that is attributable to genetic factors or sexual dimorphism, with the manifestation being more pronounced in males.



Figure 35. Pronounced genial tubercles of the mandible.

The right ulna exhibits an anatomical anomaly in the coronoid process, manifesting as bifurcated (**Figure 36**). The condition is characterized by a rare anatomical variation whose etiology is idiopathic. The scarce references in the medical literature that could offer a more comprehensive understanding of the condition are not sufficient. However, potential explanations for the observed phenomenon include congenital variations due to genetic factors or developmental anomalies during embryogenesis, rather than pathological conditions such as an elbow dislocation. In the event that a pathological etiology is to be considered, it could be a Type A fracture in the anteromedial facet of the coronoid process, as classified by Wrightington (Al-Ani et al., 2022).



Figure 36. Bifurcated coronoid process of the right ulna.

3.2.1.9.7 Paleopathologies: determination of health

3.2.1.9.7.1 Individual 1

The studied bones present several paleopathologies, including dental diseases, periostitis, osteoarthritis, and osteoporosis. The teeth present various paleopathologies, including *antemortem*

tooth loss and defects of the enamel. The tooth that has suffered *antemortem* loss is the $_1$M, and the mandible has proceeded to the reabsorption of the alveolus. The alveolus of the M_1 also presents an eroded surface. The defects in the enamel consist of linear hypoplasias present in both mandibular canines. According to the Swärdstedt (1966) equations, the enamel formation was disturbed repeatedly at the ages of 1.4, 2.2, and 3.1 years (**Table 29**). Multiple factors can cause hypoplasia, being the most common in prehistoric societies malnutrition, psychosocial stress, or infection during tooth development (Hillson, 2014).

Table 29. Measures of the enamel hypoplasia, only recorded in first superior incisors and inferior canines.

Tooth	Number of grooves	Distance from the groove to the cemento-enamel junction (in mm)	Height of the crown (in mm)
$_x$C	3	1, 2 and 3	7

The presence of periostitis, an inflammatory reaction of the periosteum (Baxarias & Herrerín, 2008; Roberts & Buikstra, 2019), has been identified in the left ribs in the form of new periosteal reactive bone formation in the caudal edges (**Figure 37**). This reaction can result from a traumatic injury or bacterial infection (Davies-Barrett et al., 2019; Ortner, 2003). This pathology has been associated with pulmonary diseases, such as tuberculosis, given the potential for lung diseases to inflame the pleura, which can affect the bone as it attaches to the visceral surfaces of the ribs, thereby causing an inflammatory reaction on the surface of the ribs (Mariotti et al., 2015; Roberts & Buikstra, 2019).



Figure 37. Left ribs with evidence of new periosteal reaction in the caudal edges.

The vertebrae of the deceased are affected by degenerative osteoarthritis. The presence of osteophytes, defined as fibrocartilage-capped bony outgrowths (Wong et al., 2016), are located in the ninth thoracic vertebrae and in the three first lumbar vertebrae in the form of claw osteophytes (Heggeness & Doherty, 1998) in the epiphyseal rings of the vertebral bodies (**Figure 38**). The lumbar vertebral bodies also exhibit signs of slight compression, suggesting that the intervertebral disks have undergone erosion over time. These injuries are attributable to degenerative osteoarthritis that comes through the aging process (Rissech et al., 2006), which can result in a reduction in mobility.

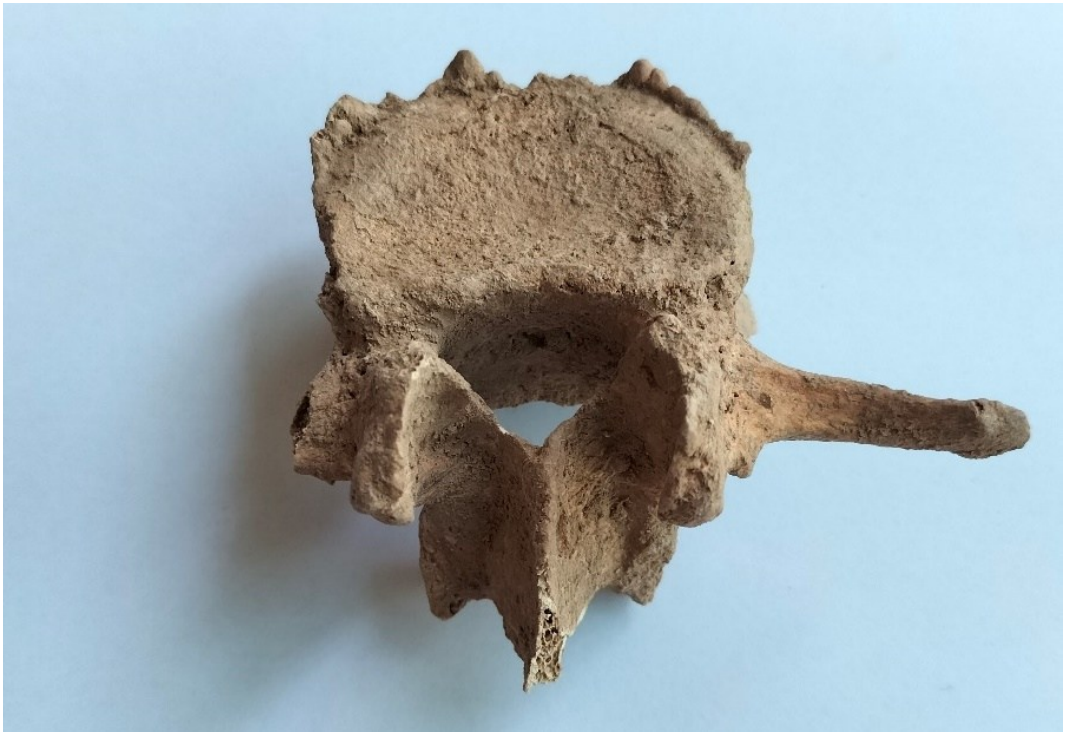


Figure 38. Claw osteophytes located in the epiphyseal ring of the vertebral body of a lumbar vertebra.

Osteoporosis is characterized by reduced bone density and microarchitectural deterioration of bone tissue, leading to increased bone fragility and a high risk of fractures (Lin & Lane, 2004). The presence of porosis is evident in the shoulder girdle, the arms, and the legs. The left clavicle is affected in the acromial facet; both humeri are affected in the distal epiphysis; both ulnae are affected in the proximal epiphysis; both radii are affected in the connection of the radial head with the radial neck; and the right tibia is affected in the tibial plateau.

3.2.1.9.7.2 Individual 2

Evidence of osteoporosis has been observed in the proximal epiphysis of the left ulna. This injury is characterized by an increased propensity for bone fragility and a high risk of fractures (Lin & Lane, 2004).

3.2.1.9.7.3 Individual 3

The presence of paleopathologies was not detected in the observed bone.

3.2.1.9.8 Enthesopathies: determination of activity markers

3.2.1.9.8.1 Individual 1

Enthesopathies have been observed in the upper limbs of the body, including the arms and the hands. The right humerus displays the presence of enthesophytes in the lateral supracondylar crest, the site of the brachioradialis muscle's attachment. This muscle is responsible for flexing the elbow. A study of the ulnae reveals the presence of enthesophytes on both the right and left sides. These enthesophytes are located in the supinator crest on the right ulna and in the lateral border of the radial tuberosity on the left ulna. The muscle that connects to both anatomical structures is the supinator muscle, which is responsible for supinating the arm when the elbow is extended. The sum of these enthesopathies suggests a repetitive use of the elbow joints.

The proximal phalanges of the right hand possess pronounced crests in the fibrous sheaths (also known as *vaginae fibrosae digitorum manus*) (see **Figure 39**). The crests are associated with a developed pulley system in the fingers, as well as increased mechanical strain on the insertions, which may result in a stronger grip (Hermann et al., 2022). This enthesopathy is frequently linked to the manipulation and holding of tools (Baxarias & Herrerín, 2008).



Figure 39. Crests in the fibrous sheaths of the right proximal hand phalanges.

3.2.1.9.8.2 Individual 2

The presence of enthesopathies was not detected in the observed bones.

3.2.1.9.8.3 Individual 3

The presence of enthesopathies was not detected in the observed bone.

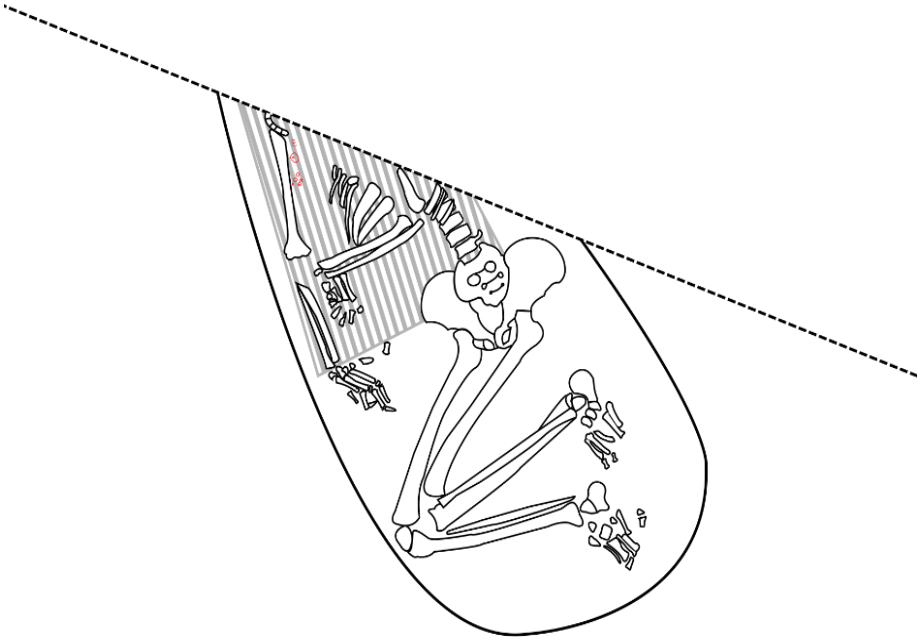
3.2.1.10 Grave 13

3.2.1.10.1 The container



Sector	3
Structure number	2023/19
Location	Locus 161.9
Period	Ninevite 5 (2900 – 2550 BCE) First half of the 3rd millennium BCE Early Bronze Age
Architectural phase	The construction of the grave occurred during the architectural phase 5A. Consequently, it can be posited that the existence of life and death within the site may have been contemporaneous.
Type of container	Simple pit
Morphology	Oval shape

3.2.1.10.2 The content

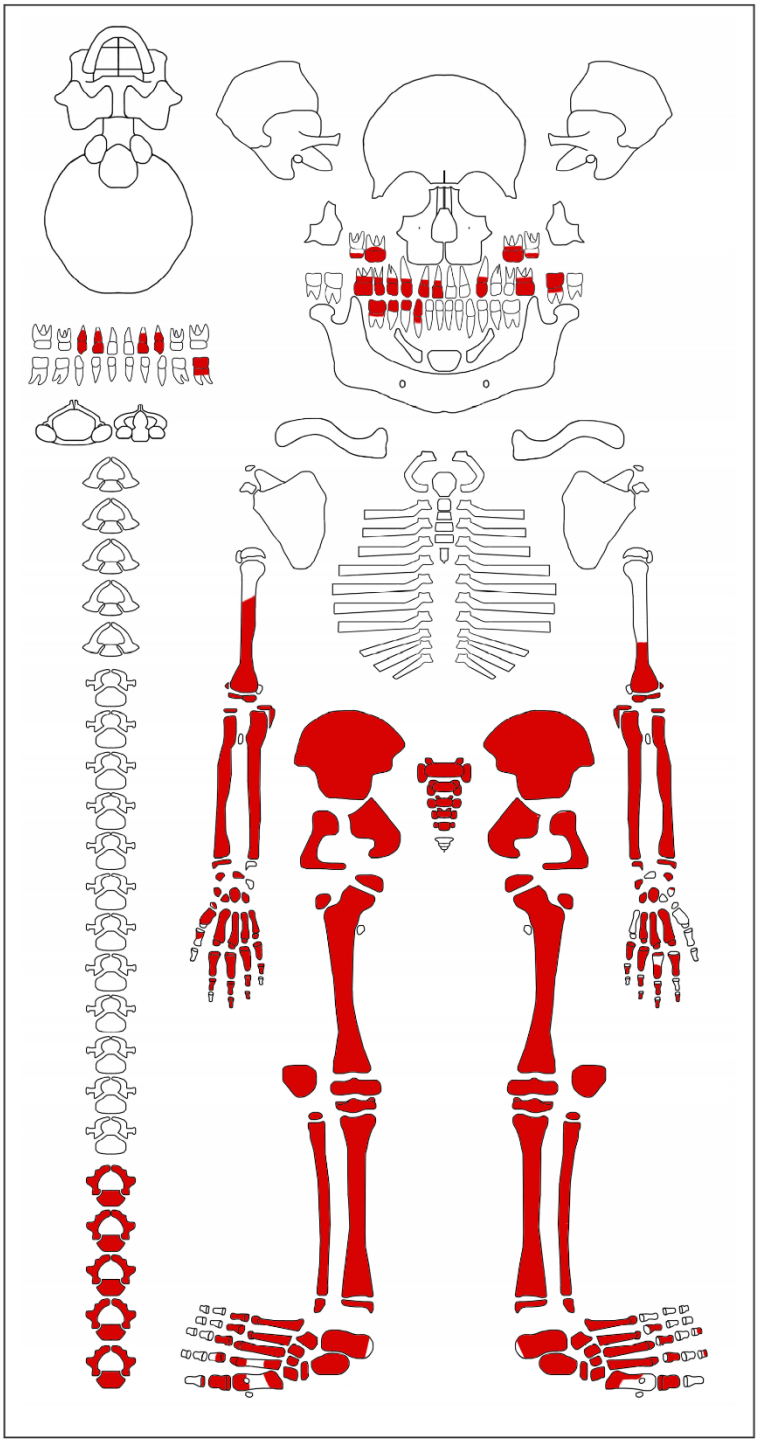


Number of buried individuals	1
Form of disposal	Primary inhumation
State of preservation	Poorly preserved
Body orientation	Northwest-Southeast
Face orientation	West
Position	Supine decubitus with the limbs flexed to the right side.
Skeletal articulation	Articulated, strictly and loose
Ornaments	One necklace made of beads of different shape and materials.
Grave goods	None

3.2.1.10.3 Osteology: bone identification

Visual recording form - Child (Roksandic, 2003)

GRAVE 13



3.2.1.10.4 Determination of sex

The absence of any sexual trait did not allow to determine the sex of the individual.

3.2.1.10.5 Determination of age

Age has been determined by tooth development according to Schour & Massler (1941), Gustafson & Koch (1974) and AlQahtani et al. (2010), and by epiphyseal fusion of the bones from the postcrania according to Schaefer et al. (2009). Tooth development provides an approximate estimated age between 7 and 8 years. Epiphyseal fusion reveals that the bones belonging to the upper and lower limbs are unfused. The arms indicate an approximate estimated age of less than 11 to 20 years; the hands, less than 14 to 16 years; the legs, less than 12 to 19 years; and the feet, less than 10 to 16 years. Consequently, the estimated age range is approximately between 7 and 8 years, a determination that is supported by the reliability of tooth development and the evidence provided by epiphyseal fusion. According to Buikstra & Ubelaker (1997), the individual is then classified as a child.

3.2.1.10.6 Stature estimation

The estimation of the stature of the buried individual was not performed due to the lack of epiphyseal fusion of the long bones. Nevertheless, the maximum length of the best-preserved and complete bones was measured (**Table 30**).

Table 30. Measures from the preserved long bones (in centimeters).

Side	Bone	Length (in cm)	Side	Bone	Length (in cm)
Right	Humerus	23	Left	Humerus	Not observable
	Radius	18		Radius	19
	Ulna	18		Ulna	19.5
	Femur	34		Femur	34
	Tibia	29		Tibia	29
	Fibula	29		Fibula	25.5

3.2.1.10.7 Paleopathologies: determination of health

The only paleopathology observed in the studied bones is a defect of the enamel. It consists of linear hypoplasias present in both maxillary canines. As no first maxillary incisors or mandibular canines were affected, the enamel hypoplasia present in the maxillary canines has been rec-

orded. According to the Swärdstedt (1966) equations, the enamel formation was disturbed repeatedly at the ages of 3.3, 4.2, and 6.1 years (**Table 31**). A multitude of factors have been identified as potential contributors to the development of hypoplasia. Among these, malnutrition, psychosocial stress, and infections during the process of tooth development have been documented as the most prevalent in prehistoric societies (Hillson, 2014).

Table 31. Measures of the enamel hypoplasia.

Tooth	Number of grooves	Distance from the groove to the cemento-enamel junction (in mm)	Height of the crown (in mm)
C^{x}	1	4	7
^{x}C	2	3 and 6	7

3.2.1.10.8 Enthesopathies: determination of activity markers

The presence of enthesopathies was not detected in the observed bone.

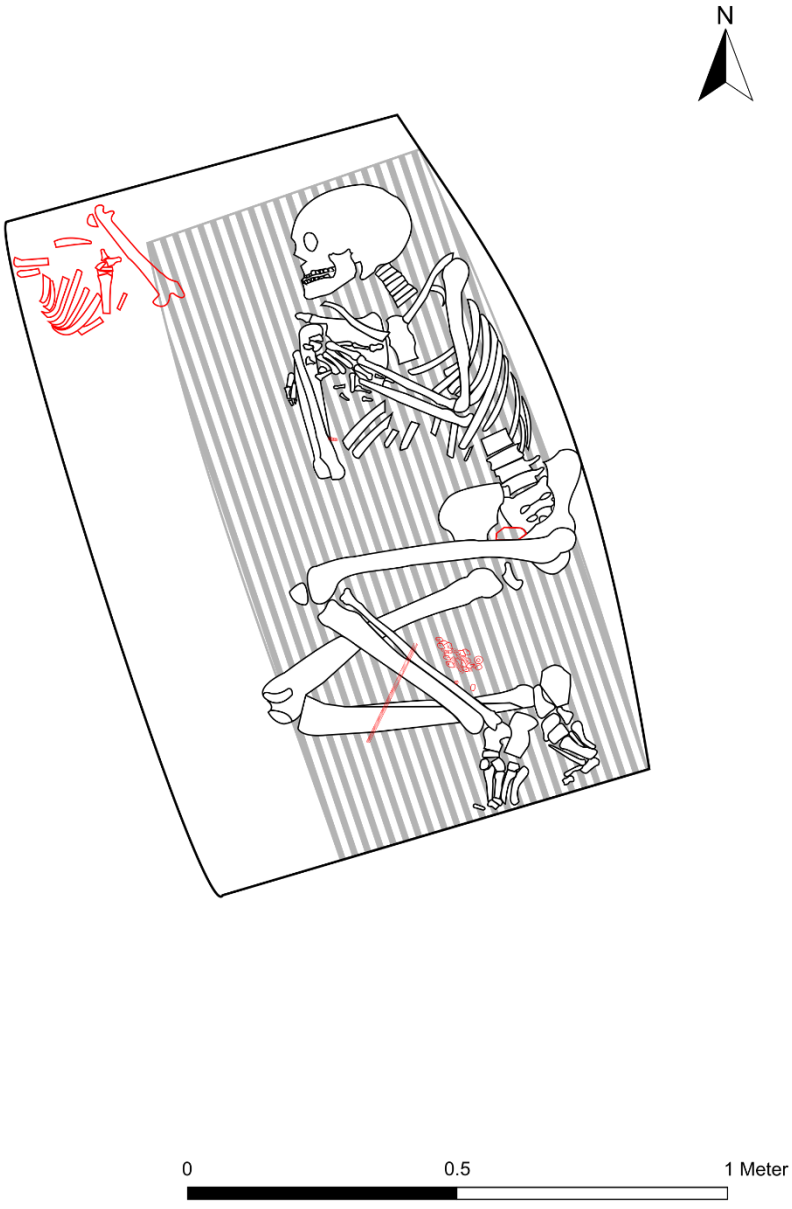
3.2.1.11 Grave 14

3.2.1.11.1 The container



Sector	3
Structure number	2023/20
Location	Locus 139.6
Period	Ninevite 5 (2900 – 2550 BCE) First half of the 3rd millennium BCE Early Bronze Age
Architectural phase	The construction of the grave occurred during the architectural phase 5A. Consequently, it can be posited that the existence of life and death within the site may have been contemporaneous.
Type of container	Mudbrick chamber
Morphology	Rectangular

3.2.1.11.2 The content



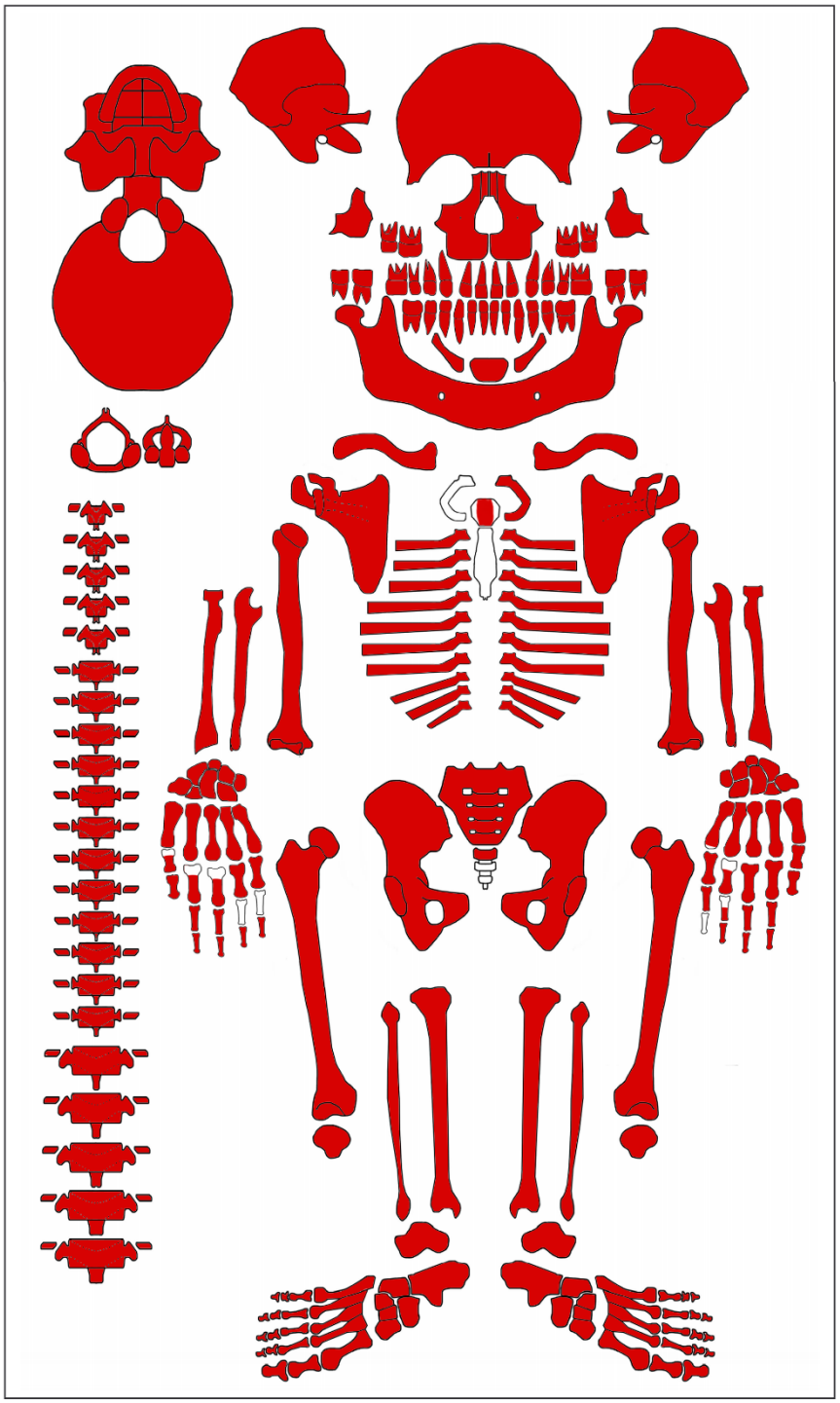
Number of buried individuals	1
Form of disposal	Primary inhumation
State of preservation	Poorly preserved
Body orientation	Southwest-Northeast
Face orientation	West
Position	Supine decubitus with the limbs flexed to the right side.
Skeletal articulation	Articulated
Ornaments	Both calves were found to have been tied up with a long necklace composed of 1,387 beads. It is composed of 802

	discoid-shaped white rock, 524 discoid-shaped black rock, 20 discoid-shaped gray rock, 5 larger discoid-shaped white rock, 33 perforated shells of the species *Engina mendicaria*, and 3 needle-eye-shaped greenish-white rock. In addition, three transparent and one green rock crystal have been identified as associated with the necklace. A second necklace composed of 67 beads was discovered in the posterior region of the calves. It is composed of 11 perforated shells of the species *Engina mendicaria*, 53 discoid-shaped white rock, 2 tubular-shaped black rock, and 1 wide tubular-shaped transparent rock.
Grave goods	One cylinder seal with geometric motives (lines and rhombs with dots inside) was placed over the right forearm, a flint tool was placed over the coccyx, and a rack and two legs of an ovicaprid were placed in front of the face.

3.2.1.11.3 Osteology: bone identification

Visual recording form - Adult (Roksandic, 2003)

GRAVE 14



3.2.1.11.4 Determination of sex

The determination of sex was based on cranial (Acsádi & Nemeskéri, 1970) and coxal (Buikstra & Ubelaker, 1997) features. The cranial features that have been preserved include the nuchal

crest, the left mastoid process, the right supraorbital margin, and the mental eminence. The preserved characteristics are indicative of a male classification (see **Table 32**). The coxal features are only observable in the right *os coxae*. The greater sciatic notch is narrow, being characteristic of a male sex. The analysis of the *os pubis* and the Phenice traits (1969) reveals the absence of the subpubic concavity, which is characteristic of male sex.

Table 32. Scores for the cranial features to determine sex.

Cranial feature	Right side	Center	Left side
Nuchal crest		5 (Male)	
Mastoid process	Not observable		4 (Probably Male)
Supraorbital margin	4 (Probably Male)		Not observable
Supraorbital ridge / Glabella		Not observable	
Mental eminence		4 (Probably Male)	

3.2.1.11.5 Determination of age

The determination of age was based on the examination of tooth wear attrition in permanent molars following Brothwell (1981), which has also been adapted in T. D. White et al. (2012). The analysis estimates an age above 45 years (**Table 33Table 22**), classifying the individual as a middle adult according to Buikstra & Ubelaker (1997).

Table 33. Scores of dental attrition in permanent molars (in anthropological notation).

Tooth	Score	Estimated age (in years)
^{1}M	5+	> 45
^{2}M	5+	> 45
^{3}M	5+	> 45
M^{1}	5+	> 45
M^{2}	5++	> 45
M^{3}	5+	> 45
$_{1}$M	5+	> 45
$_{2}$M	5+	> 45
$_{3}$M	1	17 – 25
M$_{1}$	5++	> 45
M$_{2}$	5+	> 45
M$_{3}$	5+	> 45

3.2.1.11.6 Stature estimation

In order to estimate the stature of the buried individual, the maximum length of the best-preserved and complete bones was measured (**Table 34**). The regression equations for white males, according to Trotter (1970) were employed, as well as the modification equation for individuals over 30 years of age. If the deceased was 45 years of age, the estimated stature would range between 159.6 and 216.6 centimeters, with an average of 188.1 centimeters.

Table 34. Measures from the preserved long bones (in centimeters).

Side	Bone	Length (in cm)	Side	Bone	Length (in cm)
Right	Humerus	32	Left	Humerus	32
	Radius	35.5		Radius	27.5
	Ulna	27		Ulna	31
	Femur	43		Femur	43
	Tibia	37		Tibia	37
	Fibula	36.5		Fibula	36

3.2.1.11.7 Paleopathologies: determination of health

Only two paleopathologies have been observed in the studied bones, which consist of defects of the tooth enamel and osteoporosis. The defect in the dental enamel consists of linear hypoplasias present in both mandibular canines. According to the Swärdstedt (1966) equations, the enamel formation was disturbed repeatedly at the ages of 1.4, 1.8, 3.1, and 3.5 years (**Table 35**). A multitude of factors have been identified as potential contributors to the development of hypoplasia. Among these, malnutrition, psychosocial stress, and infections during the process of tooth development have been documented as the most prevalent in prehistoric societies (Hillson, 2014).

Table 35. Measures of the enamel hypoplasia, only recorded in first superior incisors and inferior canines.

Tooth	Number of grooves	Distance from the groove to the cemento-enamel junction (in mm)	Height of the crown (in mm)
C_x	2	1 and 3.5	7
$_xC$	2	1.5 and 3	7

Osteoporosis is characterized by reduced bone density and microarchitectural deterioration of bone tissue, leading to increased bone fragility and a high risk of fractures (Lin & Lane, 2004). The presence of porosis is evident in both hands and feet. Lesions can be found in the metacarpals of the hands at the distal epiphyses, as well as in the different facets of the tarsals and in the metatarsals of the feet in both the proximal and distal epiphyses. These injuries can result in a significant reduction in the mobility and use of the hands and arms.

3.2.1.11.8 Enthesopathies: determination of activity markers

The proximal phalanges of both the right and left hands possess pronounced crests in the fibrous sheaths (also known as *vaginae fibrosae digitorum manus*) (**Figure 40**). The crests are associated with a developed pulley system in the fingers, as well as increased mechanical strain on the insertions, which may result in a stronger grip (Hermann et al., 2022). This enthesopathy is frequently linked to the manipulation and holding of tools (Baxarias & Herrerín, 2008).



Figure 40. Proximal hand phalanges of the left hand. Pronounced crests in the fibrous sheaths are observable on both sides of the palmar view of the bone.

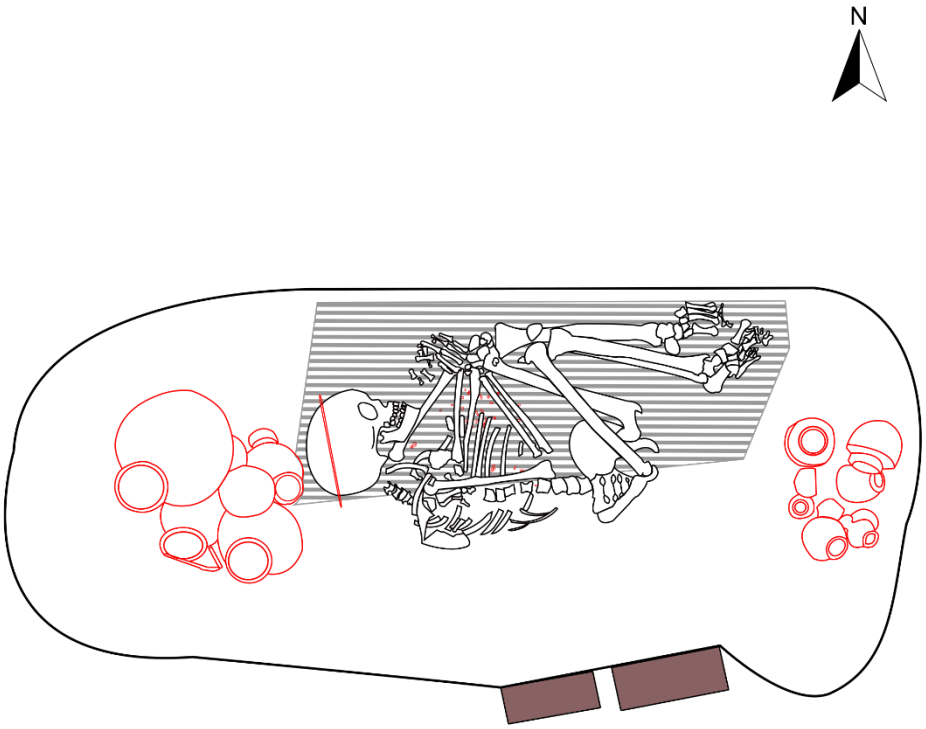
3.2.1.12 Grave 15

3.2.1.12.1 The container



Sector	3
Structure number	2023/21
Location	Locus 168.2
Period	Ninevite 5 (2900 – 2550 BCE) First half of the 3rd millennium BCE Early Bronze Age
Architectural phase	The construction of the grave occurred during the period of rapid transitional architecture, specifically phases 5A and 5B. Consequently, it can be posited that the existence of life and death within the site may have been contemporaneous.
Type of container	Simple pit
Morphology	Oval shape

3.2.1.12.2 The content



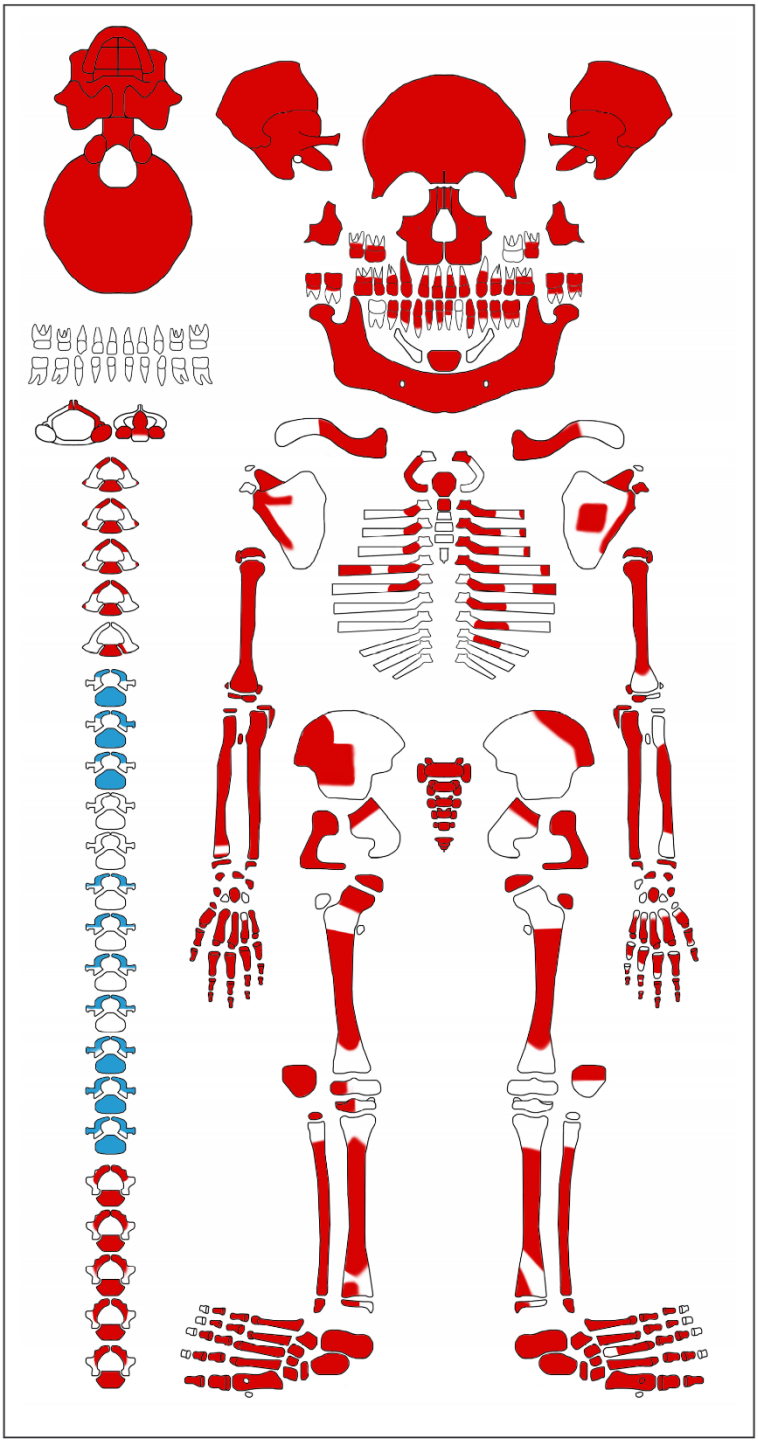
Number of buried individuals	1
Form of disposal	Primary inhumation
State of preservation	Poorly preserved and partially burned
Body orientation	West-East
Face orientation	North
Position	Supine decubitus with the limbs flexed to the left.
Skeletal articulation	Articulated
Ornaments	One bronze needle was found positioned over the right side of the skull, and a necklace composed of 78 discoid- and bi-conical-shaped beads of limestone or plaster, along with

	two discoid-shaped lapis lazuli beads, was also discovered. The beads were dispersed throughout the neck and thorax regions.
Grave goods	The first set, situated to the west of the head, comprises 6 middle-sized pottery vessels, featuring plain and incised decorations. Plain pottery corresponds to the Ninevite 5 fine ware. The incised pottery exhibits geometric motifs. Between the vessels, a bone needle was identified, characterized by a quadrangular arrow-like head and an incised neck. There were also two thick bronze needles: one curved at the proximal end and one straight with a spherical head. The second set, situated to the east of the feet, comprises 13 small-sized pottery vessels, featuring plain, painted, and incised decorations. Plain pottery corresponds to the Ninevite 5 fine ware. The incised pottery exhibits geometric motifs. The painted pottery is characterized by thick oxidized lines. The presence of sealing plaster was observed in a subset of the vessels. Inside one of the vessels a flint tool was found.

3.2.1.12.3 Osteology: bone identification

Visual recording form - Child (Roksandic, 2003)

GRAVE 15



3.2.1.12.4 Determination of sex

The determination of sex was based on cranial (Acsádi & Nemeskéri, 1970) and coxal (Buikstra & Ubelaker, 1997) features. The cranial features that have been preserved include the nuchal crest, the mastoid processes, the supraorbital margins, and the mental eminence. The preserved characteristics are indicative of a probably female classification (see **Table 36**). The coxal feature that has been preserved in the right *os coxae* is the greater sciatic notch, which is broad, being characteristic of a female sex. The analysis of the *os pubis* and the Phenice traits (1969) in the left *os coxae* reveals the presence of the ventral arc, and of a ridge in the medial aspect of the ischio-pubic ramus, which are characteristic of a female sex.

Table 36. Scores for the cranial features to determine sex.

Cranial feature	Right side	Center	Left side
Nuchal crest		Not observable	
Mastoid process	2 (Probably Female)		3 (Indeterminate)
Supraorbital margin	2 (Probably Female)		2 (Probably Female)
Supraorbital ridge / Glabella		Not observable	
Mental eminence		1 (Female)	

3.2.1.12.5 Determination of age

The determination of age was based on multiple methods, including the cranial sutures in the vault according to Meindl & Lovejoy (1985), the examination of tooth development according to Schour & Massler (1941), Gustafson & Koch (1974) and AlQahtani et al. (2010), the examination of tooth wear attrition in permanent molars following Brothwell (1981), which has also been adapted in T. D. White et al. (2012), the development of the pubic symphysis, and the epiphyseal fusion of the bones from the postcrania according to Schaefer et al. (2009)**Table 14**. The cranial sutures in the vault provide an age range between 11 to 50 years, with an average estimated age of 30.5 years (see **Table 37**).

Table 37. Cranial suture fusion sites of the vault and the given scores.

Site	Score
Midlambdoid	1
Lambda	1
Obelion	1
Anterior sagittal	1
Bregma	1
Midcoronal	1
Pterion	1
Sphenofrontal	1
Inferior sphenotemporal	1
Superior sphenotemporal	1

Tooth development indicates that the individual was between the ages of 16 and 18, while estimates of dental attrition suggest a range of 17 to 25 years (**Table 38**).

Table 38. Scores of dental attrition in permanent molars (in anthropological notation).

Tooth	Score	Estimated age (in years)
^{1}M	1	17 – 25
^{3}M	1	17 – 25
M^{1}	1	17 – 25
M^{2}	1	17 – 25
M^{3}	1	17 – 25
$_{1}$M	1	17 – 25
$_{2}$M	1	17 – 25
$_{3}$M	1	17 – 25
M$_{2}$	1	17 – 25
M$_{3}$	1	17 – 25

According to the Todd system (1920), the development of the pubic symphysis in the *os coxae* is assigned to the first phase, whose age is determined to be below 19 years. According to the Suchey-Brooks system (Brooks & Suchey, 1990), the development of the pubic symphysis in the *os coxae* in female individuals is assigned to Phase 1. The 95% age range is determined to be between 15 and 24 years, with a mean age of 19.4 years.

With regard to the epiphyseal fusion of the bones from the postcrania, it has been observed that numerous epiphyses remain not fused to the diaphyses. The epiphyseal annular ring of the thoracic vertebrae is unfused, a characteristic that enables the determination of age to be as low as 16 to 18 years. In the sternum, the mesosternal flakes are not yet fused, suggesting an age below 17 years. The development of the epiphyseal flakes of the tubercles of both the right and left

ribs provide an estimated age of 18 years. The presence of unfused medial epiphysis in both clavicles suggests an age below 18 years. The bones of the arms exhibit either the proximal or the distal epiphysis to be unfused to the diaphyses, thereby providing an estimated age range between 15 to 17 years. The development of the bones from both hands also indicates an approximate age of 15 years. The bones of the legs exhibit either the proximal or the distal epiphysis to be unfused to the diaphyses, thereby providing an estimated age range between 14 and 17 years. The calcaneus of the right foot is completely fused, indicating an age above 15–16. In the *os coxae*, the ischiatic tuberosity from the ischium is fused, indicating an estimated age between 16 to 23 years, and the iliac crest remains unfused, indicating an age below 19 years. The vertebrae of the sacrum are unfused, indicating an age below 25 years (Ríos et al., 2008). The results of the analysis of the epiphyseal fusion suggest an approximate estimated age of 16 to 17 years.

With the exception of cranial suture fusion in the vault, the development of teeth, the attrition of teeth, the development of the pubic symphysis, and the epiphyseal fusion of the bones from the postcrania are in accordance with estimates of the age of death of the individual around 16 to 17 years, thereby classifying as an adolescent, according to Buikstra & Ubelaker (1997).

3.2.1.12.6 Stature estimation

In order to estimate the stature of the buried individual, the maximum length of the best-preserved and complete bones was measured (**Table 39**). The regression equations for white males, according to Trotter (1970) were employed. The estimated range of stature varied between 152.7 and 169.6 centimeters, with an average of 161.2 centimeters.

Table 39. Measures from the preserved long bones (in centimeters).

Side	Bone	Length (in cm)	Side	Bone	Length (in cm)
Right	Humerus	30	Left	Humerus	29
	Radius	23		Radius	23
	Ulna	25		Ulna	24
	Femur	42		Femur	43
	Tibia	34		Tibia	36
	Fibula	33		Fibula	34

3.2.1.12.7 Paleopathologies: determination of health

The studied bones present several paleopathologies, including dental diseases and periostitis. The dental diseases that have been observed are related with tooth decay (caries), dental calculus (tartar), and defects of the enamel. They have various etiologies, being poor oral health and accumulation of bacteria the principal ones, causing considerable pain and difficulties in eating (Lewis, 2018). Caries is an infectious disease that progressively destroys the crown and the root structures due to microbial activity (Ortner, 2003). It has been identified in the medial surface of the $_2$M. Dental calculus consists of the buildup of hardened plaque on the surface of the tooth (Lewis, 2018), and it is present in 5 teeth. Detailed information can be seen in **Table 40**.

Table 40. Detailed information about the identified dental calculus (in anthropological notation).

Tooth	Intensity	Surface location
I_2	Slight	Lingual
M_2	Slight	Mesolingual
P^2	Slight	Mesolingual
M^1	Slight	Mesolingual
M^2	Slight	Lingual

The defects in the enamel consist of linear hypoplasias, present in the mandibular canines. According to the Swärdstedt (1966) equations, the enamel formation was disturbed repeatedly at the ages of 1.6 and 1.9 years (**Table 41**). Other teeth affected by linear hypoplasia are the maxillary second incisors and canines, as well as the first incisor of the mandible. Multiple factors can cause hypoplasia, being the most common in prehistoric societies malnutrition, psychosocial stress, or infection during tooth development (Hillson, 2014).

Table 41. Measures of the enamel hypoplasia, only recorded in first superior incisors and inferior canines.

Tooth	Number of grooves	Distance from the groove to the cemento-enamel junction (in mm)	Height of the crown (in mm)
I^1	1	4	12
C_x	1	2	11
$_xC$	1	2	11

The presence of periostitis, an inflammatory reaction of the periosteum (Baxarias & Herrerín, 2008; Roberts & Buikstra, 2019), has been identified in the right clavicle, at the costoclavicular

impression. This reaction can result from a traumatic injury or bacterial infection (Davies-Barrett et al., 2019; Ortner, 2003).

3.2.1.12.8 Enthesopathies: determination of activity markers

The presence of enthesopathies was not detected in the observed bones.

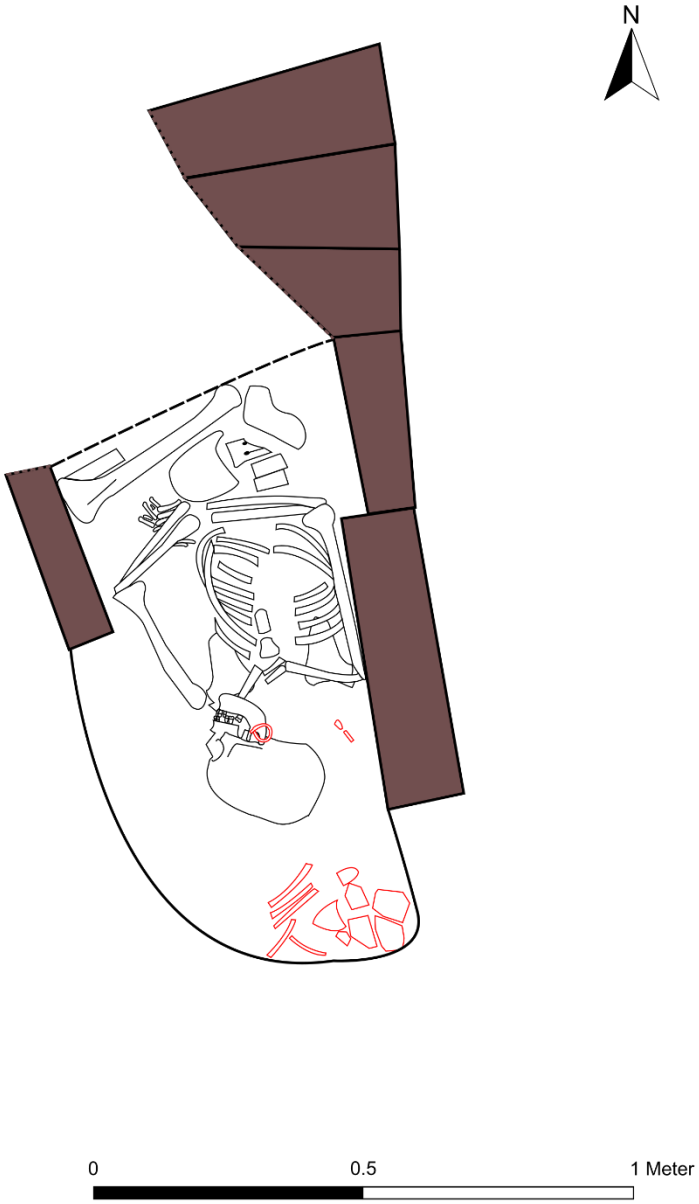
3.2.1.13 Grave 16

3.2.1.13.1 The container



Sector	3
Structure number	2024/1
Location	Locus 154.8
Period	Ninevite 5 (2900 – 2550 BCE) First half of the 3rd millennium BCE Early Bronze Age
Architectural phase	The construction of the grave occurred during the period of rapid transitional architecture, specifically phases 5A and 5B. Consequently, it can be posited that the existence of life and death within the site may have been contemporaneous.
Type of container	Simple pit
Morphology	Oval shape

3.2.1.13.2 The content



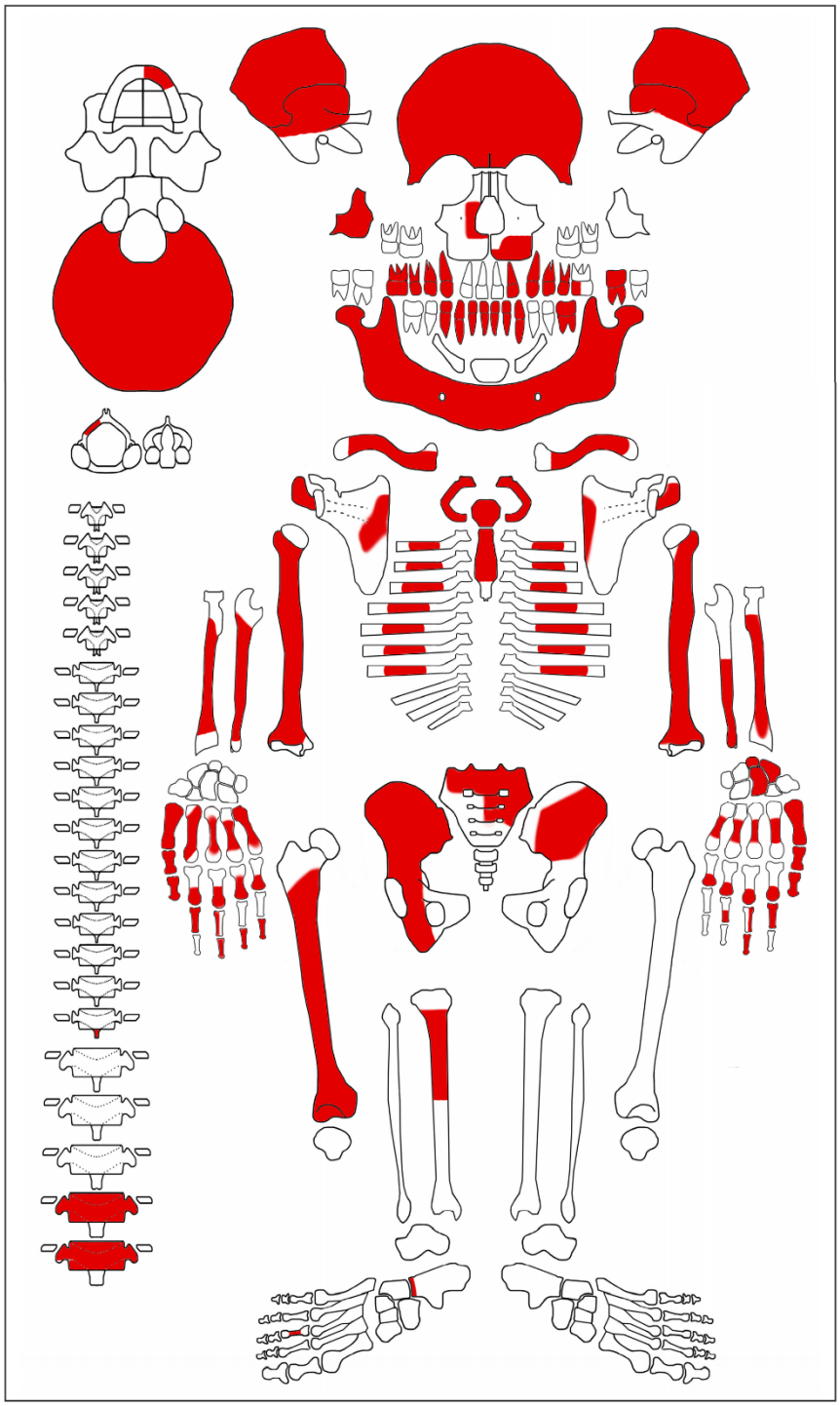
Number of buried individuals	1
Form of disposal	Primary inhumation
State of preservation	Poorly preserved
Body orientation	South-North
Face orientation	West
Position	Supine decubitus
Skeletal articulation	Articulated
Ornaments	A metallic spiral-shaped earring in the right ear.
Grave goods	A cylinder seal with geometric motifs (lines and rhombs with dots inside) and a trapezoidal-shaped pendant made of

amygdaloidal basalt are positioned to the east of the skull. South of the skull, a ribcage of an ovicaprid was placed on a burned plate with slip casting decoration.

3.2.1.13.3 Osteology: bone identification

Visual recording form - Adult (Roksandic, 2003)

GRAVE 16



3.2.1.13.4 Determination of sex

The determination of sex was based on cranial (Acsádi & Nemeskéri, 1970) and coxal (Buikstra & Ubelaker, 1997) features. The cranial features that have been preserved include the right supraorbital margin and the mental eminence. The preserved characteristics are indicative of a probable female classification (see **Table 42Table 8**). The coxal features are only observable in the right *os coxae*. The greater sciatic notch is broad, being characteristic of a female sex.

Table 42. Scores for the cranial features to determine sex.

Cranial feature	Right side	Center	Left side
Nuchal crest		Not observable	
Mastoid process	Not observable		Not observable
Supraorbital margin	3 (Indeterminate)		Not observable
Supraorbital ridge / Glabella		Not observable	
Mental eminence		2 (Probably Female)	

3.2.1.13.5 Determination of age

The determination of age was based on the by epiphyseal fusion of the bones from the postcrania according to Schaefer et al. (2009), on the examination of tooth wear attrition in permanent molars following Brothwell (1981), which has also been adapted in T. D. White et al. (2012), and on tooth wear attrition according to Lovejoy (1985) (see **Table 43**). While the system of Lovejoy proposes a large estimated age range, between 16 to 40 years, the mode is set between 20 to 24 years. Molar attrition following the system of Brothwell estimates an age range between 25 to 35 years. Due to the poor preservation of the epiphyseal fusion, a reliable age range cannot be estimated. However, the epiphyses of the long bones appear to be fused, suggesting an age of at least 15 to 19 years for female individuals. Considering all the methods employed, we suggest the individual was over 20 years old, classified as an adult according to Buikstra & Ubelaker (1997).

Table 43. Scores of dental attrition (in anthropological notation) according to the Brothwell (1981) and Lovejoy (1985) systems.

Brothwell system			Lovejoy system		
Tooth	Score	Estimated age (in years)	Tooth	Phase	Estimated age (in years)
^{1}M	4	25 – 35	C^{x}	B_1	16 – 20
M^{1}	4	25 – 35	P^{1}	C	18 – 22
$_{1}M$	4	25 – 35	P^{2}	D	20 – 24
$_{2}M$	4	25 – 35	M^{1}	G	35 – 40
			^{2}I	D	20 – 24
			^{x}C	D	20 – 24
			^{1}P	D	20 – 24
			^{2}P	D	20 – 24
			^{1}M	G	35 – 40
			I_1	D	20 – 24
			I_2	D	20 – 24
			C_x	D	20 – 24
			P_1	D	20 – 24
			$_{2}I$	D	20 – 24
			$_{x}C$	E	24 – 30
			$_{1}M$	G	35 – 40
			$_{2}M$	G	35 – 40

3.2.1.13.6 Stature estimation

In order to estimate the stature of the buried individual, the maximum length of the best-preserved and complete bones was measured (**Table 44**). The regression equations for white males, according to Trotter (1970) were employed. The estimated range of stature varied between 151 and 180 centimeters, with an average of 165.5 centimeters.

Table 44. Measures from the preserved long bones (in centimeters).

Side	Bone	Length (in cm)	Side	Bone	Length (in cm)
Right	Humerus	30.5	Left	Humerus	29
	Radius	25.5		Radius	23.5
	Ulna	24		Ulna	23.5
	Femur	41		Femur	Not observable
	Tibia	Not observable		Tibia	Not observable
	Fibula	Not observable		Fibula	Not observable

3.2.1.13.7 Paleopathologies: determination of health

The presence of paleopathologies was not detected in the observed bones.

3.2.1.13.8 Enthesopathies: determination of activity markers

The presence of enthesopathies was not detected in the observed bones.

3.2.2 Gir-e Gomel

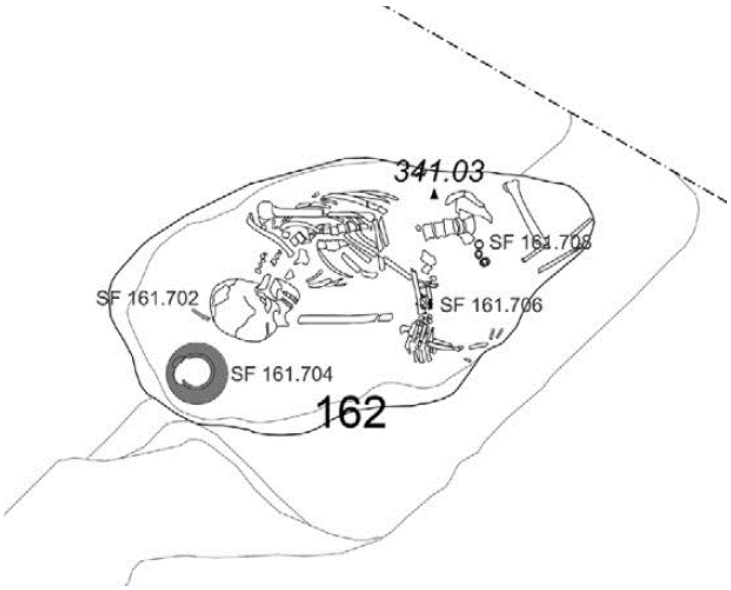
The graves of Gir-e Gomel were excavated and studied by the members of *The Kurdish-Italian Gir-e Gomel Archaeological Project (KIGAP)*, who published the data in two preliminary fieldwork reports (Morandi Bonacossi et al., 2018, 2025). A total of eight graves dating to the first half of the 3rd millennium BCE were identified, specifically from the Ninevite 5 period.

Archaeologists and anthropologists from the project documented archaeothanatological data concerning the container and the contents of the graves. The information regarding the content included a description of the type of container and its morphology. The information concerning the contents comprised the number of buried individuals, the type of disposal, the state of preservation of the skeletal remains, the orientation of the body and the face, the position of the deceased, the skeletal articulation and the presence of ornaments and grave goods. Photographs and illustrations of the graves were obtained and also published in the preliminary reports. The recovery of the data occurred in the interval between the excavation of the burials in 2012 and its publication in 2018.

The methods employed for age and sex determination have not been explicitly published; only the final assessment in cases where it was possible to recover this information has been documented. The presence of paleopathologies and enthesopathies has not been previously documented, which limits the availability of data to assess health and activity markers.

3.2.2.1 Grave 24

3.2.2.1.1 The container



Operation	1
Location	Northwestern area
Period	Ninevite 5 (2900 – 2550 BCE)
	First half of the 3rd millennium BCE
	Early Bronze Age
Type of container	Simple pit
Morphology	The simple pit is irregular in shape with an oval tendency

3.2.2.1.2 The content

Number of buried individuals	1
Form of disposal	Primary inhumation
State of preservation	Poorly preserved
Body orientation	Southwest - Northeast
Face orientation	Southeast
Position	Right lateral decubitus, with the upper and lower limbs flexed to the right.
Skeletal articulation	Not recorded

Ornaments	Two bracelets composed of white beads and worked shells (three carnelian beads may also be part of the bracelets), a diadem made of a copper or bronze band and white beads, a pendant made of a large white cylinder, a belt placed around the abdomen made of shell rings of the *Conus* species, and a toggle pin with a lanceolate head made of copper or bronze. The toggle pin is chronologically associated with the late 3rd millennium to the early 2nd millennium BCE.
Grave goods	Two pottery vessels of Excised Ware style, related to the late Ninevite 5 period.

3.2.2.1.3 Determination of age and sex

The buried individual consists of a young adult female whose age ranges from 20 to 30 years.

3.2.2.2 Grave 42

3.2.2.2.1 The container



Operation	3
Location	Beneath Grave 44
Period	Ninevite 5 (2900 – 2550 BCE) First half of the 3rd millennium BCE Early Bronze Age
Type of container	Simple pit
Morphology	The simple pit is oval in shape

3.2.2.2.2 The content

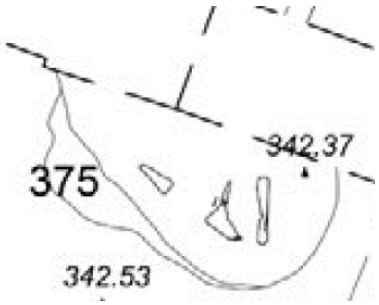
Number of buried individuals	1
Form of disposal	Primary inhumation
State of preservation	Poorly preserved
Body orientation	Southwest - Northeast
Face orientation	West
Position	Supine decubitus with the upper and lower limbs flexed to the right side.
Skeletal articulation	Not recorded
Ornaments	A toggle pin made of copper or bronze, and a ring made of a *Conus* shell.
Grave goods	A small jar belonging to the late Ninevite 5 period.

3.2.2.2.3 Determination of age and sex

The buried individual consists of a young adult male whose age ranges from 28 to 35 years.

3.2.2.3 Grave 45

3.2.2.3.1 The container



Operation	1
Location	Beneath the entrance to Grave 44
Period	Ninevite 5 (2900 – 2550 BCE)
	First half of the 3rd millennium BCE
	Early Bronze Age
Type of container	Simple pit
Morphology	The simple pit is oval in shape

3.2.2.3.2 The content

Number of buried individuals	1
Form of disposal	Primary inhumation
State of preservation	Poorly preserved
Body orientation	East - West
Face orientation	Indeterminable
Position	Left lateral decubitus with flexed upper and lower limbs.
Skeletal articulation	Disarticulated and an absent skull
Ornaments	A necklace composed of more than 100 beads and a bracelet made of 30 small rounded white beads. It has been determined that the beads made of shell belong to species that originate from the Gulf: *Dentalia*, *Engina mendicaria*, and *Nassarius*. In the hip, a belt composed of *Conus* shell rings was discovered. Twenty grey stone disc beads were distributed across the thorax and pelvis. Three pendants or amulets with zoomorphical shapes: a porcupine and a bovid

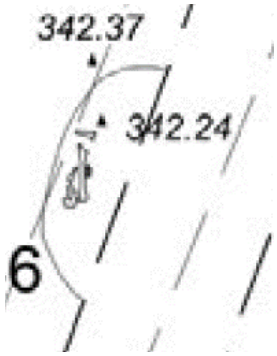
	or bear made of white stone, and a turtle made of a darker stone.
Grave goods	A glyptic element in the form of a cylinder seal of hourglass shape that features geometric motifs of concentric semicircular lines.

3.2.2.3.3 Determination of age and sex

The deceased consists of a child individual whose sex could not be determined due to an absence of identifiable sexual traits.

3.2.2.4 Grave 46

3.2.2.4.1 The container



Operation	1
Location	Beneath the eastern wall from Grave 44
Period	Ninevite 5 (2900 – 2550 BCE)
	First half of the 3rd millennium BCE
	Early Bronze Age
Type of container	Simple pit
Morphology	The simple pit is round in shape

3.2.2.4.2 The content

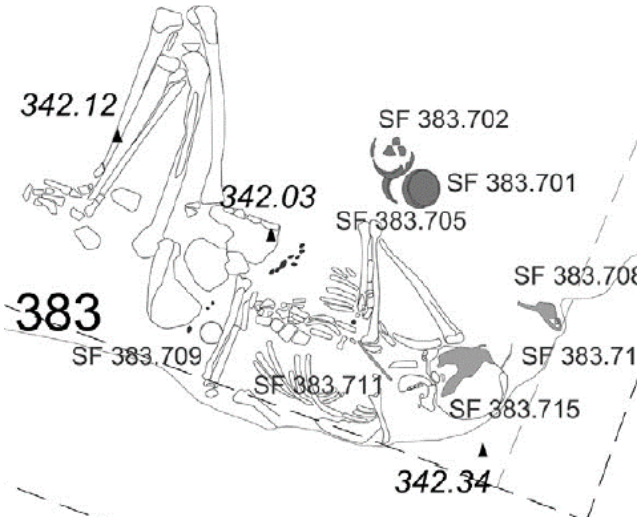
Number of buried individuals	1
Form of disposal	Primary inhumation
State of preservation	Poorly preserved
Body orientation	Indeterminable
Face orientation	Indeterminable
Position	Indeterminable
Skeletal articulation	Disarticulated
Ornaments	None
Grave goods	None

3.2.2.4.3 Determination of age and sex

Age remains indetermined and the absence of any sexual trait did not allow to determine the sex of the individual.

3.2.2.5 Grave 47

3.2.2.5.1 The container



Operation	1
Location	Beneath Grave 44
Period	Ninevite 5 (2900 – 2550 BCE)
	First half of the 3rd millennium BCE
	Early Bronze Age
Type of container	Simple pit
Morphology	The simple pit is irregular in shape with an oval tendency.

3.2.2.5.2 The content

Number of buried individuals	1
Form of disposal	Primary inhumation
State of preservation	Poorly preserved
Body orientation	East - West
Face orientation	South
Position	Right lateral decubitus with flexed upper limbs.
Skeletal articulation	Articulated
Ornaments	A diadem accompanied by a pin with a rolled head made of copper or bronze, positioned in the skull. It is hypothesized that both are part of a headpiece made of a fabric, in which the diadem is adjusted by the pin. A copper or bronze straw was found in the thorax area. Multiple beads, some made

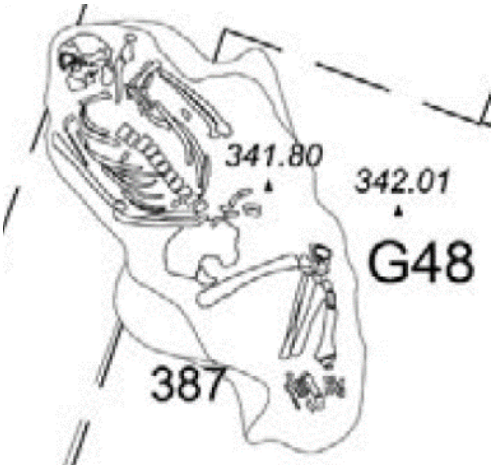
	of silver and located close to the arms and necks, may have been part of a necklace and a bracelet.
Grave goods	A copper or bronze razor and pottery bowls with beaded rims that are attributed to the late Ninevite 5 period.

3.2.2.5.3 Determination of age and sex

The buried individual consists of a young adult male whose age ranges from 21 to 22 years.

3.2.2.6 Grave 48

3.2.2.6.1 The container



Operation	1
Location	Beneath the northern area of the western wall from Grave 44
Period	Ninevite 5 (2900 – 2550 BCE) First half of the 3rd millennium BCE Early Bronze Age
Type of container	Simple pit
Morphology	The simple pit is irregular in shape with an oval tendency.

3.2.2.6.2 The content

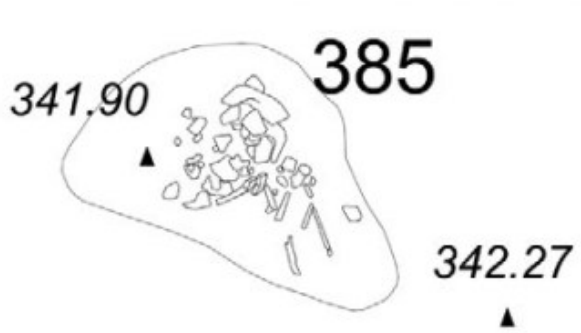
Number of buried individuals	1
Form of disposal	Primary inhumation
State of preservation	Poorly preserved
Body orientation	Northwest - Southeast
Face orientation	Southwest
Position	Supine decubitus with the upper and lower limbs flexed to the left.
Skeletal articulation	Loosely articulated
Ornaments	None
Grave goods	None

3.2.2.6.3 Determination of age and sex

The buried individual consists of a young adult male whose age ranges from 22 to 24 years.

3.2.2.7 Grave 49

3.2.2.7.1 The container



Operation	1
Location	Beneath Grave 44
Period	Ninevite 5 (2900 – 2550 BCE)
	First half of the 3rd millennium BCE
	Early Bronze Age
Type of container	Simple pit
Morphology	The simple pit is irregular in shape with an oval tendency.

3.2.2.7.2 The content

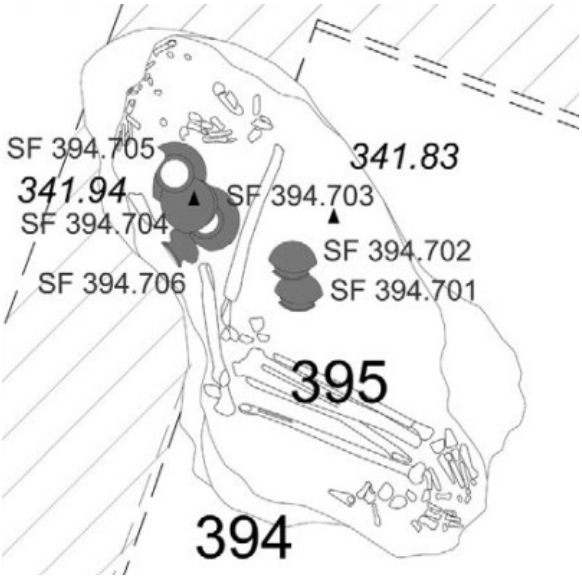
Number of buried individuals	1
Form of disposal	Primary inhumation
State of preservation	Poorly preserved
Body orientation	Indeterminable
Face orientation	Indeterminable
Position	Indeterminable
Skeletal articulation	Disarticulated
Ornaments	None
Grave goods	None

3.2.2.7.3 Determination of age and sex

The buried individual consists of an old adult whose age ranges from 45 to 55 years. Sex has been determined as a possible male.

3.2.2.8 Grave 51

3.2.2.8.1 The container



Operation	1
Location	Beneath Grave 48 and the northwestern wall from Grave 44
Period	Ninevite 5 (2900 – 2550 BCE) First half of the 3rd millennium BCE Early Bronze Age
Type of container	Simple pit
Morphology	The simple pit is irregular in shape with an oval tendency.

3.2.2.8.2 The content

Number of buried individuals	1
Form of disposal	Primary inhumation
State of preservation	Poorly preserved
Body orientation	Northwest - Southeast
Face orientation	Indeterminable
Position	Unknown decubitus with flexed upper and lower limbs.
Skeletal articulation	Disarticulated
Ornaments	None
Grave goods	Six small pottery jars, which are consistent with the late Ninevite 5 period repertoire. Four were located close to the *os coxae*, and two were in proximity to the knees.

3.2.2.8.3 Determination of age and sex

The deceased consists of an adult individual, but the absence of any sexual trait did not allow sex determination.

3.2.3 Plaça de la Gardunya

The remains of the buried individuals from Plaça de la Gardunya were stored after fieldwork at the Archaeological Archive of the Collection Centre from the Barcelona History Museum (MUHBA) in 81 boxes. Each box contained a comingle of coordinated remains belonging to different individuals, graves and sectors. The buried individuals of Plaça de la Gardunya have been studied in two previous occasions since the recovery of the remains during fieldwork. The two studies consisted of determining the minimum number of individuals, sex, age, and stature, as well as a paleopathological identification of the skeletal remains. Nevertheless, both studies encompassed only a portion of the remains, and have yet not been studied completely. The first analysis, performed in 2014 (unpublished), studied 6 stratigraphic units belonging to Graves 2 (4319) and 4 (4328, 4389, 4430, 4463) from Sector 4, as well as Grave 1 from Sector 5 (50574), determining a MNI of 67. The second analysis, performed in 2018 by Dr. Ferran Estebaranz Sánchez and Dr. Laura M. Martínez (unpublished), studied 21 stratigraphic units belonging to Graves 2 (4232, 4312, 4313, 4314, 4315, 4316, 4317, 4318, 4319, 4319 (a), 4319 ("c")) and 3/4 (4328, 4375, 4430, 4450, 4392) from Sector 4, and Graves 1 (50574, 50616) and 2 (50618, 50619, 50620) from Sector 5. The remains were stored in 30 boxes of a total of 80, and a MNI of 52 was determined.

In 2023, a team of researchers from the SAPPO-GRAMPO Research Group at the Autonomous University of Barcelona conducted an inventory of all the human remains stored in the 80 boxes. The team included Alicia Gluitz (PhD student), Biel Soriano Elias (PhD student), Olivia Orri Orri (PhD student), Àstrid Ortega Forn (undergraduate student), and Caterina Sabán Vinyals (undergraduate student). The inventory enabled the establishment of a minimum number of individuals required for the remaining 50 boxes, the contents of which had not previously been subject to anthropological analysis. Furthermore, it facilitated a re-examination of the 30 boxes that had been studied in 2018. The archaeothanatological analysis of the buried individuals at Plaça de la Gardunya has been based on data recovered from the extant published literature (Gómez et al., 2015; Velasco et al., 2017), as well as in reports elaborated by the team members of the SAPPO-GRAMPO Research Group. The graves that were studied include Graves 2, 3/4, 5, and 7 from Sector 4, as well as Graves 1 and 2 from Sector 5. Furthermore, a burial with no associated grave number located in Sector 4 has been examined, along with three burials lacking an ascribed grave or sector number. The recovery of data has been incomplete, as certain individuals have not been assigned grave and sector numbers, thereby rendering their association with any of the aforementioned graves or sectors unfeasible. The integration of anthropological data with

information pertaining to sexual and age determination has proven to be a challenging endeavor, particularly with respect to its association with specific individuals. In order to overcome the challenges posed by the scarcity of information and the inconsistencies in the data, a thorough analysis has been conducted. This analysis integrates stratigraphic data and fieldwork reports, resulting in a comprehensive interpretation of the construction and usage phases of the grave. Additionally, the minimum number of buried individuals has been identified, and taphonomic and/or anthropic processes have been determined for each grave. In instances where recovery was feasible, the type of disposal, the position and orientation of the bodies, and the presence or absence of ornaments and grave goods have been ascertained following the criteria used to describe the graves from the site of Gird Lashkir. The Minimum Number of Individuals has been determined to be 127, all belonging to the Early Bronze Age. 102 individuals were buried in Sector 4, 22 were buried in Sector 5, and 3 more individuals without an ascribed sector or grave number. In case the skeletal remains of a stratigraphic unit belong to different individuals, each one has been identified with a code, consisting in the stratigraphic unit followed by a dot and a correlative number, always starting from number 1. If the skeletal remains of each individual allowed the determination of age and sex, it has also been recorded. The comingled storage of the bones has not allowed to be very precise in terms of age assessment.

Upon completion of the archaeothanatological analysis, an anthropological analysis was conducted to determine the biological profile of the individuals. The determination of sex has been approached through cranial features (Acsádi & Nemeskéri, 1970) and coxal traits (Buikstra & Ubelaker, 1997). The determination of age in subadult individuals has been assessed through the examination of epiphyseal fusion of the bones from the postcrania (Schaefer et al., 2009). For adult individuals, age assessment has been conducted through the analysis of cranial sutures of the vault (Meindl & Lovejoy, 1985), the assessment of dental attrition through the Brothwell system (1981), and the observation of the epiphyseal fusion of the bones from the postcrania (Schaefer et al., 2009).

The present study has not yet had the opportunity to perform a comprehensive analysis of the bones. Consequently, the development of visual recording forms to associate all the remains with a specific individual has not yet been possible. The inability to isolate the individuals from the accumulation of bones hinders the estimation of their stature and the observation of paleopathologies and enthesopathies. Consequently, the relationship of these observations to a specific individual remains unattainable. However, the analysis yielded insights into a few paleo-

pathologies, which are discussed in the results section. This work is thus regarded as a preliminary investigation, with the understanding that further analyses are necessary to substantiate these pieces of evidence.

3.2.3.1 Grave 2 (Sector 4)

3.2.3.1.1 Archaeothanatological analysis

Grave 2 consists of a hypogeum containing the multiple successive inhumations of a minimum of 18 individuals (**Table 45**). The determination of individuals has led to the addition of five individuals to this grave, which was originally published as a grave with 12 inhumations (Velasco et al., 2017).

The construction of the burial chamber was followed by a series of primary inhumations, with a total of 13 individuals being buried successively. The remains were initially positioned as a primary deposit and subsequently relocated to the back of the chamber, where they were mixed with the bones of the preceding deceased individuals. The 13 individuals in question are part of the following stratigraphic units: 4312, 4313, 4214, 4315, 4316, 4317, 4319, 4319 (a), 4319 (b), and 4319 (c). Individuals 4312 and 4313 were relocated to the western area of the chamber, while the remaining individuals were positioned in the northeastern sector. The individual 4318 was positioned in a right lateral decubitus with flexed limbs. Subsequent interments resulted in the removal and repositioning of the skull of the aforementioned individual to a different location within the chamber. The last individual buried during the penultimate inhumation phase was 4232, positioned in right lateral decubitus, and exhibited an articulated connection. The body was placed in a position above the site of the previous inhumation of the individual 4318. A pottery vessel was identified as a grave good in association with 4232, which was positioned posterior to the skull. Following this burial, the space was filled with soil, thereby preserving the anatomical connection. Thereafter, the final two individuals interred were associated with the stratigraphic unit 4174. The remains were then placed in secondary deposit within a comingle of bones. The pit was subsequently covered with soil, thereby sealing the grave.

Table 45. Minimum Number of Individuals of each stratigraphic unit from Grave 2 (Sector 4).

Inhumation phase	Stratigraphic unit	Minimum Number of Individuals
1st	4312	1
	4313	1
	4314	1
	4315	1
	4316	1
	4317	1
	4319	4
	4319 (a)	1
	4319 (b)	1
	4319 (“c”)	2
2nd	4318	1
3rd	4232	1
4th	4174	2

3.2.3.1.2 Anthropological analysis. Determination of sex and age

Sex and age have been ascertained for four individuals: three adult males and one adult female. The Brothwell system (1981) has provided a more precise age estimation through the analysis of molar attrition for two individuals: 4319.2 and 4174.1 (see **Table 46**).

Table 46. Assessment of molar attrition according to Brothwell (1981).

Individual	Tooth (in anthropological notation)	Score for molar attrition	Age in years
4319.2	$_1$M	4	25-35
4174.1	$_1$M	3	17-25

Among the indeterminate individuals, three are subadults (two under 12 years of age), two are adolescent or young adult individuals, one is a young adult, and eight are adults above 20 years of age. Further details are available in **Table 47**.

Table 47. Sex and age determination for each individual buried at Grave 2 (Sector 4).

Individual	Sex	Age (in years)	Age class (Buikstra & Ubelaker, 1997)
4312	Indeterminate	> 20	Adult
4313	Indeterminate	> 20	Adult
4314	Indeterminate	> 20	Adult
4315	Male	> 20	Adult
4316	Indeterminate	< 20	Adult
4317	Male	> 20	Adult
4319.1	Indeterminate	> 20	Adult
4319.2	Indeterminate	25-35	Young adult (20-35)
4319.3	Male	> 20	Adult
4319.4	Indeterminate	< 12	Infant (0-3) or child (3-12)
4319 (a)	Indeterminate	> 20	Adult
4319 (b)	Indeterminate	> 20	Adult
4319 ("c").1	Indeterminate	> 20	Adult
4319 ("c").2	Indeterminate	< 12	Infant (0-3) or child (3-12)
4318	Female	> 20	Adult
4232	Indeterminate	18-25	Adolescent (12-20) or young adult (20-35)
4174.1	Indeterminate	17-25	Adolescent (12-20) or young adult (20-35)
4174.2	Indeterminate	< 20	Subadult

3.2.4.1 Grave 3/4 (Sector 4)

3.2.4.1.1 Archaeothanatological analysis

Grave 3/4 is comprised of a double-chambered hypogeum with an access shaft, and it has been determined that a minimum of 66 individuals were buried. The published literature ascribes this grave to 56 inhumations; however, the present analysis has identified 10 additional individuals. Chamber 4 (published as chamber A in the available literature) contains the inhumation of 41 individuals, and chamber 3 (published as chamber B in the literature) contains the inhumation of 25 individuals (**Table 48**The scarcity of information regarding individual 3402, buried within chamber 4 or A, poses a significant challenge, as it precludes the determination of the phase in which it was interred.

Table 48). The stratigraphy of both chambers reveals a prolonged burial tradition within the hypogeum, characterized by a consistent burial pattern. This pattern involved initially disposing of the deceased in a primary deposit, followed by relocating them to the back of the chamber once they were skeletonized, thereby creating space for new burials.

The first group of deceased individuals buried in chamber 4 or A consisted of 39 individuals belonging to the stratigraphic units 4291, 4379, 4389, 4391, and 4474. The bodies were buried successively in a primary deposit, which was subsequently transformed into a secondary deposit when each new deceased was disposed inside the chamber. The bodies were adorned with V-shaped perforated buttons. A total of 26 V-shaped perforated buttons, 22 of which have a rectangular shape and 4 of which have a pyramidal shape, 2 of which have *oculi* decoration motifs, have been documented but not associated with any specific individual. The skeletons were already skeletonized when they were displaced to the back of the chamber, forming a comingle of bones. Subsequent to these successive burials, individual 4473 was interred in primary deposit. Upon the completion of preparations for interment, the remains of individual 4475 were relocated to the back of the chamber, as individual 4473 had not yet undergone complete skeletonization. Consequently, its original position was maintained in a loosely articulated state. It was oriented in a southeast-northwest direction. Individual 4475 was found in primary disposal and with articulated anatomical connections. Its position was determined to be left lateral decubitus, with an orientation from southeast to northwest. The two most recent individuals to be interred were identified as 4388 and 4390, respectively, and were located in a primary deposit in close proximity to the chamber's entrance. The individual 4388 was buried first, with its bones remaining in anatomical position, with the body positioned in a left lateral decubitus with flexed limbs, oriented southeast-northwest. The individual 4390 was buried above 4388, in a left lateral

decubitus position, oriented east-west, and remained in anatomical connection. Both consist of an adult and a subadult individual, respectively.

The initial burials within chamber 3 or B were those of individuals 4450 and 4392, placed as a primary deposit at the back of the chamber and exhibiting preserved anatomical connection. Both individuals were placed in a prone decubitus position with the limbs flexed to the left. However, 4450 was oriented northwest-southeast, while 4392 was oriented southeast-northwest. Following this, two individuals from stratigraphic unit 4463 were buried. One of the deceased was positioned in a prone decubitus position, oriented west to east. Once the skeletons were partially skeletonized, the bones were relocated to the back of the chamber. The individual whose position and orientation has been identified lost the anatomical connection of the skull with the postcrania, and the other completely lost its anatomical connection. Thereafter, the burial was reopened to accommodate successive burials of 11 individuals belonging to the stratigraphic unit 4430. The initial disposal method may have entailed a primary deposit, subsequently transformed into secondary deposits as each new deceased individual was placed within the chamber. The skeletons were already skeletonized when they were moved to the back of the chamber, forming a mixture of bones. The bones were placed above the two earliest inhumations (4450 and 4392) without disturbing them. After these successive inhumations occurred, a compact sediment made of clay and sand, with carbonate nodules and mudbrick inclusions, started to slowly fill the chamber, setting the buried bones in place. Additionally, the sedimentary layer of stratigraphic unit 4410 contained skeletal remains. In the following opening of the burial, six individuals belonging to the stratigraphic unit 4328 were buried as primary deposits, with the bones comingling to the back of the chamber as new deceased were buried. The last individual interred in this burial was 4376, positioned in left lateral decubitus with flexed limbs, and oriented north-south. This burial was subsequently affected by the disturbance of the anatomical connection, resulting in the dislocation of the skull, forearms, and feet from the remainder of the body. This last phase of burials was accompanied by two pottery vessels as grave goods. After the completion of these actions, the chamber was closed, and the access shaft was sealed with a filling of medium-sized rocks.

During the Roman period, a silo was constructed, which not only cut the upper level of the access shaft but also exerted a minor influence on the adjacent areas within the most recent inhumation phases of both chambers. During the late medieval period, the construction of a wall from

the city also disturbed the grave. The most recent disturbance was the construction of a subterranean parking lot in the 1960s, which affected chamber 3 or B by removing the lower limbs of individual 4392.

The scarcity of information regarding individual 3402, buried within chamber 4 or A, poses a significant challenge, as it precludes the determination of the phase in which it was interred.

Table 48. Minimum Number of Individuals of each stratigraphic unit from Grave 3/4 (Sector 4).

Chamber	Inhumation phase	Stratigraphic unit	Minimum Number of Individuals
4 or A	1st	4291	1
		4379	2
		4389	32
		4391	1
		4474	1
	2nd	4473	1
	3rd	4475	1
	4th	4388	1
	5th	4390	1
3 or B	1st	4450	1
		4392	1
	2nd	4463	2
	3rd	4430	11
	4th	4410	1
	5th	4328	6
	6th	4321	1
	7th	4376	1
	Unclear	3402	1

3.2.4.1.2 Anthropological analysis. Determination of sex and age

A determination has been made regarding the sex and age of 21 individuals. The Brothwell system (1981) has provided a more precise age estimation through the analysis of molar attrition for twenty-two individuals (see **Table 49**).

Table 49. Assessment of molar attrition according to Brothwell (1981).

Individual	Tooth (in anthropological notation)	Score for molar attrition	Age in years
4389.11	$_1$M	3	17-25
4389.12	M$_1$	3	17-25
4389.13	M$_1$	1	17-25
4389.14	$_1$M	1	17-25
4389.15	M$_1$	3-	17-25
4389.16	M$_1$	3-	17-25
4389.17	M$_1$	2+	12-25
4389.18	M$_1$	3	17-25
4389.19	M$_1$	4	25-35
4389.20	$_1$M	3-	17-25
4389.21	M$_1$	3	17-25
4389.22	M$_1$	3-	17-25
4389.23	M$_1$	3-	17-25
4389.24	M$_1$	2+	17-25
4391	$_1$M	3+	17-25
4473	$_1$M	2	12-16
4388	M^1	4	25-35
4450	M$_1$	1	< 17-25
4328.6	M$_1$	3+	17-25
4430.7	M$_1$	3-	17-25
4430.8	$_1$M	3-	17-25
4430.9	^{1}M	4	25-35

Chamber 4 (or A) contains the inhumation of nine female individuals (six of whom are estimated to be adolescents or young adults, one young adult, and two adults) and ten male individuals (four of whom are estimated to be adolescents or young adults, one young adult, and five adults). Among the 22 indeterminate individuals, six are subadults, one is an adolescent, four are adolescents or young adults, and eleven are adults. Chamber 3 (or B) contains the remains of two individuals who were likely between the age ranges of adolescence and young adulthood. Among the 23 indeterminate individuals, one is a child, two are subadults, one is an adolescent or a young adult, one is a young adult, and eighteen are adults. For a more exhaustive overview, please refer to **Table 50**.

Table 50. Sex and age determination for each individual buried at Grave 3/4 (Sector 4).

Chamber	Individual	Sex	Age (in years)	Age class (Buikstra & Ubelaker, 1997)
4 or A	4291	Indeterminate	> 20	Adult
	4379.1	Indeterminate	> 20	Adult
	4379.2	Indeterminate	> 20	Adult
	4389.1	Indeterminate	< 20	Subadult
	4389.2	Indeterminate	> 20	Adult
	4389.3	Indeterminate	> 20	Adult
	4389.4	Indeterminate	> 20	Adult
	4389.5	Indeterminate	> 20	Adult
	4389.6	Indeterminate	> 20	Adult
	4389.7	Indeterminate	> 20	Adult
	4389.8	Indeterminate	> 20	Adult
	4389.9	Indeterminate	< 20	Subadult
	4389.10	Indeterminate	< 20	Subadult
	4389.11	Female	17-25	Adolescent (12-20) or young adult (20-35)
	4389.12	Indeterminate	17-25	Adolescent (12-20) or young adult (20-35)
	4389.13	Indeterminate	17-25	Adolescent (12-20) or young adult (20-35)
	4389.14	Female	17-25	Adolescent (12-20) or young adult (20-35)
	4389.15	Male	17-25	Adolescent (12-20) or young adult (20-35)
	4389.16	Male	17-25	Adolescent (12-20) or young adult (20-35)
	4389.17	Indeterminate	12-25	Adolescent (12-20) or young adult (20-35)
	4389.18	Female	17-25	Adolescent (12-20) or young adult (20-35)
	4389.19	Female	25-35	Young adult (20-35)
	4389.20	Female	17-25	Adolescent (12-20) or young adult (20-35)
	4389.21	Indeterminate	17-25	Adolescent (12-20) or young adult (20-35)
	4389.22	Male	17-25	Adolescent (12-20) or young adult (20-35)
	4389.23	Male	17-25	Adolescent (12-20) or young adult (20-35)

	4389.24	Female	17-25	Adolescent (12-20) or young adult (20-35)
	4389.25	Indeterminate	< 20	Subadult
	4389.26	Female	> 20	Adult
	4389.27	Female	> 20	Adult
	4389.28	Male	> 20	Adult
	4389.29	Male	> 20	Adult
	4389.30	Male	> 20	Adult
	4389.31	Male	> 20	Adult
	4389.32	Indeterminate	> 20	Adult
	4391	Female	17-25	Adolescent (12-20) or young adult (20-35)
	4474	Indeterminate	< 20	Subadult
	4473	Indeterminate	12-16	Adolescent (12-20)
	4475	Male	> 20	Adult
	4388	Male	25-35	Young adult (20-35)
	4390	Indeterminate	< 20	Subadult
3 or B	4450	Indeterminate	10-11	Child (3-12)
	4392	Indeterminate	> 20	Adult
	4463.1	Indeterminate	> 20	Adult
	4463.2	Indeterminate	> 20	Adult
	4430.1	Indeterminate	< 20	Subadult
	4430.2	Indeterminate	> 20	Adult
	4430.3	Indeterminate	> 19	Subadult
	4430.4	Indeterminate	> 20	Adult
	4430.5	Indeterminate	> 20	Adult
	4430.6	Indeterminate	> 20	Adult
	4430.7	Indeterminate	17-25	Adolescent (12-20) or young adult (20-35)
	4430.8	Male	17-25	Adolescent (12-20) or young adult (20-35)
	4430.9	Indeterminate	25-35	Young adult (20-35)
	4430.10	Indeterminate	> 20	Adult
	4430.11	Indeterminate	> 20	Adult
	4410	Indeterminate	> 20	Adult
	4328.1	Indeterminate	> 20	Adult
	4328.2	Indeterminate	> 20	Adult
	4328.3	Indeterminate	> 20	Adult
	4328.4	Indeterminate	> 20	Adult
	4328.5	Indeterminate	> 20	Adult
	4328.6	Male	17-25	Adolescent (12-20) or young adult (20-35)

4321	Indeterminate	> 20	Adult
4376	Indeterminate	> 20	Adult
3402	Indeterminate	> 20	Adult

3.2.5.1 Grave 5 (Sector 4)

3.2.5.1.1 Archaeothanatological analysis

Grave 5 consists of six simple pits with an oval morphology that contained the inhumation of a minimum number of 16 individuals (see **Table 51**). The archaeothanatological analysis has facilitated a more precise characterization of the individuals buried in the simple pits that correspond to Grave 5, which initially contained only 11 individuals.

The simple pits cut an abandoned room with an oval morphology. The first simple pit, designated as pit 4470, contained four subadult individuals associated with the stratigraphic units 4377, 4427, and 8141. These individuals were placed in a secondary deposit. The pit was filled with soil, blocks, animal remains, and pottery shards.

The second simple pit, identified by structure number 4469, was constructed in a manner that partially covered the preceding pit. The burial contained four subadult inhumations in a secondary deposit, which were associated with the stratigraphic unit 4437. The remains were found in association with a grave good composed of a pottery vessel.

The third simple pit, designated as structure 4471, yielded skeletal remains of a subadult individual, which were concomitant with the stratigraphic unit 4436. The grave goods accompanying the remains included two cattle horns and four pottery vessels.

The fourth simple pit, designated as structure 4461, contained four inhumations of subadult individuals associated with the stratigraphic unit 4462. The structure was partially disturbed in two distinct phases. Initially, it was severed by a combustion structure. Subsequently, it was further disturbed by the construction of a subterranean parking lot in the 1960s.

The fifth simple pit, designated as structure 4472, contained two subadult inhumations. These inhumations were associated with the stratigraphic unit 4384, were placed as secondary deposits and then covered by large blocks. As a grave good, a pottery vessel was found.

The sixth and last simple pit, designated as structure 4405, contained eight human remains in secondary deposit of a subadult individual associated with stratigraphic unit 4406. The pit contained no grave goods.

Table 51. Minimum Number of Individuals of each stratigraphic unit from Grave 5 (Sector 4).

Structure number	Stratigraphic unit	Minimum Number of Individuals
4470	4377	1
	4427	1
	8141	2
4405	4406	1
4472	4384	2
4471	4436	1
4469	4437	4
4461	4462	4

3.2.5.1.2 Anthropological analysis. Determination of sex and age

The determination of sexual traits in the observed bones proved unfeasible, precluding precise determination of sex. Furthermore, the age of the specimen could only be ascertained at the level of subadult. (**Table 52**).

Table 52. Sex and age determination for each individual buried at Grave 5 (Sector 4).

Individual	Sex	Age (in years)	Age class (Buikstra & Ubelaker, 1997)
4377	Indeterminate	< 20	Subadult
4406	Indeterminate	< 20	Subadult
4427	Indeterminate	< 20	Subadult
4436	Indeterminate	< 20	Subadult
4437.1	Indeterminate	< 20	Subadult
4437.2	Indeterminate	< 20	Subadult
4437.3	Indeterminate	< 20	Subadult
4437.4	Indeterminate	< 20	Subadult
4462.1	Indeterminate	< 20	Subadult
4462.2	Indeterminate	< 20	Subadult
4462.3	Indeterminate	< 20	Subadult
4462.4	Indeterminate	< 20	Subadult
8141.1	Indeterminate	< 20	Subadult
8141.2	Indeterminate	< 20	Subadult
4384.1	Indeterminate	< 20	Subadult

4384.2	Indeterminate	< 20	Subadult

3.2.6.1 Grave 7 (Sector 4)

3.2.6.1.1 Archaeothanatological analysis

A thorough anthropological analysis of Grave 7 yielded the presence of various bones from the lower body, which could potentially belong to a single individual with the stratigraphic number 8283.

3.2.6.1.2 Anthropological analysis. Determination of sex and age

The absence of sexual traits in the observed bones precludes the determination of the individual's sex. However, the remains appear to belong to an adult individual.

3.2.6.2 Burial without an ascribed grave number (Sector 4)

3.2.6.2.1 Archaeothanatological analysis

It has been determined that one stratigraphic unit, designated 4381, has not been assigned a grave number. The burial contains poorly preserved small fragments of human and animal bones, which could belong to a single individual.

3.2.6.2.2 Anthropological analysis. Determination of sex and age

The absence of sexual traits in the observed bones precludes the determination of the individual's sex. However, the remains appear to belong to an adult individual.

3.2.7.1 Grave 1 (Sector 5)

3.2.7.1.1 Archaeothanatological analysis

Grave 1 consists of a hypogeum with a single chamber, in which a minimum of 16 individuals were buried in a secondary deposit (see **Table 53**). This analysis has identified eight additional individuals in comparison to the previously published literature. The burial contains both sexes and all age ranges, exhibiting a loose or disarticulated anatomical connection. Consequently, determining the position of the bodies or the orientation of the disposal is not feasible, with the exception of individuals 50616 and 50700. It was observed that 50616 was in a right lateral decubitus position, while 50700 was in a prone decubitus position. The retrievable information is incomplete due to the disturbance of the hypogeum in the 16th century CE. A pit was excavated in the area, resulting in the destruction of the southeastern portion of the grave.

Table 53. Minimum Number of Individuals of each stratigraphic unit from Grave 1 (Sector 5).

Stratigraphic unit	Minimum Number of Individuals
50570	1
50574	13
50616	1
50700	1

3.2.7.1.2 Anthropological analysis. Determination of sex and age

Sex and age have been determined for one individual, consisting of a male young adult. The Brothwell system (1981) has provided a more precise age estimation through the analysis of molar attrition for four individuals (see **Table 54**).

Table 54. Assessment of molar attrition according to Brothwell (1981).

Individual	Tooth (in anthropological notation)	Score for molar attrition	Age in years
50616.2	M^1	4	25-35
50700	$_1M$	4+	25-35
50574.8	M^1	1	< 17 - 25
50574.9	M_1	4	25-35

Among the 15 indeterminate individuals, one is a child, one is a subadult, two are young adults, and eleven are adults. More detailed information can be seen in **Table 55**. For this grave, the anthropologists who registered the bone remains had previously assigned a code to one individual: Individual 2 was assigned the stratigraphic number 50616, even though only one individual was present for these stratigraphic units.

Table 55. Sex and age determination for each individual buried at Grave 1 (Sector 5).

Individual	Sex	Age (in years)	Age class (Buikstra & Ubelaker, 1997)
50570	Indeterminate	> 20	Adult
50574.1	Indeterminate	> 20	Adult
50574.2	Indeterminate	> 20	Adult
50574.3	Indeterminate	> 20	Adult
50574.4	Indeterminate	> 20	Adult
50574.5	Indeterminate	> 20	Adult
50574.6	Indeterminate	> 20	Adult
50574.7	Indeterminate	> 20	Adult
50574.8	Indeterminate	5-6	Child (3-12)
50574.9	Indeterminate	25-35	Young adult (20-35)
50574.10	Indeterminate	< 20	Subadult
50574.11	Indeterminate	> 20	Adult
50574.12	Indeterminate	> 20	Adult
50574.13	Indeterminate	> 20	Adult
50616.2	Male	25-35	Young adult (20-35)
50700	Indeterminate	25-35	Young adult (20-35)

3.2.8.1 Grave 2 (Sector 5)

3.2.8.1.1 Archaeothanatological analysis

The hypogeum contained the inhumations of at least six individuals (see **Table 56**). This determination contributes an additional individual to the extant published literature. The first individuals interred in Grave 2 were 50621 and 50615, which were buried as a primary deposit. Following its skeletonization, the hypogeum was opened with the purpose of accommodating two new burials, 50618 and 50620, the latter being positioned above the remains of 50621. Therefore, 50621 and 50615 were repositioned, resulting in the loss of anatomical connection, and were left in a secondary deposit. Both 50618 and 50620 exhibited no signs of disturbance and were maintained in a primary deposit. The question of whether 50618 and 5620 were buried simultaneously or successively remains unresolved, as the presence of a negligible amount of sediment between the two bodies hinders definitive determination. The last individual buried consists of 50619, which was placed above the two preceding deceased in a primary deposit. The three individuals (50618, 50619, and 50620) were buried in a southwest-northeast orientation, with the limbs flexed to the left. Individuals 50618 and 50620 were positioned in a left lateral decubitus position, while individual 50619 was positioned in a prone decubitus position. Following the burial of the deceased, the grave was sealed by filling the access shaft with rocks of a medium size. The burial remained undisturbed since the 16th century CE, when a cut disturbed the grave. In the 1960s, the site was once again disturbed when its southern area was destroyed by the construction of an underground parking lot. This destruction entailed the loss of several bones from the upper part of the skeleton from individual 50618.

Table 56. Minimum Number of Individuals of each stratigraphic unit from Grave 2 (Sector 5).

Inhumation phase	Stratigraphic unit	Minimum Number of Individuals
1st	50615	1
	50621	1
2nd	50618	2
	50620	1
3rd	50619	1

3.2.8.1.2 Anthropological analysis. Determination of sex and age

Sex and age have been determined for three individuals, consisting of a young adult female individual, and two male individuals (including one adolescent and one adolescent or young adult).

The Brothwell system (1981) has provided a more precise age estimation through the analysis of molar attrition for four individuals (see **Table 57**).

Table 57. Assessment of molar attrition according to Brothwell (1981).

Individual	Tooth (in anthropological notation)	Score for molar attrition	Age in years
50615.2	M^1	4	25-35
50618.1	M_1	3-	17-25
50620.3	M^1	4	25-35

Among the three indeterminate individuals, one is a middle adult, and two are adults. More detailed information can be seen in **Table 58**. For this grave, the anthropologists who registered the bone remains had previously assigned a code to two individuals: Individual 2 was assigned the stratigraphic number 50615, and Individual 3 was assigned the stratigraphic number 50620. However, only one individual was present for both stratigraphic units.

Table 58. Sex and age determination for each individual buried at Grave 2 (Sector 5).

Individual	Sex	Age (in years)	Age class (Buikstra & Ubelaker, 1997)
50615.2	Female	25-35	Young adult (20-35)
50621	Indeterminate	> 20	Adult
	Male	17-20	Adolescent (12-20) or young adult (20-35)
50618.2	Indeterminate	> 20	Adult
50620.3	Male	22-25	Young adult (20-35)
50619	Indeterminate	35-50	Middle adult (35-50)

3.2.8.2 Burials without an ascribed Sector or Grave number

3.2.8.2.1 Archaeothanatological analysis

Three individuals without a designated Sector or Grave have been identified while studying the skeletal remains of Plaça de la Gardunya. Each individual is assigned a unique stratigraphic unit, designated by the codes 8236, 20323, and 51091, respectively.

3.2.8.2.2 Anthropological analysis. Determination of sex and age

The absence of sexual traits in the observed bones precludes the determination of the individuals' sex. However, the remains appear to belong to adult individuals. For a more comprehensive overview, refer to ***Table 59***.

Table 59. Sex and age determination for the individuals buried at the stratigraphic units 8236, 20323, and 51091.

Individual	Sex	Age (in years)	Age class (Buikstra & Ubelaker, 1997)
8236	Indeterminate	> 20	Adult
20323	Indeterminate	> 20	Adult
51091	Indeterminate	> 20	Adult

3.3 DENTAL MICROWEAR PATTERN

3.3.1 Materials

3.3.1.1 Gird Lashkir

The site of Gird Lashkir yielded a substantial dental assemblage comprising an initial sample of 254 teeth that belong to 11 distinct individuals distributed across 10 graves. A detailed replica of each recovered tooth was created and collected during fieldwork at the site. After observation through Optical Microscopy, only one representative tooth per individual was selected, resulting in a final sample of 11 teeth (**Table 60**).

Table 60. Initial and final tooth samples from Gird Lashkir.

Individual	Initial sampled teeth	Final sample (in anthropological notation)
4	15	$_1$P
5	31	$_2$P
6.1	29	$_1$m
6.2	21	^{1}M
7	20	m$_2$
10	25	$_2$M
12.1	14	$_2$P
13	20	$_2$m
14	29	^{1}M
15	31	^{1}P
16	19	$_2$M

3.3.1.2 Gir-e Gomel

The site of Gir-e Gomel provided an initial sample of 88 teeth that belong to 6 distinct individuals. A detailed replica was created during a brief research stay in the facilities provided by Dr. Daniele Morandi Bonacossi, Principal Investigator of *The Kurdish-Italian Gir-e Gomel Archaeological Project (KIGAP)*, in the city of Duhok (Iraq) during their fieldwork campaign. After observation through Optical Microscopy, only one representative tooth per individual was selected, resulting in a final sample of 5 teeth (**Table 61**). The individual from Grave 45 was excluded due to the absence of microwear traces in the examined tooth.

Table 61. Initial and final tooth samples from Gir-e Gomel.

Individual	Initial sampled teeth	Final sample (in anthropological notation)
24	11	$_2$P
42	28	$_1$M
45	1	None
47	25	$_2$M
48	16	M^1
49	7	^{3}M

3.3.1.3 Plaça de la Gardunya

The site of Plaça de la Gardunya has yielded an initial sample of 31 first molars, each one corresponding to a different individual. Samples were collected at the Archaeological Archive of the Collection Centre from the Barcelona History Museum (MUHBA) and the copy of each tooth was performed at the Seminari d'Arqueologia Prehistòrica del Pròxim Orient (SAPPO) laboratories from the Grup de Recerca Arqueològica de la Mediterrània i del Pròxim Orient (GRAMPO) research group, which belongs to the Department of Prehistory of the Autonomous University of Barcelona (UAB). After observation through Optical Microscopy, only one representative tooth per individual was selected, resulting in a final sample of 22 teeth (**Table 62**). The individuals 4174 and 4319.2 from Grave 2 (Sector 4), 4328.6, 4430.7, 4430.9 and 4450 from Grave 3/4 (Sector 4), and 50616.2, 50574.8 and 50574.9 from Grave 1 (Sector 5) were excluded due to the absence of microwear traces in the examined tooth.

Table 62. Initial tooth samples for Plaça de la Gardunya.

Sector	Grave	Individual	Final sample (in anthropological notation)
4	2	4174	None
		4319.2	None
	3/4	4328.6	None
		4388	M^1
		4473	$_1$M
		4450	None
		4430.7	None
		4430.8	$_1$M
		4430.9	None
		4389.11	$_1$M
		4389.12	M$_1$

		4389.13	M_1
		4389.14	$_1M$
		4389.15	M_1
		4389.16	M_1
		4389.17	M_1
		4389.18	M_1
		4389.19	M_1
		4389.20	$_1M$
		4389.21	M_1
		4389.22	M_1
		4389.23	M_1
		4389.24	M_1
		4391	$_1M$
5	1	50616.2	None
		50700	$_1M$
		50574.8	None
		50574.9	None
	2	50620.3	M^1
		50618.1	M_1
		50615.2	M^1

3.3.2 Methods

First, the identified teeth from each individual were cleaned with a cotton swab with pure acetone to remove the adhered grit and dust, followed by ethanol, and left to air-dry. Due to the methodology's requirement for subjecting the samples to a metallization process, it is not suitable for use with the original samples. Consequently, replicas of the samples were produced. A negative cast was created by applying *President MicroSystem Coltène Affinis Regular Body*, a medium consistency hydrophobic polyvinylsiloxane silicone. This impression material is widely used in dental microwear research and odontological practice due to its precision and resolution (Galbany et al., 2004). The cast was filled with a *Feroca® FEROPUR PR55+E5* rigid two-component polyurethane resin in stoichiometric proportions, using a Pasteur pipette, and mixed thoroughly to prevent the formation of air bubbles on the dental surfaces. Following the fabrication of the replica, observations were conducted at 40× magnification using an *Olympus SZ61* binocular lens. This process enabled the discarding of teeth exhibiting poorly preserved microwear patterns on the buccal surfaces.

Samples with preserved microwear in the surface of the enamel underwent further preparation and observation using Scanning Electron Microscopy at the Servei de Microscopia of the Autonomous University of Barcelona. Replica of the teeth were mounted on aluminum stubs with term

fusible gum, and sputter coated with a 5 nm coat of gold-palladium with a *K250 Coater Carbon* attached to an *Emitech K550X*. Parameters were fixed at 1 minute sputtering cycle through argon gas, at a 50 mm working distance (WD), a pressure of 0.05 mbar, and an intensity of 25 mA. Samples were observed with a *Zeiss EVO ® MA 10* Scanning Electron Microscope in high vacuum mode, following standard methodology for buccal microwear analysis (Pérez-Pérez et al., 1994). Parameters were fixed at 15-kV acceleration voltage, and a ranged working distance (WD) between 15 to 30 mm. Micrographs were taken at 100× magnification, preferably on the middle third of the buccal surface of the teeth, avoiding the cervical and occlusal rims (Galbany et al., 2004), as well as 200× and 500× magnifications to observe taphonomical alterations of the enamel.

To ensure the representativeness of the sample, a standardized selection criterion was employed. From the postcanine teeth that exhibit the most preserved microwear patterns, one tooth is selected for each individual from the left side of the mandible, following the indicated sequence of preference. The first or second molar, the second premolar, the first premolar, or the third molar. In the absence of a well-preserved buccal microwear pattern on either tooth or the original absence of the sampled individual's teeth, the selection criteria involved the selection of the same teeth order, beginning with the left side of the maxilla, followed by the right side of the mandible, and concluding with the right side of the maxilla (Estebaranz et al., 2009; Gluitz et al., 2023; Lalueza et al., 1996; Pérez-Pérez et al., 1994).

Micrographs of the final selected samples were cropped to a fixed area of 0.56 mm^2 for measurement standardization (Galbany et al., 2004; Jarošová et al., 2016). Cropped images were enhanced with a High Pass Filter (HPF) and Curves adjustment in Photoshop CS6 software. The High Pass Filter has been utilized to enhance the clarity and contrast of an image by accentuating the edges during transitions in brightness and texture. Conversely, the Curves function has been employed to optimize the contrast of an image, thereby improving its visual quality. Striations that exceeded 15 µm in length and possessed a length-to-width ratio of 4:1 were meticulously counted, measured, and oriented using ImageJ software (Estebaranz et al., 2009; Martínez et al., 2020). Following the protocol of Pérez-Pérez et al. (1994), the orientations of the striations were classified in 45-degree intervals: horizontal striations (abbreviated as H) are composed of traces going from 0 to 22.5 degrees, and 157.5 to 180 degrees; vertical striae (abbreviated as V), from 67.5 to 112.5 degrees; mesio-occlusal to disto-cervical traces (abbreviated as MD) and disto-occlusal to mesio-cervical traces (abbreviated as DM) depend on the tooth's location. For MD striations, left mandibular and right maxillary molars have a degree ranging from 112.5 to 157.5, while right mandibular and left maxillary molars have a degree ranging from 22.5 to 67.5.

For DM striations, the degrees are inverted, such as left mandibular and right maxillary molars have a degree ranging from 22.5 to 67.5, while right mandibular and left maxillary molars have a degree ranging from 112.5 to 157.5 (**Figure 41**). For each striae orientation (H, V, MD and DM), the total number of striae, its average length and its standard deviation has been calculated. This results in 15 quantitative variables that define the microwear pattern of an individual. Finally, three indices were calculated: the ratio of horizontal and vertical striae (NH/NV), the ratio of horizontal striae and total striae density (NH/NT), and the ratio of vertical striae and total striae density (NV/NT) (Lalueza et al., 1996; Pérez-Pérez et al., 1994).

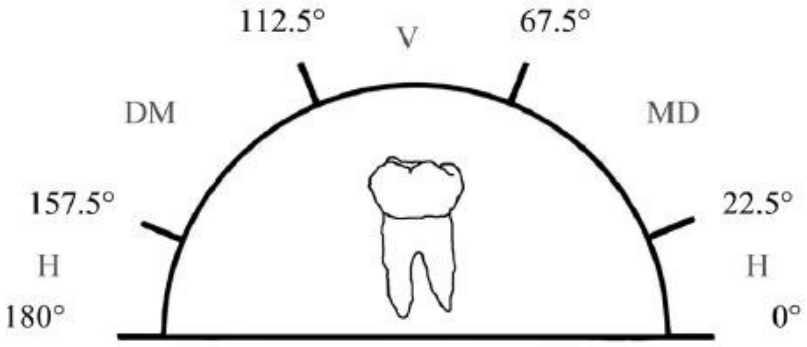


Figure 41. Schematic diagram of the striae orientations on the buccal side of the teeth. Image extracted from Zhou & Fu (2025), Figure 1.

SPSS software has been used to observe intrapopulation variability in terms of age and sex. Thereafter, the microwear pattern of the studied individuals was classified into a diet pattern following the analysis of known diets published by Lalueza et al. (1996). The known diets belong to different hunter-gatherer pastoralist and agriculturalist populations (***Table 63***). A comparative analysis has been conducted on the dietary tendencies of the individuals from Plaça de la Gardunya by examining the microwear patterns of various archaeological sites from the Iberian Peninsula. These sites range in chronology from the Neolithic to the Bronze Age, and their microwear patterns have been previously published. The sites of Cova de l'Avi (Hernando, 2024), Tossal de les Basses (Salazar-García et al., 2016), Can Gambús (Alrousan 2009) and Caserna de Sant Pau del Camp (Estebaranz-Sánchez et al., 2008) belong to the Neolithic period. Sites spanning from the Late Neolithic to the Chalcolithic include Cova de Can Sadurní (Hernando, 2024), Cova Foradada (Hernando, 2024) and Cova de la Guineu (Hernando, 2024). Ranging from the Late Neolithic to the Bronze Age is the site of Cova del Trader. Sites from the Chalcolithic period

include El Portalón de la Cueva Mayor (García-González et al., 2019), El Alto de la Huesera (García-González et al., 2019), Molinico (Romero & Juan, 2007) and Cueva El Mirador (Hernando, Willman, et al., 2020). A site ranging from the Late Chalcolithic to the Middle Bronze Age is Roc de les Orenetes (Hernando, 2024). Lastly, sites ranging from the Early to the Middle Bronze Age include Mercat de Santa Caterina (Gluitz et al., 2023), Cova de Valdavara (Hernando, Willman, et al., 2020), Cova del Gegant (Hernando, 2024), Cova dels Galls Carboners (Hernando, 2024), Cabezo Redondo (Romero & Juan, 2007), Cova dels Blaus (Romero et al., 2004) and Mar i Muntanya (Galbany et al., 2008). Lastly, post-mortem taphonomic and diagenetic alterations on tooth enamel are reported for the studied populations, including both physical and chemical effects.

Table 63. Populations with a known diet (Lalueza et al., 1996) that have been used to classify the diet of the studied individuals.

Diet	Population	Territory	*n*
Carnivore (terrestrial and marine animals)	Fuegian	Tierra del Fuego	20
Carnivore (terrestrial and marine animals)	Inuit	Arctic, Subarctic	20
Carnivore (marine animals)	Vancouver Islander	Canada	17
Carnivore (terrestrial animals)	Sámi	Norway, Sweden, Finland, Russia	5
Omnivore	Andamanese	India	18
Omnivore	Vedda	Sri Lanka	9
Omnivore	San	Southern Africa	15
Omnivore	Tasmanian	Australia	11
Omnivore	Australian	Australia	18
Vegetarian	Indian	Eastern India	20

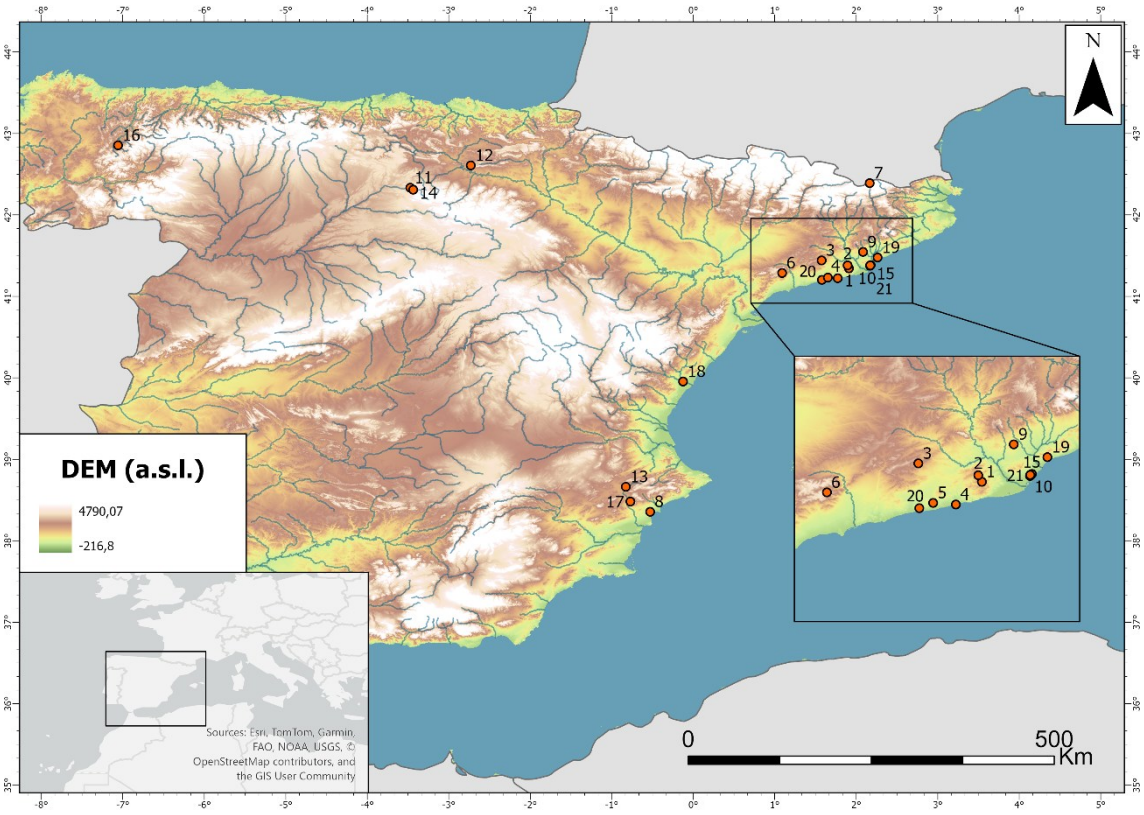


Figure 42. Archaeological sites with published dental microwear striation patterns from the buccal side of the tooth, belonging to a chronology ranging from the Neolithic to the Bronze Age. 1) Cova de Can Sadurní, 2) Cova de l'Avi, 3) Cova de la Guineu, 4) Cova del Gegant, 5) Cova del Trader, 6) Cova dels Galls Carboners, 7) Roc de les Orenetes, 8) Tossal de les Basses, 9) Can Gambús, 10) Caserna de Sant Pau del Camp, 11) El Portalón de la Cueva Mayor, 12) El Alto de la Huesera, 13) Molinico, 14) Cueva El Mirador, 15) Mercat de Santa Caterina, 16) Cova de Valdavara, 17) Cabezo Redondo, 18) Cova dels Blaus, 19) Mar i Muntanya, 20) Cova Foradada, and 21) Plaça de la Gardunya.

3.4 ZooMS

3.4.1 Materials

Sampling for ZooMS analysis consisted in collecting faunal individuals, whose species could not be determined by morphological identification, from the sites of Gird Lashkir, Gir-e Gomel, and Plaça de la Gardunya (**Table 64**). A total of 11 samples have been submitted for species identification. This determination is fundamental in order to elaborate stable isotope baselines for interpreting diet from past populations, as well as to define the trophic level of animal and human individuals.

Table 64. Ovicaprid samples for ZooMS analysis.

Site	Sample ID	Bone	Taxa	Starting mass (in mg)
Gird Lashkir	TL52	Mandible	Ovicaprid	24.60
	TL53	Mandible	Ovicaprid	22.70
	TL54	Mandible	Ovicaprid	15.10
	TL55	Phalanx	Ovicaprid	28.90
	TL56	Mandible	Ovicaprid	29.90
	TL57	Mandible	Ovicaprid	20.30
	TL58	Mandible	Ovicaprid	27.40
	TL59	Mandible	Ovicaprid	20.40
	TL60	Mandible	Ovicaprid	28.70
Gir-e Gomel	GG25	Long bone	Ovicaprid	16.80
Plaça de la Gardunya	PG93	Rib	Ovicaprid	19.50

3.4.2 Methods

Zooarchaeology by Mass Spectrometry has been performed on 11 ovicaprid samples to provide an accurate taxonomical identification, following the modified method developed by Buckley et al. (2009), in the laboratories of the Institut de Ciència i Tecnologia Ambientals from the Autonomous University of Barcelona (ICTA-UAB). This method allows to obtain the peptide mass fingerprint of Type I collagen from bone samples. A fragment of bone was powdered with an agate pestle and mortar, which were cleaned with pure ethanol between samples to avoid cross contamination. A sample size ranging between 15 and 30 mg were collected in a labeled Eppendorf tube. The powdered sample was demineralized in 250 µl of 0.6 M hydrochloric acid (HCl). After demineralization, the acid was triple washed in and a solution of 200 µl, 50 mM, and pH 8 of ammonium bicarbonate ($(NH_4)HCO_3$). Then, the sample was gelatinized for one hour in 65 °C with 100 µl ammonium bicarbonate, in order to prepare the primary amino acid structure for enzymatic digestion. When collagen extraction was complete, a 50 µl aliquot was transferred to

a new Eppendorf tube, and 0.4 µg of trypsin enzyme was added for chemical digestion during 18 hours at 37 °C. Trypsin splits the C-terminal peptide bonds or arginine (R) and lysine (K) residues and adds to each peptide the mass of a water molecule, which results in different collagen peptides that differ in mass and length between taxa (Richter et al., 2022). To stop the digestion process, 1 µl of 5% trifluoroacetic acid ($C_2HF_3O_2$, also known as TFA) was added. Afterwards, samples were desalted and purified with *ThermoScientific Pierce™* 100 µl C18 Pipette Tips filters. Finally, an aliquot of 1 µl of each sample was mixed with a matrix solution that cocrystalizes with the peptides, composed by 1 µl of α-cyano-4-hydroxycinnamic acid ($C_{10}H_7NO_3$), and then spotted in triplicate on an *AB 384 Opti-TOF™* steel target plate. The plate was then analyzed on an *Applied Biosystems/MDS SCIEX* 4800 MALDI TOF/TOF™ Analyzer, a mass spectrometer composed of a Matrix-Assisted Laser Desorption Ionization (MALDI) and a Time-Of-Flight/Time-Of-Flight ion detector. The resulting spectra were averaged and analyzed with the software package *mMass*, developed by Strohalm et al. (2008), and identified comparing the peptide mass fingerprints with published databases (Buckley et al., 2009, 2010; Kirby et al., 2013; Welker et al., 2016).

3.5 STABLE ISOTOPES

3.5.1 Materials

3.5.1.1 Gird Lashkir

Bone collagen samples have been collected for the purpose of studying dietary patterns. In the initial phase of the sampling process, only rib fragments were collected due to the fact that rib is a type of bone that does not compromise the percentage of preserved skeletal remains. Following the unsuccessful extraction of bone collagen, a second piece of rib was sampled for the purpose of extracting bone collagen. The second stage of the sampling process entailed the collection of long bones, a measure taken to account for the potential failure of bone collagen extraction. This decision was based on the anatomical characteristics of bones, wherein the cortical portion is thicker and more thoroughly preserved compared to that of ribs. A total of 24 bone samples were collected from 12 individuals, representing 11 different graves. The third and final stage of the sampling process entailed the collection of teeth, given the negligible preservation of bone collagen. Consequently, 21 tooth enamel samples have been collected to facilitate the interpretation of dietary patterns from carbonates. These tooth enamel samples were also collected in order to perform analysis on residence patterns. A comprehensive overview of the samples is provided in **Table 65**.

Table 65. Human samples collected from Gird Lashkir.

Grave	Sample ID	Bone	Tissue age	Starting mass (in mg)
4	TL21	Left rib	Last 3 to 5 years of life	279.30
	TL37	Right rib	Last 3 to 5 years of life	313.30
	TL43	Right fibula	Last 20 to 33 years of life	304.00
	TL62	LLI2	3 months to 5 years old	10.09
	TL72	LLM3	9.5 to 12 years old	5.12
5	TL22	Right rib	Last 3 to 5 years of life	247.70
	TL44	Right radius	Last 10 to 20 years of life	314.10
	TL63	LLI2	3 months to 5 years old	10.08
6.1	TL24	Right rib	Last 3 to 5 years of life	235.70
	TL34	Right rib	Last 3 to 5 years of life	338.90
	TL61	LLI2	3 months to 5 years old	10.49
	TL73	LLM3	9.5 to 12 years old	4.95
6.2	TL23	Right rib	Last 3 to 5 years of life	257.40
	TL33	Right rib	Last 3 to 5 years of life	267.00
	TL45	Right fibula	Last 20 to 33 years of life	239.90
	TL64	LLI2	3 months to 5 years old	10.48
	TL74	ULM3	9.5 to 12 years old	6.35

7	TL28	Left rib	Last 3 to 5 years of life	337.10
	TL38	Left rib	Last 3 to 5 years of life	266.40
	TL46	Right femur	Last 25 to 50 years of life	235.40
	TL65	LLI2	3 months to 5 years old	11.27
	TL75	URM3	9.5 to 12 years old	4.89
9	TL26	Left rib	Last 3 to 5 years of life	105.50
10	TL25	Right rib	Last 3 to 5 years of life	239.90
	TL35	Right rib	Last 3 to 5 years of life	309.20
	TL47	Left humerus	Last 17 to 33 years of life	247.80
	TL66	LLI2	3 months to 5 years old	16.07
	TL76	URM3	9.5 to 12 years old	5.21
11	TL27	Right rib	Last 3 to 5 years of life	259.80
	TL36	Right rib	Last 3 to 5 years of life	332.60
	TL48	Right femur	Last 25 to 50 years of life	258.70
12.1	TL67	LRI2	3 months to 5 years old	13.17
	TL77	LRM3	9.5 to 12 years old	9.02
13	TL49	Left tibia	Last 20 to 50 years of life	286.30
	TL70	LRM1	0 to 2.5 years old	10.00
	TL71	LRM1	0 to 2.5 years old	8.47
14	TL50	Right tibia	Last 20 to 50 years of life	221.10
	TL68	LLI2	3 months to 5 years old	10.70
	TL79	LRM3	9.5 to 12 years old	5.53
15	TL51	Right femur	Last 25 to 50 years of life	302.10
	TL69	LLI2	3 months to 5 years old	10.57
	TL78	ULM3	9.5 to 12 years old	4.97
16	TL89	Right femur	Last 25 to 50 years of life	386.42
	TL90	LRM1	0 to 2.5 years old	6.82
	TL91	URI1	3 months to 5 years old	11.44

A total of 23 samples of fauna have been collected to establish a local baseline, including 7 *Ovis aries*, 1 *Capra hircus*, 2 *Capra aegagrus*, 1 *Gazella* sp., *3 Gazella gazella,* 4 *Sus domesticus*, and 1 *Helicidae* (see **Table 66**).

Table 66. Faunal samples collected from Gird Lashkir.

Species	Sample ID	Bone	Starting mass (in mg)
Ovis aries	TL4	Rib	292.10
	TL32	Rib	279.30
Ovis aries	TL52	Mandible	269.38
Ovis aries	TL53	Mandible	346.61
Ovis aries	TL55	Phalanx	224.17
Ovis aries	TL56	Mandible	326.96
Ovis aries	TL57	Mandible	349.37
Ovis aries	TL60	Mandible	376.75

Capra hircus	TL83	Mandible	327.06
Capra aegagrus	TL81	Phalanx	261.71
Capra aegagrus	TL82	Mandible	253.91
Gazella sp.	TL1	Phalanx	354.70
	TL29	Phalanx	208.60
Gazella gazella	TL86	Mandible	338.50
Gazella gazella	TL87	Phalanx	279.85
Gazella gazella	TL88	Phalanx	366.51
Sus domesticus	TL2	Metapodial	436.30
	TL30	Metapodial	367.40
Sus domesticus	TL3	Rib	329.10
	TL31	Rib	449.90
Sus domesticus	TL84	Phalanx	334.15
Sus domesticus	TL85	Mandible	235.21
Helicidae	TL80	Shell	10.89

3.5.1.2 Gir-e Gomel

Bone collagen samples have been collected for the evaluation of dietary patterns. Rib fragments were collected for analysis, as they do not compromise the percentage of preserved skeletal remains. In the event that the ribs exhibited signs of poor preservation, fragments of long bones were collected for further analysis. A total of 10 bone samples were collected from 8 individuals, all belonging to different graves. To further facilitate the interpretation of dietary patterns from carbonates, 9 additional tooth enamel samples from these individuals were collected. The collection of tooth enamel samples was also undertaken for the purpose of conducting a subsequent analysis of residence patterns. A thorough overview of the samples is provided in **Table 67Table 65**.

Table 67. Human samples collected from Gir-e Gomel.

Grave	Sample ID	Bone	Tissue age	Starting mass (in mg)
24	GG15	Right rib	Last 3 to 5 years of life	296.60
	GG28	LLI1	3 months to 5 years old	10.38
	GG34	URM3	9.5 to 12 years old	6.03
42	GG16	Right rib	Last 3 to 5 years of life	225.10
48	GG17	Left rib	Last 3 to 5 years of life	239.50
	GG27	ULI2	3 months to 5 years old	12.34
	GG32	ULM3	9.5 to 12 years old	9.00
47	GG18	Right rib	Last 3 to 5 years of life	224.40
	GG29	LLI2	3 months to 5 years old	10.06

	GG33	LLM3	9.5 to 12 years old	7.23
44F/49	GG19	Right rib	Last 3 to 5 years of life	284.70
	GG20	Fibula	Last 20 to 33 years of life	301.60
	GG31	URM3	9.5 to 12 years old	8.90
50	GG11	Fibula	Last 20 to 33 years of life	356.20
51	GG13	Rib	Last 3 to 5 years of life	328.40
63	GG14	Left rib	Last 3 to 5 years of life	239.50
	GG21	Left rib	Last 3 to 5 years of life	394.30
	GG26	LLI2	3 months to 5 years old	11.52
	GG30	LRM3	9.5 to 12 years old	7.45

Six bone samples from animals were collected with the objective of establishing a local baseline, including 2 *Capra hircus*, 1 ovicaprid, and 3 *Ovis aries* (see **Table 68**).

Table 68. Faunal samples collected from Gir-e Gomel.

Species	Sample ID	Bone	Starting mass (in mg)
Capra hircus	GG5	Long bone	278.40
Capra hircus	GG10	Phalanx	222.50
Ovis aries	GG6	Metacarpal	463.50
Ovicaprid	GG7	Long bone	371.90
Ovis aries	GG8	Phalanx	292.80
Ovis aries	GG9	Phalanx	394.50

3.5.1.3 Plaça de la Gardunya

Bone collagen samples have been collected for the aim of performing analysis on dietary patterns. The bone type has been selected with the objective of collecting the maximum number of individuals per stratigraphic unit, in the event that numerous individuals are assigned the same stratigraphic unit number. Consequently, the most prevalent bone with the same laterality has been sampled in these cases. In other cases, when the individual was only identified by its skull, a fragment of skull has been collected. Furthermore, to conduct a comprehensive analysis of residential patterns, a single tooth enamel sample has been obtained from each individual. In instances where teeth and bones are found to be associated with the same individual, a bone

fragment and a tooth are collected for analysis. This approach enables the reconstruction of dietary patterns and residence patterns. The sampling process has yielded the collection of bone and/or teeth from a total of 82 individuals, which are distributed as follows: 14 individuals from Grave 2 (Sector 4), 51 individuals from Grave 3/4 (Sector 4), 1 individual from Grave 5 (Sector 4), 1 individual from Grave 7 (Sector 4), 11 individuals from Grave 1 (Sector 5), and 4 individuals from Grave 2 (Sector 5). A comprehensive overview of the samples is provided in **Table 69**.

Table 69. Human samples collected from Plaça de la Gardunya.

Sector	Grave	Individual	Sample ID	Bone	Tissue age	Starting mass (in mg)
4	2	4174	PG1	Humerus	Last 17 to 33 years of life	255.20
			PG62	LLM1	0 to 2.5 years old	7.36
			PG102	LLM1	0 to 2.5 years old	10.80
		4232	PG2	Right radius	Last 10 to 20 years of life	205.40
		4312	PG3	Skull	Last 10 to 50 years of life	320.70
		4313	PG4	Skull	Last 10 to 50 years of life	283.10
		4314	PG5	Skull	Last 10 to 50 years of life	210.10
		4315	PG6	Skull	Last 10 to 50 years of life	316.40
		4317	PG7	Skull	Last 10 to 50 years of life	250.60
		4318	PG8	Right femur	Last 25 to 50 years of life	213.60
		4319.1	PG9	Left tibia	Last 20 to 50 years of life	307.30
		4319.2	PG61	LLM1	0 to 2.5 years old	6.56
			PG101	LLM1	0 to 2.5 years old	12.15
		4319 ("c").1	PG35	Right tibia	Last 20 to 50 years of life	269.20
		4319 ("c").2	PG36	Right tibia	Last 20 to 50 years of life	319.00
		4319 (a)	PG49	Humerus	Last 17 to 33 years of life	305.20
		4319 (b)	PG50	Humerus	Last 17 to 33 years of life	312.50
	3/4	3402	PG48	Skull	Last 10 to 50 years of life	227.00
		4328.1	PG24	Left humerus	Last 17 to 33 years of life	286.10
		4328.2	PG25	Left humerus	Last 17 to 33 years of life	265.60
		4328.3	PG86	Left humerus	Last 17 to 33 years of life	212.10
		4328.4	PG87	Left humerus	Last 17 to 33 years of life	288.10
		4328.5	PG88	Left humerus	Last 17 to 33 years of life	272.70

4328.6	PG59	LRM1	0 to 2.5 years old	5.57
	PG99	LRM1	0 to 2.5 years old	10.42
4376	PG89	Right femur	Last 25 to 50 years of life	278.50
4379.1	PG53	Skull	Last 10 to 50 years of life	204.50
4379.2	PG54	Skull	Last 10 to 50 years of life	283.80
4388	PG90	Left ulna	Last 17 to 33 years of life	253.90
	PG56	URM1	0 to 2.5 years old	4.44
	PG96	URM1	0 to 2.5 years old	10.23
4389.1	PG10	Right femur	Last 25 to 50 years of life	305.40
4389.2	PG11	Right femur	Last 25 to 50 years of life	287.50
4389.3	PG12	Right femur	Last 25 to 50 years of life	299.00
4389.4	PG13	Right femur	Last 25 to 50 years of life	206.80
4389.5	PG14	Right femur	Last 25 to 50 years of life	297.00
4389.6	PG15	Right femur	Last 25 to 50 years of life	288.80
4389.7	PG16	Right femur	Last 25 to 50 years of life	243.10
4389.8	PG17	Right femur	Last 25 to 50 years of life	232.10
4389.9	PG18	Right femur	Last 25 to 50 years of life	281.70
4389.10	PG19	Right femur	Last 25 to 50 years of life	268.40
4389.11	PG71	LLM1	0 to 2.5 years old	5.55
	PG111	LLM1	0 to 2.5 years old	10.28
4389.12	PG72	LRM1	0 to 2.5 years old	6.44
	PG112	LRM1	0 to 2.5 years old	10.81
4389.13	PG73	LRM1	0 to 2.5 years old	6.93
	PG113	LRM1	0 to 2.5 years old	10.89
4389.14	PG74	LLM1	0 to 2.5 years old	7.94
	PG114	LLM1	0 to 2.5 years old	11.21

4389.15	PG75	LRM1	0 to 2.5 years old	6.89
	PG115	LRM1	0 to 2.5 years old	10.58
4389.16	PG76	LRM1	0 to 2.5 years old	5.64
	PG116	LRM1	0 to 2.5 years old	11.45
4389.17	PG77	LRM1	0 to 2.5 years old	6.77
	PG117	LRM1	0 to 2.5 years old	10.88
4389.18	PG78	LRM1	0 to 2.5 years old	7.82
	PG118	LRM1	0 to 2.5 years old	10.17
4389.19	PG79	LRM1	0 to 2.5 years old	5.38
	PG119	LRM1	0 to 2.5 years old	11.91
4389.20	PG80	LLM1	0 to 2.5 years old	6.57
	PG120	LLM1	0 to 2.5 years old	12.5
4389.21	PG81	LRM1	0 to 2.5 years old	5.89
	PG121	LRM1	0 to 2.5 years old	10.68
4389.22	PG82	LRM1	0 to 2.5 years old	6.97
	PG122	LRM1	0 to 2.5 years old	10.03
4389.23	PG83	LRM1	0 to 2.5 years old	4.94
	PG123	LRM1	0 to 2.5 years old	10.14
4389.24	PG84	LRM1	0 to 2.5 years old	7.95
	PG124	LRM1	0 to 2.5 years old	12.03
4390	PG37	Left femur	Last 25 to 50 years of life	304.60
4391	PG70	LLM1	0 to 2.5 years old	4.18
	PG110	LLM1	0 to 2.5 years old	10.51
4392	PG55	Right femur	Last 25 to 50 years of life	215.70
4430.1	PG28	Left radius	Last 10 to 20 years of life	217.70
4430.2	PG29	Right femur	Last 25 to 50 years of life	294.70

		4430.3	PG30	Right femur	Last 25 to 50 years of life	256.60
		4430.4	PG31	Right femur	Last 25 to 50 years of life	311.10
		4430.5	PG32	Right femur	Last 25 to 50 years of life	273.40
		4430.6	PG33	Right femur	Last 25 to 50 years of life	294.40
		4430.7	PG51	LRM1	0 to 2.5 years old	8.03
			PG94	LRM1	0 to 2.5 years old	13.11
		4430.8	PG52	LLM1	0 to 2.5 years old	8.26
			PG95	LLM1	0 to 2.5 years old	11.10
		4430.9	PG57	ULM1	0 to 2.5 years old	4.95
			PG97	ULM1	0 to 2.5 years old	10.24
		4450	PG27	Skull	Last 10 to 50 years of life	288.50
			PG58	LRM1	0 to 2.5 years old	6.77
			PG98	LRM1	0 to 2.5 years old	10.34
		4463	PG26	Left femur	Last 25 to 50 years of life	296.70
		4473	PG20	Skull	Last 10 to 50 years of life	302.40
			PG60	LLM1	0 to 2.5 years old	9.35
			PG100	LLM1	0 to 2.5 years old	10.22
		4475	PG85	Right femur	Last 25 to 50 years of life	228.40
	5	8141	PG39	Right femur	Last 25 to 50 years of life	222.20
	7	8283	PG21	Right femur	Last 25 to 50 years of life	273.80
5	1	50574.1	PG41	Skull	Last 10 to 50 years of life	211.50
		50574.2	PG42	Skull	Last 10 to 50 years of life	301.50
		50574.3	PG43	Skull	Last 10 to 50 years of life	291.70
		50574.4	PG44	Skull	Last 10 to 50 years of life	234.60
		50574.5	PG45	Skull	Last 10 to 50 years of life	293.20
		50574.6	PG46	Skull	Last 10 to 50 years of life	266.10

	50574.7	PG47	Skull	Last 10 to 50 years of life	235.10
	50574.8	PG68	URM1	0 to 2.5 years old	7.52
		PG108	URM1	0 to 2.5 years old	11.43
	50574.9	PG69	LRM1	0 to 2.5 years old	8.08
		PG109	LRM1	0 to 2.5 years old	11.92
	50616.2	PG23	Skull	Last 10 to 50 years of life	306.50
		PG66	URM1	0 to 2.5 years old	4.68
		PG106	URM1	0 to 2.5 years old	13.41
	50700	PG38	Femur	Last 25 to 50 years of life	213.90
		PG67	LLM1	0 to 2.5 years old	4.56
		PG107	LLM1	0 to 2.5 years old	10.69
2	50615.2	PG91	Skull	Last 10 to 50 years of life	292.00
		PG65	URM1	0 to 2.5 years old	4.24
		PG105	URM1	0 to 2.5 years old	10.08
	50618.1	PG34	Right rib	Last 3 to 5 years of life	269.80
		PG63	LRM1	0 to 2.5 years old	4.12
		PG103	LRM1	0 to 2.5 years old	10.23
	50619	PG40	Skull	Last 10 to 50 years of life	313.40
	50620.3	PG22	Skull	Last 10 to 50 years of life	255.60
		PG64	URM1	0 to 2.5 years old	4.49
		PG104	URM1	0 to 2.5 years old	10.63

A total of two faunal samples were retrieved from the animal remains at Plaça de la Gardunya, comprising one *Bos taurus* and one *Ovis aries*, thereby serving as a baseline for further analysis (**Table 70**).

Table 70. Faunal samples from Plaça de la Gardunya.

Species	Sample ID	Bone	Starting mass (in mg)
Bos taurus	PG92	Rib	281.10
Ovis aries	PG93	Ribs	325.10

3.5.2 Methods

Samples have been processed and analyzed using two different methodologies, depending on the stable isotope to be studied. Carbon and nitrogen stable isotopes have been extracted from bone collagen and analyzed with an Elemental Analyzer Isotope Ratio Mass Spectrometer (EA-IRMS). Oxygen and strontium have been extracted from tooth enamel hydroxyapatite, and carbonates have been analyzed with a GasBench II Isotope Ratio Mass Spectrometer (GC-IRMS), and a Multi Collector Inductively Coupled Mass Spectrometer (MC-ICP-MS), respectively. Carbon stable isotope from tooth enamel hydroxyapatite was also measured with an GC-IRMS in the cases in which bone collagen could not be extracted due to sample preservation.

3.5.2.1 Bone collagen extraction

Bone samples have been processed for collagen extraction. This procedure has been performed at the Laboratori d'Arqueologia i Paleoecologia Biomolecular (BIOMAP) of the Institut de Ciència i Tecnologia Ambientals, from the Autonomous University of Barcelona (ICTA-UAB). The followed protocol consisted in demineralize, gelatinize, filtrate, and lyophilize collagen from bone. Samples underwent a cleaning procedure to remove any sediment and taphonomical contaminants by using a scalpel. The spongy part of the bones was removed, leaving only the cortical part, given that sediment tends to adhere to the vascular cavities. Once clean, the bones were fractured longitudinally to obtain elongated fragments, and these were weighed on an analytical microbalance to obtain a sample range of 200-300 mg. The sample was then placed inside a labeled sterile 15 ml conical centrifuge tube to start the demineralization process. 8 ml of 0.6 M refrigerated hydrochloric acid (HCl) was added to the samples, which were and kept at 5 °C for a range of 2 to 10 days, depending on bone preservation, size, and density. The acid was changed

every three days to prevent its weakening effect. The process of bone demineralization removes minerals or mineral salts adhered to the bones, and transforms the samples from a solid to a gelatinous and lighter state (a pseudomorph). To completely remove the hydrochloric acid from the samples, a triple rinse with *Milli-Q® system* ultrapure water (Type I) was applied. Afterwards, the samples were washed once with 0.05 M sodium hydroxide (NaOH) for 20 minutes to dissolve base-soluble contaminants, such as humic acids, which can damage the samples. Samples were triple rinsed again with ultrapure water to remove the sodium hydroxide. Once the samples were demineralized and decontaminated, they were gelatinized through hydrolysis, a chemical reaction in which a water molecule breaks several chemical bonds. This process makes collagen soluble. A 0.001 M pH3 hydrochloric acid (HCl) solution was added to the samples, and then dry bathed at 80°C for 48 hours in a *Fishedbrand™ Isotemp™ Digital Dry Batch/Block Heaters*, covered with aluminum foil to prevent temperature shifts. Once gelatinized, samples were filtered with an *Ezee™* graduated polypropylene tube with a sintered polyethylene filter. This process removes insoluble residues and unwanted particles. The conical centrifuge tube was sealed with *Parafilm®* natural polyolefin thermoplastic, and frozen at -20 °C for 48 hours. Finally, samples were lyophilized to evaporate the frozen water through sublimation, transitioning from a solid to a gaseous state in a vacuum system that applies low pressures. Samples were placed in a *Telstar LyoQuest™ -55* lyophilizer with a perforated *Parafilm®* seal, and lyophilized for 48 hours. Afterwards, the weight of the conical centrifuge tube with the collagen sample was weighted on the analytical microbalance. The percentage of collagen yield was calculated with the following equation:

$$wt.\% = \frac{Collagen\ mass\ (mg)}{Bone\ mass\ (mg)} \times 100$$

3.5.2.2 Tooth enamel hydroxyapatite extraction

The sampling method has followed the guidelines of the Light Isotope Mass Spectrometry Laboratory from the Max Planck Institute for the Science of Human History. Bulk sampling has been applied to obtain a mean value of each individual. Sample preparation was performed in the laboratories of the Institut de Ciència i Tecnologia Ambientals from the Autonomous University of Barcelona (ICTA-UAB).

Empty 1.5 ml micro-centrifuge Eppendorf tubes have been weighted in an Ohaus® Explorer™ Semi-Micro Balance and labeled with the samples' IDs. In a sterile space, the surface of the tooth

enamel was cleaned using ethanol absolute and abraded with a Dremel 3000 drill, using diamond tips, at lower speed. After the cleaning, the enamel of the best-preserved side of each tooth was powdered along the entire growth axis of the crown using the drill and an agate pestle and mortar for bulk analysis. Both the drill and the pestle and mortar were cleaned with delicate task wipes and ethanol absolute between samples, while the diamond tips were discarded after being used in one sample to avoid crossed contamination. The weight of the powdered samples was recorded using the Ohaus® Explorer™ Semi-Micro Balance and then transferred to the previously labeled Eppendorf tubes.

Diamond tips for the drill were cleaned with Dichloromethane (CH_2Cl_2) and given an ultrasonic bath in an Elmasonic Select ultrasonic cleaner, in Pulse mode, for 15 minutes.

3.5.2.3 Analysis of $\delta^{13}C$ and $\delta^{15}N$ from bone collagen

A weight of approximately 0.35 mg of collagen was encapsulated in tin capsules, a material that is a good catalyst for combustion in mass spectrometers. Capsules were shaped into cubes or cylinders using sterile forceps. Encapsulated samples were placed in a polypropylene microplate, and analyzed in a *Thermo Flash 1112 Elemental Analyzer* coupled to a *Thermo Delta V Advantage* Isotope Ratio Mass Spectrometer (EA-IRMS) with a *Conflo III* interface, at the Stable Isotope Analysis Laboratory (LAIE) of the Institute of Environmental Science and Technology from the Autonomous University of Barcelona (ICTA-UAB). The stable carbon and nitrogen isotope values from the samples were measured with a precision of < 0.01‰ (1σ) and < 0.02‰ (1σ), respectively. Reproducibility was verified by duplicate analysis of some samples, and in cases of seemingly aberrant initial results, repeated analyses and sampling were performed. The reference material IAEA-600 (caffeine) was used as a control standard. Results are expressed in *Vienna Pee Dee Bee* standard (VPDB).

The reliability of the collagen isotopic values of ancient samples was addressed using four quality control indicators: collagen yield (wt%) ≥ 1%, carbon preservation percentage (%C) ≥ 13%, nitrogen preservation percentage (%N) ≥ 4.5%, and the ratio of carbon to nitrogen atoms (C:N) between 2.9-3.6 (Ambrose, 1990; DeNiro, 1985; Guiry & Szpak, 2020; van Klinken, 1999). Recent studies on collagen contamination have observed that the range of C:N atomic ratio for ancient samples proposed by DeNiro (1985) is too wide and the lower and upper limits have a direct impact on the $\delta^{13}C$ isotopic values, which undergo important shifts and cause unreliable results. Therefore, new conservative and liberal C:N ranges have been suggested for mammals, birds

and warm-water fish, aiming to keep reliable samples with an expected maximum shift of 0.5‰ to 1.0‰ in the $\delta^{13}C$ isotopic values (**Table 71**) (Guiry & Szpak, 2021).

Table 71. Suggested alternative C:N limits for ancient collagen. Modified from Guiry & Szpak (2021).

Taxa	Expected animal bone collagen $\delta^{13}C$	Conservative C:N range (0.5‰ tolerance)	Liberal C:N range (1.0‰ tolerance)
Mammals, birds,	-20.0‰	3.15 - 3.50	3.15 - 3.90
warm-water fish	-18.0‰	3.15 - 3.45	3.15 - 3.70

3.5.2.3.1 Northern Mesopotamia

Baselines for carbon and nitrogen stable isotopes have been performed using the collected faunal samples, as well as published databases from the surrounding area (***Figure 43***). Baselines for C_3 plants include $\delta^{13}C$ values from Early Bronze Age sites from the first half of the 3rd millennium, including the Syrian sites of Emar, Tell Mozan, Tell Mishrifeh, Tell el'Abd, and Tell Leilan, as well as the Lebanese site of Tell Fadous, and the Jordan site of Hirbet ez-Zeraqon (Riehl et al., 2008; Sołtysiak, 2011; Styring et al., 2017). The species that were subjected to analysis include barley (*Hordeum sativum* and *Hordeum vulgare*), wheat (*Triticum* sp.), emmer wheat (*Triticum dicoccum*), einkorn wheat (*Triticum monococcum*), lentil (*Lens culinaris*), grape (*Vitis vinifera*), fig (*Ficus carica*), and flax (*Linum usitatissimum*) (**Figure 44**). Baselines for local animals have been obtained using the samples included in the present study, as well as cattle (*Bos taurus*) and a sheep (*Ovis aries*) from the northeastern Syrian site of Tell Leilan (Styring et al., 2017). Published data about human samples from the same period have also been collected to provide a contextual framework for our data and to facilitate a more thorough interpretation of the obtained results. The sites included are northeastern Syrian sites of Tell Brak (*n* = 3) and Tell Leilan (*n* = 2), and the samples consist of adult and subadult individuals from both sexes (Sołtysiak, 2011).

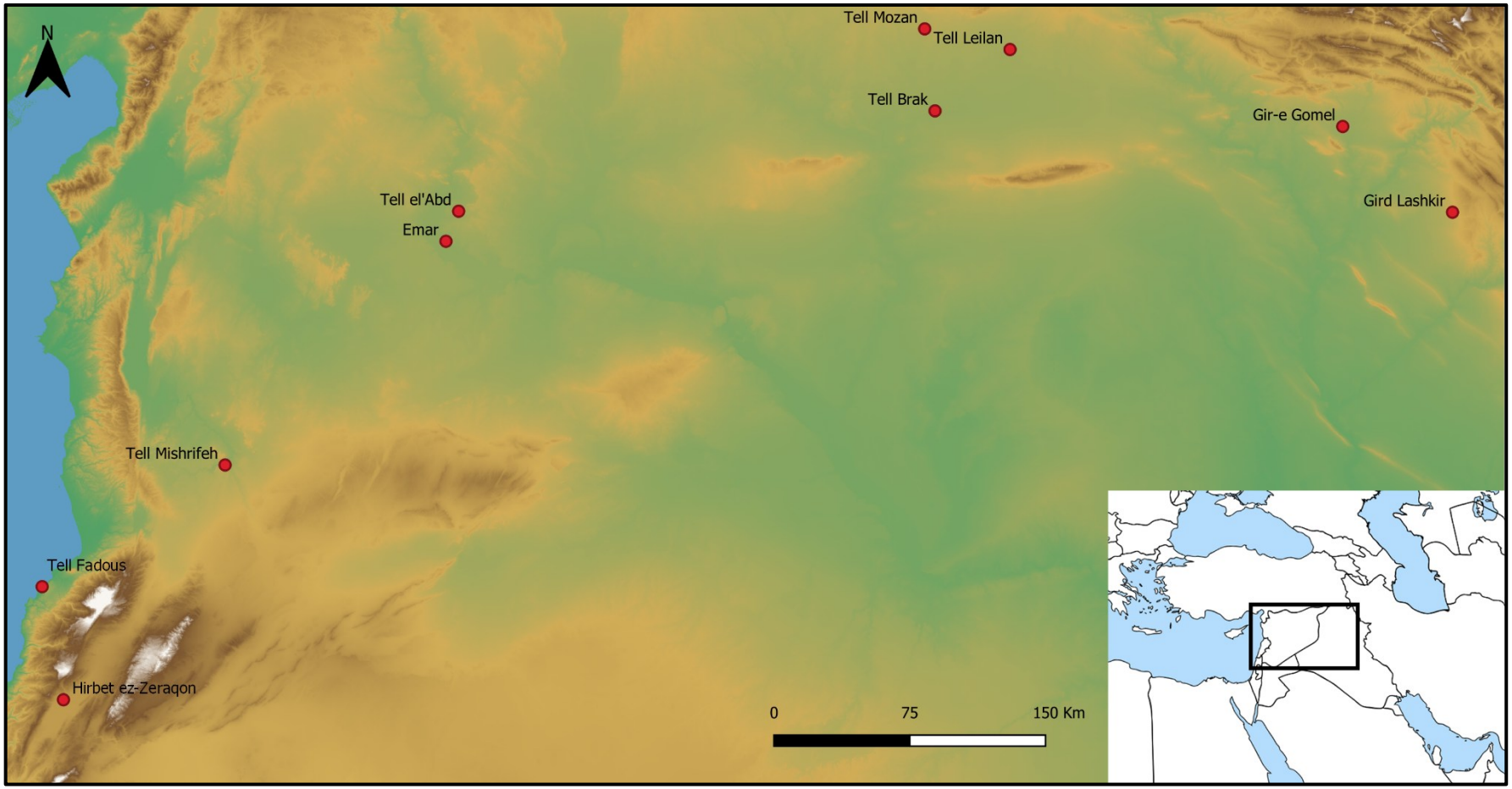


Figure 43. Archaeological sites with published $\delta^{13}C$ and $\delta^{15}N$ isotopic data included in the present study.

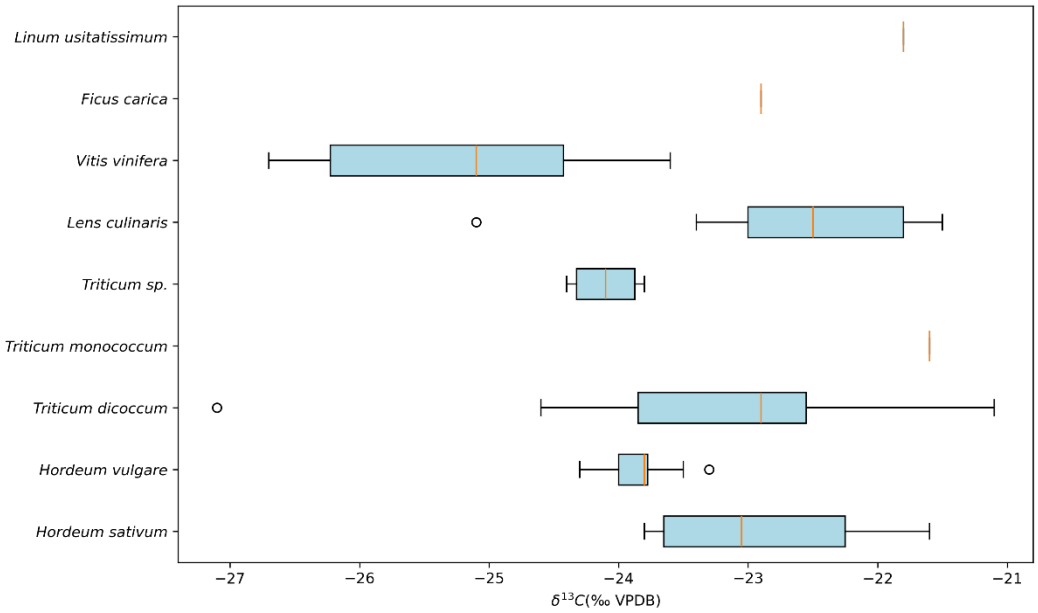


Figure 44. $\delta^{13}C$ values of C_3 plants from different Early Bronze Age sites in Northern Mesopotamia.

3.5.2.3.2 Northeastern Iberia

Baselines for carbon and nitrogen stable isotopes have been performed using the collected faunal samples, as well as published databases from the eastern region of the Iberian Peninsula (***Figure 45***). Baselines for C_3 plants include barley (*Hordeum vulgare L.*, *n* = 74) and wheat (*Triticum aestivum* and *Triticum durum*, *n* = 29) samples from the southeastern sites of La Bastida and Gatas (Knipper et al., 2020). Baselines for herbivore and omnivore animals have been obtained using the samples included in the present study, as well as from the sites of La Bastida, Gatas, and the Formentera site of Ca na Costa. The herbivore species consist of sheep (*Ovis aries*, *n* = 4), goat (*Capra hircus*, *n* = 3), cattle (*Bos taurus*, *n* = 9), and deer (*Cervus elaphus*, *n* = 4). The omnivore species consist of pig (*Sus domesticus*, *n* = 7) and dog (*Canis familiaris*, *n* = 2). Baselines for modern fish from freshwater environments include bleaks (*Alburnus Alburnus*, *n* = 1), Catalonian barbels (*Barbus haasi*, *n* = 1), pumpkinseeds (*Lepomis gibbosus*, *n* = 1), rutilus roaches (*Rutilus rutilus*, *n* = 1), and Ebro chubs (*Squalius laietanus*, *n* = 1) from the Llobregat and Besós basins, in northeastern Iberia (Cano-Rocabayera et al., 2015). Baselines for fish from marine environments include prehistoric cods (*Epinephelus marginatus*, n = 1), common pandoras (*Pagellus erythrinus*, *n* = 1), and Mediterranean barracudas (*Sphyraena sphyraena*, *n* = 1) from the site of Cova des Riuets, located in the island of Formentera. Additional samples from modern fish fished in the waters of Formentera include cods (*Epinephelus marginatus*, *n* = 2), common pandoras (*Pagellus erythrinus*, *n* = 2), Mediterranean barracudas (Sphyraena sphyraena, *n* = 2), and Mediterranean morays (*Muraena helena*, *n* = 2) (Garcia-Guixé et al., 2010).

Published data about human samples ranging from the Chalcolithic to the Late Bronze Age period have also been collected to provide a contextual framework for our data and to facilitate a more thorough interpretation of the obtained results. The sites included are southeastern sites of Cuesta del Negro (*n* = 22), Úbeda (*n* = 7), Baeza (*n* = 20), La Bastida (*n* = 19), and Gatas (*n* = 9), as well as the site of Ca na Costa (*n* = 8), located in the island of Formentera (Fuller et al., 2005; Knipper et al., 2020; Molina-González et al., 2019). Specifically, human samples from Ca na Costa belong to the Chalcolithic period. The sites of Baeza and Úbeda include samples ranging from the Late Chalcolithic to the Late Bronze Age. La Bastida and Gatas include samples from the Bronze Age, corresponding to the Argar society. And the site of Cuesta del Negro consists of samples from the Middle Bronze Age and the Late Bronze Age, which correspond to the Argaric and post-Argaric phases of the Argaric occupation, respectively.

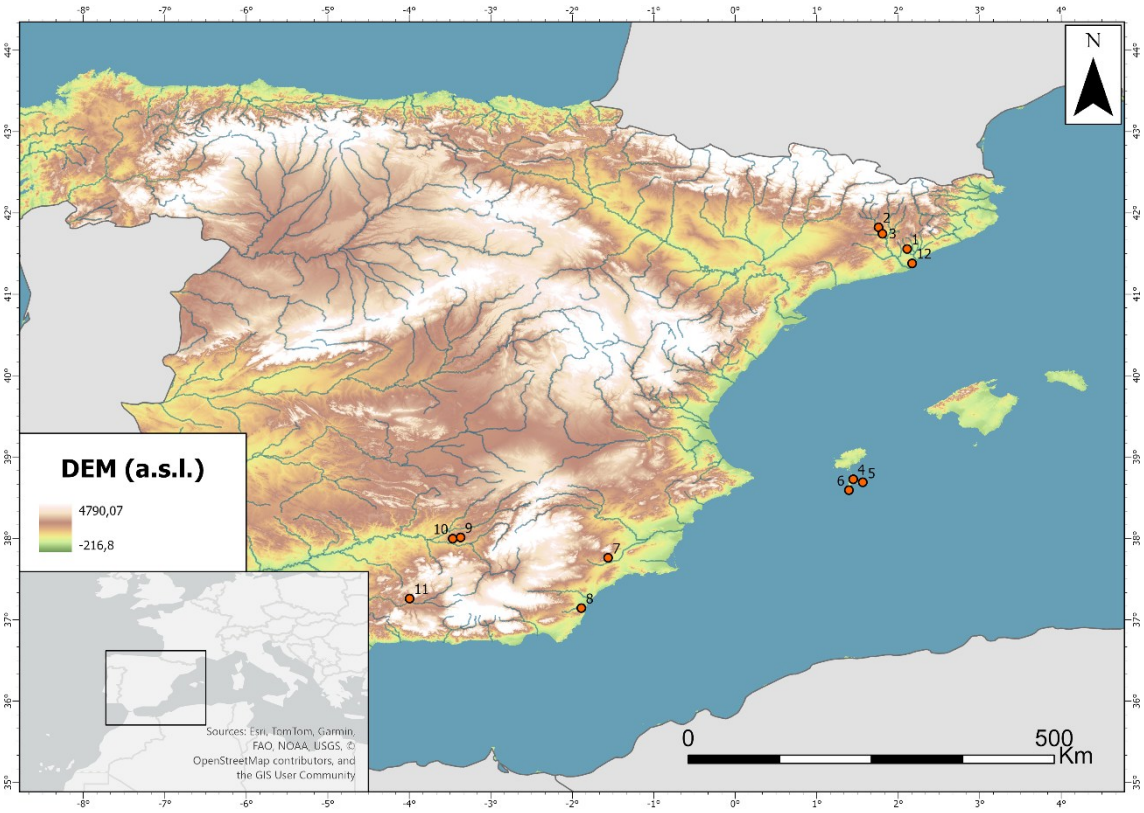


Figure 45. Archaeological sites with published $\delta^{13}C$ and $\delta^{15}N$ isotopic data included in the present study. 1) Ripoll River (Sabadell, Besós basin), 2) Cardener River (Súria, Llobregat basin), 3) Cardener River (Sant Joan de Vilatorrada, Llobregat basin), 4) Ca na Costa, 5) Cova des Riuets, 6) Formentera waters, 7) La Bastida, 8) Gatas, 9) Úbeda, 10) Baeza, 11) Cuesta del Negro, and 12) Plaça de la Gardunya.

3.5.2.4 Analysis of $\delta^{13}C$ and $\delta^{18}O$ from carbonates in tooth enamel hydroxyapatite

Carbon and oxygen sable isotope analysis were performed at the IsoTOPIK Laboratory, at the University of Burgos Scientific and Technology Centre. The used Isotope Ratio Mass Spectrometer (IRMS) was a continuous flow *Thermo Scientific Delta V Plus*, equipped with a *Thermo Scientific Gas-Bench II* carbonate sample preparation and injection system. The powdered carbonate samples were digested in He-flushed borosilicate exetainers at 70 °C using water-free 99.9% phosphoric acid. To assess the accuracy (external analytical precision) and to calibrate the obtained isotopic values, the results were measured against IAEA-603 ($\delta^{13}C$ = +2.46‰, $\delta^{18}O$ = -2.37‰) and NBS18 ($\delta^{13}C$ = -5.014‰, $\delta^{18}O$ = -23.2‰) calcite international references. The results are expressed in parts per mil relative to the *Vienna Pee Dee Belemnite* scale (‰ VPDB). The average 1σ internal precision error (ten injections per sample) is 0.03‰ for $\delta^{18}O$ and 0.03‰ for $\delta^{13}C$. According to the reference material analyses, stable carbon and oxygen isotope values were measured accurately to the nearest 0.02‰ and 0.02‰, respectively. Reproducibility was

verified by duplicate analysis of some samples, and in the case of seemingly aberrant initial results, repeat sampling and analysis was undertaken.

In order to associate the measured oxygen stable isotope values to a geographic region, data is transformed into drinking water values, given that fractionation varies between the composition of human tooth enamel and water resources (Daux et al., 2008). First, oxygen stable isotope values relative to VPDB scale have been transformed to *Vienna Standard Mean Ocean Water* (VSMOW) scale following the Coplen et al. (1983) equation:

$$\delta^{18}O_{VSMOW} = 1.03092 \times \delta^{18}O_{VPDB} + 30.92$$

Once the data has been transformed into VSMOW, it has to be transformed into drinking water values, also relative to VSMOW. The equation of Chenery et al. (2012), based on the Daux et al. (2008) equation number 4, has been followed:

$$Drinking\ water = 1.786\ \times\ \delta^{18}O_{VSMOW(carbonate)} - 54.005$$

Afterwards, the resulting drinking water values have been compared to the oxygen stable isotope values sampled in the surrounding area of the sites to establish the water resource catchment area of the studied populations.

3.5.2.4.1 Northern Mesopotamia

A baseline for carbon stable isotopes has been performed using published data from the surrounding area of the analyzed sites (***Figure 46***). One publication is the only source for 8 human samples with no detailed information about age or sex, and 2 animal samples of the *Ovis aries* species. They belong to the Early Bronze Age site of Terqa (Syria) (Tomczyk et al., 2016). The sampled tooth of human individuals provides information about early childhood.

Local isoscapes for oxygen stable isotopes have yet to be published; therefore, an exhaustive bibliographical review was performed to characterize the different available water resources from the surrounding area. These resources will serve as the reference data for the results presented in this study. The published data set includes the Tigris River in Southeastern Turkey (Dişli, 2018), the Shaqlawa-Harrir Basin in Erbil (Iraq) (Seeyan & Merkel, 2014), the Tigris River and the Little Zab in Iraq (Al-Kubaisi & Hassan, 2021), the Little Zab river in Kirkuk (Iraq) (Alabadi & Alshamma'a, 2015; Sahib et al., 2016), the Dashty-Hewler Basin in Erbil (Iraq) (Al-Naseri et al., 2022; Mamand & Mawlood, 2024), the Makook Mountains in Erbil (Iraq) (Mustafa et al., 2015), the Warmawa Sub-Basin in Sulaymaniyah (Iraq) (Salam Smail, 2023), the Shwan Sub-Basin in

Kirkuk (Iraq) (Al-Gburi et al., 2022), the Tigris River and the Tigris Channel in Baghdad (Iraq) (Abbood et al., 2024), and the Euphrates River in Central Iraq (Ali et al., 2015; Al-Paruany et al., 2017) (**Figure 47**).

A Shapiro-Wilk normality test was conducted to ascertain whether the dataset from the present study and the published hydrological data exhibited a normal distribution. In order to observe a relationship between the oxygen isotope values of human samples with a hydrological resource, an analysis of variance (ANOVA) with a Bonferroni post hoc test has been used to analyze parametric data, while a Kruskal-Wallis with a Dunn-Bonferroni post hoc test has been used to analyze non-parametric data.

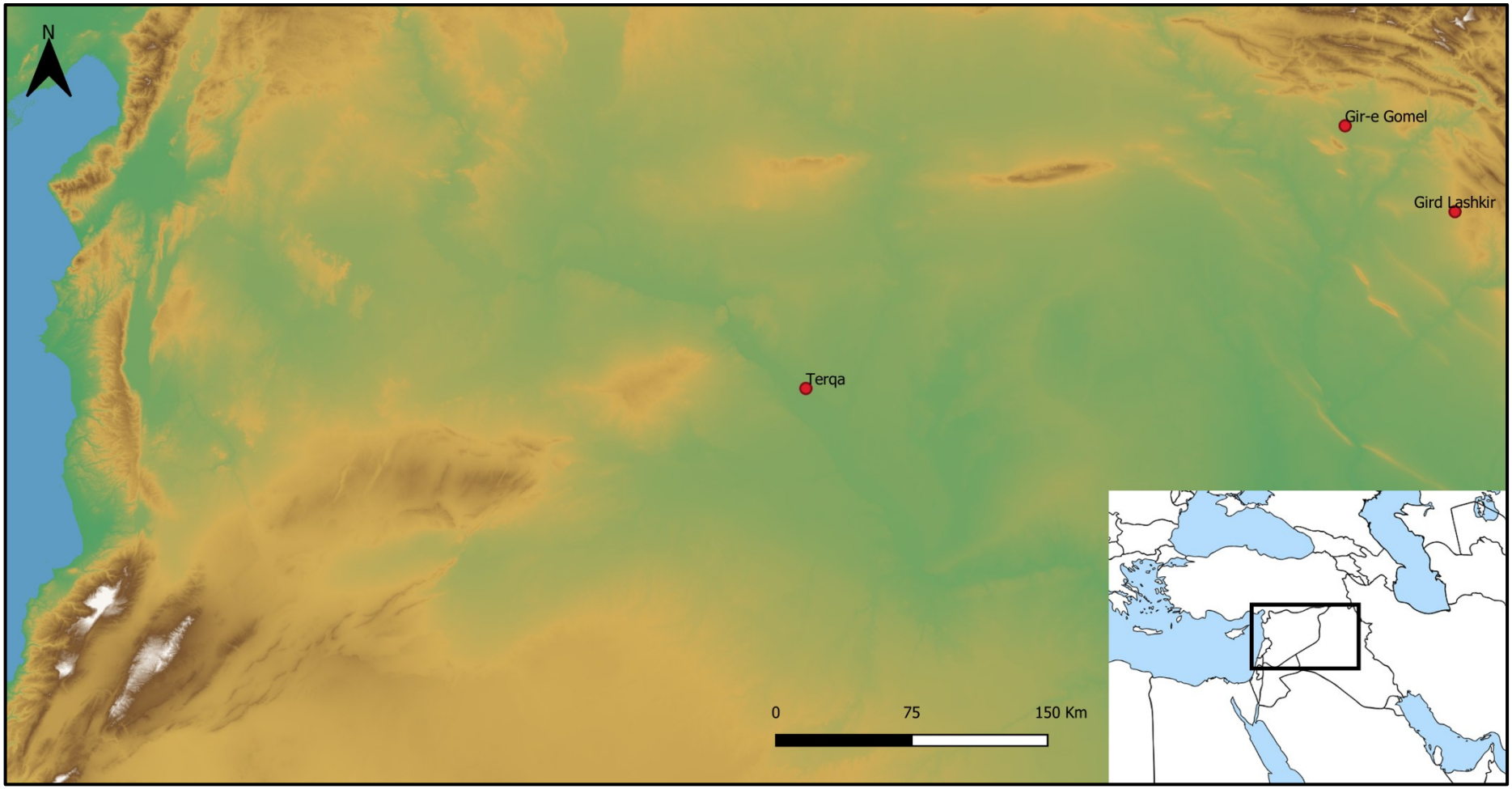


Figure 46. The archaeological site of Terqa, which has published $\delta^{13}C$ isotopic data that has been included in the present study.

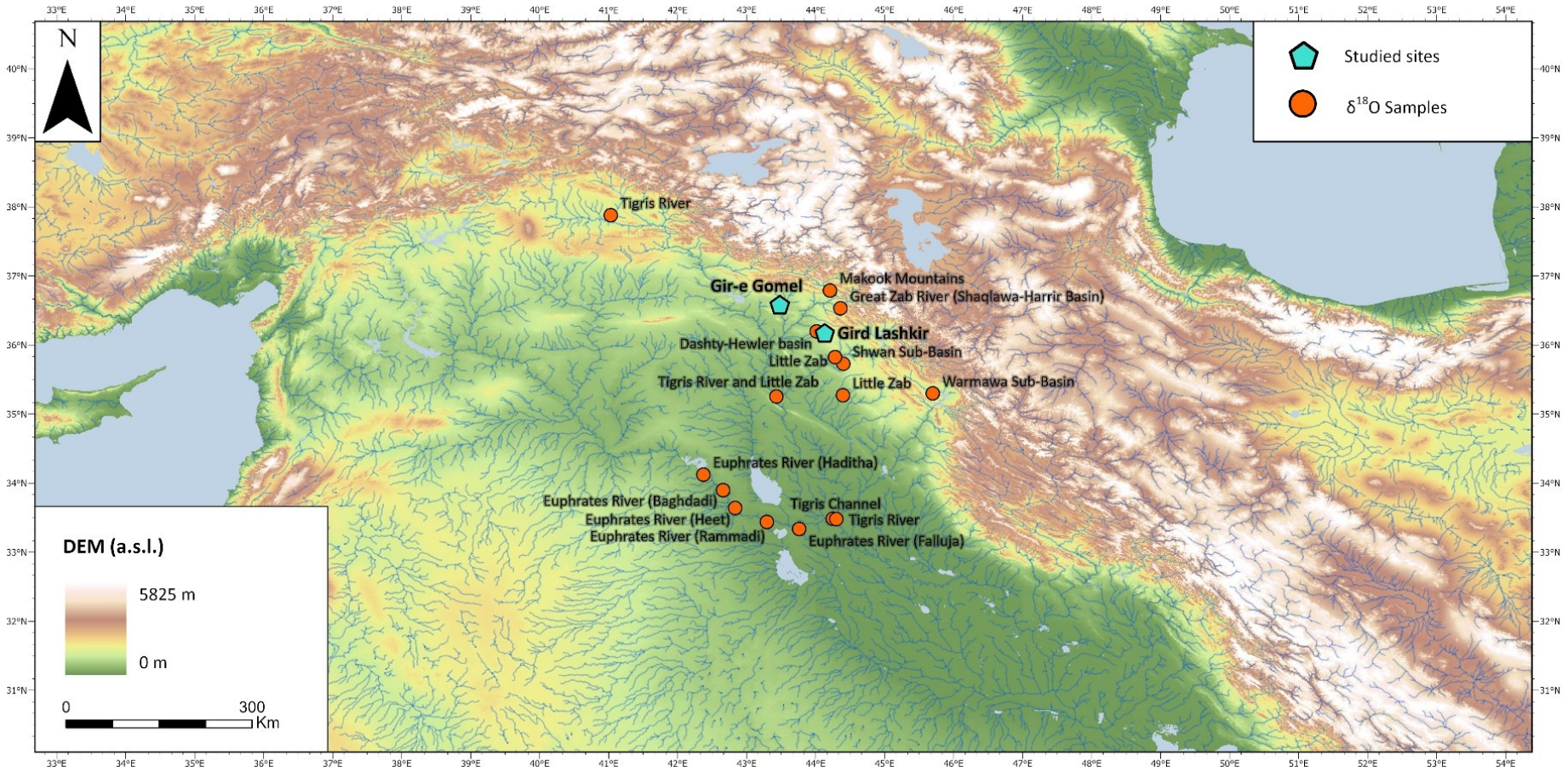


Figure 47. Sites with published $\delta^{18}O$ isotopic data included in the present study.

3.5.2.4.2 Northeastern Iberia

Published studies incorporating carbon and oxygen stable isotopes of tooth enamel hydroxyapatite from the surrounding area are pending, and thus, data from the region is not yet available. However, studies conducted in the central region of the Iberian Peninsula, particularly in the Madrid area, have yielded substantial carbon and oxygen data from 82 individuals spanning the Late Neolithic to the Bronze Age period. These studies have included not only tooth enamel hydroxyapatite samples from human and animal specimens but also bone hydroxyapatite samples. To contextualize and interpret the results of Plaça de la Gardunya's population, published data on human tooth enamel hydroxyapatite has been collected. The dataset is composed of the Late Neolithic site of La Ocañuela (*n* = 1), the Chalcolithic sites of Gózquez 047 (*n* = 2) and El Rebollosillo (*n* = 3), and the Bronze Age sites of Casa Montero (*n* = 2), Caserío de Perales 2 (*n* = 1), El Congosto (*n* = 2), El Muladar (*n* = 1), Fuente de la Mora (*n* = 1), Gózquez 085 (*n* = 8), La Dehesa Pol. 25 (*n* = 4), Los Chorrillos (*n* = 1), Pista de Motos (*n* = 1), and Los Berrocales (*n* = 33) (Díaz-del-Río et al., 2017). The oxygen stable isotopes obtained from the sampled sites were published in the VPDB scale and subsequently transformed into VSMOW. These values were then converted into drinking water values in order to maintain a cohesion with our dataset in the graphics.

Local isoscapes for oxygen stable isotopes have yet to be published; therefore, an exhaustive bibliographical review was performed to characterize the different available water resources from the surrounding area. These resources will serve as the reference data for the results presented in this study. The published data set includes oxygen stable isotope measures from several months of the year, and the collected sites belong to the northeastern area of the Iberian Peninsula, as well as from the eastern region of Valencia and the island of Mallorca in the Mediterranean sea (Díaz-Teijeiro et al., 2009; Hatvani et al., 2020; Moreno et al., 2021; Neal et al., 1992; Négrel et al., 2016; Viladés Ribera, 2013). From the northeastern region of the Iberian Peninsula, the sampled sites include the Ebro Basin and its tributaries (*n* = 27), the Llobregat Basin and its tributaries (*n* = 11), the territories of Prades (*n* = 27) and Montseny (*n* = 29), the city of Barcelona (*n* = 11), the Pyrenees (*n* = 13), the area of the airport from Girona (*n* = 19), Palma de Mallorca (*n* = 1) and Valencia (*n* = 20). Samples consist of water from rivers, streams, groundwater and rainfall.

3.5.2.5 Analysis of $^{87}Sr/^{86}Sr$ from carbonates in tooth enamel hydroxyapatite

Strontium stable isotopic analysis was performed at the Laboratori d'Isòtops Radiogènics i Ambientals (LIRA), from the University of Barcelona. Samples were dissolved in double distilled nitric acid. Following standard chromatographic techniques, strontium was purified using Tris-Kem® Sr-spec resin, which efficiently separates strontium from other interfering elements, such as Rb (rubidium). Purified samples were analyzed in a Nu Instruments Plasma 3 Multi Collector Inductively Coupled Mass Spectrometer (MC-ICP-MS) at the Centres Científics i Tecnològics from the University of Barcelona (CCiTUB). The efficiency of the chemical purification during chromatography was verified by a Sr/Rb ratio > 1000. The contribution of ^{87}Rb to the ^{87}Sr signal was corrected from the measurement of the ^{85}Rb signal, assuming a value of 0.385617 for the $^{87}Sr/^{86}Sr$ ratio. $^{87}Sr/^{86}Sr$ ratios were normalized for instrumental mass bias to $^{86}Sr/^{88}Sr = 0.1194$. A correction was also applied for instrumental drift by sample-standard bracketing using the standard reference material for strontium carbonate (SRM® 987, NIST), which has an $^{87}Sr/^{86}Sr$ ratio value of 0.710249. External analytical reproducibility was ± 0.000018 (2σ, *n* = 19).

3.5.2.5.1 Northern Mesopotamia

The scarcity of bioavailable $^{87}Sr/^{86}Sr$ baselines within the geographical area encompassed by this study has required the collection of samples from soil, plants, and animals with a brief life span. However, following consultations with multiple laboratories, only a snail shell specimen from Gird Lashkir was deemed suitable for analysis, thereby establishing a preliminary bioavailable $^{87}Sr/^{86}Sr$ baseline. Subsequent studies are currently in development to increase this baseline with a larger quantity and more diverse sample types.

Statistical analysis of human samples was conducted to observe variability both inter- and intra-group, as well as to assess affinity groups. In order to establish a strontium isotope isoscape from the surrounding area of the sites of Gird Lashkir and Gir-e Gomel, bioavailable strontium ranges from different sites have been collected, covering five contemporary countries: Iraq, Syria, Turkey, Lebanon, and Iran (**Table 72**). The bioavailable strontium from each site was classified into each country's geologic formation in the period unit. From a geological time scale perspective, the geology of the sites was formed during the Phanerozoic eon (538.8 million years ago to the present), encompassing the Paleozoic and Cenozoic eras, as well as the Cambrian and Quaternary periods. The most ancient geological period that has been sampled is the Cambrian

(538.8 to 486.9 million years ago), which is located in Iran. The subsequent period is the Carboniferous, which extends from 358.9 to 298.9 million years ago. This period is also located in Iran. Following the Cambrian period, the Permian-Triassic boundary, which occurred 251.96 million years ago, was located in Iran. The Cretaceous period, which lasted from approximately 143.1 to 66 million years ago, is geographically located in Iraq, Syria, Lebanon, and Iran. The Neogene period, spanning from 23 to 2.6 million years ago, is the most extensively sampled geological period, and its presence is documented in Iraq, Syria, Turkey, and Iran. The Quaternary period, which is the current geological time period (2.6 million years ago to the present), is found in Iraq, Syria, Turkey, and Iran (**Figure 48**).

In an effort to achieve higher analysis resolution, the bioavailable strontium from Iraq was not analyzed according to its geological formation period. Rather, it was classified as a site to ascertain whether there was a greater association with one site or another, as opposed to a larger area.

Table 72. Bioavailable strontium stable isotope baseline for the northern Mesopotamian region.

Country	Site	Geological period	Sample type	$^{87}Sr/^{86}Sr$ range	Reference
Iraq	Nineveh	Neogene	Ostrich shell	0.7082 – 0.7085	Hodos et al. (2020)
	Kirkuk	Neogene	Water	0.7077 – 0.7086	Sahib et al. (2016)
	Bestansur	Cretaceous and Quaternary	Plant	0.7077 – 0.7086	Elliott et al. (2015)
	Ur	Quaternary	Ostrich shell	0.7074 – 0.7082	Hodos et al. (2020)
Syria	Ugarit	Cretaceous	Plant	0.7078 – 0.7089	Henderson et al. (2009)
	Bab el Hawa	Neogene	Plant	0.7078 – 0.7089	Henderson et al. (2009)
	Aleppo Citadel and Aleppo Park	Neogene	Plant	0.7078 – 0.7089	Henderson et al. (2009)
	Lake Jabbūl	Neogene	Plant	0.7078 – 0.7089	Henderson et al. (2009)
	Balikh valley	Neogene	Plant	0.7078 – 0.7089	Henderson et al. (2009)
	Heraqla	Neogene	Plant	0.7078 – 0.7089	Henderson et al. (2009)
	Al-Raqqa	Neogene	Plant	0.7078 – 0.7089	Henderson et al. (2009)
	Tell Majnuna	Neogene	Soil	0.7078 – 0.7089	Sołtysiak (2019)
	Tell Brak	Neogene	Plant	0.7078 – 0.7089	Henderson et al. (2009)
	Tell Barri	Neogene	Soil	0.7078 – 0.7089	Sołtysiak (2019)
	Tell Masaikh	Neogene	Soil	0.7078 – 0.7089	Sołtysiak (2019)
	Tell Ashara	Neogene	Soil	0.7078 – 0.7089	Sołtysiak (2019)
	Wadi Barada	Quaternary	Plant	0.7069 – 0.7081	Henderson et al. (2009)

	Amara	Quaternary	Plant	0.7069 – 0.7081	Henderson et al. (2009)
	Bab Sharqi	Quaternary	Plant	0.7069 – 0.7081	Henderson et al. (2009)
	Northeast Damascus	Quaternary	Plant	0.7069 – 0.7081	Henderson et al. (2009)
	Najha	Quaternary	Plant	0.7069 – 0.7081	Henderson et al. (2009)
Turkey	Kandilli	Neogene	Volcanic rock	0.7043 – 0.7048	Kaygusuz et al. (2018)
	Lake Van and its tributaries	Quaternary	Water	0.7069 – 0.7081	Saygın et al. (2022)
Lebanon	Beirut	Cretaceous	Plant	0.7069 – 0.7081	Henderson et al. (2009)
Iran	Khalifan	Carboniferous	Granite	0.7107 - 0.8350	Bea et al. (2011)
	Tepe Silveh	Quaternary	Human bone	0.7107 - 0.8350	Khojasteh et al. (2020)
	Shahneshin	Cretaceous	Barite and country rocks	0.7065	Amin-Rasouli et al. (2021)
	Azna-Dorud	Cambrian	Metagranite	0.7061 – 0.7145	Shabanian et al. (2018)
	Abadeh	Permian-Triassic boundary	Conodont fossil	0.7070 – 0.7080	Korte et al. (2004)
	Rag-e Sefid	Cretaceous	Rock	0.7070 – 0.7080	Navidtalab et al. (2016)

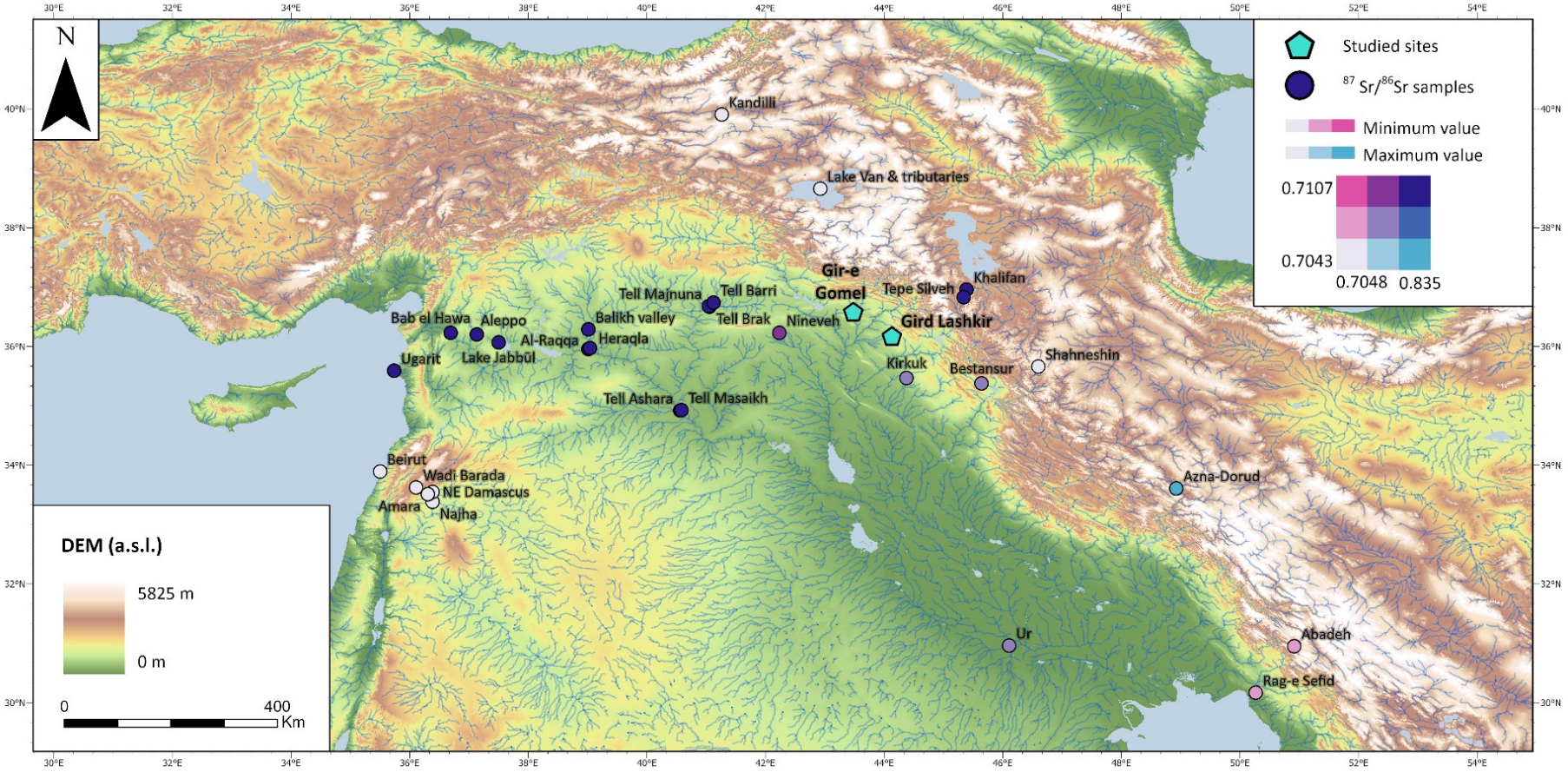


Figure 48. Map displaying the studied sites and the sampled sites of strontium stable isotope.

For this purpose, a series of tests have been conducted. Given the incompatibility of our dataset with most of these tests, a combination of them was used to infer the geological origin of the population studied. Therefore, we implemented a comprehensive statistical analysis that included descriptive statistics, normality tests (Shapiro-Wilk test), Mann-Whitney U tests, Kruskal-Wallis with Dunn-Bonferroni post hoc tests, linear discriminant analysis (LDA), and hierarchical cluster analysis (HCA). In the latter, we evaluated the efficacy of nearest-neighbor's Ward's method agglomerative clustering and Euclidian distance. LDA and HCA have been demonstrated to be the least suitable analyses to apply due to the nature of the dataset under consideration; consequently, the results of these analyses have solely been used to reinforce the interpretation of the results provided by the other statistical tests.

The use of human dental enamel for the purpose of determining local and migrant individuals has been a subject of interest in the field of anthropology. According to Price et al. (2002), subjects whose strontium isotope ratios fell within the range of the mean ± 2σ have been identified as being local to the site.

3.5.2.5.2 Northeastern Iberia

Since 2009, strontium stable isotope analyses have been conducted in the Iberian Peninsula and the Balearic Islands to investigate paleomobility patterns among past populations. The publication of strontium isotope signatures in subsequent years resulted in the establishment of a database, IDEArq-δimP, hosted by the Spanish National Research Council (CSIC). This database encompasses strontium, oxygen, nitrogen, and carbon stable isotopes from geological materials, animal remains, and human remains across a range of archaeological contexts and chronologies.

The creation of an isoscape for the Iberian Peninsula was achieved by Díaz-del-Río et al. (2022) with the publication of two isoscapes with predicted $^{87}Sr/^{86}Sr$ signatures for each geological type. The dataset used to create the isoscapes included plant remains, snails, soil, water, animal bones, and human bones, with a total of 1533 samples. While environmental samples are contemporary, archaeological remains span from the Neolithic to the Middle Ages. Two isoscapes were created: one encompassing all sample types and another exclusively including samples from archaeological contexts (***Figure 49***). The results of the analysis yielded specific strontium signature ranges for each geological zone in the Iberian Peninsula: These ranges will be used to compare and contextualize the strontium signatures from the case study of Plaça de la Gardunya.

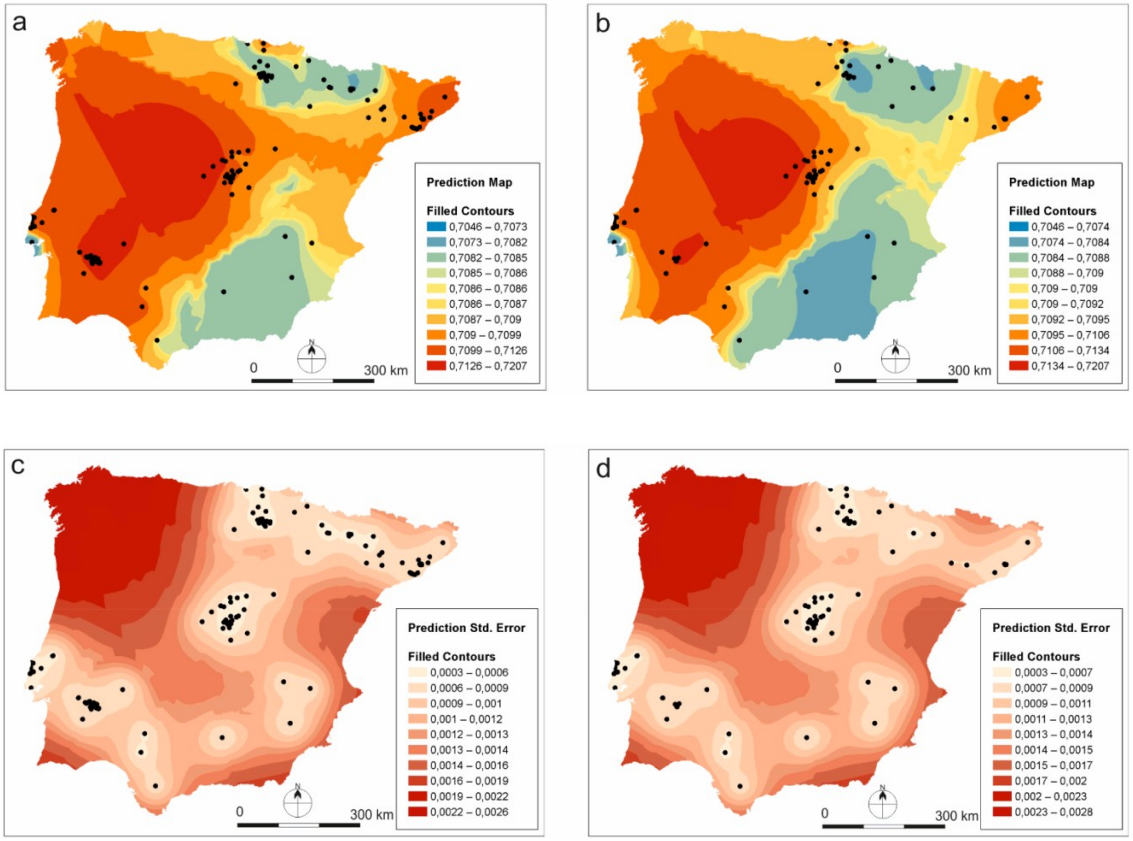


Figure 49. Isoscape models for the predicted $^{87}Sr/^{86}Sr$ signatures for each geological type. a) and c) consist of the isoscape that includes environmental and archaeological samples, as well as the standard error of the predicted ranges. b) and d) consist of the isoscape that includes solely archaeological samples, as well as the standard error of the predicted ranges.

CHAPTER 4: RESULTS

4.1 BURIAL CUSTOMS

The application of standardized protocols to the study of the graves and the anthropological assemblage from Gird Lashkir has yielded positive results in the reconstruction of the processes undergone by the burials and inhumed individuals, from their construction and deposition to subsequent taphonomic and anthropological disturbances. The potential for conducting a comprehensive analysis has been instrumental in facilitating a more profound comprehension of burial practices and the funerary customs of the community that inhabited the northern Mesopotamian region. A substantial amount of information has been obtained for Gird Lashkir, which is particularly noteworthy when compared to the information obtained for the graves and the skeletal remains from the site of Plaça de la Gardunya. The methodology employed in the fieldwork and curation of the Plaça de la Gardunya materials exemplifies the imperative for meticulous coding and classification of all the anthropological remains originating from multiple burials with mixed bones. Failure to adhere to archaeothanatological and anthropological protocols during the excavation process can result in the retrieval of only a fraction of the information that is potentially available. Notwithstanding, a thorough evaluation of all extant data has facilitated the acquisition of comprehensive archaeothanatological data. The reconstruction of the biological profile of the population has not been optimal, suggesting the necessity for further investigation. In future studies, each bone from the assemblage will be examined to ascertain the number that can be associated with specific individuals.

The interpretation of the burial customs will be performed under a processual school of thought. The theoretical framework of processualism emphasizes the analysis of funerary remains, with a particular focus on the container and its contents, as a means to explore social organization. The material register can be studied to obtain information about status markers, including richness, complexity, and social hierarchization. One criterion for establishing social inequality is the time and energy investment in the burials. The greater the time and energy expended by the community on the construction of the container and the fabrication of the grave goods accompanying the deceased, the higher in hierarchy, richness, or social status that individual will be regarded. The presence of exogenous materials, which are only available through long-distance trade, ores with a limited global presence, and large quantities and qualities of grave goods, are indicative of an individual with a high status (Flannery, 1973; Kinnes, 1975; Renfrew, 1973; Rodríguez-Corral & Ferrer Albelda, 2018; Shennan, 1975; Tainter, 1975; Valentini, 2019).

4.1.1 Gird Lashkir

The totality of the graves excavated in Sector 3 belonging to the Ninevite 5 period provided sufficient information to perform an archaeothanatological analysis and the reconstruction of the biological profile of the deceased. Graves 2 and 4 were excavated by team members from the SAPPO-GRAMPO Research Group prior to the implementation of a standardized archaeothanatological procedure; therefore, the information recovered from these graves is slightly scarcer than the information from the subsequent graves. Nevertheless, the exhaustive photographic documentation of both graves during its excavations has allowed for a more nuanced interpretation. Graves 5 to 16 were excavated during the course of the present PhD study, in which novel archaeothanatological and anthropological criteria for analysis were implemented. A substantial enhancement has been observed in the efficiency of information retrieval. The poor preservation of the human remains has caused the loss of many features that would allow for the determination of the sex and age of the individual. Once the skeleton is recovered from the burial, these features are no longer observable. A comprehensive examination during fieldwork has facilitated the refinement of age and sex assessments, thereby enabling a more precise reconstruction of the biological profile of the buried community.

4.1.1.1 Archaeothanatology of the graves

Under this section, the results of the archaeothanatological data, which were used to reconstruct the burial customs and taphonomic processes the graves underwent, are presented.

4.1.1.1.1 Grave 2

During the transitional architectural phases 4A and 3, a simple pit was excavated in phase 4A levels when they were not in use. The newborn individual was placed inside the pit within the funerary urn, which was placed sideways with the entrance facing South. At the time of excavation of the urn, the following elements were not documented: the body's orientation and facial position; the subject's posture; and the skeletal articulation. Consequently, the reconstruction of the original deposition of the deceased inside the grave, as well as the subsequent taphonomic processes, remains unfeasible.

4.1.1.1.2 Grave 4

A rectangular cut was performed in the architectural phase 4A, which had previously been abandoned. Two mudbrick walls from phase 4A are reused in the eastern and western sides of the burial. The body of the deceased was placed within the cut, and mudbricks were used to secure its position. The skull was held in place with a cushion made out of pebbles, and the postcrania could have been wrapped in a shroud because of the articulation of the skeleton.

4.1.1.1.3 Grave 5

A simple pit was excavated during the course of the architectural phase 4A, below the room L. 101. The anatomical position of the postcrania suggests that the deceased could have been wrapped in a shroud. The slight displacement of the skull could have been caused by the presence of a pillow composed of organic materials that have not been preserved.

The grave goods placed inside the burial consist of a cylinder seal with geometric motifs, as well as a trapezoidal-shaped pendant made of amygdaloidal basalt, both placed above the sacrum of the individual. It is possible that the items were stored in a small bag suspended from a belt. In the vicinity of Gird Lashkir, two distinct geological origins of amygdaloidal basalt have been identified: one in the Bekhair Anticline, in proximity to the city of Duhok in Iraqi Kurdistan (Karim et al., 2020), and another in Baska Piwaza of Halgurd Mountain, situated approximately 170 kilometers north of the city of Erbil, near the border with Iran (Ahmed et al., 2023). The amount of time required to obtain the raw material and to manufacture the pendant is significant. However, trade would only need to be conducted over short distances. The cylinder seal has suffered extensive damage due to its prolonged use, resulting in significant deterioration and poor preservation. It is regarded as a component of prestige, serving as an identifier that denotes ownership and affiliation with a shared heritage. The geometric motifs present on the seal are unique and distinct from any other found cylinder seal, suggesting the possibility of its belonging to a different lineage. From a stratigraphic perspective, this individual appears to be the most recent individual buried with the set of the cylinder seal, which features geometric motifs, and the trapezoidal-shaped pendant of amygdaloidal basalt. The same set is shared by the deceased buried in Graves 7 and 16. This suggests that the set may have been ascribed exclusively to female individuals of high status within the community.

4.1.1.1.4 Grave 6

During the course of the architectural phase 4B, a simple pit was excavated in the courtyard area. This occurred after phase 4A was no longer in use. The burial cut two fallen mudbricks from a wall located to the west of the burial. Inside the pit, a simultaneous double inhumation of a child (Individual 1 or Grave 6.1) and a female young adult (Individual 2 or Grave 6.2) was placed in a flexed position. The bones of both individuals are intertwined, indicating that the inhumation occurred simultaneously. It is evident that Individual 2 is in close contact with the younger individual, as evidenced by the placement of the right hand beneath the right coxae of Individual 1. The left foot of the child is also placed above the femur of the adult. Following the placement of the deceased, the burial was covered with soil.

Subsequent to this, when the bones from Individual 2 had not yet undergone complete skeletonization, an animal disturbed the position of the legs and feet by displacing them towards more ancient stratigraphic levels of the site. Upon the skeletonization process, a more recent cut disturbed the upper part of the skeleton, resulting in the displacement of the upper part of the thorax to the east and the disconnection of the skull from the postcrania.

4.1.1.1.5 Grave 7

A simple pit was excavated during the course of the architectural phase 4A, in a courtyard area. The deceased was placed inside the burial, which was reinforced in the eastern side with mudbricks.

The grave contains the inhumation of a child with inherited high status, as indicated by the presence of ornaments and grave goods. The necklace comprises a diverse array of rock materials and shapes. The procurement of raw materials required trade, and the fabrication of the beads was a time-consuming process, thus establishing a prestige associated with this ornament. A similar necklace has been found in Grave 13, which contains the remains of another child.

One of the beads of the necklace exhibits a similarity in size and shape to a pendant also found in Graves 5 and 16. The presence of the pendant, crafted from amygdaloidal basalt, and the cylinder seal constitute components of a set that appears to be exclusive to female individuals of a high status within the community. In the vicinity of Gird Lashkir, two distinct geological origins of amygdaloidal basalt have been identified: one in the Bekhair Anticline, in proximity to

the city of Duhok in Iraqi Kurdistan (Karim et al., 2020), and another in Baska Piwaza of Halgurd Mountain, situated approximately 170 kilometers north of the city of Erbil, near the border with Iran (Ahmed et al., 2023). The amount of time required to obtain the raw material and to manufacture the pendant is significant. However, trade would only need to be conducted over short distances. The cylinder seal exhibits an identical pattern of geometric motifs with Grave 14, which is situated stratigraphically beneath Grave 7, as well as with Grave 16. This object serves as an identifier, denoting ownership and affiliation with a shared heritage. The *cyprea* shell is also an exotic good that is sourced from the Red Sea, implying the existence of long-distance trade networks.

4.1.1.1.6 Grave 8

During the course of the architectural phase 4B, a simple pit was excavated in a courtyard area. A secondary inhumation was placed inside the pit, consisting of fragments of the skull, mandible, vertebrae, ribs, tibia, and one incisor. The preserved remains of the skull consisted of fragments from the right side, which was positioned in an inverted orientation and supported by pottery fragments and stones of small-to-medium size. The aforementioned postcrania bones were deposited in a random position inside the pit.

The disposition and conservation of the remains suggest that the burial was a secondary inhumation, affected by the erosion of the mound, rather than a primary burial profoundly impacted by the mound's erosion.

4.1.1.1.7 Grave 9

A simple pit was excavated in the architectural phase 5A, which had previously been abandoned. The excavation of the pit was conducted at what appears to be the point of entry to Locus 154, which corresponds to a room from a pluricellular dwelling. The deceased was placed in a seated position within the funerary urn, which was then covered with a lid. The urn was subsequently buried in the pit sideways, with the entrance facing North. Once the jar was covered with soil, a large stone was placed above the opening of the jar. This stone may have served as a marking sign of the grave or to secure the lid to the jar. Subsequent to the process of skeletonization, the upper portion of the body underwent a forward collapse, resulting in the disarticulation of the body.

4.1.1.1.8 Grave 10

A simple pit was excavated in the architectural phase 5A, which had previously been abandoned. In the interior of the pit, the presence of phytoliths in a vertical arrangement, exhibiting uniform widths and lengths, suggests the presence of a reed mat. This comfort element was placed along a probable pillow made of earthen materials for the deceased in the base of the burial. A significant number of phytoliths were identified surrounding the bones of the postcrania, suggesting that the body may have been wrapped in a shroud and subsequently placed within the burial. The left foot, which was found in an unnatural position, may have rotated during the burial process, as it is compressed under the right foot and leg. Additionally, the left leg exhibits no evidence of rotation. The burial was closed with earth building materials, such as large mudbricks. Following the process of skeletonization, the mandible exhibited a displacement toward the thorax. The archaeological remains found in the filling of the burial included animal remains and lithic flint tools. One of the tools had bitumen residues adhered to the unbladed side, suggesting that it was used to attach a handle. The presence of painted and plain pottery sherds indicates that the individual may have belonged to the Early Ninevite 5 period.

4.1.1.1.9 Grave 11

A simple pit was excavated during the architectural phase 5A. The pit cut slightly the western wall of the room Locus 154, which belongs to a pluricellular dwelling. A significant number of phytoliths were identified surrounding the bones of the postcrania, suggesting that the body may have been wrapped in a shroud and subsequently placed within the burial. The proximity of the burial to the mounds' slope has resulted in significant erosion of the bones, and the soil composition has led to the cementation of the bones in the lower body region due to the presence of abundant mineral concretions.

4.1.1.1.10 Grave 12

This grave is located in the plain area surrounding the mound of Gird Lashkir. The burial contains a secondary inhumation of at least three individuals, which were clearly identifiable due to the size and robustness of the different bones. The remains were interred in a manner of deposition that could be described as "comingled," within a simple pit that had been excavated in a stratum

characterized by a prevalence of pebbles formed by watercourses. The filling of the grave contained small pebbles and soil. This area appears to be susceptible to inundation from heavy rainfall and watercourses, as evidenced by the stratigraphic levels below, contemporary with, and above the grave, which were filled with medium-sized pebbles.

It has been determined that the presence of preserved bones in the archaeological context is directly associated with the modern utilization of heavy machinery, a factor that has played a significant role in altering the original state of the grave. This alteration, which entailed the destruction of approximately half of the original structure, occurred in 2022 in the course of construction activities aimed at the construction of a channel for residual waters.

4.1.1.1.11 Grave 13

From a stratigraphic and geographical perspective, this burial is situated directly beneath Grave 6. A simple pit was excavated during the architectural phase 5A, in a courtyard area. The presence of phytoliths in a vertical arrangement, exhibiting uniform widths and lengths, suggests the presence of a reed mat within the interior of the pit. A substantial quantity of phytoliths was identified in the proximity of the bones on the palmar side of both hands, indicating that the hands may have been in contact with a piece of attire (possibly gloves) or that the body may have been shrouded. Further information will be gathered following the excavation of the complete burial, as the upper portion of the body could not be excavated due to its insertion into the northern profile of the sector. One fallen mudbrick of a wall was found at the feet of the individual, being a possible element of reinforcement of the burial or a fastener to secure the body.

The grave contains the inhumation of a child with inherited high status, as indicated by the presence of a necklace composed of beads made from a variety of rock materials and shapes, as well as fine bronze rings. The procurement of the raw materials required the existence of a long-distance trade network, and the fabrication of the beads was a time-consuming process, thus establishing a prestige associated with this ornament. A similar necklace has been found in Grave 7, which contains the remains of another child.

4.1.1.1.12 Grave 14

From a stratigraphic and geographical perspective, this burial is situated directly beneath Grave 7. A big room from the pluricellular dwelling was separated by a short wall (2022/12), dividing the space into a big room (L. 140) and a smaller room (L. 139). The latter room was used as a space for the burial of the deceased, creating a mudbrick chamber from the previous walls, during the course of the architectural phase 5A. In the interior of the burial, the presence of phytoliths in a vertical arrangement, exhibiting uniform widths and lengths, suggests the presence of a reed mat.

The burial exhibits a variety of ornaments and grave goods, making it one of the burials with the richest offerings. The composition of the necklaces, which consists of a great number of beads of various materials and small dimensions, as well as the necessary long-distance trade routes to obtain the *Engina mendicaria* shells, which originate from the Red Sea or the Arabic Gulf (Then-Obłuska, 2015), are indicative of their status as elements of prestige. Another crucial element is the presence of a cylinder seal, which shares the same pattern of geometric motifs with Graves 7 and 16, which is situated stratigraphically above this grave. This object serves as an identifier, denoting ownership and affiliation with a shared heritage. Furthermore, an animal offering was placed within the burial. The nature of the offerings, in conjunction with the comfort elements incorporated into the burial, suggests that the deceased was regarded as a high-status member of the community.

4.1.1.1.13 Grave 15

A simple pit was excavated during the architectural phase 5B, in a courtyard area, partially cutting a mudbrick wall belonging to the architectural phase 7. The burial was cut in a slope manner, with the torso positioned in the deepest part of the burial and the legs and hands positioned in the shallowest part. Two mudbricks were discovered at the southernmost extent of the cut, suggesting the potential for either the collapse of a wall or the deliberate placement of mudbricks as structural supports. The presence of phytoliths in a vertical arrangement, exhibiting uniform widths and lengths, suggests the presence of a reed mat within the interior of the pit. A substantial number of ashy adhesions were identified surrounding the bones, including the skull, the ribs, the left scapula, the medial side of the right ulna, all bones from the left arm, the right hand (**Figure *50***), the hips, the legs (the left femur and both tibias), and the feet (the tarsals and metatarsals). The preservation of the remains, as well as the presence of a large bronze

needle placed above the right side of the skull, suggest that the body may have been wrapped in a shroud, secured by the needle, and subsequently placed within the burial.



Figure 50. Metacarpals and phalanges of the right hand exhibiting ashy adhesions in the palmar side.

The body was adorned with a necklace composed of 78 discoid- and biconical-shaped beads of limestone or plaster, along with two discoid-shaped lapis lazuli beads. To accompany the deceased, two sets of grave goods were placed in the burial. The first set, situated to the west of the head, comprises 6 middle-sized pottery vessels, featuring plain and incised decorations. The plain pottery corresponds to the Ninevite 5 fine ware, and the incised pottery exhibits geometric motifs. A bone needle was identified between the vessels, characterized by a quadrangular arrow-like head and an incised neck. Two thick bronze needles were also present: one curved at the proximal end and one straight with a spherical head. The second set, situated to the east of

the feet, comprises 13 small-sized pottery vessels, featuring plain, painted, and incised decorations. The plain pottery corresponds to the Ninevite 5 fine ware, and the incised pottery exhibits geometric motifs. The painted pottery is characterized by thick oxidized lines. The presence of sealing plaster was observed in a subset of the vessels. Inside one of the vessels a flint tool was also found. At the time of the discovery, the vast majority of the vessels were found to be empty of soil, suggesting that they had been covered by a sealing material in their openings. This sealing material could have taken the form of a piece of fabric secured with strings, as evidenced by the presence of burned sealing clays from other pits in the sector that exhibited fabric and string impressions.

The grave goods present in the burial consist of one of the largest ensembles among the other burials, including multiple needles of bronze. These elements collectively contribute to an overall sense of prestige. Additionally, it is important to consider the incorporation of comfort elements, such as the reed mat. The elements accompanying the deceased and their arrangement suggest that the individual was considered important to the community. The youth of the individual could also be indicative of a high degree of inherited status.

The burial was sealed with building materials, including mudbricks, and it was gradually filled with organic soils. The bones of the hands and the thorax exhibited sufficient space to disarticulate, and the beads of the necklace displaced across the neck and the thorax. Subsequent taphonomic processes significantly influenced the state of preservation of the bones. Multiple bones exhibit surface cracking, exfoliation and dark coloring, suggesting exposure to heat, as well as brown staining that occurs during contact with the burial soil and its chemical taphonomical interactions (Dupras & Schultz, 2014). Surface cracking is found in the shoulder girdle (including the clavicles and the right scapula), the humeri, the hips, and the legs (including the femurs and tibias) (**Figure *51***). The presence of soil and burning stains was observed in the following anatomical regions: the skull, the ribs, the right scapula, the bones of both arms and hands, the hips, the legs (including the left femur and both tibias), and the feet (including the tarsals and the metatarsals). A multitude of evidence indicates that the burial was exposed to elevated temperatures for a brief period, sufficient to generate ashy adhesions on the bones, surface cracking, and brown to black staining. The soil used to fill the burial in the lower part of the skeleton was also very organic and dark, suggesting ashy origins. The heat generated by a large kiln from the same architectural phase 5B (structure number 2023/26, located inside room L. 170), situated 1.5 meters south of the burial, may be the cause of the observed taphonomical damages.



Figure 51. Right clavicle with evidence of surface cracking due to heat exposure.

4.1.1.1.14 Grave 16

The burial was excavated in the architectural phase 5B, which had previously been abandoned. The grave cut a previous mudbrick wall and used the left mudbricks as a reinforcement on the eastern side. The individual was placed inside an oval shaped simple pit and filled the grave with soil. As ornaments, the deceased had a metallic earring with a spiral shape hanging from the right ear. The object does not exhibit taphonomic coloration that could facilitate the identification of the metal. Notwithstanding, the substance is non-magnetic. A set composed of a trapezoidal-shaped amygdaloid basalt pendant and a cylinder seal with geometric motifs, which is also shared with Graves 5 and 7, was placed behind the skull, on the eastern side. It is proposed that the set may have been ascribed exclusively to female individuals of high status within the community. In the vicinity of Gird Lashkir, two distinct geological origins of amygdaloidal basalt have been identified: one in the Bekhair Anticline, in proximity to the city of Duhok in Iraqi Kurdistan (Karim et al., 2020), and another in Baska Piwaza of Halgurd Mountain, situated approximately 170 kilometers north of the city of Erbil, near the border with Iran (Ahmed et al., 2023). The amount of time required to obtain the raw material and to manufacture the pendant is significant. However, trade would only need to be conducted over short distances. The cylinder seal is regarded as a component of prestige, serving as an identifier that denotes ownership and affiliation with a shared heritage, probably with Graves 7 and 14. Another element of prestige is the metallic earring, an ornament that is distinctive at the site as no other has yet appeared.

As the architectural phase 5A commenced, the room L. 154 was created through the construction of walls above the burial. In order to prepare the floor for the room, the level of use was cut, disturbing the burial and destroying the lower part of the deceased's body.

4.1.1.2 The containers

The predominant grave typology at Gird Lashkir is the simple pit with an oval shape, as evidenced by the 11 burials present at Sector 3. A total of two burials have been identified within simple pits, exhibiting a rectangular morphology. Notably, one of these burials consists of a mudbrick chamber with a rectangular shape. The simple pit has been identified as the prevailing burial pattern at the site, with no correlation observed to factors such as age, sex, or status of the interred individual. However, the mudbrick chamber has been identified as belonging to a significant member of the community, as evidenced by the presence of a middle-aged male buried with elaborate ornaments and grave goods.

4.1.1.3 Burial distribution among the site

In Sector 3, an unequal distribution of burial spaces was identified, with a preponderance of female burials (six individuals) and unsexed individuals (five subadult individuals) observed. In contrast, only two male individuals were buried, suggesting that these individuals may have been buried in other areas of the mound that have not yet been excavated.

4.1.1.4 Health and lifestyle

The population at Gird Lashkir suffered predominantly from pathologies related to the mouth, including severe tooth attrition, exposure of the dentin and the pulp chamber, dental calculus (tartar), tooth decay (caries), *antemortem* tooth loss, defects of the enamel hypoplasia and periodontitis. Linear tooth enamel hypoplasia is present in eight individuals (Graves 4, 5, 6, 10, 12, 13, 14 and 15), indicating an interruption in the enamel formation in the early stages of life, especially during the ages of 1.5 and 6, being 3.5 years the age the mode within the population. These statistics indicate a generalized repeated episodes of malnutrition or psychosocial stress among the community, independently of their social status.

The individuals with poorer oral hygiene are Graves 5, 10, 15. Caries is a disease that has been frequently encountered in civilized populations with wide spectrum economies, with its widespread origins in the Neolithic period. Caries is developed when bacteria located in the saliva

ferments dietary carbohydrates (such as sugars) and create organic acids that lead to the demineralization of the dental enamel (Larsen et al., 1991). Clinical research has observed that female individuals show higher frequencies of caries than men, which has been attributed to hormonal fluctuations related to puberty, menstruation and pregnancy. Different studies have also observed that another cause is the differential access to food among male and female individuals, in which female consume more carbohydrates than men (Pezo Lanfranco & Eggers, 2012). This may be the cause with the affected individuals at Gird Lashkir. The presence of dental calculus, also known as tartar, contributes to poor oral health by creating direct accesses to the periodontic area in which bacteria are able to act and create infections, resulting in periodontitis and gingivitis (Lewis, 2018). Antemortem tooth loss and exposition of the dentin and the pulp chamber are also easy accesses to mouth infections.

Inflammation of the periosteum, also known as periostitis (Baxarias & Herrerín, 2008; Roberts & Buikstra, 2019), is present in numerous bones of different individuals of the community (Graves 4, 5, 9, 12.1 and 15), predominantly on the ribs in form of new periosteal reactive bone formation in the caudal edges. This reaction can result from a traumatic injury or bacterial infection, and has been associated with pulmonary diseases, such as tuberculosis, given the potential for lung diseases to inflame the pleura, which can affect the bone as it attaches to the visceral surfaces of the ribs, thereby causing an inflammatory reaction on the surface of the ribs (Davies-Barrett et al., 2019; Mariotti et al., 2015; Ortner, 2003; Roberts & Buikstra, 2019).

Diseases that weaken bone density, such as osteoporosis, is present in most of the middle adult individuals, either female (Grave 5) or male (Graves 12.1 and 14), but some young adults are also affected (Graves 10 and 12.2). The most affected bones are the vertebrae, the soulder girdle, the upper and lower limbs

On the other hand, degenerative osteoarthritis is less frequent and more prevalent in female adult individuals (Graves 4 and 5), and in a male adult individual (Grave 14). The most affected bones are the vertebrae and the feet.

Lifestyle can be inferred through the observation of activity markers, which are usually manifested in the joints of young and middle adults. Some individuals present different degrees of enthesopathies related to continuous physical work with the upper limbs. The most prevalent, observed in Graves 4, 12.1 and 14, is the presence of a crest in the fibrous sheaths of the hand

phalanges, also known as *vaginae fibrosae digitorum manus*, which is associated with a developed pulley system in the fingers, as well as increased mechanical strain on the insertions, which may result in a stronger grip (Hermann et al., 2022). This enthesopathy is frequently linked to the manipulation and holding of tools (Baxarias & Herrerín, 2008). Enthesophytes and robustness in the tendon and ligament insertions of the bones are also frequent. Grave 5 presents *osteochondritis dissecans* in the right elbow, indicating a repetitive use of the right arm and/or indicative of right-handedness, and Grave 12.1 shows repetitive use of the elbow joints.

Enthesopathies in the legs and feet are also observed in Graves 4 and 5, which develop in association to frequent walking or jumping activities.

It can be posited that the appearance multiple enthesopathies related to a heavy use of the upper and lower limbs, suggesting that during life, some adult members of the community were involved in a continuous and physical work.

4.1.1.5 Social organization

A four-tier social status system has been identified based on the following criteria: the age of the buried individual, the comfort elements of the burial, the ornaments, and the grave goods accompanying the deceased. To begin with, the newborn status is to be considered. Individuals younger than three years of age were placed in a funerary urn and buried in a simple pit. The burial is characterized by the absence of grave goods and ornaments. It can be posited that Grave 2 and Grave 9 are members of this group. Secondly, a low social status is observed, in which burials are characterized by the absence of any additional items beyond the remains of the deceased individual. The majority of burials exhibited a commitment to preserving the physical integrity of the deceased, as evidenced by Graves 4, 6, and 11. In contrast, other burials involved partial burial, resulting in significant fragmentation of the skeletal remains. The latter case is exemplified in Grave 8.

Thirdly, the middle social status within the community is constituted by two graves. Grave 10, situated within the mound, features a reed mat as a comfort element and an animal offering. Grave 12 is situated in the plain area of the site. Although the grave consists of a secondary inhumation of comingled bones, it contains a large pottery vessel with incised decorations.

Finally, the high social status is characterized by the placement of prestige ornaments and grave goods within the grave, as well as the presence of comfort elements in some cases. The artifacts

in question include cylinder seals featuring geometric motifs, necklaces composed of semiprecious stones, metal objects, exotic shells, sets of pottery vessels, and bone artifacts. The following Graves are associated with this group: 5, 7, 13, 14, 15, and 16. Child individuals (Graves 7 and 13) have been observed to possess a distinctive necklace that features shared materials (carnelian, lapis lazuli, among others) and bead shapes, thereby acquiring an ascribed status. Two female individuals, Grave 5 and 15, possess a set composed of a trapezoidal-shaped pendant made of amygdaloidal basalt and a cylinder seal with geometric motifs. This set is also shared by Grave 7, whose age prevented determination of the sex. Consequently, we propose the allocation of this set exclusively to female individuals. Two additional members of the high social status, Graves 14 and 15, are notable for their lack of the set, though they exhibit a substantial quantity of grave goods and the presence of comfort elements. Grave 14 is the oldest buried member of the community and is the sole individual placed in a mudbrick cist. It can be posited that this particular individual was a prominent figure within the community, potentially assuming a significant role at the site.

The cylinder seals exhibit two distinct geometric motif patterns. One seal (Grave 5) features a handcrafted design with diagonal lines, while three others (Graves 7, 14, and 16) exhibit a combination of lines, rhombs, and dots. The significance of cylinder seals during this era is noteworthy. Their creation is associated with interpretations such as the possession of prestige objects, which facilitated the tracking and management of goods within the trading network. These seals also served as symbols of lineage or inheritance. Consequently, these individuals gained access to the economic sphere of society that governed the production and trade of goods with other communities. Nonetheless, this interpretation must be considered with a degree of caution, as no impressions of the cylinder seals found at Gird Lashkir have been discovered in the area occupied by Ninevite 5 communities.

4.1.2 Gir-e Gomel

The eight burials at Gir-e Gomel dating to the first half of the 3rd millennium BCE exhibit severely compromised preservation conditions resulting from both natural taphonomic processes and anthropogenic disturbances. The most significant post-depositional impact occurred through the intrusive construction of Grave 44, which was superimposed directly above seven of the earlier interments, causing substantial disruption to the original burial contexts and skeletal articulation. Despite these preservation challenges, the available archaeological documentation has facilitated a systematic archaeothanatological analysis, enabling the reconstruction of burial containers and the spatial organization of grave contents. This taphonomic approach has proven particularly valuable for understanding the original depositional environment and mortuary gestures.

4.1.2.1 The containers

The graves at Gir-e Gomel are characterized by simple pits that predominantly exhibit oval morphologies, though some display irregular contours that approximate oval configurations. The funerary practices of this period involved the excavation of simple pits within the *extra muros* areas, creating a well-defined necropolis spatially segregated from the settlement area. The minimal labor investment required for grave construction, evidenced by the absence of architectural elaboration or differential treatment, suggests an egalitarian approach to mortuary practices wherein social distinctions are not reflected in burial architecture. This uniformity in grave morphology indicates that status differentiation, if present within the community, was not expressed through investment in tomb construction.

4.1.2.2 Health and lifestyle

Paleopathological and enthesopathological analyses have not yet been conducted on the skeletal assemblage from this site, and the compromised preservation state of the remains presents significant limitations for comprehensive health and lifestyle assessments. The demographic profile reveals that the majority of individuals interred at this location were young adults who died between 20 and 30 years of age, with the notable exception of the individual from Grave 49, whose age at death was estimated between 45 and 55 years, as well as a child individual. This mortality pattern demonstrates consistency with previously documented demographic trends from Gird Lashkir, despite the scarcity of subadult burials in the current dataset—a lacuna

that may reflect taphonomic processes, cultural burial practices, or sampling biases inherent to the archaeological record. Future osteological investigations will focus on expanding our understanding of the health status, occupational activities, and lifeways of these ancient populations through detailed paleopathological examination and activity-related skeletal modifications analysis.

4.1.2.3 Social organization

A three-tier social status system has been identified based on the ornaments and grave goods accompanying the deceased. The lowest status is characterized by an absence of ornaments and grave goods, as evidenced in Graves 46, 48, and 49. The middle social status is characterized by an absence of ornaments, yet the presence of modest grave goods, such as the six small pottery jars evident in Grave 51. Finally, the third and highest social status is distinguished by the presence of both ornaments and grave goods. The ornaments are composed of materials that are indicative of prestige. Of particular note are the most precious items, which are crafted from silver, copper or bronze and include elements such as diadems, toggle pins, pins, straws, and beads. Semi-precious stones, including carnelian, white and gray stones, and shells, are frequently used in the fabrication of ornaments such as necklaces, pendants, bracelets, rings, and belts. The grave goods include pottery vessels and cylinder seals displaying geometric motifs.

The individuals who have been classified in the higher social class are as follows: Graves 24, 42, 45, and 47. Grave 24 is characterized by its elaborate ornamentation, including a diadem crafted from copper or bronze, white beads adorning the skull, two bracelets composed of white, carnelian, and shell beads, a pendant shaped like a white cylinder of considerable size, and a belt positioned around the abdomen made of shell rings. A copper or bronze toggle pin was also placed in the burial, suggesting its potential use as a fastening element associated with clothing. Grave 42 also possesses a copper or bronze toggle pin, as well as a ring made of shell material. Grave 47 exhibits a similar pattern, featuring a copper or bronze diadem and a pin. This combination would be consistent with a headpiece composed of fabric materials, which would have covered the deceased's head. Additionally fabricated from copper or bronze is the straw, which can be considered a constituent of a pendant given its position in the thorax. Silver beads were also unearthed in the burial, suggesting that the deceased may have worn a necklace or bracelet. A razor made of copper or bronze was found in a burial. Finally, Grave 45 displays four ornaments: a necklace composed of over 100 shell beads, three pendants featuring zoomorphical shapes (porcupine, bovid or bear, and turtle), a bracelet consisting of 30 shell beads, and a belt

crafted with shell rings. A total of up to 20 disc beads were found distributed across the thorax and the pelvis, which may have been components of some form of clothing or belt. As a grave good, a cylinder seal with an hourglass shape and geometric motifs was included in the burial. The motifs were composed of concentric semicircular lines.

Cylinder seals represent a critical category of material culture during this chronological period, functioning as multifaceted instruments that transcended purely administrative purposes. The production and circulation of these objects likely reflects their role as prestige items that simultaneously facilitated commercial transactions and served as markers of economic participation within inter-regional exchange networks. Beyond their practical applications in goods management and transaction authentication, cylinder seals worked as tangible expressions of social identity, potentially signifying lineage affiliation or hereditary status within the community hierarchy. The possession of such artifacts suggests that this individual maintained privileged access to the economic networks that regulated production cycles and facilitated trade relationships with neighboring communities.

4.1.3 Plaça de la Gardunya

Initial analysis of the comingled skeletal assemblage from Plaça de la Gardunya has successfully established minimum number of individuals estimations for each burial context and has enabled partial reconstruction of the depositional sequence of successive inhumations within the hypogea. These preliminary archaeothanatological investigations have yielded valuable insights into the mortuary practices, particularly regarding the use of collective burial spaces and the temporal organization of interments. However, the complex nature of the commingled remains has precluded the development of comprehensive biological profiles, needing future research initiatives focused on individual skeletal element attribution and demographic analysis. The current inability to associate specific skeletal elements with individual deceased has resulted in incomplete and heterogeneous demographic data, limiting assessments of age, sex, stature, and health status. Consequently, osteological analysis represents a priority that will provide essential data for understanding population demographic, health patterns, and lifestyle within this society.

4.1.3.1 The containers

Two predominant grave typologies have been identified: the hypogeum and the simple pit. Both the hypogea and the simple pits are of oval morphologies, but the hypogea are deeper, contain a greater number of buried individuals, and are used for longer periods of time than the simple pits. A tendency has been observed regarding the simple pits, as they exclusively contain the burials of subadult individuals in a secondary deposit.

Graves 2 and 3/4 from Sector 4, as well as Grave 1 and 2 from Sector 5 consist of hypogea, typically single-chambered except for Grave 3/4, which is double-chambered. Single-chambered hypogea contain less than 20 deceased, while the double-chambered hypogea has been able to contain a minimum number of 66 individuals.

The oldest buried individuals correspond to the subadults from Grave 5 (Sector 4), evidencing the first burial typology employed was the simple pit. Radiocarbon dates provide a range of use between 2200s and the 1800s cal. BCE. Only one sector of the population seems to have been buried in this excavated area, implying maybe the adults were buried in another not yet excavated area. The bones were secondary deposits of comingled and selected bones, with modest grave goods and no ornaments.

Hypogea have proven to be more recent than the simple pits, with radiocarbon dates ranging between the 1900s and the 1500s cal. BCE. This shift in the burial customs allowed to bury a larger portion of the community in a more concentrated necropolis area. An access shaft to access the chambers has only been recovered in Grave 3/4 from Sector 4 and Grave 2 from Sector 5. The absence of an access shaft could imply its nonexistence or its destruction after more recent disturbances. If their nonexistence is considered, the assignation as a hypogeum may be discarded and considered as only subterranean chambers.

4.1.3.2 Health and lifestyle

While comprehensive paleopathological and enthesopathological analyses remain to be conducted, preliminary examination of the skeletal remains has yielded significant pathological indicators that provide initial insights into the health profile of this ancient population. Most notably, skeletal evidence consistent with congenital rickets has been documented in the upper limb elements of four individuals recovered from Grave 2 in Sector 4, suggesting possible nutritional deficiencies or metabolic disorders affecting vitamin D synthesis during early development. Additionally, periosteal reactions observed on several long bone shafts indicate episodes of non-specific inflammatory processes, which may reflect infectious disease, trauma-related complications, or chronic stress responses. A comprehensive anthropological analysis incorporating systematic paleopathological assessment, demographic reconstruction, and activity-related skeletal modifications would significantly enhance our understanding of health dynamics and lifeways within this population.

4.1.3.3 Social organization

The first buried individuals at the necropolis were sixteen subadults located in six different simple pits. Their disposal was secondary, and only a selection of bones was placed inside the pits. The scarce grave goods and the absence of ornaments also play a role in the identification of the social role of these buried individuals. It seems probable that the adult portion of the community was buried elsewhere, an area not reached by excavation. The burial pattern suggests the presence of an equal society, with no great distinction between individuals, and with no importance in the preservation of the skeleton in its complete integrity. The burial process involved the previous preparation and skeletonization of the deceased, with an importance of the selection of the bones to be buried.

After the simple pits, the community started to bury their dead inside chambers and hypogea. Hypogea were architecturally more complex than chambers, as they possessed an access shaft. The complexity in architecture has demonstrated to correspond to the appearance of ornaments, being Grave 3/4 an example. The community buried all types of ages and sexes inside the chambers and hypogea, excepting fetuses or newborn individuals. The position of the buried individuals is also shared by all the individuals, preferring the lateral and the prone decubitus with flexed limbs. The generalized absence of grave goods and the buried demography suggests an equitable behavior in the funerary customs, indicating a shared social status by all the community. Only 32 individuals that have been associated with V-perforated buttons seem to be different from all the other deceased. Proposing a hypothesis of a shared lineage for these individuals without ancient DNA analysis is risky but plausible, as we observe the presence of four individuals with congenital rickets buried in Grave 2 from Sector 4, which could be part of the same family.

4.2 DENTAL MICROWEAR PATTERN

4.2.1 Gird Lashkir and Gir-e Gomel

The study of the dental microwear pattern of the buccal side of the postcanine teeth has provided the number of horizontal, vertical, mesiodistal, and distomesial striae, as well as the average length and its standard deviations for the sites of Gird Lashkir (**Table 73**), Gir-e Gomel (**Table 74**), and for both sites (**Table 75**). The average striation density (NT) of Gird Lashkir is 99.55, ranging from 70.67 to 179.67, and the average striation length (XT) is 114.68, ranging from 74.01 to 169.72. The average striation density (NT) of Gir-e Gomel is 107.54, ranging from 79.67 to 130.33, and the average striation length (XT) is 117.54, ranging from 90.80 to 155.45.

4.2.1.1 Post-mortem taphonomic effects

This study has identified physical and chemical taphonomic effects occurring post-mortem in the studied final teeth samples. Fissures have been observed in eleven teeth, six from Gird Lashkir and five from Gir-e Gomel. This weathering effect has resulted in the vertical cracking of the dental crowns (***Figure 52***). Scratches have been observed on thirteen teeth, eight from Gird Lashkir and five from Gir-e Gomel, caused by the interaction of the tooth enamel with soil particles during burial (***Figure 53***). Erosion or destruction of the enamel surface has been observed in nine teeth, five from Gird Lashkir and four from Gir-e Gomel (***Figure 54***). A total of six teeth have been observed to display an exposure of the enamel prisms, with three from Gird Lashkir and three additional cases from Gir-e Gomel. This taphonomic effect is discernible only under higher magnifications, ranging from 200× to 500× (***Figure 55***). The exposure of *perykimata* has been observed in twelve teeth. All of the final samples from Gir-e Gomel exhibit the exposure of the growing lines of enamel, while only six out of eleven final samples from Gird Lashkir do exhibit *perykimata* (***Figure 56***).

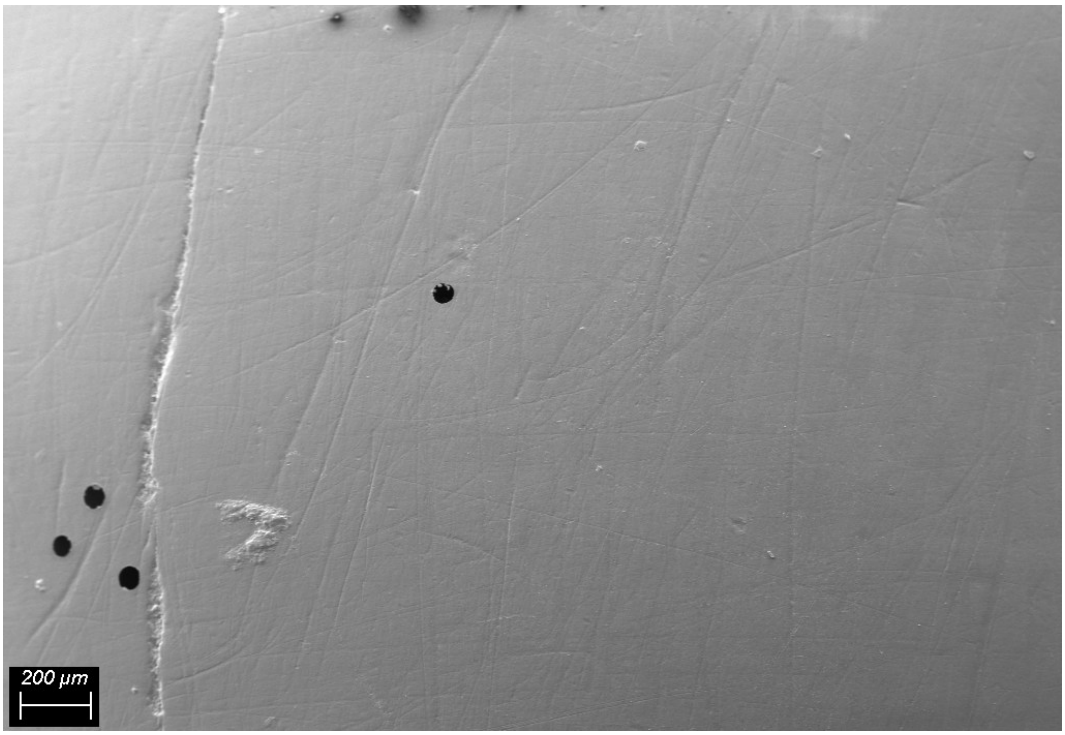


Figure 52. Micrograph at 100× magnification from a $_1$M that belongs to Grave 42 from Gir-e Gomel. A fissure is visible on the left side of the image.

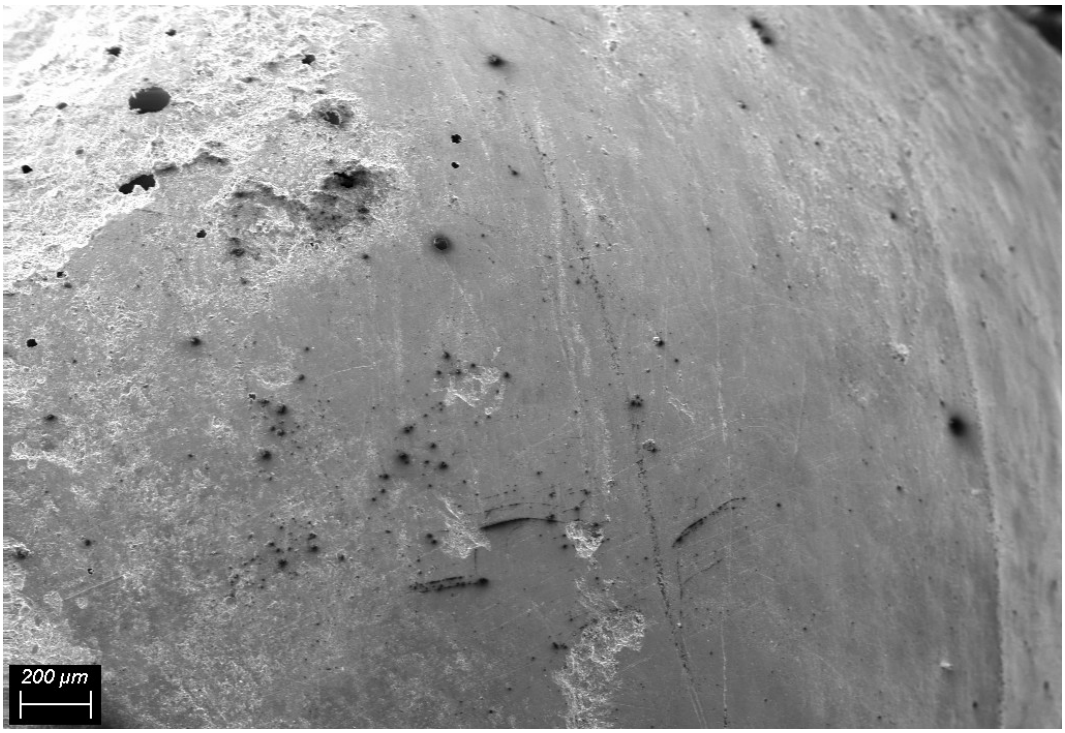


Figure 53. Micrograph at 100× magnification from a deciduous m_2 that belongs to Grave 7 from Gird Lashkir. Scratches in a diagonal orientation are visible on the lower center of the image.

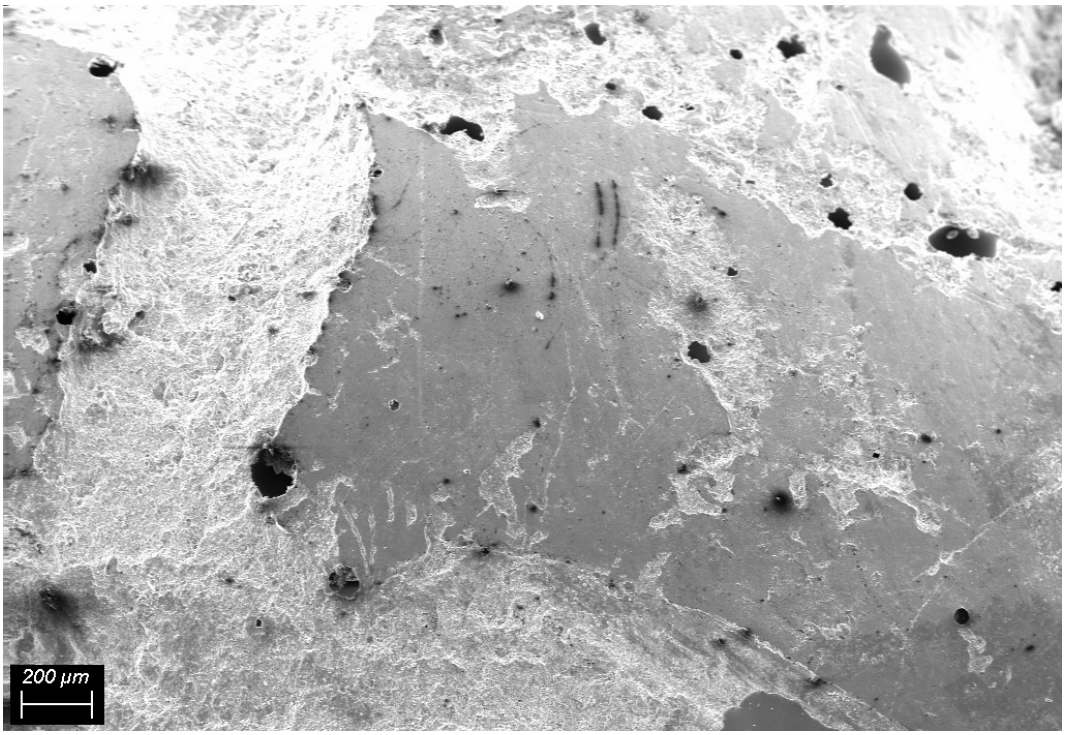


Figure 54. Micrograph at 100× magnification from a deciduous m_2 that belongs to Grave 7 from Gird Lashkir. The surface of the enamel exhibits erosion and destruction.

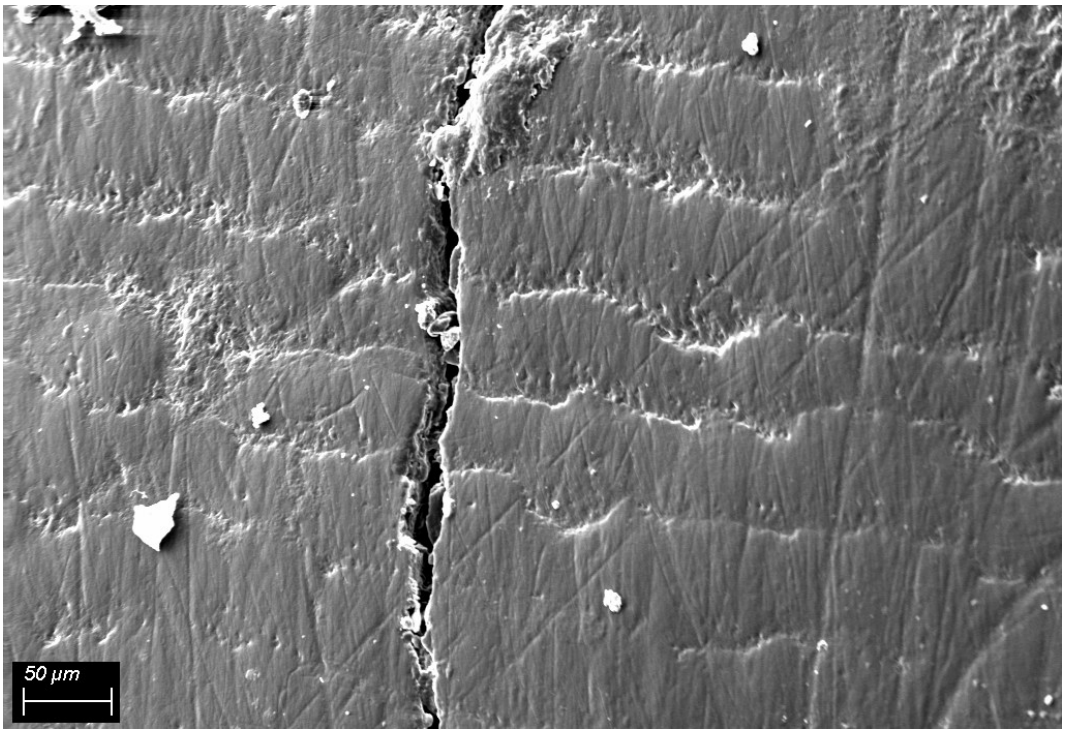


Figure 55. Micrograph at 500× magnification from a $_2$P that belongs to Grave 24 from Gir-e Gomel. Enamel prisms are exposed in the growth lines.

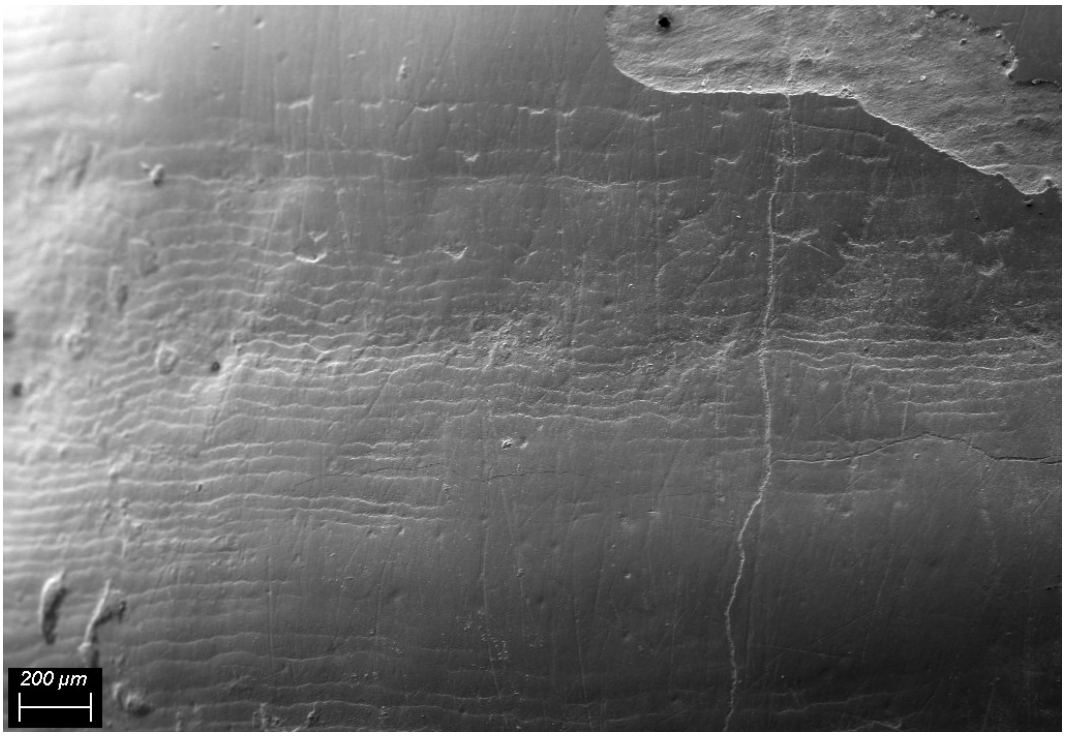


Figure 56. Micrograph at 100× magnification from a $_1$P that belongs to Grave 4 from Gird Lashkir. *Perykimata* is exposed all over the surface of the crown.

4.2.1.2 Intrapopulation variability

The values that characterize the dental microstriation pattern of the buccal side of each individual from the site of Gird Lashkir is presented in **Table 73**, and from the site of Gir-e Gomel is presented in **Table 74**. The values that characterize the entire population of Gird Lashkir and Gir-e Gomel can be seen in **Table 75**. The Shapiro-Wilk normality test has determined that the density of horizontal (p = 0.008), vertical (p = 0.03), and mesiodistal striations (p = 0.002) exhibit significant differences between individuals, suggesting that the data are not normally distributed. A Kruskal-Wallis test for the non-parametric data indicates that there are no significant differences between age or sex ($p > 0.05$). An analysis of variance (ANOVA) and a Levene post-hoc test for the normally distributed data indicates that there are no significant differences between adults and subadults ($p > 0.05$). The Bonferroni and Tukey's HSD post-hoc tests indicate no significant differences between female, male, and indeterminate individuals ($p > 0.05$). A scatter plot of the total density of striae and its average length for both female and male individuals suggests a homogeneity in their microwear pattern (***Figure 57***).

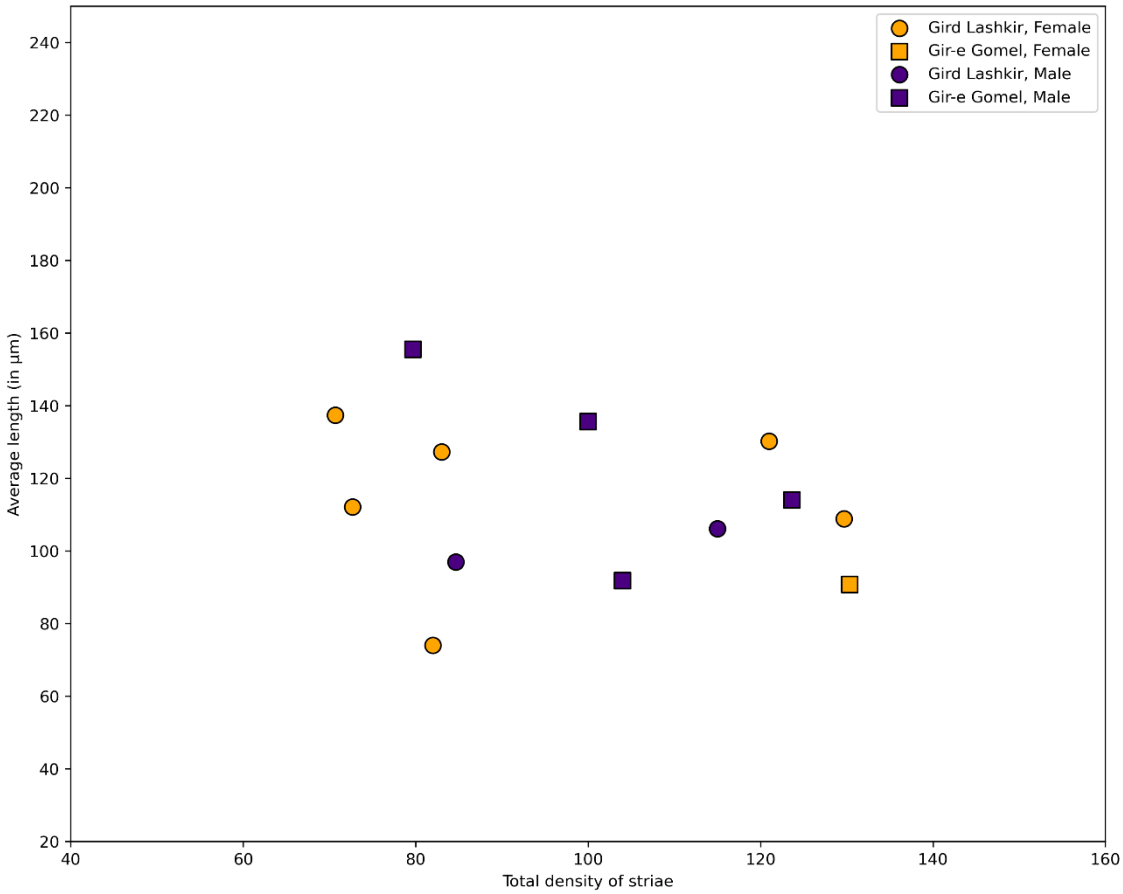


Figure 57. Scatter plot of the total density of striae and the average length (in µm) for female (in orange) and male (in purple) individuals from Gird Lashkir (represented by a circle) and Gir-e Gomel (represented by a square) individuals.

Table 73. Dental microwear pattern of Gird Lashkir's individuals.

	Number of striae					Average length				
Grave	Horizontal	Vertical	Mesiodistal	Distomesial	Total	Horizontal	Vertical	Mesiodistal	Distomesial	Total
4	35.00	8.00	3.00	24.67	70.67	151.25 ± 141.40	143.57 ± 75.94	98.15 ± 55.10	119.34 ± 94.06	137.36 ± 118.65
5	45.33	7.67	10.67	19.33	83.00	129.87 ± 117.38	171.51 ± 112.58	98.33 ± 48.82	119.74 ± 104.93	127.30 ± 108.44
6.1	57.00	6.00	27.33	22.67	113.00	101.75 ± 68.77	130.66 ± 65.47	108.20 ± 89.21	90.24 ± 55.48	102.27 ± 73.02
6.2	56.33	30.00	38.00	5.33	129.67	127.70 ± 119.95	125.72 ± 100.10	69.83 ± 59.34	81.93 ± 53.30	108.84 ± 105.09
7	27.00	5.67	8.67	2.00	43.33	175.37 ± 156.59	171.78 ± 111.40	174.32 ± 156.31	133.25 ± 34.47	169.72 ± 145.26
10	28.67	18.33	1.67	24.00	72.67	108.70 ± 80.80	129.31 ± 140.61	58.90 ± 20.62	108.38 ± 87.96	112.17 ± 98.48
12.1	50.67	28.67	3.33	32.33	115.00	132.47 ± 123.32	103.52 ± 83.38	140.97 ± 87.12	66.74 ± 42.37	106.10 ± 100.78
13	100.67	51.67	9.33	18.00	179.67	103.36 ± 77.73	97.00 ± 84	74.26 ± 63.56	65.42 ± 52.64	96.48 ± 79.30
14	43.33	23.00	17.67	0.67	84.67	97.58 ± 77.72	124.16 ± 102.47	58.24 ± 40.21	56.86 ± 43.65	96.93 ± 82.95
15	106.67	4.00	8.33	2.00	121.00	136.21 ± 108.74	112.29 ± 69.17	88.25 ± 83.73	67.88 ± 52.36	130.25 ± 106.11
16	37.00	4.00	9.33	32.00	82.33	75.52 ± 41.54	73.34 ± 18.65	77.25 ± 31.16	71.78 ± 35.12	74.01 ± 38.04

Table 74. Dental microwear pattern of Gir-e Gomel's individuals.

	Number of striae					Average length				
Grave	Horizontal	Vertical	Mesiodistal	Distomesial	Total	Horizontal	Vertical	Mesiodistal	Distomesial	Total
24	52.00	34.67	0	43.67	130.33	103.39 ± 104.62	103.01 ± 99.34	0	68.13 ± 47.98	90.80 ± 89.73
42	51.33	10.00	0.33	38.33	100.00	148.93 ± 127.03	139.61 ± 92.44	73.57	116.46 ± 93.93	135.63 ± 114.37
47	62.00	12.33	1.33	48.00	123.67	121.53 ± 112.32	131.40 ± 118.19	61.40 ± 6.46	108.03 ± 116.05	114.03 ± 114.79
48	32.33	37.00	2.33	8.00	79.67	174.55 ± 132.74	153.95 ± 126.62	88.57 ± 51.79	84.44 ± 44.93	155.45 ± 124.77
49	55.33	10.67	36.33	1.67	104.00	95.10 ± 86.33	104.52 ± 66.23	83.62 ± 73.63	36.46 ± 5.96	91.76 ± 79.83

Table 75. Dental microwear pattern of the whole population of Gird Lashkir and Gir-e Gomel.

Site	Number of striae					Average length				
	Horizontal	Vertical	Mesiodistal	Distomesial	Total	Horizontal	Vertical	Mesiodistal	Distomesial	Total
Gird Lashkir	53.42	17.00	12.48	16.64	99.55	121.80 ± 101.27	125.72 ± 87.62	95.16 ± 66.83	89.23 ± 59.67	114.68 ± 96.01
Gir-e Gomel	50.60	20.93	8.07	27.93	107.53	128.70 ± 112.61	126.50 ± 100.56	61.43 ± 26.38	82.70 ± 61.77	117.54 ± 104.70

Table 76. Indices of the relative frequency of striation, grouped into age and sex categories for the Gird Lashkir individuals.

Category	Group	*n*	NH/NT	NV/NT	NH/NV
Age	Subadults	4	0.64	0.15	4.33
	Adults	7	0.46	0.19	2.48
Sex	Females	6	0.55	0.13	4.29
	Males	2	0.47	0.26	1.82
All		11	0.54	0.17	3.14

Table 77. Indices of the relative frequency of striation, grouped into age and sex categories for the Gir-e Gomel individuals.

Category	Group	*n*	NH/NT	NV/NT	NH/NV
Age	Adults	5	0.47	0.19	2.42
Sex	Females	1	0.40	0.27	1.50
	Males	4	0.49	0.17	2.87
All		6	0.47	0.19	2.42

The results of the calculation of the indices of relative frequency of striation, grouped into age and sex categories, can be observed in ***Table 76*** and ***Table 77***, the first for Gird Lashkir's individuals and the latter for Gir-e Gomel's individuals. The indices encompass the ratio of density of horizontal and vertical striae (NH/NV), the ratio of density of horizontal striae and total striae density (NH/NT), and the ratio of density of vertical striae and total striae density (NV/NT) (Lalueza et al., 1996; Pérez-Pérez et al., 1994).

Upon examination of the NH/NV ratio (***Table 78***), subadults exhibit a nearly twice the value of adults, underscoring the considerable density of horizontal striations and the decreased density of vertical striae. Adults from Gird Lashkir display an NH/NV index of 2.48, which is similar to the 2.42 index observed in Gir-e Gomel, suggesting comparable microstriation patterns. With respect to the sex category, female individuals display slightly denser horizontal striae, while male individuals exhibit slightly denser vertical striations. A comparison of Gird Lashkir and Gir-e Gomel female individuals reveals that the former displays significantly denser horizontal striations (4.29) compared to the latter (1.50). A comparison of the female and male individuals from Gir-e Gomel reveals that the former exhibits a greater density of striae (1.50) compared to the latter (2.87). Nonetheless, the results from Gir-e Gomel in terms of sex category could be biased due to the low number for female individuals.

Table 78. Indices of the relative frequency of striation, grouped into age and sex categories for both Gird Lashkir and Gir-e Gomel individuals.

Category	Group	*n*	NH/NT	NV/NT	NH/NV
Age	Subadults	4	0.64	0.15	4.33
	Adults	12	0.47	0.19	2.45
Sex	Females	7	0.52	0.15	3.38
	Males	6	0.49	0.20	2.42
All		16	0.51	0.18	2.88

4.2.1.3 Diet classification

The studied populations with a known diet, as published by Lalueza et al. (1996), serve as reference datasets to classify the type of diet from the sites of Gird Lashkir and Gir-e Gomel. Both populations exhibit a higher density of short striations compared to the reference diets (***Figure 58***).

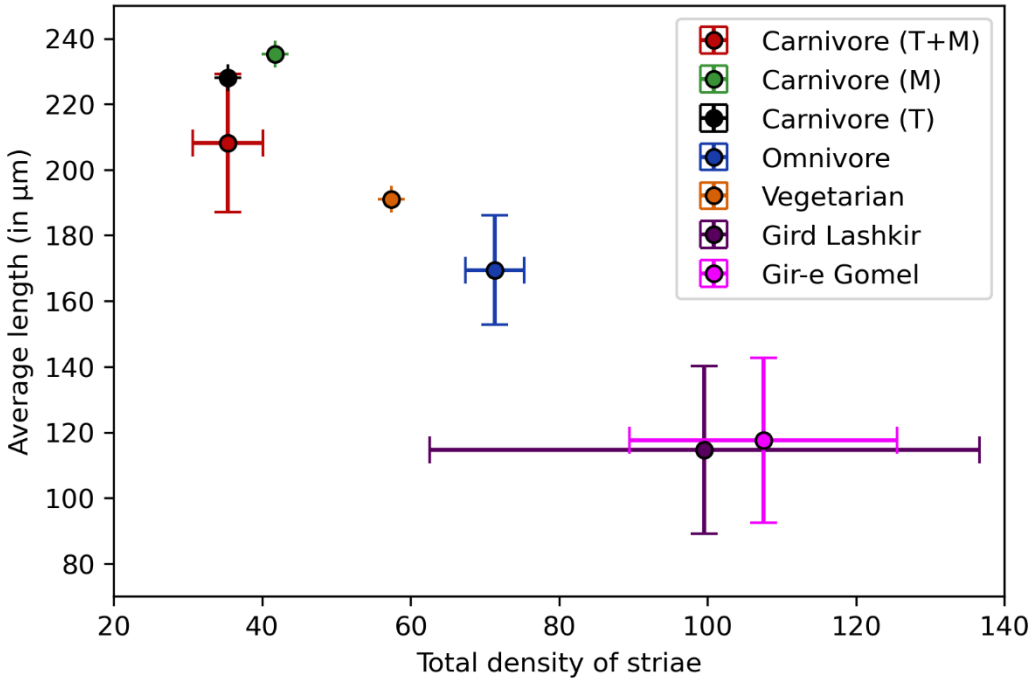


Figure 58. Scatter plot displaying the total density and the average length of striae from populations of known diets and the northern Mesopotamian populations of Gird Lashkir and Gir-e Gomel.

A **Linear Discriminant Analysis (LDA)** was performed to classify the microwear patterns of the population of Gird Lashkir and Gir-e Gomel, the subadult, the female, and the male individuals into one of five different diet groups: carnivore (differentiating the groups by the origin of their protein consumption, including marine, terrestrial, and both marine and terrestrial), omnivore, and vegetarian. The predictor variables encompassed 15 variables that characterize a microstriation pattern. It was determined that ten of the variables did not meet the requisite statistical assumptions. The canonical discriminant functions that met the requisite statistical assumptions included the density of horizontal (NH), vertical (NV), mesiodistal (NMD), and distomesial striae (NDM), as well as the average length of horizontal striations (XH). The model demonstrated a positive ability to discriminate among the five diet groups and exhibited a 100% accuracy rate in

the classification of the original grouped cases, correctly categorizing the population of Gird Lashkir and Gir-e Gomel within the omnivorous group (**Figure *59***). The canonical discriminant functions for the subadult, female and male individuals indicate that function 1 explains 90.9% of the variance, and function 2 explains 8.4%, thus summing to 99.3%. All cases have been processed, and none was excluded from the classification, exhibiting a 100% accuracy rate in the classification of the original grouped cases. The observation of the data from the subadult individuals, the analysis has provided a categorization of 25% omnivorous, and 75% vegetarians (***Figure 60***). When exploring the data of the female individuals, 28.6% were categorized as carnivores with a marine consumption, 57.1% fell into the omnivorous category, and 14.3% were identified as vegetarians (***Figure 61***). In the case of male individuals, 66.67% were categorized as omnivorous, and 33.33% were identified as vegetarians (***Figure 62***).

This analysis enables the observation of the general tendency of the population to have adopted an omnivorous diet, while the intra-population analysis allows for the observation of more subtle variations in diet (***Table 79***). Subadult individuals appear to exhibit a preferential consumption of abrasive foodstuffs. Female adults exhibit a tendency to consume a wider variety of foodstuffs, with two individuals—Graves 4 and 10 from Gird Lashkir—demonstrating a softer abrasive microstriation pattern, indicative of increased intake of protein from aquatic sources. The male individuals are predominantly classified as omnivorous, yet two individuals deviate from this pattern and exhibit a more pronounced abrasive microstriation pattern, suggesting a greater inclination toward a vegetarian diet. These individuals are Grave 14 from Gird Lashkir, the oldest individual, and Grave 48 from Gir-e Gomel, a young adult.

Table 79. Diet classification of the individuals of Gird Lashkir and Gir-e Gomel after the Linear Discriminant Analysis.

Site	Grave	Age	Sex	Classified diet
Gird Lashkir	4	Adult	Female	Carnivore (marine)
Gird Lashkir	5	Adult	Female	Omnivore
Gird Lashkir	6.2	Adult	Female	Omnivore
Gird Lashkir	10	Adult	Female	Carnivore (marine)
Gird Lashkir	16	Adult	Female	Omnivore
Gird Lashkir	15	Subadult	Female	Vegetarian
Gir-e Gomel	24	Adult	Female	Omnivore
Gird Lashkir	12.1	Adult	Male	Omnivore
Gird Lashkir	14	Adult	Male	Vegetarian
Gir-e Gomel	42	Adult	Male	Omnivore
Gir-e Gomel	47	Adult	Male	Omnivore
Gir-e Gomel	48	Adult	Male	Vegetarian
Gir-e Gomel	49	Adult	Male	Omnivore
Gird Lashkir	6.1	Subadult	Indeterminate	Omnivore
Gird Lashkir	7	Subadult	Indeterminate	Vegetarian
Gird Lashkir	13	Subadult	Indeterminate	Vegetarian

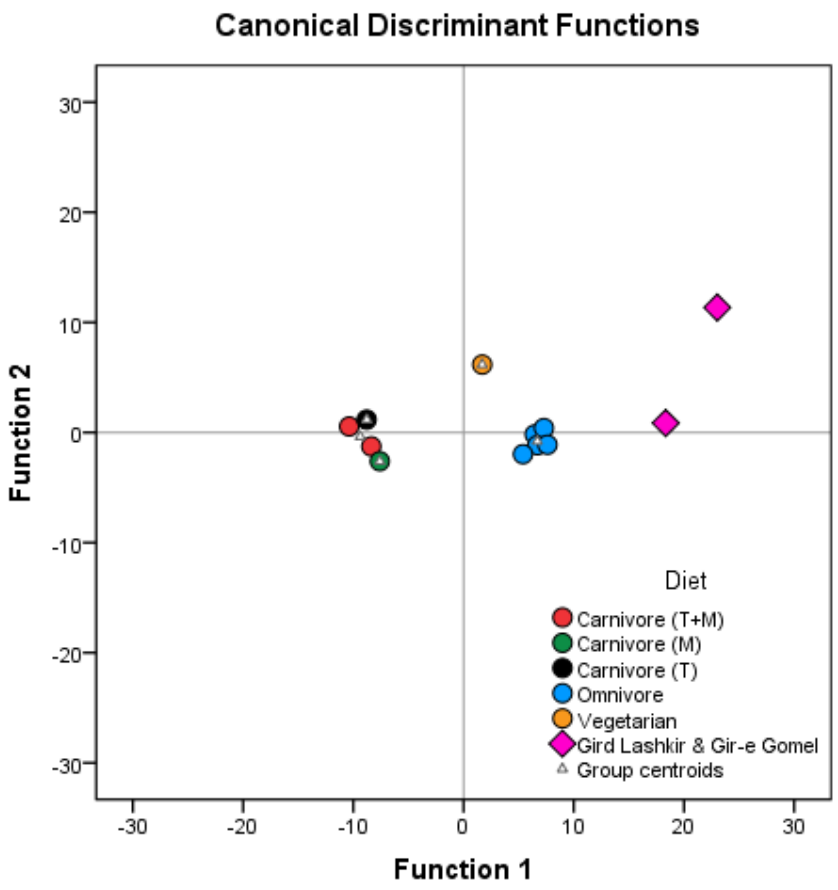


Figure 59. Scatter plot displaying the results of functions 1 and 2 of the Linear Discriminant Analysis to classify Gird Lashkir and Gir-e Gomel's population into a dietary category.

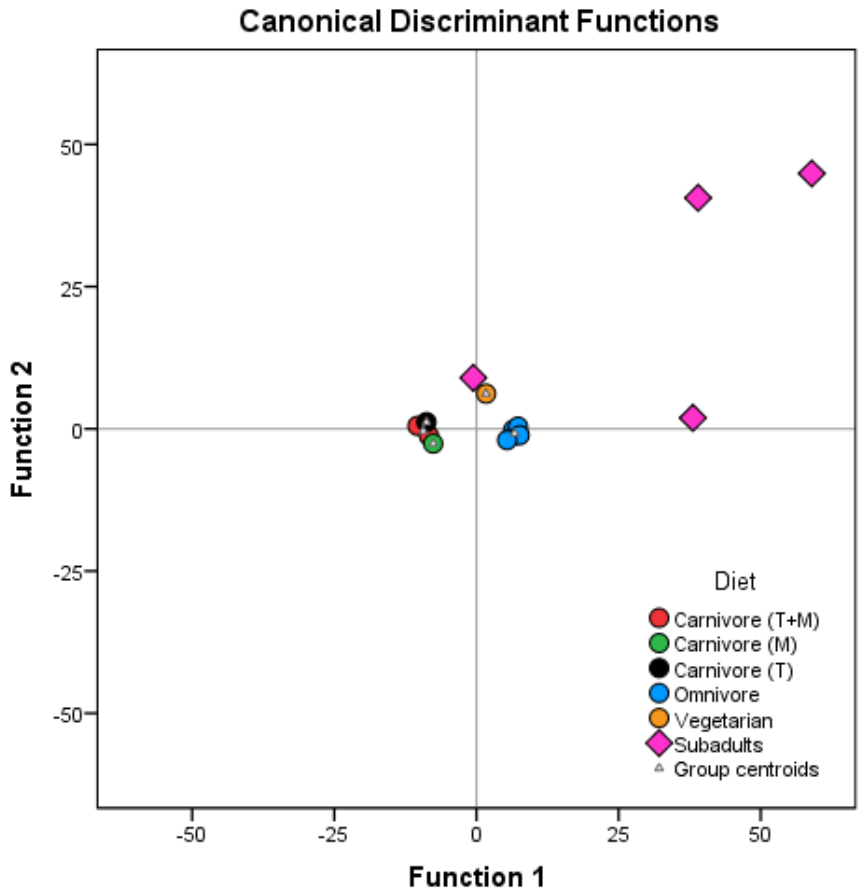


Figure 60. Scatter plot displaying the results of functions 1 and 2 of the Linear Discriminant Analysis to classify the subadult individuals from Gird Lashkir into a dietary category.

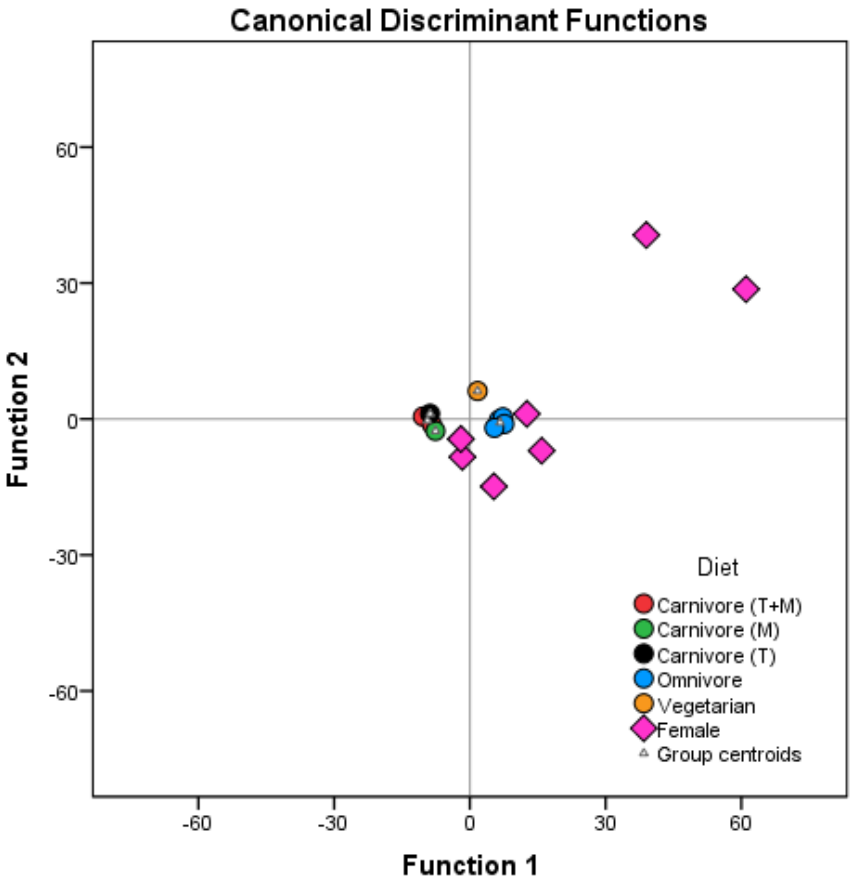


Figure 61. Scatter plot displaying the results of functions 1 and 2 of the Linear Discriminant Analysis to classify Gird Lashkir and Gir-e Gomel's female individuals into a dietary category.

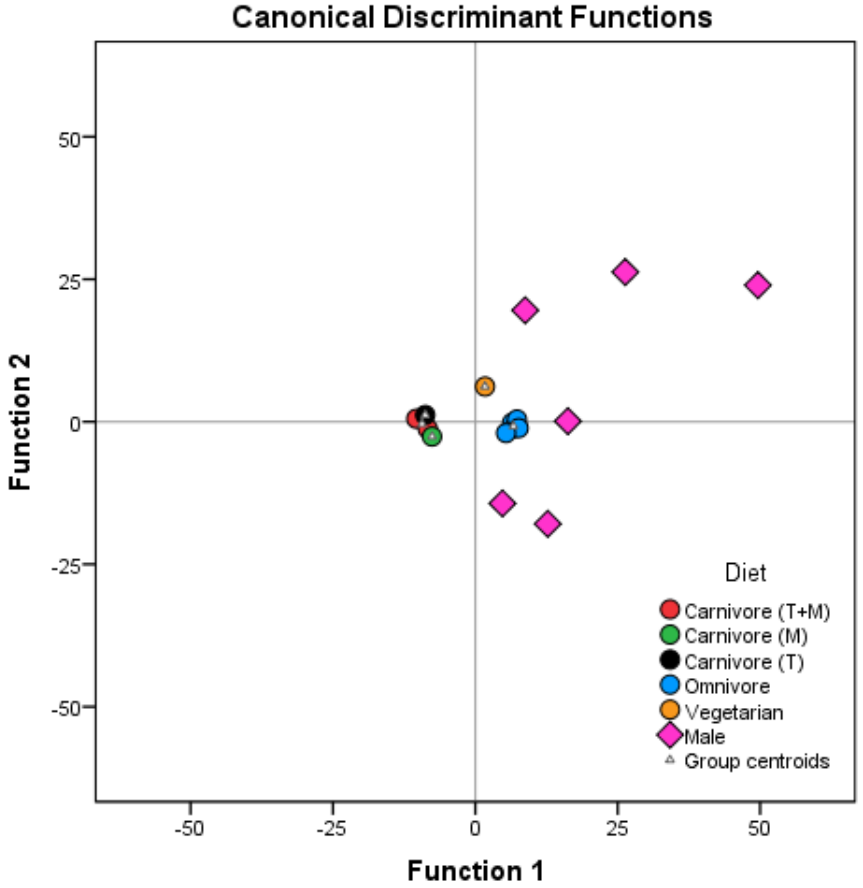


Figure 62. Scatter plot displaying the results of functions 1 and 2 of the Linear Discriminant Analysis to classify Gird Lashkir and Gir-e Gomel's male individuals into a dietary category.

4.2.1.4 Comparison with other archaeological sites

To date, traceology studies incorporating buccal microwear analysis have not been conducted for populations from the Mesopotamian region, representing a significant gap in our understanding of dietary patterns and food processing behaviors. Only a limited number of analyses have been performed on the occlusal surface (Sołtysiak, 2011). The absence of comparative datasets from other archaeological sites in the region has constrained our ability to contextualize our findings within the broader framework of Mesopotamian dietary evolution and to establish comparative baselines for understanding regional dietary patterns and their temporal variations.

4.2.2 Plaça de la Gardunya

The study of the postcanine dentition has provided the dental microwear pattern of the buccal view from the individuals of Plaça de la Gardunya. This pattern includes the number of horizontal, vertical, mesiodistal, and distomesial striae, as well as the average length and its standard deviations (**Table 80**). The values for the microstriation pattern for the entire population are provided in **Table 81**, which incorporates five individuals previously published and studied by the same author (Gluitz et al., 2023). The individuals previously examined include 4232 and 4319.3 from Grave 2 (Sector 4), 4328.6 from Grave 3/4 (Sector 4), 50616.2 from Grave 1 (Sector 5), and 50619 from Grave 2 (Sector 5). The average striation density (NT) of Plaça de la Gardunya is 140.27, ranging from 64.67 to 188.67, and the average striation length (XT) is 104.29, ranging from 56.35 to 164.57.

Table 80. Dental microwear pattern of Plaça de la Gardunya's individuals.

	Number of striae					Average length				
Grave	Horizontal	Vertical	Mesiodistal	Distomesial	Total	Horizontal	Vertical	Mesiodistal	Distomesial	Total
4430.8	75.67	17.00	3.00	39.67	135.33	106.53 ± 97.63	116.04 ± 101.92	88.91 ± 55.60	93.92 ± 75.28	103.50 ± 94.08
4388	91.00	16.00	76.67	5.00	188.67	102.31 ± 107.89	115.34 ± 111.87	106.91 ± 98.77	74.47 ± 34.56	103.56 ± 102.02
4473	56.33	23.00	3.33	49.33	132.00	91.34 ± 76.42	96.43 ± 73.37	184.08 ± 73.01	95.26 ± 64.10	95.96 ± 74.17
50618.1	32.67	11.33	18.67	2.00	64.67	90.92 ± 63.84	105.12 ± 57.61	84.54 ± 96.71	106.11 ± 35.13	91.14 ± 72.40
50620.3	57.00	11.33	4.00	72.33	144.67	106.51 ± 80.30	116.33 ± 98.91	114.76 ± 57.38	104.96 ± 101.15	106.74 ± 93.09
50615.2	60.33	9.67	3.67	49.33	123.00	119.30 ± 109.50	136.69 ± 110.93	95.72 ± 45.34	114.41 ± 89.56	117.20 ± 100.38
50700	46.33	15.33	8.33	8.33	78.33	143.98 ± 107.96	152.73 ± 110.48	93.57 ± 39.48	83.09 ± 38.86	134.24 ± 100.88
4391	39.67	12.67	6.33	35.67	94.33	160.75 ± 133.20	92.17 ± 44.63	153.24 ± 107.35	127.37 ± 101.75	138.26 ± 114.66
4389.11	46.67	39.33	23.33	85.33	99.33	98.19 ± 79.08	87.46 ± 53.89	59.87 ± 31.94	78.05 ± 46.98	56.35 ± 37.87
4389.12	67.67	37.67	6.67	17.67	129.67	133.21 ± 109.50	139.56 ± 98.87	159.51 ± 106.39	97.85 ± 69.56	131.69 ± 102.53
4389.13	40.67	21.67	20.67	2.33	85.33	102.72 ± 72.76	112.59 ± 71.73	64.79 ± 30.72	57.89 ± 27.10	94.56 ± 66.69
4389.14	35.33	13.00	7.00	20.00	75.33	89.22 ± 48.13	85.42 ± 41.80	64.82 ± 37.58	93.09 ± 81.88	87.41 ± 57.96
4389.15	45.33	24.00	13.00	2.33	84.67	106.17 ± 96.49	125.17 ± 87.01	66.04 ± 22.58	50.29 ± 10.50	103.82 ± 87.28
4389.16	48.67	28.67	35.67	3.50	115.33	109.05 ± 112.16	107.80 ± 89.38	85.57 ± 66.88	99.54 ± 88.77	101.13 ± 96.65
4389.17	36.67	23.33	10.00	1.00	70.33	123.16 ± 121.99	127.43 ± 109.17	64.34 ± 22.80	93.06	115.81 ± 110.51
4389.18	53.67	50.67	10.67	11.67	126.67	101.74 ± 69.53	99.90 ± 61.97	71.47 ± 48.10	83.50 ± 45.40	96.67 ± 63.53
4389.19	48.00	24.00	22.00	4.67	98.67	90.21 ± 56.43	107.96 ± 64.38	81.61 ± 53.56	109.22 ± 69.80	93.59 ± 60.20
4389.20	50.67	32.00	4.33	32.67	119.67	99.54 ± 79.30	99.16 ± 79.45	81.95 ± 37.51	84.55 ± 70.67	94.83 ± 76.45
4389.21	46.33	33.33	22.00	7.33	109.00	95.64 ± 68.75	109.22 ± 81.27	99.03 ± 100.94	67.06 ± 31.83	98.40 ± 78.90
4389.22	42.33	36.33	28.00	15.50	77.33	61.16 ± 51.13	89.27 ± 68.31	75.50 ± 54.08	56.48 ± 24.59	74.14 ± 50.29
4389.23	70.33	16.00	23.00	11.00	120.33	106.87 ± 92.34	102.98 ± 92.48	100.66 ± 77.32	71.27 ± 41.94	101.54 ± 89.73
4389.24	84.33	17.00	23.33	18.67	143.33	97.82 ± 102.94	133.26 ± 118.90	59.74 ± 50.69	100.11 ± 76.58	95.81 ± 97.86

Table 81. Dental microwear pattern of the whole population of Plaça de la Gardunya, including the data of a previously published study by the same author (Gluitz et al., 2023).

Number of striae					Average length				
Horizontal	Vertical	Mesiodistal	Distomesial	Total	Horizontal	Vertical	Mesiodistal	Distomesial	Total
45.31	25.32	18.90	20.49	104.75	114.53 ± 83.10	115.85 ± 84.31	100.15 ± 59.47	92.76 ± 60.34	106.25 ± 85.72

4.2.2.1 Post-mortem taphonomic effects

Post-mortem physical and chemical taphonomic effects have been observed in the studied final teeth samples. Fissures have been observed in twenty-one out of twenty-two teeth, primarily due to weathering effects that lead to the vertical cracking of the dental crowns (***Figure 63***). Scratches, resulting from the interaction between the tooth enamel and soil particles during burial, have been observed on all teeth (***Figure 64***). A total of twenty teeth have exhibited signs of erosion or destruction of the enamel surface (***Figure 65***). The exposure of the enamel prisms has been observed in a limited number of cases, with only three teeth displaying this effect when magnified between 200× and 500× (***Figure 66***). Finally, exposure of *perykimata* is evident in twelve teeth (***Figure 67***).

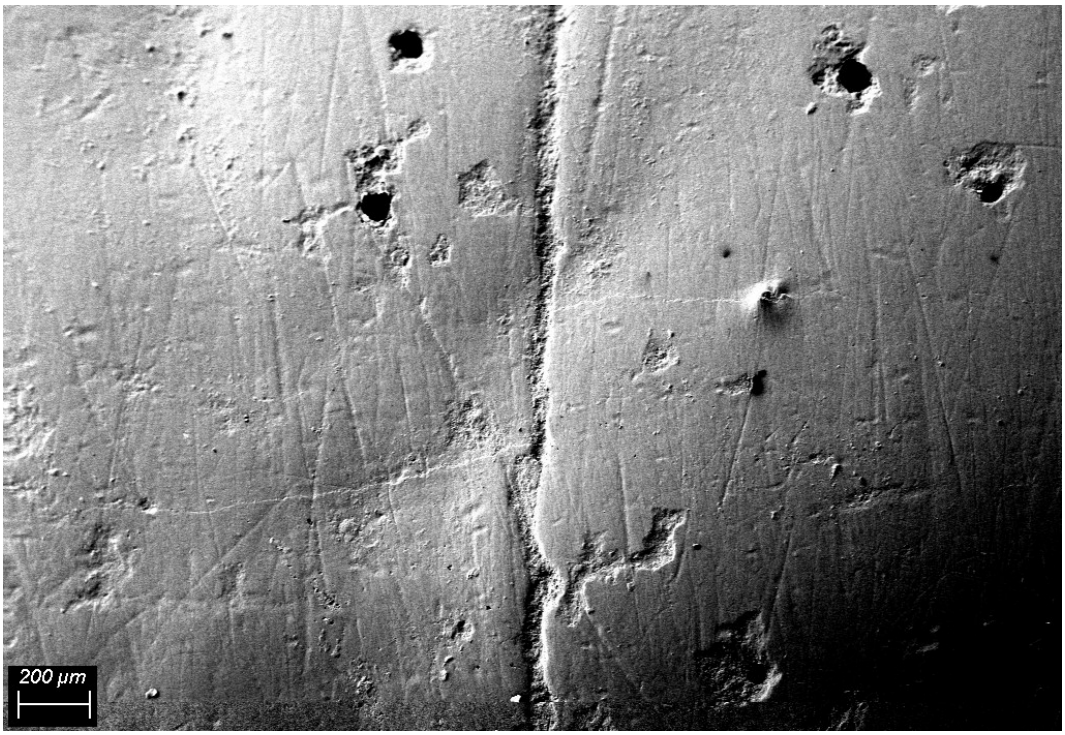


Figure 63. Micrograph at 100× magnification from a M_1 that belongs to the individual 4389.15 from 3/4 (Sector 4). A fissure is visible at the center of the image.

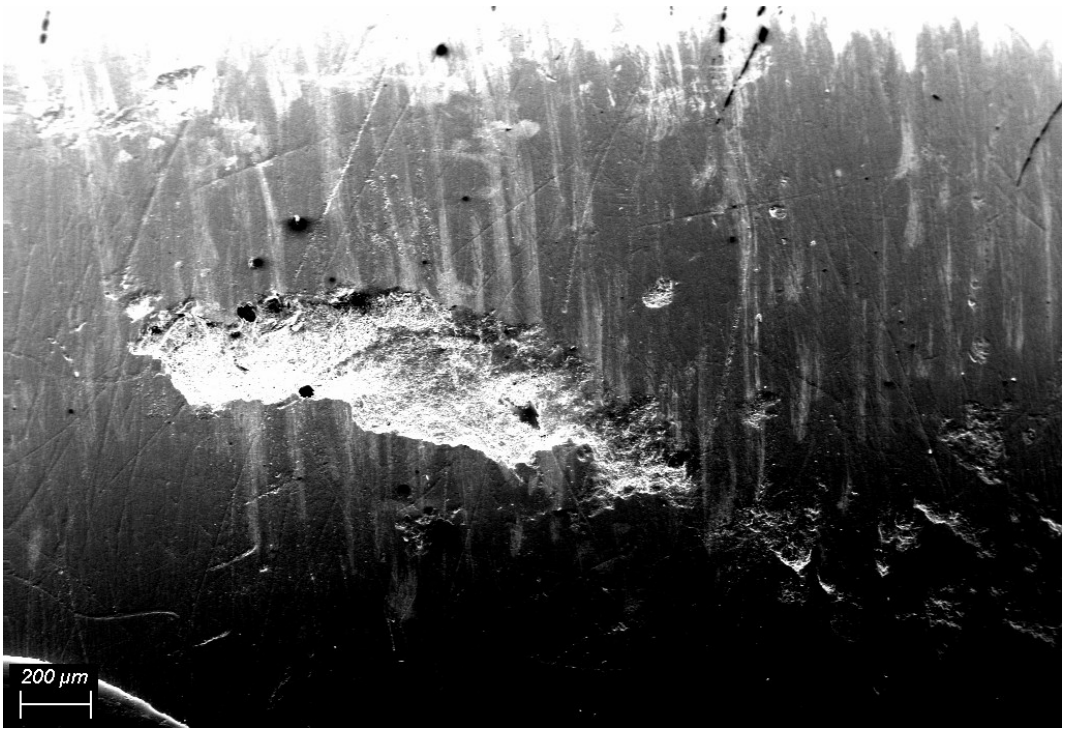


Figure 64. Micrograph at 100× magnification from a M_1 that belongs to the individual 50700 from Grave 1 (Sector 5). Scratches with a vertical orientation are visible on the enamel surface.

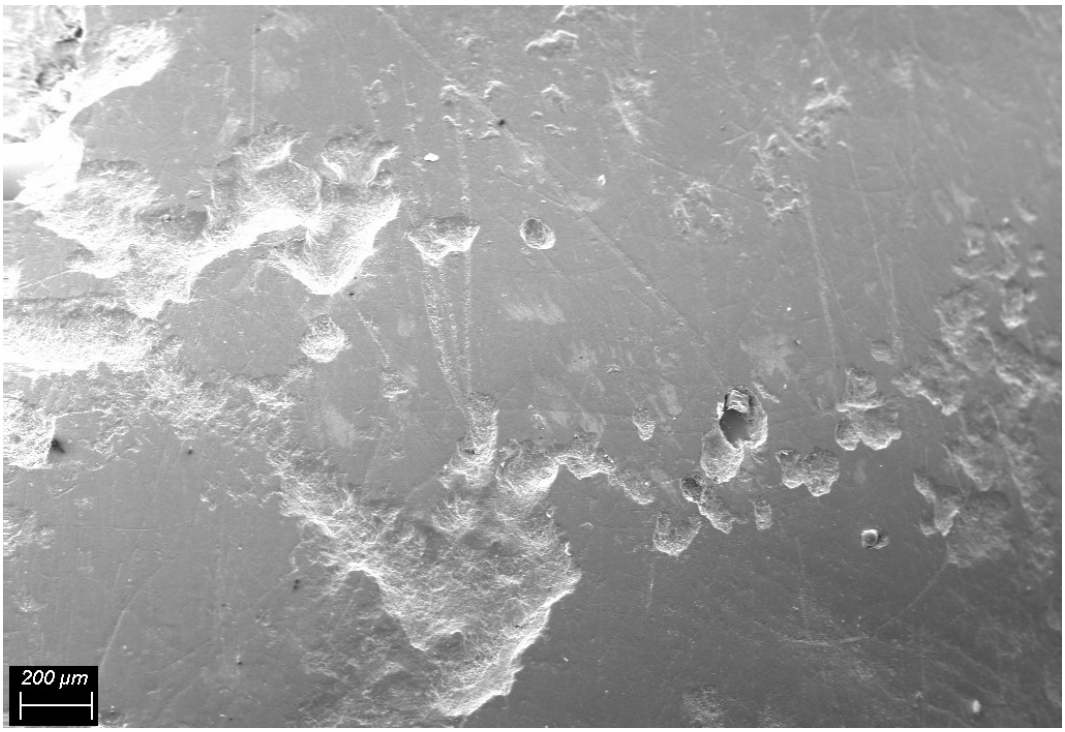


Figure 65. Micrograph at 100× magnification from a M_1 that belongs to the individual 50618.1 from Grave 2 (Sector 5). The surface of the enamel exhibits erosion and destruction.

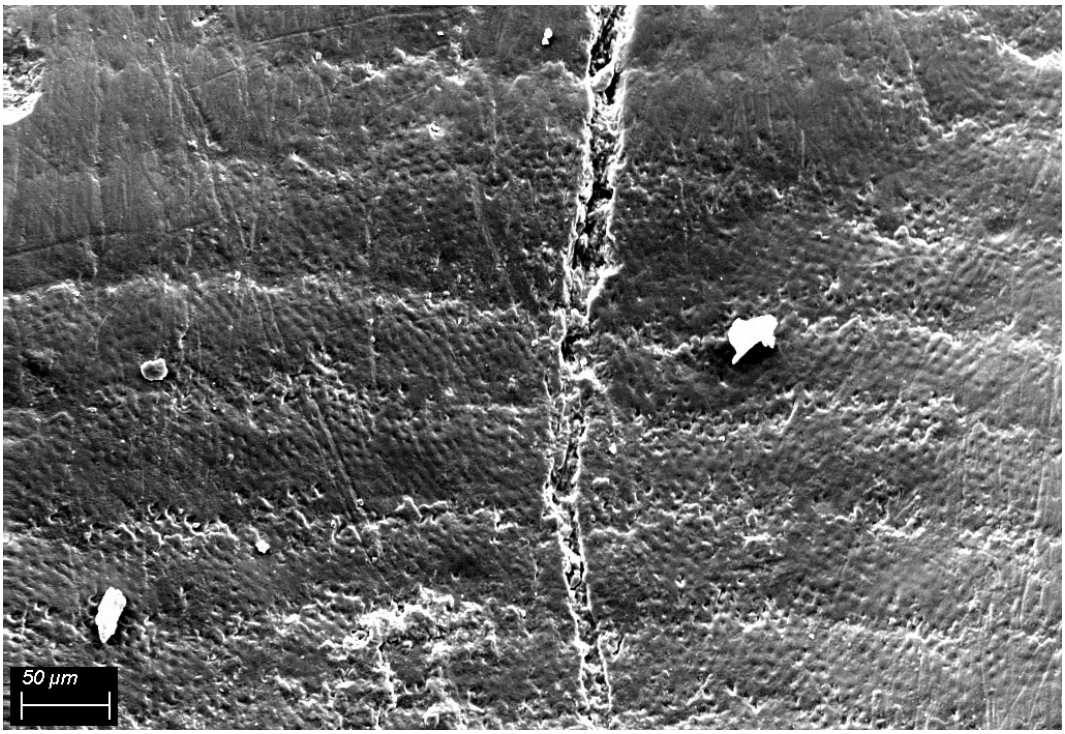


Figure 66. Micrograph at 500× magnification from a from a M_1 that belongs to the individual 4389.24 from 3/4 (Sector 4). Enamel prisms are exposed in the growth lines.

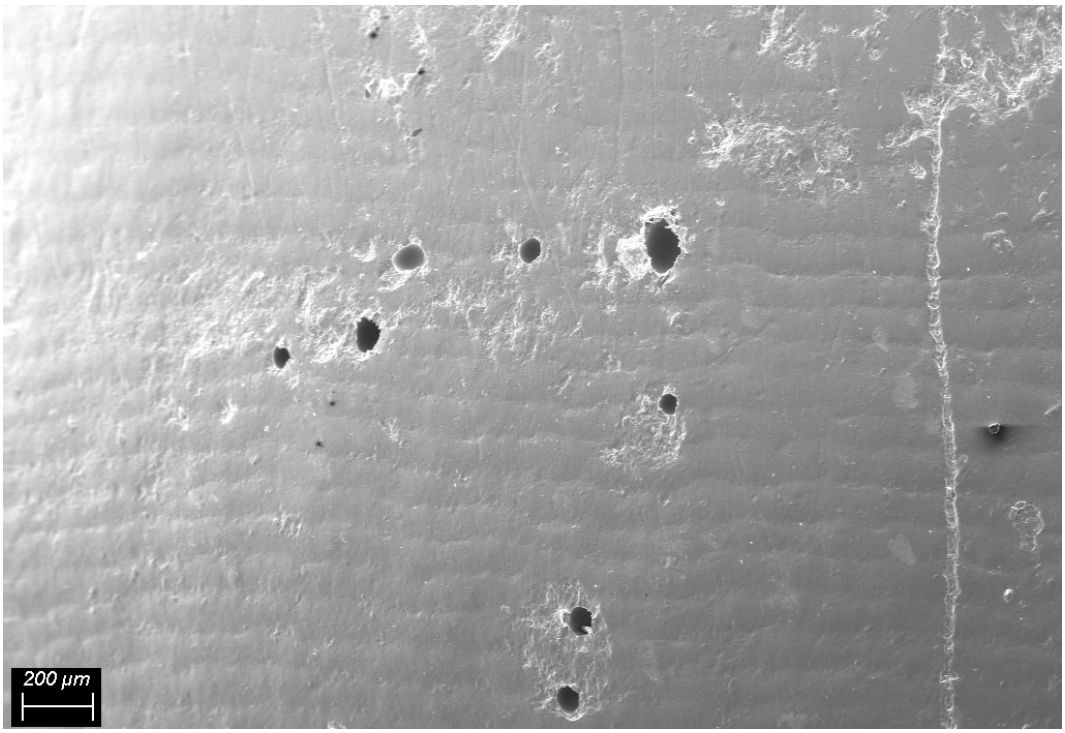


Figure 67. Micrograph at 100× magnification from a M_1 that belongs to the individual 4389.17 from Grave 3/4 (Sector 4). *Perykimata* is exposed all over the surface of the crown.

4.2.2.2 Intrapopulation variability

The Shapiro-Wilk normality test has determined that the density of vertical (p = 0.00), mesiodistal (p = 0.00) and distomesial striae (p = 0.002), as well as the average length of vertical (p = 0.001), mesiodistal (p = 0.00) and its standard deviation (p = 0.001), and all striae orientations (p = 0.00) display significant differences between individuals, suggesting that the data are not normally distributed. A Kruskal-Wallis test for the non-parametric data indicates that there are no significant differences between age or sex (p > 0.05). An analysis of variance (ANOVA) and a Levene post-hoc test for the normally distributed data indicates that there are no significant differences between adults and subadults (p > 0.05). The Bonferroni and Tukey's HSD post-hoc tests indicate that there are no significant differences between female, male, and indeterminate individuals (p > 0.05). A scatter plot of the total density of striae and its average length for female, male, and indeterminate individuals suggests a homogeneity in their microwear pattern (**Figure *68***). A slight increase in the average length of striations was observed in male individuals compared to female individuals.

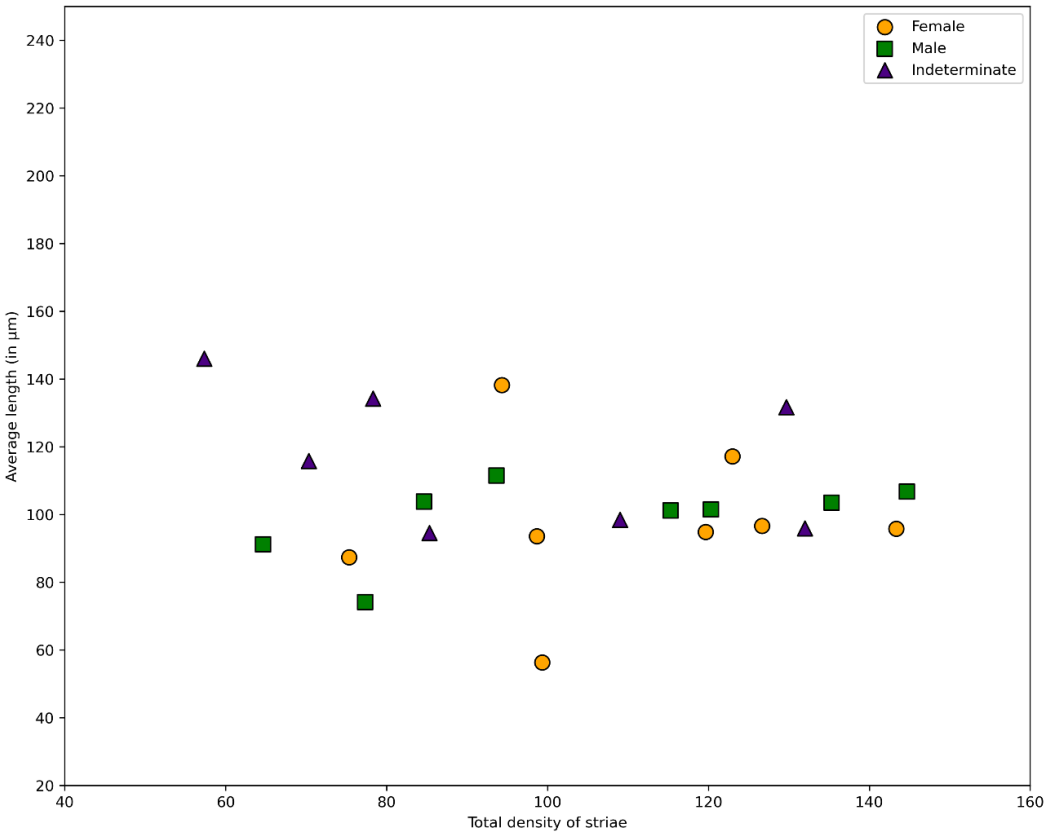


Figure 68. Scatter plot of the total density of striae and the average length (in µm) for female (represented by an orange circle), male (represented by a green circle), and indeterminate individuals (represented by a purple triangle) from Plaça de la Gardunya.

The results of the calculation of the indices of relative frequency of striation, grouped into age and sex categories, can be observed in ***Table 82***. The indices encompass the ratio of density of horizontal and vertical striae (NH/NV), the ratio of density of horizontal striae and total striae density (NH/NT), and the ratio of density of vertical striae and total striae density (NV/NT) (Lalueza et al., 1996; Pérez-Pérez et al., 1994). With respect to the age category, subadult and adult individuals display similar results for the ratio of density of horizontal striae and total striae density, as well as the ratio of density of vertical striae and total striae density. Nevertheless, the ratio of density of horizontal and vertical striae of subadults (2.18) exhibits a slight increase in comparison to adult individuals (1.75), which could be potentially biased due to the low number for subadult individuals. Regarding the sex category, female and male individuals display similar results for the ratio of density of horizontal striae and total striae density, as well as the ratio of density of vertical striae and total striae density. However, the ratio of density of horizontal and vertical striae of female individuals (2.11) exhibits a slight increase in comparison to

male individuals (1.73), suggesting a slightly denser horizontal striation pattern for females and a slightly denser vertical striation pattern for males.

Table 82. Indices of the relative frequency of striation, grouped into age and sex categories for Plaça de la Gardunya's individuals.

		n	NH/NT	NV/NT	NH/NV
Age group	Subadults	3	0.47	0.22	2.18
	Adults	24	0.43	0.24	1.75
Sex	Females	8	0.48	0.23	2.11
	Males	11	0.40	0.23	1.73
All		27	0.43	0.24	1.79

4.2.2.3 Diet classification

The studied populations with a known diet, as published by Lalueza et al. (1996), serve as reference datasets to classify the type of diet from Plaça de la Gardunya. This site exhibits a higher density of short striations compared to the reference diets (***Figure 69*****Figure 50Figure 70**).

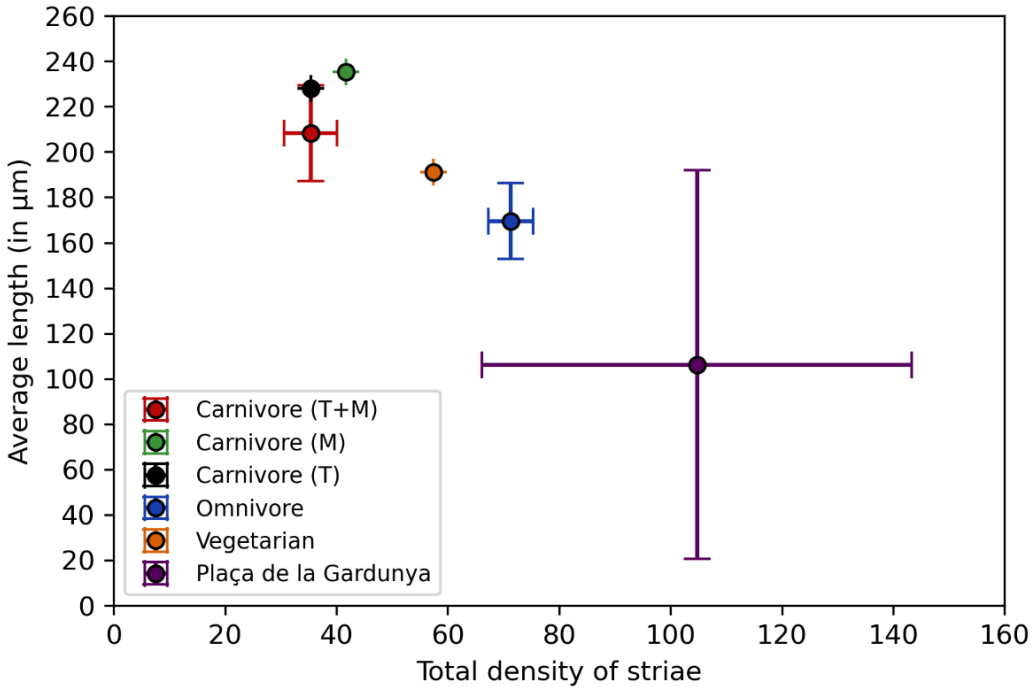


Figure 69. Scatter plot displaying the total density and the average length of striae from populations of known diets and the population of Plaça de la Gardunya.

A Linear Discriminant Analysis (LDA) was performed to classify the microwear patterns of the population of Plaça de la Gardunya, the subadult, the female, and the male individuals into one of five different diet groups: carnivore (differentiating the groups by the origin of their protein consumption, including marine, terrestrial, and both marine and terrestrial), omnivore, and vegetarian. The predictor variables encompassed 15 variables that characterize a microstriation pattern. It was determined that ten of the variables did not meet the requisite statistical assumptions. The canonical discriminant functions that met the requisite statistical assumptions included the density of horizontal (NH), vertical (NV), mesiodistal (NMD), and distomesial striae (NDM), as well as the average length of horizontal striations (XH). The model demonstrated a positive ability to discriminate among the five diet groups and exhibited a 100% accuracy rate in the classification of the original grouped cases, correctly categorizing the population of Plaça de la Gardunya within the omnivorous group (**Figure *70*Figure *59***). The canonical discriminant functions for the subadult, female and male individuals indicate that function 1 explains 90.9% of the variance, and function 2 explains 8.4%, thus summing to 99.3%. All cases have been processed, and none was excluded from the classification, exhibiting a 100% accuracy rate in the classification of the original grouped cases. The observation of the data from the subadult individuals, the analysis has provided a categorization of 33.3% omnivorous, and 55.7% vegetarians (***Figure 71***). When exploring the data of the female individuals, 87.5% were categorized as omnivores, and 12.5% were identified as vegetarians (***Figure 72***). In the case of male individuals, 81.8% fell into the omnivorous category, and 18.2% were identified as vegetarians (***Figure 73***).

Linear Discriminant Analysis has provided insights into the dietary patterns of the population of Plaça de la Gardunya, revealing an omnivorous diet characterized by a notable consumption of abrasive foodstuffs derived from plants (**Table *83***). It is noteworthy that two out of three subadults exhibit a microwear pattern indicative of a vegetarian diet. There are no significant differences between male or female individuals, nor between graves in terms of dietary tendencies, suggesting equal access to food, not subject to age, sex, or social status.

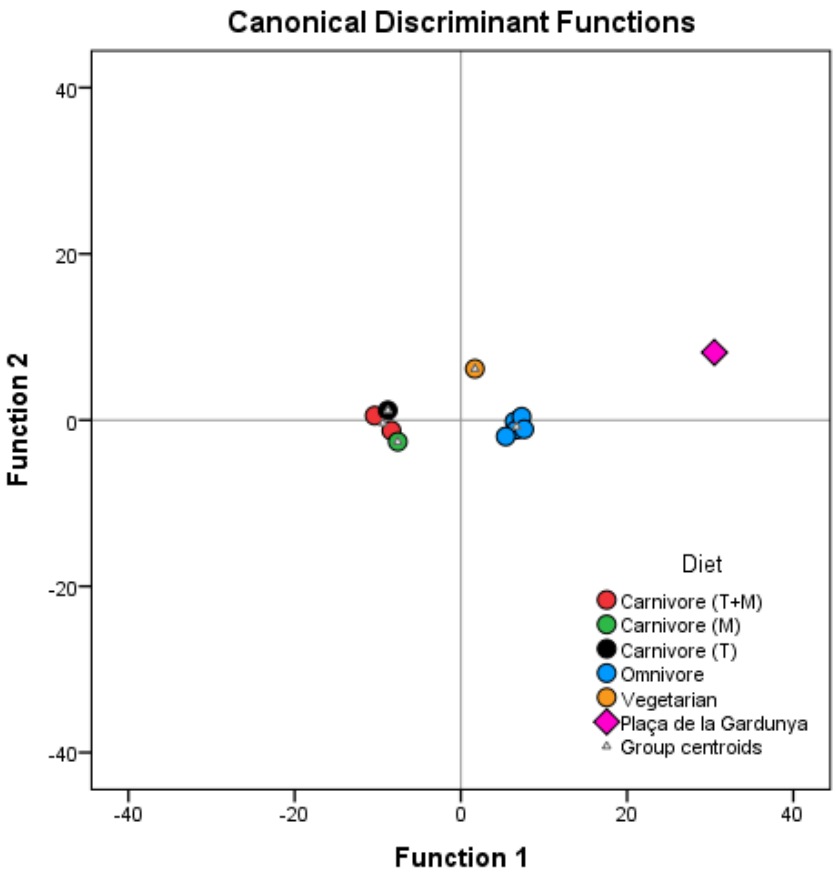


Figure 70. Scatter plot displaying the results of functions 1 and 2 of the Linear Discriminant Analysis to classify Plaça de la Gardunya's individuals into a dietary category.

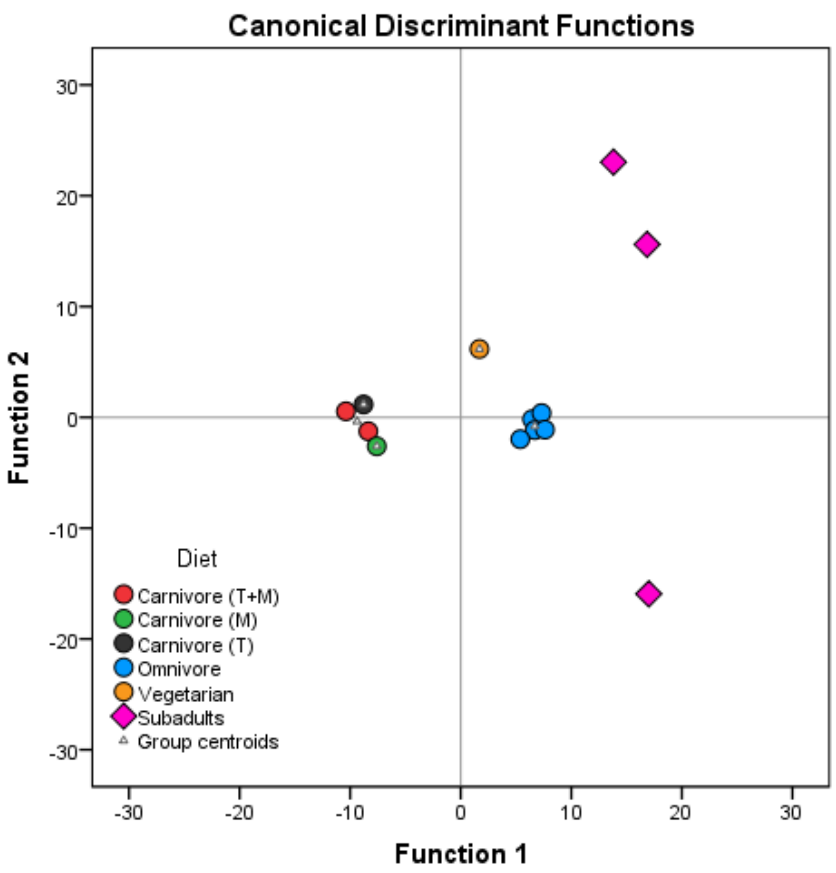


Figure 71. Scatter plot displaying the results of functions 1 and 2 of the Linear Discriminant Analysis to classify the subadult individuals from Plaça de la Gardunya into a dietary category.

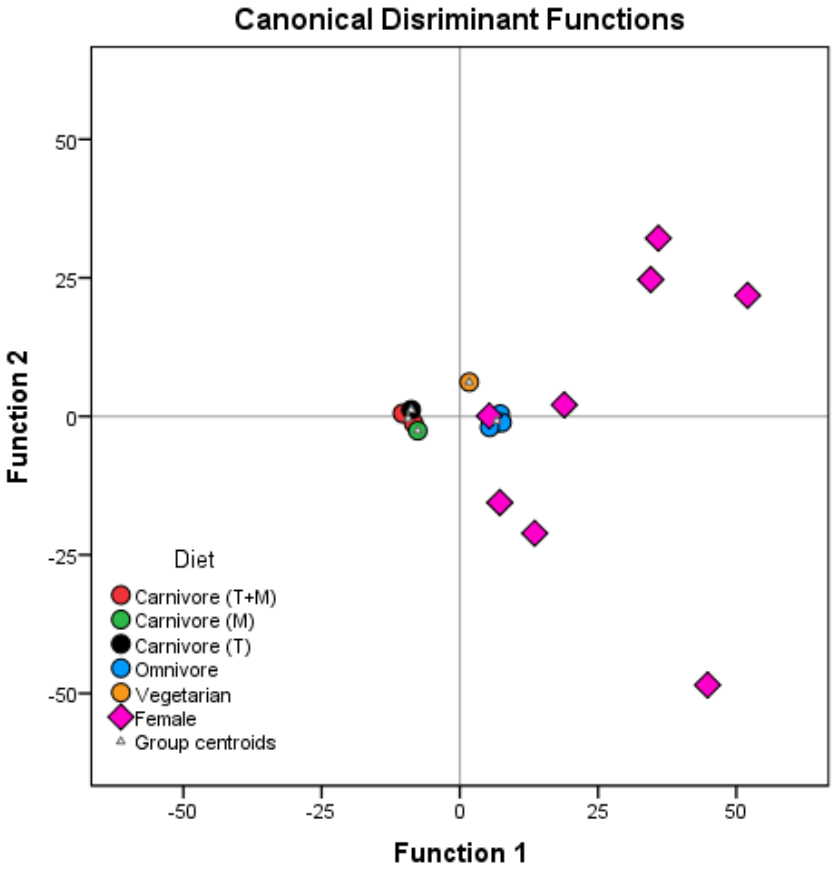


Figure 72. Scatter plot displaying the results of functions 1 and 2 of the Linear Discriminant Analysis to classify Plaça de la Gardunya's female individuals into a dietary category.

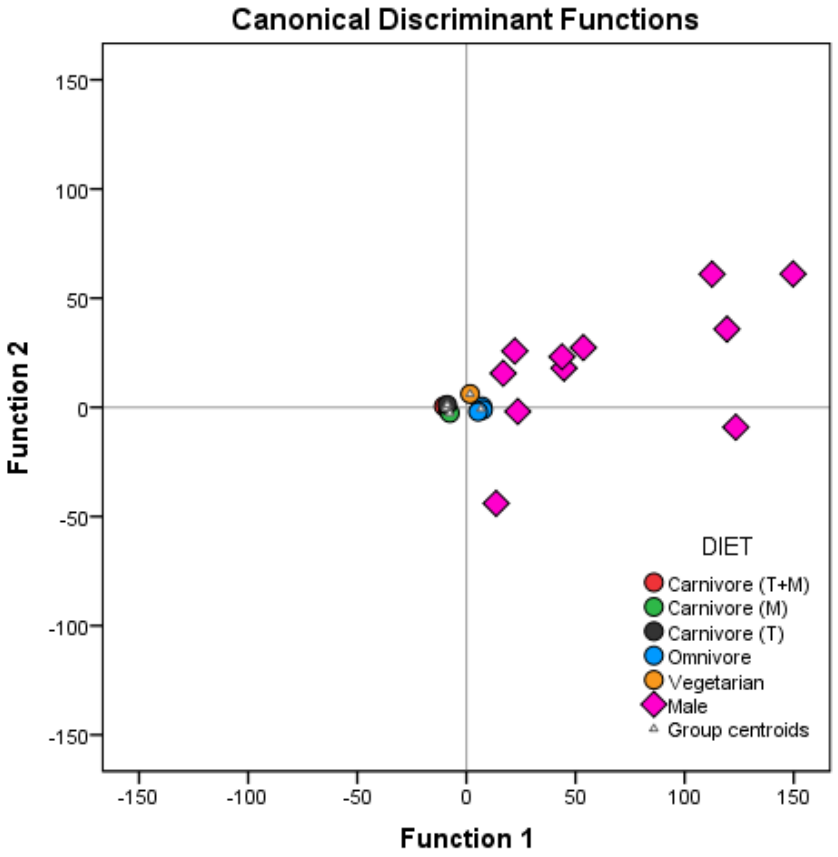


Figure 73. Scatter plot displaying the results of functions 1 and 2 of the Linear Discriminant Analysis to classify Plaça de la Gardunya's male individuals into a dietary category.

Table 83. Diet classification of the individuals of Plaça de la Gardunya after the Linear Discriminant Analysis.

Sector	Grave	Individual	Age	Sex	Classified diet
4	2	4232	Adult	Indeterminate	Omnivore
		4319.3	Adult	Male	Omnivore
	3/4	4473	Subadult	Indeterminate	Omnivore
		4389.17	Subadult	Indeterminate	Vegetarian
		4391	Adult	Female	Omnivore
		4389.11	Adult	Female	Omnivore
		4389.14	Adult	Female	Omnivore
		4389.19	Adult	Female	Omnivore
		4389.20	Adult	Female	Omnivore
		4389.24	Adult	Female	Omnivore
		4389.18	Adult	Female	Vegetarian
		4389.21	Adult	Indeterminate	Omnivore
		4389.12	Adult	Indeterminate	Vegetarian
		4389.13	Adult	Indeterminate	Vegetarian
		4430.8	Adult	Male	Omnivore
		4388	Adult	Male	Omnivore
		4389.16	Adult	Male	Omnivore
		4389.22	Adult	Male	Omnivore
		4389.23	Adult	Male	Omnivore
		4328.6	Adult	Male	Omnivore
		4389.15	Adult	Male	Vegetarian
5	1	50700	Adult	Indeterminate	Vegetarian
		50616.2	Adult	Male	Omnivore
	2	50618.1	Subadult	Male	Vegetarian
		50615.2	Adult	Female	Omnivore
		50619	Adult	Indeterminate	Omnivore
		50620.3	Adult	Male	Omnivore

4.2.2.4 Comparison with other archaeological sites

Buccal microwear analyses have been widely studied to determine the abrasiveness of human diets. These analyses have been performed on populations from different chronologies, not only limited to northeastern Iberia, but in all the Iberian Peninsula. Analysis of these datasets provides a basis for understanding the dietary patterns of different societies.

A total of twenty archaeological sites, ranging from the Neolithic to the Middle Bronze Age, have been selected for comparison and contextualization of the results obtained from the population of Plaça de la Gardunya. To date, the most extensive and comprehensive dataset has been published by Hernando (2024; Hernando et al., 2024), encompassing 88 individuals from eight distinct sites across northeastern Iberia. Her research has encompassed a comprehensive analysis of the buccal microwear values, which collectively serve to define the abrasion patterns exhibited by each individual. This multifaceted approach has not only focused on the publication of frequency ratios, total density of striae, and average length of striations from the entire population, but has also delved into the detailed examination of all 15 buccal microwear values that serve to characterize the distinct abrasion patterns exhibited by each individual. However, given that certain authors exclusively provide frequency ratios, total density of striae, and average length of striations, the present study will encompass this information from the entire population to facilitate comparisons between the sites (**Figure 74**).

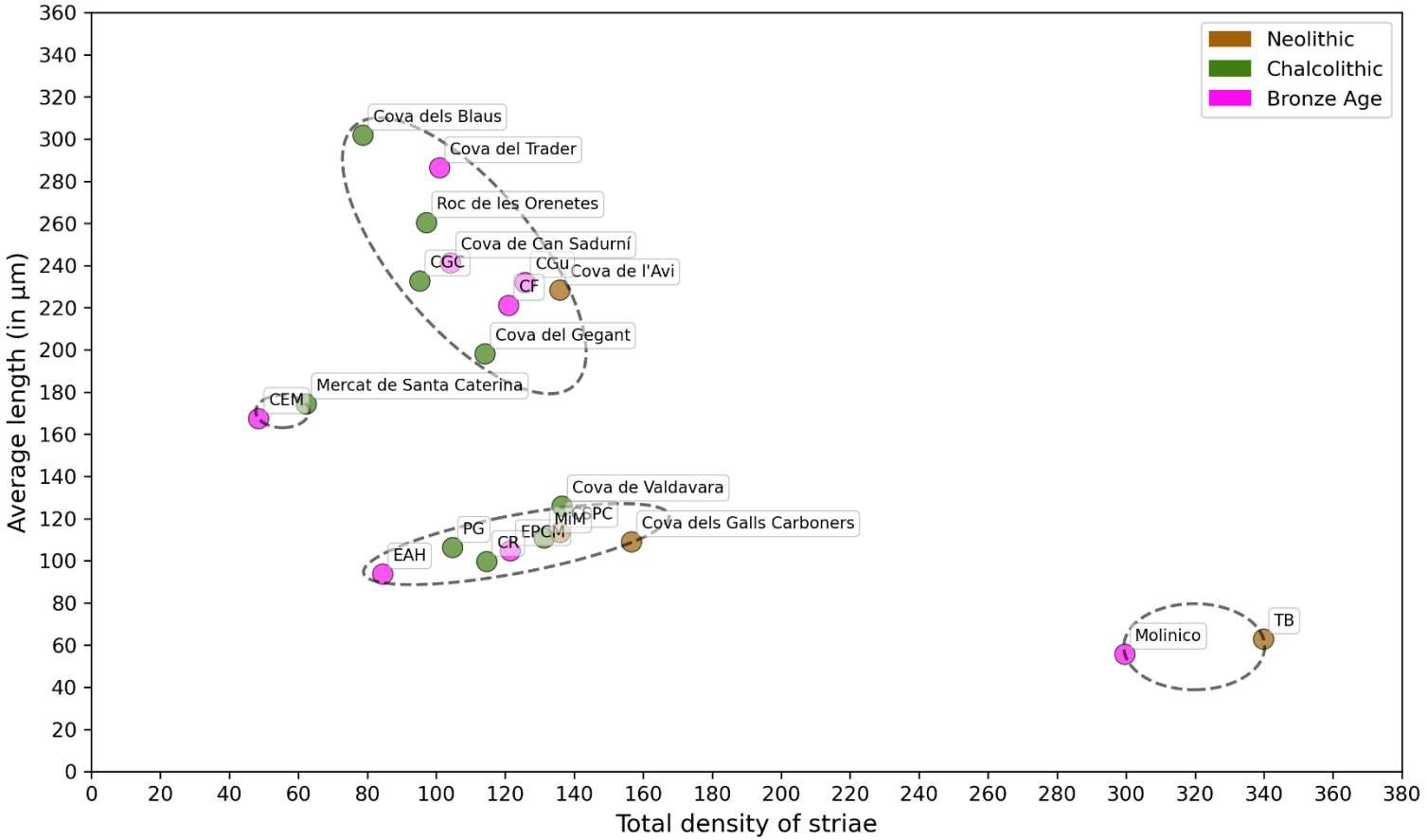


Figure 74. Scatter plot displaying the total density and the average length of striae from Plaça de la Gardunya (abbreviated as PG) and the compared archaeological sites. Some sites have been abbreviated in the graphic to tackle label superposition: Cova dels Galls Carboners (CGC), Cova de la Guineu (CGu), Cova Foradada (CF), Cueva El Mirador (CEM), El Alto de la Huesera (EAH), Cabezo Redondo (CR), El Portalón de la Cueva Mayor (EPCM), Mar i Muntanya (MiM), Caserna de Sant Pau del Camp (CSPC), and Tossal de les Basses (TB).

Upon the graphical representation of the total density and the average length of striae, four discernible clusters are identified. The microwear pattern from the first cluster, which includes the sites of Molinico and Tossal de les Basses, is characterized by a high density of short striations. This diet, characterized by its high levels of abrasiveness, has been interpreted as omnivorous, with a consumption primarily consisting of low-processed foodstuffs that have been contaminated by abrasive particles, such as grit. The pattern from the second cluster, which includes the studied site of Plaça de la Gardunya and the archaeological sites of El Alto de la Huesera, Cabezo Redondo, El Portalón de la Cueva Mayor, Mar i Muntanya, Caserna de Sant Pau del Camp, Cova de Valdavara and Cova dels Galls Carboners, is characterized by a low density and short average length of striations. A number of studies from these sites propose a variety of interpretations, yet they are largely consistent in suggesting an omnivorous diet comprising substantial amounts of animal protein (meat and milk) and plant-based foodstuffs. These plant-based foodstuffs were processed and refined through milling techniques that introduced abrasive inclusions into the consumed food (Galbany et al., 2008; García-González et al., 2019; Hernando et al., 2019; Hernando, Willman, et al., 2020; Romero & Juan, 2007). The microwear pattern from the third cluster, which includes the sites of Cueva El Mirador and Mercat de Santa Caterina, is characterized by a low density of intermediate average length of striations. A soft omnivorous diet, centered on the implementation of refined culinary techniques such as roasting, boiling, milling, fermenting, or steaming, could be a potential dietary strategy (Gluitz et al., 2023; Hernando et al., 2022). The microwear pattern from the fourth and last cluster, which includes the sites of Cova del Gegant, Cova Foradada, Cova de l'Avi, Cova de la Guineu, Cova dels Galls Carboners, Cova de Can Sadurní, Roc de les Orenetes, Cova del Trader, and Cova dels Blaus, is characterized by an intermediate density of long striations. The sites of this group with a higher density of striations, such as Cova de l'Avi, Cova del Gegant, Cova Foradada, and Cova de la Guineu, have been interpreted as exhibiting an omnivorous diet, with the consumption of abrasive particles originating from milling techniques or other processing methods, including grit particles and other environmental contaminants. Furthermore, the high frequency of caries in these populations suggests a diet consisting of sticky foods, such as processed carbohydrates in the form of porridges, which are highly cariogenic (Hernando et al., 2024; Romero et al., 2004). The sites of this group, characterized by longer striations and a low density of striae, including Cova dels Galls Carboners, Cova de Can Sadurní, Roc de les Orenetes, Cova del Trader, and Cova dels Blaus, have been interpreted to be indicative of a soft diet, comprising meat and secondary products. These sites also exhibit evidence of refined cooking techniques, suggesting the application of methods that enabled the removal of abrasive particles from foodstuffs.

4.2.3 Concluding remarks

4.2.3.1 Gird Lashkir and Gir-e Gomel

The buccal microstriation pattern exhibited by both Gird Lashkir and Gir-e Gomel has demonstrated no significant differences in terms of age and sex, suggesting that the entire society has no differential access to food resources. Evidence for slight differences is observed in the relative frequency ratios concerning the density of horizontal, vertical, and total density of striae (NH/NT, NV/NT, and NH/NV). The results obtained from these ratios suggest the presence of slight variations in dietary patterns between subadults and adults, as well as between females and males. Ratios from subadult individuals suggest a slightly more abrasive diet than adult individuals, which represents the consumption of more abrasive foodstuffs than adults. This information, in conjunction with the outcomes of the diet categorization via the linear discriminant analysis, which signifies an affinity for more vegetarian diets among subadult individuals, could be interpreted as follows. Subadult individuals may consume greater quantities of plant-based foodstuffs than adult individuals, or food contaminated by abrasive particles derived from food processing techniques such as milling. This hypothesis is substantiated by the presence of saddle querns and handstones at the sites in question (Gómez-Bach et al., 2019; Molist, Breu, et al., 2019a). The diet would also include animal protein, although in lower quantities. Adult individuals have been predominantly classified as having an omnivorous diet, with certain exceptions being designated as vegetarian or carnivorous based on a consumption of aquatic animal protein. In the case of Gird Lashkir, the relative frequency ratios indicate that female individuals tend to have diets that are more abrasive than those of male individuals. This finding appears to be at odds with the results obtained from the linear discriminant analysis. Two female adults, Graves 4 and 10 from Gird Lashkir, have been classified as having a carnivorous diet based on the consumption of aquatic animals. Both graves are notable for an absence of ornamentation and modest grave goods. This finding challenges the prevailing assumption that the consumption of softer foods with higher amounts of animal protein is predominantly observed among individuals with higher social status or males. The presence of caries in three female individuals (Graves 5, 10, and 15) also suggests the ingestion of carcinogenic elements, such as sticky plant-based foods. In the case of male individuals, the diet classification has proposed omnivore and vegetarian diets.

A comprehensive analysis of the data on buccal microwear pattern and the archaeological record from the sites indicates that the individuals inhabiting Gird Lashkir and Gir-e Gomel had equal access to food and an omnivorous diet. Furthermore, the consumption of different types

of foods did not depend on sex or social status. With respect to age, subadult individuals may have exhibited a higher consumption of plant-based and/or processed foodstuffs in comparison to adults. The consumption of aquatic animals in Graves 4 and 10 from Gird Lashkir may be indicative of the consumption of this type of meat, or it may be a bias towards the classification of diets. This is because all three types of carnivore diets (with a mixed consumption of terrestrial and aquatic animals, or with the exclusive consumption of aquatic or terrestrial animals) have similar patterns, as evidenced by the linear discriminant analyses. The results of the study provide further evidence of the consumption of the botanical and animal species found in the sites (wheat, barley, lentil, ovicaprid, pig, cattle, among others), as well as the potential consumption of aquatic animals from the nearby rivers, channels, and streams, including the Tigris, the Great Zab, and Little Zab.

Consequently, by examining the dental microwear analysis of populations from northern Mesopotamia, it can be concluded that social differences evident during the Ninevite 5 period were not attributable to differing access to food resources.

4.2.3.2 Plaça de la Gardunya

The buccal microstriation pattern exhibited by the individuals from Plaça de la Gardunya does not exhibit any significant differences in terms of age or sex. This result suggests that access to food resources is equal for all members of the population. Subtle differences are observed in the relative frequency ratios concerning the density of horizontal, vertical, and total density of striae (NH/NT, NV/NT, and NH/NV). As has been previously observed for the population of northern Mesopotamia, subadult individuals exhibit a slight increase in their abrasive pattern in comparison with adult individuals. These results could suggest the consumption of more abrasive foodstuffs than adults, but the outcomes could be potentially biased due to the low number of subadult individuals in comparison with adults. Linear discriminant analysis has been employed to differentiate dental microwear patterns according to a known dietary pattern. This analysis has revealed that subadult individuals exhibit greater dietary similarities to omnivorous and vegetarian diets. As observed in northern Mesopotamia, subadult individuals may consume greater quantities of plant-based foodstuffs or have their food processed with milling techniques that add grit. Adult individuals have been classified as either omnivores or vegetarians, indicating a balanced consumption of animal protein and plant-based foodstuffs. No differences arise for the groups buried in the same graves. A minimal distinction is observed in the relative frequency

ratios between female and male individuals, with females exhibiting slightly more abrasive microwear patterns than males.

A comparison of the buccal microwear pattern with other archaeological sites from the Iberian Peninsula reveals that Plaça de la Gardunya clusters with sites whose diets have been interpreted as omnivorous, with consumption of animal protein (primary and secondary products), as well as plant-based foodstuffs that could be processed and refined via milling techniques that introduced abrasive inclusions into the consumed food (Galbany et al., 2008; García-González et al., 2019; Hernando et al., 2019; Hernando, Willman, et al., 2020; Romero & Juan, 2007). The presence of saddle querns and grinding stones has been documented in the archaeological records of Early Bronze Age sites (Aguelo & Huertas, 2006; Bofill, 2016; Bordas, 2016; Gómez & Molist, 2016; Granados et al., 1993; Nadal & Castillo, 2010; Piera et al., 2005; Suau & Matas, 2010; Velasco et al., 2017), thus rendering it a very probable hypothesis. The provenance of the animal protein, whether it be aquatic or terrestrial, remains indistinguishable. At least, as evidenced by zooarchaeological remains, it is apparent that numerous species of terrestrial animals, including those from husbandry and hunting, were consumed (e.g., ovicaprids, bovids, pigs, equids, foxes, deer, rabbits, among others).

In summary, no evidence of differential access to food based on age or sex has been observed, suggesting equal access to food resources for the entire population.

4.3 ZooMS

Samples analyzed by ZooMS, composed by 11 ovicaprids belonging to the sites of Gird Lashkir, Gir-e Gomel and Plaça de la Gardunya, although its collagen was poorly preserved, have provided positive results, with a detailed taxonomy identification to the classification level of genus and species. The peptide mass fingerprint was obtained for 9 out of 11 samples (**Table 84**). Six samples from Gird Lashkir have been identified as the species *Ovis aries*, two samples were identified as the indiscernible genus *Ovis* or *Capra* (ovicaprid), and one sample provided no fingerprint at all. One hypothesis may be a high diagenetic alteration of the collagen or an exposure to fire in ancient times. The sample of Gir-e Gomel has been identified as the species *Capra hircus*, and the last sample corresponding to Plaça de la Gardunya, has been identified as the species *Ovis aries*.

Table 84. Results for ZooMS analysis.

Site	Sample ID	ZooMS ID
Gird Lashkir	TL52	*Ovis aries*
	TL53	*Ovis aries*
	TL54	Ovicaprid
	TL55	*Ovis aries*
	TL56	*Ovis aries*
	TL57	*Ovis aries*
	TL58	Ovicaprid
	TL59	No ID – probably burnt
	TL60	*Ovis aries*
Gir-e Gomel	GG25	*Capra hircus*
Plaça de la Gardunya	PG93	*Ovis aries*

4.4 STABLE ISOTOPES

4.4.1 Diet

4.4.1.1 Gird Lashkir and Gir-e Gomel

4.4.1.1.1 Intrapopulation variability

The results of the carbon and nitrogen stable isotope analysis of bone collagen samples, along with its quality control indicators, are presented in **Table 85**. The site of Gird Lashkir has exhibited low success rates in bone collagen extraction, suggesting poor preservation of the samples due to taphonomic and diagenetic alterations. Only one sample out of twenty-four provided reliable $\delta^{13}C$ and $\delta^{15}N$ values, corresponding to a success rate of 4.16%. The sample containing preserved collagen is from Grave 5, which has a collagen yield of 2.3%. The preservation percentages of carbon and nitrogen are 34.29 and 10.57, respectively, and the C:N ratio is 3.78. The atomic ratio exceeds the maximum range proposed by DeNiro (1985). However, when considering the recommended C:N ratio limits for ancient collagen established by Guiry & Szpak (2021), this value falls within the liberal range, with a 1‰ shift tolerance in the $\delta^{13}C$ value. Consequently, given the reliability of the isotopic results, the conclusions may be considered valid. The efficacy of the extraction process is particularly deficient for animal samples, as evidenced by the failure to extract collagen in all instances.

In comparison, the site of Gir-e Gomel has a much higher success rate. All human samples have proven to be successful in providing reliable $\delta^{13}C$ and $\delta^{15}N$ values. With the exception of Grave 42, all samples exhibited a collagen yield percentage greater than 1.52%. The preservation percentages of carbon and nitrogen are ≥ 42.39% and ≥ 14.07%, respectively, and the C:N atomic ratio ranges between 3.13 and 3.56. The implementation of these quality control indicators ensures the integrity and reliability of the results. In accordance with the conclusions of Guiry & Szpak (2021), the C:N atomic ratio is indicative of a shift in $\delta^{13}C$ values of less than 0.5‰. Animal samples from Gir-e Gomel have demonstrated a similarly favorable rate of success, with five out of six samples providing reliable results, yielding an 83.33% success rate. However, a single specimen of *Capra hircus* exhibited a collagen yield of 0.29%, while the preservation percentages of carbon and nitrogen were ≥ 42.37% and ≥ 15.33%, respectively. The C:N atomic ratio ranges between 3.11 and 3.22, with the lower limit falling below the alternative range proposed by Guiry & Szpak (2021). However, this range aligns closely with the traditional limit proposed by DeNiro (1985). These quality control indicators provide reliable $\delta^{13}C$ and $\delta^{15}N$ values, and a shift in the $\delta^{13}C$ isotopic signature greater than 1.0‰ is to be expected.

Table 85. Stable isotope values of carbon and nitrogen from human and animal bone collagen samples.

Site	Individual	Sample ID	wt%	$\delta^{13}C$ (in ‰ VPDB)	%C	$\delta^{15}N$ (in ‰ VPDB)	%N	C:N
Gird Lashkir	Grave 5	TL44	2.3	-20.48	34.29	5.92	10.57	3.78
Gir-e Gomel	Grave 24	GG15	4.08	-20.28	43.57	6.19	15.75	3.23
	Grave 42	GG16	0.80	-20.26	42.39	6.24	14.07	3.51
	Grave 47	GG18	1.52	-19.88	43.13	6.06	14.15	3.55
	Grave 48	GG17	5.34	-19.29	42.94	7.80	14.08	3.56
	Grave 49	GG20	4.54	-20.08	43.14	5.63	14.79	3.41
	Grave 51	GG13	4.87	-19.87	43.87	7.21	16.36	3.13
	Capra hircus	GG5	0.29	-20.05	42.37	5.00	15.33	3.22
	Capra hircus	GG10	13.08	-20.09	44.64	5.19	16.65	3.13
	Ovis aries	GG6	1.01	-20.93	43.73	5.24	16.03	3.18
	Ovis aries	GG8	1.33	-19.48	42.61	3.47	15.52	3.20
	Ovis aries	GG9	7.55	-19.04	44.54	3.86	16.71	3.11

The human and animal $\delta^{13}C$ values of Gird Lashkir and Gir-e Gomel, ranging from -20.93‰ to -19.04‰, are indicative of a diet comprised primarily of C_3 plants. The mean values of $\delta^{13}C$ and $\delta^{15}N$ from both Gird Lashkir and Gir-e Gomel human individuals together exhibit mean values of -20.02‰ ± 0.36 and 6.44‰ ± 0.72, respectively. The mean values of $\delta^{13}C$ and $\delta^{15}N$ of herbivores from Gir-e Gomel display mean values of -19.92‰ ± 0.71 and 4.55‰ ± 0.83, respectively. The $\delta^{15}N$ range of herbivores is established at 3.47‰ to 5.24‰, while the range of humans is determined to be from 5.63‰ to 7.80‰. A comparison of human individuals with herbivores reveals a depletion of 0.1‰ in $\delta^{13}C$ and an enrichment of 1.89‰ in $\delta^{15}N$, suggesting an increased trophic level.

When comparing the data in terms of age (**Figure 75**) or sex (**Figure 76**), two male adult individuals are found to be more enriched in $\delta^{15}N$ than subadult, female, and indeterminate individuals. This evidence could be indicative of subadult, female, and indeterminate adult individuals having a diet with lower animal protein consumption than some male individuals, specifically from local herbivores. However, the limited number of samples per age class and per sex may introduce bias, potentially affecting the interpretation of the data.

The results of the carbon stable isotope analysis of tooth enamel hydroxyapatite are presented in **Table 86**. The reliability of the $\delta^{13}C$ results obtained from both Gird Lashkir and Gir-e Gomel is likely attributable to the well-preserved inorganic fraction of tooth enamel. This approach facilitates the enhancement of the dietary analysis from Gird Lashkir, expanding it from 1 to 11 human individuals, and the incorporation of a new proxy for 4 human individuals of Gir-e Gomel whose bone collagen exhibited a well-preserved state. The range of $\delta^{13}C$ values from human samples at both sites extends from -12.57‰ to -10.82‰, indicating a shift of 7.95‰ ± 0.62 with respect to bone collagen. The mean value of $\delta^{13}C$ from the human samples collected from Gird Lashkir is -11.32‰ ± 0.37, from Gir-e Gomel, -11.93‰ ± 0.47, and from both sites combined, -11.50‰ ± 0.48. These results are indicative of a diet consisting of C_3 plants, which is consistent with the outcomes observed in bone collagen samples and the archaeobotanical analysis.

Table 86. Stable isotope values of carbon from human tooth enamel hydroxyapatite samples.

Site	Individual	Sample ID	$\delta^{13}C$ (in ‰ VPDB)	Std. Dev.
Gird Lashkir	Grave 4	TL72	-11.29	0.02
	Grave 6.1	TL73	-11.02	0.03
	Grave 6.2	TL74	-11.35	0.04
	Grave 7	TL75	-10.86	0.02
	Grave 10	TL76	-11.23	0.03
	Grave 12.1	TL77	-11.84	0.03
	Grave 13	TL71	-11.43	0.02
	Grave 14	TL79	-10.82	0.04
	Grave 15	TL78	-11.43	0.04
	Grave 16	TL90	-11.94	0.05
Gir-e Gomel	Grave 24	GG34	-11.80	0.02
	Grave 47	GG33	-12.57	0.02
	Grave 48	GG32	-11.92	0.02
	Grave 49	GG31	-11.43	0.03

To assess the variability in the $\delta^{13}C$ results, a Shapiro-Wilk normality test was conducted on tooth enamel hydroxyapatite. This analysis revealed that there were no statistically significant differences among the individuals ($p = 0.491$). This observed outcome suggests that the data is normally distributed. An analysis of variance (ANOVA) was conducted, complemented by Levene, Bonferroni, and Tukey's HSD post-hoc tests. These analyses revealed that there were no statistically significant differences between female, male, and indeterminate individuals ($p > 0.05$). When comparing the data in terms of age (**Figure 77**) or sex (**Figure 78**), no differences are observed. The results indicate that intrapopulation variability is more effectively interpreted from bone collagen, which provides $\delta^{13}C$ and $\delta^{15}N$ isotopic signatures, than from $\delta^{13}C$ values derived from tooth enamel hydroxyapatite.

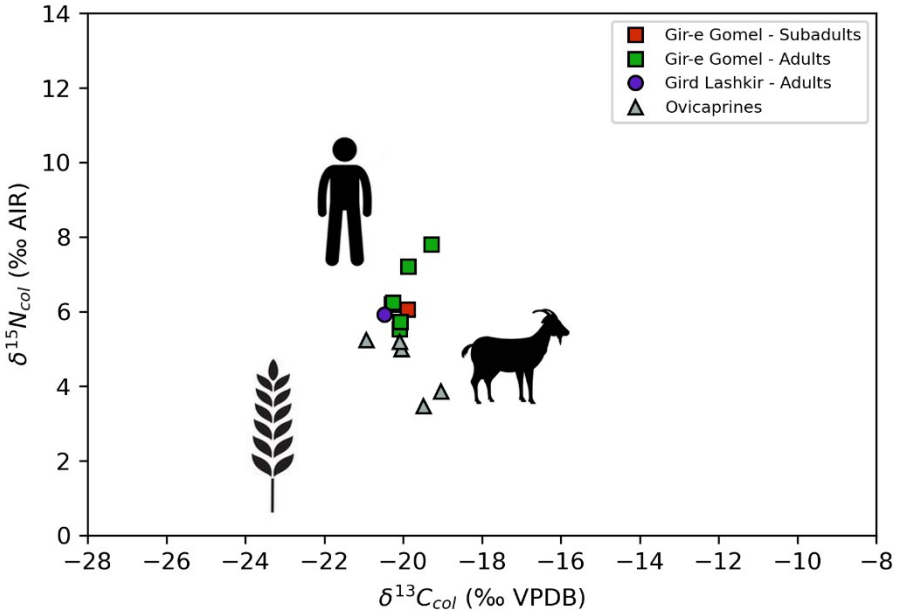


Figure 75. Carbon and nitrogen stable isotope values of human and animal bone collagen samples from Gird Lashkir and Gir-e Gomel, classified by age range.

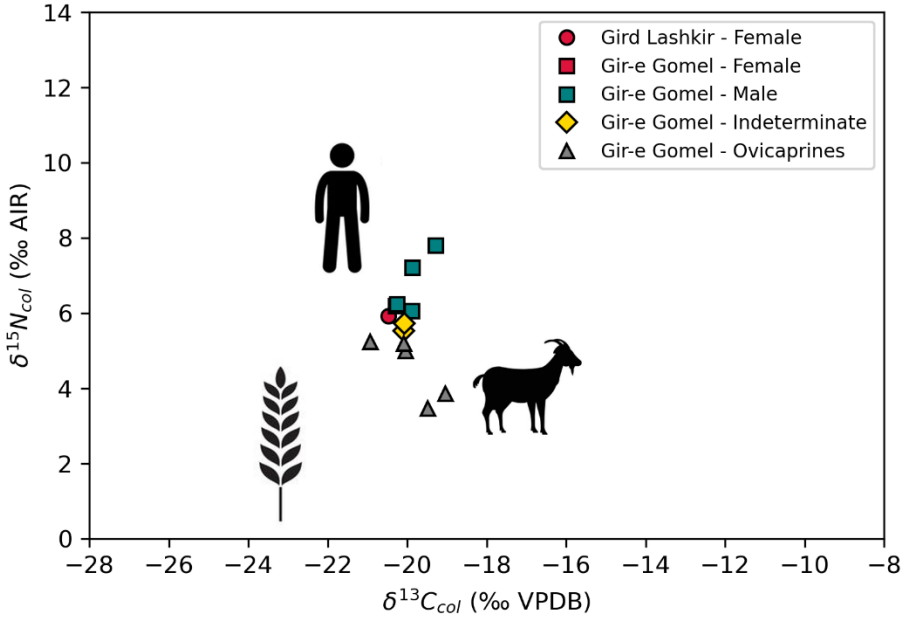


Figure 76. Carbon and nitrogen stable isotope values of human and animal bone collagen samples from Gird Lashkir and Gir-e Gomel, classified by sex.

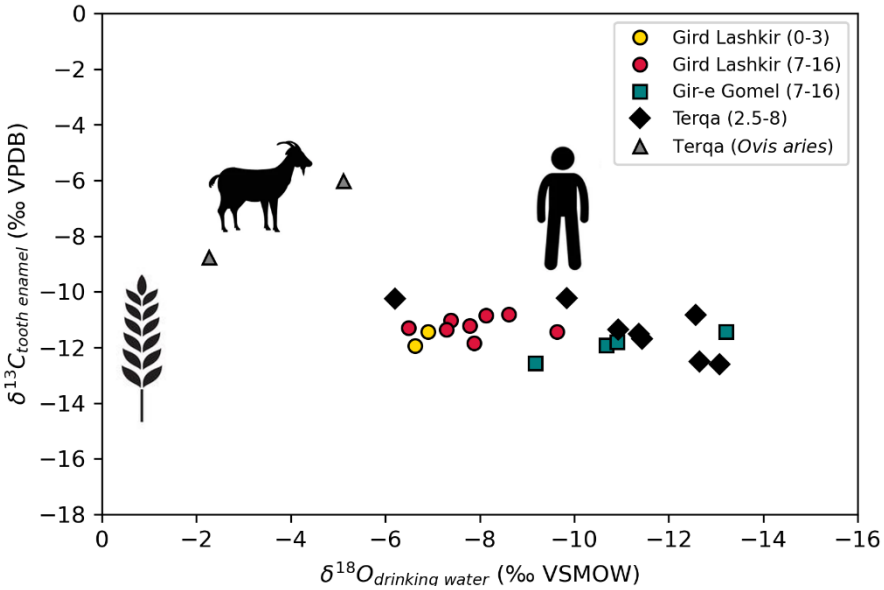


Figure 77. Carbon and oxygen stable isotope values of human and animal tooth enamel hydroxyapatite samples, classified by tissue age.

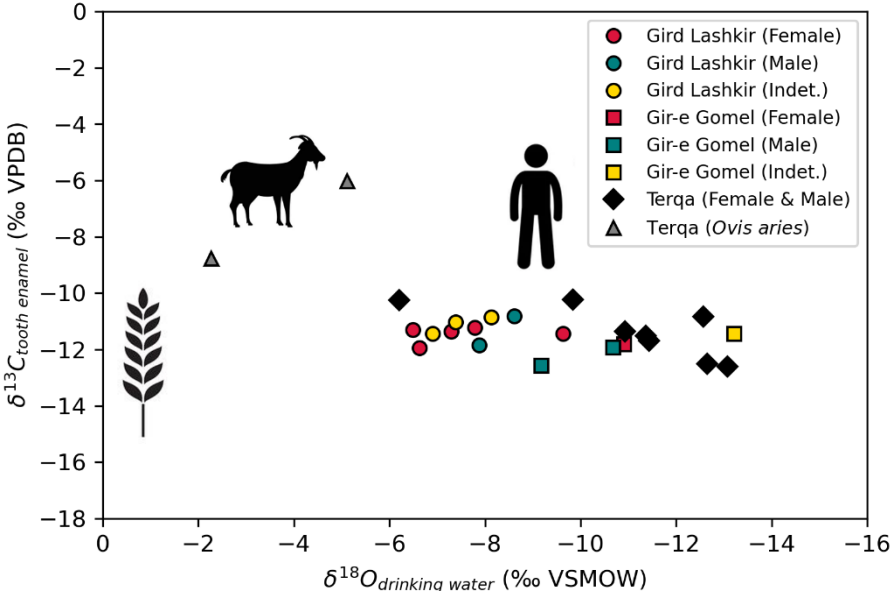


Figure 78. Carbon and oxygen stable isotope values of human and animal tooth enamel hydroxyapatite samples, classified by sex.

4.4.1.1.2 Comparison with other archaeological sites

Stable isotope analysis is not widely performed in the region of northern Mesopotamia or its surrounding territories, due to the poor preservation of organic materials. Nevertheless, some studies have been performed on charred plant remains, on herbivore animals and on human individuals belonging to the first half of the 3rd millennium in the Ninevite 5 occupied region. These studies will allow for contextualization, comparison, and interpretation of our dataset (**Figure 79**).

$\delta^{13}C$ and $\delta^{15}N$ isotopic signatures from human individuals belonging to the site of Tell Barri (northeastern Syria) have been interpreted as indicative of a diet exclusively based on the consumption of C_3 plants. Notably, one female individual demonstrated the most depleted $\delta^{13}C$ value within the complete dataset. A comparison was made between males and females, and the results indicated that males consumed a diet with a larger proportion of animal protein, likely derived from herbivorous livestock that consumed a significant amount of C_4 grasses (Sołtysiak & Schutkowski, 2015) At Tell Leilan, the stable isotope signatures of both herbivore and omnivore livestock coincided with a pure C_3 diet. This finding was interpreted as indicating that a significant portion of the diet for the herds consisted of C_3 crops, which were also consumed by the population (Styring et al., 2017). A similar scenario is observed in the individuals from Gird Lashkir and Gir-e Gomel, whose $\delta^{13}C$ isotopic values are indicative of a C_3 plant-based diet, and whose $\delta^{15}N$ isotopic signatures are associated with low consumption of animal protein derived from herds of herbivorous animals (Ellegård et al., 2019). Herbivorous animals are more likely to have been fed the same crops as human individuals. In a similar sense, male individuals exhibited slightly higher consumption of animal protein compared to adult females and subadult individuals.

The depleted $\delta^{15}N$ values exhibited by the C_3 plants provide insight into the manuring practices employed, suggesting that the crops were low-manured. A direct relationship between site size and manuring practices has been observed in the Early Bronze Age in northern Mesopotamia, in which the smaller the site, the more manured is the cultivated land (Styring et al., 2017). However, Gird Lashkir and Gir-e Gomel, which are small in size, do not align with this pattern.

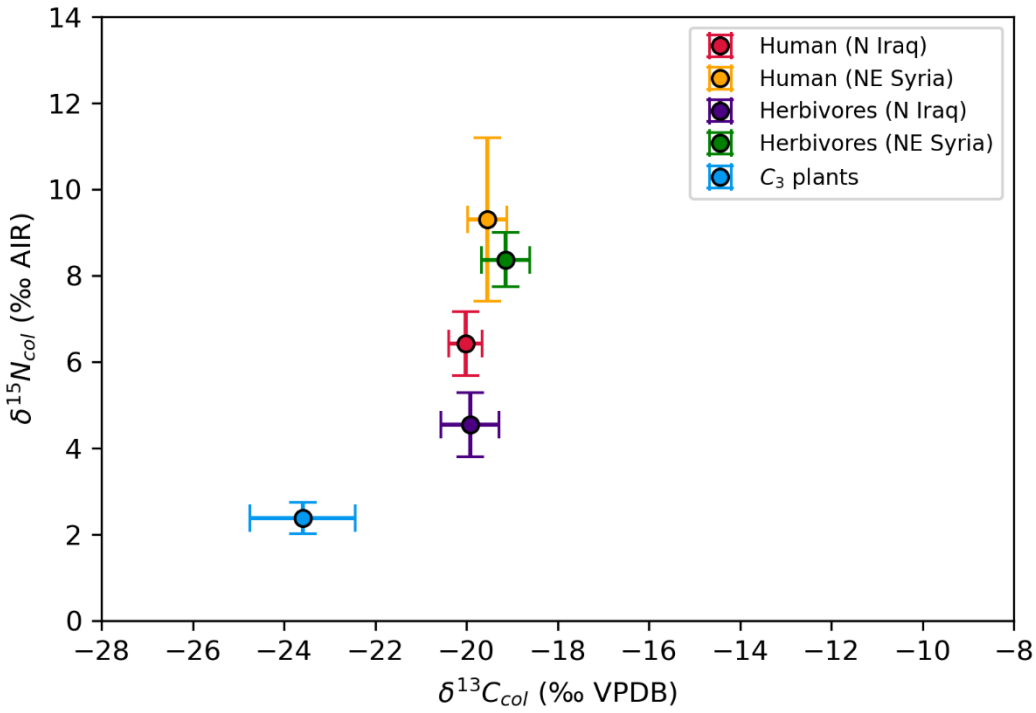


Figure 79. Mean and standard error of carbon and nitrogen stable isotopes from human and herbivores from Gird Lashkir and Gir-e Gomel sites. Data from human and herbivore animals from contemporaneous sites in northeastern Syria have been included (Sołtysiak, 2011; Styring et al., 2017). Data from C_3 plants from northern Mesopotamia has also been incorporated (Riehl et al., 2008; Sołtysiak, 2011; Styring et al., 2017).

4.4.1.2 Plaça de la Gardunya

4.4.1.2.1 Intrapopulation variability

The results of the carbon and nitrogen stable isotope analysis of bone collagen samples, along with its quality control indicators, are presented in ***Table 87***. In a total human sample size of sixty, only thirty-nine samples exhibited well-preserved collagen, yielding a 65% success rate in collagen extraction. It is noteworthy that both animal samples exhibited a 100% success rate in bone collagen extraction. The collagen yield for all the samples from Plaça de la Gardunya is ≥ 2.9, the preservation percentage of carbon is ≥ 23.37, the preservation percentage of nitrogen is ≥ 6.51, and the C:N atomic ratio ranges from 3.35 to 4.36. The cases in which the C:N exceeds the liberal range proposed by Guiry & Szpak (2021), which is 3.9 for mammals, birds, and warm-water fish with an expected $\delta^{13}C$ value of -20.00‰, have resulted in the removal of five individuals from the dataset: 4430.4, 50574.2, 4319 (b), 4328.4, and 4388. This results in a total of 36

samples that have provided reliable results. From these samples, a maximum shift tolerance of 1‰ shift tolerance in the $\delta^{13}C$ signature can be expected.

Table 87. Stable isotope values of carbon and nitrogen from human and animal bone collagen samples.

Individual	Sample ID	wt%	$\delta^{13}C$ (in ‰ VPDB)	%C	$\delta^{15}N$ (in ‰ VPDB)	%N	C:N
4174	PG1	8.7	-20.38	38.82	8.18	12.92	3.50
4232	PG2	9.2	-19.58	39.81	10.06	13.08	3.55
4312	PG3	7.4	-19.86	37.14	9.92	11.71	3.70
4314	PG5	12.1	-20.26	41.15	10.24	12.38	3.88
4315	PG6	7.6	-19.97	39.58	10.29	12.58	3.67
4317	PG7	15	-19.54	45.20	10.29	15.55	3.39
4318	PG8	18.8	-19.84	39.04	9.89	12.08	3.77
4319.1	PG9	10.6	-19.61	39.66	9.35	13.00	3.56
4389.4	PG13	10.4	-20.38	47.60	9.26	15.48	3.59
4389.10	PG19	6.5	-19.31	37.84	10.57	12.36	3.57
8283	PG21	12.1	-19.01	33.03	11.00	11.11	3.47
50620.3	PG22	5.8	-19.70	39.69	10.80	13.41	3.45
4328.1	PG24	11.6	-19.67	41.61	10.70	13.59	3.57
4328.2	PG25	8.1	-19.79	45.54	10.78	14.91	3.56
4463	PG26	10	-19.35	40.16	9.71	13.01	3.60
4450	PG27	7.3	-19.64	41.75	10.28	14.21	3.43
4430.2	PG29	7.2	-19.50	42.08	9.99	13.50	3.64
4430.4	PG31	2.9	-20.01	25.20	10.79	7.47	3.93
4430.5	PG32	13.4	-19.18	44.86	9.67	15.21	3.44
50618.1	PG34	9.8	-19.45	42.65	12.10	14.48	3.43
4319 ("c").1	PG35	10.7	-19.93	43.05	10.08	13.62	3.68
4319 ("c").2	PG36	8.2	-19.88	41.96	9.94	14.02	3.49
4390	PG37	6.3	-19.88	39.43	10.72	12.26	3.75
8141	PG39	16.1	-18.97	42.87	9.40	14.30	3.50
50619	PG40	15.2	-19.28	37.78	11.19	12.39	3.56
50574.1	PG41	4.5	-20.26	36.16	8.89	11.34	3.72
50574.2	PG42	7	-20.55	41.10	9.94	12.02	3.99
50574.3	PG43	6.3	-20.27	39.44	10.41	12.19	3.77

50574.7	PG47	13.1	-20.35	33.26	10.34	10.24	3.79
3402	PG48	7	-18.70	40.20	8.86	12.92	3.63
4319 (b)	PG50	6.3	-20.49	24.54	9.57	6.56	4.36
4379.2	PG54	8.8	-19.38	43.73	10.84	14.60	3.49
4392	PG55	8.6	-19.85	41.06	11.49	13.87	3.45
4328.3	PG86	9.4	-19.55	42.05	9.97	13.92	3.52
4328.4	PG87	3.1	-20.54	35.07	9.25	9.78	4.18
4328.5	PG88	10.2	-19.63	44.41	9.36	14.78	3.50
4376	PG89	4.9	-20.08	38.27	9.00	12.58	3.55
4388	PG90	10	-20.15	23.37	10.33	6.51	4.19
50615.2	PG91	10	-19.58	39.64	10.73	13.16	3.51
Bos taurus	PG92	9.6	-21.28	43.47	5.95	14.35	3.53
Ovis aries	PG93	17.5	-21.02	45.32	8.19	15.78	3.35

The mean $\delta^{13}C$ isotopic signature of human samples is -19.69‰ ± 0.42, with a range from -20.38 to -18.70‰. The mean of the herbivores is -21.15‰ ± 0.18, with a range from -21.28 to -21.02‰. The $\delta^{15}N$ isotopic signature of the human sample exhibited a mean value of 10.13‰ ± 0.81, with a range extending from 8.18 to 12.10‰. In contrast, the mean value of the herbivorous samples was recorded as 7.07‰ ± 1.58, with a range from 5.95 to 8.19‰. A comparison of human individuals with herbivores reveals an enrichment of 1.45‰ in $\delta^{13}C$ and an enrichment of 3.06‰ in $\delta^{15}N$, suggesting an increased trophic level in relation to herbivores. The isotopic signatures from the total population demonstrate a correlation with the consumption of C_3 plants and animal protein, derived from meat and dairy products.

To assess the variability in the $\delta^{13}C$ and $\delta^{15}N$ results, a Shapiro-Wilk normality test was conducted. This analysis yielded no statistically significant differences among the individuals (p = 0.556 and p = 0.978, respectively). The low number of female, male, and subadult individuals in the dataset precludes the possibility of conducting further analyses to ascertain statistical differences among age and sex groups. The low number of individuals per age and sex classes may also introduce bias, potentially affecting the interpretation of the data.

When the data is categorized in terms of age (***Figure 80***) or sex (***Figure 81***), adults and subadults are shown to be clustered together. This find suggests a generalized equal consumption of the same foodstuff in all age ranges. However, one male adult individual exhibits the most enriched

$\delta^{15}N$ isotopic signature among the studied population, suggesting a higher consumption of animal protein compared to the rest of the population. Three adult individuals, 4174, 3402, and 50574.1, exhibit isotopic signatures indicative of a higher consumption of plant-based foodstuffs and a lower intake of animal protein compared to the overall population.

The results of the carbon stable isotope analysis of tooth enamel hydroxyapatite are presented in ***Table 88***. The analysis of carbon stable isotopes from carbonates has allowed the enhancement of the dietary analysis from the individuals of Plaça de la Gardunya, providing additional information provided by the previous bone collagen results to the individuals 4174, 4388, 4450, 50615.2, 50618.1, and 50620.3. This analysis has enabled the extension of the study to encompass an additional 26 individuals, in addition to the 34 individuals for whom reliable results for bone collagen were previously obtained. The range of $\delta^{13}C$ values from human samples extends from -14.28‰ to -9.90‰, indicating a shift of 7.25‰ ± 0.32 with respect to bone collagen. The mean value of $\delta^{13}C$ for the entire population is -12.53‰ ± 0.91, -12.25‰ ± 0.42 for subadults, -12.56‰ ± 1.00 for female adults, -12.62‰ ± 0.91 for male adults, and -12.49‰ ± 1.04 for indeterminate adults. These results are indicative of a diet consisting of pure C_3 plants, which is consistent with the outcomes observed in bone collagen samples and the archaeobotanical analysis.

To assess the variability in the $\delta^{13}C$ results, a Shapiro-Wilk normality test was conducted on tooth enamel hydroxyapatite. This analysis yielded no statistically significant differences among the individuals ($p > 0.05$). This observed outcome suggests that the data is normally distributed. An analysis of variance (ANOVA) was conducted, complemented by the Levene post-hoc test. These analyses revealed that there were no statistically significant differences between age ranges or sex categories ($p > 0.05$). When the data is displayed in terms of age (***Figure 82***) or sex (***Figure 83***), all individuals cluster together in $\delta^{13}C$ isotopic values that are associated with the consumption of C_3 plant-based foodstuffs. The sole exception is observed in one adult with indeterminate sex, which is distinguished by its depleted $\delta^{13}C$ isotopic signature of -14.28‰, corresponding to the individual 50620.3. It is possible that the individual was introduced to fish from freshwater resources during their early childhood.

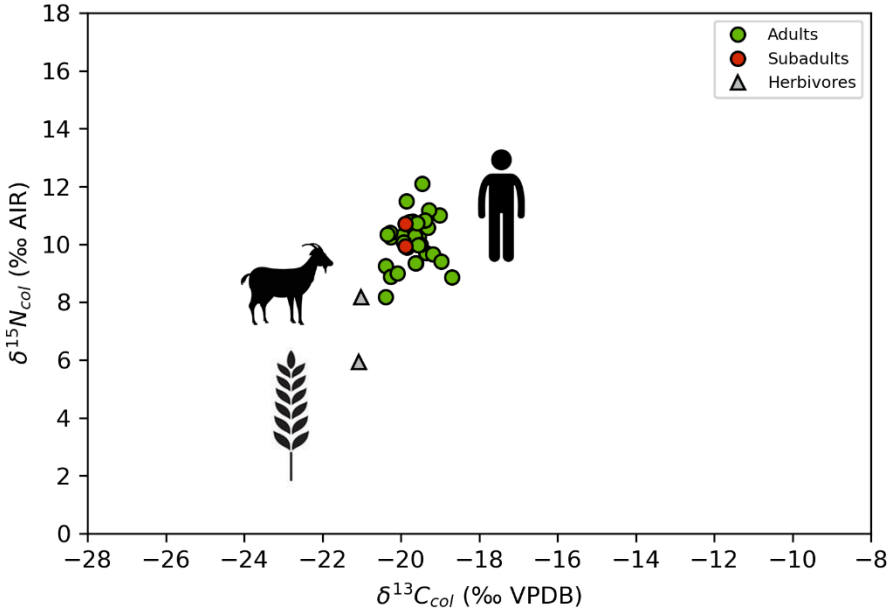


Figure 80. Carbon and nitrogen stable isotope values of human and animal bone collagen samples from Plaça de la Gardunya, classified by age range.

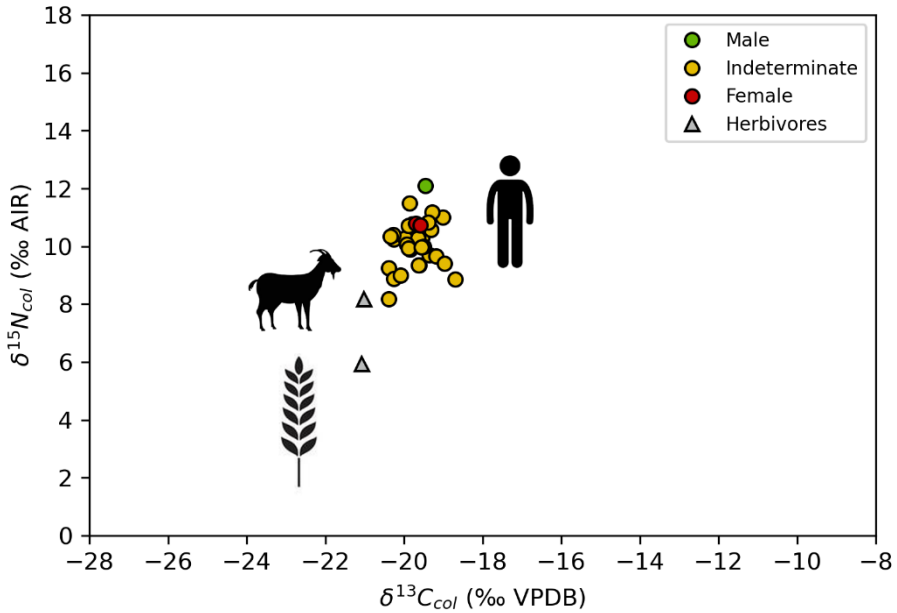


Figure 81. Carbon and nitrogen stable isotope values of human and animal bone collagen samples from Plaça de la Gardunya, classified by sex.

Table 88. Stable isotope values of carbon from human tooth enamel hydroxyapatite samples.

Individual	Sample ID	$\delta^{13}C$ (in ‰ VPDB)	Std. Dev.
4430.7	PG51	-12.29	0.03
4430.8	PG52	-12.62	0.02
4388	PG56	-13.30	0.03
4430.9	PG57	-9.90	0.05
4450	PG58	-11.76	0.02
4328.6	PG59	-13.08	0.01
4473	PG60	-12.63	0.03
4319.2	PG61	-12.89	0.02
4174	PG62	-13.53	0.03
50618.1	PG63	-12.52	0.03
50620.3	PG64	-14.28	0.01
50615.2	PG65	-14.08	0.06
50616.2	PG66	-11.98	0.03
50700	PG67	-12.41	0.02
50574.8	PG68	-11.79	0.04
50574.9	PG69	-12.93	0.04
4391	PG70	-12.49	0.05
4389.11	PG71	-11.13	0.03
4389.12	PG72	-13.16	0.03
4389.13	PG73	-12.80	0.02
4389.14	PG74	-12.63	0.05
4389.15	PG75	-12.24	0.05
4389.16	PG76	-12.73	0.04
4389.17	PG77	-12.32	0.05
4389.18	PG78	-13.24	0.01
4389.19	PG79	-12.95	0.03
4389.20	PG80	-12.80	0.02
4389.21	PG81	-13.20	0.05
4389.22	PG82	-10.75	0.02
4389.23	PG83	-12.70	0.04
4389.24	PG84	-11.18	0.04

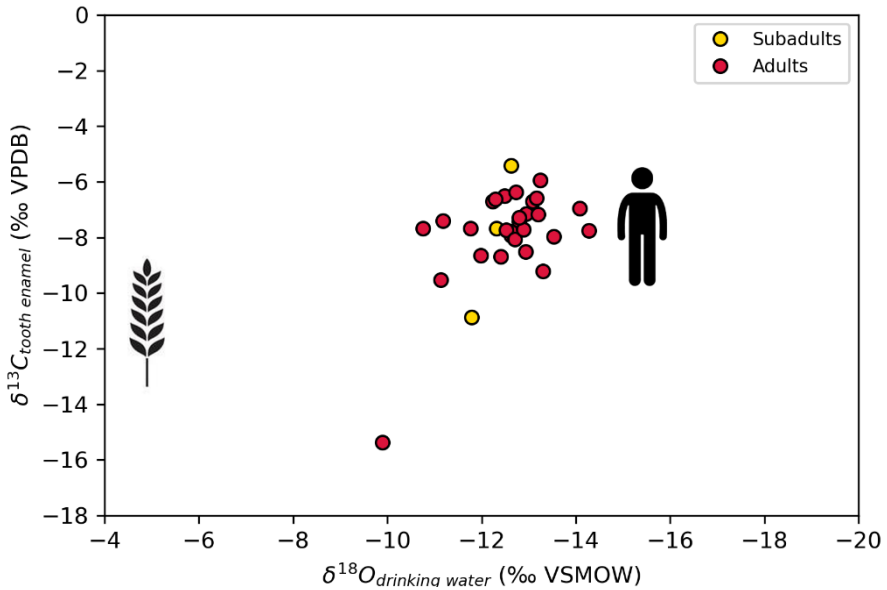


Figure 82. Carbon and oxygen stable isotope values of human tooth enamel hydroxyapatite samples, classified by tissue age (between 0-3 years of age).

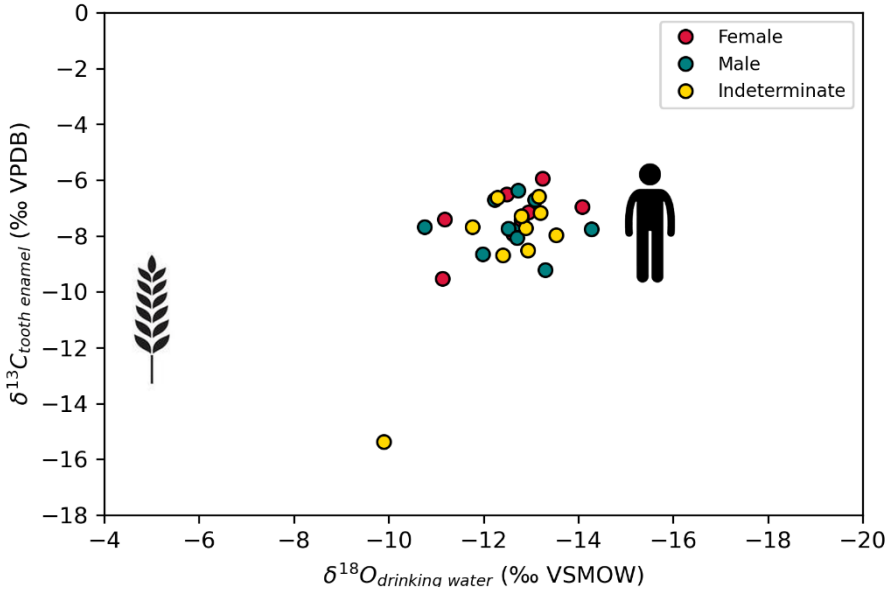


Figure 83. Carbon and oxygen stable isotope values of human tooth enamel hydroxyapatite samples, classified by sex.

4.4.1.2.2 Comparison with other archaeological sites

To contextualize, compare, and interpret the results from Plaça de la Gardunya, human and animal samples with published $\delta^{13}C$ and $\delta^{15}N$ isotopic signatures from bone collagen have been incorporated into the study. The mean and standard deviation values are displayed in ***Figure 84***. The Iberian Peninsula has been the subject of numerous dietary studies that have employed stable isotope analyses, encompassing human individuals, terrestrial animals, marine animals, and freshwater animals. The substantial corpus of published results enables the present study to expand the interpretation of the results and consider environments that were not sampled during the course of this PhD project. The data collection has been restricted to the eastern region of the Iberian Peninsula, which is in proximity to the Mediterranean Sea. Sites such as Cuesta del Negro and Gatas, which exhibit comparable mean values to those of Plaça de la Gardunya, have been interpreted as omnivorous diets comprising the consumption of C_3 plant species and terrestrial animal protein from domesticated local herbivores and omnivores, including both meat and dairy products. However, agricultural produce was of greater importance than animal protein in these contexts. The incorporation of marine animal protein could be proposed, although it should be noted that this would occur at a very sporadic pace.

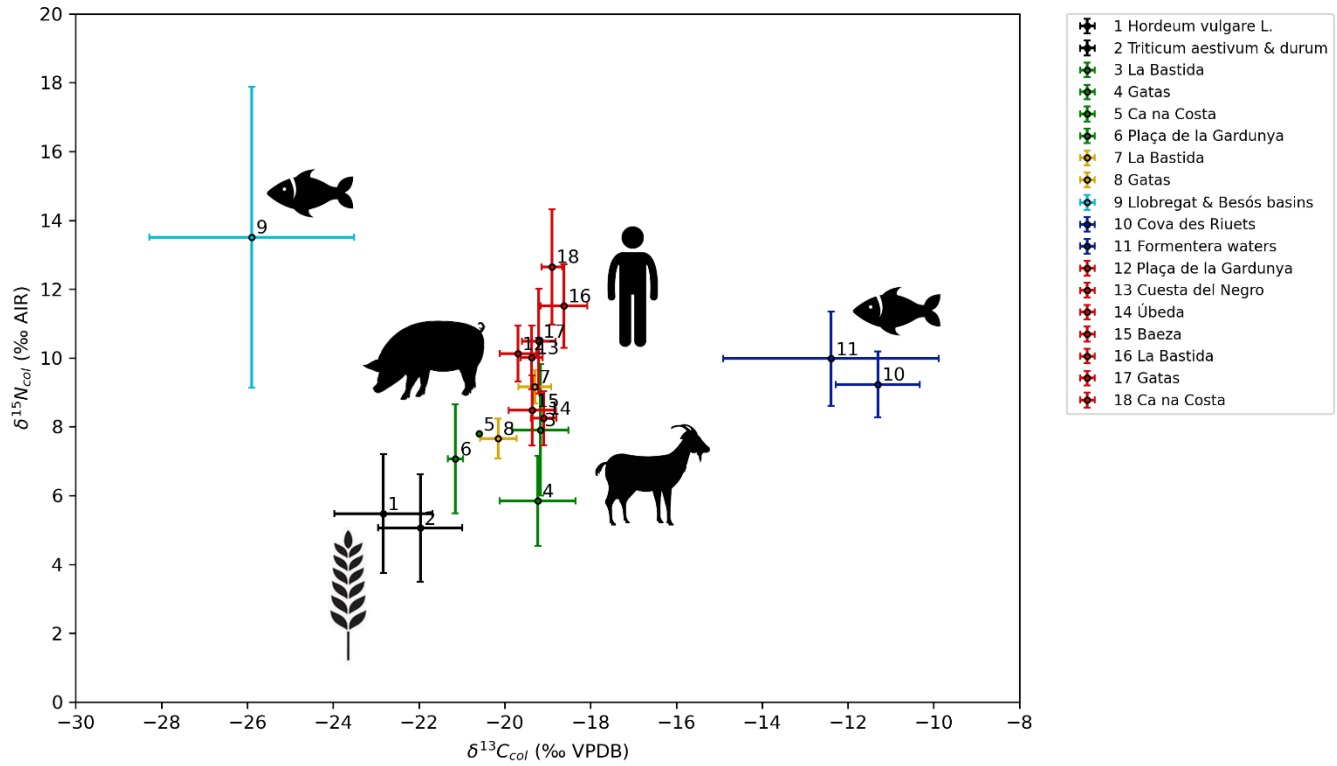


Figure 84. Mean and standard error of carbon and nitrogen stable isotopes of human and herbivore samples from the site of Plaça de la Gardunya. Included data for contextualization consists of human, herbivore, and omnivore animals from archaeological sites of the Iberian Peninsula (Fuller et al., 2005; Knipper et al., 2020; Molina-González et al., 2019). Data from modern fish from freshwater and marine environments, as well as marine prehistoric fish, have also been included (Cano-Rocabayera et al., 2015; Garcia-Guixé et al., 2010). Black represents C_3 plants, green represents herbivores, orange represents omnivores, light blue represents freshwater fish, dark blue represents marine fish, and red represents human samples.

Human samples with published $\delta^{13}C$ isotopic signatures from tooth enamel hydroxyapatite have been used to contextualize, compare, and interpret the results from Plaça de la Gardunya. The mean values from $\delta^{13}C$ and $\delta^{18}O$ are displayed in ***Figure 85***. The sites included in the study belong to the Late Neolithic, the Chalcolithic, and the Bronze Age periods from the central region of the Iberian Peninsula (Díaz-del-Río et al., 2017). A range of hypotheses have been proposed to explain the depleted $\delta^{13}C$ isotopic signatures observed at these sites. One potential factor contributing to this phenomenon is the consumption of marine animal protein. Another possibility is that the aridity of the area may affect the stable carbon isotopes assimilated during plant photosynthesis. It has been posited that the application of manure could potentially enrich the δ13C signature to a slight extent. Finally, the consumption of the earliest imported C_4 plants has also been posited. However, this hypothesis appears to be improbable, given that C_4 plant species were first introduced to the Iberian Peninsula during the Middle Bronze Age.

The depleted mean value of $\delta^{13}C$ from Plaça de la Gardunya is then encompassed within pure C_3 plant-base diets, coinciding with the archaeobotanical remains recovered to date.

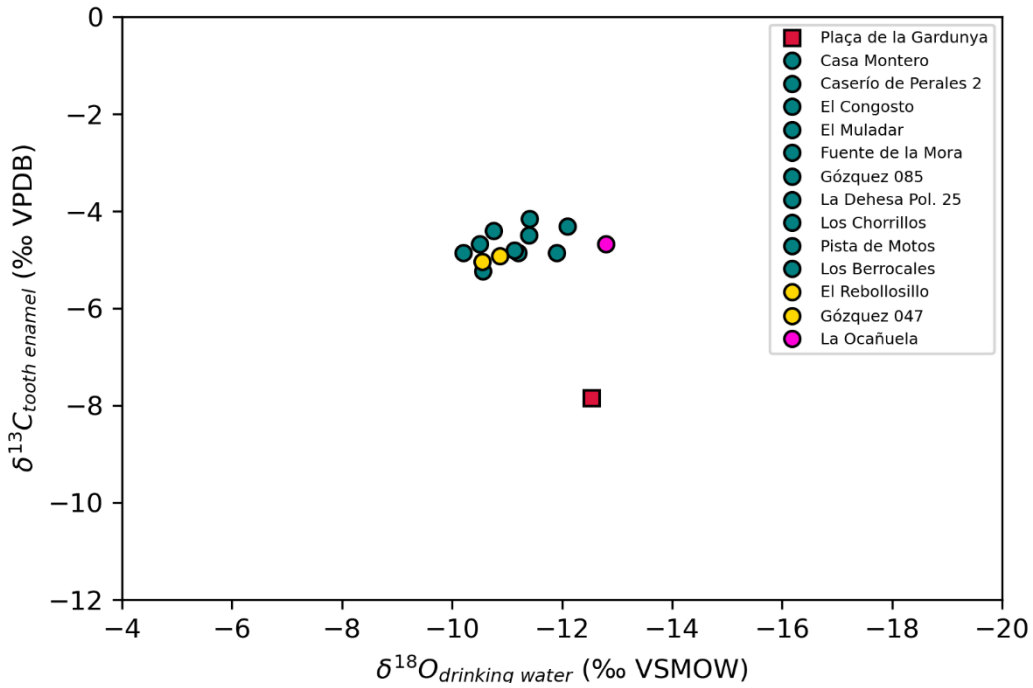


Figure 85. Mean values of carbon and oxygen stable isotopes of human samples from Plaça de la Gardunya and the archaeological sites included for comparison that belong to the Late Neolithic (in pink), to the Chalcolithic (in gold), and the Bronze Age (in teal) (Díaz-del-Río et al., 2017).

4.4.2 Residence patterns

4.4.2.1 Water catchment areas

4.4.2.1.1 Gird Lashkir and Gir-e Gomel

Tooth enamel hydroxyapatite samples have demonstrated a 100% success rate in providing reliable results of oxygen stable isotopes. The results of the $\delta^{18}O$ analysis conducted on ten individuals of Gird Lashkir are presented in **Table 89**, while the results from five individuals of Gir-e Gomel are presented in

Table 90.

Shapiro-Wilk normality test has been performed to observe if data is normally distributed. Significant values indicate that Tigris River (Southeastern Turkey), Makook Mountains (Erbil, Iraq) and Warmawa Sub-Basin (Sulaymaniyah, Iraq) are normally distributed ($p > 0.05$), whereas Shaqlawa-Harrir Basin (Erbil, Iraq), Tigris River and Little Zab (Iraq), Little Zab (Iraq), Dashty-Hewler Basin (Erbil, Iraq), Shawn Sub-Basin (Kirkuk, Iraq), Tigris River and Tigris Channel (Baghdad, Iraq), and Euphrates River (Central Iraq) are not normally distributed ($p < 0.05$). These results may be caused by the small *n* of the normal distributed water resources, and the great variability of $\delta^{18}O$ values in each water resource. The latter can be affected by different factors, such as sample type (groundwater, precipitation water, spring water, surface water…), sampling area (usually wide and include multiple sample types) and seasons (dry and wet seasons tend to have different values). The same test has been used for Gird Lashkir and Gir-e Gomel's human samples and significant values indicate they are normally distributed ($p = 0.664$ and $p = 0.950$, respectively).

Table 89. Oxygen stable isotope values from Gird Lashkir's individuals.

				$\delta^{18}O$			
Grave	Sample ID	Tooth	Tissue age	VPDB (in ‰)	Std. Dev.	Conversion to VSMOW (in ‰)	Conversion to VSMOW drinking water (in ‰)
4	TL71	$_3M$	8 - 16 y	-4.19	0.02	26.60319405	-6.49
6.1	TL73	$_3M$	8 - 16 y	-4.68	0.03	26.1000556	-7.39
6.2	TL74	^3M	7 - 16 y	-4.62	0.02	26.15572198	-7.29
7	TL75	M^3	7 - 16 y	-5.08	0.02	25.68683977	-8.13
10	TL76	M^3	7 - 16 y	-4.89	0.02	25.87846058	-7.79
12.1	TL77	M_3	8 - 16 y	-4.94	0.02	25.82814674	-7.88
13	TL71	M_1	0 - 3 y	-4.41	0.04	26.37196446	-6.9
14	TL79	M_3	8 - 16 y	-5.34	0.02	25.41600142	-8.61
15	TL78	^3M	7 - 16 y	-5.89	0.02	24.84435051	-9.63
16	TL90	M_1	0 - 3 y	-4.26	0.02	26.52504701	-6.63

Table 90. Oxygen stable isotope values from Gir-e Gomel's individuals.

				$\delta^{18}O$			
Grave	Sample ID	Tooth	Tissue age	VPDB (in ‰)	Std. Dev.	Conversion to VSMOW (in ‰)	Conversion to VSMOW drinking water (in ‰)
24	GG34	M^3	7 - 16 y	-6.59	0.01	24.1281811	-10.91
47	GG33	$_3M$	8 - 16 y	-5.64	0.05	25.10127226	-9.17
48	GG32	^3M	7 - 16 y	-6.46	0.03	24.25664198	-10.68
49	GG31	M^3	7 - 16 y	-7.84	0.03	22.84143129	-13.21

Table 91. Shapiro-Wilk normality test for the oxygen stable isotope values in sampled water resources.

		Zone	Statistic	*N*	*p*
$\delta^{18}O$ (‰ VSMOW)	Tigris River	Southeastern Turkey	0.896	5	0.387
	Shaqlawa-Harrir Basin	Erbil, Iraq	0.936	100	0.000
	Tigris River and Little Zab	Iraq	0.912	26	0.029
	Little Zab	Kirkuk, Iraq	0.683	62	0.000
	Dashty-Hewler Basin	Erbil, Iraq	0.902	29	0.011
	Makook Mountains	Erbil, Iraq	0.950	8	0.715
	Warmawa Sub-Basin	Sulaymaniyah, Iraq	0.901	10	0.223
	Shwan Sub-Basin	Kirkuk, Iraq	0.701	125	0.004
	Tigris River and Tigris Channel	Baghdad, Iraq	0.933	42	0.017
	Euphrates River	Central Iraq	0.897	26	0.014

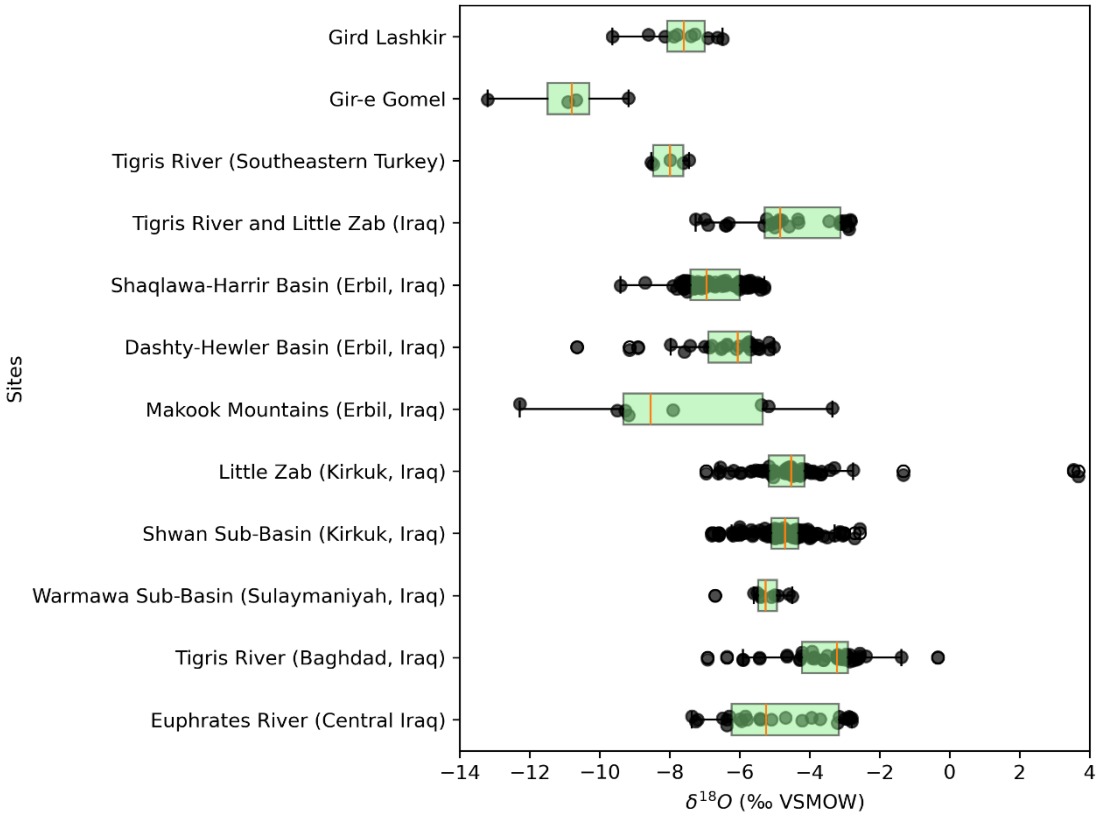


Figure 86. Boxplot of oxygen stable isotope values from human samples from Gird Lashkir and Gir-e Gomel, and water samples from the surrounding area.

Due to variability in data normality, two analyses have been performed: analysis of variance (ANOVA), usually used for equal variances, and a Kruskal-Wallis with a Dunn-Bonferroni post hoc test, usually used for non-parametric data. On the one hand, significant values in the analysis of variance (ANOVA) and post hoc analysis using Bonferroni test, indicates that $\delta^{18}O$ values from Gird Lashkir are similar to those from the Tigris River in southeastern Turkey, the Shaqlawa-Harrir Basin in Erbil (Iraq) and Makook Mountains in Erbil (Iraq), with a $p = 1$. To a lesser degree, its values resemble the ones from the Dashti-Hewler Basin in Erbil (Iraq), with a $p = 0.116$. Gir-e Gomel samples provided no correlations to any of the water resources. On the other hand, significant values in the Kruskal-Wallis with a Dunn-Bonferroni post hoc test indicate $\delta^{18}O$ values from Gird Lashkir and Gir-e Gomel are similar to those from the Tigris River in southeastern Turkey, Shaqlawa-Harrir Basin in Erbil (Iraq), Dashty-Hewler Basin in Erbil (Iraq) and the Makook Mountains in Erbil (Iraq), with a $p = 1$. To a lesser degree, its values resemble the ones from Warmawa Sub-Basin in Sulaymaniyah (Iraq), with a $p = 0.157$ for Gird Lashkir, and a $p = 0.116$ for Gir-e Gomel.

After performing both analysis of variance, Gird Lashkir's values are similar to the upper part of the Tigris River, as well as the water resources located in Erbil (Iraq), such as the Great Zab. This population drank local water resources and seem to be native from the site. Gir-e Gomel's values, on the contrary, are very different from all the water resources from Iraq and is surroundings. Nevertheless, the Kruskal-Wallis test indicates the same results as for Gird Lashkir, inferring its population was drank local water and may have drawn on water resources from the surroundings.

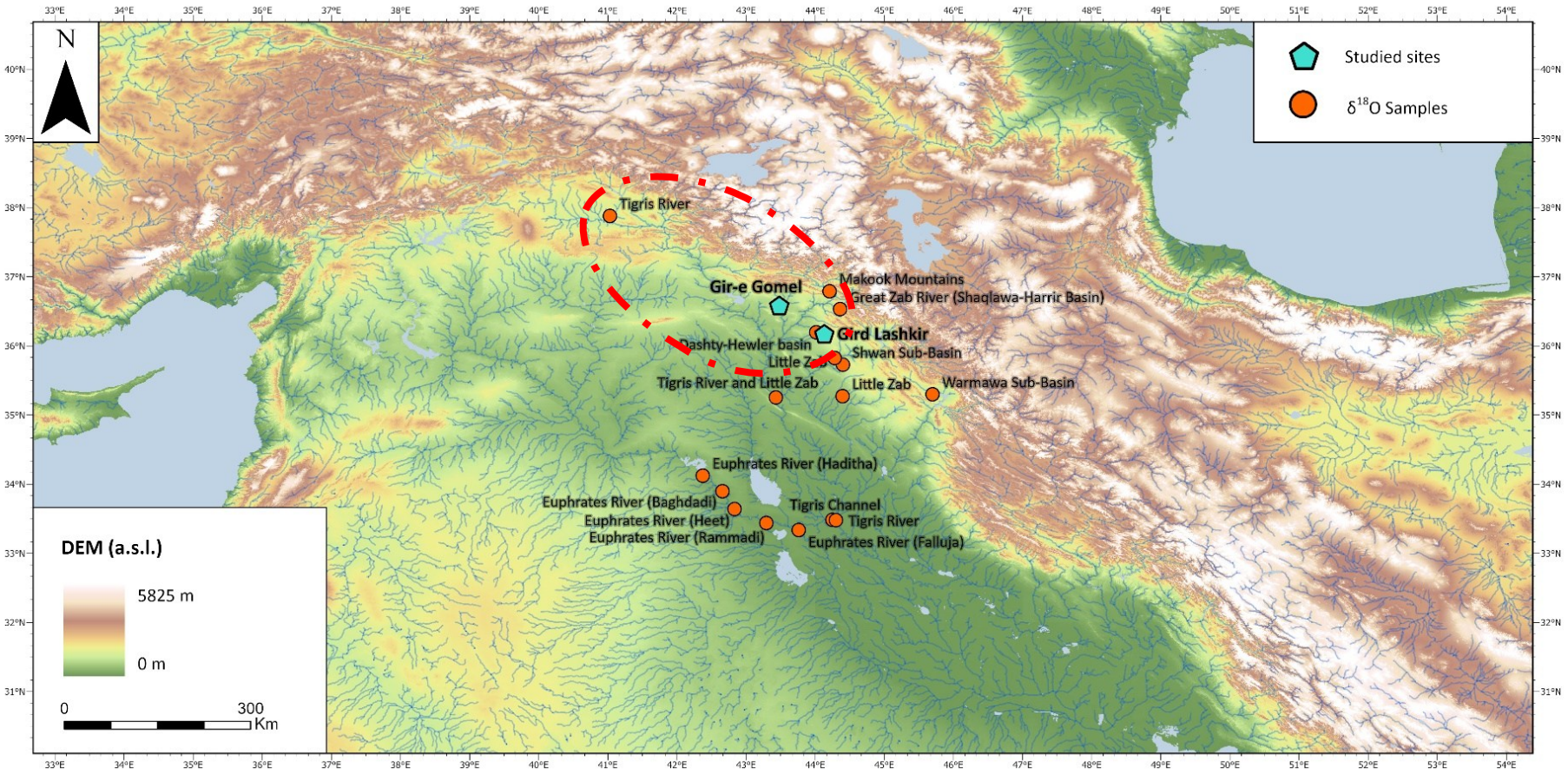


Figure 87. Water catchment areas of the individuals from Gird Lashkir and Gir-e Gomel.

4.4.2.1.2 Plaça de la Gardunya

Tooth enamel hydroxyapatite samples have demonstrated a 100% success rate in providing reliable results of oxygen stable isotopes. The $\delta^{18}O$ isotopic signature from 31 individuals of Plaça de la Gardunya are presented in **Table 92**. The mean value of $\delta^{18}O$ for the entire population is -7.84‰ ± 1.77, ranging between -15.37 and -5.42‰.

A Shapiro-Wilk normality test was conducted to ascertain the distribution of data from Plaça de la Gardunya. The results indicate statistical differences ($p < 0.05$), suggesting that the data does not follow a normal distribution. A Kruskal-Wallis analysis with a Dunn-Bonferroni post-hoc test revealed no significant differences between female, male, and indeterminate individuals, as well as between subadult and adult individuals. A Linear Discriminant Analysis (LDA) has been performed between the isotopic signature of the population from Plaça de la Gardunya and the database of published $\delta^{18}O$ isotopic signatures from rainfall, groundwater, and river water samples belonging to water resources located in northeastern Iberia. The analysis failed to classify the $\delta^{18}O$ isotopic signatures from Plaça de la Gardunya's individuals to any hydrological resource due to the variability of their $\delta^{18}O$ values throughout the year. When the isotopic signatures are displayed in a boxplot graphic (***Figure 88***), it is observed that the first quartile of Plaça de la Gardunya is compatible with the hydrological resources primarily located in the Ebro Basin and its tributaries, in Barcelona, in the Llobregat Basin and its tributaries, in Montseny, and in the Pyrenees. To a lesser extent, values are compatible with the water resources from Prades and Girona. Overall, the region of Catalonia appears to coincide with the values associated with Plaça de la Gardunya. In contrast, further territories such as Valencia or Mallorca have more depleted values. One individual is distinguished by its depleted $\delta^{18}O$ isotopic signature, which consists of an adult of indeterminate sex (4430.9), with a value of -15.37‰. Its isotopic signature demonstrates significant compatibility with the hydrological resources of the Prades region, followed by those of the Montseny area.

Table 92. Oxygen stable isotope values for Plaça de la Gardunya's individuals.

				$\delta^{18}O$			
Individual	Sample ID	Tooth	Tissue age (in years)	VPDB (in ‰)	Std. Dev.	VSMOW (in ‰)	Drinking water (in ‰ VSMOW)
4430.7	PG51	M_1	0 - 3	-4.26	0.01	26.52504701	-6.63
4430.8	PG52	$_1M$	0 - 3	-4.89	0.02	25.87417855	-7.79
4388	PG56	M^1	0 - 3	-5.66	0.02	25.08307364	-9.21
4430.9	PG57	^1M	0 - 3	-9.01	0.01	21.63175801	-15.37
4450	PG58	M_1	0 - 3	-4.83	0.04	25.94269102	-7.67
4328.6	PG59	M_1	0 - 3	-4.31	0.02	26.4790152	-6.71
4473	PG60	$_1M$	0 - 3	-3.61	0.03	27.20267815	-5.42
4319.2	PG61	$_1M$	0 - 3	-4.85	0.03	25.91806936	-7.72
4174	PG62	$_1M$	0 - 3	-4.99	0.03	25.77462137	-7.97
50618.1	PG63	M_1	0 - 3	-4.86	0.04	25.9105758	-7.73
50620.3	PG64	M^1	0 - 3	-4.87	0.02	25.8955887	-7.76
50615.2	PG65	M^1	0 - 3	-4.44	0.03	26.34520178	-6.95
50616.2	PG66	M^1	0 - 3	-5.36	0.03	25.39780279	-8.64
50700	PG67	$_1M$	0 - 3	-5.38	0.03	25.37746315	-8.68
50574.8	PG68	M^1	0 - 3	-6.57	0.03	24.14959125	-10.87
50574.9	PG69	M_1	0 - 3	-5.29	0.03	25.46738577	-8.52

4391	PG70	$_1$M	0 - 3	-4.19	0.02	26.59891202	-6.5
4389.11	PG71	$_1$M	0 - 3	-5.83	0.02	24.90536942	-9.52
4389.12	PG72	M_1	0 - 3	-4.24	0.03	26.54859817	-6.59
4389.13	PG73	M_1	0 - 3	-4.62	0.04	26.16214503	-7.28
4389.14	PG74	$_1$M	0 - 3	-4.97	0.03	25.79924304	-7.93
4389.15	PG75	M_1	0 - 3	-4.3	0.02	26.48222672	-6.71
4389.16	PG76	M_1	0 - 3	-4.12	0.04	26.6695655	-6.37
4389.17	PG77	M_1	0 - 3	-4.83	0.01	25.94055001	-7.68
4389.18	PG78	M_1	0 - 3	-3.89	0.01	26.90935914	-5.94
4389.19	PG79	M_1	0 - 3	-4.54	0.03	26.23601003	-7.15
4389.20	PG80	$_1$M	0 - 3	-4.7	0.03	26.07864545	-7.43
4389.21	PG81	M_1	0 - 3	-4.55	0.03	26.23065749	-7.16
4389.22	PG82	M_1	0 - 3	-4.82	0.01	25.94590255	-7.67
4389.23	PG83	M_1	0 - 3	-5.05	0.04	25.71788448	-8.07
4389.24	PG84	M_1	0 - 3	-4.68	0.02	26.09042103	-7.41

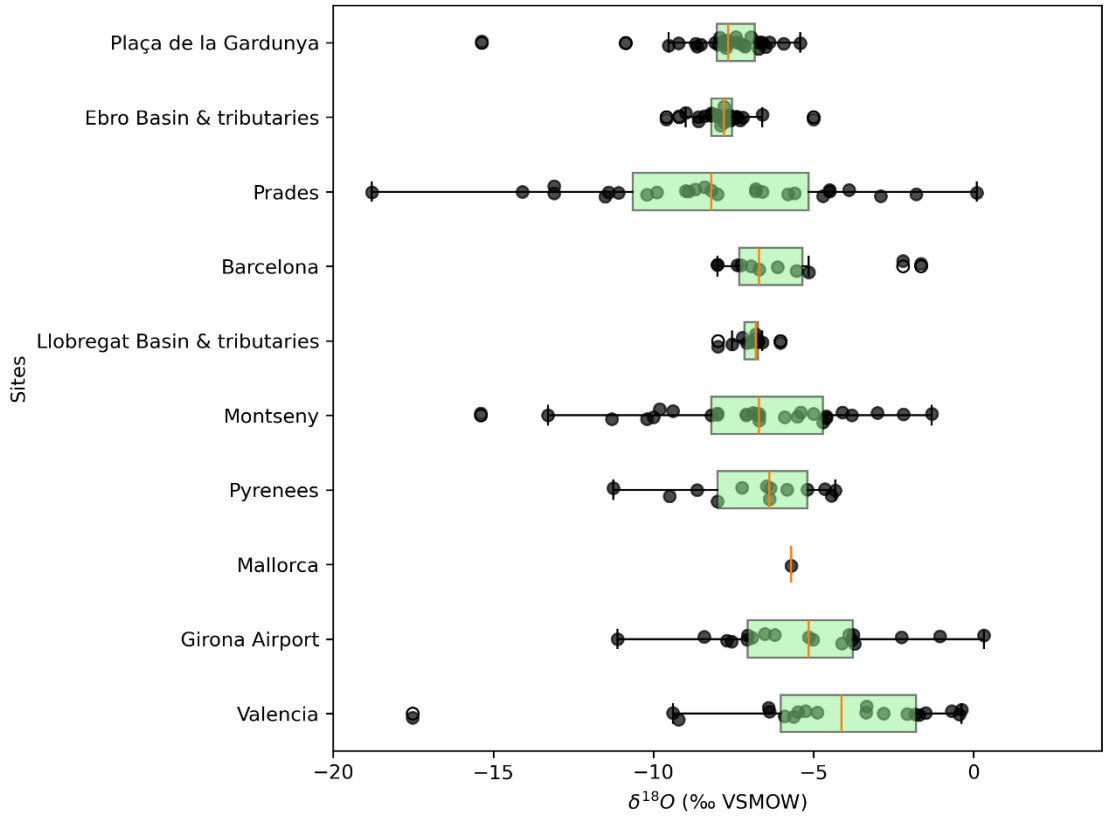


Figure 88. Boxplot of oxygen stable isotope values from human samples from Plaça de la Gardunya, and water samples from the surrounding area.

4.4.2.2 Geological areas

4.4.2.2.1 Gird Lashkir and Gir-e Gomel

Strontium isotope analysis has provided the $^{87}Sr/^{86}Sr$ values for each individual from Gird Lashkir (*n* = 11) and Gir-e Gomel (*n* = 4). Results and standard deviation are presented in **Table 93**.

Table 93. $^{87}Sr/^{86}Sr$ results from Gird Lashkir and Gir-e Gomel's individuals.

Site	Grave	Sample ID	Tooth	Tissue age	$^{87}Sr/^{86}Sr$	Std. Dev.
Gird Lashkir	4	TL62	$_2$I	3 m - 5 y	0.708220	0.000019
	5	TL63	$_2$I	3 m - 5 y	0.708220	0.000019
	6.1	TL61	$_2$I	3 m - 5 y	0.708298	0.000019
	6.2	TL64	$_2$I	3 m - 5 y	0.708193	0.000019
	7	TL65	$_2$I	3 m - 5 y	0.708203	0.000019
	10	TL66	$_2$I	3 m - 5 y	0.708196	0.000019

	12.1	TL67	I_2	3 m - 5 y	0.708139	0.000019
	13	TL70	M_1	0 - 3 y	0.708171	0.000019
	14	TL68	$_2I$	3 m - 5 y	0.708172	0.000019
	15	TL69	$_2I$	3 m - 5 y	0.708180	0.000019
	16	TL91	I^1	3 m - 5 y	0.708176	0.000019
Gir-e Gomel	24	GG28	$_1I$	3 m - 5 y	0.708070	0.000019
	47	GG29	$_2I$	3 m – 5 y	0.708087	0.000019
	48	GG27	^2I	10 m - 5 y	0.708109	0.000019

A snail shell collected from the site of Gird Lashkir has been analyzed to establish the strontium isotope signature of the local geology. The snail shell has a $^{87}Sr/^{86}Sr$ isotopic signature of 0.708152. $^{87}Sr/^{86}Sr$ ratio of Gird Lashkir's population yields a range of 0.708139 - 0.708298 and a mean of 0.708197 ± 0.000041. As for Gir-e Gomel, $^{87}Sr/^{86}Sr$ ratio yields a range of 0.708070 - 0.708109 and a mean of 0.708089 ± 0.000019. The values of Gird Lashkir's population are similar to the signature of the snail shell. When observing the values of Gird Lashkir classified by sex, male individuals have the same strontium isotope signature as the snail (see **Figure 89** and **Figure 90**), while female and indeterminate individuals have a slightly higher value of strontium.

Data has been tested to see if individuals were local or non-local. Individuals have been considered local if their strontium isotope ratios ($^{87}Sr/^{86}Sr$) fell between the range of the mean ± 2σ, 0.708170 and 0.708224, as determined by their human tooth enamel samples. Two individuals, a child individual from Grave 6 ($^{87}Sr/^{86}Sr$ = 0.708298), and a middle-adult male individual from Grave 12 ($^{87}Sr/^{86}Sr$ = 0.708139), fall outside the local stable isotope range. In Gir-e Gomel, all individuals are considered local given that their strontium isotope ratios ($^{87}Sr/^{86}Sr$) fall between the range of the mean ± 2σ, 0.707953 and 0.708161, as determined by their human tooth enamel samples.

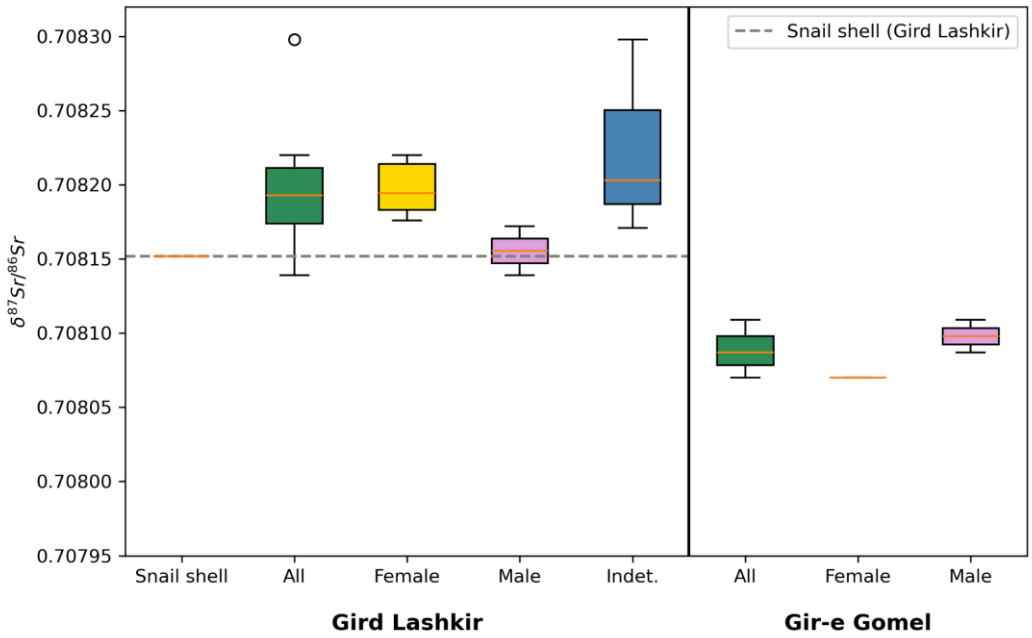


Figure 89. Boxplot of Gird Lashkir and Gir-e Gomel's human strontium stable isotopic signatures, classified by sex. Local strontium signature of the site of Gird Lashkir is shown as a discontinuous grey line.

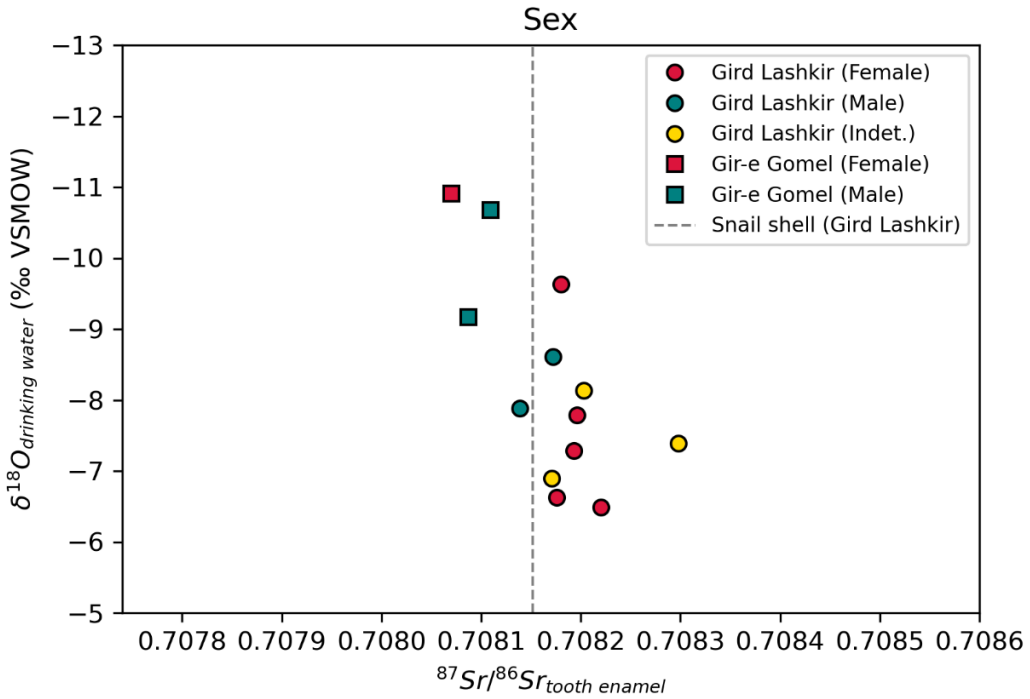


Figure 90. Oxygen and strontium stable isotope signatures from the population of Gird Lashkir and Gir-e Gomel, categorized by sex. The grey discontinuous line depicts the local strontium signature for Gird Lashkir.

In order to observe if the individuals of our dataset share affinity with a geological strontium isotope signature from its surroundings, we perform further analysis. Results are specifically interesting for observing the possible geological origin of the two non-local individuals from Gird Lashkir. Analysis based on sex are discarded to be performed due to the low number of individuals per group (5 female and 2 male individuals). Data normality for Gird Lashkir and Gir-e Gomel has been verified through the Shapiro-Wilk test and equal variance. Shapiro-Wilk p-value is < 0.05, indicating data belongs to different groups and does not possess a normal distribution. Non-parametric statistic has to be applied to our dataset. In order to observe the affinity degree of Gird Lashkir and Gir-e Gomel's individuals to a specific geological region, Mann-Whitney U tests and Kruskal-Wallis with Dunn-Bonferroni post hoc tests have been performed to compare pairs of groups. Results for the Mann-Whitney U tests show that Gird Lashkir has different degrees of affinity to different geological groups. Only one region shows the higher affinity, consisting of the north region of Syria (p = 0.852). Lower affinity is shown for the site of Azna-Dorud in Iran (p = 0.392), the site of Kurkuk in Iraq (p = 0.359), the area of Erbil (p = 0.192) and the site of Ur in Iraq (p = 0.160), followed by Beirut in Lebanon (p = 0.111). Results from the Kruskal-Wallis with Dunn-Bonferroni post hoc tests show the highest affinity degree to multiple geological regions (p = 1): the southwest region of Syria, the area of Beirut in Lebanon, and the site of Azna-Dorud in Iran. Gir-e Gomel does also show different affinity degrees to the geology of the surrounding regions. Mann-Whitney U tests provide different degrees of affinity, consisting of the site of Azna-Dorud in Iran (p = 1), and the sites of Bestansur (p = 0.773) and Ur in Iraq (p = 0.758). To a lesser degree, affinity is shown with the north Syrian region (p = 0.178), the area of Erbil in Iraq and Beirut in Lebanon (p = 0.157), and the site of Ugarit in Syria (p = 0.064). The Kruskal-Wallis with Dunn-Bonferroni post hoc tests provide the highest affinity degree (p = 1) to five geological regions: the southwest of Syria, the area of Beirut in Lebanon, the western-southwestern region of Iran, Lake Van and its tributary rivers in southeast Turkey, and the site of Ur in Iraq. Both the Mann-Whitney U tests and the Kruskal-Wallis with Dunn-Bonferroni post hoc tests provide different results and only coincide in assessing the highest affinity degree to the site of Azna-Dorud in Iran for Gird Lashkir and Gir-e Gomel, and the site of Ur in Iraq for Gir-e Gomel.

Some questions arise after the analyses performed. The results associate both the individuals from the sites of Gird Lashkir and Gir-e Gomel to regions that are very far away from the results provided by the analysis of oxygen stable isotope. Samples for strontium stable isotope represent early childhood of the individuals (up to 5 years of age), while samples for oxygen stable

isotope represent later childhood (7 to 16 years of age). A common interpretation for these differences is attributed to the consumption of foodstuffs from other regions, but carbon and nitrogen stable isotope analysis from our data reject this possibility, given that the consumption of local fauna and flora is observed. If we combine both $\delta^{18}O$ and $^{87}Sr/^{86}Sr$ results to interpret population origin, even though the highest association is not observed by the Mann-Whitney U tests and the Kruskal-Wallis with Dunn-Bonferroni post hoc tests, we should take into account the associated geological regions included in the catchment area of water resources (**Figure 91**).

When contrasting both analysis through this perspective, one can observe that individuals from Gird Lashkir are associated with the geology of site of Nineveh in Iraq, and the northeastern region of Syria. A low probability also points an affinity to the area of Kirkuk. The individuals from Gir-e Gomel would be associated to the southeastern geological region of Turkey that comprises the Lake Van and its tributary rivers, and, less probably, to the site of Bestansur in Iraq. In regard to the two non-local individuals from Gird Lashkir, observing their $^{87}Sr/^{86}Sr$ value and taking into account the most probable catchment area of water resources after the $\delta^{18}O$ analysis, the child individual of the double Grave 6 could have been spent his childhood in the region of Nineveh or northeastern Syria, while the male adult individual from the triple pit Grave 12 could be associated to both the region comprised with Lake Van in southeast Anatolia, and the southeast area of Erbil in Iraqi Kurdistan.



Figure 91. Map displaying the studied sites and the samples for strontium and oxygen stable isotopes.

4.4.2.2.2 Plaça de la Gardunya

The $^{87}Sr/^{86}Sr$ isotopic signatures of the 31 sampled individuals from Plaça de la Gardunya are presented in **Table 94**. The $^{87}Sr/^{86}Sr$ isotopic signature from the population of Plaça de la Gardunya yielded a mean value of 0.709482 ± 0.000532, ranging from 0.708622 to 0.711023.

Table 94. $^{87}Sr/^{86}Sr$ results from Plaça de la Gardunya's individuals.

Individual	Sample ID	Tooth	Tissue age (in years)	$^{87}Sr/^{86}Sr$	Std. Dev.
4430.7	PG94	M_1	0 - 3	0.709302	0.000019
4430.8	PG95	$_1M$	0 - 3	0.709267	0.000019
4388	PG96	M^1	0 - 3	0.709164	0.000019
4430.9	PG97	$_1M$	0 - 3	0.709291	0.000019
4450	PG98	M_1	0 - 3	0.709148	0.000019
4328.6	PG99	M_1	0 - 3	0.710117	0.000019
4473	PG100	$_1M$	0 - 3	0.709310	0.000019
4319.2	PG101	$_1M$	0 - 3	0.711023	0.000019
4174	PG102	$_1M$	0 - 3	0.710994	0.000019
50618.1	PG103	M_1	0 - 3	0.709259	0.000019
50620.3	PG104	M^1	0 - 3	0.709276	0.000019
50615.2	PG105	M^1	0 - 3	0.709309	0.000019
50616.2	PG106	M^1	0 - 3	0.709239	0.000019
50700	PG107	$_1M$	0 - 3	0.709258	0.000019
50574.8	PG108	M^1	0 - 3	0.709240	0.000019
50574.9	PG109	M_1	0 - 3	0.708622	0.000019
4391	PG110	$_1M$	0 - 3	0.709333	0.000019
4389.11	PG111	$_1M$	0 - 3	0.709288	0.000019
4389.12	PG112	M_1	0 - 3	0.709548	0.000019
4389.13	PG113	M_1	0 - 3	0.709807	0.000019
4389.14	PG114	$_1M$	0 - 3	0.709721	0.000023
4389.15	PG115	M_1	0 - 3	0.709184	0.000023
4389.16	PG116	M_1	0 - 3	0.709236	0.000023
4389.17	PG117	M_1	0 - 3	0.709270	0.000023
4389.18	PG118	M_1	0 - 3	0.709181	0.000023
4389.19	PG119	M_1	0 - 3	0.709572	0.000023
4389.20	PG120	$_1M$	0 - 3	0.709856	0.000023

4389.21	PG121	M_1	0 - 3	0.710531	0.000023
4389.22	PG122	M_1	0 - 3	0.709058	0.000023
4389.23	PG123	M_1	0 - 3	0.709366	0.000023
4389.24	PG124	M_1	0 - 3	0.709179	0.000023

When differences between age and sex classes are observed (***Figure 92***), a cluster with the same range of values is noted for both female and male individuals, as well as for subadult individuals. However, certain individuals exhibited higher strontium stable isotopic signatures, particularly four indeterminate individuals (one male and two female), deviating from the main cluster. One adult of indeterminate sex demonstrates lower values in comparison to the remaining members of the cluster.

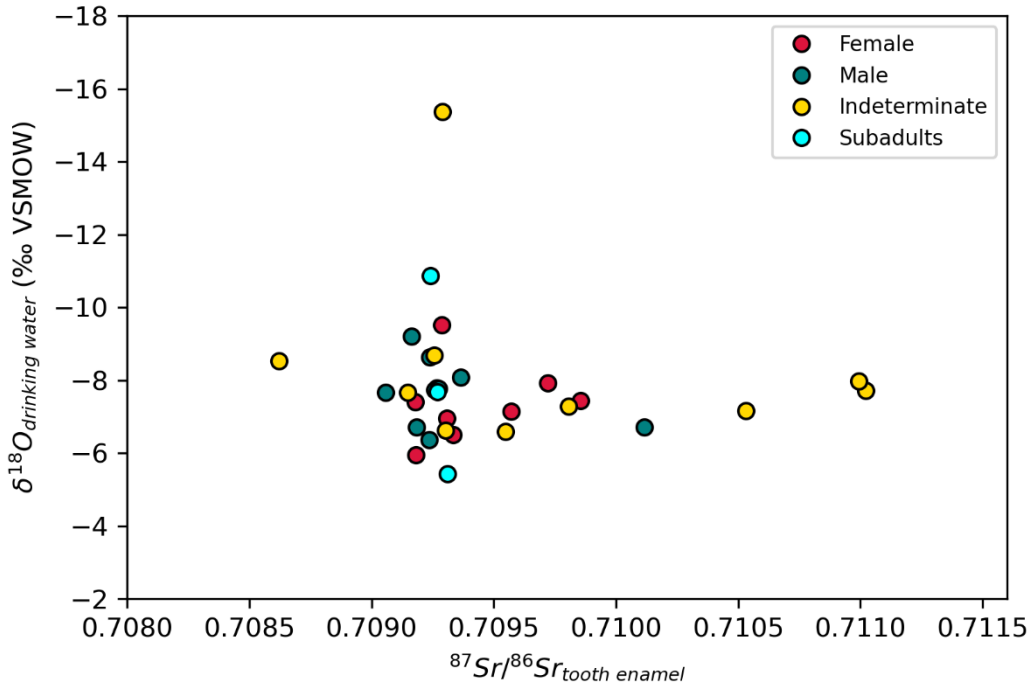


Figure 92. Oxygen and strontium stable isotope signatures from the population of Plaça de la Gardunya, categorized by sex and age.

Data has been tested to see if individuals were local or non-local. Individuals have been considered local if their strontium isotope ratios ($^{87}Sr/^{86}Sr$) fell between the range of the mean ± 2σ, 0.792870 and 0.709677, as determined by their human tooth enamel samples. Seven individuals fall outside the local stable isotope range, including 4174 ($^{87}Sr/^{86}Sr$ = 0.710994), 4319.2 ($^{87}Sr/^{86}Sr$ = 0.711023), 4389.20 ($^{87}Sr/^{86}Sr$ = 0.709856), 4328.6 ($^{87}Sr/^{86}Sr$ = 0.710117), 4389.13 ($^{87}Sr/^{86}Sr$ =

0.709721), 4389.14 ($^{87}Sr/^{86}Sr$ = 0.709721), and 4389.21 ($^{87}Sr/^{86}Sr$ = 0.710531). Two of these individuals, 4174 and 4319.2, were buried in Grave 2 from Sector 4, while the rest were buried in Grave 3/4 from Sector 4.

To associate the studied individuals with a specific geology, the predicted $^{87}Sr/^{86}Sr$ ranges for the geology of the Iberian Peninsula published by Díaz-del-Río et al. (2022) will be used. Two isoscape maps have been created: one including geological and archaeological samples, and another including solely archaeological material. The first isoscape delineates four distinct ranges for the classification of our data (***Figure 93***), while the second isoscape delineates up to six distinct ranges (***Figure 94***), thereby facilitating a more comprehensive classification.

Upon examination of the isoscape, encompassing geological and archaeological samples, the individual 50574.9 is categorized within the range of 0.7086 to 0.7087, aligning with the geology of Lleida and Alicante. The range in which the majority of individuals are associated corresponds to the values between 0.7090 and 0.7099, with 26 individuals (4388, 4389.11, 4389.12, 4389.13, 4389.14, 4389.15, 4389.16, 4389.17, 4389.18, 4389.19, 4389.20, 4389.22, 4389.23, 4389.24, 4391, 4430.7, 4430.8, 4430.9, 4450, 4473, 50574.8, 50615.2, 50616.2, 50618.1, 50620.3, and 50700). These values are characteristic of the territories of Lleida, Barcelona, and Tarragona. The final range encompasses values from 0.7099 to 0.7126. Four adult individuals, 4174, 4319.2, 4328.6, and 4389.21, exhibit strontium signatures characteristic of this range, which corresponds to the territories of Barcelona and Girona.

Upon examination of the isoscape, encompassing solely archaeological samples, the individual 50574.9 manifests a strontium signature within the predicted range of 0.7084 to 0.7088. These values are indicative of the geology characteristic of the territories of Castellón and Valencia. Six additional individuals, identified as 4388, 4389.15, 4389.18, 4389.22, 4389.24, and 4450, exhibit strontium values that are consistent with the geology of Lleida, Tarragona and Castellón, with predicted strontium signatures ranging from 0.7090 to 0.7092. Fifteen individuals, 4389.11, 4389.16, 4389.17, 4389.23, 4430.7, 4430.8, 4430.9, 4473, 4391, 50574.8, 50615.2, 50616.2, 50618.1, 50620.3, and 50700, exhibit strontium signatures ranging between 0.7092 and 0.7095, which correspond to the areas of Lleida, Barcelona, and Tarragona. The range between 0.7095 and 0.7106 includes seven individuals, 4328.6, 4389.12, 4389.13, 4389.14, 4389.19, 4389.20, and 4389.21, whose geologies correspond to the territories of Barcelona and Girona. The remaining two individuals, identified as 4174 and 4319.2, exhibit strontium signatures ranging from 0.70106 to 0.7134, which are indicative of the geology characteristic of central and western Iberia.

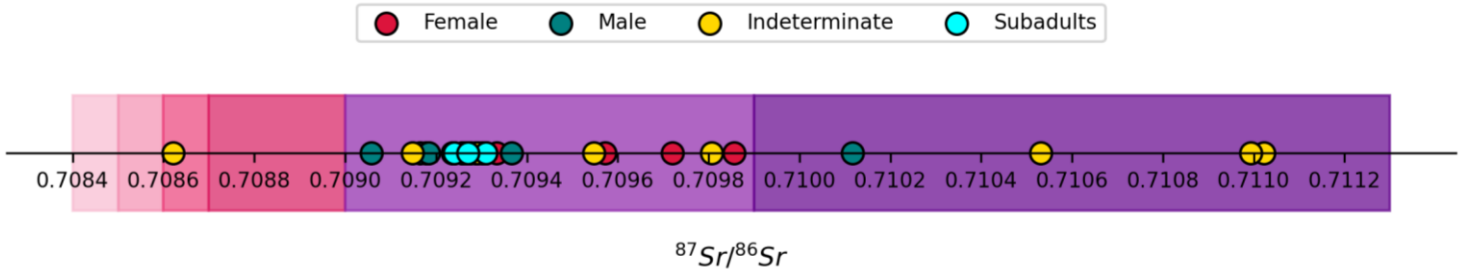


Figure 93. Isotopic signatures of strontium from the individuals of Plaça de la Gardunya classified by age and sex. The different color ranges correspond to the predicted values of the isoscape map from the Iberian Peninsula elaborated by Díaz-del-Río et al. (2022), in which geological, animal and human samples were included in the dataset.

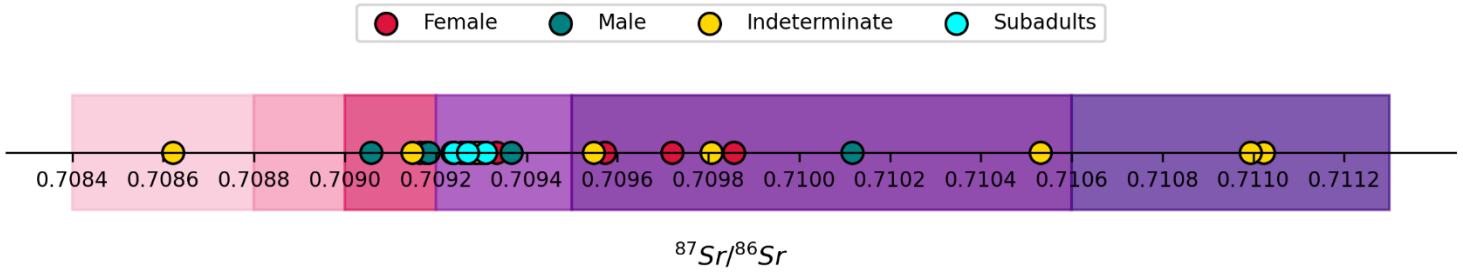


Figure 94. Isotopic signatures of strontium from the individuals of Plaça de la Gardunya classified by age and sex. The different color ranges correspond to the predicted values of the isoscape map from the Iberian Peninsula elaborated by Díaz-del-Río et al. (2022), in which archaeological samples (animal and human) were included in the dataset.

4.4.3 Concluding remarks

4.4.3.1 Diet

The employment of a sampling strategy that incorporates bone collagen and tooth enamel hydroxyapatite samples has led to a substantial expansion in the scope of analysis regarding the diet of the studied individuals. This approach has facilitated the acquisition of valuable information concerning dietary trends within the population and the existence of disparities based on factors such as age and sex. The analysis of bone collagen in 34 individuals, as well as the analysis of tooth enamel hydroxyapatite in 31 individuals, yielded dietary proxies for bone collagen and tooth enamel hydroxyapatite in a total of 34 individuals from Plaça de la Gardunya. This analysis also resulted in a final total dietary sample of 60 individuals for Plaça de la Gardunya.

The individuals studied from northern Mesopotamia, specifically from the sites of Gird Lashkir and Gir-e Gomel, demonstrated an omnivorous diet, as evidenced by their $\delta^{13}C$ isotopic values, which are indicative of a C_3 plant-based diet. Additionally, their $\delta^{15}N$ isotopic signatures suggest a limited consumption of animal protein derived from herbivorous livestock (Ellegård et al., 2019). These herbivorous animals were presumably nourished with the same agricultural products consumed by human populations. A notable finding was that male individuals exhibited slightly higher consumption of animal protein compared to adult females and subadult individuals.

An analysis of manuring practices in northern Mesopotamia (Styring et al., 2017) revealed that crops cultivated in the surrounding areas of Gird Lashkir and Gir-e Gomel received minimal manure. This characteristic demonstrates the deviation of these two sites, which are relatively small in scale, from the documented trend. Previous observations in northern Mesopotamia indicate that smaller sites during the Early Bronze Age demonstrate more intensive fertilization of their agricultural lands.

The results from the case study of Plaça de la Gardunya, located in the northeastern of the Iberian Peninsula, point to an omnivorous diet comprised of a mixture of predominantly C_3 plants, which aligns with findings from bone collagen samples and archaeobotanical analysis, alongside consumption of domestic herbivorous and omnivorous livestock in the form of meat and dairy products, with the possibility of a very sporadic consumption of animal resources from marine and freshwater environments.

Isotopic signatures of $\delta^{13}C$ and $\delta^{15}N$ from bone collagen samples have indicated a uniform consumption of similar food types across all age groups. One adult male individual (50618.1) exhibited an enriched $\delta^{15}N$ isotopic signature, indicating elevated animal protein consumption relative to the remaining population. Several adult individuals (4174, 3402, and 50574.1) exhibited isotopic signatures indicative of elevated plant-based food consumption and reduced animal protein intake in comparison to other members of the studied population. Furthermore, analysis of the $\delta^{13}C$ isotopic signatures from tooth enamel hydroxyapatite further identified an adult of indeterminate sex, exhibiting a significantly depleted $\delta^{13}C$ isotopic signature (50620.3). It has been hypothesized that the subject consumed freshwater fish during early childhood.

4.4.3.2 Residence patterns

The results of both oxygen and strontium stable isotope analyses have been combined to infer residence patterns. The analyses conducted on the study case of Gird Lashkir and Gir-e Gomel suggest that only two individuals could be exogenous from Gird Lashkir: a child individual from Grave 6 and a male adult individual from Grave 12. The strontium stable isotopic signatures exhibited by these samples fall outside the local geological range. This suggests that the child individual from Grave 6 may have spent its early childhood in the region of Nineveh or in northeastern Syria, while the male adult individual from Grave 12 could have spent its childhood in the region between Erbil in Iraqi Kurdistan and Lake Van in southeastern Anatolia. The population of Gir-e Gomel exhibits stable isotopic values associated with a vast geological territory encompassing southeastern Turkey and northeastern Iraq, specifically from the Lake Van to the site of Bestansur. However, the delineation of precise geographical boundaries for these societies remains challenging due to the complex geology of northern Mesopotamia. The strontium stable isotope values from this extensive territory exhibit very slight variations, which complicates the proposal of a detailed interpretation.

The local population from Gird Lashkir obtained their water resources from the Tigris River and its tributaries, such as the Great Zab, as well as from groundwater in the region of Erbil. The local population of Gir-e Gomel appears to have obtained its hydrological resources from the surrounding area, such as the Gomel River, among other sources, including wadis.

The analyses conducted on the study case of Plaça de la Gardunya suggest that seven individuals could be exogenous from the site, consisting of 4174, 4319.2, 4328.6, 4389.13, 4389.14,

4389.20, and 4389.21. According to the published strontium isoscapes of predicted isotopic signatures, individuals 4174, 4319.2, 4328.6, and 4389.21, exhibit strontium signatures characteristic of the territories of Barcelona and Girona. Individuals 4174 and 4319.2 could also be compatible with strontium signatures from a vast region comprising central and western Iberia. One individual, designated as local (50574.9), exhibits a strontium signature related to the territories of Lleida, Alicante, Castellón and Valencia, as depicted in the isoscape maps. The remaining individuals exhibited strontium isotope signatures which are characteristic of the northeastern territories of Iberia, comprising Lleida, Tarragona, Barcelona, and Girona, thereby aligning with the proposed interpretation of the results derived from the analysis of oxygen stable isotopes. It is suggested that the water resources obtained in the early childhood of the local individuals coincide with the oxygen stable isotopic signature of the hydrological sources from the region of Catalonia. A notable distinction is observed in the oxygen isotopic signature of a single individual, which deviates from the characteristics exhibited by the overall population. This result is noteworthy as it is the only one (4430.9) that can be directly associated with the water resources from the regions of Prades and the Montseny, indicating that the individual spent its childhood in one of these regions.

CHAPTER 5: DISCUSSION AND CONCLUSIONS

The results presented in this PhD project have yielded comprehensive analyses concerning burial customs, social structures, biological profiles, health status, lifestyles, dietary habits, and mobility patterns from three case studies: Gird Lashkir, Gir-e Gomel, and Plaça de la Gardunya. The sites, located in northern Mesopotamia and northeastern Iberia, underwent similar politico-economic processes regarding early urbanism and increasing social complexity. However, they were ruled by distinct social dynamics in very different geographic locations. These disparities have functioned as exemplary case studies, facilitating the evaluation of the efficacy of a multidisciplinary approach in elucidating the presence or absence of social inequalities reflected in human bones.

The methodologies employed have yielded favorable outcomes in achieving the objectives delineated for the present study. The subsequent sections will synthesize the results and interpretation of the data.

5.1 Burial practices

The burial customs at Gird Lashkir, Gir-e Gomel, and Plaça de la Gardunya reflect varying degrees of ritual complexity, spatial organization, and labor investment in grave typologies. In the regions of Gird Lashkir and Gir-e Gomel, the predominant grave typology consists of the simple pit, which is characterized by its oval shape. Only one mudbrick chamber has been identified at Gird Lashkir, where an elderly male of high status was interred within the walls of a disused room from a pluricellular house. Gir-e Gomel exhibits a greater prevalence of burials with an irregular shape, though these tend to an oval shape. Archaeothanatological analyses have revealed the presence of comfort elements within certain burials from Gird Lashkir and Gir-e Gomel, including reed mats and cushions.

In Plaça de la Gardunya, the simple pit is also present, but it is only in its initial use as a necropolis that it is observed. It has been established that only subadult individuals were buried in this fashion and in that specific area. The location of the adults' burials remains unknown. The development of more sophisticated graves included the construction of hypogea, which featured an access shaft, and single or double chamber. Within the chambers, successive inhumations were conducted in primary deposits, resulting in the transformation of the deceased into secondary deposits following the arrival of additional deceased individuals within the chambers. Each chamber was used for an extended period, with a minimum of 100 individuals occupying

each. A higher labor investment in the construction of the graves is observed in Plaça de la Gardunya in comparison to Gird Lashkir and Gir-e Gomel. However, the labor investment in both northern Mesopotamian sites is evidenced by their ornaments and grave goods.

5.2 SOCIAL ORGANIZATION

While evidence of an unequal social organization is present in the burials in northern Mesopotamia, northeastern Iberia exhibits no social differences in terms of age, sex, or wealth. In the case of Gird Lashkir and Gir-e Gomel, a hierarchical social status has been observed through the analysis of the ornaments and grave goods. In Gird Lashkir, the social status of newborn individuals was distinct, and they were subject to a specific burial custom. This custom entailed inhumations within funerary urns without ornaments or grave goods. The presence of low social status has been identified in both sites, as evidenced by the absence of ornaments and grave goods. The middle social status is comprised of only a few individuals, in which comfort elements and modest grave goods, such as animal offerings or pottery vessels, were placed inside the burials. The highest social status is characterized by the ownership of comfort elements, ornaments composed of copper, bronze, and silver, semi-precious stones, exotic shells (such as diadems, necklaces, pendants, bracelets, rings, and belts), along with grave goods such as pottery vessels, razors, and cylinder seals. The importation of materials that conform to the ornamental assemblage indicates complex socio-political structures in which trading networks played a crucial role in the acquisition of elements of prestige.

The possession of cylinder seals exhibiting shared geometric patterns served as symbols of lineage and of product provenance. These seals indicate that the owner played a significant role in the exchange networks of Mesopotamia and beyond. In Gird Lashkir, certain cylinder seals are found in conjunction with trapezoidal pendants crafted from amygdaloidal basalt, a distinctive feature observed primarily in female and child burials. This combination is exclusive to the highest social stratum within the community. The presence of child burials with higher status further suggests that social status was ascribed and possibly hereditary.

At Plaça de la Gardunya, funerary practices are focused on collective burial spaces, particularly hypogea, which were reused over long periods of time. The emphasis here is not on individual identity but on collective memory. No grave goods or ornaments could be associated with specific individuals, and no deceased was treated differently in any burial context. Therefore, an

equal social organization is proposed for this community. However, the presence of V-shaped perforated buttons in a subset of individuals raises the possibility of subtle status distinctions or kin affiliations that warrant further genetic investigation.

5.3 HEALTH AND LIFESTYLE

The health status and lifestyle of the individuals from Gird Lashkir have been positively assessed due to the application of standardized archaeothanatological and anthropological methodologies since the excavation process. The high prevalence of oral pathologies, including caries, dental calculus, defects of the enamel hypoplasia, tooth attrition, and periodontal disease, indicates chronic dietary stress and poor oral hygiene, potentially linked to the consumption of carbohydrate-rich foodstuffs. The presence of linear tooth enamel hypoplasias is indicative of systemic malnutrition or psychosocial stress episodes that occurred during early childhood. Caries has exhibited a higher prevalence among female than male individuals. This tendency has been observed since the Neolithic period. Hormonal fluctuations and the consumption of carcinogenic foodstuffs, such as sticky carbohydrates, have been proposed as causative factors. Pulmonary diseases were prevalent among Gird Lashkir's individuals, as evidenced by the new periosteal reactive bone formation in the caudal edges of the ribs. The presence of osteoporosis and degenerative osteoarthritis was less frequent.

Skeletal evidence indicates that adult individuals engaged in labor-intensive lifestyles. The most prevalent activities involved the upper and lower limbs, including the manipulation and holding of tools, as well as walking and jumping activities.

Due to the compromised preservation of skeletal remains at Gir-e Gomel and Plaça de la Gardunya, comprehensive paleopathological analysis was limited. Nevertheless, initial observations from Plaça de la Gardunya reveal skeletal manifestations of congenital rickets, suggesting vitamin D deficiencies and possible metabolic disorders. These conditions, coupled with periosteal reactions, indicate a community exposed to environmental or nutritional stressors, which future research may explore more thoroughly.

5.4 DIETARY PATTERNS THROUGH DENTAL MICROWEAR ANALYSIS

The analysis of the buccal microwear pattern from the populations of Gird Lashkir, Gir-e Gomel, and Plaça de la Gardunya has yielded highly favorable results. The analysis of the abrasiveness of consumed foodstuffs has facilitated the identification of distinct dietary trends. The use of datasets from known diets has enabled the classification of microwear patterns from each individual into a specific diet, including the carnivore diet, which includes the consumption of terrestrial or marine animals (or both), the vegetarian diet, and the omnivore diet. The classification at the population level has facilitated the discernment of the dietary tendencies of the distinct societies. The analysis at the individual level has also enabled the observation of dietary trends between different individuals, with the aim of investigating whether any differences arise in terms of age, sex, or social status. Conducting analyses with the potential to exceed the capacity to provide explanations for the entire population represents a significant advancement in the field of archaeology. This is due to the fact that analyses conducted at the individual level offer a greater degree of detail in defining the lives of people from the past.

The application of buccal dental microwear analysis has yielded novel insights into the dietary behaviors of the populations studied. Both Gird Lashkir and Gir-e Gomel displayed microwear patterns consistent with an omnivorous diet, characterized by medium striation densities and moderate average lengths. This aligns with archaeological expectations for agro-pastoral communities engaging in mixed subsistence strategies.

Significant intrapopulation variability was identified. At Gird Lashkir, females exhibited a broader dietary spectrum, with some individuals (Graves 4 and 10) showing microwear indicative of aquatic animal protein consumption. Males, on the other hand, exhibited patterns suggesting a stronger reliance on plant-based, abrasive foods. Subadults displayed the most abrasive patterns, likely due to the consumption of processed abrasive foodstuffs with tools that released grit material, such as saddle querns.

The Linear Discriminant Analysis (LDA) classified most individuals into the omnivorous category, with subadults and some adults trending toward vegetarianism. These findings provide a robust framework for understanding dietary variability within and between populations, contributing to broader discussions of food access, gendered consumption, and social roles in prehistoric communities.

Interestingly, individuals from Plaça de la Gardunya exhibited higher striation densities but slightly shorter average lengths, indicating a diet composed of fibrous and processed plant materials, possibly influenced by agricultural intensification or socio-cultural preferences in food preparation.

To summarize, the evidence from the three case studies indicates that differential access to food resources is not attributed to factors such as age, sex, and social status.

5.5 DIETARY PATTERNS THROUGH STABLE ISOTOPE ANALYSES

The low success rate in collagen extraction has posed significant challenges, thereby hindering the capacity to conduct comprehensive analyses on the individuals from Gird Lashkir. Gir-e Gomel has demonstrated a higher degree of efficacy in the extraction of bone collagen, with applications in both human and animal bones. This has enabled the execution of carbon and nitrogen stable isotope analysis, facilitating the interpretation of dietary patterns. Despite the fact that a number of samples do not fully align with the stipulated quality control criteria, it is imperative to acknowledge the critical nature of the preservation state of bones in this region. In order to conduct these types of analyses, it is essential to expand the range of samples available for study.

In order to interpret dietary patterns, it has been necessary to adopt an alternative sampling method consisting of tooth enamel hydroxyapatite. Given its inorganic composition and the dimensions of its crystal lattice, which renders it less susceptible to diagenetic alteration, the analysis of carbonates from tooth enamel hydroxyapatite is also appropriate. This sample type has demonstrated a 100% success rate, thereby enabling the augmentation of the sample size from 1 to 11 in the case of Gird Lashkir and from 34 to 60 individuals in the case of Plaça de la Gardunya.

For samples belonging to northern Mesopotamia, the analysis of bone collagen from humans and animals has provided $\delta^{13}C$ stable isotope signatures that are associated with values from C_3 plants. This result is coherent with the archaeobotanical species identified in sites such as Gird Lashkir, as taxonomical identification of charred botanical remains indicates the presence of an extensive cultivation of cereal crops that consists of einkorn wheat (*Triticum monococcum*), emmer wheat (*Triticum dicoccum*), and barley (*Hordeum vulgare*), lentil crops (*Lens culinaris*), and

the occasional gathering of wild legumes such as medick (*Medicago* sp.), ray-podded medick (*M. radiata*), *Trigonella* sp., milkvetch (*Astragalus* sp.), as well as fruits like fig (*Ficus carica*) (Molist, Breu, et al., 2019a). Humans and animals would consume the same plant species.

Signatures of $\delta^{15}N$ stable isotopes for human individuals are enriched in comparison to local animals, suggesting that they were consuming local domesticated herbivore species. Data is coherent with the archeozoological remains recovered at sites such as Gird Lashkir, which have identified herds of goats (*Capra hircus*), sheep (*Ovis aries*), pigs (*Sus domesticus*), cattle (*Bos taurus*), and equids (*Equus* sp., and *Equus hemionus*). The abundance of remains indicates a prevalent consumption of pig, followed by goat, and to a lesser extent, cattle and sheep were consumed (Molist et al., 2023). Slaughter patterns suggests the consumption of meat and dairy products (Molist, Breu, et al., 2019b; Molist, Gómez-Bach, et al., 2019). Not only domestic species would have been consumed, but also some hunted species such as wild goat (*Capra aegagrus*), gazelle (*Gazella gazella*), and hare (*Lepus* sp.). The consumption of gastropods, bivalves, and crustaceans has been proposed (Molist, Breu, et al., 2019b), but this hypothesis must be ruled out. A slight difference in terms of age and sex arise, as adult male individuals exhibit higher animal protein consumption than female and subadult individuals.

For samples belonging to northeastern Iberia, isotopic signatures of $\delta^{13}C$ and $\delta^{15}N$ suggest an omnivorous diet consisting of the consumption of C_3 plants, alongside with animal protein in form of meat and dairy products, originating from domestic herbivorous and omnivore livestock. These results coincide with the archaeobotanical species identified in northeastern Iberia, which consist of different varieties of wheat (*Triticum aestivum*, *Triticum durum*, *Triticum dicoccum* and *Triticum compactum*), of barley (*Hordeum vulgare* and *Hordeum vulgare nudum*), and legumes such as bitter vetch (*Vicia ervilia*), broad bean (*Vicia faba*), and pea (*Pisum sativum*) (Alonso, 1997, 2000). They also align with the animal taxa identified in the territory, which included mainly herbivore livestock composed of pigs (*Sus domesticus*), bovids (*Bos taurus*), ovicaprids (*Ovis aries* and *Capra hircus*), and equids (*Equus caballus*), as well as hunted species, such as deer (*Cervus elaphus*), fallow deer (Dama dama), rabbit (*Oryctolagus cuniculus*), hare (*Lepus* sp.), fox (*Vulpes vulpes*), and wild boar (*Sus scrofa*) (Andúgar Martínez & Saña Seguí, 2004). Isotopic signatures also align with the sporadic consumption of animal protein originating from marine and freshwater environments. The archaeological record has identified the collection of gastropods (*Patella* sp.) and bivalvia (*Glycymeris glycymeris*, and *Acanthocardia tuberculata*) species, which coincide with the results provided by the stable isotopic analysis.

5.6 RESIDENCE PATTERNS THROUGH STABLE ISOTOPE ANALYSES

The integration of oxygen and strontium isotope analyses revealed distinct mobility patterns across the examined populations. At Gird Lashkir, isotopic evidence identified two non-local individuals among the burial assemblage: a child individual from Grave 6, and an adult male from Grave 12. Their strontium signatures deviated from the local geological baseline, indicating their probable origins in geographically distant regions. Specifically, the isotopic profile of the child individual suggested early childhood residence in the Nineveh vicinity or northeastern Syrian territories, while the adult male's signature indicated an early childhood residence in the geographical area extending from Erbil in Iraqi Kurdistan to Lake Van in southeastern Anatolia.

The Gir-e Gomel population demonstrated isotopic signatures consistent with a broader geographical territory spanning from southeastern Turkey to northeastern Iraq, particularly the region from Lake Van to Bestansur. However, the complex geological composition of northern Mesopotamia presents interpretive challenges, as the strontium isotope ratios across this extensive territory exhibit minimal variation, thereby limiting the precision of geographical provenance determinations.

Regarding hydrological resources, the population of Gird Lashkir derived their water supply from the Tigris River system, supplemented by regional groundwater sources near Erbil. The local Gir-e Gomel inhabitants accessed water from proximate sources, including the Gomel River and seasonal watercourses within their immediate environment.

The isotopic analysis of the Plaça de la Gardunya assemblage identified seven individuals (4174, 4319.2, 4328.6, 4389.13, 4389.14, 4389.20, and 4389.21) as potentially non-local based on their strontium signatures. Through comparison with published strontium isoscapes, four individuals (4174, 4319.2, 4328.6, and 4389.21) exhibited signatures characteristic of the Barcelona and Girona territories. Additionally, individuals 4174 and 4319.2 demonstrated compatibility with isotopic signatures from central and western Iberian regions, suggesting possible origins across a broader geographical range. However, this last hypothesis is less probable than considering a northeastern Iberian origin.

One individual (50574.9), classified as local, displays strontium values consistent with the territories of Lleida, Alicante, Castellón, and Valencia according to isoscape projections. The remain-

ing individuals exhibit isotopic signatures characteristic of northeastern Iberian territories, encompassing Lleida, Tarragona, Barcelona, and Girona, which corroborate the interpretations derived from oxygen isotope analysis.

The oxygen isotope data suggests that local individuals obtained their childhood water resources from hydrological sources consistent with Catalonian regional signatures. A singular individual (4430.9) presented a distinctive oxygen isotopic signature that diverged from the population norm, with values directly correlating to water resources from the Prades and Montseny regions, indicating childhood residence in one of these specific geographical areas.

5.7 CONCLUSION

In summary, the burial data from Gird Lashkir, Gir-e Gomel, and Plaça de la Gardunya reveal diverse narratives of life, death, and society in prehistoric communities. This study demonstrates the efficacy of multidisciplinary approaches in elucidating complex social realities embedded within the skeletal remains of deceased individuals. The three case studies have demonstrated their suitability for all the methodologies conducted, providing reliable and detailed insights on matters of inequality and social complexity.

While archaeothanatological and anthropological analyses have observed the presence of hierarchical social statuses in northern Mesopotamia through the quantity and variety of ornaments and grave goods, dental microwear and stable isotopic analyses have determined that a generalized egalitarian access to foodstuffs was ensured in the studied communities. The study of dietary preferences reveals that male individuals exhibit a slightly higher consumption of animal protein than their female individuals. For the northeastern region of the Iberian Peninsula, archaeothanatological and anthropological analyses have determined an egalitarian social organization with no differential access to foodstuffs.

Stable isotopic analyses have been instrumental in establishing novel proxies for the animal and plant species consumed by the population at both the individual and community levels. These findings align with the archaeobotanical and archeozoological records obtained from both regional contexts. The analysis of oxygen and strontium stable isotopes has also enabled the ob-

servation of mobility patterns, thereby facilitating the differentiation between individuals considered to be local and non-local to the sites in question. The results of the study indicated a high degree of mobility within neighboring territories.

The results obtained from the various methodologies employed indicate a paucity of data for the studied territories with regard to dental microwear analyses and detailed isoscape maps. Subsequent research endeavors should prioritize the expansion of datasets from neighboring sites to enhance the interpretation of results. Complementary analyses, including ancient DNA and organic residue analyses, will be of significant importance in providing detailed information about the life of the studied communities.

REFERENCES

Abbood, A. K., Abdullah, E. J., & Al-Paruany, K. B. (2024). Distribution of Environmental Isotopes 18O and 2H in Water Resources in the Al-Taji Area, Northern Baghdad, Iraq. *Iraqi Geological Journal*, *57*(1), 111–119. https://doi.org/10.46717/igj.57.1A.10ms-2024-1-21

Acsádi, Gy., & Nemeskéri, J. (1970). *History of human life span and mortality*. Akadémiai Kiadó.

Aebersold, R., & Goodlett, D. R. (2001). Mass Spectrometry in Proteomics. *Chemical Reviews*, *101*(2), 269–296. https://doi.org/10.1021/cr990076h

Aguelo, J., & Huertas, J. (2006). *Memòria de la intervenció arqueològica al solar del Mercat de Santa Caterina, Ciutat Vella (Barcelona, Barcelonès)*.

Ahmed, M. A., Mirza, T. A., & Kalaitzidis, S. P. (2023). Petrography and geochemistry of the Baska Piwaza ore mineralization, Halgurd Mountain, Iraqi Kurdistan Region: Insights on the Genesis. *The Iraqi Geological Journal*, *56*(2B), 114–136. https://doi.org/10.46717/igj.56.2B.9ms-2023-8-18

Alabadi, M. A. A., & Alshamma'a, A. M. (2015). Using Environmental Isotopes for Water Resources Evaluation in Altun Kopri Basin, NE Kirkuk. In *Iraqi Journal of Science* (Vol. 56, Issue 2B).

Al-Ani, Z., Tham, J.-L., Ooi, M. W. X., Wright, A., Ricks, M., & Watts, A. C. (2022). The radiological findings in complex elbow fracture-dislocation injuries. *Skeletal Radiology*, *51*(5), 891–904. https://doi.org/10.1007/s00256-021-03900-x

Alcalde, G., Molist, M., Montero, I., Planagumà, L., Saña, M., & Toledo, A. (1998). Producciones metalúrgicas en el nordeste de la Península Ibérica durante el III milenio cal. AC: el taller de la Bauma del Serrat del Pont (Tortellà, Girona). *Trabajos de Prehistoria*, *55*(1), 81–100.

Al-Gburi, H. F., Al-Tawash, B. S., Al–Tamimi, O. S., & Schüth, C. (2022). Stable isotope composition in precipitation and groundwater of Shwan Sub-Basin, Kirkuk governorate, northeast of Iraq. *Water Supply*, *22*(10), 7442–7459. https://doi.org/10.2166/ws.2022.327

Ali, K. K., Al-Kubaisi, Q. Y., & Al-Paruany, K. B. (2015). Isotopic study of water resources in a semi-arid region, western Iraq. *Environmental Earth Sciences*, *74*(2), 1671–1686. https://doi.org/10.1007/s12665-015-4172-6

Al-Kubaisi, Q. Y., & Hassan, A. S. (2021). Isotopic and hydrochemical study of groundwater in an area between the lesser zab and tigris river, Northern Iraq. *Iraqi Geological Journal*, *54*(1F), 44–50. https://doi.org/10.46717/igj.54.1F.5ms-2021-06-25

Almagro-Gorbea, M. (1997). La Edad del Bronce en la Península Ibérica: periodización y cronología. *SAGVNTVM (Papeles Del Laboratorio de Arqueología de Valencia)*, *30*, 217–229.

Al-Naseri, S. K., Falih, A. H., & Kumar, U. S. (2022). Moisture sources and spatio-temporal variation of isotopic signatures in Iraqi precipitation. *Environmental Earth Sciences*, *81*(18). https://doi.org/10.1007/s12665-022-10559-7

Alonso, N. (1997). *Agricultura a la plana occidental catalana durant la protohistòria*. Universitat de Lleida.

Alonso, N. (2000). Registro arqueobotánico de Cataluña Occidental durante el II y I milenio A.N.E. *Complutum*, *11*, 221–238.

Alonso, N., & López, J. B. (2000). Minferri (Juneda, Garrigues): un nou tipus d'assentament a l'aire lliure a la plana occidental catalana, durant la primera meitat del segon mil·lenni cal. BC. *Tribuna d'Arqueologia*, *1997–1998*, 279–306.

Al-Paruany, K. B., Al-Naseri, S., & Al-Ajena, A.-H. F. (2017). Distribution of environmental isotopes in the euphrates river between qaim – Falluja, western Iraq. *Iraqi Geological Journal*, *50*(1), 12–27. https://doi.org/10.46717/igj.50.1.2ms-2017-06-24

AlQahtani, S. J., Hector, M. P., & Liversidge, H. M. (2010). Brief communication: The London atlas of human tooth development and eruption. *American Journal of Physical Anthropology*, *142*(3), 481–490. https://doi.org/10.1002/ajpa.21258

Alrousan, M., Al-Shorman, A., Galbany, J., & Pérez-Pérez, A. (2013). Buccal dental microwear and stable isotopes of El Collado: A mesolithic site from Spain. *Bulletin of the International Association for Paleodontology*, *7*(1), 4–11.

Ambrose, S. H. (1990). Preparation and characterization of bone and tooth collagen for isotopic analysis. *Journal of Archaeological Science*, *17*(4), 431–451. https://doi.org/10.1016/0305-4403(90)90007-R

Ambrose, S. H., & Norr, L. (1993). Experimental Evidence for the Relationship of the Carbon Isotope Ratios of Whole Diet and Dietary Protein to Those of Bone Collagen and Carbonate. In J. B. Lambert & G. Grupe (Eds.), *Prehistoric Human Bone* (pp. 1–37). Springer. https://doi.org/10.1007/978-3-662-02894-0_1

Amin-Rasouli, H., Moradi, M., & Baleshabadi, Z. S. (2021). Geochemistry, S and Sr isotopes and origin of the Shahneshin barite deposit, NW Kurdistan Province, Iran. *Journal of Economic Geology*, *13*(4), 789–815. https://doi.org/10.22067/ECONG.2021.51781.85753

Andúgar Martínez, L., & Saña Seguí, M. (2004). La gestió ramadera durant el segon mil·lenni. *Cypsela*, *15*, 209–228.

Arrivabeni, M. (2019). Pottery. In E. Rova (Ed.), *ARCANE - Associated Regional Chronologies for the Ancient Near East and the Eastern Mediterranean - Tigridian Region* (Vol. 5, pp. 45–129). Brepols.

Ayarzagüena Sanz, M. (2000). Surgimiento y creación del concepto de Mesolítico. *Espacio, Tiempo y Forma. Serie I, Prehistoria y Arqueología*, *13*, 11–32.

Bahn, P. (2008). *Arqueología. Conceptos clave* (C. Renfrew & P. Bahn, Eds.). Ediciones Akal S.A.

Bakr Othman, A., & Ali Mahmood, A. (2023). The Nineveh 5 pottery at Tell Lashkr (analytic and technical study). *Qalaai Zanist Scientific Journal*, *8*(1), 783–819. https://doi.org/10.25212/lfu.qzj.8.1.29

Balaguer, P., Hinojo, E., Oliart, C., & Soriano, I. (2011). Tecnología metalúrgica prehistórica en el nordeste de la Península Ibérica: el caso de las "hachas planas." In J. M. Mata-Perelló, L. Torró i Abat, & M. N. Fuentes prieto (Eds.), *Actas del V Congreso Internacional sobre minería y metalurgia históricas en el suroeste europeo (León - 2008). Libro en homenaje a Claude Domergue* (pp. 159–168). Sociedad Española para la Defensa del Patrimonio Geológico y Minero.

Barceló, J. A. (2008). La seqüència crono-cultural de la prehistòria catalana. Anàlisi estadística de les datacions radiomètriques de l'inici de l'Holocè a l'Edat del Ferro. *Cypsela*, *17*, 65–88.

Baxarias, J., & Herrerín, J. (2008). *The handbook atlas of paleopathology*. Libros Pórtico.

Bea, F., Mazhari, A., Montero, P., Amini, S., & Ghalamghash, J. (2011). Zircon dating, Sr and Nd isotopes, and element geochemistry of the Khalifan pluton, NW Iran: Evidence for Variscan magmatism in a supposedly Cimmerian superterrane. *Journal of Asian Earth Sciences*, *40*(1), 172–179. https://doi.org/10.1016/j.jseaes.2010.08.005

Bell, L. S., Lee-Thorp, J. A., & Dobney, K. (2006). Mapping Human Movement using Stable Oxygen Isotopic Ratio Mass Spectrometry: Potential Application to Forensic Science Demonstrated by a Modern Horse-Human Study. *Canadian Society of Forensic Science Journal*, *39*(2), 47–54. https://doi.org/10.1080/00085030.2006.10757136

Bernaerts, A., Vanhoenacker, F. M., Hintjens, J., Chapelle, K., Salgado, R., De Foer, B., & De Schepper, A. M. (2006). Tumors and tumor-like lesions of the jaw part II: mixed and radiopaque lesions. *JBR-BTR*, *89*(2), 35–43.

Bieliński, P. (2010). Tell Arbid. Preliminary Report on the Results of the Twelfth Season of Syrian-Polish Excavations. *Polish Archaeology in the Mediterranean*, *19*, 537–554.

Bieliński, P. (2012). Tell Arbid 2008-2009. Preliminary Report on the Results of the Thirteenth and Fourteenth Seasons of Polish-Syrian Excavations. *Polish Archaeology in the Mediterranean*, *21*, 511–536.

Blaizot, F. (2022). Methodological Guidelines for Archaeothanatological Practice. In C. J. Knüssel & E. M. J. Schotsmans (Eds.), *The Routledge Handbook of Archaeothanatology* (pp. 22–41). Routledge. https://doi.org/10.4324/9781351030625-3

Bofill, M. (2016). Les indústries macrolítiques. In A. Gómez & M. Molist (Eds.), *La prehistòria al pla de Barcelona. Documents per a una nova síntesi* (pp. 117–123). Ajuntament de Barcelona, Institut de Cultura, Museu d'Història de Barcelona.

Bolt, D., & Green, A. (2003). The Burial of the Dead. In E. Rova & H. Weiss (Eds.), *The Origins of North Mesopotamian Civilization: Ninevite 5 Chronology, Economy, Society: Vol. Subartu IX* (pp. 519–562). Brepols.

Boquer, S., Gonzálvez, L., Mercadal, O., Rodon, T., & Sáenz, L. (1990). Les estructures del Bronze Antic - Bronze Mitjà al jaciment arqueològic de Can Roqueta (Sabadell, Vallès Occidental). *Arraona*, *7, III Època*, 9–25.

Bordas, A. (2016). El jaciment de Nou de la Rambla 82. In A. Gómez & M. Molist (Eds.), *La prehistòria al pla de Barcelona. Documents per a una nova síntesi* (pp. 196–198). Ajuntament de Barcelona, Institut de Cultura, Museu d'Història de Barcelona.

Boulestin, B. (2022). A Tale of Two Worlds. Terminologies in archaeothanatology. In C. J. Knüsel & E. M. J. Schotsmans (Eds.), *The Routledge Handbook of Archaeothanatology* (pp. 42–54). Routledge. https://doi.org/10.4324/9781351030625-4

Brandt, L. Ø., Haase, K., & Collins, M. J. (2018). Species identification using ZooMS, with reference to the exploitation of animal resources in the medieval town of Odense. *Danish Journal of Archaeology*, *7*(2), 139–153. https://doi.org/10.1080/21662282.2018.1468154

Breu, A., Alcántara, R., Arnaiz, R., Colomer, F., Moya, A., & Sisa, J. (2019). Detection, recovery and analysis of visible bitumen residues in pottery from Tell Lashkir, Kurdistan, Iraq. *Los Tiempos Cambian. De La Piedra al Teclado. Actas de Las X Jornadas de Jóvenes En Investigación Arqueológica. JIA 2017 (Burgos, 7-10 de Junio de 2017)*, 566–677.

Breu, A., Rosell-Melé, A., Molist, M., & Bach-Gómez, A. (2022). Bayesian mixing models as a tool to explore Bronze Age bitumen trade from Tell Lashkir (Erbil, Iraq). *Journal of Archaeological Science*, *145*, 105643. https://doi.org/10.1016/j.jas.2022.105643

Brooks, S., & Suchey, J. M. (1990). Skeletal age determination based on the os pubis: a comparison of the Acsádi-Nemeskéri and Suchey-Brooks methods. *Human Evolution*, *5*(3), 227–238.

Brothwell, D. R. (1981). *Digging up bones: the excavation, treatment, and study of human skeletal remains* (3rd ed.). Cornell University Press.

Buckley, M. (2018). Zooarchaeology by Mass Spectrometry (ZooMS) Collagen Fingerprinting for the Species Identification of Archaeological Bone Fragments. In C. Giovas & M. LeFebvre (Eds.), *Zooarchaeology in Practice* (pp. 227–247). Springer International Publishing. https://doi.org/10.1007/978-3-319-64763-0_12

Buckley, M., Collins, M., Thomas-Oates, J., & Wilson, J. C. (2009). Species identification by analysis of bone collagen using matrix-assisted laser desorption/ionisation time-of-flight mass spectrometry. *Rapid Communications in Mass Spectrometry*, *23*(23), 3843–3854. https://doi.org/10.1002/rcm.4316

Buckley, M., Whitcher Kansa, S., Howard, S., Campbell, S., Thomas-Oates, J., & Collins, M. (2010). Distinguishing between archaeological sheep and goat bones using a single collagen peptide. *Journal of Archaeological Science*, *37*(1), 13–20. https://doi.org/10.1016/j.jas.2009.08.020

Buikstra, J. E. (Ed.). (2019). *Ortner's Identification of Pathological Conditions in Human Skeletal Remains* (3rd ed.). Elsevier. https://doi.org/10.1016/C2011-0-06880-1

Buikstra, J. E., & Ubelaker, D. H. (1997). *Standards for data collection from human skeletal remains: proceedings of a seminar at the Field Museum of Natural History, organized by Jonathan Haas* (3rd ed., Vol. 44). Arkansas Archeological Survey.

Burton, J. H., & Hahn, R. (2016). Assessing the "Local" 87Sr/86Sr Ratio for Humans. In G. Grupe & G. McGlynn (Eds.), *Isotopic Landscapes in Bioarchaeology* (pp. 113–121). Springer Berlin Heidelberg. https://doi.org/10.1007/978-3-662-48339-8_6

Burton, J., & Katzenberg, M. A. (2019). Strontium isotopes and the chemistry of bones and teeth. In M. A. Katzenberg & A. L. Grauer (Eds.), *Biological Anthropology of the Human Skeleton* (3rd ed., pp. 505–514). John Wiley & Sons, Inc. https://doi.org/10.1002/9781119151647.ch15

Calandra, I., Pedergnana, A., Gneisinger, W., & Marreiros, J. (2019). Why should traceology learn from dental microwear, and vice-versa? *Journal of Archaeological Science*, *110*, 105012. https://doi.org/10.1016/j.jas.2019.105012

Calderone, L., & Weiss, H. (2003). The End of the Ninevite 5 Period at Tell Leilan. In E. Rova & H. Weiss (Eds.), *The Origins of North Mesopotamian Civilization: Ninevite 5 Chronology, Economy, Society* (Vol. 9, pp. 193–220). Brepols.

Camacho, N. P., Rinnerthaler, S., Paschalis, E. P., Mendelsohn, R., Boskey, A. L., & Fratzl, P. (1999). Complementary information on bone ultrastructure from scanning small angle X-ray scattering and Fourier-transform infrared microspectroscopy. *Bone*, *25*(3), 287–293. https://doi.org/10.1016/S8756-3282(99)00165-9

Cano-Rocabayera, O., Maceda-Veiga, A., & de Sostoa, A. (2015). Fish fins and scales as non-lethally sampled tissues for stable isotope analysis in five fish species of north – eastern Spain. *Environmental Biology of Fishes*, *98*(3), 925–932. https://doi.org/10.1007/s10641-014-0328-6

Carlús, X., González, J., & Nadal, E. (2010). Estructures de l'Edat del Bronze tipus grill plan al litoral de Barcelona. *Cypsela*, *18*, 157–169.

Carlús, X., & Nadal, E. (2008). Carrer de la Riereta, 37-37 bis: un nou assentament prehistòric al pla de Barcelona. Primers resultats. *Cypsela*, *17*, 91–114.

Chambon, P. (2016). Les pràctiques funéraires : évolution du rituel. In A. Gómez Bach & M. Molist Montaña (Eds.), *La prehistòria al pla de Barcelona. Documents per a una nova síntesi* (pp. 141–150). Ajuntament de Barcelona, Institut de Cultura, Museu d'Història de Barcelona.

Chenery, C. A., Pashley, V., Lamb, A. L., Sloane, H. J., & Evans, J. A. (2012). The oxygen isotope relationship between the phosphate and structural carbonate fractions of human bioapatite. *Rapid Communications in Mass Spectrometry*, *26*(3), 309–319. https://doi.org/10.1002/rcm.5331

Chesson, L. A., Ehleringer, J. R., & Cerling, T. E. (2011). Light-Element Isotopes (H, C, N, and O) as Tracers of Human Diet: A Case Study on Fast Food Meals. In M. Baskaran (Ed.), *Handbook of Environmental Isotope Geochemistry* (pp. 707–723). Springer Verlag.

Coplen, T. B., Kendall, C., & Hopple, J. (1983). Comparison of stable isotope reference samples. *Nature*, *302*, 236–238.

Dahlberg, A. A., & Kinzey, W. (1962). Etude microscopique de l'abrasion et de l'attrition sur la surface des dents. *Bulletin Du Groupement International Pour La Recherche Scientifique En Stomatologie et Odontologie (Bruxelles)*, *5*, 242–251.

Daura, J., Sanz, M., Soriano, I., Pedro, M., Rubio, Á., Oliva, M., Gibaja, J. F., Queralt, I., Álvarez, R., & López-Cachero, F. J. (2017a). Objetos de oro, epicampaniforme en la cova del gegant relaciones en la costa mediterránea de la península ibérica durante la edad del bronce. *Trabajos de Prehistoria*, *74*(1), 149–167. https://doi.org/10.3989/tp.2017.12188

Daux, V., Lécuyer, C., Héran, M.-A., Amiot, R., Simon, L., Fourel, F., Martineau, F., Lynnerup, N., Reychler, H., & Escarguel, G. (2008). Oxygen isotope fractionation between human phosphate and water revisited. *Journal of Human Evolution*, *55*(6), 1138–1147. https://doi.org/10.1016/j.jhevol.2008.06.006

Davies-Barrett, A. M., Antoine, D., & Roberts, C. A. (2019). Inflammatory periosteal reaction on ribs associated with lower respiratory tract disease: A method for recording prevalence

from sites with differing preservation. *American Journal of Physical Anthropology*, *168*(3), 530–542. https://doi.org/10.1002/ajpa.23769

DeNiro, M. J. (1985). Postmortem preservation and alteration of in vivo bone collagen isotope ratios in relation to palaeodietary reconstruction. *Nature*, *317*(6040), 806–809. https://doi.org/10.1038/317806a0

Díaz-del-Río, P., Uriarte, A., Becerra, P., Pérez-Villa, A., Vicent, J. M., & Díaz-Zorita, M. (2022). Paleomobility in Iberia: 12 years of strontium isotope research. *Journal of Archaeological Science: Reports*, *46*, 103653. https://doi.org/10.1016/j.jasrep.2022.103653

Díaz-del-Río, P., Waterman, A. J., Thomas, J. T., Peate, D. W., Tykot, R. H., Martínez-Navarrete, M. I., & Vicent, J. M. (2017). Diet and mobility patterns in the Late Prehistory of central Iberia (4000–1400 cal bc): the evidence of radiogenic (87Sr/86Sr) and stable (δ18O, δ13C) isotope ratios. *Archaeological and Anthropological Sciences*, *9*(7), 1439–1452. https://doi.org/10.1007/s12520-017-0480-y

Díaz-Teijeiro, M. F., Rodríguez-Arévalo, J., & Castaño, S. (2009). La Red Española de Vigilancia de Isótopos en la Precipitación (REVIP): distribución isotópica espacial y aportación al conocimiento del ciclo hidrológico. *Ingeniería Civil*, *155*, 87–97.

Dişli, E. (2018). Evaluation of Hydrogeochemical Processes for Waters' Chemical Composition and Stable Isotope Investigation of Groundwater/Surface Water in Karst-Dominated Terrain, the Upper Tigris River Basin, Turkey. *Aquatic Geochemistry*, *24*(5–6), 363–396. https://doi.org/10.1007/s10498-019-09349-8

Duday, H. (2009). *The Archaeology of the dead : lectures in archaeothanatology / Henri Duday ; translated by Anna Maria Cipriani and John Pearce*. Oxbow Books.

Dupras, T. L., & Schultz, J. J. (2014). Taphonomic Bone Staining and Color Changes in Forensic Contexts. In J. T. Pokines & S. A. Symes (Eds.), *Manual of forensic taphonomy* (pp. 315–340). CRC Press.

Ellegård, L., Alstad, T., Rütting, T., Johansson, P. H., Lindqvist, H. M., & Winkvist, A. (2019). Distinguishing vegan-, vegetarian-, and omnivorous diets by hair isotopic analysis. *Clinical Nutrition*, *38*(6), 2949–2951. https://doi.org/10.1016/j.clnu.2018.12.016

Elliott, S., Bendrey, R., Whitlam, J., Aziz, K. R., & Evans, J. (2015). Preliminary ethnoarchaeological research on modern animal husbandry in Bestansur, Iraqi Kurdistan: Integrating animal, plant and environmental data. *Environmental Archaeology*, *20*(3), 283–303. https://doi.org/10.1179/1749631414Y.0000000025

El-Zaatari, S. (2010). Occlusal microwear texture analysis and the diets of historical/prehistoric hunter-gatherers. *International Journal of Osteoarchaeology*, *20*(1), 67–87. https://doi.org/10.1002/oa.1027

Ericson, J. E. (1985). Strontium isotope characterization in the study of prehistoric human ecology. *Journal of Human Evolution*, *14*(5), 503–514. https://doi.org/10.1016/S0047-2484(85)80029-4

Eskildsen, K. R. (2019). Christian Jürgensen Thomsen (1788–1865): Comparing prehistoric antiquities. *History of Humanities*, *4*(2), 263–267. https://doi.org/10.1086/704813

Estebaranz, F., Martínez, L. M., Galbany, J., Turbón, D., & Pérez-Pérez, A. (2009). Testing hypotheses of dietary reconstruction from buccal dental microwear in Australopithecus afarensis. *Journal of Human Evolution*, *57*(6), 739–750. https://doi.org/10.1016/j.jhevol.2009.07.007

Estebaranz-Sánchez, F., Fernández Domínguez, E., Martínez Martínez, L., Gamba, C., Alrousan, M., Turbón, D., Oms, J. I., Pérez-Pérez, A., Anfruns, J., & Arroyo-Pardo, E. (2008). Anàlisi antropològica de les restes neolítiques de la caserna de Sant Pau (biometria, dentició, ADNA i mmicroestriació dentària). *Quarhis: Quaderns d'Arqueologia i Història de La Ciutat de Barcelona, ISSN 1699-793X, No. 4, 2008, Pags. 76-82*, *4*(Època II), 76–82.

Farooq, I., Ali, S., & Anderson, P. (2021). Dental Enamel. In I. Farooq, S. Ali, & P. Anderson (Eds.), *An Illustrated Guide to Oral Histology* (pp. 15–34). Wiley. https://doi.org/10.1002/9781119669616.ch2

Finkbeiner, U., Novak, M., Sakal, F., & Sconzo, P. (Eds.). (2015). *Associated Regional Chronologies for the Ancient Near East and the Eastern Mediterranean - Middle Euphrates* (Vol. 4). Brepols.

Flannery, K. V. (1973). Tombs for the living. *Man*, *8*, 177–193.

Forest, J.-D. (2003). The Ninevite 5 Culture: Its Nature and its Origins. In E. Rova & H. Weiss (Eds.), *The Origins of North Mesopotamian Civilization: Ninevite 5 Chronology, Economy, Society: Vol. Subartu IX* (pp. 563–584). Brepols.

France, C. A. M., & Owsley, D. W. (2015). Stable Carbon and Oxygen Isotope Spacing Between Bone and Tooth Collagen and Hydroxyapatite in Human Archaeological Remains. *International Journal of Osteoarchaeology*, *25*(3), 299–312. https://doi.org/10.1002/oa.2300

Fricke, H. C., O'Neil, J. R., & Lynnerup, N. (1995). SPECIAL REPORT: Oxygen isotope composition of human tooth enamel from medieval Greenland: Linking climate and society. *Geology*, *23*(10), 869. https://doi.org/10.1130/0091-7613(1995)023<0869:SROICO>2.3.CO;2

Friedman, I., & O'Neil, J. R. (1977). *Compilation of stable isotope fractionation factors of geochemical interest* (M. Fleischer, Ed.; 6th ed., Vols. 440-KK). US Geological Survey.

Fujii, H., Yoshikawa, M., Oguchi, H., Oguchi, K., & Numoto, K. O. H. (1989). Preliminary Report on the Excavations at Tell Thuwaij, Tell Jessary (second season), and Qasr Banat. *Sumer*, *42*, 38–59.

Fuller, B. T., Fuller, J. L., Sage, N. E., Harris, D. A., O'Connell, T. C., & Hedges, R. E. M. (2005). Nitrogen balance and δ15N: Why you're not what you eat during nutritional stress. *Rapid Communications in Mass Spectrometry*, *19*(18), 2497–2506. https://doi.org/10.1002/rcm.2090

Galbany, J., Garriga, N., Majoral, M., Coll, R., & Fluxà, J. (2008). Microdesgaste y patología dental en la población de la Edad de Bronce de "Mar i Muntanya" (Alella, Barcelona). *Rev. Esp. Antrop. Fís.*, *28*, 25–36.

Galbany, J., Martínez, L. M., & Pérez-Pérez, A. (2004). Tooth replication techniques, SEM imaging and microwear analysis in primates: methodological obstacles. *Anthropologie*, *42*(1), 5–12.

García-González, R., Sánchez-Puente, Z., Arsuaga, J. L., & Carretero, J. M. (2019). Dietary inferences from dental microwear patterns in Chalcolithic populations from the Iberian Peninsula: the case of El Portalón de Cueva Mayor (Sierra de Atapuerca, Burgos, Spain) and El

Alto de la Huesera (Álava, Spain). *Archaeological and Anthropological Sciences*, *11*(8), 3811–3823. https://doi.org/10.1007/s12520-018-0711-x

Garcia-Guixé, E., Subirà, M. E., Marlasca, R., & Richards, M. P. (2010). δ13C and δ15N in ancient and recent fish bones from the Mediterranean Sea. In *Journal of Nordic Archaeological Science* (Vol. 17).

Garcia-Ramis, F. X. (2024). *Spatial analysis of the Ninive 5 culture in northern Mesopotamia (3000-2500 BCE)* [Autonomous University of Barcelona]. https://doi.org/http://hdl.handle.net/10803/693211

Garvie-Lok, S. J., Varney, T. L., & Katzenberg, M. A. (2004). Preparation of bone carbonate for stable isotope analysis: The effects of treatment time and acid concentration. *Journal of Archaeological Science*, *31*(6), 763–776. https://doi.org/10.1016/j.jas.2003.10.014

Genovés, S. (1967). Proportionality of the long bones and their relation to stature among Mesoamericans. *American Journal of Physical Anthropology*, *26*(1), 67–77. https://doi.org/10.1002/ajpa.1330260109

Gluitz, A., Martínez, L. M., Molist, M., & Estebaranz-Sánchez, F. (2023). Diet in the Early Bronze Age: a buccal microwear analysis from the plain of Barcelona (Spain). *Archaeological and Anthropological Sciences*, *15*(10), 157. https://doi.org/10.1007/s12520-023-01855-9

Gómez, A., Bordas, A., Arroyo, S., Huertas, J., Aguelo, J., Velasco, A., González, J., Nadal, J., Saña, M., & Molist, M. (2015). Evidències arqueològiques de les comunitats humanes en la transició del III al II mil·lenni cal BC al Pla de Barcelona. *Quarhis: Quaderns d'Arqueologia i Història de La Ciutat de Barcelona*, *11*, 82–96.

Gómez, A., & Molist, M. (2016). La seqüència temporal dels hàbitats. In A. Gómez & M. Molist (Eds.), *La prehistòria al pla de Barcelona. Documents per a una nova síntesi* (pp. 75–90). Ajuntament de Barcelona, Institut de Cultura, Museu d'Història de Barcelona.

Gómez, A., Nadal, J., & Molist, M. (2014). El mar i les comunitats humanes al llarg de la prehistòria al Pla de Barcelona. *Barcelona Quaderns d'Història*, *21*, 63–76.

Gómez-Bach, A., Breu, A., Sisa, J., Mylona, P., Bradosty, Z., Zebari, A., & Molist, M. (2019). Singular deposits in Gird Lashkir (Erbil, Iraqi Kurdistan) at the beginning of the Early Bronze Age. *3rd International Scientific Conference - Archaeology and Heritage of Kurdistan (ISCAHKRD)*, 1–11. https://doi.org/10.31972/ISCAHKRD19.008

Granados, O., Puig, F., & Farré, R. (1993). La intervenció arqueològica a Sant Pau del Camp: un nou jaciment prehistòric al Pla de Barcelona. *Tribuna d'Arqueologia*, *1991–1992*, 27–38.

Gron, K. J., Gröcke, D. R., Groß, D., Rowley-Conwy, P., Robson, H. K., & Montgomery, J. (2024). Neolithisation through bone: Stable isotope analysis of human and faunal remains from Syltholm II, Lolland, Denmark. *Journal of Archaeological Science: Reports*, *53*, 104384. https://doi.org/10.1016/j.jasrep.2024.104384

Grossman, K. (2014). Ninevite 5 Ceramics. In M. Lebeau (Ed.), *ARCANE Interregional. Ceramics* (Vol. 1). Brepols.

Gruber, N. (2008). The Marine Nitrogen Cycle: overview and challeges. In D. G. Capone, D. A. Bronk, M. R. Mulholland, & E. J. Carpenter (Eds.), *Nitrogen in the Marine Environment* (2nd ed., pp. 1–50). Academic Press. https://doi.org/10.1016/B978-0-12-372522-6.00001-3

Guàrdia, M., & Francès, J. (2017). Les estructures de l'edat del bronze de la Plana del Castell - Parc de l'Alba (Cerdanyola del Vallès, Barcelona). *Revista d'Arqueologia de Ponent*, *27*, 81–115.

Guiry, E. J., & Szpak, P. (2020). Quality control for modern bone collagen stable carbon and nitrogen isotope measurements. *Methods in Ecology and Evolution*, *11*(9), 1049–1060. https://doi.org/10.1111/2041-210X.13433

Guiry, E. J., & Szpak, P. (2021). Improved quality control criteria for stable carbon and nitrogen isotope measurements of ancient bone collagen. *Journal of Archaeological Science*, *132*, 105416. https://doi.org/10.1016/j.jas.2021.105416

Gustafson, G., & Koch, G. (1974). Age estimation up to 16 years based on dental development. *Odontologisk Revy*, *25*, 297–306.

Hara, A. T., Livengood, S. V., Lippert, F., Eckert, G. J., & Ungar, P. S. (2016). Dental Surface Texture Characterization Based on Erosive Tooth Wear Processes. *Journal of Dental Research*, *95*(5), 537–542. https://doi.org/10.1177/0022034516629941

Hare, P. E., & Estep, M. L. F. (1983). Carbon and nitrogen isotopic composition of amino acids in modern and fossil collagens. *Carnegie Institution of Washington*, *Year Book 82*(1982–1983), 410–413.

Hatvani, I. G., Erdélyi, D., Vreča, P., & Kern, Z. (2020). Analysis of the Spatial Distribution of Stable Oxygen and Hydrogen Isotopes in Precipitation across the Iberian Peninsula. *Water*, *12*(2), 481. https://doi.org/10.3390/w12020481

Hedges, R. E. M. (2003). On bone collagen—apatite-carbonate isotopic relationships. *International Journal of Osteoarchaeology*, *13*(1–2), 66–79. https://doi.org/10.1002/oa.660

Heggeness, M. H., & Doherty, B. J. (1998). Morphologic Study of Lumbar Vertebral Osteophytes. *Southern Medical Journal*, *91*(2), 187–189.

Helwing, B. (2012). An age of heroes? Some thoughts on Early Bronze Age funerary customs in northern Mesopotamia. *First International Symposium of the Tübingen Post-Graduate School, Tubingen, Germany*.

Henderson, J., Evans, J., & Barkoudah, Y. (2009). The roots of provenance: glass, plants and isotopes in the Islamic Middle East. *ANTIQUITY*, *83*, 414–429.

Henriksen, K., & Karsdal, M. A. (2019). Type I collagen. In M. A. Karsdal (Ed.), *Biochemistry of Collagens, Laminins and Elastin* (2nd ed., pp. 1–12). Elsevier Academic Press. https://doi.org/10.1016/B978-0-12-817068-7.00001-X

Hermann, S., Eshed, I., Sáenz, I., Doepner, N., Ziegler, K., & Hermann, K. G. (2022). Osteo-Proliferative Lesions of the Phalanges on Radiography: Associations with Sex, Age, and Osteoarthritis. *Diagnostics*, *12*(3), 1–9.

Hernando, R. (2024). A comprehensive dataset and image-set for exploring buccal dental microwear in late prehistory farming groups from northeastern Iberian Peninsula. *Data in Brief*, *57*, 110929. https://doi.org/10.1016/j.dib.2024.110929

Hernando, R., Fernández-Marchena, J. L., Willman, J. C., Ollé, A., Vergès, J. M., & Lozano, M. (2020). Exploring the utility of optical microscopy versus scanning electron microscopy for

the quantification of dental microwear. *Quaternary International*, *569–570*, 5–14. https://doi.org/10.1016/j.quaint.2020.05.022

Hernando, R., Lozano, M., Ceperuelo, D., Alonso, S., & Vaquero, M. (2019). Los niños de La Cova de Valdavara (Becerreá, Lugo): Análisis morfológico, patológico y del microdesgaste dental. *Munibe Antropologia-Arkeologia*, *2019*(3), 207–218. https://doi.org/10.21630/maa.2019.70.17

Hernando, R., Moreno-Ibáñez, M. Á., Carbonell, E., Cebrià, A., Daura, J., Díez-Canseco, C., Edo, M., Fullola, J. M., Morales, J. I., Oms, F. X., Ramírez-Pedraza, I., Sanz, M., Subirá, M. E., Tornero, C., Vergès, J. M., & Lozano, M. (2024). Eating through time: Understanding dietary practices across late prehistory in the northeastern Iberian Peninsula. *American Journal of Biological Anthropology*, *184*(4). https://doi.org/10.1002/ajpa.24950

Hernando, R., Willman, J. C., Souron, A., Cebrià, A., Oms, F. X., Morales, J. I., & Lozano, M. (2022). What about the buccal surfaces? Dental microwear texture analysis of buccal and occlusal surfaces refines paleodietary reconstructions. *American Journal of Biological Anthropology*, *178*(2), 347–359. https://doi.org/10.1002/ajpa.24509

Hernando, R., Willman, J. C., Vergès, J. M., Vaquero, M., Alonso, S., Oms, X., Cebrià, A., Morales, J. I., & Lozano, M. (2020). Inferring childhood dietary maturation using buccal and occlusal deciduous molar microwear: a case study from the recent prehistory of the Iberian Peninsula. *Archaeological and Anthropological Sciences*, *12*(1), 30. https://doi.org/10.1007/s12520-019-00997-z

Hillson, S. (2014). Dental markers of disease and malnutrition. In *Tooth Development in Human Evolution and Bioarchaeology* (pp. 162–197). Cambridge University Press. https://doi.org/10.1017/cbo9780511894916.007

Hillson, S. (2023). *Dental Anthropology* (2nd ed.). Cambridge University Press. https://doi.org/10.1017/9781108381550

Hodos, T., Cartwright, C. R., Montgomery, J., Nowell, G., Crowder, K., Fletcher, A. C., & Gönster, Y. (2020). The origins of decorated ostrich eggs in the ancient Mediterranean and Middle East. *Antiquity*, *94*(374), 381–400. https://doi.org/10.15184/aqy.2020.14

Janzen, A., Richter, K. K., Mwebi, O., Brown, S., Onduso, V., Gatwiri, F., Ndiema, E., Katongo, M., Goldstein, S. T., Douka, K., & Boivin, N. (2021). Distinguishing African bovids using Zooarchaeology by Mass Spectrometry (ZooMS): New peptide markers and insights into Iron Age economies in Zambia. *PLOS ONE*, *16*(5), e0251061. https://doi.org/10.1371/journal.pone.0251061

Jarošová, I., Vávra, J., Jiřík, J., & Horáková, M. (2016). Buccal Dental Microwear of a Barbarian Population from Prague-Zličín – a Study of the Migration Period in the Czech Republic. *Interdisciplinaria Archaeologica - Natural Sciences in Archaeology*, *7*(1), 55–70. https://doi.org/10.24916/iansa.2016.1.3

Jim, S., Jones, V., Ambrose, S. H., & Evershed, R. P. (2006a). Quantifying dietary macronutrient sources of carbon for bone collagen biosynthesis using natural abundance stable carbon isotope analysis. *British Journal of Nutrition*, *95*(6), 1055–1062. https://doi.org/10.1079/BJN20051685

Karim, K. H., Khanaqa, P. A., & Babashekh, S. M. (2020). Revisiting the “Gercus Basalt within the Eocene Gercus Formation”: Implications for sedimentary origin of a basaltic body, Kurdistan Region, Northern Iraq. *Ore and Energy Resource Geology*, *4–5*, 100008. https://doi.org/10.1016/j.oreoa.2020.100008

Katzenberg, M. A., & Waters-Rist, A. L. (2019). Stable isotope analysis: a tool for studying past diet, demography, and life history. In M. A. Katzenberg & A. L. Grauer (Eds.), *Biological Anthropology of the Human Skeleton* (3rd ed., pp. 469–504). John Wiley & Sons, Inc. https://doi.org/10.1002/9781119151647.ch14

Kaygusuz, A., Aslan, Z., Aydınçakır, E., Yücel, C., Gücer, M. A., & Şen, C. (2018). Geochemical and Sr-Nd-Pb isotope characteristics of the Miocene to Pliocene volcanic rocks from the Kandilli (Erzurum) area, Eastern Anatolia (Turkey): Implications for magma evolution in extension-related origin. *Lithos*, *296–299*, 332–351. https://doi.org/10.1016/j.lithos.2017.11.003

Kellner, C. M., & Schoeninger, M. J. (2007). A simple carbon isotope model for reconstructing prehistoric human diet. *American Journal of Physical Anthropology*, *133*(4), 1112–1127. https://doi.org/10.1002/ajpa.20618

Kelly, J. F. (2000). Stable isotopes of carbon and nitrogen in the study of avian and mammalian trophic ecology. *Canadian Journal of Zoology*, *78*(1), 1–27. https://doi.org/10.1139/z99-165

Khojasteh, R. A., Kasiri, M. B., & Abedi, A. (2020). A preliminary study on the ancient migrations in Tepe Silveh Piranshahr, (North-western Iran) based on strontium isotopes of skeletons. *Mediterranean Archaeology and Archaeometry*, *20*(2), 35–44. https://doi.org/10.5281/zenodo.3752145

Kinnes, I. (1975). Monumental function in British Neolithic burial practices. *Worls Archaeology*, *7*(1), 16–29.

Kirby, D. P., Buckley, M., Promise, E., Trauger, S. A., & Holdcraft, T. R. (2013). Identification of collagen-based materials in cultural heritage. *Analyst*, *138*(17), 4849–4858. https://doi.org/10.1039/c3an00925d

Klaus, H. D., & Lynnerup, N. (2019). Abnormal Bone: Considerations for Documentation, Disease Process Identification, and Differential Diagnosis. In J. E. Buikstra (Ed.), *Ortner’s Identification of Pathological Conditions in Human Skeletal Remains* (pp. 59–89). Academic Press. https://doi.org/10.1016/B978-0-12-809738-0.00005-3

Knipper, C., Rihuete-Herrada, C., Voltas, J., Held, P., Lull, V., Micó, R., Risch, R., & Alt, K. W. (2020). Reconstructing Bronze Age diets and farming strategies at the early Bronze Age sites of La Bastida and Gatas (southeast Iberia) using stable isotope analysis. *PLOS ONE*, *15*(3), e0229398. https://doi.org/10.1371/journal.pone.0229398

Koch, P. L., Tuross, N., & Fogel, M. L. (1997). The Effects of Sample Treatment and Diagenesis on the Isotopic Integrity of Carbonate in Biogenic Hydroxylapatite. In *Journal of Archaeological Science* (Vol. 24).

Kono, T., Sakae, T., Nakada, H., Kaneda, T., & Okada, H. (2022). Confusion between Carbonate Apatite and Biological Apatite (Carbonated Hydroxyapatite) in Bone and Teeth. In *Minerals* (Vol. 12, Issue 2). MDPI. https://doi.org/10.3390/min12020170

Korte, C., Kozur, H. W., Joachimski, M. M., Strauss, H., Veizer, J., & Schwark, L. (2004). Carbon, sulfur, oxygen and strontium isotope records, organic geochemistry and biostratigraphy across the Permian/Triassic boundary in Abadeh, Iran. In *International Journal of Earth Sciences* (Vol. 93, Issue 4, pp. 565–581). https://doi.org/10.1007/s00531-004-0406-7

Krueger, H. W. (1991). Exchange of carbon with biological apatite. *Journal of Archaeological Science*, *18*(3), 355–361. https://doi.org/10.1016/0305-4403(91)90071-V

Krueger, H. W., & Sullivan, C. H. (1984). Models for carbon isotope fractionation between diet and bone. In J. F. Turnland & P. E. Johnson (Eds.), *Stable Isotopes in Nutrition* (Vol. 258, pp. 205–222). American Chemical Society.

Krueger, K. L., Chwa, E., Peterson, A. S., Willman, J. C., Fok, A., van Heel, B., Heo, Y., Weston, M., & DeLong, R. (2021). Technical note: Artificial Resynthesis Technology for the experimental formation of dental microwear textures. *American Journal of Physical Anthropology*, *176*(4), 703–712. https://doi.org/10.1002/ajpa.24395

Lalueza, C., Pérez-Pérez, A., & Turbón, D. (1996). Dietary Inferences Through Buccal Microwear Analysis of Middle and Upper Pleistocene Human Fossils. *American Journal of Physical Anthropology*, *100*, 367–387.

Laneri, N. (2016). *Hirbemerdon Tepe Archaeological Project 2003-2013 Final Report: Chronology and Material Culture*. Bradypus.

Larsen, C. S., Shavit, R., & Griffin, M. C. (1991). Dental caries evidence for dietary change: an archaeological context. In M. A. Kelley & C. S. Larsen (Eds.), *Advances in Dental Anthropology* (pp. 179–202). Wiley-Liss.

Ławecka, D. (2019). Architecture and Settlement Trends. In E. Rova (Ed.), *Associated Regional Chronologies for the Ancient Near East and the Eastern Mediterranean - Tigridian Region* (Vol. 5, pp. 139–164). Brepols.

Lebeau, M. (Ed.). (2012). *Associated Regional Chronologies for the Ancient Near East and the Eastern Mediterranean - Jezirah* (Vol. 1). Brepols.

Lee-Thorp, J. A., Sealy, J. C., & van der Merwe, N. J. (1989). Stable carbon isotope ratio differences between bone collagen and bone apatite, and their relationship to diet. *Journal of Archaeological Science*, *16*(6), 585–599. https://doi.org/10.1016/0305-4403(89)90024-1

Lee-Thorp, J. A., & van der Merwe, N. J. (1987). Carbon isotope analysis of fossil bone apatite. *South African Journal of Science*, *83*, 712–715.

Lee-Thorp, J. A., & van der Merwe, N. J. (1991). Aspects of the chemistry of modern and fossil biological apatites. *Journal of Archaeological Science*, *18*(3), 343–354. https://doi.org/10.1016/0305-4403(91)90070-6

LeGeros, R. Z., & LeGeros, J. P. (1984). Phosphate minerals in human tissues. *Phosphate Minerals*, *12*(170), 351–385.

Leggett, S., Le Roux, P., Tinguely, C., Baranowski, U., & Sayle, K. (2024). *Carbon, Nitrogen, Sulphur, Oxygen and Strontium Isotope Analysis of Human Remains from the Early Medieval Burial at Winfarthing, Diss, Norfolk on behalf of Time Team 2023*. University of Edinburgh.

Lewis, M. (2018). Dental Disease, Defects, and Variations in Dental Morphology. In M. Lewis (Ed.), *Paleopathology of Children: Identification of Pathological Conditions in the Human Skeletal Remains of Non-Adults* (pp. 67–89). Elsevier Academic Press. https://doi.org/10.1016/b978-0-12-410402-0.00004-7

Lightfoot, E., Ballantyne, R., & O'Connell, T. C. (2024). Chapter 31 - Stable isotope analysis of seeds and bones. In R. Ballantyne, A. Cooper, D. Gibson, M. Knight, & I. R. Zeki (Eds.), *Must Farm pile-dwelling settlement: Volume 2. Specialist reports* (Vol. 2). McDonald Institute for Archaeological Research.

Lin, J. T., & Lane, J. M. (2004). Osteoporosis: A review. *Clinical Orthopaedics and Related Research*, *425*, 126–134. https://doi.org/10.1097/01.blo.0000132404.30139.f2

Longinelli, A. (1984). Oxygen isotopes in mammal bone phosphate: A new tool for paleohydrological and paleoclimatological research? *Geochimica et Cosmochimica Acta*, *48*(2), 385–390. https://doi.org/10.1016/0016-7037(84)90259-X

López-Cachero, F. J., & Rovira Hortalà, M. C. (2018). El bronze final i el ritual funerari incinerador a Catalunya. In J. Bosch, M. Borrell, & A. M. Garrido (Eds.), *La fi és el principi. Pràctiques funeràries a la Catalunya prehistòrica* (pp. 103–117). Museu d'Arqueologia de Catalunya.

Lovejoy, C. O. (1985). Dental Wear in the Libben Population: Its Functional Pattern and Role in the Determination of Adult Skeletal Age at Death. *American Journal of Physical Anthropology*, *68*, 47–56.

Luz, B., & Kolodny, Y. (1985). Oxygen isotope variations in phosphate of biogenic apatites, IV. Mammal teeth and bones. *Earth and Planetary Science Letters*, *75*(1), 29–36. https://doi.org/10.1016/0012-821X(85)90047-0

Luz, B., Kolodny, Y., & Horowitz, M. (1984). Fractionation of oxygen isotopes between mammalian bone-phosphate and environmental drinking water. *Geochimica et Cosmochimica Acta*, *48*(8), 1689–1693. https://doi.org/10.1016/0016-7037(84)90338-7

Madupalli, H., Pavan, B., & Tecklenburg, M. M. J. (2017). Carbonate substitution in the mineral component of bone: Discriminating the structural changes, simultaneously imposed by carbonate in A and B sites of apatite. *Journal of Solid State Chemistry*, *255*, 27–35. https://doi.org/10.1016/j.jssc.2017.07.025

Mahoney, P. (2006). Microwear and morphology: Functional relationships between human dental microwear and the mandible. *Journal of Human Evolution*, *50*(4), 452–459. https://doi.org/10.1016/j.jhevol.2005.11.003

Mallowan, M. E. L. (1964). Ninevite V. In K. Bittel, E. Heinrich, B. Hrouda, & W. Nagel (Eds.), *Vorderasiatische Archäologie : Studien und Aufsätze : Anton Moortgat zun fünfundsechzigsten Geburtstag gewidmet von Kollegen, Freunden und Schülern* (Mann, pp. 142–154). Verlag Gebr. Mann.

Mallowan, M. E. L. (2008). The Early Dynastic Period in Mesopotamia. In I. E. S. Edwards, C. J. Gadd, & N. G. L. Hammond (Eds.), *The Cambridge Ancient History: Vol. Volume 1, Part 2* (3rd ed., pp. 291–314). Cambridge University Press.

Mamand, B. S., & Mawlood, D. K. (2024). Identifying sources of groundwater and recharge zone using stable environmental isotopes in the Erbil basin-northern Iraq. *Kuwait Journal of Science*, *51*(1). https://doi.org/10.1016/j.kjs.2023.09.002

Mariotti, V., Zuppello, M., Pedrosi, M. E., Bettuzzi, M., Brancaccio, R., Peccenini, E., Morigi, M. P., & Belcastro, M. G. (2015). Skeletal evidence of tuberculosis in a modern identified human skeletal collection (Certosa cemetery, Bologna, Italy). *American Journal of Physical Anthropology*, *157*(3), 389–401. https://doi.org/10.1002/ajpa.22727

Martín, A., Guilaine, J., & Thommeret, Y. (1981). Estratigrafía y dataciones C14 del yacimiento de la «Cova del Frare» de St. Llorenç del Munt (Matadepera, Barcelona). *ZEPHYRVS*, *32–33*, 101–111.

Martín, A., Miret, J., Bosch, J., Blanch, R. M., Aliaga, S., Enrich, R., Colomer, S., Albizuri, S., Folch, J., Martínez, J., & Casas, T. (1988). Les excavacions al paratge de la Bòbila Madurell i de Can Feu (Sant Quirze del Vallès, Vallès Occidental). *Tribuna d'Arqueologia*, *1987–1988*, 77–92.

Martínez, L. M., Estebaranz-Sánchez, F., Ferràndez-Cañadell, C., Romero, A., Ribot, F., Galbany, J., Gibert, L., & Pérez-Pérez, A. (2020). Buccal dental-microwear and feeding ecology of Early Pleistocene Theropithecus oswaldi from Cueva Victoria (Spain). *Journal of Human Evolution*, *142*, 102736. https://doi.org/10.1016/j.jhevol.2019.102736

Martínez, L. M., & Pérez-Pérez, A. (2004). Post-mortem wear as indicator of taphonomic processes affecting enamel surfaces of hominin teeth from Laetoli and Olduvai (Tanzania): implications to dietary interpretations. *Anthropologie*, *42*(1), 37–42.

Maya, J. L. (1997). Reflexiones sobre el Bronce Inicial en Cataluña. *SAGVNTVM (Papeles Del Laboratorio de Arqueología de Valencia)*, *30*, 11–27.

Maya, J. L., & Petit, M. A. (1986). El grupo del Nordeste. Un nuevo conjunto de cerámicas con boquique en la Península Ibérica. *Anales de Prehistoria y Arqueología*, *2*, 49–71.

McCorriston, J., & Weisberg, S. (2002). Spatial and Temporal Variation in Mesopotamian Agricultural Practices in the Khabur Basin, Syrian Jazira. *Journal of Archaeological Science*, *29*(5), 485–498. https://doi.org/10.1006/jasc.2001.0741

McGrath, K., Rowsell, K., Gates St-Pierre, C., Tedder, A., Foody, G., Roberts, C., Speller, C., & Collins, M. (2019). Identifying Archaeological Bone via Non-Destructive ZooMS and the Materiality of Symbolic Expression: Examples from Iroquoian Bone Points. *Scientific Reports*, *9*(1), 11027. https://doi.org/10.1038/s41598-019-47299-x

Meier-Augenstein, W. (2010). *Stable Isotope Forensics: An Introduction to the Forensic Application of Stable Isotope Analysis* (1st ed.). John Wiley & Sons Ltd.

Meier-Augenstein, W. (2018). *Stable Isotope Forensics: methods and Forensic Applications of Stable Isotope Analysis*.

Meindl, R. S., & Lovejoy, C. O. (1985). Ectocranial suture closure: A revised method for the determination of skeletal age at death based on the lateral-anterior sutures. *American Journal of Physical Anthropology*, *68*(1), 57–66. https://doi.org/10.1002/ajpa.1330680106

Mendes Cardoso, J., Merencio, F., Villagran, X., Wesolowski, V., Estevam, R., Fuller, B. T., DeBlasis, P., Pierre-Gilson, S., Guiserix, D., Méjean, P., Figuti, L., Farias, D., Guimaraes, G., Strauss, A., & Jaouen, K. (2024). Late shellmound occupation in southern Brazil: A multi-

proxy study of the Galheta IV archaeological site. *PLOS ONE*, *19*(3), e0300684. https://doi.org/10.1371/journal.pone.0300684

Molina-González, F., Nocete-Calvo, F., Delgado-Huertas, A., Cámara-Serrano, J. A., Martínez-Sánchez, R. M., Jiménez-Brobéil, S., Miranda-León, M. T., Riquelme-Cantal, J. A., Spanedda, L., Pérez-Bareas, C., Lizcano-Prestel, R., Nieto-Liñán, J. M., Nájera-Colino, T., Granados-Torres, A., & Carrión-Méndez, F. (2019). Diet and environment in south-eastern Iberia during the Bronze Age, based on isotope analysis of human remains. *Oxford Journal of Archaeology*, *38*(2), 189–213. https://doi.org/10.1111/ojoa.12164

Molist, M., Bach, A., Zebari, A., Breu, A., Sisa, J., Gironès, I., Monforte, A., Alcàntara, R., Gluitz, A., Douché, C., Garcia, F., Abdullrahman, H., & Sulaiman, A. (2023). Arqueología en el norte del Zagros y valle del Tigris (Kurdistán iraquí). In *Informes y Trabajos: Instituto del Patrimonio Cultural de España* (Vol. 21, pp. 28–43). Ministerio de Cultura y Deporte.

Molist, M., Breu, A., Sisa, J., Alcántara, R., Cruells, W., Arnaiz, R., Gómez-Bach, A., Saña, M., Bradosty, Z., Douché, C., Mylona, P., & Zebari, A. M. (2019b). New data on the 4th-3rd millennia in Northern Mesopotamia: The ancient occupations at Gird Lashkir in their archaeological contexts. *Paléorient*, *45*(2), 191–206. https://doi.org/10.4000/paleorient.765

Molist, M., Gómez-Bach, A., Bradosky, Z., Anfruns, J., Cruells, W., Alcantara, R., Arnaiz, R., Breu, A., Moya, A., Sisa, J., Mohamad, A., & Ahmed, H. (2019). Proyecto arqueológico en Grid Lashkir (Erbil, Kurdistán, Iraq): resultados de las campañas de excavación 2015-2016. In *Informes y Trabajos: Excavaciones en el exterior* (Vol. 17, pp. 201–221). Ministerio de Cultura y Deporte.

Molist, M., Zebari, A., & Bach, A. (2024). Archaeological Excavations in Iraqi Kurdistan: Unveiling New Evidence on the Development of Complex Societies in Northern Mesopotamia at Gird Lashkir (Erbil). *Near Eastern Archaeology*, *87*(3), 188–193. https://doi.org/10.1086/731390

Morandi Bonacossi, D., Ahmad Qasim, H., Coppini, C., Gavagnin, K., Girotto, E., Iamoni, M., & Tonghini, C. (2018). The Italian-Kurdish Excavations at Gir-e Gomel in the Kurdistan Region of Iraq. Preliminary Report on the 2017 and 2018 Field Seasons. *Mesopotamia. Rivista Di Archeologia, Epigrafia e Storia Orientale Antica*, *53*, 67–162.

Morandi Bonacossi, D., Coppini, C., Gavagnin, K., & Ahmed Qasim, H. (2025). Exploring Bronze Age Urbanism in the Navkur Plain (Kurdistan Region of Iraq): Preliminary Report on the 2019 Italian-Kurdish Excavations at Gir-e Gomel. *Zeitschrift Für Orient-Archäologie*, *16*(1).

Moreno, A., Iglesias, M., Azorin-Molina, C., Pérez-Mejías, C., Bartolomé, M., Sancho, C., Stoll, H., Cacho, I., Frigola, J., Osácar, C., Muñoz, A., Delgado-Huertas, A., Bladé, I., & Vimeux, F. (2021). Measurement report: Spatial variability of northern Iberian rainfall stable isotope values – investigating atmospheric controls on daily and monthly timescales. *Atmospheric Chemistry and Physics*, *21*(13), 10159–10177. https://doi.org/10.5194/acp-21-10159-2021

Muhly, J. D., & Stech, T. (2003). The Metallurgy of Ninevite 5. In E. Rova & H. Weiss (Eds.), *The Origins of North Mesopotamian Civilization: Ninevite 5 Chronology, Economy, Society: Vol. Subartu IX* (pp. 417–428). Brepols.

Mustafa, O., Merkel, B., & Weise, S. M. (2015). Assessment of hydrogeochemistry and environmental isotopes in karst springs of makook anticline, Kurdistan Region, Iraq. *Hydrology*, *2*(2), 48–68. https://doi.org/10.3390/hydrology2020048

Nadal, E., & Castillo, R. J. (2010). *Intervenció arqueològica al C/ d'Espalter, 1b-11; C/ de Sant Pau, 66; C/ de Sant Josep Oriol, 7-11; pl. de Salvador Seguí*.

Navidtalab, A., Rahimpour-Bonab, H., Huck, S., & Heimhofer, U. (2016). Elemental geochemistry and strontium-isotope stratigraphy of Cenomanian to Santonian neritic carbonates in the Zagros Basin, Iran. *Sedimentary Geology*, *346*, 35–48. https://doi.org/10.1016/j.sedgeo.2016.10.003

Neal, C., Neal, M., Warrington, A., Ávila, A., Piñol, J., & Rodà, F. (1992). Stable hydrogen and oxygen isotope studies of rainfall and streamwaters for two contrasting holm oak areas of Catalonia, northeastern Spain. *Journal of Hydrology*, *140*, 163–178.

Négrel, P., Petelet-Giraud, E., & Millot, R. (2016). Tracing water cycle in regulated basin using stable δ18O–δ2H isotopes: The Ebro river basin (Spain). *Chemical Geology*, *422*, 71–81. https://doi.org/10.1016/j.chemgeo.2015.12.009

Numoto, H. (1993). Incised and Excised Designs of the Ninevite 5 Pottery. *Al-Rāfidān*, *14*, 69–108.

Oates, D. (1982). Tell Brak. In J. Curtis (Ed.), *Fifty rears of Mesopotamian Discovery* (pp. 62–71). British School of Archaeology in Iraq.

O'Connell, T. C., Kneale, C. J., Tasevska, N., & Kuhnle, G. G. C. (2012). The diet-body offset in human nitrogen isotopic values: A controlled dietary study. *American Journal of Physical Anthropology*, *149*(3), 426–434. https://doi.org/10.1002/ajpa.22140

O'Leary, M. H. (1988). Carbon Isotopes in Photosynthesis. *BioScience*, *38*(5), 328–336. https://doi.org/10.2307/1310735

Ortner, D. J. (2003). Infectious Diseases: Introduction, Biology, Osteomyelitis, Periostitis, Brucellosis, Glanders, and Septic Arthritis. In D. J. Ortner (Ed.), *Identification of Pathological Conditions in Human Skeletal Remains* (pp. 179–226). Academic Press.

Palastanga, N., Field, D., & Soames, R. (1989). *Anatomy and human movement: structure and function*. Heinemann Medical Books.

Pederzani, S., & Britton, K. (2019). Oxygen isotopes in bioarchaeology: Principles and applications, challenges and opportunities. *Earth-Science Reviews*, *188*, 77–107. https://doi.org/10.1016/j.earscirev.2018.11.005

Pellegrini, M., & Snoeck, C. (2016). Comparing bioapatite carbonate pre-treatments for isotopic measurements: Part 2 — Impact on carbon and oxygen isotope compositions. *Chemical Geology*, *420*, 88–96. https://doi.org/10.1016/j.chemgeo.2015.10.038

Pérez-Pérez, A., Alesan, A., & Roca, L. (1990). Measurement error: Inter-and Intraobserver Variability. An Empiric Study. *International Journal of Anthropology*, *5*(2), 129–135. https://doi.org/10.1007/BF02442082

Pérez-Pérez, A., Lalueza, C., & Turbón, D. (1994). Intraindividual and intragroup variability of buccal tooth striation pattern. *American Journal of Physical Anthropology*, *94*(2), 175–187. https://doi.org/10.1002/ajpa.1330940203

Pestle, W. J., Crowley, B. E., & Weirauch, M. T. (2014). Quantifying Inter-Laboratory Variability in Stable Isotope Analysis of Ancient Skeletal Remains. *PLoS ONE*, *9*(7), e102844. https://doi.org/10.1371/journal.pone.0102844

Pezo Lanfranco, L., & Eggers, S. (2012). Caries Through Time: An Anthropological Overview. In M.-Y. Li (Ed.), *Contemporary Approach to Dental Caries* (pp. 3–34). InTech.

Phenice, T. W. (1969). A Newly Developed Visual Method of Sexing the Os Pubis. *American Journal of Physical Anthropology*, *30*, 297–302.

Piątkowska-Małecka, J., & Smogorzewska, A. (2010). Animal economy at Tell Arbid, north-east Syria, in the third millennium BC. *Bioarchaeology of the Near East*, *4*, 25–43.

Piera, J., Moreno, I., Bordas, A., & Suau, L. (2005). *Memòria de la intervenció arqueològica a l'Illa d'en Robador: C/Robador, Sant Rafel, Sant Josep Oriol i Sadurní. Ciutat Vella, Barcelona*.

Pittman, H. (2019). Glyptic Art of the Tigridian Region. In E. Rova (Ed.), *Associated Regional Chronologies for the Ancient Near East and the Eastern Mediterranean - Tigridian Region* (Vol. 5, pp. 283–348). Brepols.

Postgate, J. (1998). *Nitrogen Fixation* (3rd ed.). Cambridge University Press.

Postgate, J. R. (Ed.). (1972). *The Chemistry and Biochemistry of Nitrogen Fixation* (1st ed.). Springer US. https://doi.org/10.1007/978-1-4684-1818-7

Postgate, J. R. (1982). Biological nitrogen fixation: fundamentals. *Philosophical Transactions of the Royal Society of London. B, Biological Sciences*, *296*(1082), 375–385. https://doi.org/10.1098/rstb.1982.0013

Price, T. D., Burton, J. H., & Bentley, R. A. (2002). The characterization of biologically available strontium isotope ratios for the study of prehistoric migration. *Archaeometry*, *44*(1), 117–135. https://doi.org/10.1111/1475-4754.00047

Price, T. D., Johnson, C. M., Ezzo, J. A., Ericson, J., & Burton, J. H. (1994). Residential Mobility in the Prehistoric Southwest United States: A Preliminary Study using Strontium Isotope Analysis. *Journal of Archaeological Science*, *21*(3), 315–330. https://doi.org/10.1006/jasc.1994.1031

Ranjitkar, S., Turan, A., Mann, C., Gully, G. A., Marsman, M., Edwards, S., Kaidonis, J. A., Hall, C., Lekkas, D., Wetselaar, P., Brook, A. H., Lobbezoo, F., & Townsend, G. C. (2017). Surface-Sensitive Microwear Texture Analysis of Attrition and Erosion. *Journal of Dental Research*, *96*(3), 300–307. https://doi.org/10.1177/0022034516680585

Renfrew, A. C. (1973). *Before Civilization: The Radiocarbon Revolution and Prehistoric Europe*. Pimlico.

Resnick, D., & Niwayama, G. (1983). Entheses and Enthesopathy. Anatomical, Pathological, and Radiological Correlation. *Diagnostic Radiology*, *146*, 1–9.

Richards, M. P. (2015). Stable Isotope Analysis of Bone and Teeth as a Means for Reconstructing Past Human Diets in Greece. *Hesperia Supplements*, *49*, 15–23.

Richards, M. P., & Trinkaus, E. (2009). Isotopic evidence for the diets of European Neanderthals and early modern humans. *Proceedings of the National Academy of Sciences*, *106*(38), 16034–16039. https://doi.org/10.1073/pnas.0903821106

Richter, K. K., Codlin, M. C., Seabrook, M., & Warinner, C. (2022). A primer for ZooMS applications in archaeology. *Proceedings of the National Academy of Sciences*, *119*(20), 1–10. https://doi.org/10.1073/pnas.2109323119

Riehl, S., Bryson, R., & Pustovoytov, K. (2008). Changing growing conditions for crops during the Near Eastern Bronze Age (3000-1200 BC): the stable carbon isotope evidence. *Journal of Archaeological Science*, *35*(4), 1011–1022. https://doi.org/10.1016/j.jas.2007.07.003

Ríos, L., Weisensee, K., & Rissech, C. (2008). Sacral fusion as an aid in age estimation. *Forensic Science International*, *180*(2–3), 111.e1-111.e7. https://doi.org/10.1016/j.forsciint.2008.06.010

Rissech, C., Estabrook, G. F., Cunha, E., & Malgosa, A. (2006). Using the Acetabulum to Estimate Age at Death of Adult Males. *Journal of Forensic Sciences*, *51*(2), 213–229.

Ristenbatt, R. R., Hietpas, J., De Forest, P. R., & Margot, P. A. (2022). Traceology, criminalistics, and forensic science. *Journal of Forensic Sciences*, *67*(1), 28–32. https://doi.org/10.1111/1556-4029.14860

Roaf, M. (1984). Excavations at Tell Mohammed 'Arab in the Eski Mosul Dam Salvage Project. *Iraq*, *46*(2), 141. https://doi.org/10.2307/4200223

Roaf, M. (1988). Problems in the Chronology of Ninevite 5. *American Journal of Archaeology*, *92*(4), 589–591. https://doi.org/10.2307/505255

Roaf, M. (2003). The Architecture of the Ninevite 5 Period. In E. Rova & H. Weiss (Eds.), *The Origins of North Mesopotamian Civilization: Ninevite 5 Chronology, Economy, Society: Vol. Subartu IX* (pp. 311–334). Brepols.

Roberts, C. A., & Buikstra, J. E. (2019). Bacterial Infections. In J. E. Buikstra (Ed.), *Ortner's Identification of Pahtological Conditions in Human Skeletal Remains* (pp. 321–439). Academic Press.

Rodríguez-Corral, J., & Ferrer Albelda, E. (2018). Teoría e interpretación en la arqueología de la muerte. *Spal - Revista de Prehistoria y Arqueología*, *27*(2), 89–123.

Roksandic, M. (2003). New Standardised Visual Forms for Recording the Presence of Human Skeletal Elements in Archaeological and Forensic Contexts. *Internet Archaeology*, *13*, 1–14. https://doi.org/https://doi.org/10.11141/ia.13.3

Romero, A., & De Juan, J. (2012). SEM, teeth, and palaeoanthropology: the secret of ancient human diets. In H. Schatten (Ed.), *Scanning Electron Microscopy for the Life Sciences* (pp. 236–256). Cambridge University Press.

Romero, A., & Juan, J. De. (2007). Intra-and Interpopulation Human Buccal Tooth Surface Microwear Analysis : Inferences About Diet and Formation Processes. *Anthropologie (1962-)*, *45*(1), 61–70.

Romero, A., Polo-Cerdá, M., & de Juan, J. (2004). Análisis por microscopía electrónica de barrido de la dentición de los individuos de la Cova dels Blaus (Vall d'Uixó, Castelló): aproximación a la paleodieta a través de la patología y patrón de microestriación dental. In M. S. Hernández Pérez & L. Hernández Alcaraz (Eds.), *La Edad del Bronce en tierras valencianas y zonas limítrofes* (pp. 158–166). Diputación Provincial de Alicante, Instituto Alicantino de Cultura Juan Gil-Albert, Ayuntamiento de Villena.

Rova, E. (2003a). Ninevite 5 Relative Chronology, Periodization and Distribution: An Introduction. In E. Rova & H. Weiss (Eds.), *The Origins of North Mesopotamian Civilization: Ninevite 5 Chronology, Economy, Society* (Vol. 9, pp. 1–10). Brepols.

Rova, E. (2003b). Tell Karrana 3: Ceramic Evidence for the Late Uruk/Ninevite 5 Transition. In E. Rova & H. Weiss (Eds.), *The Origins of North Mesopotamian Civilization: Ninevite 5 Chronology, Economy, Society* (Vol. 9, pp. 11–24). Brepols.

Rova, E. (2013). The Ninevite 5 Period in Northeast Syria. In W. Orthman, P. Matthiae, & M. al-Maqdissi (Eds.), *Archéologie et Histoire de la Syrie I. La Syrie de l'époque néolithique à l'âge du fer. Schriften Zur Vorderasiatischen Archäologie* (Vol. 1, pp. 107–119). Harrassowitz Verlag.

Rova, E. (Ed.). (2019). *Associated Regional Chronologies for the Ancient Near East and the Eastern Mediterranean - Tigridian Region* (Vol. 5). Brepols.

Rovira, M. C. (2006). El bronze inicial a Catalunya des de la perspectiva metal·lúrgica. *Cypsela*, *16*, 135–146.

Rutkowski, Ł. (2019). Metal. In E. Rova (Ed.), *Associated Regional Chronologies for the Ancient Near East and the Eastern Mediterranean - Tigridian Region* (Vol. 5, pp. 165–210). Brepols.

Sage, R. F., & Sage, T. L. (2013). C4 Plants. In S. A. Levin (Ed.), *Encyclopedia of Biodiversity* (2nd ed., pp. 361–381). Elsevier. https://doi.org/10.1016/B978-0-12-384719-5.00192-1

Sahib, L. Y., Marandi, A., & Schüth, C. (2016). Strontium isotopes as an indicator for groundwater salinity sources in the Kirkuk region, Iraq. *Science of the Total Environment*, *562*, 935–945. https://doi.org/10.1016/j.scitotenv.2016.03.185

Salam Smail, S. (2023). *Stable Isotopes in Precipitation and Groundwater in Iraqi Kurdistan Region: A Case Study in Sulaimani Governorate*. Palacký University Olomouc.

Salazar-García, D. C., Romero, A., García-Borja, P., Subirà, M. E., & Richards, M. P. (2016). A combined dietary approach using isotope and dental buccal-microwear analysis of human remains from the Neolithic, Roman and Medieval periods from the archaeological site of Tossal de les Basses (Alicante, Spain). *Journal of Archaeological Science: Reports*, *6*, 610–619. https://doi.org/10.1016/j.jasrep.2016.03.002

Sasaki, T., Takagi, M., & Yanagisawa, T. (2007). Structure and Function of Secretory Ameloblasts in Enamel Formation. In *Ciba Foundation Symposium 205 - Dental Enamel* (pp. 32–53). https://doi.org/https://doi.org/10.1002/9780470515303.ch4

Saygın, S., Polat, N., Willmes, M., Lewis, L. S., Hobbs, J. A., Atıcı, A. A., & Elp, M. (2022). Strontium isotopes in otoliths reveal a diversity of natal origins for Tarek (Alburnus tarichi) in Lake Van, Turkey. *Fisheries Research*, *255*. https://doi.org/10.1016/j.fishres.2022.106441

Schaefer, M., Black, S., & Scheuer, L. (2009). *Juvenile Osteology: A Laboratory and Field Manual*. Elsevier Academic Press. https://doi.org/https://doi.org/10.1016/B978-0-12-374635-1.X0001-X

Schmidt, C. W., Remy, A., Van Sessen, R., Willman, J., Krueger, K., Scott, R., Mahoney, P., Beach, J., McKinley, J., D'Anastasio, R., Chiu, L., Buzon, M., De Gregory, J. R., Sheridan, S., Eng, J., Watson, J., Klaus, H., Da-Gloria, P., Wilson, J., … Herrmann, N. (2019). Dental microwear

texture analysis of Homo sapiens sapiens: Foragers, farmers, and pastoralists. *American Journal of Physical Anthropology*, *169*(2), 207–226. https://doi.org/10.1002/ajpa.23815

Schour, I., & Massler, M. (1941). *Development of human dentition chart*. American Dental Association.

Schultz, M., Carli-Thiele, P., Schmidt-Schultzf, T. H., Kierdorf, U., Kierdorf, H., Teegen, W.-R., & Kreutz, K. (1998). Enamel Hypoplasias in Archaeological Skeletal Remains. In K. W. Alt, F. W. Rösing, & M. Teschler-Nicola (Eds.), *Dental Anthropology. Fundamentals, Limits and Prospects* (pp. 293–311). Springer Verlag. https://doi.org/10.1007/978-3-7091-7496-8_16

Schulz-Kornas, E., Kaiser, T. M., Calandra, I., & Winkler, D. E. (2020). A brief history of quantitative wear analysis with an appeal for a holistic view on dental wear processes. In T. Martin & W. v. Koenigswald (Eds.), *Mammalian Teeth – Form and Function* (pp. 44–53). Verlag Dr. Friedrich Pfeil.

Schwartz, G. M. (1982). *From Prehistory to History on the Habur Plains: The Operation I Ceramic Periodization from Tell Leilan*. Yale University.

Schwartz, G. M. (2003). Socio-Political Developments in the Ninevite 5 Period. In E. Rova & H. Weiss (Eds.), *The Origins of North Mesopotamian Civilization: Ninevite 5 Chronology, Economy, Society: Vol. Subartu IX* (pp. 585–592). Brepols.

Scott, R. S. (2005). Dental microwear texture analysis reflects diets of living primates and fossils hominins. *Nature*, *436*, 693–695.

Seeyan, S., & Merkel, B. J. (2014). Determination of Recharge by Means of Isotopes and Water Chemistry in Shaqlawa-Harrir Basin, Kurdistan Region, Iraq. *Journal of Waste Water Treatment & Analysis*, *05*(03). https://doi.org/10.4172/2157-7587.1000179

Shabanian, N., Davoudian, A. R., Dong, Y., & Liu, X. (2018). U-Pb zircon dating, geochemistry and Sr-Nd-Pb isotopic ratios from Azna-Dorud Cadomian metagranites, Sanandaj-Sirjan Zone of western Iran. *Precambrian Research*, *306*, 41–60. https://doi.org/10.1016/j.precamres.2017.12.037

Sheldahl, L. C., Babiy, I., & Yapp, R. A. (2020). *Histology and embryology for dental hygiene*. Open Educational Resource.

Shennan, S. (1975). The social organization at Branč. *Antiquity*, *49*(196), 279–288.

Shook, B., Nelson, K., Aguilera, K., & Braff, L. (Eds.). (2024). *Explorations: An Open Invitation to Biological Anthropology* (2nd ed.). Open Educational Resources.

Simpson, G. G. (1926). Mesozoic Mammalia, IV; the multituberculates as living animals. *American Journal of Science*, *11*(63), 228–250. https://doi.org/10.2475/ajs.s5-11.63.228

Simpson, M. G. (2019). Plant Anatomy and Physiology. In *Plant Systematics* (3rd ed., pp. 537–566). Elsevier. https://doi.org/10.1016/B978-0-12-812628-8.50010-9

Slovak, N. M., & Paytan, A. (2012). Applications of Sr Isotopes in Archaeology. In M. Baskaran (Ed.), *Handbook of Environmental Isotope Geochemistry* (pp. 743–768). Springer Verlag. https://doi.org/10.1007/978-3-642-10637-8_35

Smith, T. M. (2020). Dental Histology. In M. P. Richards & K. Britton (Eds.), *Archaeological Science: An Introduction* (pp. 170–197). Cambridge University Press. https://doi.org/DOI: 10.1017/9781139013826.008

Smogorzewska, A. (2016). The Final Stage of the Ninevite 5 Pottery: Morphological Types, Technology and Diachronic Analysis from Tell Arbid (North-East Syria). *Iraq*, *78*, 175–214. https://doi.org/10.1017/irq.2016.1

Snoeck, C., & Pellegrini, M. (2015). Comparing bioapatite carbonate pre-treatments for isotopic measurements: Part 1-Impact on structure and chemical composition. *Chemical Geology*, *417*, 394–403. https://doi.org/10.1016/j.chemgeo.2015.10.004

Sołtysiak, A. (2011). Cereal grinding technology in ancient Mesopotamia: evidence from dental microwear. *Journal of Archaeological Science*, *38*(10), 2805–2810. https://doi.org/10.1016/j.jas.2011.06.025

Sołtysiak, A. (2019). Strontium and nitrogen isotopic evidence of food import to Tell Ashara–Terqa, a Bronze Age city on the Euphrates, Syria. *International Journal of Osteoarchaeology*, *29*(1), 127–133. https://doi.org/10.1002/oa.2724

Sołtysiak, A., & Schutkowski, H. (2015). Continuity and change in subsistence at Tell Barri, NE Syria. *Journal of Archaeological Science: Reports*, *2*, 176–185. https://doi.org/10.1016/j.jasrep.2015.01.011

Soriano, I. (2013). *Metalurgia y Sociedad en el Nordeste de la Península Ibérica: (finales del IV – II milenio cal ANE)*. University of Michigan Press. https://doi.org/10.30861/9781407311180

Soriano, I. (2018). Les pràctiques funeràries durant el calcolític i el bronze antic i mitjà. In J. Bosch, M. Borrell, & A. M. Garrido (Eds.), *La fi és el principi. Pràctiques funeràries a la Catalunya prehistòrica* (pp. 79–101). Museu d'Arqueologia de Catalunya.

Soriano, I., & Chamón, J. (2012). Estudio arqueometalúrgico del punzón de Cova de la Pesseta (Torrelles de Foix, Barcelona). Datos composicionales, metalográficos, isotópicos y funcionales. *MARQ. Arqueología y Museos*, *5*, 73–89.

Soriano, I., Delgado-Raack, S., Rafel, N., Hunt, M. A., Montero, I., Andreazini, A., & Malgarejo, J. C. (2019). La primera explotació de coure a Catalunya. Dades arqueològiques i arqueomèriques de la Mina de la Turquesa (Cornudella de Montsant, Priorat). *Tribuna d'arqueologia*, *2016–2017*, 198–216.

Strohalm, M., Hassman, M., Košata, B., & Kodíček, M. (2008). mMass data miner: an open source alternative for mass spectrometric data analysis. *Rapid Communications in Mass Spectrometry*, *22*(6), 905–908. https://doi.org/10.1002/rcm.3444

Styring, A. K., Charles, M., Fantone, F., Hald, M. M., McMahon, A., Meadow, R. H., Nicholls, G. K., Patel, A. K., Pitre, M. C., Smith, A., Sołtysiak, A., Stein, G., Weber, J. A., Weiss, H., & Bogaard, A. (2017). Isotope evidence for agricultural extensification reveals how the world's first cities were fed. *Nature Plants*, *3*(6), 17076. https://doi.org/10.1038/nplants.2017.76

Suau, L., & Matas, Ò. (2010). *Memòria de la intervenció arqueològica de la zona C del projecte d'infraestructures troncals des del carrer Carders a la central de RSU, en el mercat de Santa Caterina, al districte de Ciutat Vella, de Barcelona*.

Sullivan, C. H., & Krueger, H. W. (1983). Carbon isotope ratios of bone apatite and animal diet reconstruction. *Nature*, *301*(5896), 177–177. https://doi.org/10.1038/301177a0

Sun, Y., Wang, Y., Ji, C., Ma, J., & He, B. (2024). The impact of hydroxyapatite crystal structures and protein interactions on bone's mechanical properties. *Scientific Reports*, *14*(1), 9786. https://doi.org/10.1038/s41598-024-60701-7

Swärdstedt, T. (1966). *Odontological aspects of a Medieval population in the province of Jämtland, mid-Sweden*. University of Stockholm.

Tainter, J. A. (1975). Social inference and mortuary practices: An experiment in numerical classification. *World Archaeology*, *7*(1), 1–15.

Teaford, M. F. (2007). Dental microwear and Paleoanthropology: Cautions and possibilities. In S. E. Bailey & J.-J. Hublin (Eds.), *Dental Perspectives on Human Evolution. State of the Art Research in Dental Paleoanthropology* (1st ed., pp. 345–368). Springer. https://doi.org/10.1007/978-1-4020-5845-5_23

Then-Obłuska, J. (2015). Cross-cultural bead encounters at the Red Sea port site of Berenike, Egypt. Preliminary assessment (seasons 2009–2012). *Polish Archaeology in the Mediterranean*, *1*(XXIV), 735–777.

Thomalsky, J. (2019). Lithics. In E. Rova (Ed.), *Associated Regional Chronologies for the Ancient Near East and the Eastern Mediterranean - Tigridian Region* (Vol. 5, pp. 251–266). Brepols.

Thomson, R. C., & Mallowan, M. E. L. (1933). The British Museum Excavations at Nineveh, 1931-32. *Annals of Archaeology and Anthropology*, *20*, 71–186.

Todd, T. W. (1920). Age changes in the pubic bone. *American Journal of Physical Anthropology*, *3*(3), 285–334.

Tomczyk, J., Wierzbowski, H., & Zalewska, M. (2016). Stable Isotope Record of Human and Sheep Enamel Carbonate from the Ancient Middle Euphrates Valley (Syria). *International Journal of Osteoarchaeology*, *26*(4), 599–609. https://doi.org/10.1002/oa.2449

Tonussi, M. (2019). Figurines and Small Finds. In E. Rova (Ed.), *Associated Regional Chronologies for the Ancient Near East and the Eastern Mediterranean - Tigridian Region* (Vol. 5, pp. 211–250). Brepols.

Triffit, J. T. (1980). The organic matrix of bone tissue. In M. R. Urist (Ed.), *Fundamental and Clinical Bone Physiology* (pp. 45–82). J. B. Lippincott.

Trotter, M. (1970). Estimation of Stature from Intact Long Limb Bones. In T. D. Stewart (Ed.), *Personal Identification in Mass Disasters* (pp. 71–84). Smithsonian Institution.

Trotter, M., & Gleser, G. C. (1958). A re-evaluation of estimation of stature based on measurements of stature taken during life and of long bones after death. *American Journal of Physical Anthropology*, *16*(1), 79–123. https://doi.org/10.1002/ajpa.1330160106

Tsutaya, T., Doi, N., Katagiri, C., Sawafuji, R., & Yoneda, M. (2024). Human diet of premodern mainland Japan: a meta-analysis of carbon and nitrogen stable isotope ratios. *Anthropological Science*, *132*(1), 230718. https://doi.org/10.1537/ase.230718

Ubelaker, D. H. (1984). *Human Skeletal Remains, Excavation, Analysis, Interpretation. Revised edition*. Smithsonian Institution.

Ungar, P. S. (1995). A semiautomated image analysis procedure for the quantification of dental microwear II. *Scanning*, *17*(1), 57–59. https://doi.org/10.1002/sca.4950170108

Valentini, S. (2019). Burials and Funerary Practices. In E. Rova (Ed.), *Associated Regional Chronologies for the Ancient Near East and the Eastern Mediterranean - Tigridian Region* (Vol. 5, pp. 267–282). Brepols.

van Gijn, A. (2003). The Ninevite 5 Chipped Stone Assemblage from Tell Leilan: Preliminary Results. In E. Rova & H. Weiss (Eds.), *The Origins of North Mesopotamian Civilization: Ninevite 5 Chronology, Economy, Society: Vol. Subartu IX* (pp. 401–416). Brepols.

van Klinken, G. J. (1999). Bone Collagen Quality Indicators for Palaeodietary and Radiocarbon Measurements. *Journal of Archaeological Science*, *26*(6), 687–695. https://doi.org/10.1006/jasc.1998.0385

Velasco, A., Terrats, N., Gómez, A., & Molist, M. (2017). L'assentament de la Plaça de la Gardunya a Inicis del II mil·lenni: noves dades sobre les ocupacions de l'Edat del Bronze Inicial al pla de Barcelona. *Quarhis: Quaderns d'Arqueologia i Història de La Ciutat de Barcelona*, *13*, 70–89.

Viladés Ribera, M. (2013). *Estudi de les aigües salines a la conca del Riu Llobregat i Cardener: Implicacions ambientals*. Universitat Autònoma de Barcelona.

Vogel, J. C., & van Der Merwe, N. J. (1977). Isotopic Evidence for Early Maize Cultivation in New York State. *American Antiquity*, *42*(2), 238–242. https://doi.org/10.2307/278984

Walker, A., Hoeck, H. N., & Perez, L. (1978). Microwear of Mammalian Teeth as an Indicator of Diet. *Science*, *201*(4359), 908–910. https://doi.org/10.1126/science.684415

Webb, E. C., Lewis, J., Shain, A., Kastrisianaki-Guyton, E., Honch, N. V., Stewart, A., Miller, B., Tarlton, J., & Evershed, R. P. (2017a). The influence of varying proportions of terrestrial and marine dietary protein on the stable carbon-isotope compositions of pig tissues from a controlled feeding experiment. *STAR: Science & Technology of Archaeological Research*, *3*(1), 28–44. https://doi.org/10.1080/20548923.2016.1275477

Welker, F., Hajdinjak, M., Talamo, S., Jaouen, K., Dannemann, M., David, F., Julien, M., Meyer, M., Kelso, J., Barnes, I., Brace, S., Kamminga, P., Fischer, R., Kessler, B. M., Stewart, J. R., Pääbo, S., Collins, M. J., & Hublin, J.-J. (2016). Palaeoproteomic evidence identifies archaic hominins associated with the Châtelperronian at the Grotte du Renne. *Proceedings of the National Academy of Sciences*, *113*(40), 11162–11167. https://doi.org/10.1073/pnas.1605834113

Wetterstrom, W. (2003). Ninevite 5 Period Agriculture at Tell Leilan: Preliminary Study. In E. Rova & H. Weiss (Eds.), *The Origins of North Mesopotamian Civilization: Ninevite 5 Chronology, Economy, Society: Vol. Subartu IX* (pp. 387–400). Brepols.

White, C. D., Spence, M. W., Longstaffe, F. J., & Law, K. R. (2004). Demography and ethnic continuity in the Tlailotlacan enclave of Teotihuacan: the evidence from stable oxygen isotopes. *Journal of Anthropological Archaeology*, *23*(4), 385–403. https://doi.org/10.1016/j.jaa.2004.08.002

White, T. D., Black, M. T., & Folkens, P. A. (2012). *Human Osteology* (3rd ed.). Elsevier Academic Press.

Wilhelm, G., & Zaccagnini, C. (1993). *Tell Karrana 3, Tell Jikan, Tell Khirbet Salih*. Philipp von Zabern.

Wilson, L., & Pollard, A. M. (2002). Here today, gone tomorrow? Integrated experimentation and geochemical modeling in studies of archaeological diagenetic change. *Accounts of Chemical Research*, *35*(8), 644–651. https://doi.org/10.1021/ar000203s

Wong, S. H. J., Chiu, K. Y., & Yan, C. H. (2016). Osteophytes. *Journal of Orthopaedic Surgery*, *24*(3), 403–410. https://doi.org/10.1177/1602400327

Wyllie, A. H. (1997). Apoptosis: an overview. *British Medical Bulletin*, *53*(3), 451–465.

Zanon, G., Di Vico, G., & Matteo, M. (2014). Osteochondritis dissecans of the talus. *Joints*, *2*(3), 115–123.

Zapanta LeGeros, R. (1981). Apatites in biological systems. *Progress in Crystal Growth and Characterization*, *4*(1–2), 1–45. https://doi.org/10.1016/0146-3535(81)90046-0

Zapata, J., Pérez-Sirvent, C., Martínez-Sánchez, M. J., & Tovar, P. (2006). Diagenesis, not biogenesis: Two late Roman skeletal examples. *Science of the Total Environment*, *369*(1–3), 357–368. https://doi.org/10.1016/j.scitotenv.2006.05.021

Zehr, J. P., & Capone, D. G. (2021). *Marine Nitrogen Fixation*. Springer International Publishing. https://doi.org/10.1007/978-3-030-67746-6

Zhou, Y., & Fu, Q. (2025). Morphological comparison of buccal wear marks on molars between ancient Chinese agricultural and agr-pastoralist populations. *Acta Anthropologica Sinica*, *44*(1), 92–104.